STATIC AND DYNAMIC STABILITY ASSESSMENT OF SLOPES ADJACENT TO APPURTENANT HYDRAULIC STRUCTURES AND STABILIZATION RECOMMENDATIONS

PhD Dissertation

Ahmet Ali MERT

Eskişehir 2026

STATIC AND DYNAMIC STABILITY ASSESSMENT OF SLOPES ADJACENT TO APPURTENANT HYDRAULIC STRUCTURES AND STABILIZATION RECOMMENDATIONS

Ahmet Ali MERT

PHD DISSERTATION

Department of Civil Engineering
Programme in Geotechnics
Supervisor: Prof. Dr. Ahmet TUNCAN

Eskişehir
Eskişehir Technical University
Institute of Graduate Programs
January 2026

FINAL APPROVAL FOR THESIS

This thesis titled STATIC AND DYNAMIC STABILITY ASSESSMENT OF SLOPES ADJACENT TO APPURTENANT HYDRAULIC STRUCTURES AND STABILIZATION RECOMMENDATIONS has been prepared and submitted by Ahmet Ali MERT in partial fulfillment of the requirements in "Eskişehir Technical University Directive on Graduate Education and Examination" for the Degree of PhD in Civil Engineering Department has been examined and approved on 16/01/2026.

Committee Members		**Title, Name and Surname**	**Signature**
Member (Supervisor)	:	Prof. Dr. Ahmet TUNCAN	
Member	:	Prof. Dr. Murat TÜRKÖZ	
Member	:	Assoc. Prof. Dr. Burak EVİRGEN	
Member	:	Assoc. Prof. Dr. Emrah PEKKAN	
Member	:	Assoc. Prof. Dr. Kamil Bekir AFACAN	

Prof. Dr. Harun BÖCÜK
Director of the Institute of Graduate Programs

16/01/2026

SUPERVISOR APPROVAL

PhD student Ahmet Ali MERT, whom I supervise, has completed this thesis titled STATIC AND DYNAMIC STABILITY ASSESSMENT OF SLOPES ADJACENT TO APPURTENANT HYDRAULIC STRUCTURES AND STABILIZATION RECOMMENDATIONS. According to my inspections, the work is scientifically and ethically appropriate for the student to the thesis defense exam.

Supervisor
Prof. Dr. Ahmet TUNCAN

ABSTRACT

STATIC AND DYNAMIC STABILITY ASSESSMENT OF SLOPES ADJACENT TO APPURTENANT HYDRAULIC STRUCTURES AND STABILIZATION RECOMMENDATIONS

Ahmet Ali MERT

Department of Civil Engineering
Programme in Geotechnics

Eskişehir Technical University, Institute of Graduate Programs, January 2026

Supervisor: Prof. Dr. Ahmet TUNCAN

This dissertation investigates the stability of complex excavated slopes adjacent to appurtenant hydraulic structures, addressing the critical gap between deterministic stability calculations and performance-based dynamic and hydrogeological assessments. By analyzing six case studies spanning colluvial deposits, ophiolitic mélanges, saprolitic granodiorites, and water-sensitive sedimentary sequences, this research integrates field monitoring (inclinometers, InSAR) and laboratory testing with advanced numerical modeling. Limit Equilibrium (LEM) and Finite Element (FEM) methods, including fully coupled dynamic time-history simulations with the Hardening Soil Small Strain (HS-Small) model, were employed for back-analysis and predictive stabilization.

Key findings demonstrate extreme hydro-mechanical sensitivity—where saturation drastically degrades rock mass parameters such as Geological Strength Index (GSI) and Uniaxial Compressive Strength (UCS)—as a primary driver of instability, motivating a 'Dual-State' strength characterization. Post-event dynamic evaluations of the 2023 seismic sequence and Level 2 transient seepage analyses of rapid drawdown (RDD) indicate that simplified pseudo-static and Level 1 instantaneous drawdown idealizations often dictate massive structural overdesign, conceptualized herein as the 'over-engineering trap'. Standard shallow reinforcements are kinematically incompatible with deep-seated failure geometries (14–40 m) in these 'intermediate geomaterials'; stabilization instead requires high-capacity active anchoring, proactive deep sub-drainage, or topographic restoration via massive passive weighting (e.g., rockfill buttresses) to achieve 'Absolute System Lock-in' against extreme static and seismic energy.

Ultimately, this study provides a holistic geotechnical framework and evidence-based recommendations to ensure long-term integrity and serviceability of critical hydraulic infrastructure.

Keywords: Slope stability, Appurtenant hydraulic structures, Numerical modeling, Rapid drawdown, Dynamic time-history analysis.

ÖZET

YARDIMCI HİDROLİK YAPILARA BİTİŞİK ŞEVLERİN STATİK VE DİNAMİK STABİLİTESİNİN DEĞERLENDİRİLMESİ VE STABİLİZASYON ÖNERİLERİ

Ahmet Ali MERT

İnşaat Mühendisliği Anabilim Dalı
Geoteknik Bilim Dalı

Eskişehir Teknik Üniversitesi, Lisansüstü Eğitim Enstitüsü, Ocak 2026

Danışman: Prof. Dr. Ahmet TUNCAN

Bu tez, deterministik stabilite hesaplamaları ile performansa dayalı dinamik ve hidrojeolojik değerlendirmeler arasındaki kritik boşluğu ele alarak, yardımcı hidrolik yapılara bitişik karmaşık kazı şevlerinin stabilitesini araştırmaktadır. Kolüvyal çökeller, ofiyolitik melanjlar, saprolitik granodiyoritler ve suya duyarlı tortul birimleri kapsayan altı vaka çalışmasının analiziyle, saha izleme (inklinometreler, InSAR) ve laboratuvar deneyleri gelişmiş sayısal modelleme ile entegre edilmiştir. Geri analiz ve öngörüsel stabilizasyon için, Pekleşen Zemin – Küçük Birim Şekil Değiştirme (*HS-Small*) modeliyle tam bağlaşık dinamik zaman tanım alanında simülasyonları da dâhil, Limit Denge (*LEM*) ve Sonlu Elemanlar Yöntemleri (*FEM*) kullanılmıştır.

Temel bulgular, doygunluğun Jeolojik Dayanım İndeksi (*GSI*) ve Tek Eksenli Basınç Dayanımı (*UCS*) gibi kaya kütlesi parametrelerini büyük ölçüde düşürdüğü aşırı hidro-mekanik duyarlılığın duraysızlığın birincil etkeni olduğunu ve "Çift Durumlu" (*Dual-State*) dayanım belirlemeyi gerektirdiğini göstermektedir. 2023 sismik dizisine ilişkin olay sonrası dinamik değerlendirmeler ve ani su seviyesi düşüşü (*RDD*) için Seviye 2 zamana bağlı sızma analizleri, basitleştirilmiş psödo-statik yaklaşımın ve Seviye 1 anlık düşüş varsayımının sıklıkla büyük çaplı aşırı yapısal tasarıma yol açtığını ortaya koymakta; bu olgu "aşırı tasarım tuzağı" (*over-engineering trap*) olarak kavramsallaştırılmaktadır. Standart sığ destekler, bu "ara nitelikli geomalzemelerde" görülen derin yerleşimli göçme geometrileriyle (14–40 m) kinematik olarak uyumsuzdur; stabilizasyon bunun yerine yüksek kapasiteli aktif ankraj, önetkin derin alt drenaj veya büyük ölçekli pasif ağırlıklandırma (örn. iri kaya dolgu) ile topoğrafik düzenleme yaparak "Mutlak Sistem Kilitlenmesi"ni (*Absolute System Lock-in*) sağlamayı gerektirmektedir.

Sonuç olarak bu çalışma, kritik hidrolik altyapının uzun vadeli bütünlüğünü ve hizmet edebilirliğini sağlamak için bütüncül bir geoteknik çerçeve ve kanıta dayalı stabilizasyon önerileri sunmaktadır.

Anahtar Sözcükler: Şev stabilitesi, Yardımcı hidrolik yapılar, Sayısal modelleme, Ani su seviyesi düşüşü, Dinamik zaman tanım alanı analizi.

ACKNOWLEDGEMENTS

I would like to express my deepest gratitude to my supervisor, Prof. Dr. Ahmet TUNCAN, for his guidance, encouragement, and steady support throughout this doctoral journey. His academic insight, constructive feedback, and trust in my work have been invaluable in shaping both the direction and the quality of this dissertation.

I am also sincerely grateful to my committee members, Assoc. Prof. Dr. Burak EVİRGEN and Assoc. Prof. Dr. Emrah PEKKAN, for their time, careful evaluation, and thoughtful suggestions. Their questions and recommendations helped refine the scope of the study and strengthened the rigor of the analyses.

My heartfelt thanks go to my colleagues Seçkin AYDIN, Yasemin ER and M. Çağatay KENT for their technical support and for generously sharing their experience—especially regarding time-history dynamic analyses. I would also like to thank my Branch Manager, Fatih ÇALIŞKAN, for his kindness and understanding, and Özgür ÖZTÜRK and Pelin UYGUR for sharing their knowledge and experience, as well as my other colleagues for their support and encouragement throughout this process.

I owe my greatest personal thanks to my wife, Petra, and our son, Deniz Sarp. Even when this work required me to withdraw and focus intensely for long periods, their patience, understanding, and unwavering support made it possible to continue. Their presence, love, and encouragement have been my strongest motivation.

I would also like to thank my mother, father, and brother for always standing by me and supporting my decisions. Their confidence and backing have been a constant source of strength.

Finally, I extend my appreciation to the staff of Eskişehir Technical University—which was Anadolu University during my undergraduate years—where I completed my double major in Environmental Engineering and Civil Engineering. The education and supportive academic environment I experienced there laid an essential foundation for my graduate studies.

Ahmet Ali MERT

16/01/2026

STATEMENT OF COMPLIANCE WITH ETHICAL PRINCIPLES AND RULES

I hereby truthfully declare that this thesis is an original work prepared by me; that I have behaved in accordance with the scientific ethical principles and rules throughout the stages of preparation, data collection, analysis and presentation of my work; that I have cited the sources of all the data and information that could be obtained within the scope of this study, and included these sources in the references section; and that this study has been scanned for plagiarism with “scientific plagiarism detection program” used by Eskişehir Technical University, and that “it does not have any plagiarism” whatsoever. I also declare that, if a case contrary to my declaration is detected in my work at any time, I hereby express my consent to all the ethical and legal consequences that are involved.

Ahmet Ali MERT

CONTENTS

Page

LIST OF TABLES

Page

LIST OF FIGURES

Page

LIST OF IMAGES

Page

GLOSSARY OF SYMBOLS AND ABBREVIATIONS

ADAS	:	Automated Data Acquisition Systems
AFAD	:	Disaster and Emergency Management Presidency
ALS	:	Airborne Laser Scanning (Airborne platforms)
ANN	:	Artificial Neural Networks
ASK14	:	Abrahamson et al. (2014) Ground Motion Model
ASTM	:	American Society for Testing and Materials
ATV	:	Acoustic Televiewers
BSSA14	:	Boore et al. (2014) Ground Motion Model
CAV	:	Cumulative Absolute Velocity
CB14	:	Campbell and Bozorgnia (2014) Ground Motion Model
CBA	:	Cost-Benefit Analysis
CFRD	:	Concrete-Faced Rockfill Dam
CFSGD	:	Concrete-Faced Sand-Gravel Fill Dam
CIUC	:	Consolidated Isotropic Undrained Compression
CMS	:	Conditional Mean Spectrum
CNL	:	Constant Normal Load
CNS	:	Constant Normal Stiffness
COV	:	Coefficient of Variation
CS	:	Conditional Spectrum / Cuckoo Search
CU	:	Consolidated-Undrained
CWC	:	Central Water Commission
CY14	:	Chiou and Youngs (2014) Ground Motion Model
DEM	:	Distinct Element Method / Discrete Element Method
DLO	:	Discontinuity Layout Optimization
DSM	:	Digital Surface Model

ERT	:	Electrical Resistivity Tomography
FDM	:	Finite Difference Method
FELA	:	Finite Element Limit Analysis
FEM	:	Finite Element Method
FERC	:	Federal Energy Regulatory Commission
FOS / FoS / FS	:	Factor of Safety
FOSM	:	First-Order Second-Moment
GA	:	Genetic Algorithms
GCIM	:	Generalized Conditional Intensity Measure
GLE	:	General Limit Equilibrium
GMM	:	Ground Motion Model
GSI	:	Geological Strength Index
GWT	:	Groundwater Table
H-M	:	Hydro-Mechanical
HS	:	Hardening Soil
HS-Small	:	Hardening Soil Small Strain
I14	:	Idriss (2014) Ground Motion Model
I_A	:	Arias Intensity
IBO	:	Self-Drilling Anchors
ICOLD	:	International Commission on Large Dams
IFT	:	Independent Forensic Team
IMs	:	Intensity Measures
InSAR	:	Interferometric Synthetic Aperture Radar
IPI	:	In-Place Inclinometers
ISO	:	International Organization for Standardization
ISRM	:	International Society for Rock Mechanics

LiDAR	:	Light Detection and Ranging
LM	:	Landslide Material
M-C / MC	:	Mohr-Coulomb
MCC	:	Modified Cam Clay
MCE	:	Maximum Credible Earthquake
MCMC	:	Markov Chain Monte Carlo
MDE	:	Maximum Design Earthquake
ML	:	Machine Learning
MOL	:	Minimum Operating Level
M-P	:	Morgenstern-Price
MPS	:	Modal-Pushover-based Scaling
MPM	:	Material Point Method
MRL	:	Maximum Reservoir Level
MSE	:	Mechanically Stabilized Earth
OBE	:	Operating Basis Earthquake
OMS	:	Ordinary Method of Slices
OTV	:	Optical Televiewers
PBEE	:	Performance-Based Earthquake Engineering
PGA	:	Peak Ground Acceleration
PGV	:	Peak Ground Velocity
PI	:	Plasticity Index
PINNs	:	Physics-Informed Neural Networks
PLI / PLT	:	Point Load Index / Point Load Test
PMP	:	Probable Maximum Precipitation
PMT	:	Pressuremeter Test / Menard Pressuremeter Test
P-Q	:	Pressure-Flow (curves)

P_{Sa} : Pseudo-Spectral Acceleration

PSHA : Probabilistic Seismic Hazard Analysis

PSI : Persistent Scatterer Interferometry

PT : Packer (Lugeon) Test

PWP : Pore Water Pressure

QRA : Quantitative Risk Assessment

RDD : Rapid Drawdown

RF : Random Forests

RHA : Response History Analysis

RIDM : Risk-Informed Decision Making

RMR : Rock Mass Rating

RQD : Rock Quality Designation

RQD_{wjd} : Weighted Joint Density

SAO : Surface Altering Optimization

SBAS : Small Baseline Subset

SCR : Surface Condition Rating

SDF : Single-Degree-of-Freedom

SDS : Short-Period Design Spectral Acceleration Parameter

SEE : Safety Evaluation Earthquake

SF : Scaling Factor

SMR : Slope Mass Rating

SPT : Standard Penetration Test

SR : Structure Rating

SRF : Stress Reduction Factor (Q-system) / Strength Reduction Factor (FEM)

SRM : Strength Reduction Method / Shear Strength Reduction Method

S-STAF : Seismic-Slope Topographic Amplification Factor

SVM	:	Support Vector Machines
SVR	:	Support Vector Regression
SZ	:	Shear Zone
TBDY	:	Turkish Building Earthquake Code
TC	:	Triaxial Compression
TLS	:	Terrestrial Laser Scanning (Terrestrial tripods)
UC	:	Unconfined Compression Test
UCS	:	Uniaxial Compressive Strength
UD	:	Undisturbed (Samples)
UDSM	:	User-Defined Soil Models
UHS	:	Uniform Hazard Spectrum
USACE	:	U.S. Army Corps of Engineers
USBR	:	United States Bureau of Reclamation
UU	:	Unconsolidated-Undrained
V/H	:	Vertical-to-Horizontal Spectral Ratio
VST	:	Vane Shear Test
VW	:	Vibrating Wire

GLOSSARY OF SYMBOLS

[C]	:	Damping matrix
[K]	:	Stiffness matrix
[M]	:	Mass matrix
a	:	Material constant / variable parameter for the rock mass (Hoek-Brown)
a_y	:	Yield acceleration
c / c_0	:	Cohesion
c'	:	Effective cohesion
c'_r	:	Residual effective cohesion

c'_r	:	Residual effective cohesion
c_r / s_r	:	Apparent cohesion (root reinforcement)
D	:	Excavation disturbance factor
E / Ei	:	Young's modulus / Intact elastic modulus
E / $E_{interslice}$	:	Interslice normal force (Method of Slices)
E_{50}^{ref}	:	Triaxial primary loading stiffness
E_D	:	Dilatometer modulus
E_k	:	Average deformation modulus
E_m / E_{rm}	:	In-situ deformation modulus / Menard modulus / Rock mass deformation modulus
E_{oed}^{ref}	:	Oedometer loading stiffness
E_p / E_{PMT}	:	Pressuremeter modulus
E_{ur}^{ref}	:	Triaxial unloading-reloading stiffness
e_0	:	Initial void ratio
f(x)	:	Interslice force function
F_{2D}	:	Factor of Safety from 2D analysis
F_{3D}	:	Factor of Safety from 3D analysis
f_{max}	:	Maximum oscillation frequency
F_h	:	Pseudo-static horizontal force
G	:	Shear modulus
G_0	:	Small-strain shear modulus
G_{max}	:	Small-strain stiffness indicator
H	:	Hardening parameter / Slope height
I_{s50}	:	Point Load Index (indirect strength estimation)
J_a	:	Joint alteration number
J_{Cond89}	:	Joint condition ratings
J_n	:	Joint set number

J_r	:	Joint roughness number
J_v	:	Volumetric joint count
J_w	:	Joint water reduction factor
K	:	Equivalent hydraulic conductivity
k	:	Hydraulic conductivity
K_0	:	In situ horizontal stress coefficient
K_c	:	Critical Acceleration
K_D	:	Dilatometer horizontal stress index
k_h	:	Horizontal pseudo-static seismic coefficient
k_s	:	Winkler spring coefficients
k_v	:	Vertical pseudo-static seismic coefficient
k_y	:	Critical horizontal acceleration / yield acceleration
L/H	:	Length-to-height ratio
Lu	:	Lugeon coefficient
m	:	Power-law exponent
M	:	Slope of Critical State Line (CSL)
$\bar{M}$	:	Mean Moment Magnitude
m_b	:	Reduced frictional strength (Hoek-Brown)
m_i	:	Intact rock material constant / intrinsic frictional characteristics
M_w	:	Moment Magnitude
N	:	Standard penetration test blow count / Hardening parameter
$N_{1(60)}$	:	Corrected SPT blow count
P	:	Compressional Wave
P_f	:	Creep pressure / Probability of failure
PGA_{ground}	:	Peak ground acceleration at the ground surface
$PGA_{rock,outcrop}$	:	Peak ground acceleration at outcropping rock

q_T	:	Corrected cone tip resistance
q_u	:	Uniaxial compressive strength
R	:	Drawdown rate
$\bar{R}$	:	Mean Source-to-Site Distance
R_{jb}	:	Joyner-Boore distance
R_{rup}	:	Rupture distance
r_u	:	Pore water pressure ratio
S	:	Shear Wave
s	:	Rock mass cohesion/interlocking material constant (Hoek-Brown)
S_a	:	Spectral acceleration
S_s	:	Specific Storage
s_u	:	Undrained shear strength
s_u^e	:	Mixture of s_u from UU, UC, and VST
T	:	Period
T*	:	Control period
T_s	:	Natural period of the slope
u	:	Pore water pressure / Total displacement
U_t	:	Actual dissipation of pore water pressures
V_p	:	P-wave (compressional wave) velocity
V_s	:	S-wave (shear wave) velocity
V_{s30}	:	Time-averaged shear wave velocity in the top 30 meters
W	:	Weight of the sliding mass
X	:	Interslice shear force (Method of Slices)
$Z_{1.0}$ / $Z_{2.5}$	:	Depths to the 1.0 km/s and 2.5 km/s isosurfaces
Z_{hyp}	:	Hypocentral depth
Z_{tor}	:	Depth-to-top of rupture

α (Alpha)	:	Mass-proportional Rayleigh damping coefficient
β (Beta)	:	Stiffness-proportional Rayleigh damping coefficient / Reliability index
Γ (Gamma)	:	Critical state parameter
γ (Gamma)	:	Unit weight
$\gamma_{0.7}$	:	Threshold shear strain parameter
γ_s / γ_{sat}	:	Saturated unit weight
Δ (Delta)	:	Maximum element size
$\bar{\varepsilon}$ (Epsilon)	:	Logarithmic standard deviations
κ (Kappa)	:	Swelling index
λ (Lambda)	:	Compression index / Unknown scaling factor
ν (Nu)	:	Poisson's ratio
ξ (Xi)	:	Damping ratio
σ_1 (Sigma 1)	:	Major principal stress
σ_2 (Sigma 2)	:	Intermediate principal stress
σ_3 (Sigma 3)	:	Minor principal stress
σ'^{max}_3	:	Upper limit of confining stress
σ_{ci} (Sigma_ci)	:	Uniaxial compressive strength of intact rock
σ_n (Sigma_n)	:	Total normal stress
σ_n' (Sigma_n')	:	Effective normal stress
ΣM_{sf}	:	Safety factor (PLAXIS / RS2)
τ (Tau)	:	Shear strength / Shear stress
φ / ϕ (Phi)	:	Angle of internal friction
φ' / ϕ' (Phi')	:	Effective angle of internal friction
φ_b (Phi_b)	:	Angle of shear strength increase with suction

φ_{cv} (Phi_cv)	:	Constant-volume friction angle
χ (Chi)	:	Dilatancy parameter
ψ (Psi)	:	Dilation angle / State parameter
ω (Omega)	:	Frequency

1. INTRODUCTION

Slope instability around appurtenant hydraulic structures constitutes a multidisciplinary geotechnical problem at the intersection of engineering geology, hydro-mechanical behavior, seismic response, and infrastructure safety. The design, construction, and long-term operation of such critical water infrastructure require a rigorous understanding of the complex interactions between large engineered structures and their surrounding geological environments. As global infrastructure development extends into increasingly difficult terrains—characterized by transitional geological formations, pronounced hydro-mechanical fluctuations, and heightened seismic demand—the combined effects of complex geomaterials, excavation-induced stress redistribution, and operational loading histories give rise to failure mechanisms that are not adequately captured by traditional, isolated analytical methodologies. Accordingly, a rigorous assessment of these slopes requires not only a sound understanding of site-specific conditions but also an advanced, multi-methodological framework capable of bridging the gap between conventional static approaches and the dynamic, time-dependent conditions reflected in observed field performance. Within this context, the present chapter introduces the fundamental problem addressed by the dissertation, formulates the principal research hypotheses, defines the purpose and scope of the study, outlines the methodological framework adopted, and highlights the main scientific contributions and organizational structure of the thesis.

1.1. Problem Definition

The stability of slopes surrounding appurtenant hydraulic structures—such as dam abutments, spillway excavations, and diversion tunnel portals—represents a critical component in the overall safety and operational longevity of water infrastructure. These engineered and natural slopes frequently consist of complex "intermediate" geological materials, including thick heterogeneous colluvium, advanced weathering profiles (saprolites), and tectonically disturbed "block-in-matrix" (bimrock) units. Such heterogenous formations are highly susceptible to failure under a combination of adverse boundary conditions, particularly severe hydro-mechanical sensitivity, rapid reservoir level fluctuations, and extreme seismic excitation. Globally, failures in these zones have caused catastrophic damage, ranging from spillway blockages and tunnel portal closures to dam overtopping caused by landslide-generated waves.

The profound challenge in analyzing these slopes stems from their unique and multifaceted operational environment. Unlike generic natural slopes, slopes near hydraulic structures are subjected to high hydraulic gradients, transient rapid drawdown (RDD) effects, and stringent spatial constraints due to the proximity of rigid concrete structures. Traditionally, geotechnical stability assessments have relied heavily on deterministic static analyses or simplified pseudo-static seismic coefficients (k_h). However, recent historical precedents, such as the 2008 Wenchuan earthquake and documented post-seismic field performances in Türkiye, emphasize that conventional static and pseudo-static methods systematically fail to capture transient hydrogeological behaviors (such as "pore pressure lag") and dynamic hysteretic damping. Consequently, this reliance on simplified methodologies often leads to two extreme outcomes: either catastrophic failure due to the non-recognition of deep-seated residual kinematics, or massive, financially crippling "over-engineering" mandated by overly conservative screening assumptions.

Therefore, this thesis addresses a critical gap in geotechnical engineering practice where individual analysis modes are often applied in isolation. There is an urgent necessity for a comprehensive framework that evaluates hydraulic slopes under the full spectrum of their lifecycle loading—static, pseudo-static, and fully dynamic time-history—to accurately capture the kinematics of complex mass movements and prevent the limitations of conventional analytical paradigms from compromising critical infrastructure.

1.2. Research Hypotheses

To directly challenge the analytical limitations identified in geotechnical practice and establish a rigorous framework for stability assessment, this dissertation postulates the following core hypotheses:

1. Analytical Conservatism and the "Over-Engineering Trap" in Transient States: It is postulated that conventional "instantaneous" (Level 1) Rapid Drawdown assumptions, which neglect time-dependent drainage, are fundamentally overly conservative for low-permeability sedimentary clays. Implementing rigorous transient seepage (Level 2) numerical models will demonstrate that the inherent "phreatic lag" is often managed naturally,

thereby neutralizing the need for redundant, massive structural interventions.

2. Kinematic Incompatibility of Standard Support in Deep-Seated Failures: In geomaterials exhibiting deep weathering profiles, thick colluvial deposits, or bimrock characteristics, standard shallow pattern bolting (e.g., 3.0–6.0 m) is kinematically incompatible, acting merely as "floating" elements within the active sliding mass. Stabilization in such regimes strictly requires high-capacity actively prestressed anchors socketed deep into competent bedrock or massive passive topographic restoration.
3. Dynamic Resilience vs. Pseudo-Static Overestimation: A fundamental discrepancy exists between conventional pseudo-static predictions and true physical seismic performance. Highly damped, clay-rich ophiolitic matrices can sustain extreme peak ground accelerations (e.g., 0.48g) without catastrophic collapse, indicating that traditional pseudo-static coefficients may drastically neglect the hysteretic energy dissipation capabilities of these complex units.
4. The "Safety Factor Gap" and Absolute System Lock-in: A quantifiable divergence exists between Limit Equilibrium Methods (LEM) and Finite Element Methods (FEM) when applied to complex tectonic geometries. Advanced FEM modeling utilizing sophisticated constitutive models (e.g., HS-Small) will uniquely demonstrate that massive passive mass weighting (rockfill buttressing) can absorb extreme inertial forces, achieving an "Absolute System Lock-in" where pre-seismic safety margins are perfectly preserved post-earthquake.

1.3. Purpose and Scope of the Study

The primary purpose of this Ph.D. dissertation is to develop and demonstrate a robust, multi-methodological framework for evaluating and mitigating slope instabilities around appurtenant hydraulic structures. This research directly aims to bridge the gap between deterministic Limit Equilibrium Factor of Safety (FS) calculations and advanced, performance-based dynamic and hydrogeological numerical assessments.

The scope of this study encompasses six detailed case studies located in Türkiye, each rigorously selected to represent distinct geological "intermediate" materials and varied triggering mechanisms:

- Case 1: Deep Rotational Slide in Colluvial Soil (Spillway Excavation) - Analyzes a failure triggered by steep 1V:1H excavations and restricted natural drainage (r_u=0.15) caused by surface shotcrete, mitigated through 15-35 m active prestressed anchors to maintain permanent seismic displacements within tolerable serviceability limits (≤1.0 m).
- Case 2: Massive Mass Movement in Radiolarite-Limestone-Mudstone Sequence (CFRD Left Abutment) - Evaluates a 435 m long tectonic mélange geohazard mobilized by excavation and 0.6g-0.7g seismic sequences, successfully stabilized via a massive rockfill buttress that ensures Absolute System Lock-in.
- Case 3: Atmospheric Weathering and Portal Stability in Ophiolitic Mélange - Investigates rapid argillization and subsequent tunnel portal closure upon atmospheric exposure, contrasting theoretical pseudo-static failure (0.48g) with observed physical stability, remediated via a cut-and-cover topographic restoration.
- Case 4: Flysch Facies Landslide Induced by Poor Drainage and Surcharge - Examines a deep flow-type slide in highly weathered flysch triggered by a 10 m uncontrolled spoil surcharge and snowmelt, resolved through rigorous geometric flattening (1V:3H), surcharge removal, and sealing the soil-structure contact.
- Case 5: Spillway Excavation in Highly Weathered (Arenized) Granodiorite - Addresses a critical static state (FS = 1.14) in 20 m deep friable saprolite, stabilized using a zoned support strategy combining 1V:1.33H flattening, 12 m rock bolts, and hydrogeological management.
- Case 6: Rapid Drawdown (RDD) in Clayey Sedimentary Units and Analysis Hierarchy - Compares a theoretical Level 1 instantaneous drawdown screening against a Level 2 transient seepage model, mathematically proving that intrinsic pore pressure dissipation neutralizes the necessity for 12.0 m rock anchors in a submerged portal.

1.4. Method and Approach

This research establishes a multi-pronged methodological framework combining meticulous field characterization, laboratory testing, and advanced computational modeling.

- Site characterization and laboratory testing
  Field investigations integrated extensive core drilling, Menard pressuremeter tests (PMT), Standard Penetration Tests (SPT), and Lugeon/hydraulic conductivity tests. This was supplemented by state-of-the-art geophysical surveys, including seismic refraction and Electrical Resistivity Tomography (ERT), alongside long-term displacement tracking via InSAR and LiDAR. The laboratory program quantified intact parameters via Uniaxial Compressive Strength (UCS), Point Load Index (PLT), and triaxial shear tests. To transition from intact rock to rock mass behavior, empirical classification systems including RQD, RMR, the Q-system, and the Geological Strength Index (GSI) were employed, ultimately deriving non-linear strength envelopes via the Generalized Hoek-Brown failure criterion factoring in the excavation disturbance factor (D).
- Advanced computational framework

  The analytical architecture seamlessly integrates dual numerical approaches:
  - Limit Equilibrium Method (LEM): Utilizing Spencer and Morgenstern-Price algorithms within Slide2 to calculate rigorous global static and pseudo-static Factors of Safety, employing advanced search strategies (e.g., Cuckoo and Particle Swarm) to identify governing non-circular mechanisms along heterogeneous soil-rock contacts.
  - Finite Element Method (FEM): Employing the Shear Strength Reduction (SSR) technique in PLAXIS 2D and RS2 to capture stress-strain compatibility and complex soil-structure interactions without predefined geometric assumptions.
  - Dynamic Time-History Analysis: Performing fully coupled dynamic time-history simulations utilizing the advanced Hardening Soil Small Strain (HS-Small) constitutive model to capture hysteretic damping and strain-dependent stiffness. Target design spectra were generated using the PEER NGA-West2 framework, and selected seed earthquake records (including AFAD database events) were spectrally matched via SeismoMatch for precise dynamic loading.

- Back-Analysis and Calibration: A fundamental step in this methodology involved the rigorous calibration of active failure mechanisms. Residual shear strength parameters of critical slip surfaces were iteratively established using inclinometer data to bring the numerical system to a verified limit state of $FS \approx 1.0$ prior to remediation design.

1.5. Gap in the Literature and Contribution of the Thesis

A notable gap exists in current geotechnical literature regarding the holistic, coupled analysis of appurtenant hydraulic structure slopes subjected to combined operational and extreme loading conditions. Most existing studies focus heavily on single-trigger factors or idealized, homogeneous rock mass geometries. This thesis explicitly contributes to the field by providing a novel, integrated comparison of analytical approaches applied directly to complex, real-world hydraulic slopes, moving beyond theoretical mechanics to practical execution.

Key scientific and practical contributions of this research include:

- Validating performance-based seismic design: Correlating simplified pseudo-static outcomes with dynamic FEM analyses to empirically prove the high damping capacity of clay-rich ophiolitic matrices, and establishing the concept of "Absolute System Lock-in" via massive passive rockfill reinforcement.
- Resolving the RDD "over-engineering trap": Moving beyond empirical screening charts by demonstrating that Level 2 coupled transient seepage analyses physically neutralize the theoretical hazards and exorbitant shoring costs artificially created by Level 1 instantaneous drawdown assumptions.
- Characterization of "intermediate" geomaterials: Expanding the geotechnical knowledge base regarding bimrocks, arenized saprolites, and colluvial mixtures. The research illustrates how these materials dictate entirely different, deep-seated kinematic stability responses that render shallow pattern bolting obsolete, requiring instead specialized deep-anchoring or topographic restoration.

1.6. Thesis Organization

This thesis is structured into six logically progressive chapters designed to seamlessly connect the defined problem to the ultimate stabilization solutions:

- Chapter 1 (Introduction) outlines the problem definition, specific research hypotheses, core objectives, and the overarching multi-methodological approach.
- Chapter 2 (Literature Review) establishes the theoretical foundation for slope stability, intermediate geomaterial behavior, hydro-mechanical coupling, and advanced numerical analysis paradigms.
- Chapter 3 (Methodology) thoroughly details the site characterization techniques, laboratory testing protocols, empirical parameter derivation, and the specific computational framework (Slide2, RS2, PLAXIS 2D) applied to each distinct case study.
- Chapter 4 (Case Studies and Analyses) presents the empirical field data and numerical modeling results of the six specific sites, focusing on site-specific back-analyses, failure mechanism identification, and structural remediation validations under static and dynamic loading.
- Chapter 5 (Discussion) synthesizes the kinematic findings, hydro-mechanical parameter sensitivities, and numerical methodology discrepancies across all cases, explicitly evaluating the reliability of the integrated analysis framework.
- Chapter 6 (Conclusions and Recommendations) directly links back to the research hypotheses outlined in this introduction, concluding the study with definitive static and dynamic findings, practical design recommendations emphasizing the Observational Method, and targeted trajectories for future research.

2. LITERATURE REVIEW

This chapter presents a comprehensive review of the academic and technical literature pertinent to the stability of soil slopes. It begins by outlining the fundamental factors that govern slope stability, including soil properties, hydrogeological conditions, and seismic effects. It then describes the primary mechanisms of landslide failure and details the spectrum of analytical methods used for their assessment, from traditional to state-of-the-art (Duncan et al., 2014; Varnes, 1978). Finally, it reviews common slope stabilization techniques and summarizes relevant case studies from the literature.

The assessment of slope stability has evolved significantly over the past century, building upon foundational theories and analytical frameworks that continue to underpin modern geotechnical practice (Duncan, 1996; Duncan et al., 2014). The theoretical underpinnings of modern slope stability analysis are deeply rooted in the early 20th-century developments in soil mechanics, particularly the work of Karl Terzaghi on effective stress and shear strength (Terzaghi, 1943). These principles provided the basis for quantifying the forces that resist and drive slope movement. The evolution of slope stability methodologies reflects an ongoing pursuit of improved safety measures and design practices, addressing both traditional techniques and innovative analytical frameworks (Chakraborty and Dey, 2022; Tanchev, 2014).

The failure of slopes associated with dams, whether in the main embankment or in excavated spillway channels, can lead to catastrophic outcomes, including significant economic loss and loss of life (Fell et al., 2014; Fell et al., 2005). Consequently, a robust understanding of historical failures, analytical precedents, and rehabilitation performance is essential for advancing the state of practice (Fell et al., 2014; Duncan et al., 2014). This evolution is illustrated in Figure 2.1.

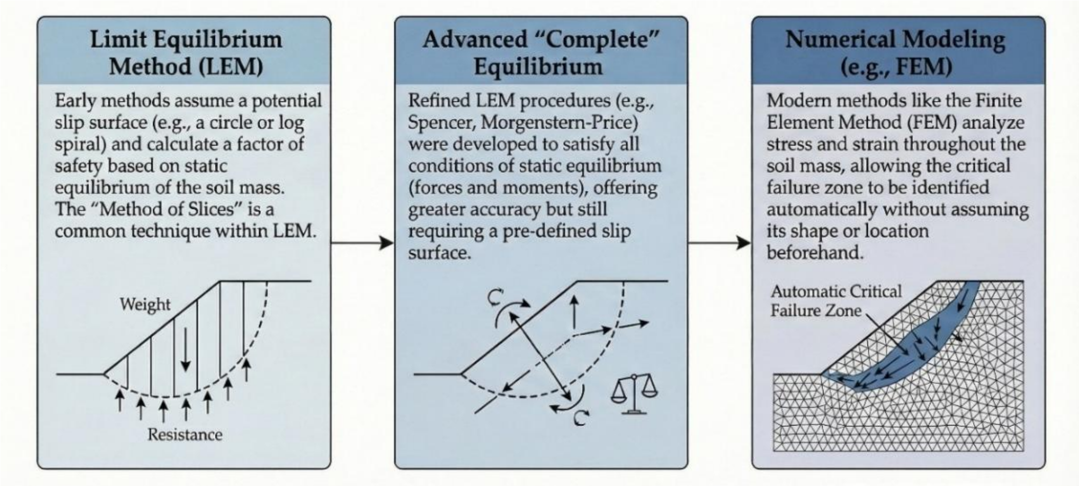

Figure 2.1. *Schematic illustration of the evolution of slope stability analysis methods from limit equilibrium to advanced numerical modeling (Duncan et al., 2014)*

The practice of slope stability analysis is founded on a rich history of theoretical development. This section traces the intellectual lineage of the discipline, beginning with the foundational concepts that underpin modern practice. It critically examines the assumptions, evolution, and inherent limitations of the primary analytical frameworks used to assess the stability of soil slopes and rock masses.

2.1. Factors Affecting Slope Stability

Slope stability is influenced by both static and dynamic factors, many of which are characterized by uncertainty and spatial variability (Xu et al., 2023; Zerouali et al., 2024). Instability occurs when the driving forces that promote downslope movement exceed the resisting forces provided by the shear strength of the soil or rock mass (Terzaghi, 1950). The reliability of any slope stability analysis, whether static, pseudo-static, or dynamic, is fundamentally dependent on the accuracy of the input parameters used to characterize the geomaterials and the geological setting (Phoon and Kulhawy, 1999; Baecher and Christian, 2003). The analysis of this balance requires a thorough understanding of the material properties, site conditions, and external loads. Slope stability is influenced by several external factors, such as (Abramson et al., 2002; Duncan et al., 2014; Wyllie and Mah, 2004):

- Geological and material properties: These include soil/rock type, unit weight, cohesion, friction angle, and structural discontinuities such as faults, joints, and bedding planes, all of which strongly influence slope stability and failure mode.

Weak layers, clay-rich interbeds, and fractured rock can significantly reduce stability. (Nanehkaran et al., 2022; Kolapo et al., 2022; Zhuang et al., 2024).

- Geometric attributes: Slope gradient and height strongly affect stability; steeper and higher slopes generally experience greater driving shear stress, and geometric relations between the slope face and potential failure planes influence kinematic feasibility. (Raghuvanshi, 2017; Lin et al., 2024).
- Hydrological conditions: Rainfall infiltration and groundwater fluctuations can increase pore-water pressure and reduce effective stress and shear strength. Reliable rainfall and hydrologic information are therefore important for landslide early warning systems. (Raghuvanshi, 2017; Guzzetti et al., 2020; Mirus et al., 2025).
- External loadings: Earthquakes can induce dynamic instability, and slopes that are stable under static conditions may become unstable under seismic loading. (Bayati et al., 2025; Raghuvanshi, 2017).
- Human activities and weathering: Construction, excavation/unloading, and long-term weathering can alter slope geometry and degrade material strength, thereby contributing to instability (Qu and Dang, 2022; Liu et al., 2024). Figure 2.2 illustrates interacting forces on a slope.

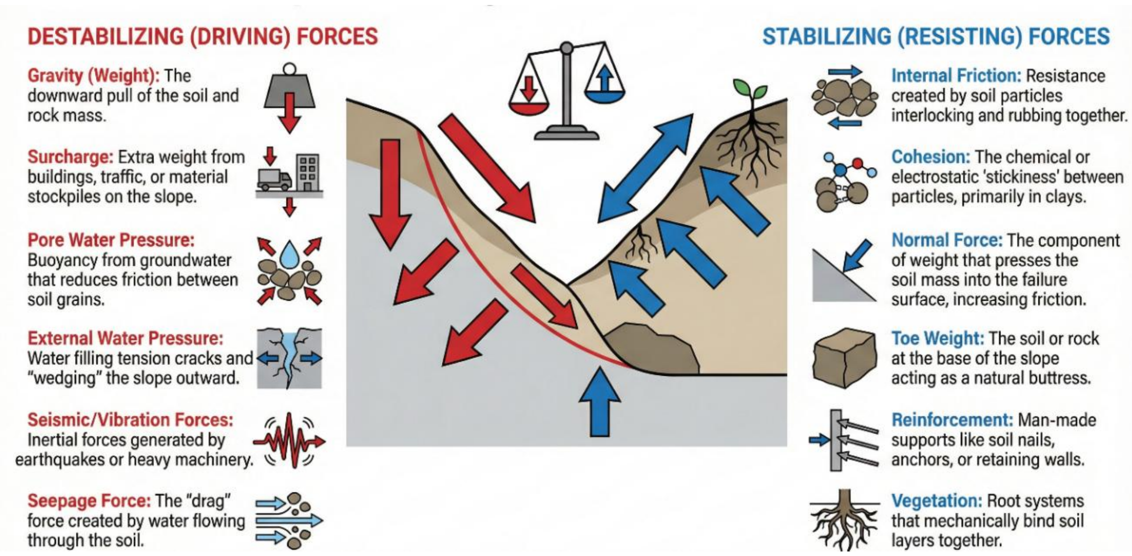

Figure 2.2. *Conceptual diagram illustrating the interaction of destabilizing forces and stabilizing forces on a slope cross-section (Abramson et al., 2002)*

Uncertainty in these factors (e.g., pore water pressure, geomaterial characteristics, slope geometry, and strength properties) is a major deficiency in traditional empirical and statistical assessments, often leading to increased error rates in stability analysis (Nanehkaran et al., 2023; Xu et al., 2023).

2.1.1. Soil properties and site conditions

The shear strength of soil is the single most critical and often the most uncertain parameter in stability analysis (Stark et al., 2005). For most geotechnical problems, the shear strength (τ) of a soil is described by the Mohr-Coulomb failure criterion (Terzaghi, 1943), which relates the strength to the effective normal stress (σ_n') on the failure plane through the effective stress cohesion (c') and the effective angle of internal friction (ϕ'):

$$\tau = c' + (\sigma_n - u)\tan(\varphi') \tag{2.1}$$

Where σ_n is the total normal stress and u is the pore water pressure (Duncan et al., 2014).

The selection of appropriate strength parameters is paramount. For cohesive soils, particularly overconsolidated clays and clay shales, it is crucial to distinguish between different strength states. The fully softened strength is considered applicable to intact, stiff clays that have not previously failed, whereas the residual strength applies to slopes containing pre-existing shear surfaces, such as those in ancient landslides or along sheared bedding planes (Stark et al., 2005). For analyses involving residual or fully softened conditions, it is a common and conservative recommendation to assume the effective cohesion (c') is zero, with all resistance derived from friction (Stark et al., 2005). The corresponding failure envelopes are plotted in Figure 2.3.

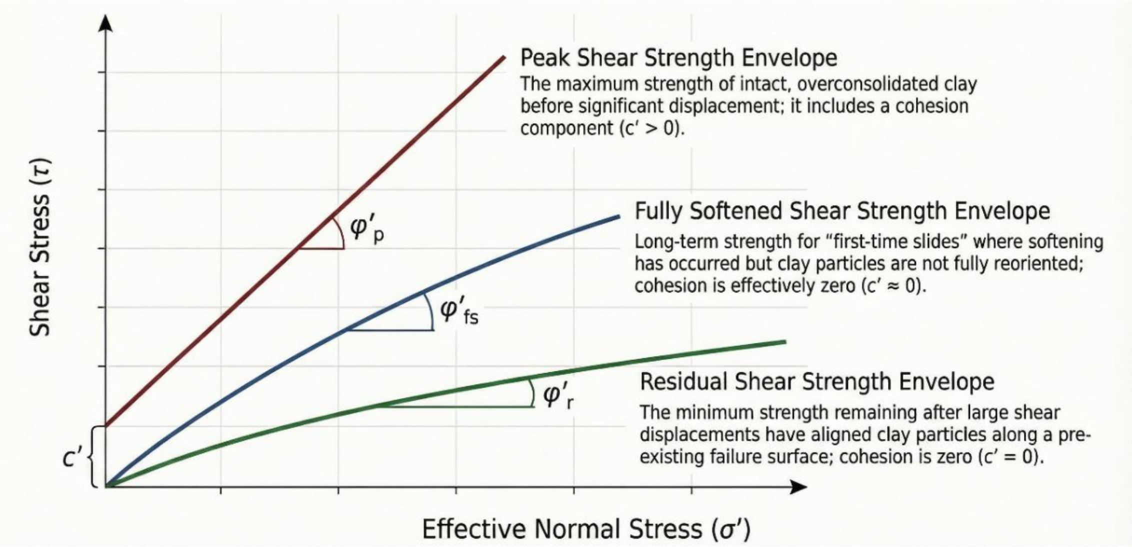

Figure 2.3. *Shear stress vs. normal stress plot illustrating the Mohr-Coulomb failure envelopes for peak, fully softened, and residual shear strengths in overconsolidated clays (Stark et al., 2005)*

The accurate characterization of soil and rock properties is a cornerstone of reliable slope stability assessment. These properties, including but not limited to cohesion, friction angle, Young's modulus, Poisson's ratio, and hydraulic conductivity, exhibit inherent spatial variability due to natural geological processes. Capturing this variability is a significant challenge (Phoon and Kulhawy, 1999; Baecher and Christian, 2003). This spatial variability means that a single, deterministic value for a soil property may not adequately represent the conditions across a slope, potentially leading to inaccurate stability assessments. For instance, the presence of weak layers or discontinuities, if not identified and characterized properly, can strongly influence the governing failure mechanism and the calculated factor of safety. A defensible stability analysis therefore depends on thorough site characterization, including stratigraphy and lithology, structural features such as faults and adversely oriented joints, the degree of weathering, groundwater conditions, and field evidence of past instability (U.S. Army Corps of Engineers [USACE], 2003; Washington State Department of Transportation [WSDOT], 2022).

Case studies reveal the critical importance of geology. The Rampac Grande landslide in Peru involved an earth slide-earth flow mechanism on slopes composed of weathered argillite rocks and tuffs. The landslide material was characterized as fine gravelly very coarse silt sediment with a high content of secondary carbonates (20-57%) and, in some instances, smectite clay minerals (up to 29%), which can significantly reduce shear strength. Similarly, the Charvak Reservoir area in Uzbekistan is characterized by limestone, sandstone, and shale, overlain by thick loess and loess-like rocks which are prone to losing strength upon contact with precipitation (Khakimov et al., 2024). Landslides in interbedded rock formations, like the one on the G104 Jinglan Line in China, are challenged by weak interlayers (e.g., mudstone) that act as preferential failure surfaces (Zhuang et al., 2024). Ophiolite units, like at the Bolango Ulu Dam in Indonesia, consist of highly fractured and sheared rock masses prone to instability when excavated (Wibowo and Purnomo, 2021). A major challenge in practice is the inherent spatial variability of these properties. Natural soil and rock deposits are never truly homogeneous; their properties vary, often significantly, from point to point (Whitman, 2000). Geomaterials are inherently variable—properties like shear strength, unit weight, and permeability can change significantly across a site.

A major challenge in slope stability is determining what set of parameters to use in analysis. A slope may have zones of weaker material (e.g., a thin clay seam) that govern stability, or spatial trends (soil getting softer with depth, etc.). Conventional deterministic analyses typically simplify this complexity by using single, representative values (e.g., a conservative average) for an entire soil layer. This approach, however, fails to capture the fact that a failure surface may preferentially seek out interconnected paths of weaker material zones, a possibility that is ignored when using average properties. As Whitman (2000) noted, the variability of soil properties horizontally and vertically is especially important in problems like long embankment stability. If an embankment extends over several kilometers, one might reasonably expect some weaker pockets—the probability of failure might be controlled by the worst pocket. Site investigation should aim not just to find average properties, but to detect such weak zones or significant stratigraphic changes. This often means more boreholes or geophysical surveys for large slopes (Phoon and Kulhawy, 1999; Baecher and Christian, 2003; Duncan et al., 2014).

Table 2.1 provides a comprehensive summary of the coefficients of variation (COV) for standard geotechnical design parameters, including unit weight (γ), friction angle (φ), and undrained shear strength (s_u).

Figure 2.4 represents the variation of average stress conditions for soil elements mobilized along a circular slip plane, emphasizing the need for location-specific laboratory testing to accurately assess slope stability. As the failure mechanism develops, the principal stress directions rotate continuously along the sliding mass:

- Active Zone (Crest): In the upper section of the slope, the vertical overburden acts as the major principal stress (σ_1), while the lateral earth pressure acts as the minor principal stress (σ_3). The failure plane develops at an angle of $45° + \phi/2$. To replicate this stress state in the laboratory, a triaxial compression test is the most appropriate method.
- Central Zone (Horizontal sliding): Along the middle segment of the slip surface, the principal stress directions rotate, and failure is predominantly governed by shear stress (τ). This localized stress condition is best simulated using a direct shear test or a simple shear test.
- Passive Zone (Toe): At the toe of the slope, the lateral resistance forces the horizontal stress to become the major principal stress (σ_1), reducing the vertical stress to the minor principal stress (σ_3). The resulting failure plane is inclined at $45° - \phi/2$. This complex stress path and principal stress reversal are most accurately modeled by a triaxial extension test. Consequently, relying solely on standard compression testing may not fully capture the varied shear strength behaviors along the entire critical slip surface, particularly in the passive regions at the toe.

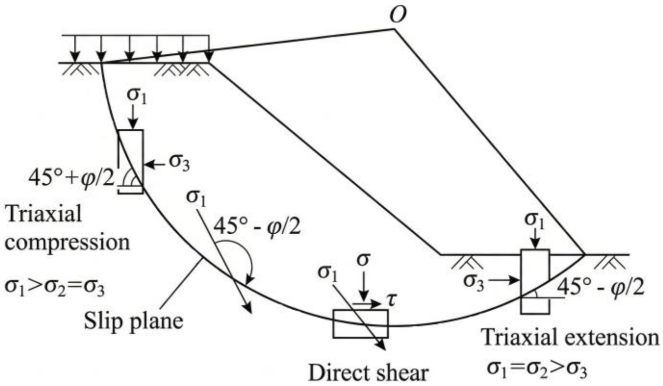

Figure 2.4. *Idealized stress states and corresponding laboratory test methods along a circular slip plane (Liu, 2009)*

Table 2.1. *Summary of coefficients of variation (COV) for common geotechnical design parameters (e.g., unit weight, friction angle, undrained shear strength) (Phoon and Kulhawy, 1999)*

Design Property[a]	Test[b]	Soil Type	Point COV (%)	Spatial average COV[c] (%)	Correlation Equation
s_u (UC)	Direct (lab)	Clay	20–55	10–40	—
s_u (UU)	Direct (lab)	Clay	10–35	7–25	—
s_u (CIUC)	Direct (lab)	Clay	20–45	10–30	—
s_u (field)	VST	Clay	15–50	15–50	14
s_u (UU)	q_T	Clay	30–40[d]	30–35[d]	18
s_u (CIUC)	q_T	Clay	35–50[d]	35–40[d]	18
s_u (UU)	N	Clay	40–60	40–55	23
s_u[e]	K_D	Clay	30–55	30–55	29
s_u (field)	PI	Clay	30–55[d]	—	32
φ	Direct (lab)	Clay, sand	7–20	6–20	—
φ (TC)	q_T	Sand	10–15[d]	10[d]	38
φcv	PI	Clay	15–20[d]	15–20[d]	43
Ko	Direct (SBPMT)	Clay	20–45	15–45	—
Ko	Direct (SBPMT)	Sand	25–55	20–55	—
Ko	K_D	Clay	35–50[d]	35–50[d]	49
Ko	N	Clay	40–75[d]	—	54
E_{PMT}	Direct (PMT)	Sand	20–70	15–70	—
E_D	Direct (DMT)	Sand	15–70	10–70	—
E_{PMT}	N	Clay	85–95	85–95	61
E_D	N	Silt	40–60	35–55	64

[a]ED, dilatometer modulus; E_{PMT}, pressuremeter modulus; K_0, in situ horizontal stress coefficient; s_u, undrained shear strength; s_u (field), corrected s_u from
vane shear test; φ, effective stress friction angle; φcv, constant-volume φ; TC, triaxial compression; UC, unconfined compression test.
[b]KD, dilatometer horizontal stress index; N, standard penetration test blow count; PI, plasticity index; q_T, corrected cone tip resistance.
[c]Averaging over 5 m.
[d]COV is a function of the mean; refer to COV equations in the text for details.
[e]Mixture of s_u from UU, UC, and VST.

Vanmarcke (1977, 1983) developed statistical descriptions of spatial variability (e.g., correlation lengths) which can be used to estimate how likely it is that a large volume of soil is below a certain strength. Another aspect is parameter selection: an engineer must choose characteristic values for analysis. Rather than picking a single "factor of safety" soil strength, probabilistic methods encourage treating the inputs as random variables with distributions (Whitman, 2000). For example, cohesion might be Normal (μ=20, σ=4 kPa), friction angle Triangular (30°, 32°, 34°). These distributions can come from lab data or literature on similar soils. Even before doing probabilistic analysis, one can use these to do sensitivity analysis—see which parameters F is most sensitive to (Baecher and Christian, 2003).

2.1.1.1. In-situ deformation characterization

In geotechnical formations where obtaining undisturbed samples is difficult, such as blocky colluvium or weathered rock masses, the Menard Pressuremeter Test (PMT) serves as a robust alternative to Standard Penetration Tests (SPT). Conducted according to ASTM D4719 (2020), the PMT measures the volumetric change of a probe against applied pressure to derive the Menard Modulus (E_m) and limit pressure (P_L). Baguelin et al. (1978) highlight that E_m provides a more direct and reliable assessment of the in-situ stiffness for soil-rock mixtures compared to correlation-based methods. Consequently, PMT parameters are frequently utilized as the basis for deriving Winkler spring coefficients (k_s) in soil-structure interaction analyses.

2.1.1.2. Degradation potential

To assess the degradation potential of weak sedimentary units (e.g., mudstones and claystones) upon exposure to atmospheric conditions and wetting-drying cycles, Slake Durability Index (I_d) tests are standardly performed as per ASTM D4644 (ASTM International, 2016). This test quantifies the resistance of the rock to disintegration, a critical parameter for slope stability in excavation zones where fresh rock is exposed. These results are utilized to justify the use of degraded strength parameters in stability models for scenarios involving long-term exposure or saturation, as the breakdown of the argillaceous matrix significantly reduces the geological strength index (GSI) over time (Franklin and Chandra, 1972).

2.1.2. Water content, precipitation, and groundwater

Next to gravity, water is the most significant factor influencing slope stability (Hopkins et al., 1975). The presence of water within a soil mass has several detrimental effects. Primarily, it generates positive pore water pressure (u), which reduces the effective normal stress between soil particles and, consequently, diminishes the frictional component of shear strength, as shown in the Mohr-Coulomb equation (Duncan et al., 2014). Groundwater can significantly alter the effective stress in soil, leading to increased pore pressure and reduced stability. The Aberfan disaster in Wales involved the catastrophic flow slide of a coal waste tip and was primarily caused by a build-up of water within the tip, which was constructed on a natural spring and lacked proper drainage (http-1[1]). The Highland Towers landslide in Malaysia was also attributed to inadequate drainage, where prolonged rainfall led to increased pore water pressure within the slope, reducing its shear strength and ultimately triggering the failure (Tan and Lee, 2017).

Rainfall infiltration is a primary trigger for landslides worldwide (Gariano and Guzzetti, 2016). As rainwater percolates into a slope, it increases the degree of saturation, which raises pore water pressures in the saturated zone and reduces matric suction (negative pore water pressure) in the unsaturated zone. Both effects contribute to a reduction in the soil's shear strength (Ali et al., 2022). The hydro-mechanical response of a slope to a rainfall event is complex and depends on the intensity and duration of the precipitation, antecedent moisture conditions, and the soil's hydraulic properties, particularly its saturated hydraulic conductivity (Ali et al., 2022). The combined effects of rainfall and seismic events have been shown to drastically impact slope stability. For example, increased water content within a slope can significantly reduce its shear strength, especially when coupled with high seismic acceleration. This interaction poses a heightened risk during intense rainfall events, necessitating careful consideration in stability analyses and designs (Jia et al., 2024).

For slopes associated with hydraulic structures, the operational regime of reservoirs is also a major factor. The condition of rapid drawdown represents a critical stability scenario (Al-Zayadi, 2022). During rapid drawdown, the external confining pressure from the reservoir water is removed more quickly than the pore water pressure within the upstream slope can dissipate. This creates a temporary but significant outward hydraulic gradient and high internal pore pressures, which can lead to a substantial reduction in the factor of safety and potentially trigger failure (Alonso and Pinyol, 2016). This drawdown scenario is depicted in Figure 2.5.

[1]http-1:https://www.ice.org.uk/what-is-civil-engineering/infrastructure-projects/aberfan-disaster-lessons-learned (accessed June 14, 2025).

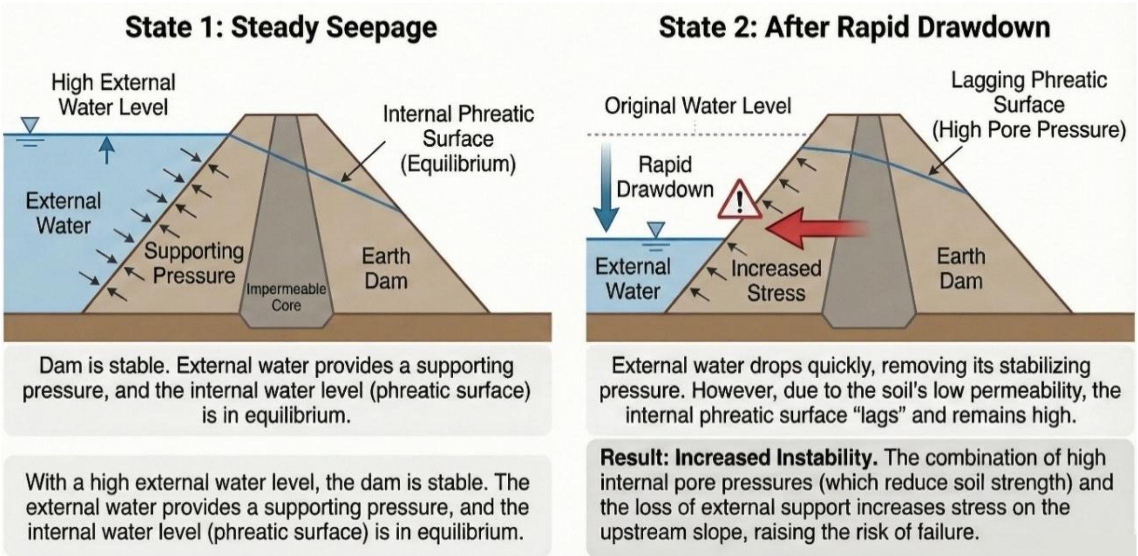

Figure 2.5. *Cross-section of an earth dam illustrating the phreatic surface lag and pore pressure distribution during rapid drawdown conditionsed from Duncan et al. (2014)*

At the Tablachaca Dam in Peru, a pre-existing rock slide was likely reactivated due to infiltration from the reservoir (Millet et al., 1992). At the Charvak Reservoir, water level fluctuations of up to 40 meters have been a significant factor in the reactivation and intensification of slope gravitational processes, leading to increased abrasion, gully erosion, and the activation of landslides due to the backup of groundwater from the reservoir (Ermatov and Ermatova, 2023). In Iran, a landslide that had been stable began moving in 2013 during the impoundment of a nearby water reservoir, with the final collapse attributed to the reservoir filling to its maximum recorded level combined with an exceptional precipitation event (Vassileva et al., 2023).

Beyond the inherent variability of soil properties, the determination of pore pressure conditions presents significant challenges due to inherent uncertainties. For instance, establishing the critical phreatic surface during extreme storm events remains a primary source of geotechnical risk (Phoon and Kulhawy, 1999; Baecher and Christian, 2003).

2.1.2.1. Hydraulic characterization

For the hydraulic characterization of fractured bedrock units, Lugeon (Packer) tests are executed following the guidelines of BS 5930 (2015). This in-situ test measures the volume of water injected under constant pressure into a sealed section of the borehole, providing a direct assessment of the rock mass hydraulic conductivity in Lugeon units (1 Lugeon ≈ 10^{-7} m/s). The test is fundamental for defining the secondary permeability controlled by discontinuity networks (Houlsby, 1976). Accurate Lugeon values are essential for transient seepage analyses, specifically for modeling rapid drawdown scenarios where the permeability contrast between the rock mass and the overlying colluvium dictates the pore pressure dissipation rates.

2.1.3. Seismic loading and earthquake-induced effects

Earthquakes impose complex dynamic loads on slopes, which can lead to instability through several mechanisms. The ground shaking induces cyclic inertial forces within the soil mass, which act as additional driving forces that temporarily increase the shear stresses along potential failure surfaces (Kramer, 1996). Seismic slope stability analysis is essential for assessing the ability of slopes to withstand seismic forces without failing. This analysis is particularly important in earthquake-prone regions where ground shaking can trigger landslides and other slope failures, leading to significant damage to infrastructure and potential loss of life (Feng and Yin, 2025). Multiple factors influence slope stability during seismic events, including soil properties, groundwater conditions, and the specific loading conditions experienced during an earthquake.

Beyond the inertial effects, cyclic loading can cause a progressive degradation of the soil's strength and stiffness, a phenomenon known as cyclic softening, which is particularly pronounced in sensitive clays (Seed and Lee, 1966; Idriss and Boulanger, 2008). In loose, saturated, cohesionless soils such as sands and silty sands, the cyclic shear strains induced by an earthquake can cause a tendency for volume reduction. In undrained conditions, this tendency translates into a rapid buildup of excess pore water pressure. If the pore pressure rises to equal the total confining stress, the effective stress drops to zero, and the soil loses nearly all of its shear strength. This process, known as liquefaction, is a principal cause of catastrophic slope failures and embankment dam failures during major earthquakes (Seed and Idriss, 1971).

The physical mechanism driving the saturated sand liquefaction process is delineated in Figure 2.6.

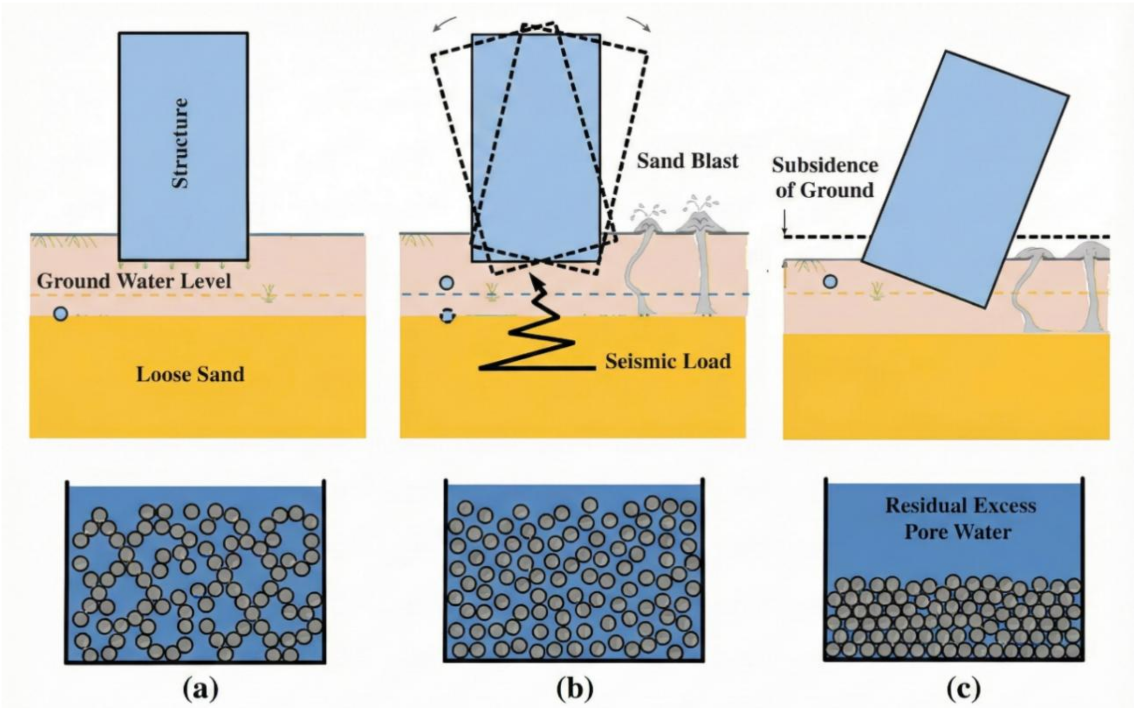

Figure 2.6. *Schematic of saturated sand liquefaction process. a) Before earthquake, b) during liquefaction, c) after earthquake (Xue and Yang, 2013)*

Additionally, Figure 2.7 charts triggering correlations.

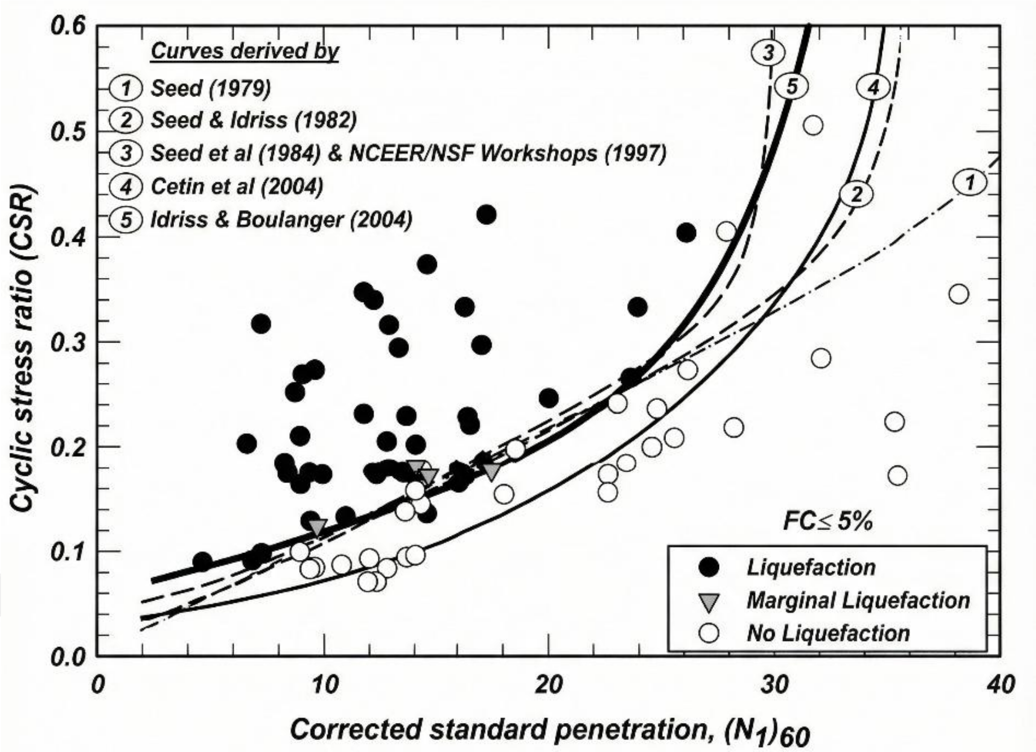

Figure 2.7. *Liquefaction triggering correlation for cohesionless soils based on SPT data (Idriss and Boulanger, 2008)*

Table 2.2 presents a concise summary of historical slope failures documented in existing literature, specifically categorizing their unique failure mechanisms and primary triggering factors.

Table 2.2. *Summary of selected historical slope failures cited in literature, characterizing failure mechanism and triggering factors*

Case Study Location	Failure Mechanism	Triggering Factor	Reference
Rampac Grande, Peru	Earth slide-earth flow	Weathered argillite/precipitation	Gaidzik et al. (2020)
Charvak Reservoir, Uzbekistan	Landslides/Collapses	Reservoir fluctuation & seismicity	Ermatov and Ermatova (2023),
Aberfan, Wales	Flow slide	Pore pressure buildup	(http-1[2])
Highland Towers, Malaysia	Slope failure	Rainfall/Inadequate drainage	Tan and Lee (2017)
Tablachaca Dam, Peru	Reactivated rockslide	Reservoir infiltration	Millet et al. (1992)

The interaction of environmental factors such as water content and seismic activity with slope stability is evident from case studies. The Charvak Reservoir area is located within the XII-Pskom-Tashkent seismogenic zone, and seismic impacts on the slope's

[2](http-1).

weak materials can trigger landslides and collapses (Ermatov and Ermatova, 2023). The Peruvian Andes are similarly characterized by high seismic activity, which contributes to numerous slope instabilities (Gaidzik et al., 2020). In the Safuna Lakes area of Peru, slope stability calculations considering a rock avalanche found that while full water saturation could decrease the factor of safety to critical levels, the combination of seismic shaking and full saturation further significantly lowered stability (Klimeš et al., 2021).

Furthermore, earthquake loading is probabilistic by nature (one can use a hazard curve to say there's X% chance of exceeding a certain PGA in Y years). Slope reliability studies increasingly couple geotechnical uncertainty with hazard uncertainty. For example, one might compute probability of failure as an integral over all earthquake shaking scenarios weighted by their occurrence probability—essentially folding the seismic hazard curve into the slope fragility curve (a performance-based engineering approach) (Cornell, 1968; Kramer, 1996; Baecher and Christian, 2003; Jibson, 2011).

2.1.4. Site investigation, characterization, and monitoring methods

The assessment of slope stability for critical hydraulic appurtenant structures—encompassing spillway cuts, tunnel portals, intake towers, and outlet works—demands a level of rigor in site characterization that significantly exceeds standard civil engineering practice. Unlike static infrastructure, these structures operate within a dynamic hydro-mechanical environment characterized by high hydraulic gradients, rapid pore pressure fluctuations, and the potential for catastrophic consequences in the event of failure. Consequently, the geological model underpinning any stability analysis must be derived from a multi-faceted investigation program that integrates traditional subsurface exploration with advanced in-situ testing, real-time hydrogeological monitoring, and remote sensing technologies. This section synthesizes the state-of-the-art methodologies for characterizing rock mass properties, hydraulic conductivity, and slope performance, emphasizing their specific applicability to the complex interactions between fluid dynamics and rock mechanics inherent in hydraulic projects.

2.1.4.1. Subsurface exploration and logging

The fundamental basis of any geotechnical design model remains the direct observation of the subsurface through drilling and core logging. For hydraulic structures, where the presence of a single permeable discontinuity can dictate the stability of a spillway foundation or the seepage regime around a tunnel portal, the exploration program must be designed to capture the structural fabric of the rock mass with high fidelity. Federal and international guidelines, such as those promulgated by the Federal Energy Regulatory Commission (FERC) and USACE, mandate a phased approach evolving from preliminary reconnaissance to final design investigations, ensuring that data density increases commensurate with design maturity (FERC, 1991).

Advanced Drilling and Recovery Techniques: While standard rotary drilling is ubiquitous, the characterization of fractured rock masses typical of tunnel portals requires specialized techniques to maximize core recovery and minimize drilling-induced disturbance. The use of double-tube and triple-tube core barrels is considered industry best practice for these applications (FERC, 1991). Triple-tube systems, which utilize a split inner liner, allow for the extraction and inspection of the core in a near-in-situ condition. This is particularly critical for preserving soft joint infillings, clay seams, and highly weathered zones that are frequently washed away by the drilling fluid in conventional single-tube or standard double-tube operations. The loss of such material can lead to a dangerous overestimation of rock mass shear strength and an underestimation of permeability. Furthermore, the diameter of the core significantly influences the representativeness of the rock quality data. For robust rock mass characterization, N-size core (approximately 54 mm diameter) or larger is generally recommended to capture a representative sample of discontinuity spacing and to provide sufficient volume for laboratory testing (FERC, 1991).

Borehole Imaging and Virtual Core Orientation: To overcome the limitations of blind core orientation and the loss of kinematic data in broken zones, borehole televiewer technology has become an indispensable tool in high-value hydraulic projects. Optical Televiewers (OTV) utilize a downhole camera and a conical mirror to generate a continuous, high-resolution, 360-degree oriented color image of the borehole wall (http-2[3]). This "virtual core" allows for the precise measurement of the dip and dip direction of discontinuities, lithological contacts, and foliation planes, even in zones of zero core recovery. Complementing optical methods, Acoustic Televiewers (ATV) employ a rotating ultrasonic transducer to image the borehole wall via the amplitude and travel time of reflected acoustic pulses. ATV systems offer the distinct advantage of functioning in

[3]http-2:https://www.epa.gov/environmental-geophysics/borehole-optical-televiewer-otv (accessed September 25, 2025).

turbid borehole fluids where optical visibility is compromised (http-3[4]). Moreover, the acoustic data provides qualitative information on fracture aperture and wall condition; low-amplitude returns typically indicate open fractures or soft infilling, while high-amplitude returns suggest healed or tight fractures. This distinction is vital for developing hydrogeological models for spillway foundations, where open fractures represent potential seepage pathways (http-3[5]). The integration of televiewer data facilitates the reorientation of core runs and the construction of detailed stereonets, which are essential for the kinematic stability analyses of steep cut slopes and tunnel portals (Li et al., 2013).

2.1.4.2. In-situ testing (SPT, Lugeon, pressuremeter)

In-situ testing bridges the gap between small-scale laboratory element testing and the large-scale behavior of the rock mass. It allows for the characterization of material response under stress and hydraulic conditions that are difficult, if not impossible, to replicate in the laboratory, particularly regarding scale effects and boundary conditions.

Standard Penetration Test (SPT) in weak rock

While the Standard Penetration Test (SPT) is primarily a soil investigation tool, it retains utility in characterizing the overburden, saprolite, and highly weathered rock transition zones often encountered at tunnel portal excavations. The blow count (N-value) provides a semi-empirical index of relative density in granular soils and consistency in cohesive soils, which can be correlated to shear strength and compressibility parameters (North Carolina Department of Transportation [NCDOT], 2021). In the context of embankment dams and appurtenant structures, SPT data is frequently used to assess liquefaction potential in foundation soils (WSDOT, 2013). However, the application of SPT in gravelly soils or weak, fractured rock requires caution; the presence of large particles can artificially inflate blow counts, leading to an overestimation of density and strength. In such transitional geomaterials, alternative dynamic cone penetration methods or large-diameter penetrometers may be required to obtain reliable data.

[4]http-3:https://www.epa.gov/environmental-geophysics/borehole-acoustic-televiewer-atv (accessed September 25, 2025).

[5](http-3).

Lugeon test (water pressure test)

For hydraulic structures, the characterization of rock mass hydraulic conductivity is paramount for assessing seepage losses, designing grout curtains, and evaluating uplift pressures beneath spillways and dams. The Lugeon test, also known as the packer test, is the standard in-situ method for this purpose. The test involves isolating a specific section of the borehole using inflatable packers and injecting water at constant pressure steps while measuring the flow rate (Vaskou et al., 2019). A Lugeon Unit (LU) is empirically defined as a flow of 1 liter per minute per meter of borehole test interval at an injection pressure of 1 MPa (approximately 10 bars) (Vaskou et al., 2019). Although originally an index of groutability, the Lugeon value is now routinely converted to equivalent hydraulic conductivity (K), with 1 LU approximating 1.3×10^{-7} m/s (Deravi et al., 2021). The interpretation of Lugeon tests extends beyond the calculation of a single permeability value; the analysis of pressure-flow (P-Q) curves over five pressure steps (loading and unloading) provides diagnostic information on the hydraulic behavior of the fractures. A linear P-Q relationship indicates laminar flow, whereas deviations from linearity can signal turbulent flow, fracture dilation (opening of joints under high pressure), fracture wash-out (erosion of infilling), or void filling (Deravi et al., 2021). In spillway foundations, high Lugeon values (>10 LU) or evidence of wash-out are critical indicators necessitating extensive grouting, drainage galleries, or cut-off walls to ensure stability against hydraulic uplift and piping (Vaskou et al., 2019).

Pressuremeter testing (PMT)

The Pressuremeter Test (PMT) provides a method for measuring the in-situ stress-strain response of the rock mass. The test involves inflating a flexible cylindrical probe against the borehole wall and monitoring the volumetric expansion as a function of applied pressure. Unlike the Lugeon test which focuses on hydraulic properties, the PMT yields mechanical parameters: the pressuremeter modulus (E_p), the limit pressure (P_L), and the creep pressure (P_f) (Briaud, 1989). In weak, jointed, or weathered rock masses where obtaining intact core for laboratory stiffness testing is challenging or impossible, the PMT is uniquely capable of measuring the in-situ deformation modulus (E_m) (Birid, 2015). This in-situ modulus accounts for the closure of micro-fractures and the compliance of the rock mass structure, which are often lost in small-scale laboratory specimens. The PMT results are typically interpreted to identify the pseudo-elastic linear phase of deformation, from which the shear modulus (G) and Young's modulus (E) can be derived using cavity expansion theory (Birid, 2015). For critical hydraulic structures, such as intake towers or heavy spillway weirs, accurate settlement calculations and soil-structure interaction analyses rely heavily on the stiffness parameters derived from high-pressure PMT testing (Failmezger et al., 2005).

Table 2.3 summarizes the primary in-situ tests (Lugeon, Pressuremeter, Dilatometer, P-S Logging) utilized in geotechnical investigations, outlining their target parameters, typical depths of investigation, and specific relevance to hydraulic structure design (e.g., seepage control, settlement analysis, and dynamic response). Limitations regarding scale effects and rock mass quality are also highlighted to support informed stabilization recommendations.

Table 2.3. *Comparison of in-situ testing methods for rock mass characterization in hydraulic structures*

Primary In-Situ Tests	**Target Parameters**	**Typical Depths of Investigation**	**Relevance to Hydraulic Structure Design**	**Limitations Regarding Scale Effects and Rock Quality**	**Source(s)**
Lugeon (Water-Pressure/ Packer Test)	Hydraulic conductivity, transmissivity, and Lugeon coefficient (Lu).	Typically 1-3 m intervals; standard 30-40 m for dams (up to 150 m).	Evaluates seepage, dictates grouting requirements, and verifies grout curtains. Crucial for predicting groundwater inflow and dissolution risks.	Limited to approx. 10 m radius; biased by near-borehole conditions. May miss vertical fractures. Risks hydrojacking. Assumes isotropic laminar flow.	(USBR, 2001; Sadeghiyeh et al., 2013; USACE, 1986, 1997; Ulusay, 2015)
Pressuremeter/ Borehole Jack (e.g., Goodman Jack)	In-situ stress, shear strength, rock mass stiffness, and deformation modulus (E).	Variable depths across the borehole; typically uses 76 mm (NX) boreholes.	Assesses settlement and dam stability. Determines rock mass stiffness for tunnel and foundation design.	Significant scale effects; yields lower moduli than lab tests due to fractures. Tests a small volume (~0.1 m³). Highly sensitive to local heterogeneities and borehole deviations.	(ASTM, 1988; Bieniawski, 1978; Montiel and Chable, 2012; Palmström and Singh, 2001; Ulusay, 2015)

Table 2.3. (Continued) *Comparison of in-situ testing methods for rock mass characterization in hydraulic structures*

Primary In-Situ Tests	**Target Parameters**	**Typical Depths of Investigation**	**Relevance to Hydraulic Structure Design**	**Limitations Regarding Scale Effects and Rock Quality**	**Source(s)**
Dilatometer (Flexible, Stiff, or Volumetric)	In-situ deformability, anisotropy, and deformation moduli (E_m, E_k).	Borehole-based continuous profiling; depth limited only by equipment.	Predicts deformation for underground structures. Essential for stress-strain analysis and modeling concrete arch dam foundations.	Tests a small volume (~0.1 m^3). May miss fractures parallel to the borehole. Measures average deformation; cannot detect directional anisotropy. Membranes prone to damage.	(ASTM, 2020; USBR, 2001; Palmström and Singh, 2001; USACE, 1997; Yow, 1993)
P-S Logging (Acoustic/ Seismic/ Geophysical)	Density, porosity, Poisson's ratio, dynamic elastic moduli, and P- and S-wave velocities.	Continuous borehole measurement; profiling covers large areas.	Crucial for seismic design and dynamic stress analysis. Identifies weakness zones, joint density, and weathering profiles.	Requires fluid-filled boreholes. Accuracy affected by signal attenuation and fracture geometry. Dynamic moduli differ from static values. May miss thin weak zones.	(USBR, 2001; Sari et al., 2020; Ulusay, 2015; USACE, 1997)

2.1.4.3. Hydrogeological monitoring (piezometers, groundwater level)

The stability of slopes adjacent to reservoirs is inextricably linked to the pore water pressure regime. Accurately monitoring the phreatic surface and pore pressure response to external loading events—such as rapid drawdown or flood surcharge—is essential for validating stability models and ensuring operational safety.

Piezometer technologies and response characteristics

The selection of appropriate piezometer technology depends on the permeability of the ground and the required response time.

- Open standpipe (Casagrande) piezometers: These instruments consist of a screened pipe installed within a sand filter zone in a borehole. While robust, simple to read, and reliable for measuring static groundwater levels in permeable strata, they suffer from a significant "hydrodynamic time lag" (http-4[6]). This lag represents the time required for a sufficient volume of water to flow into or out of the standpipe to equalize with the formation pressure. In low-permeability materials, such as clay cores or tight rock masses, this lag can be substantial, rendering open standpipes unsuitable for monitoring rapid transient pore pressure changes typical of rapid drawdown events (Central Water Commission [CWC], 2017).
- Vibrating wire (VW) piezometers: VW piezometers measure pore water pressure via a diaphragm that changes the tension (and thus the resonant frequency) of a steel wire. Because they require an infinitesimal volume change to register a pressure change, they exhibit a near-instantaneous response time (http-5[7]). This characteristic makes them the instrument of choice for monitoring transient pressures in low-permeability environments. Furthermore, VW sensors output a frequency signal that is robust against electrical noise and suitable for long-distance transmission to Automated Data Acquisition Systems (ADAS), enabling real-time monitoring and alarm generation for critical slopes (http-6[8]).

---

[6]http-4:https://www.usbr.gov/tsc/techreferences/mands/rockmanual/green_uniqueUSBR/6515.pdf (accessed September 10, 2025).
[7]http-5:https://www.precisiondrillingaustralia.com.au/blog/vibrating-wire-pizeometer (accessed September 10, 2025).
[8]http-6:https://smemonitoring.co.za/a-practical-guide-for-geotechnical-and-groundwater-monitoring (accessed December 20, 2025).

Installation methodologies

The shift to fully grouted:

Traditionally, piezometers were installed in sand filter packs sealed with bentonite pellets to isolate the test interval. A significant advancement in monitoring practice is the adoption of the "fully grouted" installation method. In this approach, the VW piezometer is embedded directly within a cement-bentonite grout column that fills the entire borehole (http-7[9]). Research and field practice have confirmed that, provided the grout permeability is appropriately matched to or lower than the surrounding ground, the sensor accurately tracks the formation pressure without the need for a sand filter. This method simplifies installation, reduces the risk of cross-communication between aquifers, and facilitates the installation of multiple sensors in a single borehole (nested piezometers) to measure vertical hydraulic gradients (http-7[10]).

Monitoring objectives for hydraulic structures

For spillway cuts and tunnel portals, the primary objectives of hydrogeological monitoring include tracking the phreatic surface response to reservoir level fluctuations, detecting the development of perched water tables in distinct geological units, and verifying the performance of drainage measures such as adits or relief wells. The data collected is indispensable for calibrating the transient seepage models used in coupled hydro-mechanical stability analyses, ensuring that the pore pressure assumptions in the design are validated by field performance (Desjarlais, 2022).

2.1.4.4. Geophysical methods (seismic refraction, ERT, MASW, PS-logging)

Geophysical methods provide a non-invasive means to interrogate the subsurface volume between boreholes, offering a continuous spatial characterization of stratigraphy, saturation, and rock mass quality.

Seismic refraction

Seismic refraction measures the travel time of compressional (P) waves refracted along subsurface interfaces where velocity increases with depth. It is a standard tool for

---

[9]http-7:https://www.geosense.com/wp-content/uploads/2021/04/Piezometers-In-depth-V1.0.pdf (accessed September 10, 2025).

[10](http-7).

mapping the depth to competent bedrock, identifying paleo-channels, and delineating zones of low-velocity rock indicative of shearing or intense weathering (Coe et al., 2018). However, the method is limited by the requirement that velocity must increase with depth; it often fails to detect low-velocity layers beneath high-velocity caps (the hidden layer problem), which can be a critical omission in slope stability investigations involving buried weak seams.

Electrical resistivity tomography (ERT)

ERT measures the spatial distribution of subsurface electrical resistivity by injecting current and measuring potential differences through an array of electrodes. Since resistivity is highly sensitive to pore fluid content, porosity, and clay mineralogy, ERT is particularly effective at identifying groundwater tables, saturation zones within landslide masses, and clay-rich fault gouge (Zhang et al., 2023). In the context of slope stability, ERT can help delineate the geometry of slip surfaces where there is a contrast in moisture content or lithology between the sliding mass and the stable bedrock (Zhang et al., 2023). Advanced applications involve time-lapse ERT, which monitors changes in resistivity over time to track moisture dynamics and infiltration fronts during rainfall events or reservoir filling sequences (Paz et al., 2020).

Multichannel analysis of surface waves (MASW)

MASW utilizes the dispersive nature of Rayleigh waves (surface waves) to derive shear wave velocity (V_s) profiles of the subsurface. Unlike seismic refraction, MASW does not require a velocity increase with depth and can effectively detect velocity inversions, such as a stiff layer overlying a soft, weathered zone (Glueer et al., 2024). The shear wave velocity is directly related to the small-strain shear modulus (G_0) of the ground, providing a direct measurement of stiffness. By combining MASW with ERT, researchers have successfully characterized complex landslide geometries where MASW defines the mechanical stiffness boundaries and ERT defines the hydrological conditions, thereby reducing the non-uniqueness inherent in individual geophysical inversion methods (Zhang et al., 2023).

P-S suspension logging

For deep characterization of rock masses, particularly for tunnel alignments and deep foundations, P-S suspension logging is considered the gold standard. This borehole geophysical method involves lowering a probe containing a source and receivers into a fluid-filled borehole to measure P-wave and S-wave velocities directly at high vertical resolution (typically every 0.5 to 1.0 meter) (http-8[11]). Unlike downhole or crosshole seismic methods, P-S logging allows for testing in a single borehole at great depths (up to 600 m or more) and provides accurate measurements of V_s and V_p. These velocities are essential for calculating dynamic elastic moduli (Poisson's ratio, Young's modulus) required for seismic deformation analysis and soil-structure interaction modeling (Sasanakul and Gassman, 2019).

2.1.4.5. Laboratory testing (rock/soil; ASTM/ISRM/ISO/EN/TS frameworks)

Laboratory testing transforms physical samples into the constitutive parameters required for numerical modeling. The selection of appropriate testing standards—ASTM, ISRM, or ISO/EN—can significantly influence the derived parameters due to subtle differences in specimen preparation, loading rates, and failure definitions.

Comparative frameworks

ASTM vs. ISO/EN: The American Society for Testing and Materials (ASTM) standards are predominant in North American practice. Standards such as ASTM D7012-14 for compressive strength of rock and ASTM D4767 for soil triaxial testing emphasize rigorous procedural control and precise equipment specifications to ensure reproducibility (http-9[12]). In contrast, the ISO 17892 series (for soil) and the International Society for Rock Mechanics (ISRM) Suggested Methods (for rock) often focus more on functional requirements and the interpretation of results within a geological context (International Organization for Standardization [ISO], 2019). For instance, in particle size analysis, differences in sieve sizes and sedimentation theories between ASTM D422 (or D6913) and ISO 17892-4 can yield slightly different soil classifications for borderline materials (Norbury, 2016).

[11]http-8:https://www.conetec.com/services/geophysical-testing/p-s-logging (accessed September 16, 2025).

[12]http-9:https://forneyonline.com/simple-guide-astm-d7012/ (accessed September 15, 2025).

Rock mechanics testing standards

For rock mechanics specifically, the ISRM Suggested Methods serve as the de facto global standard. They provide specialized procedures for determining parameters critical to slope stability, such as fracture toughness, slake durability, and joint shear strength (http-10[13]). The ASTM D7012-14 standard has unified the methods for determining both elastic moduli and compressive strength of intact rock cores, mandating strict tolerances for specimen planarity (ends flat to within 0.02 mm) to ensure accurate modulus measurement (http-9[14]). These stringent preparation requirements are essential for reducing experimental error in the high-stiffness materials typical of hydraulic structure foundations.

In-situ and laboratory testing standards

The empirical classifications and numerical models discussed above rely on robust input data derived from standardized testing. The literature emphasizes the integration of the following methods:

- *Pressuremeter testing (PMT):* Menard pressuremeter tests (ASTM D4719) are pivotal for determining in-situ deformation modulus (E_m) and limit pressure (P_L) in weak rock masses or soil-rock mixtures where core recovery is poor.
- *Uniaxial compressive strength (UCS):* Standardized testing (e.g., TS EN 1926) defines the σ_{ci} parameter, the scalar for the Hoek-Brown criterion.
- *Point load test (PLT):* Provides an indirect strength estimation (Is_{50}), which is correlated to UCS (e.g., $\sigma_c \approx 24 \times Is_{50}$), allowing for extensive data collection from core samples.
- *Triaxial compression:* Essential for determining the intrinsic frictional characteristics (m_i) of the intact rock.

Advanced hydro-mechanical coupling tests

Modern geotechnical design for hydraulic structures increasingly relies on coupled hydro-mechanical analysis. This requires advanced laboratory testing capabilities, such as triaxial tests with independent control of pore water pressure and confining pressure to determine the Biot coefficient and Skempton’s B-parameter (Kasani and Selvadurai,

[13]http-10:https://isrm.net/isrm/page/show/1305 (accessed November 15, 2025).
[14](http-9).

2023). Furthermore, the behavior of rock joints is tested under Constant Normal Stiffness (CNS) conditions rather than the traditional Constant Normal Load (CNL). CNS testing better simulates the behavior of non-planar joints in confined environments—such as behind a concrete tunnel lining or within a rock slope reinforced with passive dowels—where joint dilation is restricted by the stiffness of the surrounding rock mass, leading to an increase in normal stress and shear strength (http-11[15]).

2.1.4.6. Remote sensing & surface monitoring (InSAR, LiDAR/photogrammetry)

The spatial scale of reservoirs and the attendant slope hazards necessitates monitoring technologies that offer broad coverage without sacrificing resolution. Remote sensing has revolutionized this field by enabling the detection of millimeter-scale deformations over vast areas.

LiDAR (Light detection and ranging)

LiDAR technology, deployed from terrestrial tripods (TLS) or airborne platforms (ALS), generates dense 3D point clouds of the ground surface. By differencing sequential LiDAR scans—a technique known as change detection—engineers can identify subtle morphological changes, quantify rockfall volumes, and detect slope bulging with centimeter-level accuracy (http-12[16]). Beyond deformation monitoring, LiDAR is invaluable for the virtual mapping of rock mass structure on inaccessible steep cut slopes. Algorithms can automatically extract discontinuity orientation, persistence, and spacing from the point cloud data, mitigating the safety risks associated with manual mapping of high spillway cuts (Riquelme et al., 2014).

InSAR (Interferometric synthetic aperture radar)

Satellite-based InSAR measures ground deformation by comparing the phase of radar signals reflected from the earth's surface across multiple satellite passes. Advanced processing techniques, such as Persistent Scatterer Interferometry (PSI), track the displacement of stable natural or man-made reflectors (e.g., rock outcrops, concrete structures) over long periods. This technology can resolve displacements on the order of

[15]http-11:https://www.usbr.gov/tsc/techreferences/mands/rockmanual/rockmanual.html (accessed September 15, 2025).

[16]http-12:https://www.tensarinternational.com/resources/articles/remote-sensing-in-geotechnics (accessed November 12, 2025).

millimeters per year, providing long-term settlement or creep histories for dams and reservoir slopes (Ran et al., 2026). InSAR is particularly well-suited for monitoring reservoir rims, where it can identify slow-moving landslides that may threaten reservoir capacity or generate impulse waves, long before they manifest visually (Dwitya et al., 2024).

Data fusion and integration

The integration of LiDAR and InSAR represents the frontier of slope monitoring. This data fusion leverages the high spatial resolution and vegetation penetration of LiDAR with the extreme displacement sensitivity and high temporal frequency of InSAR. In a comprehensive monitoring program, LiDAR provides the detailed geometric context and identifies rapid, localized failures, while InSAR tracks the slow, precursor deformations that often precede catastrophic instability (Sánchez-Fernández et al., 2025). This complementary approach ensures a multi-scale understanding of slope kinematics, critical for the early warning systems protecting hydraulic infrastructure.

2.1.5. Rock mass classification systems and parameterization

This section provides a comprehensive review of the theoretical frameworks and analytical formulations used to characterize the geomechanical behavior of rock masses. The literature establishes that accurate slope stability and tunneling analysis requires integrating empirical rock mass classification systems with advanced constitutive modeling to bridge the gap between intact rock properties and the large-scale behavior of in-situ rock masses. These empirical classification systems provide a necessary framework for scaling intact rock properties to the rock mass scale, a step that is essential for preliminary design and for validating the inputs used in numerical models.

2.1.5.1. Rock quality designation (RQD)

The Rock Quality Designation (RQD), originally introduced by Deere in the mid-1960s, serves as a fundamental index for quantifying the degree of fracturing in rock cores. It is defined as the cumulative length of intact core pieces longer than 100 mm (4 inches) expressed as a percentage of the total length of the core run.

$$RQD = \left(\frac{\sum \text{Length of core pieces} > 100\text{ mm}}{\text{Total core run length}}\right) \times 100\% \qquad (2.2)$$

While RQD is a standard parameter in logging, it is often considered insufficient on its own due to inherent scale and orientation biases. RQD is a directionally dependent metric; its value is intrinsically linked to the orientation of the borehole relative to the dominant discontinuity sets. A borehole drilled parallel to the primary joint set will encounter few fractures and yield a high RQD, suggesting a massive and competent rock mass. Conversely, a borehole drilled perpendicular to the same joint set in the same rock mass may encounter closely spaced fractures, yielding a low RQD and suggesting poor quality (Narimani et al., 2025). This directional bias can lead to erroneous estimates of rock mass modulus and strength if not explicitly accounted for in the geotechnical model. Furthermore, RQD is highly sensitive to the arbitrary threshold value of 10 cm. A rock mass with a uniform joint spacing of 9 cm would theoretically yield an RQD of 0%, while a similar rock mass with a spacing of 11 cm would yield an RQD of 100%. This binary sensitivity fails to capture the mechanical similarity between these two conditions and ignores the contribution of blocks smaller than 10 cm to the overall frictional strength of the rock mass (Narimani et al., 2025).

To address these deficiencies, modern characterization often employs modifications such as the "Weighted Joint Density" (RQD_{wjd}) or correlations with the volumetric joint count (J_v). These metrics attempt to provide a more orientation-independent assessment of fracturing by considering the spacing of all joint sets within a representative volume, rather than a single linear dimension (Narimani et al., 2025). Consequently, it is increasingly being replaced or supplemented by volumetric fracture counts (J_v) in advanced characterization workflows to provide a more isotropic measure of rock quality (Narimani et al., 2025). It is often necessary to estimate rock quality in surface exposures where drilling data is absent. Palmström (1982) proposed a correlation utilizing the volumetric joint count (J_v), which allows for the estimation of RQD from surface mapping data. This relationship is widely cited in rock engineering literature (e.g., Bieniawski, 1989) for converting mapping data into a usable index:

$$RQD = 115 - 3.3J_v \tag{2.3}$$

Where J_v is the sum of the number of joints per unit volume (joints/m³). The measurement methodology is outlined in Figure 2.8.

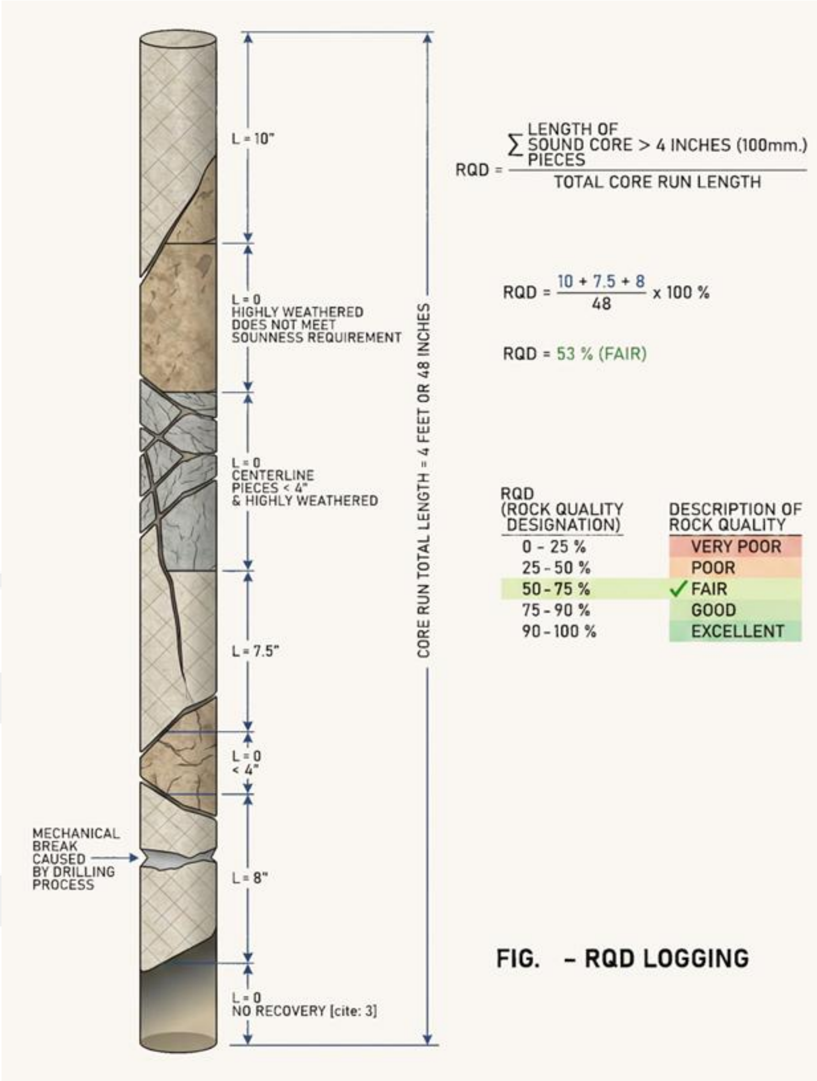

Figure 2.8. *Figure illustrating the measurement procedure for RQD, distinguishing between mechanical breaks and natural fractures (Deere and Deere, 1989)*

2.1.5.2. Rock mass rating (RMR) and slope mass rating (SMR)

The Geomechanics Classification, or Rock Mass Rating (RMR) system, developed by Bieniawski (1973, 1989), is one of the most widely employed empirical systems for estimating rock mass quality and preliminary support design. The system creates a summation of ratings for five primary parameters: (1) Strength of intact rock (UCS), (2) RQD, (3) Spacing of discontinuities, (4) Condition of discontinuities (persistence, aperture, roughness, infilling, weathering), and (5) Groundwater conditions. This derives a basic RMR value (RMR_{basic} ranging from 0 to 100), which is subsequently adjusted for the favorability of discontinuity orientation depending on the engineering application (tunnels, slopes, or foundations). Part of these rating parameters are detailed in Table 2.4.

Table 2.4. *General RMR classification parameters and their ratings (A) (Bieniawski, 1989)*

Parameter	Description	Range/Value
Strength of Intact Rock	Based on Uniaxial Compressive Strength (UCS) or Point Load Index.	0–15
RQD	Quantitative index of fracturing (Drill core quality).	3–20
Spacing of Discontinuities	Linear distance between discontinuity surfaces.	5–20
Condition of Discontinuities	Assessment of persistence, aperture, roughness, infilling, and weathering.	0–30
Groundwater Conditions	Inflow rate or pore pressure ratio.	0–15
Orientation Adjustment	Penalty for unfavorable strike/dip relative to excavation axis.	Tunnel: 0 to -12 Foundation: 0 to -25 Slope: 0 to -60

Slope Mass Rating (SMR)

Recognizing RMR's limitations specifically for slope stability analysis, Romana (1985) extended the system by introducing the Slope Mass Rating (SMR). This modification introduces specific adjustment factors (F_1, F_2, and F_3) that penalize the basic RMR based on the parallelism of joint strikes to the slope face (F_1), the joint dip angle (F_2), and the relationship between joint dip and slope face dip (F_3). A fourth factor, F_4, accounts for the method of excavation (e.g., smooth blasting versus poor blasting) (Lorig, 2009). These modifications make the RMR system a viable tool for the kinematic stability assessment of portal cuts and engineered slopes.

2.1.5.3. The Q-system

The Q-system, developed by Barton, Lien, and Lunde (1974) at the Norwegian Geotechnical Institute, is a quantitative classification system originally designed for tunnel support estimation. It groups six parameters into three quotients, representing block size, inter-block shear strength, and active stress conditions.

$$Q = \frac{RQD}{J_n} \times \frac{J_r}{J_a} \times \frac{J_w}{SRF} \tag{2.4}$$

Where:

- RQD: Rock Quality Designation.
- J_n: Joint set number (representing the number of discontinuity sets).
- J_r: Joint roughness number.
- J_a: Joint alteration number (representing filling and weathering).
- J_w: Joint water reduction factor.
- SRF: Stress Reduction Factor.

The Q-system uniquely accounts for prevailing stress through the SRF, making it highly valuable for deep tunnels or high-stress portals where stress-induced fracturing is a concern. Additionally, the quotient J_r/J_a precisely represents the inter-block shear strength, a parameter that is crucial for analyzing the sliding potential of wedges in jointed rock (Satıcı and Ünver, 2015).

2.1.5.4. Geological strength index (GSI)

The Geological Strength Index (GSI), introduced by Hoek (1994) and continuously refined (Hoek et al., 1995; Hoek and Brown, 2019), was developed specifically to support the Hoek-Brown failure criterion and overcome deficiencies in using RMR or Q for determining input parameters for numerical modeling. Unlike earlier systems, GSI characterizes the rock mass as a material continuum, focusing on the visual assessment of the interlocking of rock blocks (lithology and structure) and the condition of the discontinuity surfaces. Unlike RMR or Q, GSI intentionally avoids the "double-counting" of intact rock strength and groundwater, as these factors are handled separately within the Hoek-Brown constitutive equations (Bieniawski, 1989).

For complex geological formations like ophiolitic mélange or tectonized flysch, traditional classification systems like RMR may prove insufficient. The Geological Strength Index (GSI), developed by Hoek and Marinos (2000), addresses this gap by focusing on the blockiness and surface conditions of discontinuities. The GSI system is explicitly designed to handle rock masses that act as a continuum rather than a set of discrete blocks. It functions as a scalar to reduce intact rock properties to rock mass properties, serving as a necessary input for the Generalized Hoek-Brown failure criterion (Hoek et al., 2013).

For heterogeneous rock masses, such as ophiolitic mélanges or flysch sequences, standard classification charts are often inadequate. Marinos and Hoek (2001) developed specific GSI charts for these tectonically disturbed and heterogeneous formations.

Furthermore, for weak rock masses prone to degradation upon saturation (e.g., clay-bearing marls), adjustments to the GSI value to account for moisture content have been proposed by Sönmez and Ulusay (2002). Quantitative estimation of GSI has been proposed to reduce subjectivity. Hoek et al. (2013) quantified the GSI chart using RQD and joint condition ratings (J_{Cond89}), providing the following relationship:

$$GSI = 1.5\, J_{Cond_{89}} + \frac{RQD}{2} \tag{2.5}$$

Figure 2.9 visualizes this classification system.

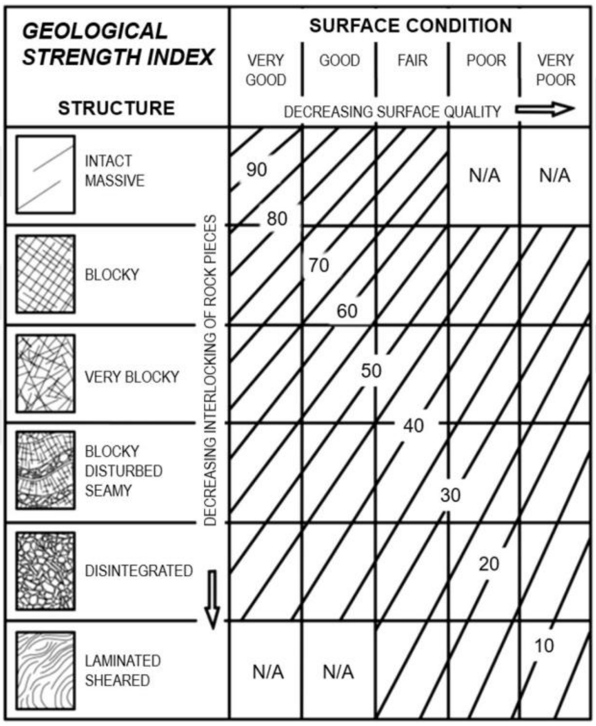

Figure 2.9. *Visual GSI Chart for Jointed Rocks showing the matrix of "Structure" (Blocky, Very Blocky, Disintegrated) vs. "Surface Conditions" (Good, Fair, Poor, Very Poor) (Hoek, 1999; Hoek and Marinos, 2000)*

Geotechnical characterization of intermediate geomaterials and the dual-state GSI approach

The geotechnical characterization of 'intermediate' geomaterials—encompassing block-in-matrix (bimrock) structures, saprolitic rock masses, and tectonic mélanges—presents a formidable challenge due to their profound heterogeneity and complex internal architectures. Traditional rock mass classification systems are often inadequate for these materials, necessitating specific adaptations of the Geological Strength Index (GSI) to capture their geomechanical reality. For highly heterogeneous tectonic mélanges and flysch formations, Marinos and Hoek (2001) established that GSI is only applicable when tectonic disruption destroys the continuity of bedding surfaces, yielding a macroscopically isotropic mass. They cautioned against a "double penalty" on the intact rock strength (σ_{ci}) caused by testing inherently flawed core samples, advocating instead for point load testing or qualitative estimates of the intact blocks (Marinos and Hoek, 2001). This framework was significantly advanced by Marinos (2019), who proposed a revised GSI classification system that categorizes these tectonically disturbed rock masses into 11 distinct geomechanical types (Types I to XI). In this updated paradigm, as tectonic disturbance intensifies and the geomaterial degrades into a chaotic broken formation or true mélange (Types X and XI), the GSI rating is systematically shifted toward the lower quadrant (GSI 5–25), and the global Hoek-Brown strength parameters are mathematically weighted to reflect the dominance of the sheared, incompetent argillaceous matrix rather than the isolated competent blocks (Marinos, 2019).

Beyond their initial structural complexity, the long-term mechanical stability of clay-bearing intermediate geomaterials is fundamentally governed by their extreme sensitivity to environmental moisture. Upon moisture exposure, the argillaceous matrices of saprolites and tectonic mélanges undergo severe mechanical degradation and slaking, driven by the hydration and volumetric expansion of constituent clay minerals such as smectite and illite (Erguler and Ulusay, 2009; Wang and Wittel, 2026). This hygro-mechanical swelling induces progressive micro-fracturing that destroys the intact matrix while simultaneously softening discontinuity infillings to low-friction clay slurries, thereby eradicating both structural interlock and joint shear resistance (Gokceoglu et al., 2000). Consequently, a drastic reduction in the assigned GSI value is necessitated to reflect this degraded state. Sönmez and Ulusay (2002) provided the quantitative justification for this reduction through their modifications to the Hoek-Brown criterion. By introducing continuous mathematical functions for the rock mass parameters, a and s—and explicitly eliminating the flawed historical assumption that s strictly equals zero for GSI < 25—their framework allows engineers to accurately calculate the residual strength of slaked, very poor-quality rock masses (Sönmez and Ulusay, 2002). Under saturated conditions, the quantitative Surface Condition Rating (SCR) and Structure Rating (SR) plummet, mathematically forcing the GSI rightward and downward on the classification chart and accurately yielding the highly convex, low-cohesion failure envelopes characteristic of slaked geomaterials (Sönmez and Ulusay, 1999; Sönmez and Ulusay, 2002).

Synthesizing the structural adaptations formalized by Marinos (2019) with the quantitative degradation mechanics articulated by Sönmez and Ulusay (2002) provides the theoretical justification for implementing a 'Dual-State GSI' methodology in slope stability analyses. Intermediate geomaterials are highly dynamic systems; assigning a single, static GSI value invariably leads to either uneconomical over-design or the failure to predict delayed catastrophic landslides (Marinos et al., 2005). The Dual-State GSI concept resolves this by defining a baseline GSI for intact/dry conditions—capturing the initial inter-block tortuosity, matric suction, and undisturbed matrix strength that permit steep initial excavation angles.

Conversely, a significantly degraded GSI is assigned to model saturated/weathered conditions, reflecting the inevitable matrix slaking, loss of block interlock, and friction angle reduction along wetted discontinuities. By transitioning the geomechanical parameters from the baseline GSI to the degraded GSI within finite element or limit equilibrium models, practitioners can rigorously simulate time-dependent strength degradation, thereby ensuring that stabilization measures are optimally designed to mitigate the specific delayed failure mechanisms inherent to moisture-sensitive tectonic mélanges and clay-bearing bimrocks.

2.1.5.5. Rock mass deformation modulus (E_{rm})

A critical application of the RMR system in numerical analysis is the estimation of the rock mass deformation modulus (E_m). Serafim and Pereira (1983) proposed a correlation (2.6) that extends the applicability of earlier RMR-based equations to poor quality rocks (RMR<50), providing a continuous relationship for a wide range of rock masses:

$$E_m = 10^{\frac{RMR-10}{40}}(\text{GPa}) \tag{2.6}$$

Estimating the in-situ deformation modulus is essential for numerical modeling of displacements. Hoek and Diederichs (2006) proposed a generalized equation based on a large database of in-situ measurements, incorporating both GSI and the disturbance factor D:

$$E_{rm} = E_{\mathrm{i}} \left(0.02 + \frac{1 - \frac{D}{2}}{1 + e^{\frac{60 + 15D - GSI}{11}}} \right) \qquad (2.7)$$

Where E_i is the intact rock modulus obtained from laboratory testing.

2.2. Landslide Mechanisms and Failure Types

Landslides are classified based on the material involved (rock, debris, or earth) and the type of movement, in accordance with widely accepted systems such as those developed by Varnes (1978) and updated by Cruden and Varnes (1996). The primary types of movement relevant to soil slopes are slides and flows. Static slope stability analysis considers several types of potential slope failures, including rotational failure, translational failure, and irregular surfaces of sliding. Understanding the characteristics of these failure modes is essential for effective slope stabilization and design (WSDOT, 2022). Table 2.5 provides an abbreviated classification of slope movements, identifying various landslide types based on the material involved and the character of the motion.

Table 2.5. *Abbreviated classification of slope movements (Varnes, 1978)*

Type of Movement	**Type of Material**		
	Bedrock	**Engineering Soils**	
		Predominantly Coarse	**Predominantly Fine**
Falls	Rockfall	Debris fall	Earth fall
Topples	Rock topple	Debris topple	Earth topple
Slides (Rotational/ Translational)	Rock slide	Debris slide	Earth slide
Lateral Spreads	Rock spread	Debris spread	Earth spread
Lateral Spreads	Rock spread	Debris spread	Earth spread
Flows	Rock flow (deep creep)	Debris flow (soil creep)	Earth flow (soil creep)
Complex	Combination of two or more principal types of movement		

Figure 2.10 categorizes various landslide types within a comprehensive framework based on material composition and movement.

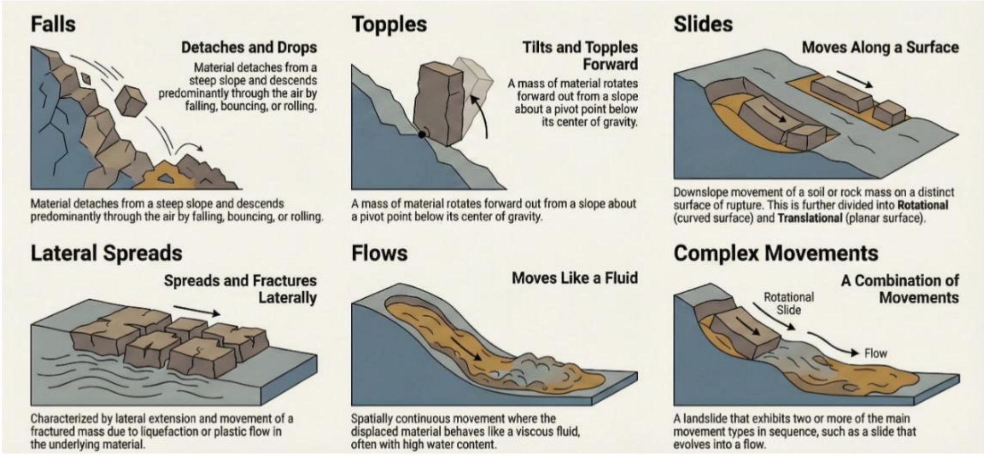

Figure 2.10. *Classification of landslide types based on material and movement mechanism (Varnes, 1978)*

2.2.1. Rotational slides

These failures are characterized by movement along a deep-seated, curved, concave-upward (listric) slip surface. They are most common in relatively homogeneous, cohesive soil deposits. The movement is rotational about an axis parallel to the slope, often resulting in a characteristic backward tilting of the top of the slide mass, forming a depression or "graben" at the main scarp (Varnes, 1978). In soil slopes, failures are broadly categorized by their geometry and movement characteristics. Rotational failures, or slumps, are common in homogeneous, cohesive soils like clays and silts, where the sliding mass moves along a concave, spoon-shaped slip surface (Duncan et al., 2014). These failures can be shallow, intersecting the slope face (face failure), or deep-seated, passing through the toe (toe failure) or into the foundation material below (base failure) (Duncan et al., 2014; Wyllie and Mah, 2004).

2.2.2. Translational slides

These involve downslope movement of a soil mass along a relatively planar or gently undulatory surface of weakness. The failure surface is often controlled by a geological discontinuity, such as a weak bedding plane, a fault, or the interface between soil and more competent bedrock. The moving mass undergoes little to no rotation and can travel considerable distances (Varnes, 1978). Translational failures involve the downslope movement of a soil mass along a relatively planar or gently undulating surface, often a weak layer or interface between different soil strata (Duncan et al., 2014). These are typical of infinite slopes, where a layer of weaker soil overlies a stronger, less permeable stratum.

2.2.3. Flows

These landslides behave like a viscous fluid, with movement occurring through continuous internal deformation of the mobilized mass. Debris flows are rapid, channelized flows of water-saturated soil, rock, and organic matter that originate on steep slopes, often triggered by intense rainfall (Cruden and Varnes, 1996). Earthflows are typically slower movements of plastic, fine-grained soils, often forming a distinctive hourglass shape with a source area, a narrow track, and a depositional lobe (Cruden and Varnes, 1996). Flows occur when a soil mass loses its structural integrity and moves as a viscous fluid, a phenomenon often triggered by the liquefaction of granular soils during earthquakes or the complete saturation of fine-grained soils during intense rainfall (Cascini et al., 2010).

2.2.4. Progressive failure

This type of failure, where a localized failure gradually propagates through a soil or rock mass, is a complex phenomenon that is not always adequately captured by traditional slope stability analyses. It occurs when the shear strength of the material degrades from its peak value to a residual value along parts of the failure surface before overall instability is reached. This phenomenon is particularly relevant for stiff clays, jointed rock masses, or sensitive soils. Numerical methods are better equipped to simulate progressive failure by modeling the reduction in shear strength after the peak is reached (Skempton, 1964). Progressive failure is a critical concept where localized overstressing and yielding at one point within the soil or rock mass leads to a redistribution of stress, causing failure to propagate and coalesce into a large-scale slip surface (http-13[17]). This process is particularly relevant in brittle materials or slopes containing pre-existing shear surfaces with low residual strength. Figure 2.11 highlights this strength transition.

[17]http-13:https://www.ciria.org/CIRIA/news/CIRIA_news2/Beyond_the_boundaries_-_slope_design_and_management.aspx (accessed October 18, 2025).

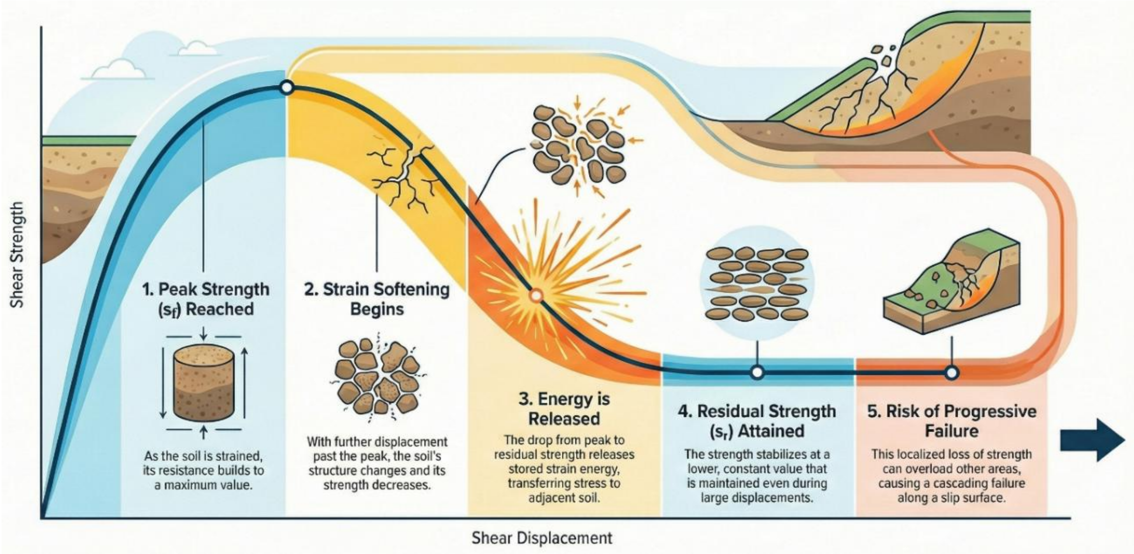

Figure 2.11. *Idealized stress-strain curves for stiff clays showing the transition from peak to residual strength associated with progressive failure (Skempton, 1964)*

In rock slopes, failure mechanisms are predominantly controlled by the orientation, spacing, and shear strength of pre-existing geological discontinuities such as joints, faults, and bedding planes (Hoek and Bray, 1981; Wyllie and Mah, 2004).

2.2.5. Planar failure

Planar failure occurs when a discontinuity plane dips out of the slope face at an angle shallower than the slope face itself, allowing a block to slide along this single surface (Hoek and Bray, 1981; Wyllie and Mah, 2004).

2.2.6. Wedge failure

Wedge failure is kinematically possible when two intersecting discontinuity planes form a wedge-shaped block whose line of intersection daylights in the slope face (Hoek and Bray, 1981; Wyllie and Mah, 2004).

2.2.7. Toppling failure

Toppling involves the forward rotation of rock columns or blocks, typically formed by steeply dipping discontinuities, about a pivot point at the base (Hoek and Bray, 1981; Wyllie and Mah, 2004). These kinematic conditions are projected in Figure 2.12.

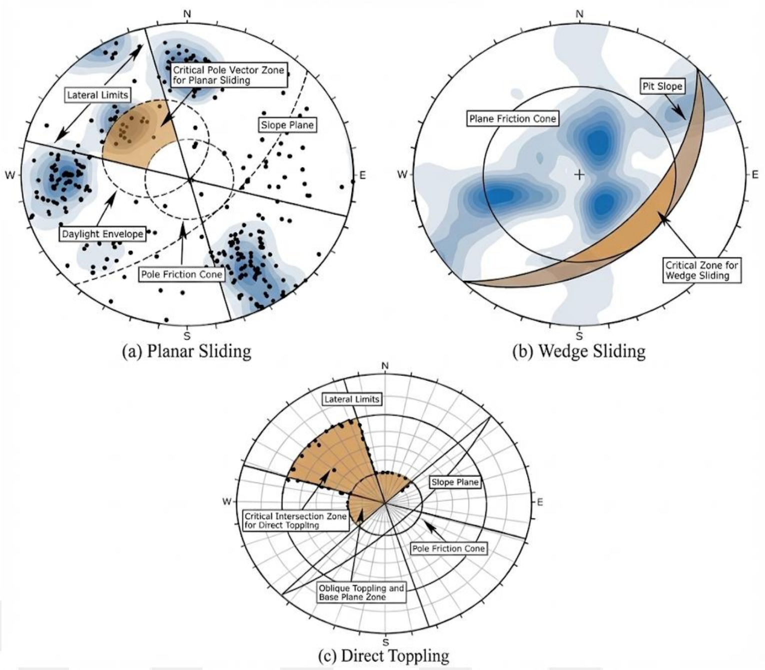

Figure 2.12. *Stereographic projection analyses for rock slope stability assessment. (a) Planar sliding kinematic analysis using pole vectors, illustrating the critical zone defined by the daylight envelope and friction cone. (b) Wedge sliding kinematic analysis identifying critical intersection points falling within the failure envelope. (c) Direct toppling analysis illustrating the critical intersection zone and lateral limits for base plane poles (Hoek and Bray, 1981)*

2.2.8. Specific mechanisms from case studies

Specific mechanisms from case studies include:

- Quick Clay Landslides: The Rissa landslide in Norway is a classic example. Highly sensitive marine clays lost almost all their shear strength upon disturbance from a small excavation, transforming into a liquid-like mass and retrogressing rapidly over a large area (Liu et al., 2021).
- Flow Slides: The Aberfan disaster involved the catastrophic flow slide of a saturated coal waste tip that liquefied and flowed down the mountainside as a slurry (http-1[18]). The Rampac Grande landslide in Peru was an earth slide-earth flow with a very rapid flow phase (Klimeš et al., 2024).
- Deep-Seated Rotational/Slump Failures: The reactivation of the landslide at Tablachaca Dam involved a deep-seated slump. The Vajont Dam disaster was a massive rockslide on a pre-existing ancient landslide surface with weak clay interbeds (Paronuzzi et al., 2021).

[18](http-1).

- Colluvial Failures: Landslides in colluvial units are often triggered by a rise in the groundwater table. The failure mechanism depends on the depth of the colluvium layer: deep-seated failures are possible with thick colluvium, while shallower failures occur with thinner layers (Amarasinghe et al., 2024).

2.3. Analysis Approaches

Slope stability evaluation is a central task in geotechnical engineering, and a wide range of analytical and numerical methods has been developed for this purpose. Slopes must be assessed under both long-term static loading and transient seismic excitation. Conventional practice has long relied on limit-equilibrium procedures, whereas modern analyses increasingly employ finite-element and other numerical stress–deformation methods. In seismic applications, assessment ranges from pseudo-static and displacement-based procedures to advanced nonlinear dynamic analyses (Duncan, 1996; Duncan et al., 2014; USACE, 2003; Kramer, 1996; Bray and Macedo, 2023; Liu et al., 2015). The selection of an appropriate method depends on the complexity of the slope geometry and soil conditions, the potential failure modes, and the availability of input parameters.

2.3.1. Limit equilibrium methods

Limit Equilibrium Methods (LEMs) are the most widely used techniques in geotechnical practice for slope stability analysis (USACE, 2003) and represent a cornerstone in slope stability analysis, providing a practical and widely adopted framework for assessing the stability of soil and rock masses. For over a century, the dominant analytical paradigm has been the Limit Equilibrium Method (LEM). The core principle of LEM is to evaluate the stability of a soil or rock mass by considering its equilibrium at the moment of incipient failure. The analysis focuses on a potential sliding mass, bounded by a predefined or assumed slip surface, and determines the conditions under wich this mass will begin to move under the influence of gravity and other external forces (Duncan, 1996). Early slope stability analysis relied on limit equilibrium concepts and the method of slices. They are widely used due to their simplicity and computational efficiency (Fellenius, 1936*)*. LEM has become a standard practice in geotechnical analysis, focusing on balancing driving and resisting forces. These methods operate on the fundamental principle of comparing the forces or moments that tend to cause a slope to fail (disturbing forces) with those that resist failure (resisting forces) along an assumed or known potential slip surface. LEMs assume the soil mass is on the verge of failure (limit equilibrium) and use a single factor of safety (F) applied uniformly along the slip surface; all slices share this factor of safety by definition (Duncan et al., 2014).

The central output of a limit equilibrium analysis is the Factor of Safety (FS), a dimensionless number that provides a quantitative measure of a slope's stability. The FoS is defined as the ratio of the available shear strength of the soil along the slip surface to the shear stress required to maintain equilibrium (Duncan et al., 2014). An FOS greater than 1.0 typically indicates a stable slope, while a value less than 1.0 signifies instability (Transportation Research Board, 1978). Design standards typically require a minimum FoS between 1.3 and 1.5 for static conditions, depending on the loading case and the level of uncertainty (Huang, 2014).

A fundamental assumption common to all limit equilibrium methods is that the shear strength of the geomaterials along the potential failure surface is governed by a defined failure criterion. The most widely adopted criterion in practice is the linear Mohr-Coulomb failure criterion, which relates the shear strength (τ) to the effective normal stress (σ') on the failure surface via the material's effective cohesion (c') and effective angle of internal friction (φ') (Duncan et al., 2014).

The most common technique for applying LEM is the "method of slices," in which the potential sliding mass is discretized into a series of vertical slices (Fellenius, 1936). This approach allows for the analysis of slopes with complex geometries, heterogeneous material properties, and variable pore water pressure conditions. This discretization, however, introduces a critical theoretical challenge: the problem becomes statically indeterminate. The number of unknown forces—specifically the normal and shear forces acting on the vertical boundaries between slices (the interslice forces)—exceeds the number of available equations of static equilibrium (i.e., summation of forces in two orthogonal directions and summation of moments) (Whitman and Bailey, 1967; Fredlund and Krahn, 1977).

Consequently, assumptions must be made about these interslice forces to solve for the factor of safety, and it is these assumptions that differentiate the various limit equilibrium methods developed over the past century. Early analytical methods, such as the Swedish Slip Circle method, were fundamentally based on limit equilibrium principles, which assume that failure occurs along a distinct surface and that the state of the slope can be evaluated by comparing the moments or forces causing failure to those resisting it. Fellenius's (1936) "Swedish circle" method introduced dividing the sliding mass into slices and assumed a circular failure surface. Subsequent refinements allowed arbitrary slip shapes and considered both force and moment equilibrium. The forces involved are presented in Figure 2.13.

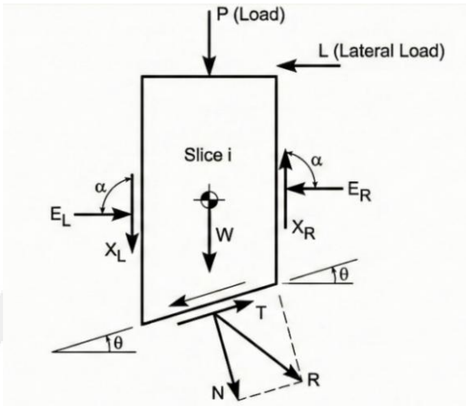

Figure 2.13. *Forces acting on a typical slice in a limit equilibrium analysis (Fredlund and Krahn, 1977)*

2.3.1.1. Method variants

The history of the method of slices is a narrative of progressive refinement, with each subsequent method seeking to satisfy more conditions of static equilibrium by making increasingly sophisticated, and arguably more realistic, assumptions about the interslice forces. This evolution reflects a quest for greater accuracy and applicability to more complex geotechnical problems. Numerous LEM formulations have been developed, differing primarily in the assumptions made regarding the magnitude and direction of the interslice forces (the forces between adjacent slices) and which conditions of static equilibrium (force and/or moment) are explicitly satisfied. The choice of method can influence the calculated FoS, with differences of up to 6% reported between various methods for the same problem (Fredlund and Krahn, 1977).

Swedish (Fellenius/Ordinary) method

The earliest methods prioritized simplicity to render the statically indeterminate problem solvable by hand. The Ordinary Method of Slices (OMS), also known as the Fellenius method (Fellenius, 1936), is the simplest approach. It achieves determinacy by assuming the resultant of the interslice forces is parallel to the base of each slice, which effectively means both interslice normal and shear forces are ignored when summing moments. While this simplification allows for a direct solution, it satisfies only overall moment equilibrium and violates force equilibrium. This omission leads to significant inaccuracies, particularly in effective stress analyses of slopes with high pore water pressures or deep circular failure surfaces, where the FS can be underestimated by as much as 60% (Whitman and Bailey, 1967). It is known to be overly conservative and is now rarely used (Griffiths and Lane, 1999; Azeze, 2020).

Bishop's simplified method

A major advance was made with Bishop's Modified method (Bishop, 1955) by Alan W. Bishop of Imperial College. This method assumes that the shear forces between slices are zero (X=0) but accounts for the interslice normal forces (E). By summing forces for each slice in the vertical direction, Bishop derived an expression for the normal force at the base of the slice that is dependent on the FS itself. This method satisfies overall moment equilibrium and vertical force equilibrium for each slice, but not horizontal force equilibrium. The resulting equation for FS is non-linear and must be solved iteratively. Despite its assumptions, Bishop's Modified method has proven to be remarkably accurate for circular failure surfaces, with calculated FS values typically falling within a few percent of more rigorous solutions. Its primary limitations, however, are its strict applicability to circular failure surfaces and the assumption of zero interslice shear, which may not be valid in all cases (Bishop, 1955; Fallah and Noferesti, 2015; Griffiths and Lane, 1999).

Janbu's simplified and generalized methods

Developed concurrently, Janbu's method (Janbu, 1954) was designed specifically to analyze slopes with non-circular failure surfaces, which are frequently observed in stratified soils or where failure is controlled by planes of weakness. The Janbu's Simplified method satisfies only force equilibrium and neglects moment equilibrium. Recognizing this limitation, Janbu later introduced an empirical correction factor, f_0, which accounts for interslice shear forces and is dependent on the geometry of the slide and the soil type. The Janbu's Corrected method provides a reasonably accurate FS for many non-circular failure mechanisms and is particularly useful for analyzing shallow slides (Janbu, 1954). Janbu's Generalized Procedure uses an assumed line of thrust to define the location of the interslice normal force.

Spencer's method

The search for methods that satisfy all conditions of static equilibrium led to the development of "rigorous" methods. The Spencer method (Spencer, 1967) satisfies all conditions of equilibrium (both force and moment) by assuming that the resultant of the interslice forces has a constant inclination (i.e., is parallel) throughout the sliding mass. The method solves for both the FS and this constant inclination angle, θ. It is considered one of the most rigorous LEM techniques because it satisfies all conditions of static equilibrium—both force and moment equilibrium—for each slice (Griffiths and Lane, 1999; Azeze, 2020; Babar et al., 2021; Fallah and Noferesti, 2015).

Morgenstern-Price method

The Morgenstern-Price (M-P) method (Morgenstern and Price, 1965) is arguably the most general and robust of the conventional LEMs. It also satisfies all conditions of static equilibrium for a failure surface of any arbitrary shape. It achieves this by introducing a flexible functional relationship between the interslice shear (X) and normal (E) forces, expressed as $X = \lambda f(x)E$. In this formulation, f(x) is a user-defined function that describes how the direction of the interslice forces varies across the slip surface, and λ is an unknown scaling factor that is solved for along with the FS. The flexibility of the f(x) function (e.g., constant, half-sine, trapezoidal) allows the method to model a wide range of conditions, making it a benchmark for slope stability analysis (Morgenstern and Price, 1965). It is applicable to slip surfaces of any shape and is generally preferred for complex problems (Griffiths and Lane, 1999; Azeze, 2020; Babar et al., 2021; Fallah and Noferesti, 2015).

General limit equilibrium (GLE) framework

The General Limit Equilibrium (GLE) method, often associated with Fredlund and Krahn (1977), is conceptually similar to the Morgenstern-Price method and also satisfies all equilibrium conditions. A framework that encompasses both Spencer and M-P methods.

Sarma method

The Sarma method is particularly useful for seismic slope-stability analysis and for problems involving complex non-circular failure surfaces represented by multiple wedges or non-vertical slices (Sarma, 1973, 1975). Instead of vertical slices, it can accommodate inclined slices or wedges, making it suitable for rock slopes where failure is often controlled by discontinuities. It applies the shear strength criterion to the sides and bottom of each slice/wedge and can provide either the FOS or the critical horizontal acceleration required to cause failure (k_y). Table 2.6 summarizes the comparison of common limit equilibrium methods.

Table 2.6. *Comparison of common limit equilibrium methods (Abramson et al., 2002; Duncan et al., 2014; Fredlund and Krahn, 1977)*

Method	Failure Surface	Interslice Force Assumptions	Equilibrium Conditions Satisfied	Typical Application/ Key Limitations
Ordinary Method of Slices (Fellenius, 1936)	Circular	Ignored (assumed parallel to slice base).	Moment only.	Simple but overly conservative for high pore pressures. Violates force equilibrium; inaccurate (Whitman and Bailey, 1967).
Simplified Bishop (1955)	Circular	Zero shear forces.	Moment & vertical force.	Widely used & accurate for circular surfaces. Violates horizontal force equilibrium.
Simplified Janbu (1954)	Non-Circular	Zero shear forces. Uses empirical correction factor.	Horizontal & vertical force.	For non-circular surfaces. Inaccurate without correction factor; violates moment equilibrium.
Spencer (1967)	Any Shape	Parallel forces (constant inclination).	Full (Force & Moment).	Rigorous for all shapes. Constant inclination assumption may be unrealistic.
Morgenstern-Price (M-P, 1965)	Any Shape	Inclination defined by an arbitrary function, f(x).	Full (Force & Moment).	Highly accurate rigorous method. Requires an assumed function, f(x).
General Limit Equilibrium (GLE)	Any Shape	Encompasses Spencer and M-P methods.	Full (Force & Moment).	Generalized formulation common in modern software.
Sarma Method (1975)	Any Shape	Shear strength applied to slice sides & bottom.	Full (Force & Moment).	Ideal for complex failure surfaces and seismic analysis.

2.3.1.2. Advantages and limitations

The evolution from Fellenius to Morgenstern-Price shows a clear trajectory from crude simplification to mathematical integrity. The limitations of one method directly motivated the development of the next, more comprehensive approach. LEMs provide a robust and often sufficiently accurate framework for many slope stability problems. While rigorous methods like Spencer and Morgenstern-Price offer more comprehensive solutions, simpler methods like Bishop's Modified method remain popular for routine analyses due to their relative simplicity and generally good agreement with more complex methods for many common slope configurations. The primary strengths of LEM are its simplicity, computational efficiency, and long history of use, which has made it a well-understood and accepted standard in the industry (Duncan, 1996; Abramson et al., 2002). The required input parameters, such as soil unit weight, cohesion (c), and angle of internal friction (φ), are readily obtainable from standard laboratory and field tests (Huang, 2014; Azeze, 2020). They became widely used due to their simplicity and reasonably accurate results (typically within 5-10% of "exact" solutions for static cases) (Duncan, 1996; Griffiths and Lane, 1999).

Despite their widespread use, LEMs are not without limitations. To compute F, one must assume a shape/location of the failure surface and make assumptions about interslice forces (Griffiths and Lane, 1999). A primary criticism is the need to assume a priori the shape and location of the failure surface, although modern software often includes sophisticated search algorithms to find the critical surface with the lowest FOS. Results can be sensitive to the assumed failure surface shape; engineers often must try circular, planar, or non-circular surfaces to find the critical one. All these Limit Equilibrium Methods (LEMs) require assumptions about interslice force distribution or neglect certain interactions, which is a key limitation. Different LEM formulations (e.g., Bishop vs. Janbu vs. Morgenstern-Price) vary in which equilibrium equations are enforced and what is assumed about interslice normal and shear forces (Fredlund and Krahn, 1977). The assumptions made about interslice forces are simplifications of a complex stress state, and different methods can yield varying FOS values for the same problem.

More fundamentally, LEMs are based on static equilibrium and do not inherently consider the stress-strain behavior of the soil or rock, deformations prior to failure, or the progressive nature of failure (Duncan, 1996). These assumptions mean LEM does not explicitly consider the stress-strain behavior of soil—it satisfies equilibrium but ignores deformations. Even the most rigorous LEMs are constrained by a fundamental deficiency: they rely on an assumed failure mechanism and analyze the statics of a rigid body at the point of failure. They cannot account for the stress-strain behavior of the soil, the process of strain localization, or the development of progressive failure, where strength loss is not simultaneous along the entire slip surface (e.g., Griffiths and Lane, 1999). This limitation is particularly acute in brittle or strain-softening materials. Furthermore, the accuracy of any LEM is contingent on the user's ability to identify the most critical potential slip surface, which can be a challenging task in complex geologic settings.

It has inherent limitations in addressing local stress variations. LEM also cannot capture progressive failure (strength changing along the surface) since a single F and peak strengths are typically used everywhere. Furthermore, LEMs are generally not well-suited for analyzing slopes where internal deformation, brittle fracture, progressive creep, or liquefaction of weaker layers are the dominant failure mechanisms. Despite these limitations, LEMs became entrenched in practice due to their conceptual simplicity and the advent of computers in the 1960s which enabled iteration for more rigorous solutions. LEM is incapable of computing deformations or providing insight into stress-strain distributions, soil-structure interaction, or complex failure modes like progressive failure (Transportation Research Board, 1978; Li et al., 2024).

2.3.1.3. Advanced critical surface search strategies

In the application of Limit Equilibrium Methods (LEM) for slope stability, the calculation of the Factor of Safety (FS) is mathematically trivial compared to the geometric problem of locating the critical slip surface that yields the minimum FS. For the complex 3D geological structures typical of tunnel portals and spillway cuts—often governed by intersecting faults, bedding planes, and joint sets—the critical surface is rarely a simple sphere or ellipsoid. Consequently, modern analysis has shifted away from traditional grid search methods toward metaheuristic optimization algorithms. These algorithms mimic natural biological processes to explore the solution space more efficiently and robustly, avoiding the trap of local minima in the complex FS landscape.

Cuckoo search (CS)

The Cuckoo Search algorithm is a nature-inspired metaheuristic based on the obligate brood parasitism behavior of some cuckoo species. In the context of slope stability optimization, a "nest" represents a potential solution (a specific slip surface geometry). The algorithm generates new solutions using Lévy flights—a random walk characterized by a heavy-tailed probability distribution of step lengths (Azizi et al., 2020). The Lévy flight mechanism allows the search to alternate between local exploitation (short steps clustering around a current best solution) and global exploration (long jumps to entirely new regions of the search space). The algorithm operates on three rules: (1) Each cuckoo lays one egg at a time in a randomly chosen nest; (2) The best nests with high-quality eggs (lowest FS) are carried over to the next generation; (3) The number of available host nests is fixed, and a host bird can discover an alien egg with a probability p_a. If discovered, the nest is abandoned, and a new nest is built in a new location (Azizi et al., 2020). Comparative studies indicate that CS outperforms other algorithms like Particle Swarm Optimization (PSO) and Genetic Algorithms (GA) in terms of convergence speed and the ability to locate lower FS values in multimodal landscapes (Azizi et al., 2020). The heavy-tailed step distribution ensures that the search does not stagnate in local minima, a common failure mode for grid searches in complex geology.

Particle swarm optimization (PSO)

PSO simulates the social behavior of bird flocking or fish schooling. A population of candidate solutions ("particles") moves through the search space with velocities that are dynamically adjusted according to their historical behavior. Each particle adjusts its trajectory based on its own best known position (local best) and the best known position of the entire swarm (global best) (http-14[19]). While effective, standard PSO can sometimes struggle with the highly discontinuous objective functions found in rock slope stability, where kinematic constraints (e.g., infinite strength along a non-daylighting wedge) create abrupt changes in the FS surface.

Surface altering optimization (SAO)

SAO is typically employed as a local refinement technique following a global search. Once a metaheuristic algorithm (like CS or PSO) identifies the general location of the critical failure mode, SAO modifies the geometry of the slip surface using spline control points to further minimize the FS. This hybrid approach ensures that the global

[19]http-14:https://www.rocscience.com/learning/facilitating-geotechnical-engineering-problems-using-metaheuristic-optimization-algorithms (accessed October 22, 2025).

minimum is located via metaheuristics and then refined to a kinematically admissible shape that may be non-circular or non-ellipsoidal, better conforming to the specific geological weaknesses of the site (http-14[20]).

2.3.1.4. Back-analysis in limit equilibrium methods

Back-analysis is the inverse process of slope stability assessment: determining the geomechanical properties of a slope at the moment of failure, under the assumption that the Factor of Safety (FS) was unity (1.0). For hydraulic structures, this technique is frequently employed to determine the residual shear strengths of bedding planes or fault gouge after a slide has occurred, providing calibrated parameters for the design of remedial stabilization works.

Probabilistic and Bayesian Approaches: Deterministic back-analysis is mathematically indeterminate; infinite pairs of cohesion (c') and friction angle (φ') can result in an FS of 1.0 for a given failure geometry. To resolve this non-uniqueness, probabilistic frameworks, particularly Bayesian updating, have gained prominence in advanced research.

- Bayesian Framework: This method treats geotechnical parameters not as fixed constants but as random variables described by probability density functions. It updates "prior" knowledge (derived from laboratory tests, regional geology, or engineering judgment) with "likelihood" information derived from the observed failure event (geometry, water levels) to produce a "posterior" distribution of the parameters (Parmar, 2025).
- Markov Chain Monte Carlo (MCMC): MCMC simulation is the computational engine used to sample from the complex, high-dimensional posterior distributions typical of slope stability problems. It allows for the rigorous quantification of uncertainty and the correlation between parameters (e.g., the strong negative correlation typically observed between back-analyzed c' and φ') (Wang, 2013).
- Maximum Likelihood Estimation: This technique identifies the set of parameters that maximizes the probability of observing the actual slope behavior (e.g., the specific failure surface geometry or displacement magnitude observed) (Wang, 2013).

[20](http-14).

These probabilistic methods transform back-analysis from a simple curve-fitting exercise into a rigorous tool for risk assessment. They allow designers to determine not just a single "best fit" value for strength, but a full probability distribution that informs reliability-based design for remediation, explicitly accounting for the uncertainties in the ground model (Hu et al., 2024).

2.3.2. Finite element methods

The field of slope stability analysis has witnessed a significant evolution from reliance on purely analytical and LEMs towards the adoption of sophisticated numerical modeling techniques, encompassing both continuum and discontinuum approaches. The inherent limitations of analytical methods, particularly their inability to model stress-strain behavior and complex failure processes, spurred a paradigm shift toward computational mechanics. This transition, made possible by the exponential growth in computing power since the 1960s, has allowed for increasingly realistic simulations of slope behavior. As computing power grew, geotechnical engineers moved beyond LEM to more fundamental numerical methods (Zienkiewicz et al., 1975; Duncan, 1996; Griffiths and Lane, 1999).

The Finite Element Method (FEM) provides a more powerful and versatile approach to stability analysis. The Finite Element Method (FEM) and the Finite Difference Method (FDM) are two prominent numerical techniques that have significantly advanced the analysis of slope stability. Both are continuum-based approaches, meaning they model the soil or rock mass as a continuous medium (Zienkiewicz et al., 1975). Unlike LEM, these methods discretize the entire problem domain—the slope, foundation, and any structural elements—into a mesh of smaller elements and solve the governing equations of motion and material behavior for the entire system (Zienkiewicz et al., 1975; Shlash, 2024). They are based on stress-strain constitutive relationships (e.g., the Mohr-Coulomb model) and can simulate the behavior of the soil and rock mass under various loading conditions (Israr et al., 2022; Li et al., 2024). Numerical methods offer more comprehensive simulations of complex geological conditions, including the effects of pore water pressure and groundwater flow on slope stability (Tanchev, 2014). For slope stability analysis, FEM has gained wider acceptance and application, largely due to its flexibility in handling complex geometries, material heterogeneity, and various boundary conditions (Griffiths and Lane, 1999).

Unlike LEM, FEM does not require any a priori assumptions regarding the shape or location of the failure surface; the failure mechanism develops naturally through the zones of highest shear stress and strain (Fredlund and Krahn, 1977). Furthermore, FEM computes the complete state of stress and deformation throughout the soil mass, providing valuable information on serviceability performance that LEM cannot (Griffiths and Lane, 1999).

The work of O.C. Zienkiewicz and colleagues (1975) was seminal in establishing FEM as a valid and powerful tool in geomechanics. Their influential textbook, *The Finite Element Method in Engineering Science*, provided the core theoretical basis for its application to a wide range of engineering problems, including geomechanics. A key contribution was the paper by Zienkiewicz et al. (1975), which formally proposed the use of FEM coupled with the shear strength reduction (SSR) technique to calculate a factor of safety for slopes. They analyzed a homogeneous c-phi slope and found good agreement between the FEM-predicted failure surface and factor of safety and those from LEM (Zienkiewicz et al., 1975; Griffiths and Lane, 1999). By the 1980s, finite element slope stability analysis was further validated (Griffiths, 1980; Matsui and San, 1992), cementing its credibility. This approach is now a standard feature in most commercial geotechnical software.

The core differences between Limit Equilibrium Methods (LEM) and Finite Element Methods (FEM) for slope stability analysis are contrasted in Table 2.7.

Table 2.7. *Comparison of limit equilibrium and finite element methods*

Feature	Limit Equilibrium Method (LEM)	Numerical Methods (FEM/FDM)
Fundamental Principle	Analyzes static equilibrium of a predefined sliced sliding mass (Transportation Research Board, 1978).	Solves stress-strain equations for a continuum mesh (Zienkiewicz et al., 1975).
FS Calculation	Ratio of resisting to driving forces along an assumed slip surface (Duncan et al., 2014).	Shear Strength Reduction (SSR) factor at numerical collapse (Griffiths and Lane, 1999).
Failure Mechanism	Predefined by user; identifies the most critical among tested surfaces (Duncan et al., 2014).	Develops naturally via localized shear strain; no prior assumption needed (Griffiths and Lane, 1999).
Stress-Strain Behavior	Ignored. Deformations cannot be calculated; implicitly controlled by FS (Transportation Research Board, 1978).	Explicitly modeled (e.g., Mohr-Coulomb); predicts stresses, strains, and deformations (Zienkiewicz et al., 1975).
Soil-Structure Interaction	Difficult to model; approximated via external loads.	Inherently modeled; simulates complex interactions (e.g., walls, anchors) (Griffiths and Lane, 1999).
Data Requirements	Requires strength parameters (c, φ) and unit weight (γ) (Huang, 2014; Azeze, 2020).	Requires strength and deformation parameters (E, ν) (Serra, 2013).
Key Strengths	Simple, computationally fast, widely accepted, and requires fewer inputs (Duncan, 1996; Azeze, 2020).	Rigorous, unbiased failure mechanism, calculates deformations, and models progressive failure (Griffiths and Lane, 1999; Li et al., 2024).
Key Limitations	Requires assumed failure surface, lacks deformation analysis, and can be non-conservative (Duncan, 1996; Transportation Research Board, 1978).	Computationally intensive, requires advanced expertise, needs more inputs, and is sensitive to mesh quality (Duncan, 1996; Shlash, 2024).
Common Software	Slope/W, Slide2, GEO5.	PLAXIS, FLAC, RS2.

2.3.2.1. Strength reduction and deformation analyses

The most common technique for calculating a factor of safety using FEM is the Shear Strength Reduction (SSR) method, also known as the Strength Reduction Method (SRM) or the phi-c reduction technique. The strength reduction method offers a way to determine slope safety factors using continuum mechanics (finite element modeling) rather than slice-by-slice statics. Originally hinted at by Zienkiewicz et al. (1975), this approach gained popularity in the 1990s (Griffiths and Lane, 1999). The fundamental principle of SRM involves systematically reducing the shear strength parameters of the geomaterials (cohesion, c, and friction angle, φ) until the slope model reaches a state of failure. The concept is to gradually reduce the shear strength parameters of the soil by a factor until the numerical model fails to converge, indicating instability (Griffiths and Lane, 1999). The Factor of Safety (FOS) is then defined as the ratio of the material's actual (or initial) shear strength to the reduced shear strength at the point of failure (Dawson et al., 1999).

In an SSR analysis, the material's shear strength parameters, cohesion (c') and the tangent of the friction angle (tan(ϕ')), are systematically and progressively reduced by a common factor, termed the Strength Reduction Factor (SRF). A series of finite element analyses are run with progressively increasing SRF values. The FoS is taken as the critical SRF at which the numerical model fails to achieve a converged solution, which is interpreted as the onset of slope collapse (Griffiths and Lane, 1999). The relationship (2.8) is given by:

$$FS = SRF_{\text{failure}} = \frac{c'_{\text{initial}}}{c'_{\text{failure}}} = \frac{\tan(\varphi'_{\text{initial}})}{\tan(\varphi'_{\text{failure}})} \tag{2.8}$$

This method offers a significant advantage over traditional LEMs as it does not require a priori assumptions regarding the shape or location of the failure surface. Instead, the critical failure surface emerges naturally from the analysis as the zone where the applied shear stresses exceed the reduced shear strength of the material or as the zone of maximum shear strain (Griffiths and Lane, 1999). This resulting failure mechanism is shown in Figure 2.14.

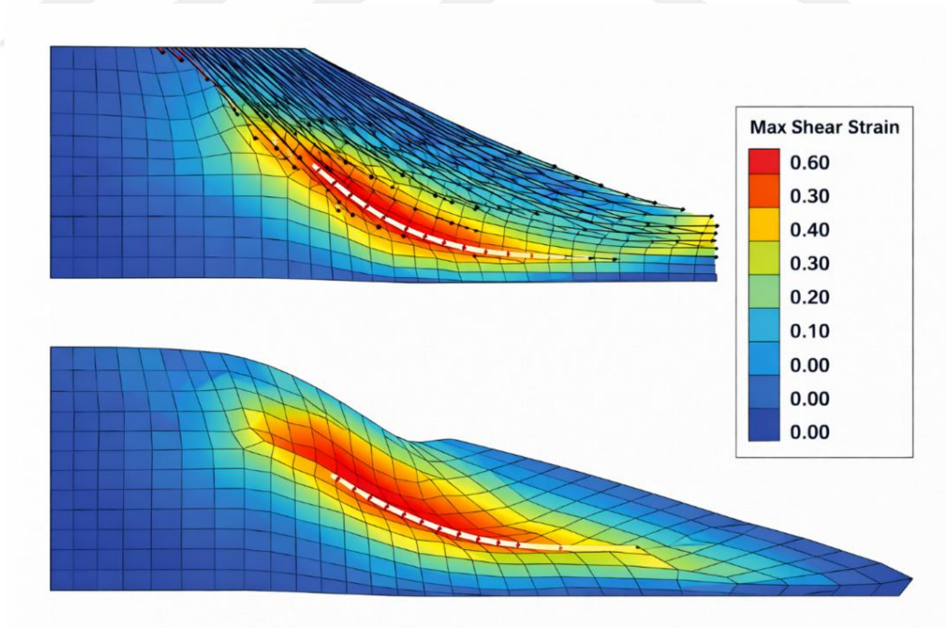

Figure 2.14. *Deformed mesh and shear strain vectors indicating slope failure mechanism (Griffiths and Lane, 1999)*

In SRM, the finite element method computes the full stress-strain response of the slope as strength is reduced, inherently finding the critical failure surface as the zone of yielded elements that propagate through the slope. This makes it a more objective and often more realistic method for identifying complex failure mechanisms. SRM can also capture progressive failure and stress redistribution within the slope, offering a more realistic representation of slope behavior compared to traditional LEM (Dawson et al., 1999). The SRM is generally considered accurate, robust, and simple enough for routine use, with FOS values obtained from SRM often being within a few percent of those derived from LEM (Griffiths and Lane, 1999).

One of the most significant advantages of FEM over LEMs is its ability to model the stress-strain behavior of geomaterials and predict deformations prior to and at failure. In contrast, FEM can simulate the entire load-deformation response of a slope, offering insights into the development of plastic strains, the formation of shear bands, and the progressive nature of failure (Griffiths and Lane, 1999). Another advantage is the ability to obtain deformations at working stress levels and factors of safety consistently from one model (Griffiths and Lane, 1999). It essentially bridges limit equilibrium with numerical analysis, providing a factor of safety along with a deformed mesh and a potential failure deformation pattern.

In the context of finite element analyses performed in commercial codes like PLAXIS, this method yields a safety factor termed ΣM_{sf}. It is explicitly noted that ΣM_{sf} represents the ratio of the available shear strength to the shear strength required for equilibrium, making it numerically equivalent to the Factor of Safety (FS) calculated in Limit Equilibrium Methods (Griffiths and Lane, 1999).

2.3.2.2. Constitutive models

The accurate prediction of slope stability hinges on the faithful representation of geomaterial behavior under various loading conditions. Constitutive models, which mathematically describe the stress-strain relationship of soils and rocks, are fundamental to both analytical and numerical analyses. The predictive power of any numerical stability analysis is fundamentally limited by the ability of the chosen constitutive model to represent the true stress-strain behavior of the soil or rock. This section critically examines the spectrum of available models relevant to the intermediate geomaterials and rock masses encountered in this study, highlighting the persistent trade-off between realism and practicality. The accuracy of an FEM analysis is highly dependent on the chosen constitutive model. Figure 2.15 contrasts these fundamental behaviors.

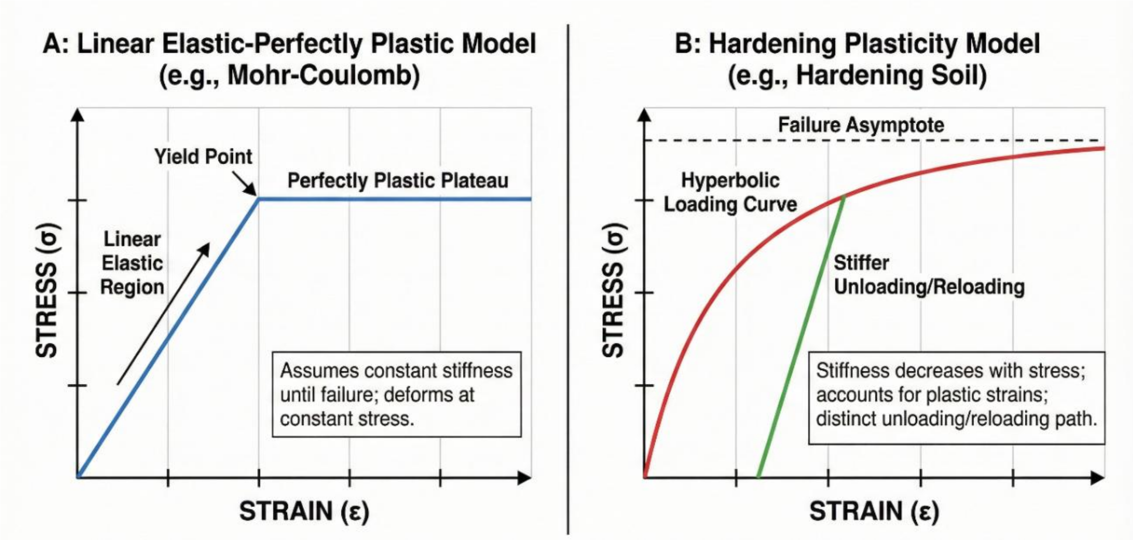

Figure 2.15. *Comparison of stress-strain behavior in constitutive models: (a) Linear elastic-perfectly plastic behavior (Mohr-Coulomb); (b) Hyperbolic stress-strain relationship (Hardening Soil) (Schanz et al., 1999)*

Mohr-Coulomb (M-C) model

The Mohr-Coulomb (M-C) model is one of the simplest and most widely used constitutive models in geotechnical engineering. It is a linear-elastic, perfectly-plastic model that combines Hooke's law with the Mohr-Coulomb failure criterion, which defines the limiting shear stress a material can withstand as a function of normal stress, cohesion (c), and the angle of internal friction (φ) (Duncan et al., 2014). It requires only five inputs: two elastic parameters (Young's modulus, E, and Poisson's ratio, ν) and three strength parameters (effective cohesion, c′, effective friction angle, ϕ′, and dilation angle, ψ) (Brinkgreve, 2021). Its appeal lies in simplicity—only a few parameters that have clear physical meaning and can be obtained from common lab tests. In numerical analysis, M-C is often implemented as a perfectly plastic model with a linear yield surface in shear stress-normal stress space. However, this simplicity comes at the cost of realism.

The M-C model has several significant limitations that restrict its applicability for advanced analyses: it assumes a linear failure envelope, which is often a poor approximation for real soils and rocks over a wide range of confining stresses (*Duncan, 1996)*; it assumes stiffness is constant, independent of the stress level, contrary to the fundamental fact that the stiffness of soils generally increases with confining pressure; it neglects the influence of the intermediate principal stress (σ_2) on yielding; and as a perfectly-plastic model, it cannot capture strain-hardening or softening behavior. This renders it incapable of modeling the accumulation of plastic strain before failure or the progressive failure mechanisms common in brittle materials. This can lead to an overprediction of the undrained shear strength (s_u) and unrealistic predictions, such as heave behind retaining walls during excavation. The corresponding yield surfaces are compared in Figure 2.16.

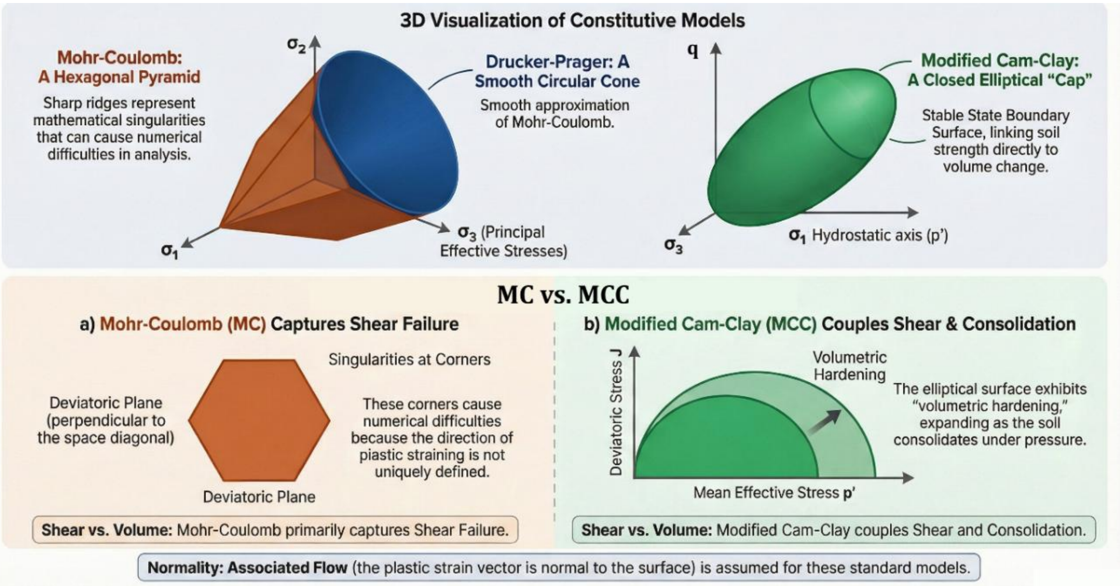

Figure 2.16. *Comparison of yield surfaces in principal stress space: (a) Mohr-Coulomb hexagonal yield surface, showing singularities at corners; (b) Modified Cam-Clay elliptical yield surface, capturing volumetric hardening (Potts and Zdravkovic, 1999)*

Hardening soil (HS) model

To overcome these limitations, advanced models like the Hardening Soil (HS) model have been developed (Schanz et al., 1999; Brinkgreve, 2021). The HS model is an advanced elastoplastic model that incorporates stress-dependent stiffness, different moduli for primary loading and unloading/reloading, and can simulate both shear and volumetric hardening (Schanz et al., 1999). As formulated by Schanz et al. (1999), it provides a significant improvement over M-C for a wide range of soils. Its key features make it highly suitable for modeling complex loading scenarios, such as those around excavations and hydraulic structures: Stress-Dependent Stiffness, Dual Hardening Mechanisms, and Distinct Loading/Unloading Stiffness (Schanz et al., 1999). Unlike M-C, the HS model defines different stiffness moduli for primary loading (E_{50}^{ref}), unloading-reloading (E_{ur}^{ref}), and oedometer loading (E_{oed}^{ref}), with each modulus decreasing as confining stress decreases via a power-law exponent m (Brinkgreve, 2021). It reproduces non-linear stress-strain curves and the memory of preloading, giving more accurate predictions. Figure 2.17 provides a detailed representation of the various stiffness moduli utilized within the Hardening Soil model.

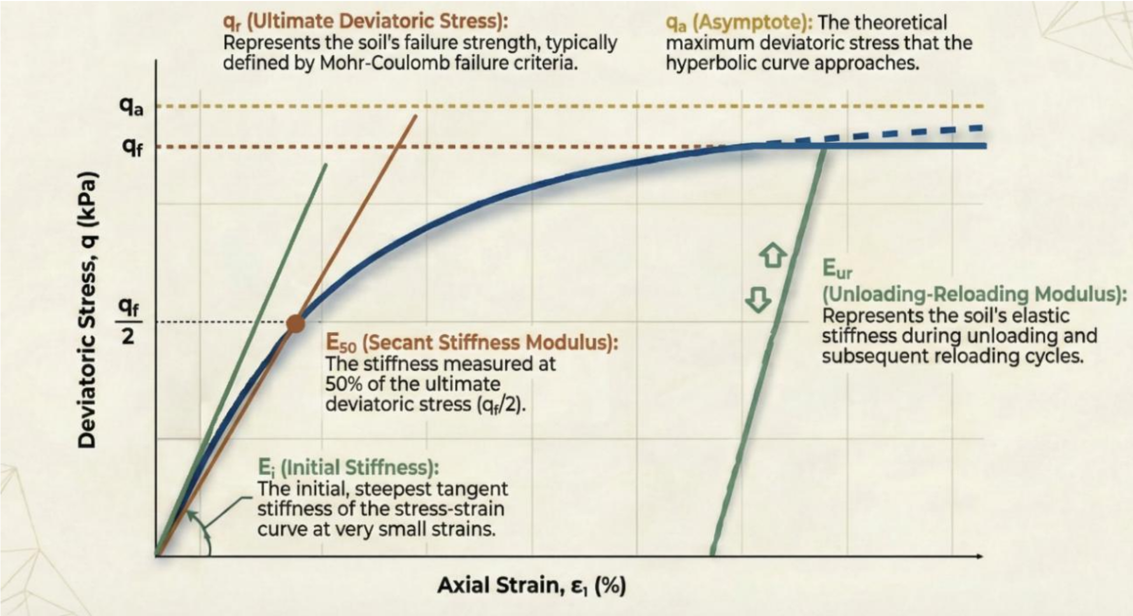

Figure 2.17. *Definition of stiffness moduli in the Hardening Soil model (Schanz et al., 1999)*

Studies have shown that the HS model can provide more reliable estimates of the factor of safety compared to the MC model (Schanz et al., 1999). The Hardening Soil model with small-strain stiffness (HS-Small) further refines this by accounting for the very high stiffness at small strain levels, leading to more realistic deformation predictions (Brinkgreve, 2021). Calibration requires more parameters (typically 5 elasticity parameters plus strength parameters), which can be obtained from triaxial and oedometer tests or estimated from correlations (Brinkgreve, 2021).

While standard elastoplastic models capture failure envelopes, they often overestimate damping at small strains. The Hardening Soil Small Strain (HS-Small) model, an extension based on Benz (2007), addresses this by incorporating the very small strain stiffness (G_0) and its non-linear degradation. By explicitly modeling hysteretic damping through a threshold shear strain parameter ($\gamma_{0.7}$), the HS-Small model provides a physically consistent decay of stiffness during dynamic loading. Brinkgreve (2021) emphasize that this feature is critical for accurate displacement prediction in seismic finite element analyses.

Generalized Hoek-Brown failure criterion

The mechanical behavior of jointed rock masses is frequently modeled using the Generalized Hoek-Brown failure criterion (Hoek et al., 2002). This non-linear criterion is superior to linear models in capturing the curvature of the failure envelope at low confining stresses, a typical condition in slope stability problems. The generalized criterion is expressed as:

$$\sigma_1' = \sigma_3' + \sigma_{ci}\left(m_b\,\frac{(\sigma_3')}{\sigma_{ci}} + s\right)^a \tag{2.9}$$

Where σ'_1 and σ'_3 are the major and minor effective principal stresses at failure. σ_{ci} is the uniaxial compressive strength of the intact rock. m_b, s, and a are material constants for the rock mass.

Derivation of Material Constants: The rock mass constants are derived from the GSI and the intact rock constant m_i using formulations that incorporate the degree of rock mass damage. Hoek et al. (2002) defined these as follows:

Reduced frictional strength:

$$m_b = m_i \exp\left(\frac{GSI - 100}{28 - 14D}\right) \tag{2.10}$$

Rock mass cohesion/interlocking:

$$s = \exp\left(\frac{GSI - 100}{9 - 3D}\right) \tag{2.11}$$

Variable parameter:

$$a = \left(\frac{1}{2}\right) + \left(\frac{1}{6}\right)\left(e^{-\frac{GSI}{15}} - e^{-\frac{20}{3}}\right) \tag{2.12}$$

The criterion introduces the Disturbance Factor (D), ranging from 0 to 1, to theoretically account for stress relief and blast damage typically induced during excavation. A critical advancement in the 2002 edition of the criterion was the explicit inclusion of the Disturbance Factor (D) to account for stress relaxation and blast damage caused by excavation processes. The factor D ranges from 0 to 1:

- D=0: Represents undisturbed in-situ rock masses or excellent quality controlled blasting (e.g., TBM tunnels).

- D=0.7: Often applied to mechanically excavated slopes in weak rock where ripping and dozing cause some disturbance.
- D=1.0: Represents significant production blast damage (e.g., large open pit slopes) or heavy stress relief.

Appropriate selection of D is vital, as it significantly degrades the calculated rock mass strength and deformation modulus. As noted by Hoek (2019), incorporating D is essential for accurately representing the reduced strength parameters in the relaxation zone surrounding rock cuts. Estimation guidelines are provided in Table 2.8.

Table 2.8. *Table illustrating guidelines for estimating the Disturbance Factor D with visual examples of rock mass appearance (Hoek and Brown, 2019)*

The disturbance factor should never be applied to the entire rock mass surrounding an excavation.		
Appearance of rock mass	Description of rock mass	Suggested value of D
	Excellent quality-controlled blasting or excavation by a road-header or tunnel boring machine results in minimal disturbance to the confined rock mass surrounding a tunnel.	$D = 0$
	Mechanical or manual excavation in poor quality rock masses gives minimal disturbance to the surrounding rock mass.	$D = 0$
	Where squeezing problems result in significant floor heave, disturbance can be severe unless a temporary invert, as shown in the photograph, is placed.	$D = 0.5$ with no invert
	Poor quality of drilling alignment, charge design and detonation sequencing results in very poor blasting in a hard rock tunnel with severe damage, extending 2 or 3 m, in the surrounding rock mass.	$D = 1.0$ at the surface with a linear decrease to $D = 0$ at about 2 m into the surrounding rock mass
	Small scale blasting in civil engineering slopes results in modest rock mass damage when controlled blasting is used, as shown on the left-hand side of the photograph.	$D = 0.5$ for controlled presplit or smooth wall blasting
	Uncontrolled production blasting can result in significant damage to the rock face.	$D = 1.0$ for production blasting
	In some weak rock masses, excavation can be carried out by ripping and dozing. Damage to the slopes is primarily due to stress relaxation.	$D = 0.7$ for mechanical excavation
	Very large open pit mine slopes suffer significant disturbance due to heavy production blasting and stress relaxation from overburden removal.	$D = 1.0$ for production blasting

Hoek–Brown to equivalent Mohr–Coulomb parameterization

Although the Hoek-Brown criterion defines the non-linear strength of rock, many Limit Equilibrium Method (LEM) analyses and numerical modeling software packages (such as standard FEM codes) still require Mohr-Coulomb (MC) parameters (cohesion c' and friction angle φ') because their plasticity algorithms are formulated in MC space. To facilitate this, equivalent parameters can be derived by fitting a linear relationship to the non-linear Hoek-Brown envelope over a specific stress range (σ'_{3max}) relevant to the specific engineering problem (Bieniawski, 1989). The critical step in accurate parameterization is selecting the correct upper limit of confining stress (σ'_{3max}) for the curve fitting. Since the strength envelope is non-linear, the tangent friction angle changes with confinement.

For slopes, the relevant stress range is relatively low. Hoek et al. (2002) suggest calculating σ'_{3max} based on the slope height (H) and rock mass unit weight (γ):

$$\frac{\sigma'_{3_{\mathrm{max}}}}{\sigma'_{\mathrm{cm}}} = 0.72 \left(\frac{\sigma'_{\mathrm{cm}}}{\gamma H}\right)^{-0.91} \tag{2.13}$$

Conversely, for deep tunnels where confinement is significantly higher, this formula must be adjusted accordingly to capture the strength behavior at higher stress levels (Hoek et al., 2002). Hoek et al. (2002) provided the exact analytical solution for this curve-fitting process using the specifically determined σ'_{3max}:

$$\varphi' = sin^{(-1)}\left(\frac{\left(6am_b\left(s + m_b\sigma'_{(3n)}\right)^{(a-1)}\right)}{\left(2(1+a)(2+a) + 6am_b\left(s + m_b\,\sigma'_{(3n)}\right)^{(a-1)}\right)}\right) \tag{2.14}$$

$$c' = \left(\frac{\sigma_{ci}\left[(1+2a)s + (1-a)m_b\sigma'_{(3n)}\right]\left(s + m_b\sigma'_{(3n)}\right)^{(a-1)}}{(1+a)(2+a)\sqrt{1 + \dfrac{6am_b\,(s\ +\ m_b\sigma'_{3n})^{a-1}}{(1+a)(2+a)}}}\right) \tag{2.15}$$

Where $\sigma'_{3n} = \sigma'_{3max} / \sigma_{ci}$.

This linearization is highly stress-dependent; therefore, selecting the correct σ'_{3max} relevant to the tunnel depth or slope height is critical for accurate stability assessment. Utilizing these specific stress-dependent equivalent parameters guarantees that the linear MC model closely approximates the true non-linear rock mass behavior in the anticipated zone of potential failure. Failure to meticulously adjust these parameters for the specific stress range of the slope can lead to significant errors in the calculated Factor of Safety (FS) (Song et al., 2023).

The choice of a constitutive model involves a fundamental and enduring trade-off between theoretical sophistication and practical usability. While advanced models like the HS model and its small-strain extension (HS-Small) offer a much more realistic representation of soil behavior, they require a greater number of input parameters. These parameters often necessitate specialized, high-quality, and expensive laboratory tests (e.g., triaxial tests with local strain measurement, oedometer tests) that may not be available on a typical commercial project. This trade-off is a significant source of uncertainty in advanced numerical modeling. The choice of a constitutive model is therefore dictated by the specific physical phenomena that must be captured to produce a meaningful analysis, which for this thesis involves accurately modeling the behavior of cohesive soils and rock masses under static, dynamic, and transient seepage conditions.

Consequently, justifying the adoption of an advanced model requires not only demonstrating the inadequacy of simpler models for the problem at hand, but also presenting a credible and rigorous strategy for parameter calibration. Therefore, a phased approach is adopted in this study: starting with Mohr-Coulomb for a baseline stability assessment, and subsequently refining the analysis with advanced models for the final evaluation of critical slopes adjacent to hydraulic structures. This parameter calibration is graphed in Figure 2.18.

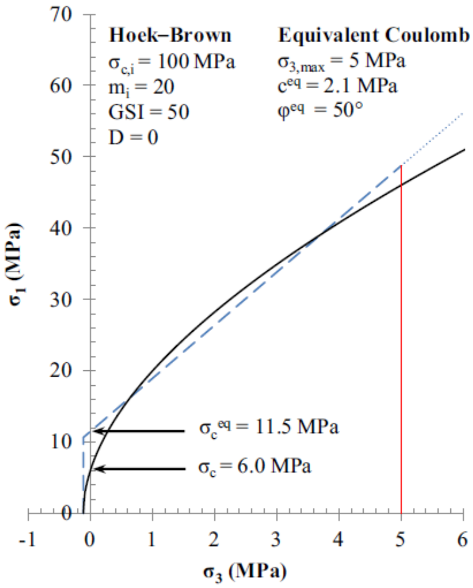

Figure 2.18. *Graph showing the curve-fitting process between the non-linear Hoek-Brown envelope and the linear Mohr-Coulomb envelope over a specific stress range (5 MPa) (Rafiei Renani and Cai, 2022)*

While critical state models such as Modified Cam Clay (MCC) (Schofield and Wroth, 1968) provide robust frameworks for normally consolidated soft clays, and advanced models like Nor-Sand (Jefferies, 1993) or UBC3D-PLM are indispensable for dynamic liquefaction analysis in saturated loose sands, they fall outside the specific geomechanical scope of this study. The intermediate geomaterials, highly compacted earthfills, and fractured rock masses adjacent to the hydraulic structures investigated herein are governed by different failure kinematics and stiffness degradation mechanics. Therefore, rather than utilizing liquefaction- or critical-state-specific models, this research deliberately adopts the Hardening Soil (HS) and Generalized Hoek-Brown frameworks to more accurately capture the stress-dependent stiffness, complex hardening, and non-linear shear strength behavior crucial for these specific boundary value problems. Table 2.9 provides a comprehensive overview of constitutive soil models, distinguishing their specific applications in both static and dynamic geotechnical analysis.

Table 2.9. *Overview of constitutive soil models for static and dynamic analysis (Bentley Systems, 2023; Brinkgreve, 2021; Schanz et al., 1999; Jefferies, 1993; Schofield and Wroth, 1968)*

Model	Key Characteristics	Primary Application	Key Parameters	Parameterization Challenge
Mohr-Coulomb (MC)	Linear-elastic, perfectly plastic with constant stiffness.	Baseline for SSR analyses; first-order approximation of soil behavior.	Young's modulus (E), Poisson's ratio (ν), effective cohesion (c'), effective friction angle (φ'), dilatancy angle (ψ).	Low; however, it often yields physically unrealistic results for deformation analyses.
Hardening Soil (HS)	Non-linear elastic with plastic hardening and stress-dependent stiffness.	Predicts realistic static load deformations for sands and stiff clays (e.g., excavations, embankments).	Reference secant stiffness (E_{50}^{ref}), oedometer loading stiffness (E_{oek}^{ref}), unloading/reloading stiffness (E_{ur}^{ref}), strength parameters (c', φ', ψ), power exponent (m).	High; demands advanced triaxial and oedometer testing for accurate calibration (Schanz et al., 1999).
Modified Cam Clay (MCC)	Critical state framework incorporating volumetric hardening and stress history.	Ideal for normally consolidated clays and large-scale settlement analyses.	Compression index (λ), swelling index (κ), critical state line slope (M), Poisson's ratio (ν), initial void ratio (e_0).	Medium; necessitates high-quality oedometer and triaxial testing (Schofield and Wroth, 1968).
Nor-Sand	Critical state model utilizing the state parameter (ψ) to control dilation/contraction and liquefaction.	Analyzes static and dynamic liquefaction in granular soils (sands).	Critical state parameters (Γ, λ), CSL slope (M), hardening parameters (H, N), dilatancy parameter (χ).	High; requires a comprehensive suite of drained and undrained triaxial tests to capture state-dependency (Jefferies, 1993).
UBC3D-PLM	Effective stress, non-linear plasticity model featuring densification and post-liquefaction rules.	Advanced dynamic modeling of liquefaction and cyclic mobility in sands.	Corrected SPT blow count ($(N_1)_{60}$), relative density, and elastic/plastic moduli.	High; demands specialized dynamic testing or extensive empirical correlations.

2.3.2.3. Advantages and limitations

The shift towards numerical modeling was motivated by the need to analyze complex slope geometries, heterogeneous material properties, and intricate boundary conditions that are difficult to accommodate within the simplifying assumptions of LEMs (Duncan, 1996). The key benefit of FEM/FDM is that no assumption about failure surface location or shape is needed—the soil can "choose" where to fail based on constitutive behavior (Griffiths and Lane, 1999). Numerical methods can identify potential failure mechanisms without prior assumption of their shape or location, a significant advantage over LEMs. Moreover, complex geometries, stratigraphies, and support systems can be modeled with relative ease in FEM. Furthermore, because there is no concept of "slices" in FEM, there is no need for assumptions regarding interslice forces, which are a major source of uncertainty among LEMs (Griffiths and Lane, 1999). They provide valuable information on slope deformations under working load conditions, long before failure is reached. This is critical for serviceability assessments of slopes near sensitive structures. Provided an appropriate strain-softening constitutive model is used, FEM/FDM can simulate the entire failure process, from the onset of local yielding to the propagation of shear bands and ultimate overall collapse. In summary, FEM/FDM approaches overcome many LEM limitations, especially for highly non-homogeneous or non-linear soil conditions, at the cost of more complex analysis and computation. Figure 2.19 visually demonstrates this difference.

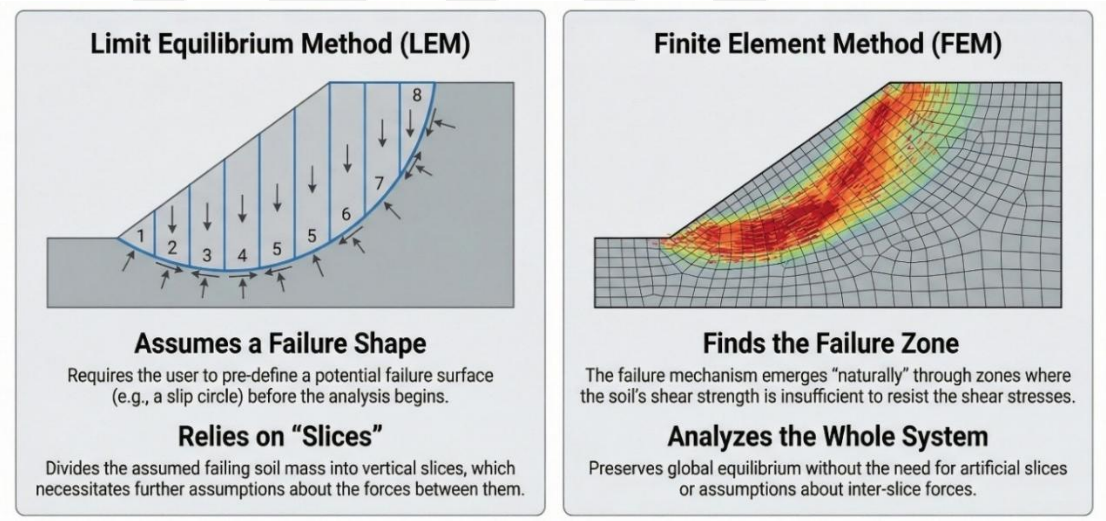

Figure 2.19. *Visual comparison of limit equilibrium method (slice assumption) versus finite element method (shear strain concentration) (Griffiths and Lane, 1999)*

Despite the advantages, the adoption of FEM was initially hampered by intense computational requirements and the challenges in accurately determining the stress-strain characteristics of soils (Liu and Feng, 2023; Wang et al., 2023). However, with the dramatic increase in computing power and the development of more user-friendly software, these hurdles have been largely overcome (Claret et al., 2024). In contrast, numerical methods offer greater flexibility in dealing with complex geometries and material behaviors, though they can be constrained by input data availability and computational resources (Azadi and Momayez, 2024). A limitation of FEM is the need for detailed input, including a constitutive model and parameters, and expertise to interpret results. The increased sophistication of advanced models comes with its own challenges: they require a larger number of input parameters that can be difficult to determine, and their calibration is a critical and time-consuming process. One limitation is that the SRM can sometimes have numerical issues in highly brittle materials or yield non-unique failures. While LEMs still hold relevance for simpler problems, FEM offers a more powerful and versatile tool for detailed and critical slope stability assessments. The main limitations of numerical methods are their significantly higher computational cost and the greater level of user expertise required to build appropriate models and interpret the results (Duncan, 1996; Shlash, 2024). They also require more detailed input parameters, including deformation properties like Young's modulus and Poisson's ratio, in addition to strength parameters (Serra, 2013).

Comparative studies often find that numerical methods yield a lower, more conservative FoS than LEM, though this is not universal (Babar et al., 2021). For example, a study on the Mohmand Dam found FEM-based FoS values to be 11-19% lower than LEM for static conditions (Babar et al., 2021). However, the same study found LEM to be more conservative for pseudo-static analysis (Babar et al., 2021). These differences often arise because numerical methods can identify more complex and critical failure mechanisms that are missed by the geometric constraints of LEM (Babar et al., 2021).

2.3.2.4. Staged construction & support installation modeling

The stability of slopes at tunnel portals and spillway cuts is inherently path-dependent; the specific sequence of excavation and support installation fundamentally alters the stress state, deformation trajectory, and ultimate stability of the rock mass. Finite Element Method (FEM) modeling must explicitly simulate these construction stages to capture the true mechanical behavior.

Stress Redistribution and Relaxation: Excavation removes the confining stress from the rock mass, leading to elastic rebound and, if stresses exceed strength, plastic yielding. In FEM, this is modeled by progressively removing elements and applying equivalent nodal forces to simulate the release of in-situ stresses. A critical modeling nuance is the timing of support installation. If support is installed "instantaneously" (in the same calculation step as the excavation), the model assumes the support carries 100% of the relaxation load, which is physically unrealistic as deformation occurs during excavation before support can be installed. Advanced modeling uses a "load split" or "core softening" approach, where a percentage of the stress relaxation (e.g., 40-50%) is allowed to occur before the support elements are activated, simulating the physical delay between cutting and supporting (Hoek, 2007).

Active vs. passive support modeling

- *Active anchors:* Prestressed anchors apply a positive clamping load to the rock face, increasing normal stress on potential slip planes. In FEM, this is modeled by applying equal and opposite forces at the anchor head and bond length nodes, simulating the tensioning process. This active load modifies the stress field before further deformation occurs (Sabatini et al., 1999).
- *Passive support:* Untensioned dowels or shotcrete only mobilize resistance in response to rock mass deformation. The model must simulate the accumulation of shear strain that engages the dowel, often requiring interface elements that allow for bond-slip behavior (Sabatini et al., 1999).

Interface elements and bond-slip behavior

The interaction between the grout, the steel reinforcement, and the surrounding rock is governed by bond stiffness and shear strength. Sophisticated FEM models utilize interface elements between the structural elements (truss or beam elements representing bolts) and the rock mesh. These interfaces allow for relative slip once the bond strength is exceeded, preventing the unrealistic transmission of infinite loads to the support and capturing potential pull-out failure modes which are common in weak rock (Sabatini et al., 1999).

Sequential excavation modeling

For large spillway cuts, excavation is typically performed in benches. The numerical model must simulate this top-down sequence. The removal of upper benches unloads the lower rock mass, potentially causing valley rebound or the opening of horizontal sheeting joints due to stress relief. Staged analysis captures the cumulative plastic strains and the progressive mobilization of shear strength on discontinuities—

phenomena that a single-step "gravity turn-on" analysis would completely miss (Potts and Zdravković, 2001).

2.3.2.5. Structural-geotechnical interaction

The structural verification of conduits and hydraulic appurtenances is typically performed using numerical codes (such as SAP2000), employing a soil-structure interaction approach. The soil support is modeled using the Winkler Spring approximation, where the ground is represented by a bed of independent, linear elastic springs. The modulus of subgrade reaction (k_s) for these springs is derived directly from in-situ Menard Pressuremeter moduli (E_m), providing a site-specific representation of the ground stiffness (Bowles, 1996). This coupled approach allows for the calculation of internal forces within structural liners under realistic non-uniform soil pressure distributions.

2.3.2.6. Transient seepage & rapid drawdown coupling in FEM

One of the most critical loading cases for slopes adjacent to reservoirs is rapid drawdown—the fast lowering of the external water level. This creates a severe destabilizing condition where the external stabilizing hydrostatic pressure is removed while high pore water pressures remain locked within the low-permeability rock or soil mass. This phenomenon presents a critical stability challenge, primarily governed by the delayed dissipation of these internal pore-water pressures—commonly termed 'phreatic lag' (Duncan et al., 2014). The rigor of the stability analysis heavily depends on the ratio of hydraulic conductivity (k) to the drawdown rate (R). If the k/R ratio is low, undrained behavior dominates, leaving the slope subjected to elevated internal pressures while the external support is lost.

In these scenarios, the principles of unsaturated soil mechanics are essential for understanding the transition from a saturated to an unsaturated state, where delayed pore-water pressure dissipation is fundamentally linked to the development of matric suction in the soil pores (Fredlund and Rahardjo, 1993). Advanced constitutive models (such as unsaturated soil mechanics models extended to rock joints) are required to handle the negative pore water pressures (matric suction) that develop in the unsaturated zone above the phreatic surface, which can contribute significantly to the temporary stability of the slope (Moradi et al., 2024). Although matric suction theoretically contributes to the available shear strength, its beneficial stabilizing effects are complex and can be readily destroyed by environmental infiltration, making it a highly sensitive variable in characterizing the true stress state of low-permeability clays during RDD (Fredlund and Rahardjo, 1993; USACE, 2003).

Historically, the design philosophy for RDD has relied heavily on Level 1 (Instantaneous) analyses, which postulate a condition where the drawdown is so rapid that absolutely no drainage occurs within low-permeability materials (Duncan et al., 2014; USACE, 2003). While this assumption simplifies stability computations by allowing the use of undrained shear strengths linked to pre-drawdown effective consolidation stresses, it inherently introduces a profound degree of conservatism that completely fails to account for any partial drainage or shear-induced pore pressure changes during realistic drawdown timelines (Duncan et al., 2014; USACE, 2003). Consequently, this Level 1 assumption represents an extreme, often unrealistic worst-case scenario that artificially mandates redundant and massive structural interventions—a phenomenon conceptualized in this thesis as the 'over-engineering trap' (Duncan et al., 2014; USACE, 2003). The rigid application of this instantaneous model ignores actual dissipation rates governed by the soil's consolidation characteristics, pushing the calculated stability artificially low and leading to highly uneconomical design dictates (Duncan et al., 2014).

To resolve the conflict between conservative approximations and economical design, a Level 2 design philosophy utilizing transient seepage analysis is strictly necessary. Transient seepage analysis couples the continuity equation with flow laws to compute the actual dissipation of pore water pressures (U_t) over time. Incorporating the specific hydraulic conductivity (k) and storage of the material accurately captures the "lag" in pore pressure response, providing a more realistic representation of the effective stresses within the slope during reservoir fluctuations (Fredlund and Rahardjo, 1993). However, the implementation of this transient approach can be divided into two distinct numerical strategies: uncoupled and fully coupled methodologies.

Uncoupled analysis

In standard practice, seepage is calculated first using a transient seepage analysis, and the resulting pore pressure fields at specific time steps are imported into a separate stress-deformation model (or LEM) to calculate stability. This approach assumes that the deformation of the rock skeleton does not affect the pore pressure (VandenBerge et al., 2015). While computationally efficient and often sufficient for high-permeability materials, this uncoupled approach ignores the "undrained" generation of pore pressures due to stress changes (the Skempton B-effect).

Fully coupled hydro-mechanical (H-M) analysis

This advanced approach solves the equations of equilibrium and fluid flow simultaneously, often using the u-p formulation (where u is displacement and p is pore pressure). It accounts for the compressibility of both the pore fluid and the soil/rock skeleton (Alonso and Pinyol, 2009). Alonso and Pinyol (2016) explicitly demonstrate that traditional instantaneous undrained methods are "conservative, but very unrealistic," as natural and compacted soils do not behave as perfectly rigid or entirely undrained masses during RDD. In a fully coupled analysis, the reduction in total stress on the slope face during drawdown can induce an immediate decrease in pore pressure (unloading effect) in the rock mass, which acts to stabilize the slope. Uncoupled analyses ignore this mechanical effect and often yield overly conservative results for rapid drawdown in compressible materials (VandenBerge et al., 2015). Conversely, in dilatant rock masses, shearing can reduce pore pressures (suction), temporarily increasing stability, while in contractive materials, shearing can generate excess pore pressures leading to failure. Only fully coupled FEM can capture these complex interactions (Alonso and Pinyol, 2009).

Ultimately, by integrating momentum balance, mass balance, and the mechanical stress-strain response of the soil skeleton, a fully coupled transient analysis accurately captures the simultaneous dissipation of pore-water pressures alongside the physical deformation of the slope (Alonso and Pinyol, 2016). These fully coupled hydro-mechanical analyses prevent the 'over-engineering trap' by providing a much more realistic calculation of the Factor of Safety (FS), effectively capturing the damping effect of soil stiffness and actual permeability, thereby justifying its use in modern stability assessments for critical hydraulic structures (Alonso and Pinyol, 2016). This theoretical framework directly underpins the methodological transition from Level 1 to Level 2 RDD analyses conducted in Case 6 of this study, rigorously demonstrating how advanced numerical coupling can eliminate the safety factor gap caused by traditional pseudo-static assumptions.

2.3.3. Static, pseudo-static and time-dependent dynamic analysis

The assessment of slope stability is tailored to the specific loading conditions expected over the life of the structure. This section reviews the analytical frameworks developed for static, pseudo-static, and full dynamic scenarios, tracing their evolution from simple, index-based approaches to comprehensive, physics-based simulations. Seismic stability analysis can be performed at several levels of complexity. True dynamic analysis entails applying actual or synthetic acceleration time histories to a slope to compute the response. This can capture amplification effects, multi-directional shaking, and dynamic stress redistribution.

2.3.3.1. Static analysis principles

Static analysis refers to evaluating slope stability under steady conditions—typically gravity loading and perhaps steady-state pore pressures, without any transient forces. The baseline assumptions are that loads (self-weight, any surface loads) are constant and that pore pressure distribution is stable (e.g., long-term drained conditions for a sustained water table, or undrained if looking at short-term end-of-construction in clay). In static analysis, one often aims to compute a factor of safety F—the ratio of available shear strength to the shear stress required for equilibrium along a potential failure surface. Classical approaches (LEM, FEM-SRM) described earlier primarily apply to static analysis. The goal is to ensure F is above a required minimum (commonly 1.3-1.5 for permanent slopes under static conditions, per many codes) (e.g., USACE, 2003).

Baseline assumptions include: no inertial forces, no rapid changes in pore pressure (i.e., fully drained for slow loading or fully undrained for rapid loading, but in a static sense we're not solving time-dependent changes). If undrained (total stress) analysis is used for clay slopes, it's assumed that the peak undrained shear strength is mobilized simultaneously (which can be unconservative if progressive failure occurs). Static analysis is often the starting point—if a slope can't pass static stability criteria, it clearly won't be stable under seismic or other transient conditions. For slopes around appurtenant hydraulic structures, static analysis includes cases like steady seepage (water forces in the slope). For example, an embankment by a spillway canal would consider the static water level and seepage forces in a static stability check. Modern static analyses can be 2D or 3D; 2D is conservative in many cases as discussed later (Duncan et al., 2014). Overall, static analysis forms the foundation, providing insight into likely slip surfaces and safety margins under normal conditions.

The baseline for any stability assessment is a static analysis, which evaluates the long-term stability of the slope under various operational loading conditions. These include the end-of-construction case, steady-state seepage under normal and flood reservoir levels, and conditions of rapid or slow drawdown of the reservoir (Irinyemi et al., 2021; USACE, 2003). These analyses are performed using the limit equilibrium or numerical methods described in the previous section to ensure the slope meets the required factors of safety for non-seismic conditions.

2.3.3.2. Pseudo-static analysis principles

Pseudo-static analysis represents a simplified approach to evaluate the stability of slopes under seismic loading conditions. Before computers enabled full dynamic simulations, geotechnical engineers developed a simplified method to account for seismic loading on slopes: the pseudo-static method. First explicitly applied to slopes by Terzaghi (1950), the method idealizes the complex, transient inertial forces from an earthquake into a single, constant, unidirectional static force applied at the centroid of the potential sliding mass. This pseudo-static force is calculated as the product of the weight of the mass (W) and a seismic coefficient (k). The horizontal force, $Fh=k_h \cdot W$, is the most critical component as it both increases the driving forces and decreases the resisting forces (Terzaghi, 1950). These forces are then included in a standard limit equilibrium analysis to calculate a pseudo-static Factor of Safety (FOS) (Kramer, 1996). The force distribution is exhibited in Figure 2.20.

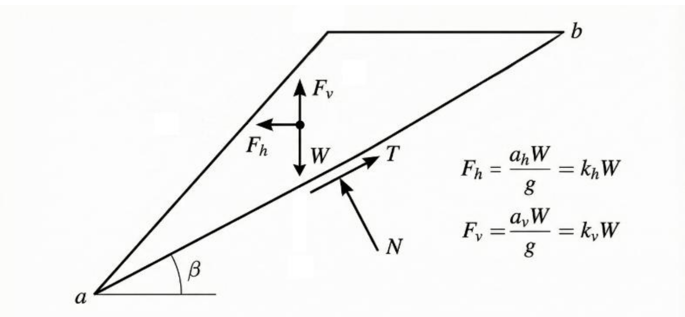

Figure 2.20. *Forces acting on a sliding soil mass during pseudo-static analysis (Kramer, 1996)*

The selection of an appropriate horizontal seismic coefficient, k_h, is the most critical and controversial aspect of the method. It is universally accepted that k_h should not be equal to the normalized peak ground acceleration (PGA), as the peak acceleration is transient and the slope material is not a rigid body (Seed, 1979; Kramer, 1996). The debate over its appropriate value has evolved over decades:

Early guidance

Terzaghi (1950) proposed values based on qualitative earthquake severity, e.g., k_h =0.1 for "severe" earthquakes and k_h=0.2 for "very severe" earthquakes, but noted that the representation of earthquake effects was "very inaccurate, to say the least".

Experience from dam engineering

Seed (1979) reviewed the performance of dams during earthquakes and noted that those designed with k_h values between 0.1 and 0.15 and a minimum FS of 1.15 generally performed well. This established the practice of using a k_h a fraction of PGA. Hynes-Griffin and Franklin (1984) concluded that if FOS $\geq$ 1.0 with k_h=0.15, the slope likely won't experience massive sliding.

Modern guidance

Researchers such as Kramer (1996) have summarized that k_h is often taken as a fraction (e.g., one-third to one-half) of the PGA, but have strongly emphasized that this is not a general rule and that the selection requires significant engineering judgment based on specific site conditions and performance requirements (Israr et al., 2022; Ranysakol, 2023; Wicaksono and Suhendra, 2023).

The primary advantage of this method is its simplicity. However, its simplicity also leads to significant limitations. The pseudo-static approach is now widely recognized as a crude simplification with severe limitations (Kramer, 1996). It provides no information on deformations and cannot directly capture phenomena like amplification, dynamic pore pressure buildup (liquefaction), or the directionality of shaking (Kramer, 1996). It does not account for the cyclic and transient nature of earthquake shaking, the dynamic response and amplification of ground motions through the dam or slope, the duration of shaking, or the progressive degradation of soil strength under cyclic loading (Fallah and Noferesti, 2015). Case studies by Seed (1979) showed earth dams that failed during earthquakes despite having pseudo-static FOS values well above 1.0, often due to strength degradation or liquefaction, a phenomenon to which the method is blind. The selection of

k_h should consider that the maximum acceleration acts for only a very short duration, and the pseudo-static approach is generally not suitable for soils that may lose significant strength during seismic shaking (Kramer, 1996). It remains in use as a screening tool: if $F_{ps}>1$ with a reasonably chosen k_h, the slope is likely stable with minor movements; if $F_{ps}<1$, one should expect movements and do more detailed analysis (Seed, 1979; Hynes-Griffin and Franklin, 1984; Kramer, 1996).

2.3.3.3. Newmark sliding block concept

The obvious shortcomings of the pseudo-static method (*Terzaghi, 1950; Kramer, 1996)* drove the development of dynamic analysis techniques that explicitly consider the time-varying nature of seismic loading and the dynamic response of the slope (Kramer, 1996; WSDOT, 2022). Figure 2.21 demonstrates the fundamental concept of the displacement of a rigid block on a rigid base under applied forces.

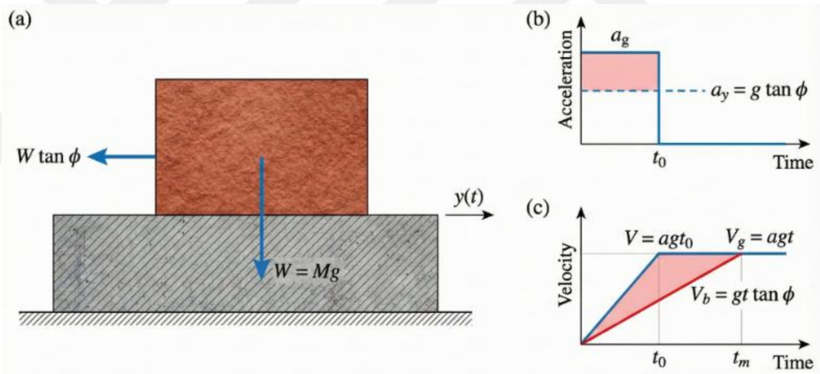

Figure 2.21. *Displacement of rigid block on rigid base: (a) block on moving base; (b) acceleration plot; (c) velocity plot (Newmark, 1965)*

Newmark's sliding block analysis, first proposed in 1965 (Newmark, 1965), stands as a foundational method for estimating permanent seismic displacements. This method shifted the paradigm from assessing stability based on a minimum factor of safety to assessing performance based on the magnitude of calculated permanent seismic displacement (Newmark, 1965). The principle is to model the potential sliding mass as a rigid block resting on an inclined plane with a resistance represented by its yield acceleration (a_y or k_y), which is the horizontal acceleration that brings the factor of safety to 1.0 (Kramer, 1996). Displacement initiates when the earthquake-induced inertial forces exceed the resisting forces. During an earthquake acceleration time history, whenever the downslope seismic acceleration exceeds this yield threshold, the block will begin to slide.

The permanent displacement is then calculated by double-integrating the portions of the earthquake acceleration time history that exceed this yield acceleration (Newmark, 1965). Figure 2.22 exemplifies the numerical integration of an earthquake acceleration time-history to calculate the resulting permanent displacement of the mass.

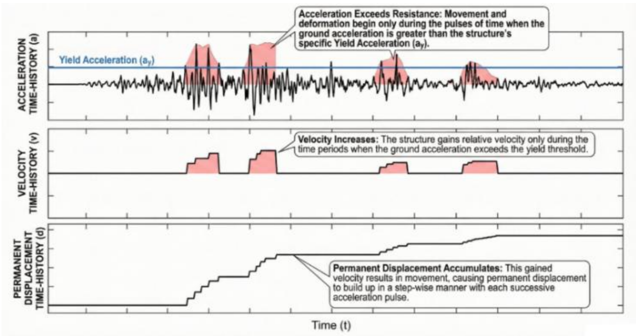

Figure 2.22. *Integration of earthquake acceleration time-history to determine permanent displacement (Newmark, 1965)*

Newmark's method thus "bridges the gap" between overly simplistic pseudo-static analyses and computationally intensive full dynamic stress-deformation analyses by providing an estimate of deformation (Makdisi and Seed, 1978; Kramer, 1996; Rathje and Saygili, 2008; Rathje and Bray, 1999, 2000). This method marked a philosophical shift from a strength-based FoS to a performance-based assessment of tolerable deformation. Its strengths are its focus on displacement and its use of the full acceleration time history, thus accounting for duration and frequency content. Weaknesses include the assumption of a rigid block and constant resistance; real slopes may weaken as they deform, so Newmark could underestimate displacement in such cases (Kramer, 1996). The basic model assumes rigid-plastic behavior and does not account for the dynamic response of a deformable slope or pore pressure generation. A study by Chen and Xia (2016) proposed a real-time dynamic Newmark method based on limit analysis, which updates the yield acceleration and other dynamic parameters as the sliding mass rotates and deforms (Kramer, 1996).

A key development in this area has been the demonstration that models incorporating not only Peak Ground Acceleration (PGA) but also Peak Ground Velocity (PGV) in their displacement predictions yield more accurate results. Rathje and Saygili (2008) showed that using PGA and PGV together significantly reduces the uncertainty in predictions compared to models based on PGA alone. This is because PGV provides indirect information about the frequency content of the earthquake motion, and displacement is sensitive to both acceleration amplitude and frequency content.

Researchers soon recognized that the rigid-body assumption was inappropriate for flexible earth slopes, which have a natural period and respond dynamically during an earthquake. This dynamic response affects the distribution of accelerations within the slope. Building on Newmark's (1965) sliding-block concept, Seed and Martin (1966) introduced dynamic seismic coefficients for deformable earth dams, and Makdisi and Seed (1978) later formalized the use of the time history of average acceleration of the potential sliding mass, $k_{av}(t)$, as input to a sliding-block displacement analysis (Newmark, 1965; Seed and Martin, 1966; Makdisi and Seed, 1978). This approach is known as a "decoupled" analysis, because the dynamic response calculation and the sliding displacement calculation are done in separate steps (Makdisi and Seed, 1978). Later, "coupled" analyses were developed that compute the dynamic response and sliding simultaneously, accounting for the fact that when sliding occurs, the stresses at the slip surface cannot exceed the soil strength (Rathje and Bray, 1999; 2000). Rathje and Bray (2000) concluded that while the coupled analysis is more rigorous, for most engineering projects the decoupled approach provides an acceptable and often conservative estimate. As with rigid block analyses, surrogate models have been developed for flexible blocks. Rathje and Antonakos (2011) presented a unified model that incorporates both the flexibility of the slope (through its natural period Ts) and the characteristics of the earthquake motion (PGA and PGV).

2.3.3.4. Fully dynamic (time-history) analysis

This is the most rigorous method for seismic slope stability assessment (Kramer, 1996; WSDOT, 2022). It involves solving the full equations of motion for a finite element or finite difference model of the slope subjected to an earthquake acceleration time-history applied at the model's base (Gou et al., 2012). Dynamic slope stability analysis involves a more rigorous approach to seismic loading, considering the time-dependent nature of earthquake forces and the dynamic response of the soil-structure system. Dynamic analysis simulates the response of slopes to seismic loading, capturing complex behaviors such as nonlinear soil response and pore pressure generation (Griffiths and Lane, 1999). These analyses typically employ numerical methods such as FEM or FDM to simulate the propagation of seismic waves through the slope, the generation and dissipation of pore pressures, and the resulting deformations (Gou et al., 2012; Irinyemi et al., 2021). Common numerical modeling approaches for this analysis include Finite Element Method (FEM) and Finite Difference Method (FDM) techniques, which allow for the evaluation of slope stability under varying seismic conditions (WSDOT, 2022).

In a full dynamic analysis, an actual earthquake acceleration time history, selected or generated to be representative of the site's seismic hazard, is applied to the base of the numerical model (Israr et al., 2022; Irinyemi et al., 2021). The software then solves the equations of motion over time, simulating the propagation of seismic waves through the foundation and the dam structure and capturing the resulting dynamic response. The power of this approach lies in its ability to capture a wide range of complex, interacting phenomena critical to seismic performance: seismic wave propagation and amplification effects within the slope; non-linear soil stress-strain behavior; soil-structure interaction; and, most importantly for slopes near hydraulic structures, the generation, redistribution, and dissipation of excess pore water pressures when performed as a coupled, effective stress analysis (Kramer, 1996).

This approach provides a wealth of performance data, including permanent deformations, dynamic stresses, and the potential for liquefaction. It is the preferred method for final design and safety assessment of high-hazard dams (FERC, 2017; WSDOT, 2022). Case studies on dams like Kockopru and Mohmand have utilized full dynamic analysis to assess performance under design earthquake scenarios (Babar et al., 2021). While these analyses require more computational and characterization effort than sliding block methods, they are becoming increasingly common in engineering practice. Recently, surrogate models based on the results of these advanced analyses have also begun to be developed (e.g., Cho and Rathje, 2022). These models are preferred as they are based on the fewest simplifying assumptions for predicting slope performance (Rathje, 2025).

Dynamic analysis of slopes under seismic loading requires meticulous treatment of the model boundaries and energy dissipation mechanisms to prevent artificial wave reflections and unrealistic resonance that can invalidate the simulation.

Absorbing boundaries

In a finite element model of a slope, the mesh represents a truncated portion of a semi-infinite geological medium. Standard "fixed" boundaries reflect outgoing seismic waves back into the model, trapping energy and artificially amplifying the dynamic response. To mimic the radiation of energy into the infinite far field, "absorbing" or "quiet" boundaries are required.

- *Lysmer-Kuhlemeyer (viscous) boundaries:* This is the standard approach in rock mechanics FEM. It involves placing dashpots (viscous dampers) at the normal and tangential directions of the boundary nodes (Kouroussis et al., 2011). The dashpot coefficients are defined as $C_n = \rho V_p A$ and $C_s = \rho V_s A$, where ρ is the rock density, V_p and V_s are the P-wave and S-wave velocities, and A is the contributory area of the node. These boundaries absorb the energy of body waves impinging on the boundary at normal incidence, simulating radiation damping (Zhao et al., 2024). To prevent spurious wave reflections from the artificial boundaries of the finite element mesh back into the model domain, viscous absorbent boundaries are routinely employed. Following the method proposed by Lysmer and Kuhlemeyer (1969), normal and shear dashpots are applied at the model boundaries. These dashpots absorb the energy of outgoing waves, effectively simulating the radiation damping of an infinite medium. This boundary condition is mandatory for performing accurate time-history analyses, ensuring that the computed dynamic response is strictly a function of the input motion and the site response, free from "box effect" artifacts.
- *Free-field boundaries:* For earthquake simulation, simple viscous boundaries are insufficient because they would also absorb the input seismic motion. Instead, "free-field" columns are modeled at the lateral boundaries. These columns simulate the 1D propagation of shear waves from the base to the surface in the far field (infinite half-space) and apply the resulting motions to the main grid boundaries via the viscous dashpots. This technique allows the model to enforce the correct free-field motion while still absorbing scattered waves generated by the slope topography or structure (Itasca, 2024a; Lysmer and Kuhlemeyer, 1969).

Damping mechanisms

Real geological materials dissipate energy through internal friction and plasticity. However, numerical models often require additional algorithmic damping to ensure stability and account for small-strain dissipation not captured by the constitutive model (especially in linear elastic phases).

- *Rayleigh damping:* This is the most common viscous damping formulation in time-domain FEM. The damping matrix [C] is constructed as a linear combination of the mass [M] and stiffness [K] matrices: [C] = α [M] + β [K] (Itasca, 2024b; Chiaradonna, 2022). Mass-proportional (α) damps low-frequency vibrations (e.g., sloshing, rigid body modes) and represents friction against the external environment. Stiffness-proportional (β) damps high-frequency noise and oscillations, which is physically analogous to internal material viscosity. A critical pitfall of Rayleigh damping is its frequency dependence. The damping ratio ξ varies with frequency ω. Engineers must carefully select a "target frequency" (usually the fundamental frequency of the slope) to ensure the correct damping ratio (e.g., 5%) is applied to the dominant modes. Outside this range, the model may be under-damped (at low frequencies) or over-damped (at high frequencies), potentially leading to inaccurate peak accelerations or suppressing higher-mode failure mechanisms (Zhao et al., 2024). In addition to the hysteretic damping provided by the constitutive models, Rayleigh damping is introduced to simulate energy dissipation at very small strains and to dampen high-frequency numerical noise. The coefficients α and β are calibrated to provide a target damping ratio centered around the fundamental natural frequencies of the slope-structure system (Idriss et al., 2019). This ensures that the model correctly dissipates energy across the relevant frequency bandwidth of the seismic input.
- *Hysteretic damping:* For large-strain dynamic problems involving plasticity, hysteretic damping (energy loss through stress-strain hysteresis loops) is preferred. It is frequency-independent and naturally arises from the nonlinear constitutive behavior of the rock mass, providing a more realistic representation of energy dissipation during strong ground motion (Itasca, 2024b).

The specific features of various software packages, including their supported constitutive models and numerical solvers, are evaluated in Table 2.10.

Table 2.10. *Comparison of commercially available software capabilities for static and dynamic slope stability analysis*

Software Name	Numerical Method	Dynamic Capability	Pore-pressure Coupling	Constitutive Models Supported
Rocscience Slide2/3 (http-15[21])	Limit Equilibrium (LEM)	Pseudo-static; Newmark displacement (rigid/coupled/de-coupled); critical acceleration (K_c).	Uncoupled; one-way seepage coupling (FEA to LEM); \bar{B} parameter for excess PWP; steady/transient states.	Mohr-Coulomb (MC), Barton-Bandis (BB), generalized Hoek-Brown (GHB), SHANSEP, anisotropic, and power curve models.
Rocscience RS2 (Phase2)/ RS3 (http-16[22])	Finite Element (FEM)	Full dynamic time-domain and SSR-dynamic stability; advanced liquefaction assessment (Finn, PM4Sand, NorSand).	Fully coupled static consolidation; partly coupled dynamic effective stress via generation models.	Hardening Soil (HS), (Modified) Cam-Clay (CC/MCC), NorSand, bounding surface models (BBM, Dafalias-Manzari), MC, and GHB.
Bentley PLAXIS 2D (http-17[23])/3D (http-18[24])	Finite Element (FEM)	Full dynamic time-history and vibration analysis; advanced liquefaction modeling (UBC3D-PLM, PM4Sand).	Fully coupled flow-deformation, consolidation, and unsaturated transient analyses (SWCC).	HS-Small, Soft Soil Creep, advanced liquefaction models (UBC3D-PLM, PM4Silt), NorSand, MCC, and UDSM.
Itasca FLAC (http-19[25])/ FLAC3D (http-20[26])	Finite Difference (FDM)	Full non-linear dynamic time-domain; liquefaction; utilizes absorbing and free-field boundaries.	Fully coupled hydro-mechanical; two-phase flow and thermal coupling; volumetric strain-induced PWP.	26+ built-in models including PM4Sand, NorSand, IMASS, Ubiquitous-joint, Cysoil, and user-defined UBCSAND.
Seequent SLOPE/W (http-21[27])	LEM / FEM	Pseudo-static; Newmark integration (via SLAMMER); utilizes QUAKE/W for dynamic stresses.	Uncoupled and one-way coupled hydro-mechanical (SEEP/W integration); supports saturated/unsaturated flow.	MC, HB, unsaturated shear strength (φ^b), SHANSEP; advanced models via SIGMA/W integration.

[21]http-15: https://www.rocscience.com/help/slide2/overview/technical-specifications (accessed July 16, 2025).

[22]http-16:https://www.rocscience.com/help/rs2/overview/technical-specifications (accessed July 16, 2025).

[23]http-17:https://www.seequent.com/products-solutions/plaxis-2d/ (accessed July 16, 2025).

[24]http-18:https://www.seequent.com/products-solutions/plaxis-3d/ (accessed July 16, 2025).

[25]http-19:https://www.itascainternational.com/software/flac-constitutive-models (accessed July 16, 2025).

[26]http-20: https://docs.itascasoftware.com/itasca900/flac3d/docproject/source/modeling/introduction/generalfeatures.html (accessed July 16, 2025).

[27]http-21:https://www.seequent.com/products-solutions/geostudio-2d/ (accessed July 16, 2025).

Table 2.10. (Continued) *Comparison of commercially available software capabilities for static and dynamic slope stability analysis*

Software Name	Numerical Method	Dynamic Capability	Pore-pressure Coupling	Constitutive Models Supported
Fine Software Geo5 (http-22[28]/ http-23[29])	LEM / FEM	Pseudo-static and dynamic earthquake modules; modal analysis and accelerogram generation.	Uncoupled (PWP isolines) or coupled consolidation and transient water flow integrations.	HS, Soft Soil, hypoplastic clay, HB, CC/MCC, MC, and Drucker-Prager.
Itasca 3DEC (http-24[30])/ UDEC (http-25[31])	Distinct Element Method (DEM)	Full dynamic time-history analyzing block interactions, wave propagation, and rockfall.	Fully coupled hydro-mechanical analysis for both intact matrix and jointed networks.	Continuously Yielding joints, BB, Coulomb slip, MC, Power Law Creep, IMASS, and C++ User-Defined Models.
Ensoft UTEXAS4 (http-26[32])	Limit Equilibrium (LEM)	Strictly pseudo-static (horizontal seismic accelerations); lacks internal Newmark integration.	Uncoupled; relies on piezometric lines, gridded data, or pore pressure ratio (r_u).	Linear/curved MC and undrained strength profiles (s_u = c).

All data compiled from official software documentation and user manuals. s_u, undrained shear strength; φ^b, angle of shear strength increase with suction; r_u, pore-pressure ratio; PWP, pore water pressure; SSR, shear strength reduction.

2.3.3.5. Comparison of approaches for hydraulic structure slopes

While pseudo-static analysis is straightforward, it does not account for the transient nature of earthquake loading, the dynamic response of the slope, or pore pressure generation (Kramer, 1996; Fallah and Noferesti, 2015; Bolla and Paronuzzi, 2021). The Newmark method provides a more realistic estimate of seismic-induced deformations than a simple FOS. Fully dynamic analysis is the most rigorous, capturing complex phenomena like liquefaction, but is also the most computationally intensive. The choice of method depends on the criticality of the structure, the seismic environment, and the soil conditions (WSDOT, 2022). For soils susceptible to strength loss, a pseudo-static

[28]http-22:https://www.finesoftware.eu/geotechnical-software/slope-stability/ (accessed July 16, 2025).

[29]http-23:https://www.finesoftware.eu/geotechnical-software/fem-earthquake/ (accessed July 16, 2025).

[30]http-24: https://docs.itascacg.com/flac3d700/3dec/docproject/source/theory/3dectheory/theory_background.html (accessed July 16, 2025).

[31]http-25:https://www.itascacg.com/software/udec (accessed July 16, 2025).

[32]http-26:https://www.ensoftinc.com/products/utexas/ (accessed July 16, 2025).

approach can be unconservative (Bray and Travasarou, 2007) and a post-earthquake stability analysis using reduced shear strength parameters or a full dynamic analysis might be more appropriate. For high-consequence slopes (like those abutting spillways or dam abutments), current best practice is to perform at least a Newmark analysis if not a full dynamic analysis, especially if FOS from pseudo-static analysis is marginal (Bray and Travasarou, 2007; WSDOT, 2022; FERC, 2017). Figure 2.23 depicts the structured hierarchy of seismic slope stability analysis methods, ranging from simplified procedures to complex numerical simulations.

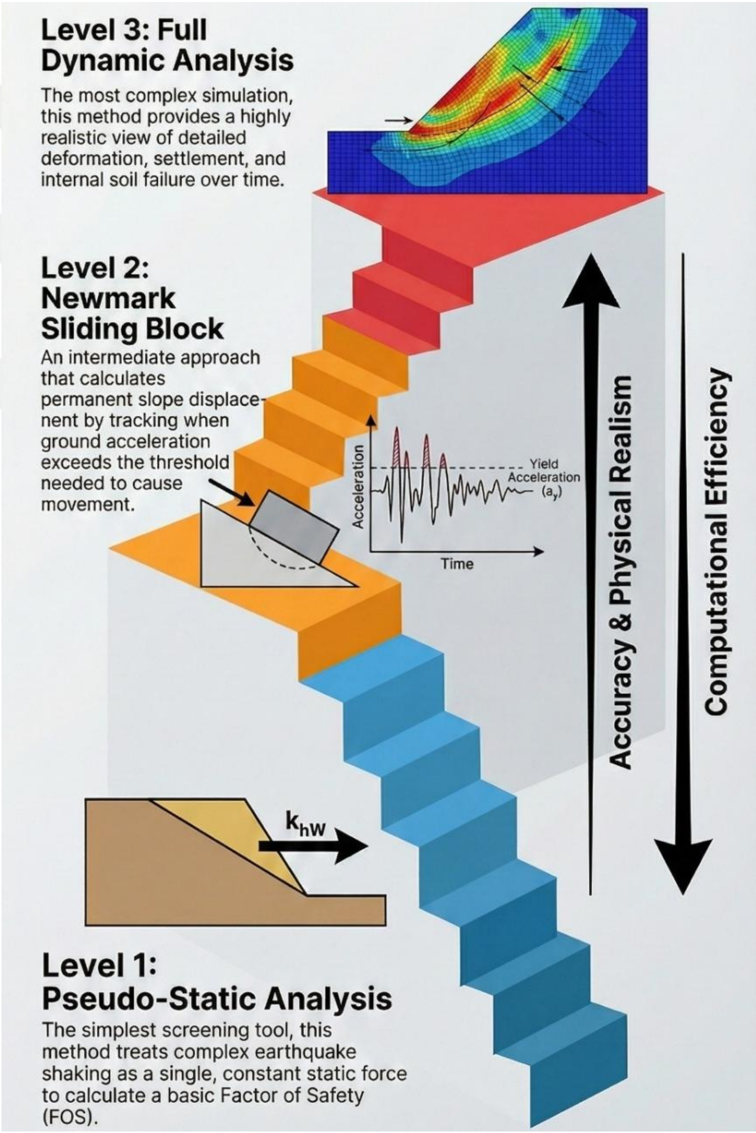

Figure 2.23. *Hierarchy of seismic slope stability analysis methods*

Pseudo-dynamic analysis represents an intermediate step between the pseudo-static and full dynamic approaches. It improves upon the pseudo-static method by considering the time-dependent and spatial variation of seismic forces and the time-dependent behavior of the structure and its foundation (http-27[33]). The analysis simulates the dynamic response by dividing the seismic motion into a series of small time steps and incrementally computing the forces and displacements, accounting for the structure's stiffness, mass, and damping properties (http-27[34]). It can account for factors like wave propagation and dynamic amplification through the slope (Steedman and Zeng, 1990).

A key advantage is its ability to incorporate the interaction between the dam and the foundation soil more realistically than a simple static force application (http-27[35]). However, while conceptually important as a bridge between simpler and more complex methods, the provided research material lacks specific documented case studies of the pseudo-dynamic method being applied to the stability of spillway excavation slopes. This absence suggests that in practice, engineers often proceed from the simpler pseudo-static method directly to full dynamic analysis for critical assessments, indicating that the pseudo-dynamic approach has not achieved widespread adoption in this specific application area. Table 2.11 provides a comprehensive comparison of different seismic slope stability analysis methods, highlighting their underlying assumptions and computational requirements.

[33]http-27:https://damtoolbox.org/wiki/Pseudo-Dynamic_Analysis (accessed September 9, 2025).
[34](http-27).
[35](http-27).

Table 2.11. *Comparison of seismic slope stability analysis methods*

Method & Source(s)	Principle & Primary Output(s)	Key Inputs	Time & Deformation Modeling	Advantages (+) & Limitations (-)	Typical Application
Pseudo-Static (Bolla and Paronuzzi, 2021; Fallah and Noferesti, 2015)	Models the earthquake as a permanent static force to calculate the Factor of Safety (FS).	Strength (c, φ), geometry, seismic coefficients (k_h, k_v).	Strictly static; stability is inferred from FS without modeling internal deformation.	(+) Simple and fast. (-) Ignores dynamic shaking and amplification.	Preliminary designs and low-hazard slope assessments.
Newmark Sliding Block (Newmark, 1965; Fallah and Noferesti, 2015)	Calculates cumulative permanent displacement of a rigid block on an inclined plane.	Yield acceleration (a_y), acceleration time history.	Dynamic integration; yields mass displacement but ignores internal slope deformations.	(+) More informative than FS alone. (-) Assumes rigid block behavior.	Estimating deformations for well-defined slip surfaces.
Pseudo-Dynamic (http-27[36]); Steedman and Zeng, 1990)	Simulates dynamic response to incrementally compute time-dependent forces and displacements.	Time history, stiffness, mass, and damping.	Incremental static steps; deformations are calculated incrementally over time.	(+) Captures time-dependency. (-) Computationally complex for standard practice.	Intermediate advanced analyses bridging static and full dynamic.
Full Dynamic Time-History (Kramer, 1996; Israr et al., 2022; Irinyemi et al., 2021; Bolla and Paronuzzi, 2021; Finn, 1988)	Solves equations of motion for a continuum model yielding time histories of deformations and stresses.	Acceleration histories, dynamic moduli, damping, advanced constitutive models.	Fully dynamic time domain; explicitly models both internal and permanent deformations.	(+) Most rigorous and realistic method. (-) Highly computationally intensive.	Final designs, liquefaction assessments, and forensic research.

[36](http-27).

2.3.4. Selection and scaling of seismic inputs

The accurate prediction of seismic performance for critical infrastructure, such as dams and associated appurtenant structures (spillway cut slopes, tunnel portals), relies fundamentally on the selection and conditioning of appropriate earthquake ground motion time histories (NEHRP Consultants Joint Venture, 2011). This process serves as the vital link between Probabilistic Seismic Hazard Analysis (PSHA) and rigorous Performance-Based Earthquake Engineering (PBEE) using nonlinear Response History Analysis (RHA) (Dhakal et al., 2007; Cornell, 1968; McGuire, 2004; Baker, 2013). This section provides a detailed, methodology-driven framework for establishing hazard-consistent seismic inputs, emphasizing techniques that account for the complex, cumulative failure mechanisms typical of large geotechnical systems.

2.3.4.1. Definition of the target seismic input spectrum

The initial phase in selecting and scaling ground motions requires establishing a precise target spectral acceleration (S_a) that is consistent with the site-specific seismic hazard level derived from PSHA (Lee et al., 2025).

Probabilistic seismic hazard analysis (PSHA) and the uniform hazard spectrum (UHS)

PSHA is the standard framework for quantifying seismic risk, integrating information on seismic sources, recurrence intervals, and ground motion prediction models (GMPMs) to determine the annual frequency of exceedance for various ground motion levels (FERC, 2014; Lee et al., 2025; Bazzurro and Cornell, 1999). The resulting ground motion level associated with a specified return period (e.g., the Maximum Design Earthquake, MDE) is often expressed as the Uniform Hazard Spectrum (UHS) (Lee et al., 2025). The UHS plots S_a values for different periods (T) where each spectral ordinate corresponds to the same probability of exceedance.

A key limitation of the UHS stems from its probabilistic derivation, which aggregates hazard contributions from numerous seismic scenarios, potentially including large, distant earthquakes and smaller, nearby earthquakes (Somerville et al., 2016). Consequently, the UHS tends to be "broadband," exhibiting unrealistically high spectral amplitudes across an unrealistically wide range of periods. This broadband characteristic means the UHS does not represent the response spectrum of any single, physically realistic seismic event (Somerville et al., 2016). Using the UHS directly as the target spectrum for ground motion selection in RHA, particularly for nonlinear analysis, can lead to overly conservative and inaccurate predictions, as the structure is forced to respond simultaneously to energy peaks that would not occur together in nature. This inconsistency compromises the fundamental objective of RHA: accurately modeling structural performance under a credible extreme loading event.

Deaggregation of seismic hazard and causal earthquake scenarios (M, R, and ε)

To transition from the statistical construct of the UHS to a realistic physical input, the PSHA results must undergo deaggregation. Deaggregation identifies the mean values of the dominant causal earthquake parameters—Moment Magnitude ($\bar{M}$), Source-to-Site Distance ($\bar{R}$), and the number of logarithmic standard deviations ($\bar{\varepsilon}$)—that contribute most significantly to the hazard at the site for the control period (T*) (Baker, 2011; Lin et al., 2013; Bazzurro and Cornell, 1999).

The ε value, or Epsilon, is particularly critical. It quantifies how much the observed or target spectral acceleration at T* deviates from the median S_a predicted by a GMPM for the specific $\bar{M}$ and $\bar{R}$ (Lin et al., 2013). A large, positive ε signifies a ground motion with an unusually rich spectral content at T* relative to the average motions for that M and R scenario. The deaggregation process provides the essential parameters necessary to define a hazard-consistent target response spectrum that closely resembles the spectral characteristics of the dominating scenario earthquake (Baker, 2011). Figure 2.24 explores the results of a PSHA deaggregation plot, identifying the relative contributions of earthquake magnitude and source-to-site distance to the total seismic hazard.

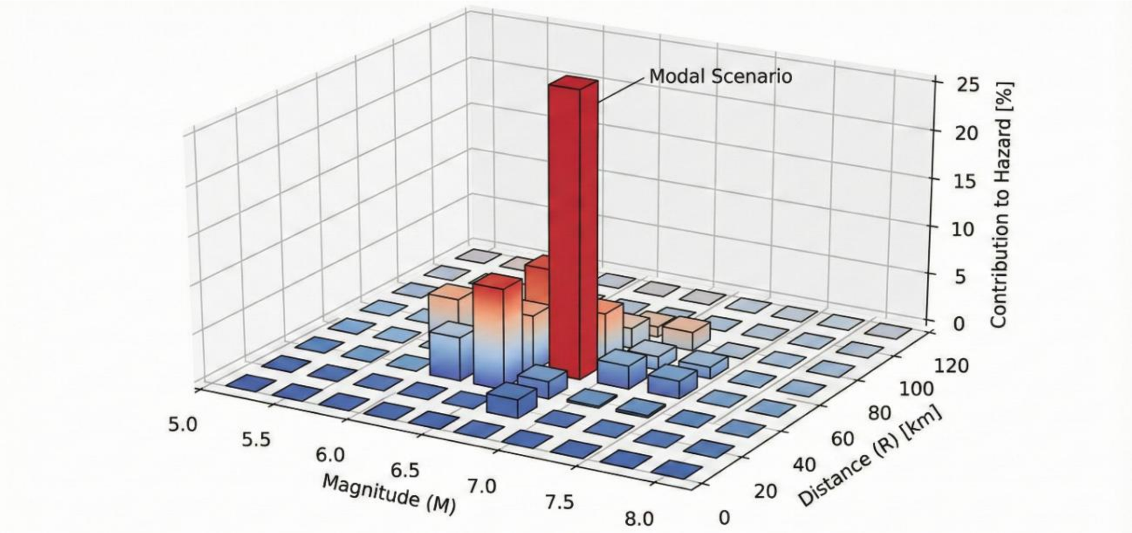

Figure 2.24. *Example of a PSHA deaggregation plot showing contributions of magnitude and distance to seismic hazard (Baker, 2008)*

The conditional mean spectrum (CMS) as a hazard-consistent target

The Conditional Mean Spectrum (CMS) resolves the limitations of the UHS by defining the expected (mean) response spectrum conditioned on the occurrence of the target spectral acceleration $S_a(T^*)$ at a selected period of interest (Baker, 2011; Baker and Cornell, 2006). The period T* is typically chosen as the fundamental period of the structure being analyzed.

The CMS calculation utilizes the deaggregated $\bar{M}$, $\bar{R}$, and $\bar{\varepsilon}(T^*)$ as inputs (Lin et al., 2013). The procedure first establishes the mean and standard deviation of the response spectrum based on $\bar{M}$ and $\bar{R}$ (Baker, 2011). Then, the correlation of the spectral residuals (Epsilon) across different periods is used to adjust the spectral ordinates at periods $T_i \neq T^*$ (Baker, 2011). This calculation produces a spectrum that is consistent with the level of hazard defined by PSHA, specifically at T*, but is significantly less broadband than the UHS, resulting in a more realistic spectral shape representative of a single, physical event (Somerville et al., 2016). This methodology ensures consistency between the PSHA results and the subsequent selection of ground motion records (Baker, 2011). Figure 2.25 contrasts the characteristics of the Uniform Hazard Spectrum (UHS) and the Conditional Mean Spectrum (CMS) for seismic ground motion characterization.

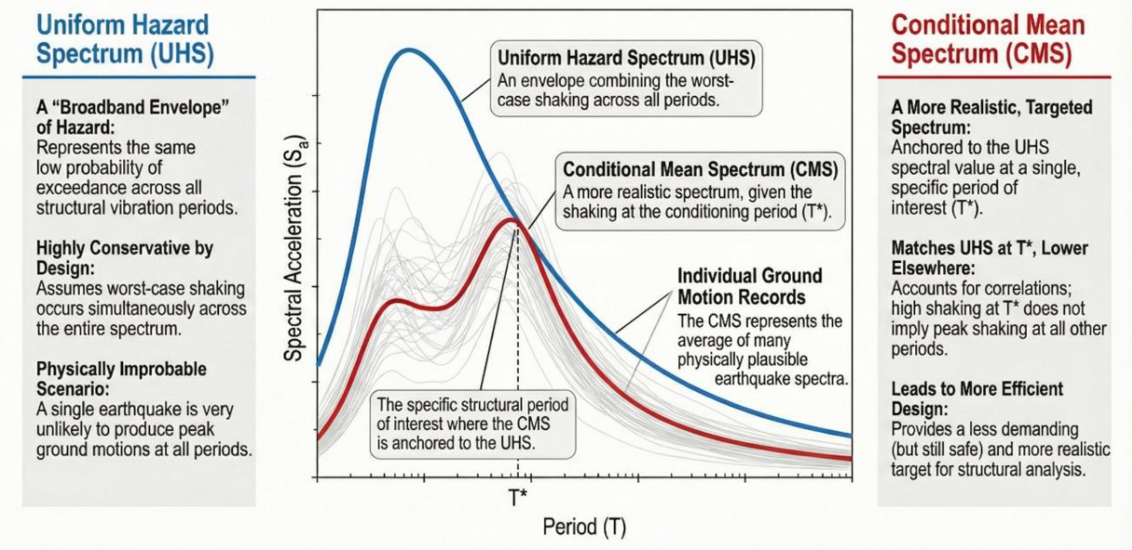

Figure 2.25. *Comparison of uniform hazard spectrum (UHS) and conditional mean spectrum (CMS) (Baker, 2011)*

Alternative conditional spectra approaches (CS and GCIM)

While the CMS provides the mean target spectrum, structural fragility assessment often requires incorporating the inherent randomness (aleatory variability) of ground motion. The Conditional Spectrum (CS), and its extensions, were developed to provide not only the mean response spectrum but also the proper dispersion characteristics, addressing a recognized deficiency in the original CMS definition (Kwong and Chopra, 2015).

A further generalization is the Generalized Conditional Intensity Measure (GCIM) approach (Bradley, 2010; Kwong and Chopra, 2015). The GCIM conditions the target spectrum not merely on a single spectral acceleration value, but on a vector of intensity measures (IMs) (Bradley, 2014). This allows the analyst to simultaneously constrain the ground motion selection criteria based on spectral acceleration, duration metrics, and energy metrics. For structures like earth dams and steep cut slopes, where failure is often governed by cumulative damage processes rather than peak inertial force alone, a holistic approach that ensures consistency across multiple IMs—such as S_a and Arias Intensity (I_A)—is theoretically the most rigorous method for developing seismic input (Bradley, 2010; Kwong and Chopra, 2015).

2.3.4.2. Ground motion record selection methodologies

The process of identifying suitable time histories ("seed motions") must prioritize the physical characteristics of the target earthquake scenario.

Selection criteria based on causal parameters (M, R, and Site Classification)

Initial selection typically involves filtering existing databases of recorded ground motions based on the deaggregated parameters: magnitude M, distance R, and site classification, often characterized by the time-averaged shear wave velocity in the top 30 meters (V_{s30}) (Haselton et al., 2010). For instance, a selection ensemble might target events with M ≥ 6.5 at closest fault distances $R_{cl} \leq 12$ km, corresponding to specific NEHRP site classes (C and D) (Haselton et al., 2010).

However, historical investigations comparing different ground motion selection approaches have consistently demonstrated that matching the target spectral shape is a more significant parameter for predicting structural response than matching the causal parameters M and R (Kwong and Chopra, 2015). While M and R define the overall hazard environment, the specific spectral shape determines the dynamic energy input to the structure. Site conditions also influence spectral shape; for example, spectral shapes recorded at rock sites tend to have lower predominant periods compared to those at soft-soil sites (Haselton et al., 2010). The selection process must therefore transition quickly from simple causal filtering to spectral compatibility verification, using the CMS as the primary selection target.

Incorporating non-spectral intensity measures (IMs) in selection

For nonlinear RHA, particularly for geotechnical structures, intensity measures beyond spectral acceleration are crucial for capturing failure mechanisms related to cumulative damage, fatigue, and energy absorption (Spiga et al., 2022).

- Duration metrics: The duration of strong shaking significantly influences structural response (Spiga et al., 2022; Dobry et al., 1978). Metrics such as significant duration or bracketed duration measure the time interval during which the majority of seismic energy is released. Ground motions, such as those characterized by near-fault effects, often contain distinct velocity pulses and have uniquely short, high-intensity durations (Haselton et al., 2010; NEHRP Consultants Joint Venture, 2011). Selecting records with duration characteristics consistent with the target $\bar{M}$ and $\bar{R}$ scenario is necessary to avoid underestimating the cyclic demand capacity of the structure (Foschaar et al., 2012).
- Energy metrics: Energy-based IMs quantify the total seismic energy input into the system. Metrics like Arias Intensity (I_A) and Cumulative Absolute Velocity

(CAV) are computed directly from the acceleration time history (Foschaar et al., 2012; Spiga et al., 2022; Arias, 1970; Campbell and Bozorgnia, 2010).

The strong correlation between energy metrics and cumulative damage demands renders them indispensable for geotechnical analyses. Specifically, the permanent displacement of slopes and earth dams is commonly estimated using Newmark's sliding block analysis (Chen et al., 2024). Research confirms a very strong non-linear correlation between calculated Newmark displacement and Arias Intensity (Jibson, 2007; Liu et al., 2025; Li et al., 2021; Hsieh and Lee, 2011; Yuan et al., 2016). The fundamental relationship between Arias Intensity (I_a) and Newmark sliding block displacement is illustrated in Figure 2.26.

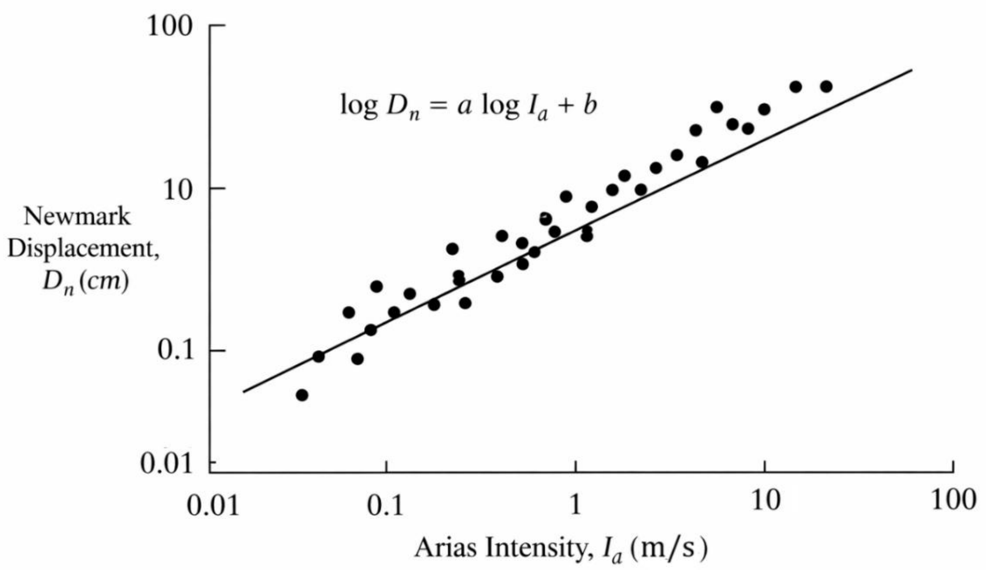

Figure 2.26. *Correlation between Arias intensity and Newmark sliding block displacement (Jibson, 2007)*

This physical link means that for geotechnical dynamic analyses, I_A is elevated from a secondary check to a primary selection constraint. A robust selection methodology, therefore, must ensure that the chosen ground motion ensemble, even after being scaled to match the S_a target (CMS), exhibits I_A and duration values that are representative of the target seismic hazard scenario. If selection were based purely on S_a, the resulting I_A could be underrepresented, leading to an unconservative estimate of permanent deformation.

Utilizing simulated and three-component records

When recorded ground motions suitable for a specific hazard scenario are limited, analysts may incorporate simulated strong-motion records (Cao et al., 2019; NEHRP Consultants Joint Venture, 2011). While simulation techniques (e.g., hybrid methods) can generate spectra-compatible motions, they carry inherent drawbacks. Artificial records may exhibit an unnaturally large number of strong motion cycles and often possess increased total energy content compared to real ground motions, potentially overestimating nonlinear demands (Cao et al., 2019). This is frequently linked to unrealistic phasing and peaks introduced during the generation process (Cao et al., 2019).

Furthermore, for large structures like dams, the seismic input must be defined in three dimensions. The RHA requires the simultaneous application of two horizontal components and one vertical component (NEHRP Consultants Joint Venture, 2011). For structures sensitive to vertical acceleration, such as high arch dams, the selected record set must ensure that the vertical component is hazard-consistent, typically maintaining an appropriate vertical-to-horizontal (V/H) spectral ratio throughout the selection and scaling procedure (Liang et al., 2023).

2.3.4.3. Strong motion processing

Raw strong motion records invariably contain non-physical noise and instrumental drift that require rigorous signal processing before use in dynamic numerical modeling. Standard practice involves baseline correction to eliminate low-frequency errors which, if left uncorrected, integrate into unrealistic drifts in velocity and displacement time histories (Boore, 2005). Furthermore, applying acausal bandpass filters (e.g., Butterworth, 1930) —a core capability of specialized processing suites like SeismoSignal— is necessary to remove high-frequency aliasing. These processing steps are theoretically fundamental to ensuring that the input motion represents a physically admissible displacement history, a prerequisite for the stability of any time-domain integration scheme (Kramer, 1996).

2.3.4.4. Techniques for scaling ground motion time histories

Once appropriate seed motions are identified, they must be adjusted to match the intensity level of the target spectrum (CMS or UHS) across the critical period range relevant to the structure (Naeim et al., 2004). Two high-level approaches are generally accepted for developing acceleration time series to fit a design response spectrum: linear amplitude scaling and spectrum matching (NEHRP Consultants Joint Venture, 2011).

Simple amplitude scaling (linear scaling)

Simple amplitude scaling involves multiplying the entire acceleration time history by a constant scaling factor (SF). This technique offers the advantage of preserving the inherent time-domain characteristics of the original record, including the relative frequency content, duration, and the complex phasing structure (Cao et al., 2019).

However, because real earthquake records possess unique spectral characteristics, simple scaling rarely achieves a close fit to the target spectrum across the entire period range of interest. This mismatch introduces significant variability in the structural response results, known as response dispersion (NEHRP Consultants Joint Venture, 2011). To manage this uncertainty and achieve a stable mean response determination, simple scaling typically requires a larger ensemble of records than spectrum matching (NEHRP Consultants Joint Venture, 2011).

Spectrum matching techniques (frequency and time domain adjustment)

Spectrum matching adjusts the seed ground motion through frequency or time domain modifications to achieve a near-perfect match with the target spectrum over a user-specified period range (NEHRP Consultants Joint Venture, 2011). Comprehensive guidance exists for implementing this technique, often specifying the target period range based on the structure's dynamic characteristics (e.g., from $0.2T_1$ to $1.5T_1$) (NEHRP Consultants Joint Venture, 2011).

The primary advantage of spectrum matching is its ability to produce time histories whose response spectra closely align with the design spectrum, thereby minimizing the response variability in the dynamic analysis results (Huang et al., 2011; NEHRP Consultants Joint Venture, 2011; Dávalos and Miranda, 2019). This can increase confidence in the determination of the mean response, though the influence of time history characteristics other than the elastic response spectrum necessitates careful application (NEHRP Consultants Joint Venture, 2011). To ensure accuracy, the aggregate fit between the spectra of the selected records and the design spectrum should be calculated using a sufficient density of spectral ordinates, often recommended to be around 100 points per logarithmic cycle of period or frequency, to prevent undetected spectral peaks and valleys between computation periods (NEHRP Consultants Joint Venture, 2011).

Spectral matching is a pivotal procedure in seismic hazard analysis, particularly when site-specific time histories are required. Among various techniques, the wavelet-based algorithm proposed by Abrahamson (1992) and refined by Hancock et al. (2006) —which constitutes the core computational engine of specialized software such as SeismoMatch— is widely recognized for its efficacy. Unlike simple amplitude scaling, which may fail to capture the spectral shape across the entire period range, wavelet-based matching adjusts the time history in the time-frequency domain. This method allows the response spectrum to closely match a target spectrum while preserving the non-stationary characteristics (e.g., duration and phase content) of the reference motion (Al Atik and Abrahamson, 2010). Such precision is essential for preventing the loss of realistic ground motion features during dynamic analysis. Figure 2.27 reveals the spectral matching effect.

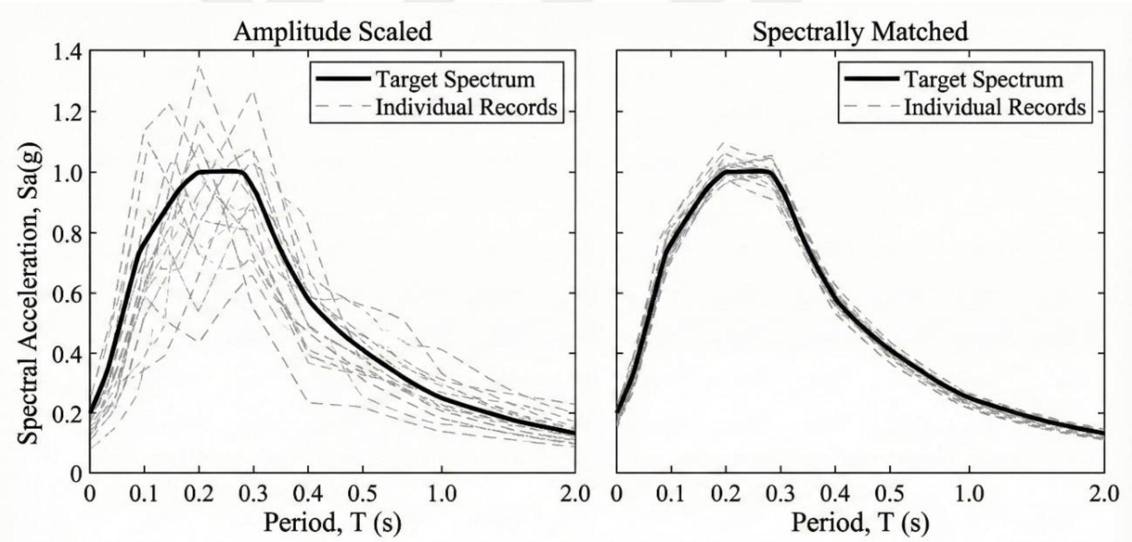

Figure 2.27. *Comparison of response spectra for amplitude scaled vs. spectrally matched ground motions (NEHRP, 2011)*

Guidance on the required number of records for dynamic analysis

Regulatory guidelines and professional standards specify minimum record counts to ensure a statistically robust determination of structural response, particularly in nonlinear analysis where dispersion can be substantial (NEHRP Consultants Joint Venture, 2011).

- For linear dynamic analysis, a minimum of three time-history records should be used (NEHRP Consultants Joint Venture, 2011).

- For nonlinear dynamic analysis (RHA), at least five time-history records are required (NEHRP Consultants Joint Venture, 2011).

If the analysis reveals that the structural response is highly sensitive to the characteristics of the selected records, or if a high level of confidence in the mean response is required for high-risk structures like dams, the number of time histories must be increased (NEHRP Consultants Joint Venture, 2011). While spectrum matching often reduces dispersion, it is generally recommended not to relax the criteria for the number of records even when using this method, due to the potential influence of non-spectral characteristics (NEHRP Consultants Joint Venture, 2011).

2.3.4.5. Critical assessment of scaling effects on nonlinear structural response

The application of scaling techniques, particularly spectrum matching, introduces complexities that require critical assessment, especially when performing nonlinear RHA, which is sensitive to factors beyond just the peak elastic spectral acceleration (NEHRP Consultants Joint Venture, 2011).

Effects of Spectrum Matching on Ground Motion Characteristics

Spectrum matching modifies the seed motion by adjusting its Fourier spectrum, which inevitably affects the amplitude, frequency content, and—critically—the phase spectrum (Cao et al., 2019). The phase spectrum determines the time non-stationarity and the temporal shape of the ground motion (Ding et al., 2024a). Altering the phase angles, even if the spectral match is achieved, can profoundly change the time history, potentially rendering it non-physical or inconsistent with the seismic source mechanism (Cao et al., 2019).

Furthermore, spectrum matching often results in an increase in the number of strong-motion cycles and, consequently, an increase in the total input energy compared to the original recorded motion (Cao et al., 2019). This manipulation, particularly in the input energy, can lead to potentially conservative estimates of cumulative damage measures and nonlinear deformation in structural or geotechnical systems (Cao et al., 2019). The tension lies in the trade-off: spectrum matching reduces response dispersion by ensuring spectral fidelity, but at the risk of generating a modified signal whose cumulative characteristics (duration, phasing, energy) may not reflect the actual seismic hazard (Huang et al., 2011).

Analysis of amplitude-scaling bias in nonlinear RHA

The appropriateness of scaling in RHA has been subject to considerable debate. Some studies suggest that when ground motions are selected appropriately (e.g., based on CMS) and scaling is implemented judiciously, amplitude scaling does not introduce systematic bias in the estimation of nonlinear structural response compared to unscaled records (Huang et al., 2011; Zhou et al., 2025; Dávalos and Miranda, 2019; Bradley, 2012).

However, caution is warranted concerning the use of excessive scaling factors (SFs) (Liang et al., 2023). Bias is introduced when analysts select low-amplitude, far-field records and apply a large SF (e.g., SF ≥ 5) to match a high-intensity target spectrum. Such highly scaled records, although spectrally compatible, lack the intrinsic characteristics—such as velocity pulse shape, duration, and energy content—of the actual near-fault or high-magnitude design event (Liang et al., 2023). This selection of low-amplitude records that are highly scaled is known to significantly overestimate the nonlinear response of structures, such as high arch dams (Zhou et al., 2025). To mitigate this risk, it is recommended practice to establish a maximum acceptable scaling factor (e.g., typically limited to 2.0 or 3.0) and to select records whose mean estimated response remains independent of the SF, a condition often observed when using Liang et al., 2023; NEHRP Consultants Joint Venture, 2011).

Strategies for mitigating scaling bias and reducing response dispersion

To optimize ground motion selection and scaling for nonlinear analysis, advanced techniques focusing on inelastic response may be employed. One such approach is the Modal-Pushover-based Scaling (MPS) method (Haselton et al., 2010). Instead of scaling to match the elastic response spectrum, the MPS method scales ground motions to match a target value of inelastic deformation determined from the first-mode inelastic single-degree-of-freedom (SDF) system equivalent to the structure (Haselton et al., 2010). This approach ensures that the ground motion intensity is appropriately matched to the inelastic performance target, offering demonstrably superior accuracy and efficiency compared to older scaling procedures, especially for first-mode dominated structures (Haselton et al., 2010).

Analysts performing RHA must also monitor key cumulative IMs, such as I_A and CAV, post-scaling to ensure that the modifications imposed by spectrum matching do not excessively deviate these critical values from the target hazard distribution, thereby ensuring the integrity of geotechnical and structural component checking (Huang et al., 2011).

2.3.4.6. Specific application to dams and appurtenant structures

The design and safety evaluation of dams and their appurtenant structures involve complex soil-structure-fluid interaction, making the selection and application of seismic input highly specialized.

Regulatory and engineering guidance (USACE, FERC, ICOLD)

The seismic evaluation of dams must adhere to established technical guidelines aimed at promoting consistency in dam performance evaluation and assuring dam safety (Bozovic, 1989). Federal agencies, such as USACE and the Bureau of Reclamation (USBR), provide detailed technical requirements and standards for design professionals (USBR, 2021; USACE, 2024).

The USACE guidelines are recognized as highly comprehensive, providing detailed rules for both simple-scaled and spectrally matched ground motions, often being more detailed than those developed for conventional buildings or bridges (NEHRP Consultants Joint Venture, 2011). These standards mandate the establishment of design ground motions that consider safety, economics, and operational functions, generally defined by the Operating Basis Earthquake (OBE) and the Maximum Design Earthquake (MDE) (USACE, 2016). Furthermore, adherence to these policies requires the installation and maintenance of strong-motion instruments on dam structures to record site-specific earthquake response, providing essential data for post-event assessment and model validation (USACE, 2024). Table 2.12 defines these regulatory criteria.

Table 2.12. *Comparison of seismic performance criteria and earthquake definitions for dams by regulatory agencies*

Agency & Structure Class	Seismic Design Criteria (OBE vs. MDE/SEE)	Performance Goal (MDE/SEE)
USACE (Critical Feature/ High Hazard)	OBE: 475 years [1].MDE/SEE: Greater of 2,475 years or MCE (extensible to 10,000 years based on risk) [2].	Prevents loss of life and catastrophic failures (e.g., uncontrolled release) [3].
FERC (High Consequence)	OBE: N/A (transitioning to RIDM) [4].MDE/SEE: Evaluates a full range of return periods via RIDM (including MCE and 10,000-year events) [5].	Maintains stability under a Risk-Informed Decision Making (RIDM) framework [6].
USBR (High Consequence)	OBE: Not utilized (relies on Public Protection Guidelines) [7].MDE/SEE: Evaluates a full range of return periods without specific deterministic limits [8].	Satisfies Public Protection Guidelines through a risk-informed framework [9].
ICOLD (Extreme / High Consequence)	OBE: 145 years (50% probability in 100 years) [10].MDE/SEE: 10,000 years (probabilistic) or 84th percentile MCE (deterministic) [11].	Strictly prevents uncontrolled water release from the reservoir [12].

[1] 145 yrs is for non-critical features.

[2,3] Based on Army Corps seismic design criteria and safety standards.

[4,5,6] FERC is increasingly moving toward Risk-Informed Decision Making (RIDM).

[7,8,9] USBR relies on total risk estimates rather than a single earthquake event.

[10,11,12] Interrnational Commission on Large Dams (ICOLD) Bulletin guidance.

Importance of selection for geotechnical permanent deformation

For earth dams, embankment stability, and large excavated slopes (e.g., spillway cut slopes), the primary concern during an earthquake is the accumulation of permanent, inelastic displacement (Deoda et al., 2020). Dynamic analysis, such as nonlinear finite element or finite difference methods, often rely on predictive models like the Newmark sliding block methodology, which explicitly requires an accurate measure of cumulative input energy.

As established previously, Arias Intensity (I_A) exhibits a robust, non-linear correlation with Newmark displacement (Li et al., 2021; Liu et al., 2025; Hsieh and Lee, 2011; Jibson, 2007; Yuan et al., 2016). Given this strong relationship, I_A must be treated as a primary constraint in the record selection process for geotechnical RHA. If the CMS selection process yields a set of records whose I_A values are inconsistent with the hazard, the predicted permanent displacements may be unreliable. Therefore, selecting records using a vector-valued IM approach (like GCIM) or vetting the I_A and duration characteristics of the CMS-matched records is critical to accurately estimate geotechnical failure modes, particularly those involving cyclic loading and degradation (Foschaar et al., 2012).

Consideration of topographic amplification for spillway cut slopes and tunnel portals

Appurtenant structures are often situated in complex terrain, involving steep cut slopes for spillways or excavations near tunnel portals (Han et al., 2017). These irregular geometries modify the incoming seismic wave field, a phenomenon known as topographic amplification (Brabhaharan, 2010; Das and Maheshwari, 2022).

Numerical studies show that ground motion is amplified at the crests and ridgelines of slopes. The Seismic-Slope Topographic Amplification Factor (S-STAF), defined as the ratio of seismic response near the slope to the free-field response, increases with both the slope angle (β) and the frequency of excitation (Das and Maheshwari, 2022; Geli et al., 1988; Ashford and Sitar, 1997; Paolucci, 2002). This amplification increases the inertial forces acting on the stability-critical regions of the slopes and surrounding structures (Brabhaharan, 2010). This topographic phenomenon is schematized in Figure 2.28.

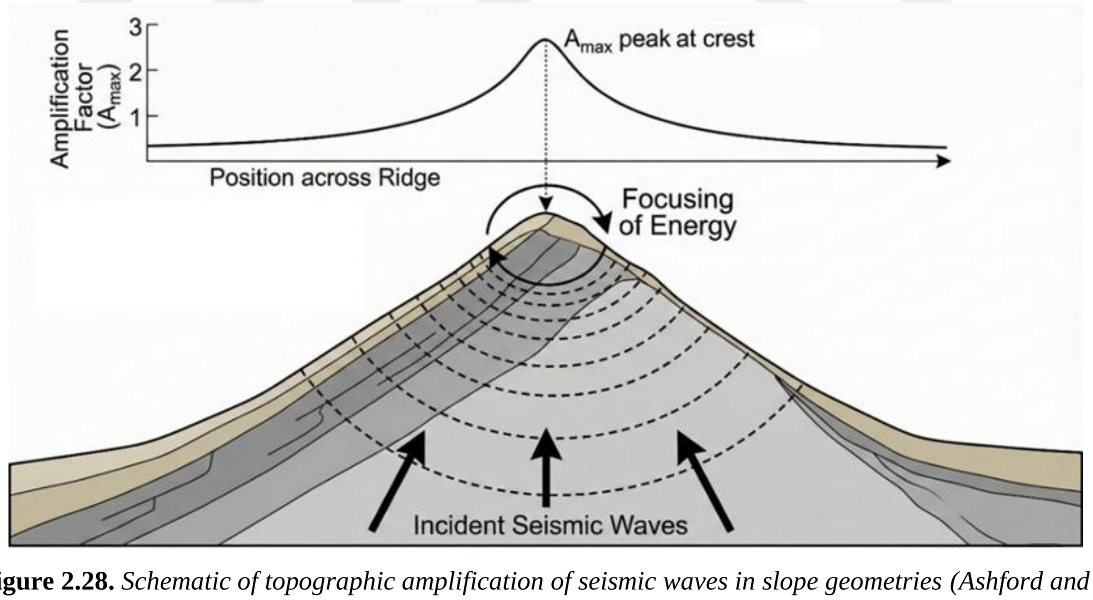

Figure 2.28. *Schematic of topographic amplification of seismic waves in slope geometries (Ashford and Sitar, 1997)*

For dynamic modeling of these features (e.g., using 2D or 3D Finite Element/Difference analysis), the methodology should account for this effect intrinsically. The scaled, hazard-consistent ground motion (derived from the CMS, representing the input at the bedrock level) is applied at the base of the numerical model

(Chen et al., 2024). The model itself, incorporating the actual site geometry and material properties, calculates the complex, frequency-dependent modification and amplification of the motion as it propagates through the slope mass to the ground surface or the structure's location (e.g., tunnel portal) (Song et al., 2024; Das and Maheshwari, 2022). For tunnel portals, the interaction between the excavation and the sloping topography can result in asymmetric surface deformation (subsidence), further emphasizing the need for 2D/3D numerical fidelity in applying the seismic input (Han et al., 2017; Song et al., 2024).

2.3.4.7. Synthesis of methodologies

The selection and conditioning of seismic inputs require balancing probabilistic rigor with physical realism. As detailed in the preceding sections, current best practices favor a move away from broadband spectral envelopes toward scenario-specific targeting. The following tables summarize the critical methodological shifts inherent in this process for high-consequence infrastructure.

Table 2.13 contrasts the target spectra definitions, highlighting the transition from the Uniform Hazard Spectrum (UHS) to the Conditional Mean Spectrum (CMS) and Generalized Conditional Intensity Measure (GCIM) to better capture the specific spectral shape of the dominant rupture scenario. Table 2.14 subsequently delineates the trade-offs between amplitude scaling and spectrum matching, emphasizing that while spectral fit reduces statistical dispersion, it must not come at the cost of altering the fundamental physical characteristics of the ground motion.

Table 2.13. *Comparison of target response spectra for ground motion selection*

Spectrum Type	Basis/Derivation	Key Characteristic	Suitability for Dynamic Analysis (RHA)	Source Reference
Uniform Hazard Spectrum (UHS)	Integrated result of PSHA across all causal scenarios (M, R).	Broadband, highly conservative; represents hazard but not a physical earthquake.	Adequate for elastic design; generally discouraged for nonlinear RHA due to overconservatism.	(Somerville et al., 2016; Lee et al., 2025)
Conditional Mean Spectrum (CMS)	PSHA deaggregation conditioned on magnitude (M), distance (R), and ε at T^*.	Narrowband, hazard-consistent; reflects the expected spectrum of the dominant scenario.	Optimal target for modern RHA; minimizes response dispersion and maintains probabilistic rigor.	(Baker, 2011)
Generalized Conditional Intensity Measure (GCIM)	Multivariate distribution conditioned on a vector of IMs (e.g., S_a, I_A).	Ensures consistency across cumulative (energy/duration) and peak (acceleration) metrics.	Essential for geotechnical RHA (dams/slopes) where performance depends on multiple IMs.	(Bradley, 2010; Kwong and Chopra, 2015)

Table 2.14. *Critical comparison of ground motion scaling techniques for rha*

Technique	Mechanism	Primary Advantage	Key Concern/ Bias Risk	Mitigation Strategy
Simple Amplitude Scaling	Linear factor applied uniformly to time history.	Preserves physical characteristics (phasing, duration, energy ratios).	Poor spectral fit across period range; results in high variability (dispersion) in structural response.	Use a larger number of records (≥ 5 to 7 for nonlinear RHA) to stabilize the mean response.
Spectrum Matching	Iterative modification in frequency/time domain to match target spectrum.	Excellent spectral fit; significantly reduces elastic and inelastic response dispersion.	Manipulation of energy and duration content; potential introduction of non-physical phasing or "energy bloating."	Limit the scaling factor (SF < 2–3); use MPS or vet cumulative IMs (like Arias Intensity) post-match.

2.3.4.8. Conclusions

The selection and scaling of seismic input for dams and appurtenant structures necessitates a rigorous approach rooted in modern PBEE principles. The analysis presented demonstrates a clear methodological progression required for doctoral-level research and high-stakes engineering practice:

- Target consistency: The Uniform Hazard Spectrum (UHS) is generally unsuitable for accurate nonlinear RHA due to its broadband nature. The use of the Conditional Mean Spectrum (CMS), derived from PSHA deaggregation of $\bar{M}$, $\bar{R}$, and $\bar{\varepsilon}$, is the required standard for defining a hazard-consistent spectral shape (Baker, 2011; FERC, 2014). For advanced analysis, particularly in geotechnical systems where performance is governed by multiple demands, the Generalized Conditional Intensity Measure (GCIM) provides the most holistic selection methodology.
- Geotechnical demand control: Earthquake records must be selected based primarily on spectral shape compatibility rather than strict causal parameter matching (Kwong and Chopra, 2015). For earth dams and slopes, Arias Intensity (I_A) has been shown to correlate strongly with permanent seismic deformation, including Newmark displacement, making it an important constraint in ground-motion selection alongside spectral acceleration for the target design scenario (Armstrong et al., 2021; Hsieh and Lee, 2011; Bradley, 2010; 2011; Macedo et al., 2019).
- Judicious scaling: Spectrum matching techniques are highly effective in minimizing response dispersion and achieving regulatory spectral fit (NEHRP Consultants Joint Venture, 2011). However, the analyst must mitigate the potential for bias by rejecting poorly chosen seed records and limiting the amplitude scaling factor (SF) to low values (typically SF $\leq$ 3). The use of excessive scaling on low-amplitude records is known to introduce significant, non-conservative bias in nonlinear response estimation (Liang et al., 2023; Zhou et al., 2025).
- Site effects integration: For appurtenant structures located on steep terrain, the input motion must account for topographic amplification. The most appropriate method involves applying the scaled, un-amplified bedrock motion at the base of the dynamic numerical model (FEA/FDA), allowing the model to naturally capture the complex, frequency-dependent Seismic-Slope Topographic Amplification Factor (S-STAF) specific to the site geometry (Das and Maheshwari, 2022).

2.3.5. Probabilistic and reliability-based approaches

Deterministic analyses produce a single FoS based on fixed input parameters. In contrast, probabilistic methods explicitly account for the inherent uncertainty and spatial variability of geotechnical properties by treating them as random variables defined by statistical distributions (Phoon and Ching, 2018). The recognition of these uncertainties has led to a fundamental shift in geotechnical practice, a move away from purely deterministic analyses toward probabilistic and reliability-based approaches. Recent advancements have integrated probabilistic analysis into slope stability studies, allowing engineers to quantify uncertainties associated with input parameters such as soil and rock properties (Chakraborty and Dey, 2022). These methods aim to quantify the uncertainty in input parameters and propagate it through the analysis to evaluate the probability of failure or the reliability index of a slope, rather than just calculating a single factor of safety (Whitman, 2000).

A single, deterministic *Factor of Safety (FS)* can give a false sense of security (Whitman, 1984). It provides no information on the probability of failure or the level of confidence in the stability assessment (Whitman, 1984). For example, a slope with a calculated FS of 1.5 but high uncertainty in its soil strength parameters may in fact pose a greater risk than a slope with an FS of 1.3 but well-defined, low-variability parameters.

Since the 1990s, there's been a growing emphasis on quantifying uncertainty in geotechnical design. Whitman (1984, 2000) championed the idea that we should compute not just FOS but the probability of failure P_f. A common approach is Monte Carlo simulation: run a large number (thousands) of slope stability analyses with input parameters sampled from their statistical distributions, then see how often failure occurs (FOS<1) (Harr, 1987). This gives an estimated P_f. The simulation workflow is captured in Figure 2.29.

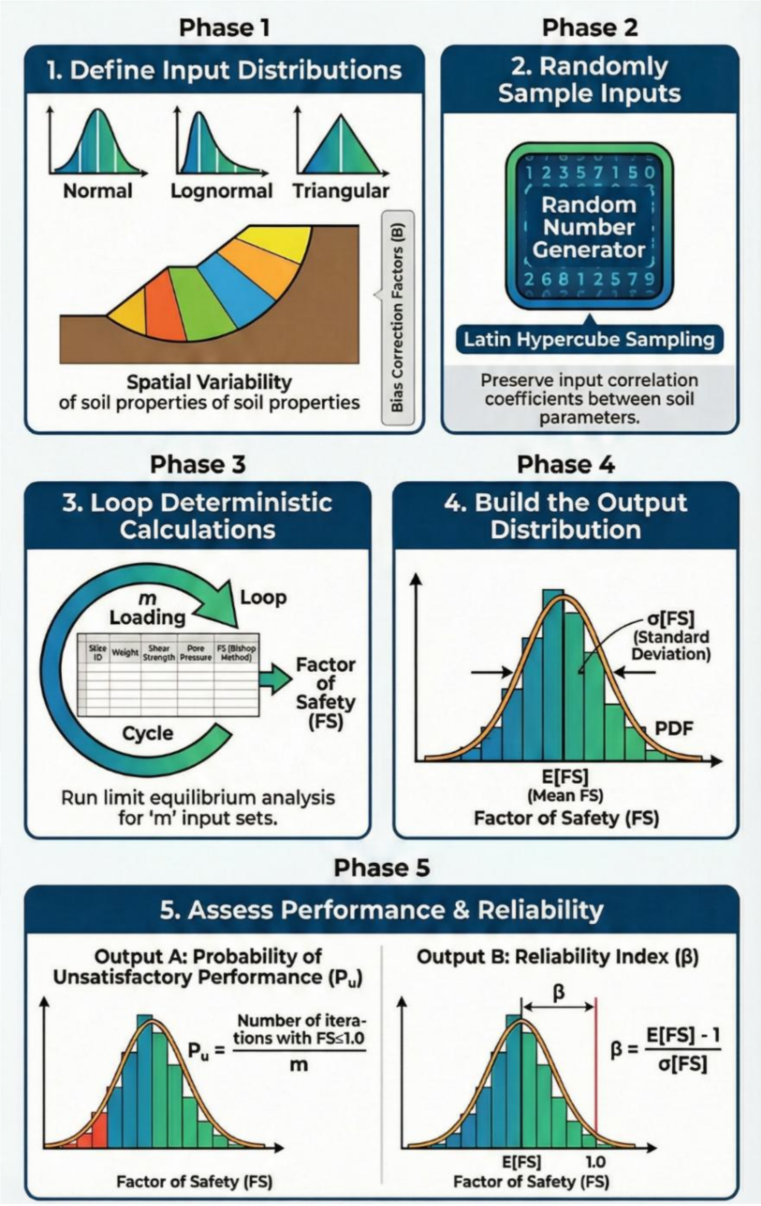

Figure 2.29. *Monte Carlo simulation workflow for probabilistic slope stability analysis (El-Ramly, et al., 2002)*

For example, if cohesion and friction vary, Monte Carlo would sample each from its distribution for each run. El-Ramly et al. (2002) did this for an embankment slope, using 10,000 simulations to get a stable estimate of failure probability. Such analyses often reveal that P_f is non-zero even if deterministic FOS>1, due to parameter uncertainty—which is expected. The question then becomes: is the probability tolerable? Whitman (2000) suggested that for routine slopes a failure probability on the order of 1% might be acceptable, whereas for extremely critical structures we want much lower (e.g., 0.1% or less). Reliability-based design codes (such as Eurocode 7) are beginning to incorporate these ideas, although full probabilistic slope stability design is not yet mainstream in all places (EN 1997-1, 2004; Phoon and Ching, 2018). The mathematical correlation between the reliability index (β) and the corresponding probability of failure (P_f) is depicted in Figure 2.30.

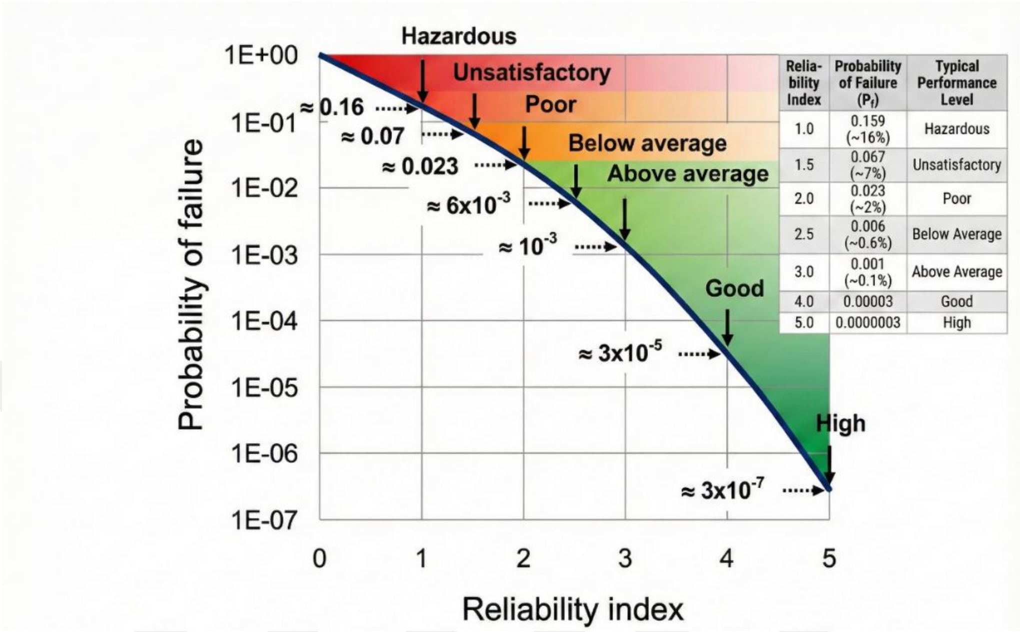

Figure 2.30. *Relationship between reliability index (β) and probability of failure (P_f) (USACE, 1997)*

Another method is the First-Order Second-Moment (FOSM) method, which linearizes the problem around mean values to estimate variance in FOS (Ang and Tang, 1975). This is less computationally heavy than Monte Carlo but can be less accurate for highly nonlinear problems. Recent research uses advanced simulation techniques like Latin Hypercube sampling or subset simulation to efficiently compute small probabilities of failure (Ji et al., 2010).

One significant source of uncertainty is incomplete knowledge (epistemic) vs. natural variability (Baecher and Christian, 2003). For example, "random testing errors" and limited samples can cause us to misjudge the mean strength of a formation (Whitman, 2000). Careful data analysis can reduce this—e.g., remove obvious outliers (possibly bad tests) and use statistical inference to estimate the true mean and confidence intervals (Whitman, 2000). Spatial correlation means that if you do more tests in the same layer, you don't get a proportional increase in information (beyond a certain point you are just finding the same value repeatedly if correlation length is long) (Vanmarcke, 1977). So designing the exploration program optimally is important—sometimes a few well-placed borings in suspected weak zones is better than many borings in the already characterized typical zones (Wu et al., 1989). Wu et al. (1989) provided an example of evaluating exploration programs by their impact on the reliability of the project.

A shift in design philosophy is emerging: rather than concluding that a slope is "safe" solely because a deterministic factor of safety exceeds a prescribed threshold (e.g., $FoS = 1.3 > 1.2$), the outcome may be framed in probabilistic terms—such as an estimated 2% probability of failure over a 50-year service life—and then judged against explicit risk acceptance criteria. This perspective is especially pertinent for slopes adjacent to critical infrastructure. For example, failure of a spillway slope may not directly threaten the structural integrity of a dam, yet it could obstruct spillway capacity and therefore represents a consequential risk that is more appropriately managed within a probabilistic decision framework. In quantitative risk assessment, such decisions are supported by combining the likelihood of failure with its consequences to rank and prioritize mitigation measures (Fell et al., 2005). Whitman (1984) advocated this risk-informed approach in geotechnical engineering, noting that traditional practice often applied uniform ("blanket") safety factors without adequately differentiating among consequence classes. Probabilistic outputs can also guide efficient allocation of investigation effort: if uncertainty in the strength of a specific stratum dominates the computed failure probability (Pf), targeted additional testing in that layer can reduce uncertainty and, in turn, decrease Pf (Baecher and Christian, 2003). This rationale aligns with the broader "value of information" concept in site characterization. The probabilistic slope-stability formulation based on the overlap between driving and resisting force distributions is illustrated in Figure 2.31.

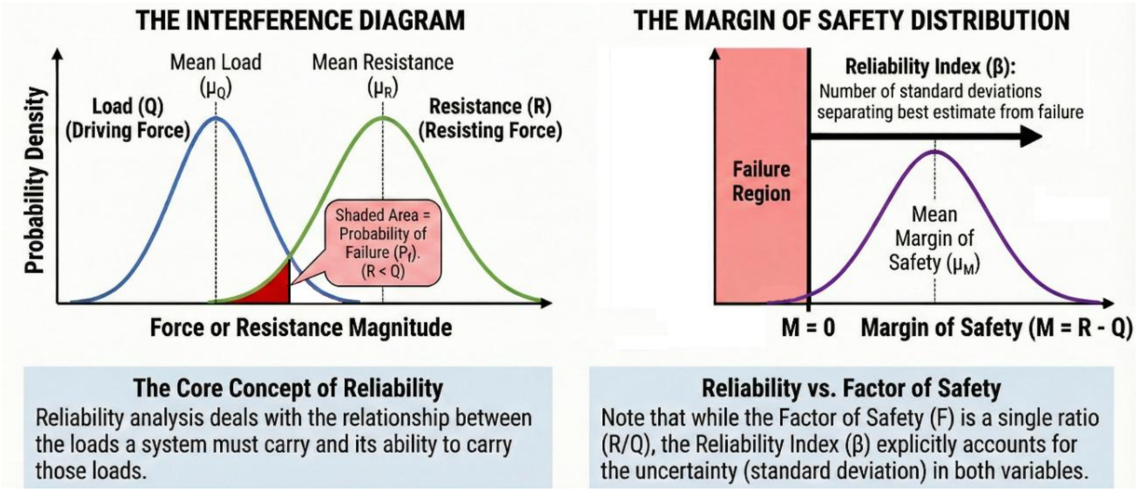

Figure 2.31. *Probabilistic definition of slope stability: the reliability index (β) and probability of failure (P_f) defined by the overlap of driving and resisting force distributions (Baecher and Christian, 2003)*

One approach that has made it into practice is the partial factor method (in Eurocode, for example): instead of one FOS, apply partial safety factors to different inputs (e.g., reduce c and tanφ by certain factors, increase loads by certain factors) (EN 1997-1, 2004). These factors are often calibrated to achieve target reliability indices (β) (Christian et al., 1994; Griffiths and Fenton, 2004). In essence, they are a deterministic wrapper around a probabilistic target. Monte Carlo studies (e.g., by Christian et al., 1994) on slope stability have shown how variability in cohesion vs. friction affects reliability. For long slopes, spatial variation means a longer potential failure surface has more "chances" to go through weak spots, which tends to lower FOS and increase variance—so long 2D slopes are less reliable than short slopes with identical mean properties. Probabilistic methods can explicitly capture that by modeling the random field of strength along the slope (Griffiths and Fenton, 2004).

In summary, site investigation and uncertainty analysis form a feedback loop: better site investigation (more data) reduces parameter uncertainty, which can markedly lower calculated probability of failure or at least narrow the confidence bounds on FOS. Whitman (2000) illustrated that systematically selecting parameter values (mean, variance) and using them in reliability analysis gives a more complete picture of stability. Engineering decisions (to remediate or not, to allocate budget for more drilling, etc.) can then be made with an understanding of both safety margins and confidence levels. This is particularly relevant to appurtenant structures: by their nature (often one-off designs in variable terrain), the slopes around them might not fit standard "rule of thumb" designs, so quantifying uncertainties can justify design choices and contingency plans.

2.3.6. Limit analysis

Limit analysis, rooted in the theory of plasticity, provides a rigorous alternative to LEM. Instead of making assumptions about interslice forces, it uses the lower-bound and upper-bound theorems of plasticity to bracket the true collapse load or factor of safety (Chen, 1975). In parallel to LEM, plastic limit analysis provides a rigorous framework to bracket slope stability solutions without a priori assuming a slip surface shape.

2.3.6.1. The lower-bound theorem

The lower-bound theorem states that a slope will be stable if a statically admissible stress field can be found that satisfies equilibrium everywhere within the soil mass and does not violate the yield criterion at any point (Chen, 1975). This theorem provides a conservative estimate of the factor of safety.

2.3.6.2. The upper-bound theorem

The upper-bound theorem states that the slope will collapse if any kinematically admissible failure mechanism (a compatible velocity field) can be devised for which the rate of work done by external and body forces exceeds the rate of internal energy dissipation along the slip surface. This provides an upper-bound (non-conservative) estimate of the failure load. In slope stability, the upper-bound theorem is more commonly applied, often with an assumed rotational failure mechanism such as a logarithmic spiral, which satisfies the kinematic requirements of plasticity theory (Chen, 1975).

Figure 2.32 compares the discretization techniques of lower bound stress fields and upper bound velocity fields within the framework of finite element limit analysis.

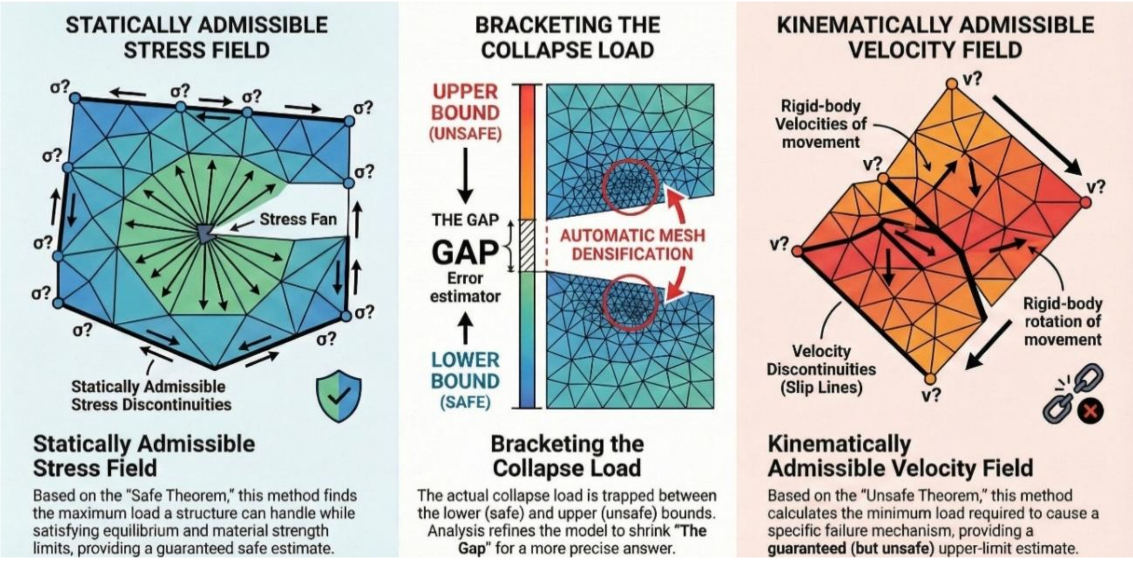

Figure 2.32. *Comparison of lower bound (stress field) and upper bound (velocity field) discretization in finite element limit analysis (Sloan, 2013)*

When the upper- and lower-bound solutions converge, they yield the exact solution for an ideal rigid-perfectly plastic material (Chen, 1975). The method inherently assumes a rigid-perfectly plastic material behavior. The advantage is rigor—no assumption of slice forces or empiricism—but at the cost of more complex computation. Modern numerical implementations, such as Finite Element Limit Analysis (FELA) and Discontinuity Layout Optimization (DLO), have made these powerful methods practical for complex geotechnical problems (Sloan, 2013). However, while limit analysis provides an excellent theoretical bracket for the true collapse load, it inherently assumes a rigid-perfectly plastic material behavior. Consequently, it yields little information regarding pre-failure deformations, stress redistributions, or progressive yielding, which are critical for the complex soil-structure interaction problems and transient seepage conditions addressed in this thesis. For this reason, elastoplastic FEM remains the preferred numerical tool for this study.

2.3.7. Empirical and observational methods

Empirical methods are based on correlations derived from extensive databases of past slope performance and failures (Hoek and Bray, 1981). For simple, homogeneous soil slopes, stability charts can provide a rapid, preliminary estimate of the FoS (Taylor, 1937). For rock slopes, empirical classification systems such as the Slope Mass Rating (SMR) and Q-slope are commonly used to assess stability based on geological and structural parameters (Azarafza et al., 2020). Taylor's traditional stability charts are reproduced in Figure 2.33.

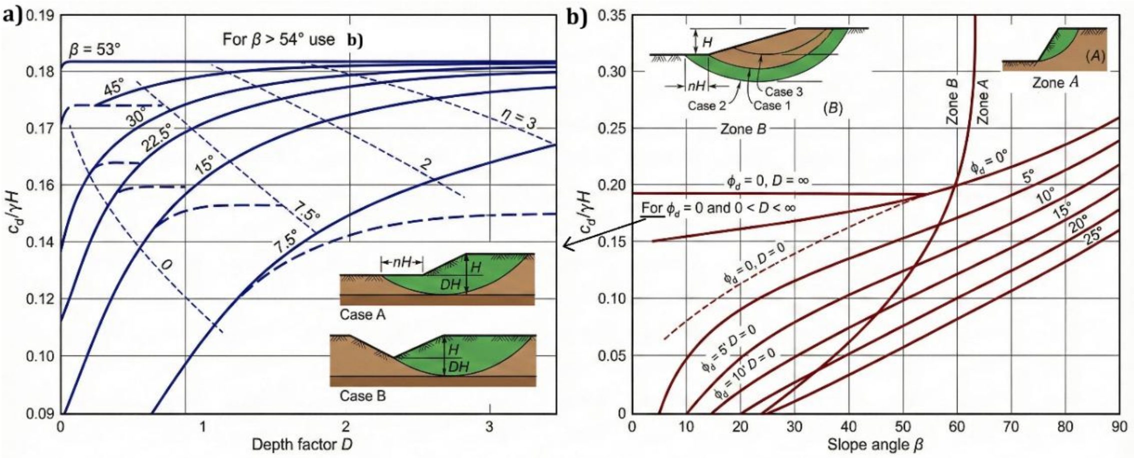

Figure 2.33. Reproduction of *Taylor's stability charts; (a) for soils with zero friction angle, (b) for soils with friction angle (Taylor, 1948)*

Observational methods utilize data from actual slopes. The most powerful of these is the back-analysis of a failed slope (Duncan and Stark, 1992). Since a failed slope has, by definition, a factor of safety of 1.0, the analysis can be used to solve for the operational shear strength parameters that must have been mobilized at the time of failure. This provides a highly reliable, site-specific estimate of soil strength for use in redesigning the slope or analyzing similar slopes in the same geological formation (Duncan and Stark, 1992).

2.3.8. Data-driven, machine learning, and hybrid methods

Although the primary methodology of this research relies on deterministic, physics-based numerical modeling, it is important to acknowledge that in recent decades, Machine Learning (ML) has emerged as a transformative approach in geotechnical engineering (Harle and Wankhade, 2025; Xu et al., 2023). Data-driven models—such as Artificial Neural Networks (ANN), Support Vector Machines (SVM), and Random Forests (RF)—excel at processing large datasets and predicting the Factor of Safety (FS) without relying on the explicit physical formulations of LEM or FEM (Pardeshi et al., 2023; Gordan et al., 2016). However, since this thesis strictly utilizes numerical and limit equilibrium approaches, detailed ML algorithms fall outside the current scope and are primarily viewed as a promising future trajectory for slope stability assessment (Zerouali et al., 2024; Nguyen, 2021).

Rather than data-driven surrogates, modern slope analysis within the context of this study increasingly relies on physics-based hybrid and coupled methods. One prominent example is coupling seepage analysis with stability. Ng and Shi (1998) performed a numerical investigation of unsaturated soil slopes under transient rainfall infiltration. By coupling a transient seepage FE analysis with strength reduction stability analysis, they showed how infiltration can drastically reduce the factor of safety (FS) over time. Other hybrid approaches include combining LEM and FEM, or static-dynamic coupling. These advanced numerical integrations allow engineers to investigate "what-if" scenarios with far more fidelity than was previously possible, directly establishing the theoretical foundation for the multi-stage stability assessments and transient rapid drawdown (RDD) analyses conducted in the subsequent chapters of this thesis.

2.3.9. Discontinuum and hybrid methods

For problems involving jointed rock masses, where behavior is dominated by discontinuities, the Discrete Element Method (DEM) is often more appropriate. DEM is a discontinuum-based method that models the rock mass as an assembly of distinct blocks or particles that interact at their contacts. Pioneered by Cundall and Strack (1979), it is exceptionally well-suited for analyzing large-deformation problems, such as rockfalls, and for investigating the complex failure mechanisms of heavily jointed rock masses. It allows for the explicit modeling of joint networks and can directly simulate the influence of joint connectivity, orientation, and shear strength on the failure process. Some formulations treat the rock as blocks connected by springs, satisfying all equilibrium and compatibility conditions and allowing for the modeling of progressive failure (Cundall, 1988). Figure 2.34 distinguishes FEM and DEM approaches.

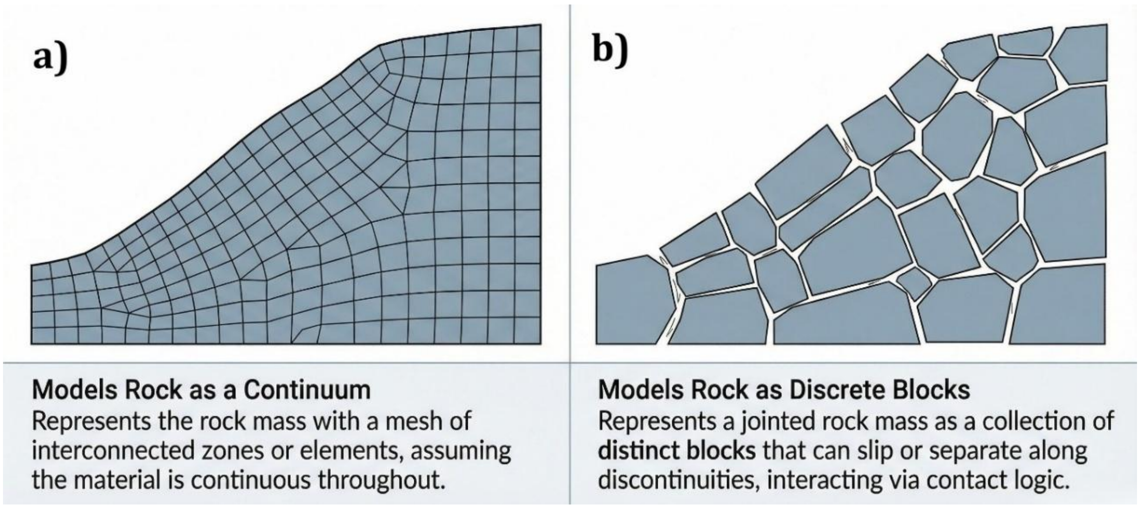

Figure 2.34. *Comparison of numerical discretization approaches. (a) finite element method (FEM) mesh representing a continuum. (b) distinct element method (DEM) representation of a jointed rock mass as discrete blocks interacting via contact logic (Wyllie and Mah, 2004)*

While DEM is exceptionally well-suited for analyzing large-deformation rockfalls, it requires extensive micro-parameter calibration and significant computational resources, making it frequently impractical for field-scale stability assessments of highly weathered intermediate geomaterials and mélanges, where continuum approximations (like the Generalized Hoek-Brown criterion) are more efficient.

The Material Point Method (MPM) is a more recent numerical technique that combines the advantages of both Eulerian and Lagrangian formulations (Sulsky et al., 1994). The material is discretized into a set of Lagrangian particles (material points) that move through a fixed Eulerian computational grid. This unique framework allows MPM to handle problems involving extremely large deformations, such as landslides, debris flows, and dam breaches, without the mesh distortion issues that can limit traditional FEM analyses (Sulsky et al., 1995). Figure 2.35 evaluates the performance of FEM mesh distortion against the particle flow capability of the MPM during large deformation run-out simulations.

MPM is particularly well-suited for simulating the entire failure process, from initiation and progressive failure to the post-failure run-out stage. Case studies have demonstrated its capability in modeling complex events like the Fundão Dam failure (Zhang et al., 2019) and the Aznalcollar dam failure (Yerro et al., 2013), capturing the development of failure surfaces and subsequent large-scale material flow (Yerro et al., 2021; Zabala and Alonso, 2011).

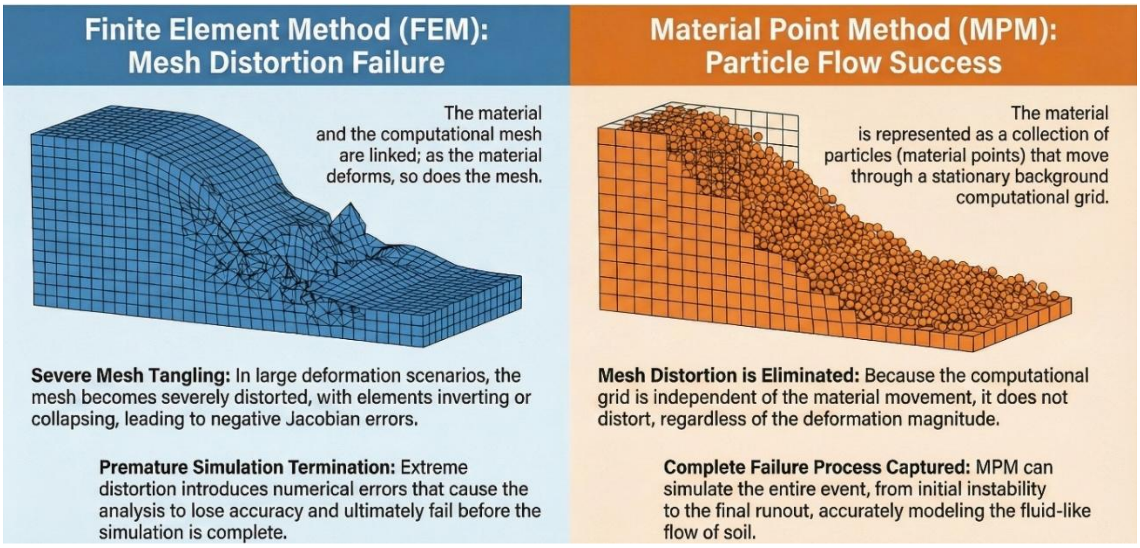

Figure 2.35. *FEM mesh distortion vs. MPM particle flow capability in large deformation run-out*

Recent developments have seen MPM coupled with FEM in hybrid approaches, leveraging FEM for the initial failure analysis and MPM for the subsequent runout simulation (Sordo et al., 2024). Despite its superiority in simulating the post-failure run-out stage and avoiding mesh tangling, a primary limitation of MPM in standard geotechnical practice is that it does not directly calculate a traditional Factor of Safety (FS). Because establishing a comparative deterministic framework (FS correlation between LEM and FEM) is the core objective of the case studies in this thesis, MPM is acknowledged as a powerful future tool but is not utilized in the present stability evaluations.

2.4. Support and Slope Improvement Methods

The stabilization of slopes adjacent to critical hydraulic structures requires a systems-based approach tailored to the specific failure kinematics of the geomaterial (Cornforth, 2005). As demonstrated in historical precedents, shallow constructive reinforcement is often kinematically incompatible with deep-seated failures typical of thick colluvial deposits and ophiolitic mélanges. Consequently, contemporary stabilization strategies for intermediate geomaterials prioritize either deep active reinforcement (e.g., high-capacity pre-stressed anchors transferring loads to competent bedrock) or massive passive geometric restoration (e.g., rockfill buttresses and cut-and-cover conduits) to achieve absolute system lock-in against both static and extreme dynamic forces (Holtz and Schuster, 1996).

Slope stability can be improved through a wide spectrum of interventions ranging from simple drainage or regrading to high-cost engineered structures. These methods are generally classified as non-structural measures (which reduce driving forces or enhance natural resistance without major engineered structures) and structural measures (which add external support or reinforcement) (Abramson et al., 2002; Holtz and Schuster, 1996). This section covers key slope stabilization techniques organized in order of increasing general cost and complexity, from low-cost, low-tech solutions to advanced engineering methods that are particularly relevant to the case studies analyzed in this thesis.

2.4.1. Non-structural and low-cost approaches

2.4.1.1. Drainage systems

One of the simplest and most cost-effective measures to improve slope stability is the control of water through drainage. Excess water is a major factor in slope failures, as it adds weight and elevates pore-water pressures, thereby reducing soil shear strength (Holtz and Schuster, 1996). By removing surface water and lowering groundwater levels, drainage both reduces the driving forces (by lightening the slope mass) and increases resisting forces (by raising effective stress and soil strength) (Holtz and Schuster, 1996). In fact, drainage is often cited as the single most important stabilization method for many landslides. Proper drainage is universally recommended as part of any landslide remediation plan, since its stabilization efficiency relative to cost is very high (Holtz and Schuster, 1996; Cedergren, 1989). Drainage measures are applicable to a wide range of failure mechanisms - from shallow erosion and surficial slips to deep rotational slides - wherever water infiltration or high groundwater is a contributing cause of instability (e.g. rainfall-triggered failures, slope failures in weak saturated soils, etc.). Common usage scenarios include natural slopes in rainy climates, highway cut slopes with seepage, and earth dams or embankments where internal water pressure must be controlled.

Surface drainage

Surface drainage aims to intercept and divert runoff before it can infiltrate into a slope. Simple measures such as graded surface slopes, swales, and diversion ditches at the top or mid-slope prevent water from ponding or flowing down the slope face (Geotechnical Control Office, 1984). Gutters, berms, and paved channels can safely convey runoff to stable outlets. By keeping infiltration minimal, surface drainage is particularly effective for preventing shallow failures (e.g. infinite slope or sheet failures caused by rainfall) and erosion flows. Surface drainage requires minimal engineering design and is relatively easy to implement (Geotechnical Control Office, 1984). For example, constructing a diversion berm and interceptor ditch along a slope can significantly reduce the risk of rainfall-induced landslides. Cedergren (1989) documented numerous highway slopes where simple measures like surface ditches and culverts successfully mitigated recurrent shallow landslides. In practice, road maintenance programs often include clearing and grading of surface drains as a first line of defense against slope failures.

Subsurface (underground) drainage

Subsurface drainage targets the internal groundwater by providing pathways for water to escape from within the slope. This can dramatically improve the stability of slopes prone to high pore pressures or elevated water tables (common in deep-seated rotational landslides or large translational slides in soil). Techniques include drainage trenches and blankets, drainage wells, and sub-horizontal drains (Holtz and Schuster, 1996). Trench drains are typically backfilled with free-draining gravel or geosynthetic drains and placed perpendicular to the slope to intercept shallow groundwater, often doubling as shear keys in weak layers (Holtz and Schuster, 1996). Horizontal drains (also called sub-horizontal or "hydraugers") are small-diameter perforated pipes drilled laterally into a slope to bleed off water from a potential sliding mass. They can extend tens of meters into a hillslope and are commonly used in residual soil slopes or clay slopes that fail during heavy rain.

Vertical relief wells or drain shafts may be drilled into unstable hillsides or at the toes of landslides to lower the water table by pumping or gravity flow. More elaborate systems like drainage galleries (adits) tunnels driven into a slope with weep holes have been used in large landslides or dam abutments to systematically drain a sliding area. Subsurface drains are effective for failures where a distinct weak zone is saturated; by lowering the phreatic surface, they improve the factor of safety significantly. For instance, horizontal drains installed in a rain-induced slope failure in Putrajaya, Malaysia, lowered groundwater and improved stability at low cost (Ahmed et al., 2012). In France, a system of vertical siphon drains successfully dropped the water table under a highway embankment by 6 m (from 2 m to 8 m depth), halting recurrent slide movements

(Jessberger, 1979; Boynton and Blacklock, 1985). Such a drainage configuration is sketched in Figure 2.36.

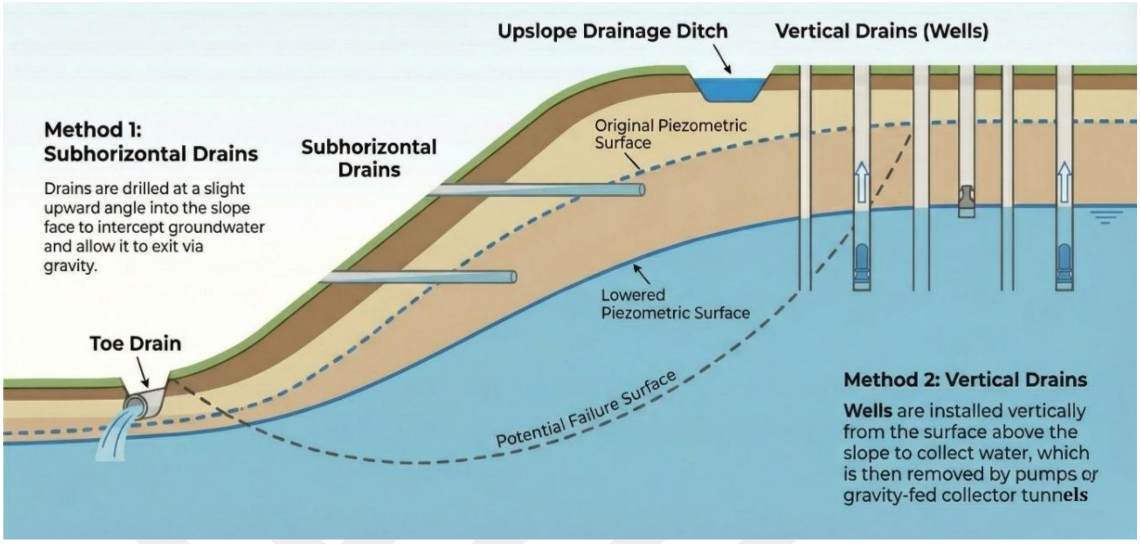

Figure 2.36. *Schematic cross-section of a slope stabilization system utilizing subhorizontal and vertical drains to lower the phreatic surface around the critical slip plane (Gedney and Weber, 1978)*

Design and maintenance considerations

Subsurface drainage should be designed based on hydrogeology; its effectiveness varies with soil permeability and drainage length (Blacklock and Wright, 1986). Drains generally function by gravity, though pumps are used if gravity outlets are unavailable (Baez et al., 1992). Incorporating filters (e.g. graded gravel or geotextile filters) is essential to prevent clogging by soil particles (Hiller and MacNeil, 2001). Maintenance of drainage systems (flushing of horizontal pipes, clearing of obstructions in ditches) is vital for long-term performance (Dennis and Nguyen, 2015). A known limitation is clogging of drains over time by sediment or bio-fouling, which can reduce their efficacy (Holtz and Schuster, 1996). Nevertheless, when properly installed and maintained, drainage can provide an immediate increase in slope stability at relatively low cost. In many cases, drainage alone has been sufficient to stabilize slopes that would otherwise require expensive structural solutions (Holtz and Schuster, 1996; Norrish et al., 1998).

2.4.1.2. Excavation and geometric modification

Modifying the geometry of a slope is a direct way to improve stability by reducing the driving forces or unfavorable geometry that contribute to failure. These methods are generally low-tech and involve earthwork to change the shape or mass distribution of the slope. Geometric modifications are most effective for slopes whose instability is due to steepness or overloading, and they are commonly applied in new construction (to design stable cut or fill angles) as well as in remedial works on existing landslides.

Typical applicable failure modes are rotational and translational slides in soil or weathered rock, where a reduction in slope angle or removal of weight will reduce the tendency for the mass to slip. They are less applicable for rock wedges or structurally controlled failures where geometry is dictated by discontinuities (though benching can help in those as well). The main techniques include: (a) flattening the slope angle, (b) removing or redistributing mass (especially at the crest), (c) creating benches or steps in the slope, and (d) removing and replacing weak materials. These approaches all aim to lower the ratio of driving forces to resisting forces on the potential failure surface (Holtz and Schuster, 1996).

Flattening the slope angle

Flattening (or laying back) the slope means regrading a steep slope to a gentler incline. By decreasing the slope angle, the downslope component of gravity (driving force) is reduced, and the resisting force (from soil strength along a now flatter potential slip surface) is increased. Even a modest flattening can significantly raise the factor of safety for a marginal slope. This method is widely used for both natural and man-made slopes if land space permits. For example, in highway engineering, cut slopes in soil are often designed with a safe flat angle (e.g. 2H:1V or gentler) to preempt failures; if a cut slope is initially over-steep and shows instability, one remedy is to regrade it to a flatter profile.

Applicable failure types: Flattening is effective for rotational failures (making the circular slip surface longer and shallower, thus more stable) and for translational slides or infinite slopes (reducing shear stress along the planar failure). It is less effective if a deep weak layer exists that cannot be altered by re-grading the surface (since the failure may daylight in the middle of the slope regardless of surface angle). Usage scenarios: Flattening is common in stabilizing highway embankments and cuts, open-pit mine slopes, and engineered fill slopes.

For instance, Peck and Ireland (1953) described the stabilization of the Cameo landslide in Colorado by partially removing and flattening the slope, which raised the factor of safety from 1.0 (at failure) to above 1.3 (Peck and Ireland, 1953). Advantages:

This method is conceptually simple and uses on-site material (cut-and-fill) without needing special materials. Limitations: It requires additional right-of-way or land at the toe to extend the slope, which may not be available in constrained sites (e.g. along road corridors or urban slopes). Also, large-volume earthworks can be costly or disruptive. In some cases, flattening alone might not achieve the desired stability if the soil is very weak or the required angle is too gentle to be practical. Still, flattening is often the first remedial option considered due to its straightforward nature.

Reducing slope or crest load

Overloading at the top of a slope can drive failures, so another strategy is to remove or reduce loads near the slope crest or upper slope. This is essentially the inverse of buttressing (which adds load at the toe): here we lighten the head of the slide. Common implementations include removing fill that was placed near a slope edge, relocating stockpiles or heavy objects away from the slope, or even demolishing or underpinning structures at risk that add stress to the slope. By unloading the top, the driving moment and shear forces along the potential failure surface are reduced.

Applicable failure modes: This is especially helpful for rotational slides where a heavy surcharge at the head pushes the mass downslope, or for translational block slides where a stiff layer might be sliding on a weaker layer - removing the weight can reduce the shear driving the slide. It also benefits compound failures where tension cracks indicate a heavy driving mass that could be trimmed.

Usage: This technique is often used in emergency landslide responses—for example, if a slope with houses on top shows movement, removing soil behind the scarp or even removing the house (if condemned) can stabilize the situation. In open-pit mines or quarries, controlled blasting or excavation at the rim can relieve pressure on a slope that is beginning to fail.

A classic example is the Vaiont landslide in Italy (1963), where post-failure analyses indicated that the natural slope might have been stabilized earlier by removing a portion of the rock at the crest (although in that case, the scale was enormous) (Müller, 1964; http-28[37]; Paronuzzi et al., 2021; Alonso and Pinyol, 2010; Dykes and Bromhead, 2021). On a smaller scale, highway engineers sometimes opt to shift a road away from a

[37]http-28:https://blogs.agu.org/landslideblog/2008/12/11/the-vaiont-vajont-landslide-of-1963/ (accessed September 13, 2025).

slide-prone embankment or remove excess fill that was unintentionally placed too near a creek bank, as recounted by Ritchie (1963) in case studies of road slope failures.

Limitations: Reducing crest load is not always feasible if infrastructure exists (buildings, roads) that cannot be moved. Also, the amount of load removal needed may be significant - partial unloading might not sufficiently increase stability if the main problem is deep-seated. In such cases, load removal may need to be combined with toe berms or other measures. Nonetheless, when practicable, unloading is a low-cost measure (essentially just earth removal) with immediate effect on stability.

Benching (terracing)

Benching involves cutting the slope into a series of steps or terraces instead of one continuous incline. Each bench removes material and provides a horizontal or gently inclined platform. Benching has multiple stabilizing effects: it breaks up the slope into shorter slope segments (interrupting a potential long failure surface), it reduces the overall steepness by adding intermediate catchments, and it can improve drainage by capturing runoff on the benches. In effect, benching can be seen as repeated local flattening of the slope and is especially useful in long or high slopes where a single flat slope might be impractical.

Applicable failure modes: Benching is effective for both soil and rock slopes that experience shallow slides or sloughing. In over-steep clay slopes, shallow slumps often start and run a short distance before hitting a bench, which can stop their progress. In rock slopes, benches catch falling rocks and reduce the likelihood of progressive failure from toe to crest. Geotechnically, benches can act like small counter-berms, providing additional weight at intervals down the slope to resist deeper failures, and can serve as keys if filled with competent material.

Usage: Terraced slopes are commonly seen in highway cuttings and open-pit mines, where benches are mandated for safety. For example, many highway cuts in mountainous terrain employ a design of, say, 3m vertical faces separated by 2m wide benches, to ensure no continuous 10m tall failure plane can form. In landslide repairs, a technique called staged excavation with berms may be used: the failed slope is excavated in steps, benching into stable strata, then rebuilding each stage. Benching is also used on large earth dams during construction to improve stability of the fill by compacting in horizontal layers (essentially creating fine benches).

Case example: In Oregon, a large ancient landslide reactivated under a highway was stabilized by excavating the moving mass in a series of benches and recompacting the soil with improved drainage (Holtz and Schuster, 1996).

Advantages: Benches improve maintenance access (you can inspect drains, vegetation, etc., from the benches) and reduce erosion velocity of runoff.

Disadvantages: Bench construction can be extensive and may require more excavation volume than a simple flattening. Also, if not properly drained, benches can accumulate water and add weight - thus they must be graded to drain out and not become seepage zones. If benches are too narrow or too few, their benefit is limited; design guidelines often specify bench width and spacing for given slope heights (Collin et al., 2005).

Figure 2.37 outlines various geometric slope stabilization techniques.

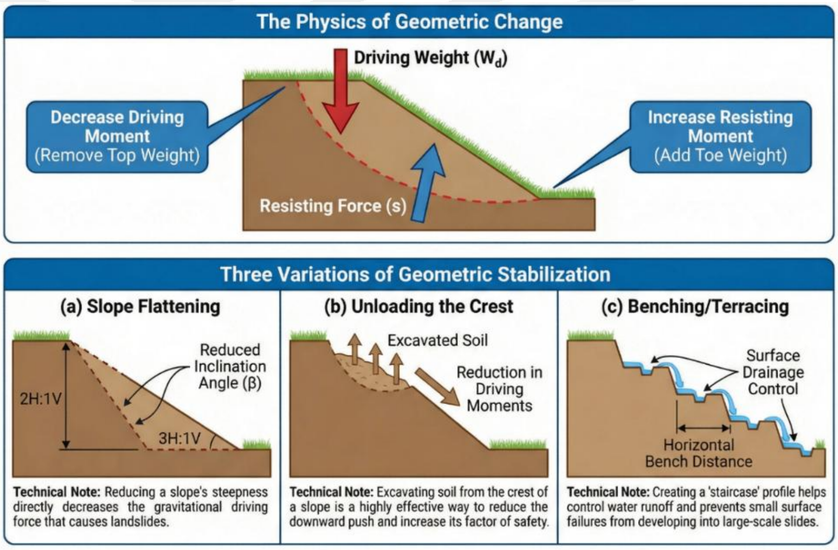

Key Comparison Table

Method	Primary Benefit	Mechanism
Slope Flattening	Decreases Gravitational Driving Force	Reduces inclination angle (β) to balance forces.
Crest Unloading	Reduces Downward Push & Increases Factor of Safety	Removes weight from the top to lessen driving moments.
Benching/Terracing	Controls Water Runoff & Prevents Small Failures	Creates a "staircase" profile to manage water and reduce slope length.

Figure 2.37. *Schematic representation of geometric slope stabilization methods: (a) slope flattening to reduce the inclination angle, (b) unloading the crest to reduce driving moments, and (c) benching to control surface drainage and reduce effective slope length (Abramson et al., 2002)*

Removal and replacement of failed material

When a slope has already failed or contains a distinct weak layer, a reliable solution is removal and replacement that is, excavating the unstable soil or rock and replacing it with stronger material (or compacting the in-situ material if possible). By removing the failed mass, you eliminate the driving block that was driving the landslide. Replacing it with competent fill (free-draining granular fill, engineered compacted soil, or even rock fill) then creates a stable configuration that can support the slope. This method essentially treats the problem by excavating out the failure surface. It is commonly used for relatively shallow failures (depth of a few meters), such as small slides on road cuts or slumps on embankment slopes.

Usage scenarios: Highway maintenance crews frequently employ this fix - they "dig out" a landslide and rebuild the slope. For example, if a 3 m deep rotational slip occurs on a roadway embankment, the repair might involve digging out the slipped clay, installing a geotextile or drain at the base, and then rebuilding with compacted gravel or well-compacted fill.

This was the approach in many small slope "pop-out" repairs on highways, as noted by Holtz and Schuster (1996) contractors would excavate the failed zone and refill it during construction or maintenance (Holtz and Schuster, 1996). The method has also been used on larger scales: for instance, the ancient landslide at Cucumaco in Honduras (case described by Abramson et al., 2002) was stabilized by excavating a portion of the landslide debris and replacing it with an engineered fill buttress.

Applicable failure types: Best suited for shallow rotational slips or planar failures where the weak material is near the surface and removable. In deep-seated failures, complete removal is usually infeasible, but partial removal of the head combined with replacement at the toe can be done.

Advantages: This method results in essentially a "reset" of the slope with known material properties - the new fill can be compacted to high strength, and often a drainage layer is added at the interface to prevent pore pressure buildup. It also permanently removes the problematic soil (e.g. highly plastic clay or loose colluvium) that may have been predisposed to fail.

Limitations: The removal itself can temporarily destabilize the slope further careful construction staging is needed so that the slope is not left unsupported for long. It can also be costly and time-consuming if large volumes are involved, especially if hauling material off-site is required. Environmental disturbance is another consideration (large excavation can scar the landscape). Additionally, a reliable source of good replacement material is needed; if poor fill is used, the problem may recur.

In one notable case in England, a reactivated landslide was repaired by recompacting the landslide debris itself after mixing in lime and reinforcing geogrids (Boynton and Blacklock, 1985). This innovative approach saved cost by reusing site material: lime treatment improved the soil strength, and geogrids provided reinforcement, leading to a stable slope without importing large quantities of new fill (Boynton and Blacklock, 1985).

2.4.1.3. Buttressing and reinforced fills

When removing material is not sufficient or feasible, the opposite approach can be taken: adding material to key parts of the slope to stabilize it. A buttress is an engineered fill placed typically at the toe of a slope (or sometimes mid-slope) to provide additional weight and resistance against sliding. Similarly, counterweight fills or toe berms are embankments constructed to press against the foot of a landslide, counteracting the outward movement. Buttressing falls under the concept of increasing resisting forces - by placing a heavy, stable mass of earth in the path of the potential failure, the slope's shear resistance is improved (Holtz and Schuster, 1996). Figure 2.38 details the mechanics and interaction involved in stabilization via a rockfill toe buttress.

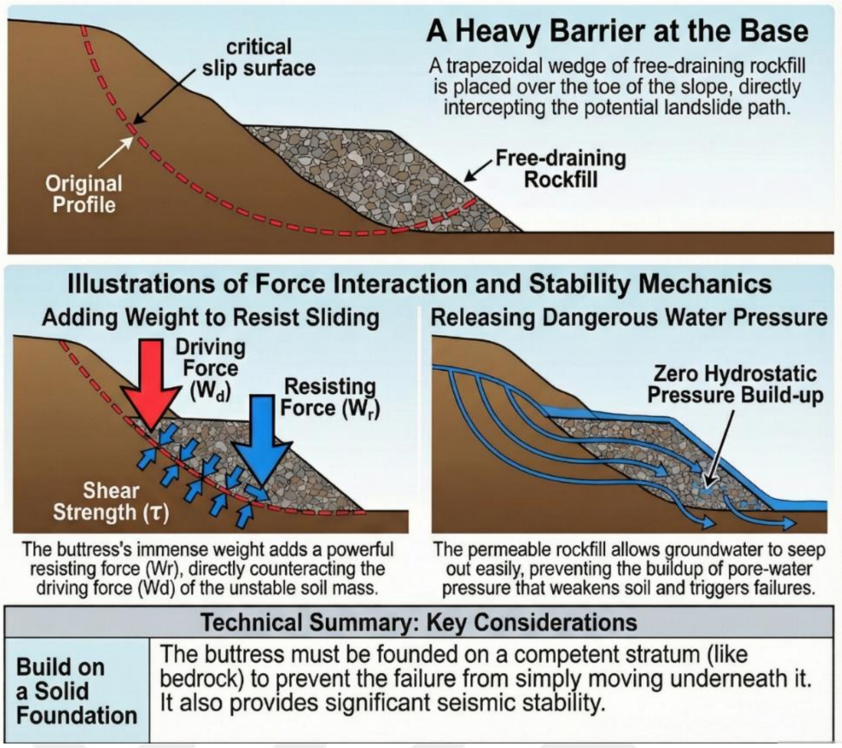

Figure 2.38. *Stabilization via rockfill toe buttress: mechanics and interaction (Cornforth, 2005)*

This method is particularly effective for deep-seated rotational failures or large landslide masses where a strong resisting force at the toe will prevent the slide from propagating. It can also help translational slides by providing a physical block at the toe. Buttresses are considered semi-structural but generally use simple materials (soil, rock) rather than concrete or steel, so they are often moderate in cost compared to built retaining walls.

Earth buttresses and toe berms

The principle behind an earth buttress or toe berm is to place sufficient additional weight at the slope's toe such that the downslope movement is resisted by the buttress's weight and strength (Holtz and Schuster, 1996). Essentially, the buttress increases the normal force on the potential slip surface near the toe (increasing frictional resistance) and provides a counter-pressure to hold the sliding mass. Design of a buttress fill is analogous to a gravity retaining wall: it must be sized so it will not slide, overturn, or fail bearing capacity on its foundation (Holtz and Schuster, 1996).

Common construction materials for buttresses are blasted rockfill, coarse gravel, boulders, or even compacted earth materials with high shear strength and weight (Holtz and Schuster, 1996). Often, cheap or locally available materials are used; for instance, quarry rock waste or demolition rubble can become buttress fill. Buttresses are placed after some excavation of the toe area to ensure good contact with firm ground, effectively creating a new, stable toe. Counter berms are essentially smaller-scale buttresses, sometimes placed slightly upslope from the toe or as a series of stepped fills to incrementally stabilize a slide. The term "berm" often implies a long, extended fill along the slope, whereas "buttress" might be a shorter, more targeted fill but the mechanism is the same. Usage: Buttresses are commonly employed in large landslide remediation where other solutions are too costly or impractical.

An example is a landslide in southern Colorado that was stabilized by constructing a rockfill buttress at the toe - the added weight provided the needed resisting force and stopped the movement (Holtz and Schuster, 1996). Millet et al. (1992) describe a very large buttress (nearly 500,000 m3 of granular material) built to stabilize a massive landslide threatening the Tablachaca hydroelectric dam in Peru (Millet et al., 1992). The buttress in that case was designed to be heavy enough to prevent any further sliding of the enormous mass. On a smaller scale, toe berms are often used by highway departments to fix slumps: for instance, Kropp and Thomas (1992) used buttress fills to successfully stabilize an active landslide in California (Kropp and Thomas, 1992). In the U.K., Edil (1992) reported using a terraced counter-berm made of crushed concrete debris to shore up an unstable slope along Lake Michigan (Edil, 1992), showcasing how waste materials can be repurposed as effective stabilization fills.

Counter-dams

Counter-dams are used to increase slope strength by cutting material from the slope's convex top and placing it at the toe, thereby reducing the overall gradient.

Reinforced Fills

In some cases, the stability of a buttress or new fill itself can be enhanced by internal reinforcement (e.g., geogrids or geotextiles) to form a steep reinforced slope, often called a mechanically stabilized earth (MSE) berm. By reinforcing the fill, the buttress can be made steeper and use less footprint, which is useful if space at the toe is limited. While the prompt lists "reinforced fills" in this category, the concept overlaps with the "reinforced fill walls" discussed later.

Typically, when a buttress must be built on a slope but a gentle stable angle would be too large, geosynthetics or even metallic reinforcements can be layered into the fill to allow a steeper face (even near-vertical), thereby acting as a hybrid between a buttress and a retaining wall (Koerner, 2012). For example, the use of geogrid-reinforced earth was combined with lime stabilization to rebuild a failed slope in England, achieving stability with a steep profile that a purely unreinforced fill might not have allowed (Boynton and Blacklock, 1985).

Failure modes addressed: Buttresses are most suited for deep rotational failures where the critical circle passes through the toe the buttress effectively loads the toe to prevent rotation. They also counteract shallow slips if placed appropriately. However, if a failure plane is very deep (below where a practical buttress can reach) or if the buttress material is weaker than the slide mass, internal failure can occur (e.g., a buttress could shear within itself if not properly designed) (Holtz and Schuster, 1996). Engineers must check that the buttress fill is internally stable and does not slide along its base (hence sometimes keys or trench toe-in are used for buttress fills).

Advantages: Buttressing uses relatively inexpensive materials and common earthwork construction techniques (dumping, spreading fill) rather than sophisticated equipment. It can be built relatively quickly for emergency stabilization. Also, buttresses can be made aesthetically unobtrusive if contoured and vegetated.

Limitations: They require space at the downslope side. In developed areas, adding a large fill may encroach on property or streams. The weight of a buttress can also cause settlement or instability if the foundation soil is weak, so sometimes ground improvement or a stability berm is needed to support the buttress itself (Holtz and Schuster, 1996). In highly sensitive or saturated soils, the added weight must be placed carefully to avoid triggering a new failure during construction.

Despite these considerations, buttress fills remain a common and effective solution, often chosen when "stiff" structural methods (like rigid walls) are not feasible due to cost or the need to accommodate some ongoing movement.

2.4.1.4. Vegetation and bioengineering Techniques

Vegetation

The use of vegetation and bioengineering is an environmentally friendly approach to slope stabilization that harnesses the reinforcing effects of plant roots and the hydrological benefits of transpiration. Vegetation is generally a low-cost, low-impact measure suitable for shallow slope failures, erosion control, and long-term stabilization of surficial soils.

The mechanical contribution of root systems to soil stability through apparent cohesion (c_r) along a potential shear plane is illustrated in Figure 2.39.

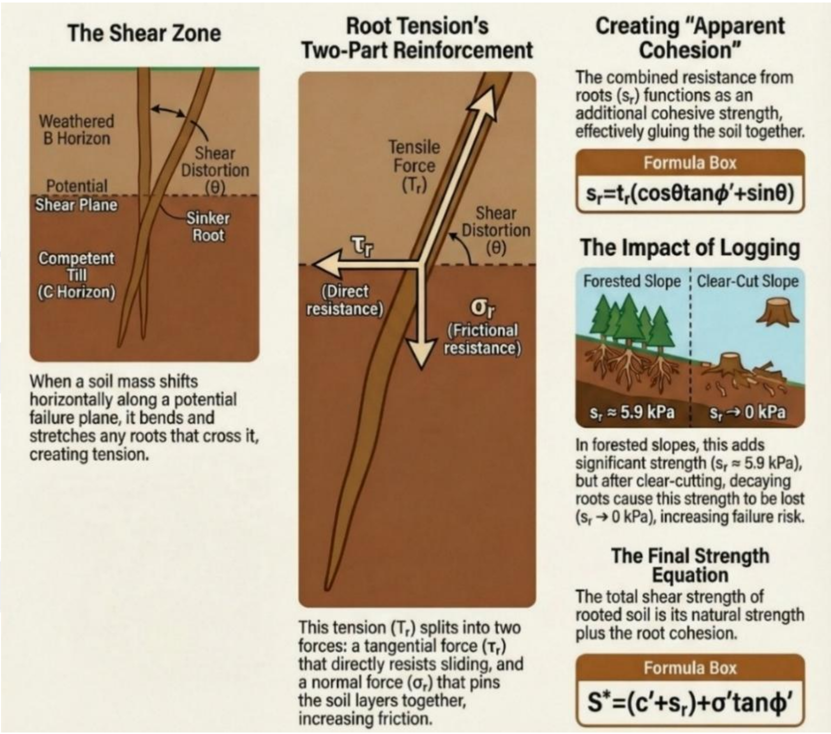

Figure 2.39. *Mechanics of root reinforcement: diagram illustrating the apparent cohesion (s_r) provided by root systems crossing a potential shear plane (Wu et al., 1979)*

The presence of plant roots can significantly increase the shear strength of near-surface soil by binding the soil matrix (akin to a natural soil reinforcement), and the canopy and root water uptake can reduce soil moisture levels, thereby lowering pore-water pressures. However, vegetation is usually supplemental to other measures for larger or immediate stability problems, as it takes time to establish and primarily influences the shallow soil zone (often the top 1-3 meters).

Principles of effectiveness: The stabilizing influence of vegetation occurs through two main mechanisms: root reinforcement and hydrological effects (Gray and Sotir, 1996). Roots, especially those of trees and shrubs, form an interlocking network that increases soil cohesion and anchors the soil layer to deeper substrate. This is particularly helpful against shallow rotational slips, infinite slope failures on steep hillsides, and surficial erosion or shallow debris flows. Studies have shown that densely rooted soil can have markedly higher apparent cohesion than bare soil for example, Wu et al. (1979) quantified how tree roots in silty clay contributed additional cohesion that raised slope stability in the Appalachians.

Meanwhile, vegetation also affects slope hydrology: plant foliage intercepts rainfall, reducing the direct erosive impact and infiltration, and root uptake (transpiration) depletes soil water, which can lower the groundwater table or at least reduce periods of saturation after storms (Wu et al., 1979). This reduction in pore pressure increases the soil's shear strength (since effective stress is higher in drier soil). In essence, plants act as natural pumps and reinforcements. Grasses and groundcovers mainly aid in erosion control and shallow binding, whereas deep-rooted species (trees, shrubs, certain vetiver grasses) can penetrate to the failure plane of shallow slides and provide mechanical stabilization.

Applicable failure types: Vegetative stabilization is most effective for shallow failures and erosion. Typical scenarios include: cut-and-fill slopes along highways that experience surficial sloughs or raveling; steep natural slopes in clay or silt that are marginally stable and prone to shallow landslides in wet seasons; embankment slopes where shallow slips occur due to surface water. Vegetation is a key component in controlling infinite slope failures in colluvial soils on hills (common in tropical regions where root mat depth correlates with slide depth). However, vegetation alone cannot stabilize deep-seated landslides or large rotational failures that extend beyond the root zone those require engineering interventions, though vegetation can be used as a complementary measure to improve surficial stability and reduce erosion after engineering works are completed.

Bioengineering techniques

Beyond simply planting grass or trees, civil engineers have developed specific bioengineering methods that combine live plant material with minor structures to stabilize slopes. Some examples: live staking or live poles (driving live willow or other quick-rooting cuttings into the slope, which sprout and root to bind the soil), brush layering (alternating layers of plant cuttings and soil in a regraded slope, which creates a reinforced slope as roots grow), root wads and vegetated geogrids (using live woody debris and geosynthetics seeded with plants), and vegetated crib walls (wooden crib frames filled with soil and plants) (Gray and Sotir, 1996).

These methods provide immediate physical support (from the structure) and longer-term biological reinforcement. For instance, live willow poles were used on a highway cutting in the UK (A249 Iwade scheme) to improve a clay slope's stability; the willows rooted and helped dry the slope, contributing to a measured increase in stability over time (Hiller and MacNeil, 2001). Another common application is on riverbanks or coastal slopes, where combinations of vegetation and simple structures (like coir logs or fascines) stabilize against washout.

Advantages: Vegetation solutions are cost-effective, sustainable, and provide ancillary benefits such as improved aesthetics, wildlife habitat, and erosion control. A vegetated slope can recover to a natural appearance, which is often desirable in parks, roadside landscapes, or residential areas. Unlike rigid structures, vegetation-reinforced slopes can often better accommodate small movements roots can stretch or new roots can grow if minor slope adjustments occur, giving a form of flexible reinforcement. Also, vegetation can improve slope resilience by continuous regeneration (e.g., even if some plants die, others can grow, maintaining some level of root reinforcement).

Limitations: There are important limitations. Vegetation typically requires a suitable climate and maintenance (irrigation during establishment, protection from grazing, etc.). In arid or cold regions, or on very steep rocky slopes, establishing vegetation dense enough for meaningful reinforcement can be challenging. Moreover, there can be a trade-off: plants need moisture to survive, yet engineering wants the soil to be dry for stability (Gray and Sotir, 1996). Poorly planned planting can sometimes retain unwelcome moisture in slopes (e.g., irrigation or watering of ornamental plantings on a slope can trigger failures a known problem in residential hillside areas).

Root penetration is finite large deep failures are beyond the reach of most plants. Additionally, during the time vegetation is growing, the slope might remain vulnerable; it could take several seasons for roots to develop the desired strength gains. Therefore, engineers often pair vegetation with structural measures (e.g., hydroseeding over a geotechnically stabilized slope) for immediate and long-term benefit.

Case Studies: Many case studies demonstrate the value of vegetation on slopes. In Hong Kong, a region with heavy rains, the government mandates greening of man-made slopes, and studies have shown that a cover of grass and shrubs significantly reduces erosion and shallow slippage on these slopes over decades (Geotechnical Control Office, 1984). In the Pacific Northwest, timber harvest and forest clearing have long been associated with increased shallow landsliding because of reduced root reinforcement (Sidle et al., 1985; Montgomery et al., 2000). On roadside cut and fill slopes, revegetation with deep-rooted shrubs and trees is used as a stabilization measure (Landis et al., 2005; Forbes and Broadhead, 2013).

The Oregon Department of Transportation successfully used willow staking and seeding on a regraded landslide slope, finding that the areas with established vegetation had far fewer erosion gullies and no shallow slumps compared to adjacent bare regraded areas (Gray and Sotir, 1996). As another example, in Nepal and Malaysia, vetiver grass (with very deep root systems) has been planted on steep embankments to prevent rainfall-induced slips; results showed improved slope stability and reduced maintenance costs (Greenwood et al., 2004). These cases illustrate that while vegetation may not solve major instabilities alone, it is a potent tool in the slope stabilization arsenal for minor to moderate issues and for enhancing other measures.

2.4.2. Conventional structural methods

Structural stabilization refers to the use of engineered structures (typically made of concrete, steel, masonry, or composites) to physically retain or reinforce a slope. These methods are generally higher in cost and complexity but are indispensable when passive measures (like drainage or regrading) are insufficient (Hausmann, 1990). Structural solutions are often used in constrained sites (where there's no room to flatten the slope or add a buttress) or when dealing with higher or steeper slopes and larger failure masses.

Broadly, structural techniques can be divided into two categories: externally stabilizing systems (structures that hold the slope from the outside, such as retaining walls or piles acting as barriers) and internally stabilizing systems (reinforcement installed within the slope mass, such as soil nailing or geogrids, which strengthen the slope from within) (Holtz and Schuster, 1996). In many cases, modern slope stabilization uses a combination of both: for example, a retaining wall (external support) anchored with tie-backs (internal reinforcement).

One key consideration is that rigid structural elements typically cannot tolerate large deformations - they work best when slopes are prevented from moving in the first place, or when only small movements occur (Holtz and Schuster, 1996). Thus, for actively creeping landslides, structural measures might need to be very robust or combined with ground improvement to reduce movement.

Below, the main structural methods are discussed, including retaining walls (of various types), gabion walls, reinforced soil walls, anchors and rock bolts, piles and micropiles, sheet pile walls, and soil nailing. Geosynthetics (geotextiles, geogrids, geocells) are also covered here, as they often serve a structural reinforcement role in slopes.

2.4.2.1. Retaining walls

Retaining walls are structures built at the toe or cut face of a slope to retain the earth behind them, essentially providing an external resisting force to counteract the tendency of the soil to slip or collapse. They are one of the oldest forms of slope stabilization. There are various types of retaining walls, but three common categories are: gravity walls, cantilever walls, and anchored walls (Das, 2010). These structural profiles are featured in Figure 2.40.

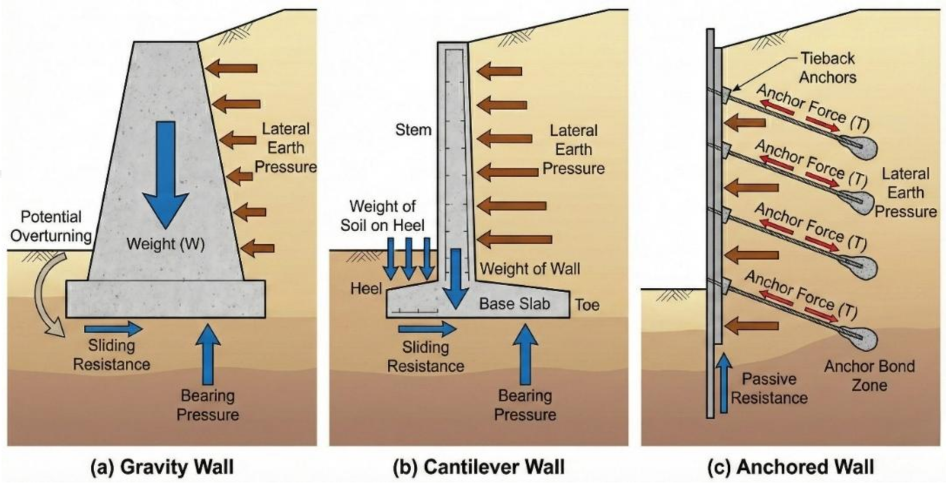

Figure 2.40. *Comparative cross-sections of common retaining wall types: (a) Gravity Wall, (b) Cantilever Wall, and (c) Anchored Wall, illustrating load transfer mechanisms (Das, 2010)*

Gravity walls

Gravity walls resist earth pressures predominantly by their own weight. Classic examples are mass concrete walls, masonry block walls, or crib walls (interlocking concrete or timber units filled with soil or rock). These walls are thick and heavy, usually leaning into the slope. They are suitable for relatively low to medium heights (say up to 3-6 m typically for unreinforced gravity walls) and are often used along roads and property boundaries where minor slopes need support.

Example: A stone gravity wall 4 m high might be used to stabilize the toe of a cut slope along a roadway, preventing small slides from reaching the road. Gravity walls can also include gabion walls (discussed separately below) which function on the gravity principle.

Cost/complexity: Gravity walls use a lot of material, which can be costly, but they are relatively simple to construct (stacking blocks or pouring concrete). They can tolerate some deformation (e.g., rock-filled cribs have some flex). A limitation is that for high walls, the base becomes very wide if relying purely on self-weight (Clayton et al., 1993).

Cantilever walls

Cantilever walls are usually made of reinforced concrete (or sometimes steel) in an L- or T-shaped cross-section. The wall has a thin stem and a base slab; the weight of backfill on the heel of the base slab provides stability against overturning. These walls leverage structural bending resistance - the stem acts like a vertical cantilever beam fixed at the base (Das, 2010). Cantilever RC walls were a workhorse of highway projects in the mid-20th century for supporting cuts and fills up to about 8-10 m high. They use less material than gravity walls but require good engineering design and skilled construction (formwork, steel reinforcement). They are generally stiff; thus, the backfill must be properly drained to avoid undue pressure. For slopes, cantilever walls are often placed at the toe of an unstable slope to hold it in place. Example: A 6 m high cantilever wall might be built to support the bottom of a landslide-prone slope adjacent to a building.

Limitations: Large cantilever walls can be expensive and need a stable foundation. They are not very tolerant of differential settlement or large ground movement failure can occur if the toe footing shifts. In earthquake-prone areas or on yielding ground, cantilever walls may need anchors or a relieving platform.

Anchored (tie-back) walls

Anchored (tie-back) walls are retaining walls (which could be gravity or cantilever type in section) that are additionally tied into the slope with anchors, usually steel tendons grouted into stable ground behind the failure zone (Berg et al., 2009). By anchoring, the wall's capacity is greatly increased without making it massive. Anchored walls can be constructed in situ, such as a sheet pile or soldier pile wall that is then tied back with prestressed anchors at intervals. Or they can be pre-built concrete walls that are later anchored. Usage: Anchored walls are common for high excavation supports (10-20+ m deep excavations) and for steep slope stabilization where a high wall is needed but a gravity/cantilever alone would be impractical (Berg et al., 2009).

For landslides, anchored walls have been used at the toe of large slides in combination with berms. For instance, at the Tablachaca Dam site in Peru, tie-back anchors were installed in a concrete retaining wall as part of the stabilization of a large landslide (in conjunction with a buttress fill) (Millet et al., 1992). Anchored walls can also be used mid-slope - sometimes a series of smaller anchored walls in steps can terrace a slope. Complexity/cost: High - anchor drilling and tensioning require specialized equipment and careful quality control. But they enable solutions that otherwise would not be possible (like holding back very deep soil pressures). Table 2.15 presents a comparative summary of various retaining wall systems used for slope stabilization, specifically detailing their respective height limitations and mechanical stabilization mechanisms.

Table 2.15. *Comparative summary of retaining wall systems for slope stabilization, detailing height limitations and stabilization mechanisms (Berg et al,. 2009; Holtz and Schuster, 1996)*

Wall Type	**Typical Height Limit (m)**	**Stabilization Mechanism**	**Primary Application**
Gravity (Concrete / Crib)	3–6 m	Dead weight resists overturning and sliding.	Toe support for small cuts; highway widening projects.
Cantilever (Reinforced Concrete)	6–10 m	Structural bending resistance; weight of backfill on heel adds stability.	Medium-height cut slopes; urban areas with space constraints.
Anchored (Tieback)	> 20 m	High-strength steel tendons transfer lateral load to a stable zone.	Deep excavations; landslide remediation; very high slopes.
Gabion	4–8 m	Gravity-based support; flexible wire mesh baskets filled with rock.	Erosion control; wet slopes (high permeability).

Selection of wall type depends on site-specific geotechnical conditions, available space, and economic feasibility. Height limits are indicative for preliminary design and may vary based on soil parameters and structural engineering.

Applicable failure modes: Retaining walls address primarily shallow to moderate depth failures where a defined slope face or toe needs support. A retaining wall essentially increases the resisting force at the foot of a potential failure. For a rotational slide, a wall at the toe can prevent the toe from kicking out and thus support the slide mass. For a translational failure on a planar surface, a properly founded wall can buttress the sliding layer. However, if the failure plane is deep-seated (well below the bottom of the wall), then a wall on the surface has limited effect the failure might occur beneath and behind it. In such cases, deep foundations or anchors would be needed to engage the stable layer. Retaining walls are not typically used for flow failures or very deep landslides due to scale; those require other measures. They are very effective for containing rockfall and wedge failures in rock slopes e.g., a crib wall at the base of a rocky slope can catch falling blocks and prevent toe erosion that could trigger a larger wedge slide.

Advantages: Walls provide immediate and clear support; they can be designed to exact requirements and give a sense of security. They also can be constructed in relatively tight spaces (especially tied-back or cantilever walls) without need for large footprints, which is crucial in urban or roadside sites. Modern design methods (e.g., using geotechnical finite element analysis or limit equilibrium with groundwater pressure considered) allow fairly optimized and safe wall solutions.

Drawbacks: As noted, stiff walls cannot accommodate large movements if a landslide is moving inches per year, a rigid wall might crack or tilt unless it's heavily anchored. Walls also often require drainage behind them to avoid water pressure build-up (weeping holes, drainage blankets), which adds maintenance needs. Cost is a major factor: tall retaining walls, especially with anchors, can be among the most expensive slope fixes per unit length. They can also be visually intrusive, though aesthetics can be improved (e.g., textured finishes, terraced walls with planters).

Gabion walls

Gabion walls are a specific type of gravity retaining wall constructed from gabions - rectangular wire mesh baskets filled with stones or rock. They are a flexible, permeable, and often cost-effective solution for supporting slopes and preventing erosion (Hausmann, 1990). Gabion walls rely on the weight of the stone fill to resist sliding and overturning, similar to a conventional gravity wall, but they differ in that the gabion structure can deform slightly without losing integrity, and water can drain through them, relieving hydrostatic pressure naturally.

Usage scenarios: Gabions are widely used along highway embankments, riverbanks, and landslide repairs where moderate wall heights (typically up to 5-6 m, though multiple tiers can go higher) are needed. For example, along a road cut in a hilly area, if a section of slope fails, a common repair is to excavate the failed material and then build a gabion retaining wall at the toe to support the slope above while reconstructing the roadway platform. Gabions have been used in mountainous areas for landslide stabilization as well - in Nepal and India, stepped gabion check walls are often built to stabilize road cut slopes that frequently slip in monsoon rains. Because gabions are permeable, they suit slopes with seepage; water can exit through the wall instead of building pressure behind it (Holtz and Schuster, 1996; Abramson et al., 2002).

Applicable failure modes: Similar to other retaining walls, gabions address shallow to medium-depth failures, by buttressing the toe. They are not meant for deep landslide stabilization on their own. They excel in conditions of erosional failures or undercutting (like stream bank sloughing) because they both retain soil and protect against erosion. Gabions also perform well for slopes that undergo repeated small failures - the flexible nature means even if minor settlement or movement happens, the gabion structure can conform without collapsing (unlike a rigid concrete wall which might crack).

Advantages: Gabion walls are relatively low-cost because they use simple materials (often on-site rock fill can be used if it's durable enough) and labor that does not require highly skilled trades (workers fill and lace the baskets, which is labor-intensive but straightforward). They require less foundation preparation than concrete walls a simple leveled gravel base is often enough because their flexibility tolerates minor differential settlement. They also integrate well with the environment: vegetation can grow in the gaps between rocks, making the wall more visually appealing over time and even stronger as roots bind it. Their permeability eliminates the need for dedicated weep holes or extensive backdrains.

Disadvantages: The lifespan of gabions depends on the durability of the wire mesh in corrosive environments, the galvanized coating can deteriorate and baskets can fail after some decades (PVC-coated or stainless-steel mesh can mitigate this). If water flow is too great, they can be susceptible to internal erosion if fine particles wash out from behind (filter fabric backing is often used to prevent this). Gabions are not suitable for extremely high walls unless engineered in multiple tiers with geogrid tie-backs, which complicates design. Aesthetic acceptance can vary some consider them unsightly rock cages, though newer designs and plantings help. Structurally, one must ensure the base row of gabions is well-anchored and the toe is protected from scour or being pushed out, as failure of the bottom units would destabilize the wall.

Case examples: In Italy's Amalfi Coast, where small landslides occur on road cuts, gabion walls are frequently built to quickly restore slope support; they have performed well under moderate slides and even seismic shaking due to their flexibility (Agostini et al., 1987). In Washington State (USA), a 4-tier gabion wall system was used to stabilize a 12 m high riverbank that was sliding it stabilized the bank and also served as a permanent erosion control measure (Holtz and Schuster, 1996). Many national parks use gabions for slope stabilization to maintain a "natural" look compared to concrete.

2.4.2.2. Reinforced fill walls (mechanically stabilized earth)

Reinforced fill walls, also known as Mechanically Stabilized Earth (MSE) walls or reinforced soil slopes, are structures where soil is reinforced internally by layers of tensile materials (like steel strips, geogrids, or geotextiles) to create a coherent gravity mass that can retain the slope or embankment behind it. Unlike a conventional retaining wall which is a separate structure holding back soil, an MSE wall's strength comes from the composite action of the soil and reinforcements together. These systems have become very popular since the 1970s due to their cost-effectiveness and versatility. They can be built as vertical walls (with facing panels or wrapped geotextile) or as steepened slopes (e.g. 70° slope face with vegetation) (Berg et al., 2009; Holtz and Schuster, 1996; Vidal, 1969).

Components: A typical reinforced fill wall has alternating layers of compacted fill and reinforcement (steel strip or polymer geogrid) placed horizontal into the fill. At the face, there may be precast concrete facing panels (common in Reinforced Earth™ walls), wire mesh facing (with erosion control mats), or wrapped geotextile that eventually is covered with vegetation. The reinforcements tie the soil together and extend deep into the backfill, such that the active pressure that would normally cause failure is resisted by tension in the reinforcements which anchor into the stable part of the soil block. Effectively, the failure surface is forced to develop a larger, deeper arc that has to pull out all those reinforcements, which is made sufficiently difficult by design (Berg et al., 2009; Holtz and Schuster, 1996).

Usage scenarios: Reinforced soil walls are widely used for highway embankments, bridge abutments, and road cut widening where a near-vertical slope is needed but a conventional concrete wall is too expensive (Berg et al., 2009; Holtz and Schuster, 1996). They are also used to rebuild failed slopes by constructing an MSE buttress. For example, if a landslide took out part of a road embankment, engineers might reconstruct that section using geogrid layers in compacted fill, producing a stable 80∘ slope that replaces the failed mass. Reinforced slopes can reach considerable heights (over 30 m in some projects) when properly designed. A famous early application was the repair of a large landslide on Interstate 70 in Oregon in the 1980s: lightweight fill combined with geogrid reinforcement was used to rebuild the slope with a steep face, avoiding further failure (Holtz and Schuster, 1996). Another example: in Nice, France, the airport extension was built on MSE walls into the sea about 15 m high (Holtz and Schuster, 1996).

Applicable failure modes: MSE walls primarily address fill slope stability issues they are ideal for preventing or repairing failures of an embankment by essentially building a new internally strong embankment. They can also help stabilize the toe of a landslide (acting as a weighted buttress, but lighter because of reinforcement or even using light fill). Reinforced soil technology is best for rotational failures in that it increases the internal shear strength of the soil mass (so the factor of safety against circular slips is raised). They have been used in seismic areas with success, as the flexible nature can withstand quake-induced strains better than rigid walls (Elias and Juran, 1991). However, like other toe solutions, if the failure plane in an existing landslide is deep and passes under the bottom of an MSE wall, the wall could slide as a whole unit, so usually MSE repairs are combined with other measures (like deep drainage or a key into bedrock at the toe) (Berg et al., 2009; Holtz and Schuster, 1996; Elias and Juran, 1991).

Advantages: MSE walls are cost-effective, often 20-50% cheaper than an equivalent concrete retaining wall for the same height (especially for heights above 3-4 m) (Elias and Juran, 1991). They use simple construction techniques (layered filling and compaction) and can tolerate differential settlement without structural distress (the facing might deform slightly but not fail). They also allow for greener and more aesthetic finishes - e.g., vegetated reinforced slopes blend into the environment. Many agencies have standardized design methods for MSE (e.g., FHWA guidelines) making their design and approval relatively straightforward (Berg et al., 2009).

Limitations: They require good quality backfill (typically granular fill with certain gradation and friction angle) for optimal performance; using poor soils can reduce effectiveness. Water management is critical - while they handle some movement, saturation can cause internal pore pressure and reduce the pullout resistance of reinforcements. Therefore, drainage layers or toe drains are needed. Reinforcement corrosion (for steel strips) or durability (polymer geogrids can creep over time or be damaged by ultraviolet during construction) must be addressed by choosing the right material and protective coatings. Very steep MSE slopes (>70°) need facing elements to hold the face during construction and control erosion. There is also a height limit beyond which design gets very conservative due to compound failure surfaces (though this limit is quite high, e.g.>30 m) (Berg et al., 2009; Holtz and Schuster, 1996).

Case studies: The Reinforced Earth Company (Vidal's system) has documented hundreds of successful projects worldwide (Holtz and Schuster, 1996; Vidal, 1969). One classic case was the Rainier Avenue landslide repair in Seattle, where a 9 m high failed slope threatening homes was stabilized by an 8 m tall geogrid-reinforced wall combined with surface drainage; this prevented further movement and was landscaped nicely (Walker, 1987). In India, geogrid-reinforced retaining walls have been used to protect mountain highways from landslides, such as on NH-22 in the Himalayas after installation, slopes survived monsoon rains that previously caused slips. These examples highlight that reinforced fill walls are a mainstream solution in modern slope engineering (Chaturvedi and Dutt, 2015).

2.4.2.3. Anchors and rock bolts

Anchors and rock bolts are long rod or tendon systems grouted or driven into the ground to tie unstable slope material to deeper stable strata. They work in tension (and sometimes shear) to provide internal stabilization of a rock mass or soil slope. While retaining walls and buttresses fight the slide from outside, anchors go into the slide to hold it together or pin it down. Rock bolts typically refer to shorter, untensioned or lightly tensioned bars used mostly in rock engineering for example, steel rods 2 to 6 m long installed in a rock face to secure loose blocks or increase the coherence of jointed rock.

They often work by creating friction or mechanical interlock (with expansion shells or resin grout) across rock discontinuities. Anchors (or tie-back anchors) usually refer to longer, actively tensioned tendons (steel strands or bars) that are anchored in a stable formation and stressed to apply a clamping force. In soil, these might be called soil anchors or ground anchors. The distinction can blur, but generally anchors are high-capacity, post-tensioned elements, whereas rock bolts are passive or locally tensioned elements (Holtz and Schuster, 1996; Littlejohn and Bruce, 1977; Sabatini et al., 1999).

In ground conditions characterized by collapsing boreholes or running ground—specifically within saturated mélange formations—traditional anchor installation methods often prove unfeasible. Consequently, stabilization designs frequently adopt Self-Drilling Anchors (IBO). This technology utilizes a hollow bar equipped with a sacrificial drill bit, allowing drilling, flushing, and grouting to be performed in a single operation without casing removal (FHWA, 2015). The grout acts as both the flushing medium and the bonding agent, ensuring continuous ground contact and immediate stabilization of the borehole wall, which is critical for the rapid reinforcement of unstable slopes. Figure 2.41 frames these load mechanisms.

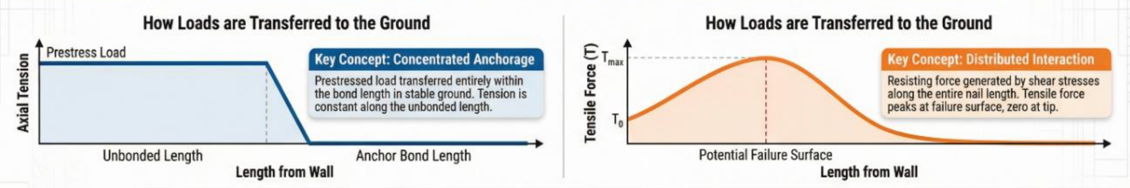

	Active Ground Anchor	Passive Soil Nail
Load Status	**Active:** Prestressed to 75-100% of design load before soil movement.	**Passive:** Load is developed only as the soil deforms.
Unbonded Length	**Required:** A specific unbonded length is critical to transfer load to stable ground.	**None:** The nail is fully bonded along its entire length to reinforce the soil mass.
Construction	**Flexible;** can be installed "Top-down" or "Bottom-up".	**Strictly** "Top-down" in sequential excavation lifts.
Testing	**100% Tested:** Every production anchor is performance-tested to verify its load capacity.	**~5% Tested:** Typically only a small fraction of production nails are tested.

Figure 2.41. *Conceptual comparison of load transfer mechanisms in (a) Pre-stressed ground anchors (active) and (b) Soil nails (passive) (Post-Tensioning Institute [PTI], 2004; British Standards Institution, 2018; Sabatini et al., 1999; Lazarte et al., 2015; Porterfield et al., 1994)*

Usage scenarios: Anchors and bolts are extremely versatile and used in both rock and soil slopes:

- In rock slopes, rock bolts are a standard solution for stabilizing potentially unstable blocks and wedges. By bolting, one can prevent wedges defined by intersecting joints from sliding out, effectively creating a reinforced rock mass that acts monolithically. For example, in highway rock cuts or tunnel portals, patterns of rock bolts (often with mesh and shotcrete on the surface) are used to stabilize the face.

- In soil slopes or weathered rock, longer ground anchors can be installed from the surface, typically inclined downward and anchored beyond the slip surface, to hold a slide in place. These might be used where a retaining wall alone is insufficient or where one wants to avoid a large wall. An anchored system often includes a waler beam or facing at the surface to distribute the load of multiple anchors along the slope face.
- Anchors are also used in conjunction with retaining walls (as discussed earlier) - effectively converting them into anchored walls or with shear piles (anchoring piles to add capacity) (Holtz and Schuster, 1996; Sabatini et al., 1999).

Applicable failure types: Anchors and bolts are especially useful for planar or wedge failures in rock (e.g. tying a potentially sliding rock wedge to the stable rock behind it). For soil, they can help stabilize translational slides or add resistance to rotational slides by providing extra anchoring force that counters the driving moment. One scenario is an active slide plane at, say, 10 m depth on a hillside one can drill anchors 15 m long that cross the slide plane and anchor in firm ground, then lock them off, essentially stitching the moving mass to the stable ground. They are also used to stabilize cuts where space for slope layback is limited: e.g., an excavation for a road widening where a steep temporary cut is stabilized by driven soil nails or anchors (soil nailing is covered separately, but conceptually similar to passive anchors) (Holtz and Schuster, 1996; Sabatini et al., 1999).

Case example: At the Vajont landslide site in Italy (prior to the disastrous 1963 failure), engineers had attempted to use tensioned cables (an early form of anchors) to hold the slope, but the scale was too vast for the technology then (Alonso et al., 2020; Paronuzzi et al., 2021; Müller, 1964). However, in more moderate cases, anchors have prevented failures. In Japan, large active landslides in volcanic soil have been stabilized by installing dozens of long anchors in a grid pattern through the moving layer into bedrock, coupled with drainage - drastically slowing or halting movements (Holtz and Schuster, 1996; Japan Landslide Society, 2008). In Hong Kong, rock bolts are used on virtually every engineered rock slope; a notable case was the stabilization of a 60 m high cut slope in hard granite where 20 m long rock anchors were installed to secure a large potential wedge that could have impacted a housing development - the anchors have performed through heavy rains and the slope stayed intact (Wyllie and Norrish, 1996).

Design and function: Anchors are designed to have a "free length" (unbonded length that stretches elastically) and a "bond length" (grouted length in the stable zone). They are tensioned to a specified load, thereby applying a compressive force to the slope mass via the anchor head/plate at the surface. This counters part of the destabilizing force. Rock bolts, if untensioned (sometimes called dowels), act once movement begins, they resist by developing tension as the rock tries to move. Tensioned rock bolts (common in mines) actively clamp joints (Sabatini et al., 1999).

Advantages: Anchors and bolts can stabilize slopes without large visible structures, maintaining a natural appearance (especially if the heads are buried or shotcreted over). They can target specific unstable elements (like a particular rock block) precisely. In many cases, they are the only feasible solution for very steep or vertical slopes where you cannot place a buttress or wall. They also have the advantage of being installable from the top or accessible side of a slope, which in some emergencies is critical (you can act without having to excavate the slide) (Holtz and Schuster, 1996).

Limitations: The need for strong stable material for anchorage is crucial - if the ground behind the slide is weak or the rock is heavily fractured, the anchors may not hold (pullout failure or creep can occur). Installation requires drilling, which can be challenging in hard rock or great depths, and alignment control is needed to ensure anchors intercept the right zone. Anchors can be prone to corrosion if not properly protected (especially steel in aggressive ground; modern practice uses epoxy-coated or encapsulated strands). Over time, tensioned anchors can lose load due to stress relaxation or ground deformation, so periodic testing or re-tensioning might be needed (permanent anchors are often designed with lock-off loads and corrosion protection for 50+ year life). Cost is moderate to high per anchor, and a pattern of many anchors might be needed, adding up cost (Littlejohn and Bruce, 1977; Sabatini et al., 1999).

Innovations: In rock, newer technologies like self-drilling hollow bar anchors can speed up installation (the bar itself serves as the drill rod and then stays in place as the bolt). There are also fiber-reinforced polymer rock bolts being tested to avoid corrosion issues. For soil anchors, there are "smart anchors" with load monitoring. An emerging variant is the helical anchor (screw anchors) for shallow slides - they can be screwed into the ground without grout, providing resistance via helices - used for temporary works or to stabilize failing road shoulders with relatively small equipment (helical piles were noted in some DOT literature as quick fixes for shallow slope failures) (Wyllie, 2018).

Overall, anchors and rock bolts provide a means to actively stabilize a slope from within, and when combined with other methods (drainage, modest grading), they can bring a factor of safety above 1.0 for slopes that otherwise would keep moving.

2.4.2.4. Piles and micropiles

Piles and micropiles are deep foundation elements that can be used to stabilize slopes by transferring loads to deeper, more stable layers and by providing shear resistance along a potential failure plane. When installed in a slope or along the toe, piles act as passive barriers or dowels that intercept the sliding mass, while anchored or braced pile systems can also actively hold a slope (Holtz and Schuster, 1996; Ito and Matsui, 1975).

Slope stabilization piles come in various forms:

- Large-diameter bored concrete piles (e.g., drilled shafts up to 1-2 m in diameter) installed in a row along the slope toe or within the slope.
- Driven piles (steel H-piles, pipe piles) driven into the ground in a closely spaced row.
- Micropiles, which are small-diameter (typically 100-300 mm) drilled, grouted piles with steel reinforcement, installed in arrays. These can be vertical or inclined.
- Secant or tangent pile walls, where overlapping drilled shafts create a continuous rigid wall in the ground.

Pile and anchor hybrids, where piles are additionally tied back with anchors for more capacity Cornforth (2005).

Mechanism: Piles increase stability by increasing the shear resistance that a sliding soil mass must overcome. As the landslide pushes against the piles, the shear strength and bending resistance of the pile element itself are mobilized to bridge the weak layer, transferring the load down to a firm stratum. If long enough, the bottom of the pile is in firm ground and provides an anchor. Pile rows can also function as retaining systems if there's an exposed height (like a drilled soldier pile wall supporting a cut). In contrast, micropiles often work in groups or networks to reinforce a soil mass (sometimes called 'pinning' a slope); rather than relying solely on individual pile stiffness, this approach improves the overall coherence of the soil mass as the elements collectively share the load (Poulos, 1995; Bruce and Juran., 1998).

Usage scenarios: Piles are typically used when a slope is too large or too sensitive to fully excavate or grade, and other solutions (drainage, walls, etc.) might not provide enough capacity. They are common in stabilizing landslides that threaten infrastructure: for example, protecting a road on a hillside by installing a row of piles along the downslope edge of the road to prevent the road from sliding away. Another scenario is protecting buildings above a creeping slope by installing piles below the building to stop the creep. Piles have been used under dams or at dam abutments to stop movements as well. Micropiles are favored in difficult access sites or where minimal disturbance is desired (since they can be installed with relatively small drilling rigs and cause little vibration). They have been used to stabilize historic landslides in areas where heavy equipment can't easily go - by drilling a pattern of inclined micropiles into the slope to create a composite reinforced ground (Bruce and Juran, 1998; Holtz and Schuster, 1996).

Applicable failure modes: Piles can address deep rotational slides and translational slides. If a slip surface is, say, 10-15 m deep, a properly designed pile that extends a good embedment below that depth can effectively "pin" the sliding layer. For flow-type failures or very weak soils, piles may not be as effective unless used in combination with other measures, because extremely soft soils might just flow around piles (though closely spaced piles can act like a wall). Piles are also used in liquefiable slope mitigation a closely spaced grid of piles can act to stiffen the ground and prevent large deformations during earthquake liquefaction (though this is more in the realm of seismic design). For rock slopes, piles are less common (rock anchors are used instead), but sometimes piles are used to stabilize talus or debris deposits at the foot of rock slopes (Ito and Matsui, 1975; Poulos, 1995).

Design considerations: The spacing and diameter of piles are key. If spaced too far apart, the failing soil can flow between them (like "bowing" through the gaps). So analyses of pile-soil interaction are done, often using methods that model the pressure against the pile and ensure the pile can take the bending moment. Empirical and analytical solutions (e.g., Ito and Matsui method) exist to compute the stabilizing force of pile rows (Ito and Matsui, 1975). Micropiles rely on their steel core and grout to resist tension/compression; they often are used in an integrated way with a footing or beam connecting them at the top (pile cap or grid beam). There are also reticulated micropile systems (root pile systems) where many micropiles are installed at different inclinations that intersect, forming a lattice through the soil this was pioneered in Italy (the "reticulated micropile" technique) to stabilize landslides by creating a 3D mesh of mini piles through the slide mass (Holtz and Schuster, 1996; *Ito and Matsui, 1975; Poulos, 1995*).

Case studies: A classic example of slope stabilization with piles is the 1983 Landslide on I-80 (California) - a landslide threatened the highway and a row of 1 m diameter drilled shafts was constructed at the toe which arrested the slide. In Hong Kong, where slopes are steep and space limited, steel H-piles have been driven at close centers to reinforce fill slopes under buildings. The Eureka Valley landslide in California was stabilized by an array of 25 cm diameter pin piles (micropiles) in a grid pattern, significantly slowing the movement (Bruce and Juran, 1998). As a large-scale case, at the Shanhui landslide in China (a massive landslide), engineers installed over 300 micropiles along with anchors and drains as part of a stabilization plan, demonstrating the viability of micropiles for even very large slides (Bruce and Juran, 1998).

Advantages: Pile solutions can be installed incrementally, targeting the most critical section of a slope, and can work in limited right-of-way conditions (all construction is vertical downwards). They add virtually no disturbance to the overall slope shape (except some drilling spoils), so they are good for preserving the environment or existing features. They provide a firm "hard" solution that can be calculated to resist known forces, giving confidence in factor of safety. Also, piles can last a long time (especially concrete piles) with minimal maintenance (Abramson et al., 2002; Holtz and Schuster, 1996).

Limitations: The cost is usually high per unit - deep drilling or driving is expensive, and a large number of piles may be required. For example, to stabilize a 50 m wide landslide, one might need a row of piles spaced 2-3 diameters apart, meaning perhaps 20-30 piles, each maybe 15 m deep a significant investment. Construction challenges include achieving the required embedment in possibly difficult ground (boulders, hard rock) and handling drilling on slopes. Vibration from pile driving can be problematic, so drilled shafts or micropiles are often preferred in sensitive settings. There is also uncertainty in load distribution: not all piles will take equal load if the slide isn't uniform, so some factor of safety or robust design is needed to account for load concentration. Monitoring is often done via inclinometers in some piles to see how they are performing over time (Abramson et al., 2002; Poulos, 1995). In summary, piles and micropiles serve as an internal structural backbone for slopes, preventing movement by sheer physical resistance. They are a go-to solution when simpler measures cannot ensure stability, despite their higher cost.

2.4.2.5. Sheet piles

Sheet piles are interlocking steel (or occasionally vinyl or timber) sheets driven into the ground to form a continuous vertical wall or cutoff. They are commonly used for excavation shoring and waterfront retention, but in slope stabilization, sheet piles can be used to support the toe of a slope or to cut off a shallow failure plane. They represent another externally stabilizing structure, but one that is relatively thin and can be installed with low footprint (Abramson et al., 2002; Holtz and Schuster, 1996).

Usage scenarios: Sheet pile walls are typically used for shallow slope failures or erosion control. For example, along a riverbank that is slumping, steel sheet piles can be driven along the bank to both retain the bank material and prevent further scour at the toe. In highway slopes, sheet piles have been used as emergency measures: if a road embankment starts to slide, a row of sheet piles at the toe (sometimes tied back with a deadman anchor or tie-rod) can arrest the movement by holding the lower part in place. They have also been used to stabilize loose sandy slopes by effectively serving as a buried wall that the sand behind cannot easily slide past. Because sheet piles can be driven relatively quickly with the right equipment, they are useful when a rapid intervention is needed and the failure is not too deep (Abramson et al., 2002).

Depth and capacity: Sheet piles are limited by practical driving depth (usually on the order of 10-15 m for common section lengths, though splicing can go deeper). Thus, they are suitable for slides or cuts up to perhaps 5-8 m high effectively, where the failure plane can be intersected by that depth of wall. For deeper failures, sheet piles alone wouldn't reach the critical surface. However, sheet piles can be combined with anchors (an anchored sheet pile wall) to increase their moment capacity and stability for taller applications (Abramson et al., 2002).

Applicable failure modes: Best for shallow translational slides, localized slumps, or to prevent toe erosion failures. For instance, an embankment resting on soft ground that is starting to spread at the toe can be constrained by sheet piles. They are also effective at controlling groundwater in some cases: by acting as a cutoff, they can prevent water from seeping into a slope from one side (lowering pore pressures on the retained side). But usually in slope apps, drainage is still needed as water can flow around or over. In sandy coastal bluffs, sheet pile walls have been driven at the bluff toe to stop coastal slides, working both as a retaining structure and as a seawall (Holtz and Schuster, 1996).

Advantages: Sheet pile installation is relatively quick and does not require excavation of the slope (the wall is driven in). It can be done from the top or bottom of the slope if access is possible. Steel sheet piles have high strength and can be extracted later if needed (like for temporary works). They also create a continuous barrier, so they can handle conditions where soil might otherwise escape between discrete piles. For temporary stabilization (e.g., holding a slope for a season until a permanent fix), sheet piles are very handy. They also have the benefit of being both a structural support and a potential water cutoff (some use them to isolate unstable saturated zones) (Abramson et al., 2002).

Disadvantages: Driving sheet piles can cause vibrations and noise problematic near buildings or in sensitive soils (risk of liquefaction or settlement). In very hard or stony ground, driving may not reach the design depth. If the required penetration is beyond standard lengths, splicing sheets is possible but cumbersome. Also, sheet piles left in place permanently are susceptible to corrosion, especially in aggressive soils or fluctuating water tables (coatings or cathodic protection might be needed for long life). From a capacity standpoint, very high walls develop large bending moments that might require thick sections or additional anchoring beyond a certain height it's not economical to rely solely on sheet pile strength (Abramson et al., 2002).

Case example: A notable use of sheet piles for slope stabilization was in Japan along canals: to prevent canal bank failures (which are like slope failures into water), long stretches of sheet pile walls were driven, and in some cases, these were enough to prevent slides after heavy rains. In the UK, a railway embankment that was sliding into a marsh was stabilized by two rows of sheet piles (one at the toe, one set back a few meters) connected by tie rods - essentially forming a braced underground wall that held the lower part of the embankment in place; it successfully stopped the movement and allowed the railway to remain operational (Holtz and Schuster, 1996).

In summary, sheet piles provide a slender but stiff retaining element that is well-suited for halting shallow slope failures quickly, bridging the gap between simple earthworks and more involved structural solutions.

2.4.2.6. Soil nailing

Soil nailing is a technique of reinforcing an existing slope or excavation by installing closely spaced, relatively slender reinforcing elements (steel bars or similar) into the ground, typically from the exposed surface, and often in a top-down manner. It creates an in-situ reinforced soil mass that has improved stability. In essence, soil nailing turns a natural slope into a sort of internally reinforced wall by adding a grid of steel bars (nails) that act in tension to hold the soil together (Lazarte et al., 2003).

Installation: Soil nails are usually steel bars (e.g., 25-40 mm diameter rebar or threaded rod) that are inserted into drilled holes (usually inclining slightly downward for drainage) and then grouted in place. The process is top-down: one excavates or exposes a section of slope (usually a near-vertical cut a few meters high), installs nails in a pattern (say, 1.5 m apart each way), applies a temporary facing (like shotcrete) to hold the soil between nails, then proceeds to excavate further and repeat for lower sections. For an existing slope (not an excavation), the nails can be drilled from the slope face without full excavation, and then a facing is applied. The finished system often has a shotcrete or concrete veneer that also bears on plates on the nail heads, tying it all together (Elias and Juran, 1991; Lazarte et al., 2003).

Mechanism: The nails increase the shear strength of the soil by adding tensile resistance to potential failure surfaces. If the slope tries to deform, the nails, anchored in stable soil behind, pick up tension and restrain the movement (functioning similarly to roots or geogrids, but installed post-construction). Soil nailing essentially increases the internal stability (in contrast to a retaining wall which provides external stability) (Holtz and Schuster, 1996). The reinforced zone can be treated as a coherent gravity mass in design.

Usage scenarios: Soil nailing has been used extensively for stabilizing steep cuts for highways and railways, steepening existing slopes to gain space, and for landslide remediation in some cases. It is particularly attractive for temporary excavation support (and has become common for deep excavations in urban areas) (Elias and Juran, 1991), but is also used for permanent applications. For natural slopes, soil nailing is typically applied to slopes that are standing but marginally stable or have experienced minor failures it's a way to retrofit reinforcement without complete rebuild.

For example, a highway cut slope that started to bulge can be stabilized by soil nailing it in place rather than regrading (useful if property beyond the slope is limited). In Vancouver, Canada, one of the first uses in the 1970s was to stabilize a steep road cut in granular soil that otherwise would have needed a retaining wall (Holtz and Schuster, 1996). Since the 1990s, many countries have adopted soil nailing for slope stabilization on highway projects; FHWA issued guidelines (Elias and Juran, 1991) for its use (Elias and Juran, 1991).

Construction sequence for a soil nail wall is displayed in Figure 2.42.

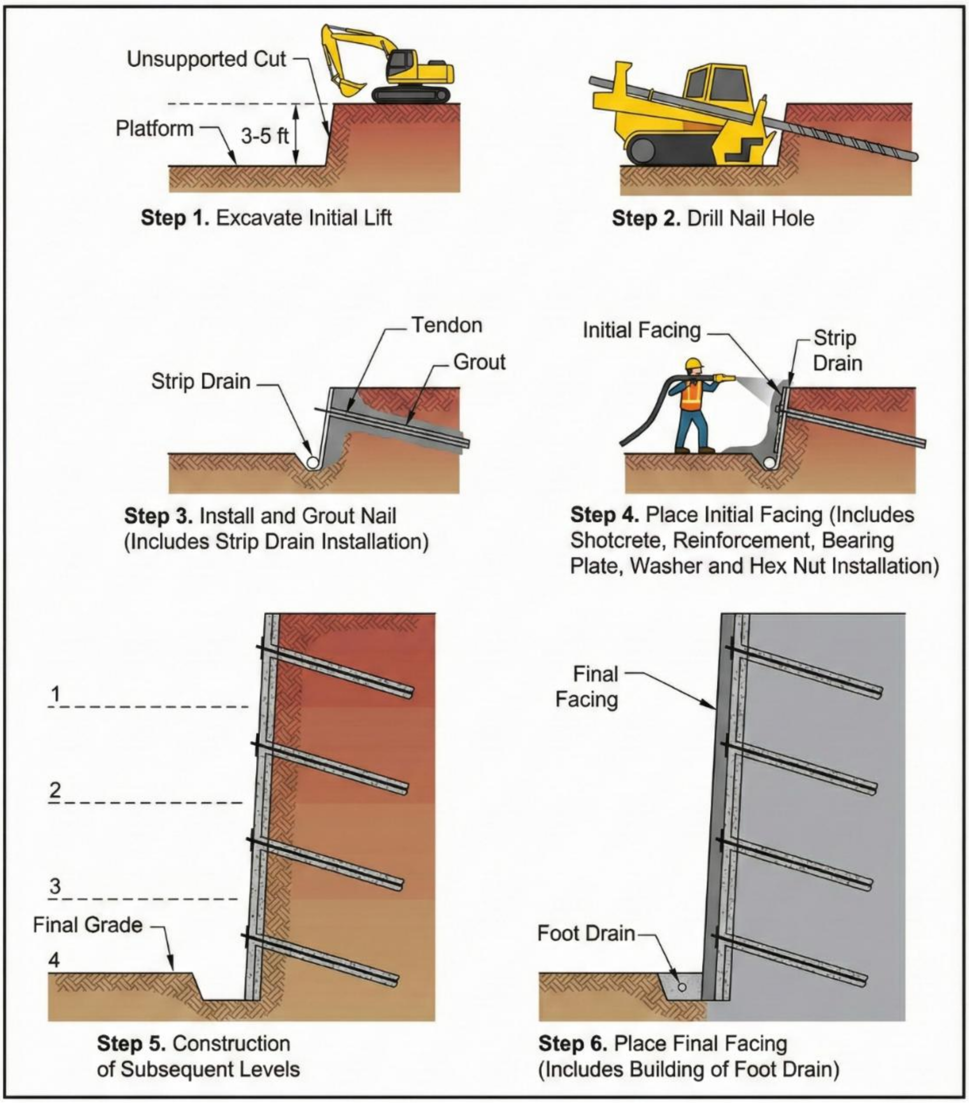

Figure 2.42. *Typical cross-section and construction sequence of a soil nail wall, illustrating top-down excavation, nail installation, and shotcrete facing application (Porterfield et al., 1994)*

Applicable failure types: Soil nailing is most applicable to soil or weathered rock slopes, not usually to hard rock (where rock bolts are used instead). It works best in materials that can stand unsupported briefly while nails are installed (i.e., cohesive soils or rocks that won't immediately collapse). Rotational slips can be prevented by nails that cut through the potential circular arc, adding resistance along it. Shallow planar failures are also addressed by nails since they pin the surface layer to the stable stuff beneath. Soil nailing is often not suitable for very deep failures because nails typically are on the order of 5-20 m long; deeper slides would require unreasonably long nails and multiple rows (in such cases, tieback anchors or piles might be better). So, nail walls are common up to maybe 10-15 m height slopes (though projects up to 20 m have been done with multiple rows).

Also, soil nailing is not ideal if large ongoing movement is happening - it's better as a preventative measure or for stabilizing a slope that's essentially at rest but needs a higher safety margin (Elias and Juran, 1991). In fact, it has mostly been used for cut slopes and excavations rather than actively moving landslides (Holtz and Schuster, 1996), although there are some case histories for landslides too.

Advantages: Soil nailing can be more economical and faster than building a retaining wall for the same slope. It uses the in-situ soil as part of the structure, requiring less new material. Construction has a relatively small footprint, all done from the exposed face, which is great for tight sites (e.g., widening a road by cutting into a slope and nailing instead of laying back or building a big wall). It creates a distributed reinforcement, which gives the system flexibility and resilience - it's not a single rigid structure that fails if one point yields; nails can yield in one area while others hold, giving ductility.

This also means soil nail systems have shown good performance under seismic loads (Elias and Juran, 1991) (their flexibility and reinforcing grid can accommodate shaking better). Another advantage is that nails can be installed with relatively light drilling equipment (track-mounted drills) which can work on steep slopes, minimizing heavy equipment needs.

Limitations: The method requires a stable construction sequence - the soil must stand long enough to drill and grout nails. In very soft or loose soils, this is problematic, so sometimes soil nailing is not feasible without temporary support (like forepoling or shotcrete first). Also, verifying the capacity of nails in the ground can be tricky; typically some nails are load-tested in tension to ensure the bond is good.

Long-term durability of nails (corrosion) needs to be managed by using corrosion-protected bars (double corrosion coating for permanent jobs). Another limitation is that for permanent applications, the aesthetic of a shotcrete wall might be a concern, though it can be sculpted or faced later. There are also patent or proprietary aspects historically (like the French Clouterre techniques) but nowadays it's standard practice with no major restrictions (Schlosser and Unterreiner, 1991). Soil nailing may be less effective in high groundwater conditions unless combined with drainage, because high pore pressures can still cause failure in between nails or along nail interfaces if not relieved.

Case studies: Aside from the early Vancouver case, France widely adopted soil nailing by the 1980s (the Clouterre project; Schlosser and Unterreiner (1991) reported on numerous French projects (Schlosser and Unterreiner, 1991)). In the U.S., one case is the stabilization of a slope on Interstate 70 in Colorado in the 1990s: a cut slope was oversteepened, and soil nailing allowed it to remain at a 1H:4V inclination with a sculpted shotcrete finish - it handled freeze-thaw and heavy rain successfully. Another is a landslide on Route 23 in Tennessee, where nails up to 9 m were installed after a 5 m deep slide, and it effectively stopped further movement (Norrish et al., 1998). While mostly used for temporary excavation, permanent soil-nailed slopes have proven stable over decades when properly designed.

In summary, soil nailing is a powerful technique for reinforcing slopes from within, particularly useful when you want to avoid large excavation or structure construction. It turns potentially unstable ground into a composite material capable of self-support.

2.4.3. Ground improvement techniques

Ground improvement methods aim to increase the strength or reduce the deformability of the soil itself, thereby stabilizing slopes by treating the problematic ground. These techniques often involve altering the soil's properties through physical, chemical, or other means. They are usually high in cost and complexity, reserved for when the native soil is too weak or unstable for conventional fixes, or when extremely high reliability is required (e.g., critical infrastructure on marginal soils).

While various techniques exist—such as deep soil mixing, stone columns, electro-osmosis, and thermal stabilization—these are often disconnected from the massive geometric or deep-anchored stabilization philosophies required for hydraulic structures in complex geologies. However, certain targeted grouting methods remain relevant. Grouting involves injecting fluid or particulate materials (such as cement slurry or polyurethane) into the soil/rock to fill voids, bind particles, or displace and compact the ground (Karol, 2003; Lazarte et al., 2003).

For slope stabilization, permeation grouting might be used to solidify a narrow zone (e.g., along a potential slip plane) or to create an impermeable barrier to cut off seepage paths, thereby controlling pore water pressures (http-29[38]). Although ground improvement is a recognized geotechnical field, the primary focus for stabilizing the deep-seated, complex failures analyzed in this thesis relies heavily on the structural and geometric interventions discussed in the preceding sections.

2.4.4. Performance of stabilization techniques under dynamic conditions

The performance of stabilization measures under seismic loading is a critical design consideration in active regions. Dynamic loads from an earthquake can significantly increase the lateral earth pressures acting on retaining walls and place high cyclic demands on anchors and soil nails (Kramer, 1996). The combination of strong ground shaking and elevated moisture / pore-pressure effects associated with rainfall can represent the most severe loading condition for a slope and its stabilization system (Jia et al., 2024; Wang et al., 2024). Therefore, remedial measures such as anti-slip piles must be designed to withstand these compounded effects to ensure slope stability (Jia et al., 2024). If rockfill buttresses are adopted, their design should also satisfy the controlling seismic stability and deformation requirements of the upgraded slope or embankment (Mejia et al., 2005).

Table 2.16 aggregates the slope stabilization methods.

Table 2.16. *Comparative Summary of Slope Stabilization Methods (Compiled from Holtz and Schuster, 1996; Abramson et al., 2002; and other cited sources)*

Method / Technique (Cost; Complexity)	**Primary principle**	**Best suited for (failure modes / typical scenarios)**
Surface Drainage (L; E)	Reduce infiltration; control erosion	Surficial erosion, shallow slumps; highway cuts/fills, disturbed slopes
Subsurface Drainage (L–M; M)	Lower pore pressure → ↑effective stress	Rotational, translational, flows; natural slopes, embankments, landslide remediation
Flattening / Regrading (L–M; E)	Reduce driving forces	Rotational, translational; highway cuts/fills, large embankments
Unloading Crest (L–M; E)	Reduce driving moment	Rotational; cut slopes, natural slopes
Benching (L–M; M)	Reduce driving forces; control erosion	Rotational, planar, rockfall; high cut/fill (soil & rock), mining
Removal & Replacement (M; M)	Replace weak with stronger material	All (if excavatable); landslide repair, weak foundation soils
Vegetation & Bioengineering (L; E–M)	Near-surface reinforcement; erosion control; drainage aid	Surficial erosion, shallow translational/rotational; embankment faces, stream banks, highway slopes

[38]http-29:https://ncfi.com/case-studies/neshoba-spillway-rehabilitation (accessed May 30, 2025).

Table 2.16. (Continued) *Comparative Summary of Slope Stabilization Methods (Compiled from Holtz and Schuster, 1996; Abramson et al., 2002; and other cited sources)*

Method / Technique (Cost; Complexity)	**Primary principle**	**Best suited for (failure modes / typical scenarios)**
Earth Buttress / Berm (M; M)	Increase toe resistance	Rotational, translational; landslide repair, embankment stabilization
Gabion Walls (M; M)	Gravity support; ↑resisting forces	Rotational, translational, erosion; retaining, channel linings, buttresses
Reinforced Fill (MSE) (M; M)	Internal reinforcement of soil mass	Internal/compound/global; steep slopes, retaining walls, embankments
Gravity / Cantilever Walls (M–H; M–H)	External lateral support	Rotational, translational; grade separation, cut/fill support
Anchored Walls (H; H)	External support via anchors	Deep-seated rotational/translational; deep excavations, constrained sites
Soil Nailing (M–H; H)	Internal passive reinforcement	Rotational, translational; excavation support, slope stabilization
Anchors / Rock Bolts (H; H)	Active compressive force	Planar/wedge/toppling (rock); deep rotational; rock slopes, retaining walls
Piles / Micropiles (H; H)	Shear/bending resistance across slip plane	Deep-seated rotational/translational; landslides, foundation support
Sheet Piles (M–H; M)	Lateral support; groundwater cutoff	Rotational, translational; waterfronts, temporary excavations
Grouting (H; H)	↑strength; ↓permeability	Various (method-dependent); fractures, soil strengthening
Preloading & PVDs (M–H; M)	Consolidation of soft soils → ↑strength	Base failure under embankments; soft clays/silts under new embankments
Deep Soil Mixing (H; H)	Soil–cement elements (high strength)	Rotational/translational/base failure; soft ground, liquefaction mitigation
Stone Columns (M–H; M)	Densify/reinforce; provide drainage	Rotational, base failure, settlement; soft clays/silts under embankments/structures
Electro-osmosis (VH; H)	Dewater/consolidate low-k soils	Failures in silts/clays; fine-grained consolidation (often temporary)
Thermal Stabilization (VH; VH)	Property change via heat/cold	Various (method-dependent); freezing for excavation support, soil strengthening

Legend: Cost = L (Low), M (Medium), H (High), VH (Very High). Complexity = E (Easy), M (Moderate), H (High), VH (Very High)

2.5. Selected Case Studies in the Literature

The geotechnical literature is rich with case studies of slope failures, which provide invaluable lessons for engineering practice (Keefer, 1984; Kramer, 1996; Tanchev, 2014). The advancement of slope stability analysis methodologies is deeply rooted in the lessons learned from both catastrophic failures and successful stabilization projects. Studying notable landslide case histories has been vital in understanding failure mechanisms and validating analysis methods.

Case studies in slope stability analyses play a critical role in identifying and understanding the complexities involved in the design and management of appurtenant hydraulic structures. By employing real-world scenarios, researchers and engineers can validate theoretical models and approaches while also addressing the unique challenges posed by specific site conditions and geotechnical factors. These cases illustrate the complex interplay of geology, hydrology, and loading that leads to instability. Case studies have shown that failures often arise from insufficient analysis or misestimation of parameters, emphasizing the importance of comprehensive stability evaluations in project design and execution (Tanchev, 2014; http-30[39]).

Several notable earthquakes have demonstrated the necessity of rigorous slope stability assessments. Historical events where slope failures caused extensive damage have highlighted the need for improved seismic design methodologies (Keefer, 1984; Jibson, 1993; Kramer, 1996). Case studies involving successful seismic slope design illustrate the importance of advanced numerical modeling and careful design considerations, showcasing how detailed site investigations and soil reinforcement strategies can enhance slope stability in seismic regions (Malhotra and Lee, 2008).

A recurring theme across major failures is the existence of long-standing, inherent weaknesses that remained dormant for years or even decades. At Oroville, the flawed design and poor foundation geology existed for 50 years, and the spillway had survived even larger floods than the one that triggered its failure (http-31[40]; Independent Forensic Team, 2018). At Guajataca, the active landslide and associated creep movements were a known condition for its entire 90-year life (http-32[41]; Cepero, 2023). At Teton, the inadequately treated foundation was a defect from the moment of construction (http-33[42]). These trigger events—the floods and the first filling—did not create the vulnerabilities; they merely exposed them. This implies that the safety of a dam cannot be judged solely by its past performance or the absence of visible distress. A system can appear stable while harboring a critical, hidden flaw.

---

[39]http-30:https://damsafety.org/dam-failures (accessed July 22, 2025).

[40]http-31:https://damfailures.org/case-study/oroville-dam-california-2017/ (accessed July 11, 2025).

[41]http-32:https://damfailures.org/case-study/guajataca-dam-puerto-rico-2017/ (accessed September 09, 2025).

[42]http-33:https://damfailures.org/case-study/teton-dam-idaho-1976/ (accessed August 05, 2025).

The safety and stability of dams and their appurtenant structures, such as spillways and outlet works, are of paramount importance in civil engineering infrastructure because these components are fundamental to dam safety and, although failure probabilities are generally low, failures can cause severe loss of life, property damage, and environmental harm (Fluixá-Sanmartín et al., 2018; Assaad and El-Adaway, 2020; Fu et al., 2018).

A thorough understanding of failure mechanisms is the foundation upon which robust design, analysis, and dam safety programs are built. Forensic analyses of past incidents reveal that failures are seldom attributable to a single, isolated cause. Instead, they often result from a complex and interconnected series of events involving latent design vulnerabilities, unrecognized geological hazards, construction deficiencies, and long-term degradation. This section deconstructs several prominent case studies of spillway and dam failures to establish a foundational understanding of how and why these critical structures fail, moving beyond a simple recounting of events to analyze the intricate interplay of physical, human, and organizational factors.

2.5.1. Case studies by trigger type (rainfall, seismic, drawdown, etc.)

2.5.1.1. Systemic & multi-faceted failure (Oroville Dam, 2017)

The failure of the main service spillway initiated on February 7, 2017, during a period of high reservoir inflow. The failure did not occur at a peak or unprecedented discharge, but at a flow of approximately 52,500 cfs (http-31[43]). The incident began with the sudden uplift and failure of a section of the concrete chute slab, which exposed the underlying, poor-quality foundation rock to the erosive power of the high-velocity flow, resulting in a rapid, progressive, head-cutting erosion (Independent Forensic Team, 2018; Phillips, 2020). The critical structural components and the sequence leading to the collapse of the Oroville Dam spillway are detailed in Figure 2.43.

[43](http-31).

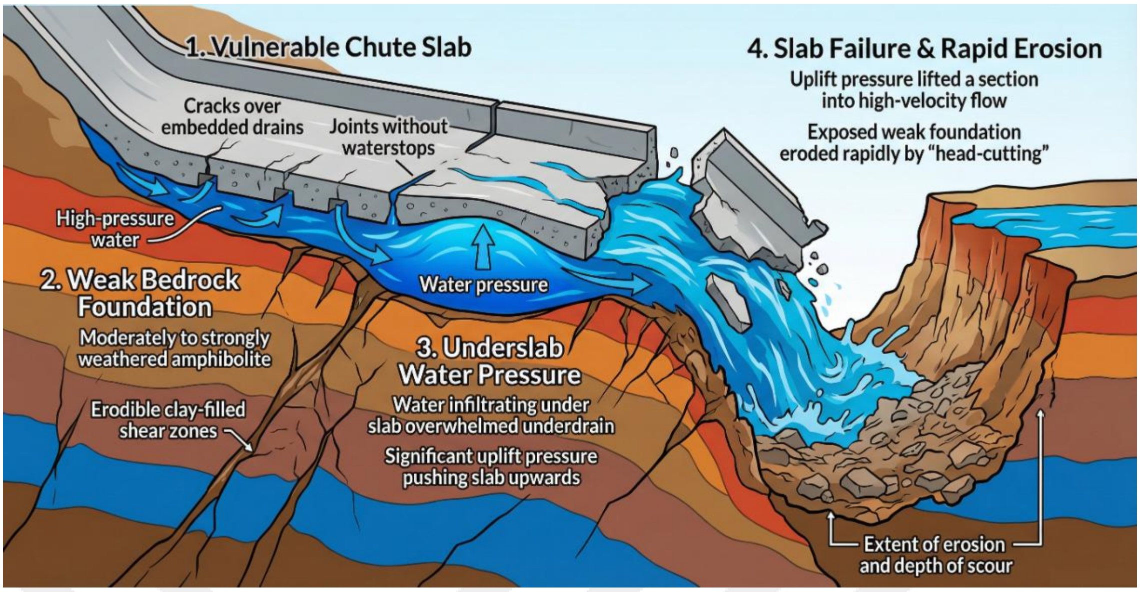

Figure 2.43. *Anatomy of the Oroville Dam spillway failure (Independent Forensic Team, 2018)*

The ultimate physical failure mechanism was identified as hydraulic jacking. Water, injected through cracks and unsealed joints in the chute slab, created uplift pressures that exceeded the combined structural strength and anchoring capacity of the slab, causing it to lift and fail (Independent Forensic Team, 2018; Harrison and Hepler, 2019). The subsequent use of the emergency spillway resulted in unexpectedly severe erosion of its unarmored hillside, prompting mass evacuations (http-31[44]). The post-incident investigation by the Independent Forensic Team (IFT) concluded that there was no single root cause but rather a "long-term systemic failure" involving a complex interaction of physical, human, and organizational factors, including inherent design vulnerabilities such as a thin, lightly reinforced concrete slab and an inadequate underdrainage system, which were not properly adapted to the site's geology (Independent Forensic Team, 2018).

2.5.1.2. Geologically controlled & rainfall triggered (Guajataca Dam, 2017)

The failure of the Guajataca Dam spillway in Puerto Rico, following extreme rainfall from Hurricane Maria, stands as a stark reminder of the controlling influence of geology. The lower half of the spillway chute was destroyed by flows estimated between 10,000 and 15,000 cfs (http-32[45]). The fundamental cause of the failure was the spillway's precarious location atop a large, actively deforming translational landslide complex (http-

[44](http-31).
[45](http-32).

32[46]). Over decades, relentless creep movement (a few millimeters per year) resulted in significant cracking and distortion of the spillway's concrete slabs, creating pathways for water to infiltrate and erode the weak, underlying landslide materials (http-32[47]). The failure mechanism was a multi-stage process driven by this underlying vulnerability, initiating with erosion of weak landslide material at the spillway toe and progressing via internal erosion and head-cutting failure, leading to a massive scour hole (http-32[48]; Wahl and Heiner, 2024).

2.5.1.3. Internal erosion & foundation deficiency (Teton Dam, 1976)

The catastrophic failure of Teton Dam during its initial reservoir filling is a foundational case study on the dangers of internal erosion. The failure progressed from small, clear seeps to a full catastrophic breach in a matter of days (http-33[49]). The most probable physical failure mode was internal erosion (piping) of the dam's impervious silty-sand core, initiated by hydraulic fracturing (http-33[50]). The critical failure mechanism of Teton Dam, specifically focusing on piping through the key trench and the inadequate grout curtain within the jointed rhyolite, is illustrated in Figure 2.44.

[46](http-32).
[47](http-32).
[48](http-32).
[49](http-33).
[50](http-33).

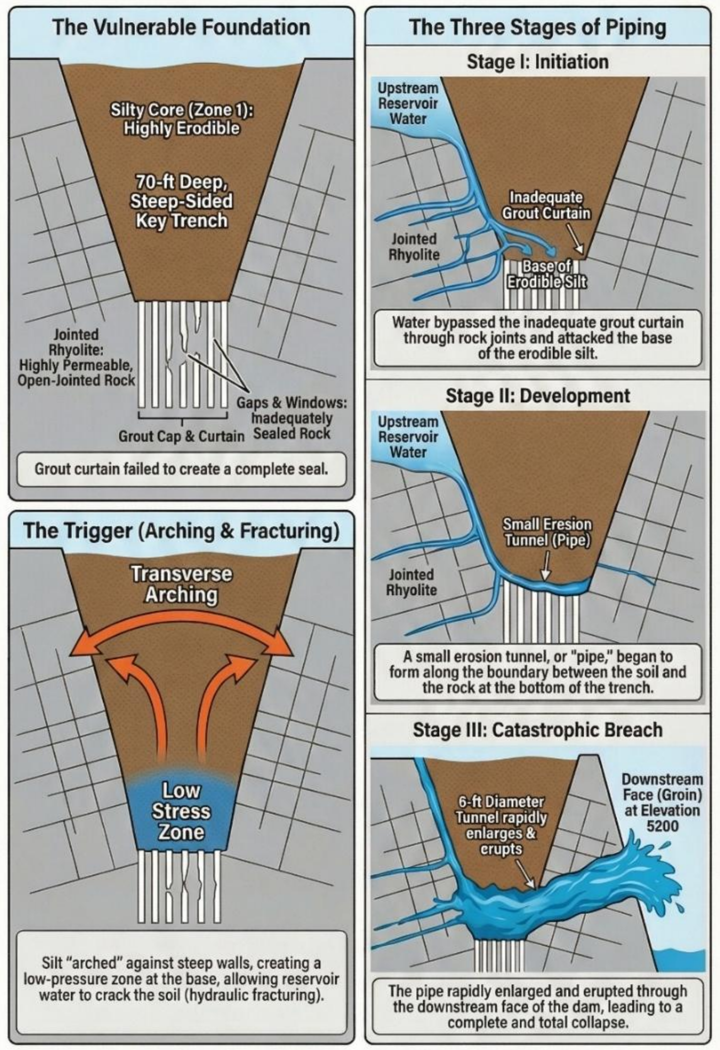

Figure 2.44. *Schematic cross-section of Teton Dam illustrating the failure mechanism: piping through the key trench and the inadequate grout curtain in the jointed rhyolite foundation (Seed and Duncan, 1981; http-33[51])*

This was enabled by a series of critical design and construction deficiencies related to the dam's foundation, which was sited in a canyon with highly pervious and jointed volcanic rock that was inadequately treated. An insufficient grout curtain left open pathways for pressurized water to contact the erodible core material, initiating the piping process (http-33[52]). The incident also highlighted systemic risk, as the main outlet works were not yet operational, leaving no means to drawdown the reservoir once distress was observed (http-33[53]).

[51](http-33).
[52](http-33).
[53](http-33).

2.5.1.4. Construction expediency & hydraulic misdirection (Sugar Creek Dam, 2007)

The near-failure of the Sugar Creek Watershed Dam illustrates how minor as-built modifications can introduce catastrophic failure modes (Richards et al., 2017). During an extreme rainfall event, the vegetated auxiliary spillway was activated. High tailwater from a blocked downstream culvert saturated the spillway exit channel. When the tailwater dropped rapidly, the flow was redirected toward the main dam embankment, causing severe erosion that nearly breached the structure (Anderson and Bass, 2008).

A post-incident investigation revealed that during original construction, the spillway's alignment had been shifted closer to the embankment and rotated towards the dam, likely to simplify excavation. This modification placed the spillway's training dike directly over a near-vertical sandstone outcrop. When overlying erodible soils were stripped away during the flood, this rock feature acted like a ramp, deflecting the high-velocity flow directly at the vulnerable downstream toe of the main embankment (http-34[54]; Anderson and Bass, 2008).

2.5.1.5. Rainfall-induced failures

Many documented failures have been directly attributed to intense or prolonged rainfall events that led to the development of high pore water pressures. Case studies from Greece and Trinidad demonstrate failures occurring after periods of intense rainfall, highlighting the role of both antecedent moisture and the triggering storm (Gariano and Guzzetti, 2016). In some cases, rainfall-induced landslides have been large enough to block major rivers, forming hazardous landslide dams (Fan et al., 2019).

Overtopping of embankment dams during extreme flood events, often associated with intense rainfall and inadequate spillway capacity, is one of the most common dam-failure modes. (Foster et al., 2000; Zhong et al., 2021; Lempérière, 2017). The Highland Towers landslide (1993) in Malaysia serves as a stark example of the catastrophic consequences of poor drainage systems. Prolonged rainfall led to increased pore water pressure, triggering the failure (Tan and Lee, 2017). The Aberfan disaster (1966) in Wales was a man-made colliery spoil heap failure. After heavy rain, a waste tip composed of fine coal waste slumped into a flow slide, engulfing a school and killing 144 people. The flow slide was primarily caused by a build-up of water within the tip, which was placed

[54]http-34:https://damfailures.org/case-study/sugar-creek-watershed-dam-no-l-44-oklahoma-2007/ (accessed April 20, 2025).

over porous sandstone with springs and lacked proper drainage, turning the base into a slurry (http-1[55]). The mechanism is best described as static liquefaction.

Expanding upon the mechanisms of precipitation-triggered instability, understanding the dynamic relationship between hydrological changes and soil mechanics remains fundamental to evaluating slope performance. In this context, Taşkıran and Aslan Fidan (2019) conducted a semi-parametric study to evaluate the impact of rainfall intensity, duration, and hydraulic conductivity on unsaturated slope stability. By employing numerical methods to determine rainfall-induced matric suction changes, and limit equilibrium methods to account for the resulting reduction in shear strength, they successfully elucidated the primary triggering mechanisms of wet-season slope failures in elevated topographies.

2.5.1.6. Seismically-induced failures

Major earthquakes have historically caused widespread and catastrophic slope failures (Keefer, 1984; Jibson, 1993; Kramer, 1996). The 1971 San Fernando earthquake caused the near-failure of the Lower San Fernando Dam due to liquefaction of its hydraulic fill embankment (Sykora, 2019). More recently, the 2011 Tohoku earthquake in Japan triggered the failure of the Fujinuma Dam (http-35[56]). Other cases, such as the Hebgen Dam incident during the 1959 Montana earthquake, illustrate the complex effects of ground shaking, including seiche waves, crest settlement, and damage to spillways (http-36[57]).

Studies of seismic landslides show a tendency for failures to initiate near ridge-crests, where topographic amplification of ground motion is most pronounced (Havenith et al., 2003). In the Safuna Lakes area, Peru, it was found that a combination of seismic shaking and full water saturation significantly lowered slope stability (Klimeš et al., 2012). The Charvak Reservoir area, Uzbekistan, is highly seismic, and earthquakes are a known trigger for landslides (Havenith et al., 2003).

The profound impact of seismic loading on earth structures necessitates rigorous dynamic evaluation, particularly concerning pore pressure generation and post-peak

[55](http-1).

[56]http-35:https://damfailures.org/lessons-learned/dams-located-in-seismic-areas-should-be-evaluated-for-liquefaction-cracking-potential-fault-offsets-deformations-and-settlement-due-to-seismic-loading (accessed July 22, 2025).

[57]http-36:https://damfailures.org/case-study/hebgen-dam-montana-1959/ (accessed July 22, 2025).

strength reduction. Investigating the dynamic response of structural fills, Bakır and Akış (2005) analyzed the complete collapse of a highway embankment subjected to severe near-fault ground motions during the 1999 Düzce earthquake. Their comprehensive evaluation—utilizing a series of static, pseudo-static, and fully coupled non-linear dynamic analyses—revealed non-brittle behavior for the coarse-grained fill, suggesting negligible post-peak shear strength reduction.

Further exploring these dynamic impacts in cohesive soils, Olgun and Acar (2009) incorporated earthquake-induced horizontal forces, excess pore water pressure generation, and corresponding shear strength reductions into their numerical stability models. Their findings highlighted that under dynamic loading conditions, cyclic shear stresses lead to substantial increases in pore water pressure, drastically lowering the factor of safety—particularly when compounded by high groundwater levels and increased slope heights. The compounding nature of hydro-mechanical and dynamic triggers is further validated in regional mass movements. Utilizing back-analysis for a mass movement in Van, Türkiye, Gör (2021) evaluated both static and dynamic conditions, ultimately concluding that while seismic forces act as a catalyst, soil saturation remains the primary driver of slip initiation. To ensure long-term dynamic resilience in such saturated domains, the study proposed and numerically validated the use of reinforced concrete retaining structures.

The seismic modification project for the B.F. Sisk Dam in California provides an excellent example of the practical application of different analysis methods. Initial 2D limit equilibrium analyses of temporary excavation slopes for shear keys yielded low factors of safety near or below unity. However, a more realistic 3D numerical model, which could account for the buttressing effect of confining topography and hillside geometry, verified that the excavation slopes would remain stable, demonstrating how simplified 2D analysis can lead to overly conservative results for complex 3D geometries (Rogers et al., 2020; Tsai et al., 2018).

The stability analysis of the spillway excavation for the Gabric Dam in Iran illustrates a standard workflow for assessing jointed rock slopes. Kinematic and limit equilibrium analyses highlighted the critical influence of both water and seismic loading, with the factor of safety for a potential wedge failure dropping from 3.7 (dry, static) to 0.0 (saturated, or when subjected to combined saturation and seismic loading) (Ghafoori et al., 2011; Maleki Javan et al., 2015).

2.5.1.7. Rapid drawdown failures

The 1965 incident at Fontenelle Dam in the US has been cited as a near-failure event where uncontrolled seepage and potential instability were major factors, illustrating the risks associated with reservoir operations (http-37[58]). The Mandali Dam in Iraq serves as a case study illustrating the impact of rapid drawdown on earth dam stability. Analysis revealed a dramatic decrease in the stability of the upstream slope under this condition (Al-Ameri and Al-Ameri, 2018).

2.5.1.8. Reservoir impoundment/fluctuation

The Vaiont (Vajont) Dam disaster (1963) in Italy is one of the most tragic landslides in history. During the filling of the Vaiont reservoir, an enormous rockslide (~270 million cubic meters) detached from the valley wall and plunged into the reservoir, generating a mega-tsunami that overtopped the dam and caused ~2,500 deaths (Paronuzzi et al., 2021). The disaster was attributed to a combination of unfavorable geological conditions (a prehistoric landslide reactivated along bedding planes in limestone and clay/shale layers) and the rise in pore water pressures due to reservoir impoundment and fluctuations.

The structural geology of the Vaiont Landslide, emphasizing the synclinal bedding, the role of clay seams, and the slide volume relative to the reservoir, is presented in Figure 2.45.

[58]http-37:https://damsafety.org/content/dam-failure-case-study-fontenelle-dam-wyoming-1965 (accessed July 22, 2025).

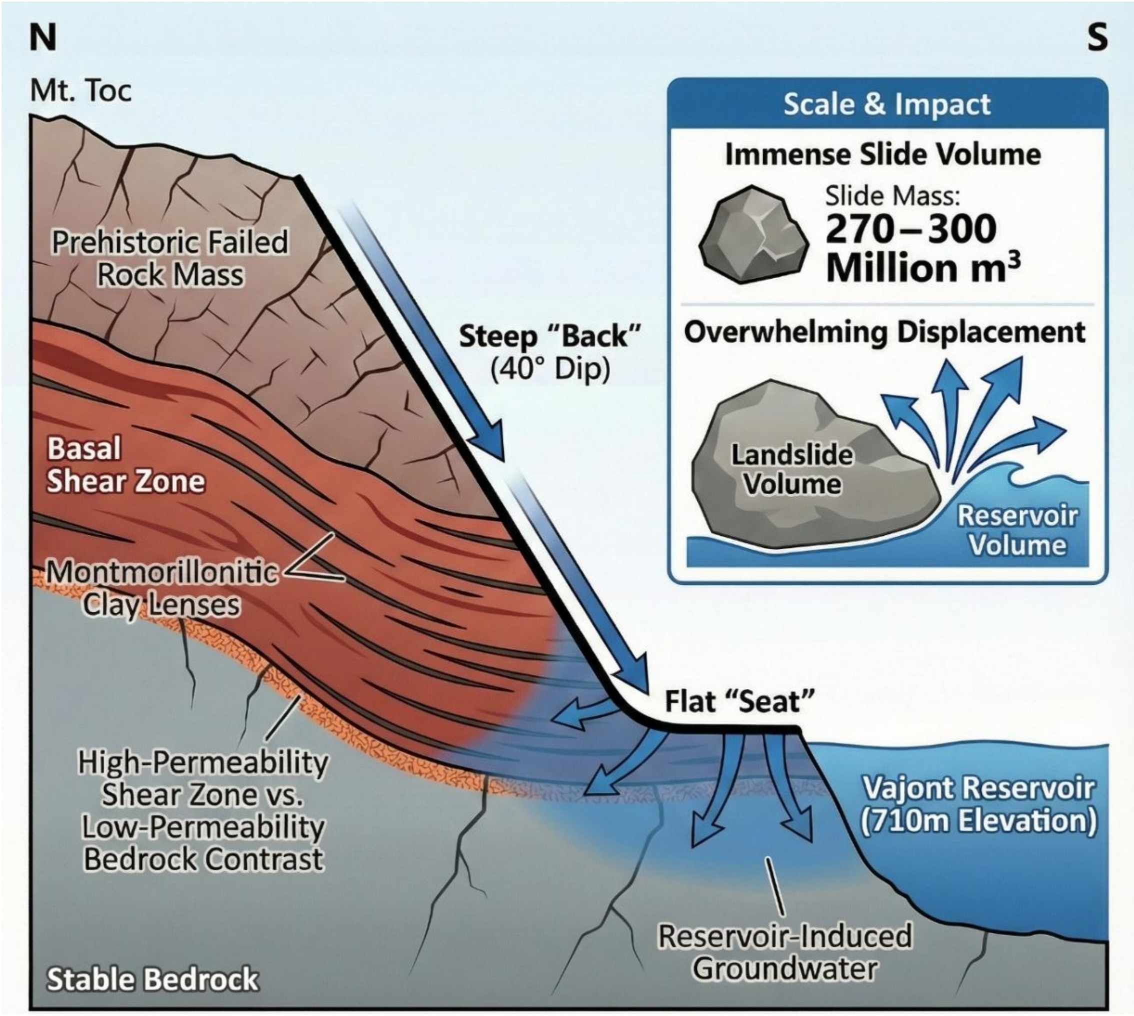

Figure 2.45. *The geological anatomy of the Vaiont Landslide, highlighting the synclinal structure, the position of the clay seams, and the slide mass volume relative to the reservoir (Paronuzzi et al., 2013)*

The Tablachaca Dam in Peru experienced the reactivation of a rock slide in its right abutment, likely due to infiltration from the reservoir (Chávez et al., 2016). In Iran, a landslide that had been stable began moving in 2013 and ultimately collapsed due to reservoir filling to its maximum recorded level combined with an exceptional precipitation event (Shobeir et al., 2017).

2.5.1.9. Excavation

Excavation for spillways in dam projects often involves significant alteration of natural slopes, potentially leading to instability, especially in complex geological settings. The Wudongde Hydropower Station on the Jinsha River provides a valuable case study for understanding the long-term deformation and stability of layered rock slopes subjected to such excavations and the influence of hydrogeological conditions (Ding et al., 2024b). While not explicitly a 'slope improvement scenario' in the sense of a pre-planned remediation, the study's findings on the behavior of excavated slopes offer insights into potential challenges and the effectiveness of analysis methods.

During the construction of Wudongde Hydropower Station, safety and stability issues arose due to geological structures, rock unloading, and large deformations in the excavated areas. The study utilized field displacement monitoring and 3D finite difference method combined with the strength reduction method to analyze the slope stability. It revealed that the layered slopes in the dam reservoir area were prone to deformation under the combined action of long-term construction disturbance and fissure water seepage. The artificial excavation areas, particularly below 1070m elevation, showed significant rock mass deformation and surface displacement.

The study highlights that while construction disturbance strongly influences the excavated areas, seepage plays a more dominant role in the deformation of higher elevation areas. The consistency between field deformation data and numerical calculations underscores the importance of comprehensive monitoring and advanced numerical modeling for predicting and managing slope stability during and after large-scale excavations like those for spillways (Ding et al., 2024b).

Beyond deep rock excavations for hydropower infrastructure, near-surface linear excavations can similarly reactivate dormant, pre-existing geohazards. Demonstrating this vulnerability, Poşluk et al. (2014) analyzed mass movements and paleo-landslide reactivations along the Ankara-Istanbul High-Speed Railway line that were triggered following earthwork and excavation activities. Utilizing limit equilibrium back-analyses, the researchers determined the necessary shear strength parameters for both static and seismic (0.2*g*) loading conditions. The study concluded that mitigating excavation-induced reactivation and ensuring long-term stability necessitates a holistic remediation approach encompassing toe fills, targeted mass unloading, and the implementation of robust retaining structures.

Beyond the massive rock slopes characteristic of mega-hydropower projects, standard excavation and construction activities frequently alter the in-situ state of stress, often reactivating dormant failures. Demonstrating the impact of such infrastructural tunneling, Özyürek et al. (2022) documented the severe geotechnical challenges encountered at the Bahçe Portal of the Bahçe-Nurdağ tunnel, where avoiding a paleo-landslide mass was impossible. Their study outlined the complex failure mechanism and presented a successfully implemented barrette pile support system, proving its efficacy in mitigating large-scale instabilities.

Focusing directly on hydraulic infrastructure, Akın (2013) presented a case study detailing slope stability issues during the construction of two reinforced concrete water reservoirs on a steep hill in Manisa, Türkiye. Utilizing back-analysis based on the non-linear Hoek-Brown failure criterion, the study demonstrated that long-term stability could be securely achieved through the implementation of a permanent toe buttress. Further reinforcing the need for integrated support systems to counteract excavation-induced stress relief, Ün and Yıldız (2021) employed both finite element and limit equilibrium methods alongside back-analysis to derive failure surface parameters. Their findings recommended bored pile walls coupled with surface water drainage as the optimal remediation strategy.

This conclusion aligns directly with the research of Kaya (2019), who investigated similar construction-induced stability issues during hospital earthworks in Artvin. By utilizing 2D and 3D FEM-SSR analyses, Kaya (2019) ultimately validated and recommended bored pile applications to stabilize the mobilized talus deposits overlying the Eocene Kabaköy Formation.

The critical role of mitigating excavation-induced stress relief through localized drainage and toe support is further emphasized in near-surface civil infrastructure. Gör (2022) highlighted these vulnerabilities in an industrial zone in Diyarbakır, where toe excavation compounded by environmental water ingress triggered significant mass movements. Dynamic analyses indicated that geometric benching and systematic environmental water drainage were sufficient for stabilization. Similarly, Topal and Akın (2009) evaluated remedial measures for a natural gas pipeline adjacent to a ruptured line in Karacabey, Bursa. They determined that preventing reactivation required a multifaceted approach: partial removal of the landslide material, construction of toe buttresses, slope flattening, and comprehensive surface drainage.

The necessity for targeted structural intervention during active earthworks is exemplified by Topsakal and Topal (2015), who assessed an active landslide during intersection construction in Artvin. By determining the exceedingly low shear strength parameters of the failure surface ($c=0$ kPa and $\phi=10^{o}$), they established prestressed anchors as the most suitable and immediate remediation technique. Beyond immediate construction impacts, the long-term viability of excavated slopes is governed by progressive environmental degradation. Investigating twenty cut slopes in the North-Western Black Sea region of Türkiye, Ersöz (2017) demonstrated how physical and chemical weathering progressively alter crucial engineering parameters such as cohesion, internal friction angle, and porosity. Consequently, the study concluded that the periodic maintenance of drainage channels is a vital, ongoing requirement to mitigate surficial failures in cut slopes.

2.5.2. Case studies by geology (unit/formation)

The geological setting is a primary controlling factor in slope stability. Many failures are associated with specific, predictable geological conditions (Stark et al., 2020; Stead and Wolter, 2015). Case studies have documented failures along adversely dipping weak seams of organic silt or bentonite, in deep deposits of colluvial soils where natural drainage paths were blocked by construction (Stark et al., 2020), and in sensitive post-glacial clays that exhibit strain-softening behavior (Stark and Hussain, 2013).

2.5.2.1. Ophiolite units

Appurtenant hydraulic structures, such as diversion tunnels, often involve significant excavation into natural slopes, which can trigger or reactivate landslides, particularly in complex geological settings like ophiolite units. A study on the Bolango Ulu Dam diversion tunnel in Indonesia provides a relevant case study for analyzing the stability of natural slopes at tunnel inlet and outlet portals (Wibowo and Purnomo, 2021). Ophiolites are geological formations consisting of oceanic crust and underlying mantle rocks, often characterized by highly fractured and sheared rock masses, making them prone to instability.

In this case, the natural slopes at the tunnel portals were initially considered stable, but subsequent analyses using both Circular Failure Chart (CFC) and Limit Equilibrium Methods (LEM) revealed critical conditions, especially at the inlet section. The portal slopes consisted of diorite and residual soil. While the outlet section showed stable conditions (FOS values around 1.29-1.30), the inlet section exhibited critical stability (FOS values around 1.01-1.07), indicating a need for stabilization measures to prevent failures under static and earthquake loads. This case study highlights the importance of thorough geotechnical investigations and stability analyses, even for seemingly stable slopes, particularly when significant civil engineering interventions like tunnel construction are involved in complex geological environments.

Further illustrating the geotechnical complexities of ultramafic rock masses within ophiolitic sequences, Şeker (2010), building upon the preliminary findings of Toker et al. (2006), investigated the failure mechanisms developed within weathered serpentinite units. Their comparative evaluation utilizing both limit equilibrium and finite element analyses demonstrated a high degree of consistency in the predicted circular slip surfaces. To ensure long-term operational stability within these degradation-prone units, Şeker (2010) subsequently recommended regrading the slope to a 3H:1V inclination, coupled with the implementation of robust surface drainage measures.

2.5.2.2. Interbedded mudstone/limestone

Landslides in interbedded rock formations, particularly those involving weak layers like mudstone, present complex challenges due to the anisotropic and heterogeneous nature of the rock mass. A recent study investigated the stability of a rocky slope with a weak interbedded layer under rainfall infiltration conditions, using a landslide on the G104 Jinglan Line in Shengzhou City, China, as an example (Zhuang et al., 2024). The geological setting of such slopes often involves alternating layers of strong (e.g., limestone, radiolarite) and weak (e.g., mudstone, fill) materials, where the weak interlayers can act as preferential failure surfaces, especially when subjected to water infiltration.

The analysis revealed that the presence of a weak interlayer, a fault, and extreme rainfall were the main factors contributing to the landslide. The weak interlayer was easily disturbed, and the deformation trend of deep displacement was consistent with rainfall patterns, indicating the significant role of hydro-mechanical coupling.

The study utilized numerical analysis (Strength Reduction Method) to calculate the stability of the landslide under natural and extreme rainstorm conditions, and compared the stability before and after treatment measures. This case study highlights the importance of considering the complex geological structure and the weakening effect of water on weak interlayers when assessing the stability of interbedded rock slopes, and provides insights into effective treatment measures such as excavation unloading and prestressed anchors.

The profound influence of structural geometry and weak substrata in interbedded formations is further illuminated when subjected to dynamic loading. Pinyol et al. (2022) provided critical insights into the kinematic evolution of a landslide driven by a synclinal flysch formation overlying a weaker marl substratum. By conducting a comparative assessment between a two-block Newmark analysis and a two-dimensional elastoplastic finite element approach under both static and dynamic conditions, their research emphasized that the inherent geological geometry dictates the multi-stage kinematic response of stratified landslide systems.

The vulnerabilities inherent to interbedded formations are also acutely observed in industrial and regional mass-wasting contexts where weak seams act as primary failure planes. Regarding material-specific failures, Karaman et al. (2015) investigated large-scale planar failures in a limestone quarry in Trabzon, Türkiye. The instability was directly attributed to the presence of weak clay seams intersecting with excessive slope angles, high bench heights, uncontrolled blasting, and heavy rainfall. In a broader regional context, Baron et al. (2004) reconstructed deep slope failures in the Czech Republic, identifying the complex interplay of a stratified flysch-bedrock structure. Their findings highlighted that deep weathering via faulting, compounded by smectite swelling within the weak interlayers and heavy rainfall, served as the primary contributing factors driving the deep-seated kinematics.

2.5.2.3. Colluvial units

Landslides in colluvial units, particularly those triggered by rainfall, present unique challenges due to the heterogeneous and often loose nature of colluvial soils. These soils, formed by the downslope movement and accumulation of weathered material, can exhibit highly variable geotechnical properties. A recent study investigated two landslide failure case studies in colluvial soils, analyzing their failure patterns using both finite element (FE) and limit equilibrium (LE) slope stability analysis methods under unsaturated conditions (Amarasinghe et al., 2024).

The study highlighted that failure in these colluvial slopes occurred primarily due to a rise in the groundwater table, emphasizing the critical role of hydro-mechanical coupling in such events. It also revealed that significant disparities can exist in pore water pressure profiles when comparing fully coupled hydro-mechanical models with sequentially coupled hydrological and mechanical models. The research further suggested that the depth of the colluvium layer influences the failure mechanism: deep-seated failures along the overburden-bedrock boundary are possible with thick colluvium, while shallower failures along the colluvium-weathered rock surface occur with thinner layers. This case study underscores the importance of advanced numerical modeling and accurate hydrogeological characterization for predicting and mitigating landslides in colluvial terrains.

The hydrogeological sensitivity of colluvial deposits is further corroborated by Jeng and Lin (2011), who examined the hydrological behavior of a highly permeable, heterogeneous colluvium soil cover in the Ta-Lun mountainous region. Because the underlying groundwater table fluctuates rapidly, the pore water pressure exhibits dynamic variations in response to weathering. Their study specifically focused on quantifying the variation of matric suction within the colluvial matrix under varying vegetation and rainfall conditions.
Furthermore, the vulnerability of colluvium is exacerbated when subjected to anthropogenic loading. Focusing on engineered fills, Al-Homoud et al. (1997) performed parametric and back-analyses on an artificial embankment failure in Jordan triggered by heavy rainfall. Their analyses considered various piezometric conditions and evaluated both shallow circular and deep block slip surfaces.

The results revealed that the instability was primarily driven by embankment overloading, construction over colluvial deposits, and the subsequent softening of the underlying colluvium due to water ingress. Remediation necessitated a combination of vertical height reduction and horizontal realignment.

In a preceding study within the same Wadi Es-Sir project, Al-Homoud and Tal (1995) analyzed non-circular slope failures in colluvium during reservoir construction, ultimately recommending the partial or complete replacement of the existing colluvial material with free-draining rockfill to achieve acceptable factors of safety.

The profound hydro-mechanical sensitivity of colluvial deposits is particularly problematic when natural vulnerabilities are compounded by anthropogenic excavation. Ehrlich et al. (2018) analyzed a highway excavation in Brazil that dramatically exacerbated pre-existing creep movements within a colluvial matrix. Through extensive field monitoring and theoretical analyses, the researchers demonstrated that the initially proposed deep horizontal drains were functionally insufficient to permanently lower the groundwater table and arrest the mobilized creep. Consequently, the study highlighted that highly permeable, actively deforming colluvial sites often necessitate alternative, significantly more aggressive dewatering and structural remediation strategies, especially following subsequent heavy rainfall events.

Given the inherent variability and hydro-mechanical sensitivity of colluvial matrices, acquiring reliable engineering parameters is a critical challenge. Synthesizing site investigation methodologies, Karikari-Yeboah and Gyasi-Agyei (2000) discussed the comprehensive evaluation of colluvium slopes, directly comparing in-situ and laboratory testing methods. Based on their derived parameters, they advocated for a multi-faceted remediation approach to counteract rainfall-induced instabilities in colluvium, encompassing the concurrent use of horizontal and vertical drains, partial or total mass excavation, and piled foundations to secure long-term structural integrity.

2.5.2.4. Quick clays

The Rissa landslide (1978) in Norway is a classic and famous example of a quick clay landslide and flow slide. In April 1978, a minor excavation triggered the collapse of a quick clay deposit. The initial failure retrogressed dramatically, liquefying a huge volume of clay; ultimately ~330,000 m² of land was consumed as about 6 million cubic meters of clay slid into the lake. These highly sensitive marine clays can liquefy upon disturbance, leading to rapid, retrogressive flow slides (Liu et al., 2021). The mechanism involves the clay losing virtually all its strength when disturbed, leading to a classic progressive failure where the head scarp migrates backward. Table 2.17 extracts synthesis of selected critical historical lessons.

Table 2.17. *Synthesis of critical lessons learned from some of the selected landmark failures*

Case history (Year)	Mechanism + key contributing factors	Main lesson for geotechnical practice
Vaiont (1963)	High-speed slide on pre-existing low-strength clay seams; high pore pressures from reservoir filling; inadequate recognition of controlling 3D geology and prehistoric slide (Müller, 1964)	3D geological/hydrogeological investigation is essential; pore water pressure is often the primary stability control
Rissa (1978)	Progressive/retrogressive failure and liquefaction of quick clay; high sensitivity and strain-softening; small initial disturbance at toe	Peak-strength methods can be unsafe for brittle soils; use residual/softened strength and model progressive failure

Table 2.17. (Continued) *Synthesis of critical lessons learned from some of the selected landmark failures*

Case history (Year)	Mechanism + key contributing factors	Main lesson for geotechnical practice
Aberfan (1966)	Flowslide via static liquefaction of saturated coal spoil; tipping onto active springs; ignored high pore pressures; lack of drainage and oversight	Drainage and pore-pressure control are fundamental; ethical responsibility and effective oversight are critical
Oroville Dam (2017)	Hydraulic jacking of spillway slabs → progressive headcutting erosion; poor foundation rock; unsealed joints; thin/lightly reinforced slabs; inadequate underdrainage; organizational/systemic deficiencies	Design must reflect site geology; joint integrity and underdrainage maintenance are critical; risk assessment must include systemic/human factors
Guajataca Dam (2017)	Internal erosion/headcutting initiated at spillway toe; spillway founded on active translational landslide complex; long-term creep cracked slabs enabling infiltration	Siting controls performance: avoid rigid structures on actively deforming landslide complexes; account for creep-induced cracking/infiltration pathways
Teton Dam (1976)	Internal erosion (piping) of core initiated by hydraulic fracturing; pervious/jointed volcanic foundation insufficiently treated (inadequate grout curtain); outlet works not operational during filling	Foundation treatment in jointed rock is paramount; outlet works must be operational for emergency drawdown during initial filling
Sugar Creek Dam (2007)	Downstream-toe erosion due to redirected flow; as-built modification shifted spillway alignment; flow deflected by rock outcrop toward dam	Minor construction changes can create catastrophic modes; as-built hydraulics must be checked and controlled
Highland Towers (1993)	Rainfall-induced landslide; prolonged rainfall increased pore pressures; inadequate drainage	Drainage capacity is critical for stability under high-precipitation loading
Lower San Fernando Dam (1971)	Liquefaction of embankment; seismic shaking of hydraulic fill	Hydraulic-fill dams are highly vulnerable to seismic liquefaction; seismic evaluation and retrofitting are required
B.F. Sisk Dam (Seismic Mod.)	Temporary excavation-slope stability (analysis case); complex topography/confinement; 2D analysis gave falsely low FoS	2D simplifications can misrepresent complex geometries; 3D modeling may be necessary to capture topographic buttressing
Wudongde Hydropower Station	Rock-mass deformation/displacement in excavated slopes; geological structure; unloading; fissure water seepage on layered slopes	Seepage can dominate high-slope deformation; prioritize comprehensive monitoring and 3D FEM assessment
Bolango Ulu Dam	Potential tunnel-inlet slope failure; complex ophiolite geology (fractured/sheared rock), residual soil over diorite; previously assumed stable	Ophiolite slopes demand rigorous investigation; excavation can render "stable" slopes critical
G104 Jinglan Line (Interbedded)	Landslide along weak interlayer; alternating strong/weak strata (mudstone/limestone); rainfall infiltration; softening of weak layers	Hydro-mechanical coupling can critically weaken interlayers; unloading and anchoring can be effective in interbedded rock
Mandali Dam	Upstream slope instability under rapid drawdown	Rapid drawdown is a critical condition that can drastically reduce upstream stability

2.5.3. Instrumentation and monitoring approaches

Field instrumentation and performance monitoring are essential for validating design assumptions, controlling construction, and providing early warning of impending instability. The standard of practice involves a suite of instruments to measure key parameters. Piezometers are used to monitor pore water pressures, while inclinometers and survey monuments are used to measure subsurface and surface displacements, respectively. A comprehensive monitoring program is a critical component of risk management for any significant natural or engineered slope (Dunnicliff, 1993). Effective seismic slope stability design incorporates several best practices, including comprehensive site characterization, seismic hazard assessment, and ongoing monitoring strategies (Malhotra and Lee, 2008).

Long-term monitoring of the Charvak earth dam using spaceborne Synthetic Aperture Radar Interferometry (InSAR) has been conducted to track deformation associated with reservoir water-level changes. Sentinel-1-based observations and numerical analysis have shown a cause-and-effect relationship between reservoir level and dam deformation (Salyamova et al., 2023). In the Safuna Lakes area, InSAR analysis detected ongoing surface movements up to 45 mm/year in the depletion zone of a 2002 avalanche, years after the event (Klimeš et al., 2021). In Iran, multi-sensor satellite time-series analysis revealed that a landslide began moving during the impoundment of a nearby reservoir, demonstrating the power of remote sensing in monitoring pre-failure deformation (Vassileva et al., 2023). At the Wudongde Hydropower Station, field displacement monitoring was used in conjunction with 3D finite difference method to analyze slope stability (Ding et al., 2024b).

The performance evaluation of aging anchors is a significant concern for dam safety. The case study of the John Day Dam is particularly instructive (Bruce and Wolfhope, 2007; Bruce, 2012). Anchors installed in 1981 with what would now be considered inadequate Class II protection were investigated decades later. The investigation revealed visible corrosion and broken strands at the anchor heads. Crucially, lift-off tests, which involve re-stressing the anchor to measure its existing load, were found to be essential for a true assessment of their condition. The tests showed that visual inspection of the anchor heads significantly underestimated the actual degree of deterioration and load loss.

Beyond case histories in the field, physical modeling and centrifuge tests have been a cornerstone of validating slope stability theories (Schofield, 1980; Zeng and Steedman, 1993). By testing small-scale models in a centrifuge at, say, 50-100 times Earth's gravity, researchers can simulate the stress conditions of a much larger prototype and observe failure mechanisms directly. A.N. Schofield (1980) at Cambridge was a pioneer in promoting centrifuge testing for geotechnical problems. In slopes, centrifuge tests have been used to study everything from simple clay cut slopes to reinforced slopes and earthquake loading on slopes. For example, centrifuge tests on clay slopes have demonstrated progressive failure and retrogression much like in real sensitive clay slides, thus validating analysis methods that incorporate strain-softening (Schofield, 1980; Zeng and Steedman, 1993).

Schofield (1980) and others showed how a centrifuge model of an embankment could produce failures that matched the Spencer or Morgenstern-Price predictions in terms of slip surface shape and FOS when properly scaled. Importantly, centrifuge tests have shed light on 3D effects and scale effects: e.g., small-scale 1g tests often couldn't replicate true failure because of dominance of surface tension or incorrect stress scaling, whereas centrifuge tests do. They have been used to validate FEM codes—for instance, a centrifuge slope failure under earthquake shaking (performed by researchers like Zeng and Steedman in the 90s) provided data on accelerations and displacements that matched well with Newmark analysis predictions for that model earthquake. Centrifuge modeling has also allowed testing of remedial measures (e.g., how effective a berm or a drain is in preventing failure) by direct observation (Fang et al., 2023).

For example, to design stabilization for a landslide-prone spillway abutment, a centrifuge model could be built with and without counterforts or nails to see the difference in behavior, thus giving confidence in the design approach. Overall, physical modeling serves as a critical check on our analytical and numerical methods—a way to see failure in the lab rather than waiting for nature's full-scale "testing," which is often destructive and unpredictable. The continued correspondence between well-instrumented centrifuge tests and numerical simulations (when both are carefully done) bolsters our trust in those computational methods for design.

2.6. Synthesis of Literature on Stabilization Methods

2.6.1. The systems approach to stabilization

A recurring theme throughout the literature is that durable and effective slope stabilization rarely relies on a single, isolated technique. Instead, the most successful solutions adopt a holistic, systems-based approach that addresses the multiple factors contributing to instability (Cornforth, 2005). Slope failure is a complex process driven by the interplay of geology, geometry, hydrology, and external loads. Consequently, remediation must be multifaceted. For instance, a landslide triggered by high pore water pressures in a steep slope of weak soil cannot be permanently stabilized by simply installing a retaining wall at the toe.

While the wall may provide immediate support, it does not address the underlying cause of instability—the high pore water pressure. A more robust and resilient solution would combine multiple methods: subsurface drainage (e.g., horizontal drains) to lower the piezometric surface and increase the soil's effective strength, geometric modification (e.g., unloading the crest) to reduce driving forces, and a structural element (e.g., a buttress or reinforced fill) at the toe to increase resisting forces (Cornforth, 2005). This integrated approach ensures that both the causes and symptoms of instability are addressed, leading to a higher overall Factor of Safety and improved long-term performance.

2.6.2. The role of cost-benefit and risk analysis

The selection of a stabilization strategy has historically been driven by initial construction cost and the achievement of a minimum deterministic Factor of Safety. However, a modern, more sophisticated approach, increasingly supported by the literature, advocates for a framework based on whole-life cost-benefit analysis (CBA) and quantitative risk assessment (QRA) (Robson et al., 2024). The "cheapest" solution is not necessarily the most "cost-effective." A low-initial-cost method that has a higher probability of failure or requires significant ongoing maintenance may have a much higher whole-life cost than a more expensive but more reliable and durable solution (Robson et al., 2024).

Recent research by Robson et al. (2024) provides a compelling methodology for such an analysis. By coupling probabilistic stability models with hydrological models, they estimate the frequency of failure for different stabilization measures. This allows for the calculation of an expected annual cost of failure, which, when combined with initial capital and maintenance costs, provides a true measure of a solution's cost-efficiency over its design life (Robson et al., 2024).

Their case study in Nepal demonstrated that a high-initial-cost anchoring system was ultimately more cost-effective than a low-initial-cost mortared masonry wall because of its significantly higher reliability and lower long-term failure risk (Robson et al., 2024). This highlights a crucial point: the optimal engineering solution is one that achieves an acceptable level of risk for the lowest whole-life cost.

2.6.3. Emerging trends and knowledge gaps

The field of slope stability engineering continues to evolve, with several key trends and corresponding knowledge gaps pointing the way for future research.

2.6.3.1. Proactive vs. reactive management

There is a clear trend towards proactive slope management, enabled by advances in remote sensing and monitoring technologies. Techniques like satellite-based Interferometric Synthetic Aperture Radar (InSAR), terrestrial laser scanning (LiDAR), and drone-based photogrammetry allow for the monitoring of slope movements over large areas with high precision. This, combined with real-time in-situ instrumentation (e.g., inclinometers, piezometers), facilitates a move from reacting to failures after they occur to identifying and mitigating hazards before they become critical (Stead and Wolter, 2015).

2.6.3.2. Sustainability and environmental integration

There is growing emphasis on more sustainable and environmentally sensitive stabilization techniques, including soil bioengineering and biotechnical stabilization, which can provide structural stabilization while also improving landscape and habitat values (Lewis, 2000). It also involves the innovative use of marginal or recycled materials in fills, which can offer significant cost and environmental savings by reducing waste and the need to transport virgin materials, though this requires more advanced design considerations for drainage and long-term performance (http-38[59]).

[59]http-38:https://www.ciria.org/CIRIA/News/blog/reusing_poor_marginal_soil.aspx (accessed October 09, 2025).

2.6.3.3. Performance data and cost analysis

A significant knowledge gap identified in the literature is the lack of robust, publicly available data on the long-term performance and whole-life costs of many stabilization techniques (Fay et al., 2012). Such data is essential for calibrating design models and conducting meaningful cost-benefit analyses. A concerted effort to instrument and monitor stabilized slopes over their design life would provide invaluable data to the engineering community, allowing for the refinement of design methods and more informed decision-making.

2.6.3.4. Advancements in Numerical Modeling

While numerical methods like FEM are powerful, there remains a need for continued research to better model complex soil behaviors. This includes improving constitutive models for unsaturated soils to more accurately capture hydro-mechanical coupling during rainfall infiltration, and refining models to simulate progressive failure mechanisms and the post-failure behavior of landslides, which are critical for hazard assessment (Fredlund and Rahardjo, 1993).

In conclusion, the effective stabilization of slopes requires a deep understanding of the underlying failure mechanisms and a comprehensive toolkit of potential solutions. The optimal approach is not a one-size-fits-all prescription but rather a carefully designed system tailored to the specific geotechnical, hydrological, and economic constraints of a project. Future progress in the field will depend on leveraging new monitoring technologies for proactive management, embracing sustainable and integrated design principles, and closing critical knowledge gaps related to long-term performance and cost.

2.7. Conflicting Viewpoints and Ongoing Debates

The field of slope stability analysis, despite significant advancements, is characterized by several conflicting viewpoints and ongoing debates. These discussions often revolve around the appropriateness of certain assumptions, the selection of key parameters, and the applicability of specific methods to complex real-world scenarios. Addressing these debates is crucial for refining analytical techniques and improving the reliability of stability assessments for critical infrastructure like appurtenant hydraulic structures. This section synthesizes some of the major unresolved questions that continue to engage researchers and practitioners.

Geotechnical engineers often debate certain issues in slope stability where there is no one-size-fits-all answer. Key ongoing debates include the applicability of 2D vs. 3D analysis, the selection of seismic coefficients, how to handle progressive failure, and whether to use effective or total stress approaches in various scenarios.

2.7.1. 2D vs. 3D slope analysis

Traditional slope stability analyses are done in two dimensions (planar cross-section), assuming a "unit width" slice of slope and implicitly that the slope extends infinitely or that failure is uniform along the third dimension, but in reality, many slides are three-dimensional, with a roughly hemispherical or ellipsoidal failure surface. Generally, a 3D failure allows more resistance because of "side constraints"—the material outside the failure cylinder provides extra support—and thus, 3D analyses often find a higher factor of safety than comparable 2D analyses, especially for localized slides in otherwise laterally uniform slopes (Stark and Eid, 1998; Kalatehjari and Ali, 2013).

Hungr et al. (1989) extended Bishop's and Janbu's methods into 3D and found that F3D could be significantly higher than F2D for cohesive soils or confined failures. Most research and case studies indicate F3D>F2D, with the ratio often being 1.05-1.3 when the slide width is limited (Hungr et al., 1989), and this difference is more pronounced for smaller aspect ratios (width/depth of slide). The influence of failure surface geometry on the discrepancy between 2D and 3D calculated factors of safety (FS) is illustrated in Figure 2.46.

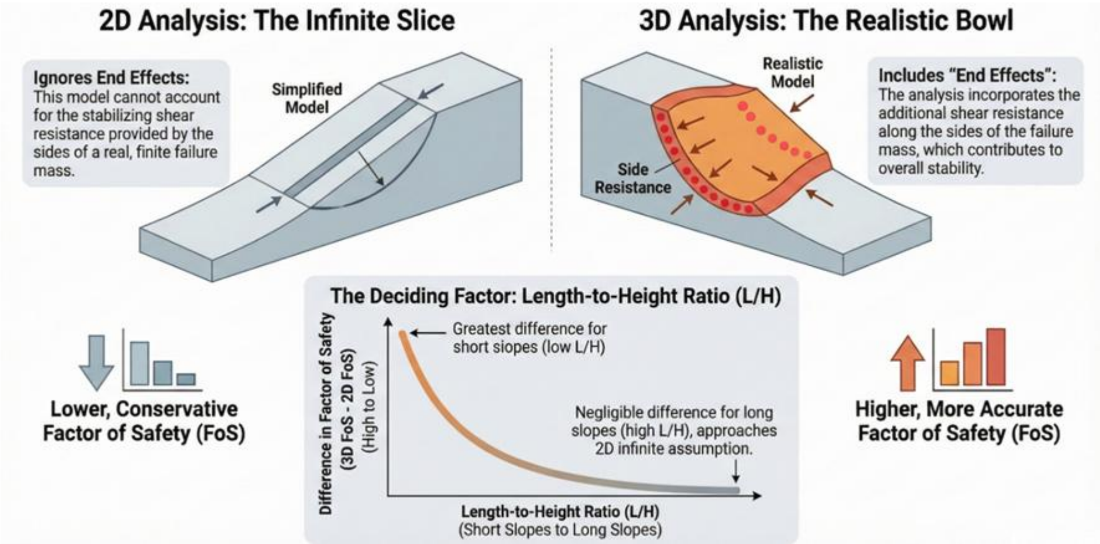

Figure 2.46. *Effect of failure surface geometry on the difference between 2D and 3D calculated factors of safety (Duncan et al., 2014)*

A general consensus is that 2D analyses are usually conservative (lower FOS) compared to 3D (Kalatehjari and Ali, 2013), although for very long homogeneous slopes like a long river embankment, a 2D plane strain analysis is more accurate as the infinite extent assumption is reasonable. However, applying 3D analysis requires more data and tools, and design codes may implicitly expect a 2D-based FOS, though some codes, like Chinese codes, allow a reduced FOS if a 3D analysis is performed.

Hungr (1987) suggested that a 2D analysis can be overly conservative, and incorporating 3D effects can explain why some slopes stand when 2D analysis predicts failure. On the flip side, there are cases like valley or ridge slopes where a 2D analysis on the worst section might overestimate stability by ignoring irregularities that could focus failure in 3D.

The debate often reduces to when 3D is necessary; generally, if the slope is highly non-uniform along its length (e.g., a corner of an excavation) or if the potential failure width is limited (like a slide between rock buttresses), then 3D is worth considering (Hungr, 1987). With increasing computational power, 3D FEM is becoming more common for critical project analysis, and comprehensive research compares 2D and 3D stability to quantify the conservatism of 2D (Kalatehjari and Ali, 2013). A remaining challenge is how to present 3D results to regulators used to 2D-based safety factors, which is an ongoing conversation in geotechnical practice.

Justification for Two-Dimensional Stability Analysis: Although slope failures in geotechnical engineering are inherently three-dimensional phenomena, two-dimensional

(2D) plane strain analyses remain the standard practice for design and assessment, primarily due to their conservative nature. Extensive research demonstrates that factors of safety calculated using 3D methods (F_{3D}) typically exceed those derived from 2D analyses (F_{2D}), thereby providing an inherent margin of safety. For homogeneous slopes, Gens et al. (1988) established that as the length-to-height ratio (L/H) of a failure mass increases, the 3D end effects diminish, causing the results to converge toward the 2D plane strain solution. In cases involving translational failures, Stark and Eid (1998) observed that 2D methods often underestimate the factor of safety by neglecting the shear resistance mobilized along the vertical sides of the slide mass, further confirming the conservatism of the 2D approach.

Conversely, for specific rotational or symmetric slip geometries, such as the ellipsoidal surfaces analyzed by Hungr et al. (1989), the calculated F_{3D} was found to show "very good correspondence" with 2D results, being only marginally higher than the minimum F_{2D}. Therefore, provided that the most critical cross-section is identified and analyzed, 2D methods yield a safe, lower-bound estimate of stability that is sufficiently accurate for practical engineering applications near dam appurtenant structures. Table 2.18 presents these comparative findings.

Table 2.18. *Summary of case studies and geometries comparing 2D and 3D factors of safety*

Case / geometry + soil	FoS (2D / 3D; ratio)	Reference	Key note
Spherical slip, R = 24.4 m; frictionless	1.402 / 1.422; 1.014	Hungr et al. (1989)	Matches closed-form (1.402); CLARA mesh
Critical ellipsoidal slip (AR = 0.66); soil not stated	1.03 / 1.23; 1.19	Hungr et al. (1989)	Compared to Leshchinski et al. (1985) log-spiral 3D FoS = 1.25
Lodalen Slide (slump); clay	1.05 / 1.01; 0.96	Sevaldson (1956)	CLARA 3D surface closely matched observed failure surface
90° convex turning corner (vertical cut); homogeneous	1.57 / 1.53; 0.97	Zhang et al. (2013)	FDM shows FoS_3D can be lower than FoS_2D in steep convex geometries
90° concave turning corner (vertical cut); homogeneous	1.57 / 1.65; 1.05	Zhang et al. (2013)	Ratio increases to 1.16 under Rough–Rough boundary conditions
San Diego Landslide (Oceanside Manor); claystone	0.92 / 1.02; 1.11	Stark and Eid (1998)	Vertical side resistance included (Janbu simplified)
Cincinnati Landfill Failure; natural soil under MSW	1.00 / 1.30; 1.30	Stark and Eid (1998)	Ignoring side resistance led to ~30% overestimation of friction angle

Table 2.18. (Continued) *Summary of case studies and geometries comparing 2D and 3D factors of safety*

Case / geometry + soil	FoS (2D / 3D; ratio)	Reference	Key note
Cylindrical center with planar/curved ends; soil not stated	— / —; 1.03–1.30	Gens et al. (1988)	General trend: 3D FoS exceeds 2D by ~3–30%
Symmetrical slopes (ellipsoidal slip); homogeneous	— / —; 1.043	Xing (1990)	Max +4.32% (homogeneous); up to ~1.10 with weak layers
Conical heaps; symmetrical homogeneous	— / —; 1.00–1.60	Baker and Leshchinsky (1987)	Ratio decreases with cohesiveness; purely frictional soils: 2D ≈ 3D

F_{2D} = Factor of Safety from 2D analysis; F_{3D} = Factor of Safety from 3D analysis; Ratio = F_{3D}/F_{2D}; FDM = Finite Difference Method; MSW = Municipal Solid Waste. Values with "—" indicate that only relative ratios were reported in the summary text.

2.7.2. Seismic coefficient selection

As discussed previously, choosing the horizontal seismic coefficient k_h is a contentious issue. There's no universal value; it should relate to the seismicity of the site and performance objectives. Different experts use different approaches: a fraction of PGA (e.g., 0.5 or 0.65 PGA), a value corresponding to a tolerable Newmark displacement (Bray and Travasarou, 2009), or historical guidance like Seed's (1979) recommendation of k_h=0.1−0.15 for M~7.5 earthquakes.

Another debate is whether pseudo-static analysis should consider duration—obviously it doesn't directly, but some argue that if the earthquake is very short, a slightly larger k_h could be sustained without failure, whereas a long earthquake might fail at a lower k_h due to fatigue or pore pressure buildup. This is partly addressed by Newmark methods, but not in pseudo-static. The vertical coefficient (k_v) is also debated; many practitioners omit it for conservatism, though some older guidelines used k_v=+-0.5k_h. Omitting it is conservative if one is worried about vertical acceleration reducing weight (which would be stabilizing when upward). If anything, a conservative approach is to include a downward (increasing weight) k_v for quasi-static analysis, but that's very conservative and rarely done. Current Eurocode type approaches ignore k_v.

Kramer (1996) and other texts emphasize that pseudo-static analysis is highly sensitive to k_h choice, which is essentially judgment. So the debate continues: should we calibrate k_h to case histories? For example, Hynes-Griffin and Franklin (1984) did so and recommended 0.15g as a screening value—if FOS≥1 with that, likely <5 cm displacement; if not, do more analysis.

Bray and Travasarou (2009) introduced a more nuanced method (pseudo-static coefficient tied to allowable displacement). Perhaps the consensus now is: Use pseudo-static with caution, and preferably in conjunction with displacement methods (e.g., Newmark), as performance-based design replaces purely factor-of-safety checks for seismic design. But there's still disagreement—some design codes in low-to-moderate seismic areas might still mandate a single k_h (like 0.1) for slope checks, which some feel is too low or too high depending on context.

2.7.3. Progressive failure and strength selection (peak vs. residual)

A classic debate in clay slope analysis is whether to use peak strength (for first-time failures) or residual/fully-softened strength (for existing large landslides or long-term conditions). Terzaghi and Peck (1967) noted long ago that many slopes that stand apparently stable with a Factor of Safety (FOS) > 1 (using peak strengths) eventually fail because of a progressive reduction of strength along a developing shear surface. Bjerrum (1967) showed that using fully softened (post-peak) strength in sensitive clays was necessary to predict large landslides in Norway.

The debate extends to less sensitive soils, such as heavily overconsolidated fissured clays, where laboratory peak strength may be much higher than what can be mobilized in the field at a large scale because the failure will localize in weak fissures at lower stress. There is also the concept of progressive failure in long slopes: if one end of a potential slip surface yields (e.g., at the toe), it may locally reach residual strength, which then puts more stress on adjacent segments, propagating the failure upward.

Limit equilibrium analysis (LEM) typically cannot handle this because it assumes a uniform factor of safety and often uses one set of strengths. Some practitioners manually adjust strengths along a slip surface (using residual at the toe and peak at the top) to simulate progressive failure (Bjerrum, 1967; Conte et al., 2014), but that requires knowing where the failure will start. Modern numerical methods like the Finite Element Method (FEM) with strain-softening models allow for more direct simulation of progressive failure, but results are sensitive to the mesh and softening law, which are non-trivial to calibrate. In practice, the debate is whether engineers should routinely reduce strengths to account for progressive failure. Some recommend using a reduced "mobilized" ϕ' for long slopes in stiff fissured clay; Skempton (1970) suggests using the fully softened ϕ' as a safe value. Others argue that if a slope has stood for ages, it has likely already undergone some progressive failure and found an equilibrium, so using peak strength is non-conservative.

A common compromise is to use peak strength for first-time analyses but also check what the FOS would be with residual or softened strengths; if the FOS falls far below 1, caution is advised. Progressive failure is particularly important for long, gentle slopes in stiff clay where a failure surface can slowly grow, whereas, in a steep slope, failure may occur all at once at peak strength. Field monitoring, such as inclinometers in slopes showing small shear strains long before failure, also informs this debate. The topic remains an area of active research, especially with the advent of the Material Point Method (MPM) being used to simulate progressive landslides. In summary, there is no universal agreement, but there is a consensus that ignoring progressive failure can be unconservative. The prudent path is to recognize situations prone to it (e.g., sensitive or fissured clays, brittle rockfills) and adjust the analysis approach or design with a higher FOS accordingly.

2.7.4. Effective stress vs. total stress analysis

This is a fundamental question for short-term stability in saturated soils, where the debate centers on which analysis method is appropriate for a given scenario: Total Stress Analysis versus Effective Stress Analysis. A Total Stress (undrained) Analysis uses the undrained shear strength, s_u, which is the cohesion intercept in a ϕ=0 analysis, without explicitly considering pore pressure. In contrast, an Effective Stress Analysis uses the effective stress strength parameters, c' and ϕ', along with pore pressures. Table 2.19 differentiates these two approaches.

Table 2.19. *Comparison of total stress vs. effective stress analysis approaches in slope stability*

Aspect	Total stress (short-term / undrained) vs Effective stress (long-term / drained)
Strength parameters	Total: undrained shear strength, s_u • Effective: c′ and φ′
Pore-water pressure	Total: implicitly captured in s_u • Effective: explicitly modeled (u)
Typical application	Total: end-of-construction in clay; rapid drawdown (partial) • Effective: long-term stability; slow construction; excavations in sand
Advantages	Total: simpler inputs (no pore-pressure prediction) • Effective: more rigorous; captures water-table changes
Limitations	Total: cannot capture pore-pressure evolution during loading; limited stress paths • Effective: requires reliable in-situ pore-pressure estimation

s_u, undrained shear strength; c′, effective cohesion; φ', effective friction angle; u, pore water pressure. Analysis selection depends on the drainage conditions and time-dependent behavior of the soil mass.

For short-term loading of clay slopes, such as at the end of construction or during a rapid drawdown where an undrained response is expected, total stress analysis is often performed. This is because the low-permeability soil does not have time to drain, so the undrained shear strength, s_u, from laboratory tests is used. This can be acceptable if the clay is intact and not undergoing significant changes in its structure or strength. However, a total stress approach has limitations and problems can arise if conditions change during the undrained loading. For example: during an earthquake, clay might generate negative or positive pore pressure, which a total stress approach cannot capture; or if different parts of a slope have different consolidation states, a single s_u value may not be representative of the entire soil mass.

An overconsolidated clay under undrained loading tends to generate negative pore pressures, making it stronger in the undrained state than an effective stress prediction using c′ and ϕ′ might show, because s_u is high. Conversely, a normally consolidated clay will generate positive pore pressure, making it weaker in the undrained state than its drained strength might suggest. A total stress test implicitly accounts for these behaviors, but only for the initial stress path of that specific test. If conditions deviate due to factors like large shear strains causing softening or cyclic loading, the total stress approach falls short. Effective stress analysis with coupled pore pressure is more general, but it requires knowing or assuming the pore pressures. For rapid loading, an estimate of the excess pore pressure must be inputted.

There was a notable debate in the 1960s and 1970s regarding the use of ϕ=0 analysis for the end-of-construction stability of clay fills. While Broms and Bennermark (1967) advocated for the utility of total stress analysis, Bjerrum (1973) demonstrated that it could overestimate stability in soft clays unless empirical correction factors based on plasticity were applied. It is now understood that both approaches are two sides of the same coin if performed correctly; undrained strength is simply a function of the effective stress and pore pressure conditions.

Current engineering practice is often to use total stress analysis for short-term conditions, with appropriate s_u values that may include adjustments for anisotropy or strain rate effects, and use effective stress analysis for long-term conditions with steady-state pore pressures (Duncan et al., 2014). In "transient" cases like rapid drawdown, engineers may run both total and effective analyses. For instance, one might assume undrained behavior during the drawdown (total stress analysis) and then effective stress conditions after some pore pressure dissipation has occurred.

The drawdown method from USACE specifies a procedure that combines both undrained strengths immediately after drawdown and effective strengths after consolidation. The debate between the two methods is essentially one of simplicity versus accuracy. Effective stress analysis is theoretically superior and makes the role of pore pressure explicit, which is beneficial in design. For example, it allows a designer to see if a slight increase in the water table would cause failure and design drainage accordingly, whereas a total stress analysis might hide that sensitivity. However, it demands more input, such as pore pressure conditions.

Total stress analysis is more straightforward if reliable lab strength tests are available, but it can be dangerously oversimplified if the in-situ loading conditions deviate from those of the test. A particularly contentious scenario is dynamic loading. Some have performed total stress dynamic analyses using a constant s_u, which ignores pore pressure generation and can be unconservative if liquefaction or softening could occur. On the other hand, effective stress dynamic analysis requires a complex constitutive model for pore pressure, which is not always available.

Consequently, a variety of approaches are seen; some practitioners use total stress analysis with reduced shear strengths to account for expected softening in a pseudo-effective approach. For example, consider a slope in a clayey dam during an earthquake. A total stress approach might use undrained strengths from monotonic triaxial tests. However, the earthquake loading could cause pore pressure buildup (softening) that those tests did not capture. If the slope's factor of safety is marginal, it could fail even if the static analysis with s_u yielded a value greater than 1.15. This relates to the observation by Seed (1979) that pseudo-static analyses can be misleading if dynamic strength loss is not considered (Bray and Travasarou, 2011).

In that context, an effective stress approach with a model for cyclic softening would be necessary to foresee the failure. The engineering community generally agrees to use effective stress analysis whenever feasible, particularly for long-term and complex scenarios. Total stress analysis should be used with caution for cases of short-term loading in low-permeability soils, with a full understanding of its assumptions.

Ultimately, slope stability analysis is not a "black box" computation. Engineering judgment is required to choose the right method and input values for each situation. Two engineers might legitimately approach the same slope differently, especially if the slope is subject to multiple complex factors (e.g., a steep, anisotropic clay slope subject to earthquakes and rapid drawdown). The way forward is often to perform multiple analyses (sensitivity studies) to see the range of possible outcomes and then design conservatively against the most critical ones.

2.8. Industry Practices and Perspectives from Professional Surveys

Key Informant Interviews (KII) were conducted using structured questionnaires aimed at gathering insights from experts in the field of slope stability, particularly within Nepal's hydropower projects. A total of 44 participants, including civil engineers and geologists, were selected to ensure diverse perspectives based on varying academic and professional backgrounds, as well as years of experience in the sector. This stratification allowed for an analysis of the differences in perceptions concerning slope stability challenges and methodologies (Regmi and Dahal, 2024).

Case studies have systematically reviewed slope stability issues across various hydropower projects, identifying significant geological and anthropogenic factors contributing to slope failures. Natural factors such as high relief, poor rock conditions, high rainfall, and seismic activity were noted, alongside anthropogenic influences like deforestation and improper land use (Regmi and Dahal, 2024). The importance of integrating new geotechnical methods and analytical tools has been highlighted in surveys conducted among professionals in the field. A notable acceptance of numerical modeling methods was observed, reflecting a collective dissatisfaction with current investigation techniques and an eagerness for advancements in slope stability analysis (Regmi and Dahal, 2024).

Participants in the KII highlighted the importance of ongoing monitoring and the need for increased budgets for slope stability assessments. This feedback emphasizes the necessity for future research to explore advanced monitoring technologies and the development of early warning systems to enhance predictive capabilities concerning slope failures. Additionally, improved data quality and acquisition processes are recommended to ensure that slope stability assessments are based on accurate and reliable information (Nguyen, 2021; Regmi and Dahal, 2024).

2.9. Synthesis of the Slope Stability Assessment Framework

The extensive literature reviewed in this chapter establishes a highly integrated, multi-disciplinary framework necessary for the static and dynamic stability assessment of slopes adjacent to appurtenant hydraulic structures. The paradigm of geotechnical engineering has decisively shifted from simplified, deterministic calculations toward advanced numerical, probabilistic, and data-driven methodologies designed to manage the profound epistemic uncertainties inherent in geological materials. Appurtenant structures, such as spillway cuts and tunnel portals, operate in highly complex hydro-mechanical environments characterized by transient pore pressure regimes, topographic irregularities, and stringent performance requirements. Consequently, modern slope stability assessment requires a cohesive synthesis of high-resolution site characterization, sophisticated numerical modeling, hazard-consistent dynamic analysis, and a systems-based approach to stabilization.

Key Takeaways from the Literature:

- Multi-scale site characterization and parameterization: The foundation of any reliable stability assessment is a robust 3D geological model. The literature emphasizes moving beyond basic drilling by integrating advanced in-situ testing (e.g., high-pressure Pressuremeter, Lugeon tests) and continuous geophysical profiling (ERT, MASW, P-S logging) to capture the true stress-strain and hydraulic properties of the rock or soil mass. Furthermore, remote sensing technologies (LiDAR and InSAR) are now indispensable for defining surface kinematics and tracking pre-failure deformations. Translating intact properties to the rock mass scale demands rigorous use of the Geological Strength Index (GSI);

critically, the Disturbance Factor (D) must be meticulously calibrated to the excavation method, and Hoek-Brown to Mohr-Coulomb equivalent conversions must be calculated using a strictly defined, application-specific confining stress range (σ'_{3max}) to avoid severe estimation errors.

- Evolution of analytical paradigms: While Limit Equilibrium Methods (LEM) remain practical tools, they are fundamentally constrained by rigid-body assumptions and a priori failure surface estimations. To overcome this in complex geological terrains, metaheuristic algorithms like Cuckoo Search and Particle Swarm Optimization (PSO) are replacing traditional grid searches to efficiently locate non-circular, 3D critical slip surfaces. However, the industry standard for critical infrastructure has firmly shifted to continuum mechanics via the Finite Element Method (FEM) and Finite Difference Method (FDM). Using the Shear Strength Reduction (SSR) technique, these numerical platforms inherently capture strain localization, staged construction relaxation, and progressive failure mechanisms without assuming failure geometries.
- Constitutive realism and hydro-mechanical coupling: The rudimentary Mohr-Coulomb model is often inadequate for capturing realistic deformations or strain-softening behavior. State-of-the-art assessments require advanced constitutive models (e.g., Hardening Soil with small-strain stiffness, Nor-Sand, UBC3D-PLM) to simulate stress-dependent stiffness, critical state behavior, and susceptibility to static or dynamic liquefaction. Moreover, for operational scenarios like rapid reservoir drawdown, traditional uncoupled seepage analyses can be dangerously non-conservative. Fully coupled hydro-mechanical (u-p) formulations are mandatory to capture the immediate stress-induced pore pressure generation (Skempton B-effects) and subsequent transient dissipation within compressible or fractured slopes.
- Hazard-consistent dynamic rigor: Evaluating seismic stability has progressed far beyond the crude simplifications of pseudo-static analysis. For high-consequence hydraulic structures, fully dynamic time-history analysis is required. A critical consensus in modern earthquake engineering is that broadband Uniform Hazard Spectra (UHS) overestimate multi-period energy. Therefore, target spectra must be defined using the Conditional Mean Spectrum (CMS) or Generalized Conditional Intensity Measures (GCIM) to accurately represent the physical

causal earthquake scenario. Furthermore, cumulative energy metrics, particularly Arias Intensity (I_A), exhibit a robust correlation with Newmark permanent displacement and must act as a primary constraint when selecting and scaling ground motions. Numerically, dynamic models must accurately capture Seismic-Slope Topographic Amplification (S-STAF) while preventing artificial wave reflection through the strict implementation of absorbing boundaries (Lysmer-Kuhlemeyer) and properly calibrated frequency-dependent Rayleigh damping.

- Probabilistic frameworks and data-driven innovations: A fundamental philosophical shift is underway from utilizing a single, deterministic Factor of Safety to adopting reliability-based design computing the Probability of Failure (Pf) via Monte Carlo simulations and Bayesian updating. This explicitly quantifies spatial variability and epistemic uncertainty. Concurrently, Machine Learning (ML) techniques—including Artificial Neural Networks (ANN), Support Vector Regression (SVR), and Random Forests (RF)—are increasingly functioning as powerful surrogate models, enabling rapid, non-linear pattern recognition for Factor of Safety prediction and dynamic risk classification.
- Systems approach to slope stabilization: Remediation is transitioning from isolated fixes to a holistic systems approach that integrates non-structural and structural interventions. Depending on the failure mechanism, stabilization requires a synergistic combination of pore pressure reduction (subsurface drainage), geometric modification, structural reinforcement (anchors, micropiles, soil nailing, reinforced fill walls), and advanced ground improvement (Deep Soil Mixing, stone columns). The selection of these systems is no longer dictated solely by initial capital expenditure; rather, optimal engineering solutions are now evaluated through a whole-life cost-benefit analysis (CBA) and quantitative risk assessment (QRA), balancing upfront costs against long-term reliability and expected annual failure costs.
- Lessons from historical precedents and ongoing debates: Forensic analyses of catastrophic failures, such as Oroville, Guajataca, Vajont, and Teton, reinforce that failures are rarely singular events; they are systemic cascades often triggered by unrecognized 3D geological flaws, long-term creep, and internal erosion acting on vulnerable infrastructure. These lessons highlight ongoing debates, such as the conservatism of 2D versus 3D analyses. While 2D analyses offer safe, lower-

bound estimates, 3D modeling is essential for evaluating confined geometries like tunnel portals and evaluating complex topographic buttressing effects. Furthermore, the validation of numerical models against physical centrifuge testing remains a critical step in bridging the gap between theoretical mechanics and actual field performance.

In summary, the synthesized literature dictates that assessing and stabilizing slopes adjacent to appurtenant hydraulic structures cannot rely on simplified legacy methods. It requires an integrated framework that merges high-fidelity geological modeling, fully coupled dynamic numerical analysis, probabilistic risk assessment, and holistic stabilization strategies. This comprehensive framework forms the robust theoretical and methodological foundation for the subsequent analytical research and stabilization recommendations developed in this thesis.

3. METHODOLOGY

This chapter delineates the multi-methodological framework adopted to investigate the stability of slopes surrounding appurtenant hydraulic structures. The research integrates field characterization, laboratory testing, and advanced numerical simulations to bridge the gap between deterministic safety factor calculations and performance-based dynamic assessments.

By systematically combining the Limit Equilibrium Method (LEM) and the Finite Element Method (FEM), this study ensures a robust evaluation of slope behavior. While static and pseudo-static analyses were applied universally across all case studies, the framework extended to specific advanced conditions where relevant: full time-history dynamic analysis was conducted for Case 2, and transient seepage (rapid drawdown) analysis was performed for Case 6.

3.1. Case 1 – Landslide in Colluvium

This section details the methodological framework employed for the geotechnical characterization and analytical design of stabilization measures for a deep-seated landslide within a heterogeneous colluvial slope at a major dam construction site. The methodology integrates site characterization through field monitoring, laboratory rock mechanics testing, empirical rock mass classification, and a dual-approach numerical modeling scheme to define failure mechanisms and validate stabilization measures.

Limit Equilibrium (LEM) analyses using Slide2 and Finite Element (FEM) simulations in PLAXIS 2D were utilized to calibrate residual shear strength parameters via back-analysis and to validate the performance of the remedial anchored beam system under both static and seismic loading. The design workflow incorporated a hybrid reinforcement strategy—combining active anchors and passive soil nails in accordance with BS 8081 and FHWA guidelines—integrated with deep drainage measures, while construction sequence simulations were performed to verify deformation-based serviceability limits by benchmarking results against the site-specific upper-bound empirical limit (derived for the N/A critical acceleration ratio) and the broader ≤ 1.0 m catastrophic threshold defined by Hynes-Griffin and Franklin (1984) and evaluate sensitivity to drainage efficiency.

3.1.1. Field investigation and monitoring program

To establish the subsurface stratigraphy and monitor the kinematics of the instability, a systematic site investigation program was implemented.

3.1.1.1. Subsurface profiling

Rotary boreholes were drilled to facilitate geological logging and the recovery of core samples for laboratory characterization.

The drilling program integrated appropriate drilling techniques depending on material type, including methods suited for overburden units (colluvium) and core drilling for competent rock masses. Borehole logging procedures included systematic recording of recovery ratios and rock mass quality indices (e.g., RQD) where applicable. Drilling operations utilized T-76 wireline core barrels to ensure high-quality recovery in the bedrock units. However, within the heterogeneous colluvial overburden, the non-plastic and blocky nature of the matrix precluded the recovery of undisturbed (UD) samples and rendered Standard Penetration Tests (SPT) unreliable. The frequent refusal on rock blocks resulted in artificially high blow counts that did not represent the weaker matrix properties. Consequently, in-situ characterization of the shear strength and deformation parameters for this unit relied primarily on Menard pressuremeter tests, following ASTM D4719 standards.

3.1.1.2. Deformation monitoring

Biaxial inclinometers were installed within the boreholes. The monitoring protocol involved periodic readings to track cumulative displacements and pinpoint the depth of the shear interface. Inclinometer installation and monitoring procedures were executed in accordance with ASTM D6230-21 standards to ensure accurate measurement of earth and structural movement.

3.1.1.3. Hydrogeological monitoring

Groundwater conditions were tracked using PVC observation wells installed in selected boreholes.

3.1.1.4. Surface mapping

Field mapping and visual inspections were conducted to document surface manifestations of instability, such as tension cracks on shotcreted faces and upper benches, and to identify active groundwater seepage points at the slope toe.

3.1.2. Laboratory testing program

Laboratory testing was conducted to characterize the intact strength properties of the sedimentary bedrock units. This data serves as the baseline for deriving rock mass design parameters.

3.1.2.1. Uniaxial compressive strength (UCS) tests

A comprehensive series of UCS tests were performed on rock core samples from both the Chalky Limestone and Clayey Limestone units to quantify the intact rock strength required for geomechanical modeling (TS EN 1926/2013).

3.1.2.2. Point load tests (PLT)

To supplement the UCS data and account for potential sample disturbance in weaker rock zones, point load tests were executed (TS 699). The Point Load Index (I_{s50}) was correlated to the uniaxial compressive strength using the following conversion formula:

$$\sigma_c = 10 \cdot I_{s50} \tag{3.1}$$

3.1.2.3. Triaxial compression tests (TC)

Furthermore, Triaxial Compressive Strength Tests were conducted on cylindrical rock specimens in accordance with TS 699 and ISRM standards to determine the shear strength parameters. The experimental data were utilized to plot the failure envelope, from which the internal friction angle and cohesion parameters of the intact rock material were defined.

3.1.2.4. Supplementary laboratory tests

Additionally, the testing suite included the determination of physical properties (density, porosity, and water absorption) and elastic constants (Young’s modulus and

Poisson’s ratio) following TS EN 1936 and TS EN 1926 standards. Direct Shear Tests were also performed on disturbed soil samples in accordance with TS 1900-2 standards to assess shear strength properties. However, due to the high coarse fraction and blocky nature of the heterogeneous colluvial units, these laboratory results were considered non-representative for the blocky rock mass matrix and were not directly utilized for those zones.

3.1.3. Empirical rock mass classification

The geomechanical properties of the fractured rock mass were scaled from laboratory-scale intact values to field-scale parameters using established empirical systems.

3.1.3.1. Geological strength index (GSI)

The GSI system was utilized to quantify the rock mass quality based on the degree of fracturing and the condition of joint surfaces observed in the field and core samples.

3.1.3.2. Generalized Hoek-Brown criterion

This non-linear failure criterion was adopted to model the strength of the bedrock units. To account for blasting and excavation effects, an excavation disturbance factor (D) was incorporated into the analysis. Hoek-Brown parameter derivation was supported through standardized rock mass characterization workflows (e.g., GSI-based parameterization and software-assisted derivation where applicable) to ensure consistency in rock mass strength scaling.

3.1.4. Analytical and numerical modeling framework

The stability of the slope was evaluated using a dual-methodology approach to ensure the rigorous validation of failure mechanisms and the proposed remedial designs. The dimensioning and capacity verification of the remedial support elements adhered to internationally recognized codes: specifically, BS 8081:1989, FHWA-IF-99-015, and recommendations by Xanthakos (1991) and Wyllie (1992) for ground anchor design and bond lengths in rock; FHWA-NHI-14-007 for soil nail walls; and ASTM A416 for prestressed steel strands.

3.1.4.1. Limit equilibrium method (LEM)

Analyses were performed using the Simplified Bishop, Spencer, and GLE/Morgenstern-Price methods within the Slide2 (v9.038) software environment. This method, which satisfies both force and moment equilibrium, was used to calculate the Factor of Safety (FS) under both static and pseudo-static conditions.

In Slide2, advanced critical surface search workflows such as Cuckoo and Particle Swarm Search were applied where needed to identify governing non-circular failure mechanisms, particularly near soil–rock contact interfaces.

3.1.4.2. Finite element method (FEM)

Numerical simulations were conducted using PLAXIS 2D under plane strain conditions. The ϕ-c reduction method was employed to determine the Strength Reduction Factor (M_{Sf}). FEM was specifically used to analyze deviatoric strain localization and to verify the failure geometry. Furthermore, advanced FEM (PLAXIS 2D) analyses were specifically targeted at the critical alignments (Section 4 and Section 5) where the colluvial deposit is thickest and continuous, and where potential ground displacements directly impact the adjacent cut-and-cover tunnel. In these critical zones, FEM was strictly required to evaluate complex soil-structure interactions and to quantify permanent ground displacements, thereby addressing the limitations of traditional LEM in capturing dynamic serviceability.

3.1.4.3. Seismic analysis

A pseudo-static approach was integrated into both LEM and FEM models. Horizontal seismic coefficients (k_h) were selected based on site-specific seismic hazard criteria. For deformation-based assessments, the computed numerical displacements were benchmarked against established empirical sliding-block criteria (e.g., Hynes-Griffin and Franklin, 1984) to verify structural serviceability limits.

3.1.4.4. Hydrogeological modeling

The influence of groundwater was simulated using both phreatic surfaces and pore pressure ratios (r_u). While the phreatic surface method was applied in both LEM and FEM calculations to define hydrostatic pressures, the r_u coefficient was utilized specifically within LEM sensitivity analyses. This parameter was adjusted to represent various saturation levels of the sliding mass, allowing for the simulation of diverse seepage conditions.

3.1.5. Back-analysis and parameter calibration

An iterative back-analysis procedure was employed to calibrate the shear strength parameters of the colluvium. The objective was to develop a numerical model that accurately replicates the observed state of instability. The procedure followed these stages:

- Baseline Modeling: Testing initial design parameters under dry conditions.
- Pore Pressure Integration: Introducing the r_u parameter to reflect observed seepage.
- Parametric Refinement: Iteratively adjusting the bulk colluvium cohesion (c') and internal friction angle (ϕ') until the model reached a critical state (FS ≈ 1.0).
- Interface Characterization: Defining a discrete residual shear zone at the bedrock interface with fully mobilized residual strength parameters (c'_r, ϕ'_r) to match the failure depth identified by inclinometer data.

3.1.6. Remedial design and stabilization methodology

The stabilization strategy was developed through a holistic design workflow that prioritized geometric modification (mass reduction) and aggressive groundwater control, supplemented by structural reinforcement to address deep-seated instability mechanisms. The design methodology followed an iterative process of dimensioning, capacity verification, and performance validation using both limit equilibrium and finite element analyses.

3.1.6.1. Design strategy and geometric modification

The primary intervention involved revising the slope geometry to reduce gravitational driving forces. The design incorporated a multi-benched excavation profile, optimized to unload the unstable upper colluvial mass while maintaining stability for the spillway infrastructure.

3.1.6.2. Drainage system design

To mitigate the primary triggering mechanism—pore water pressure accumulation at the lithological contact—a comprehensive drainage system was designed. The methodology involved sizing and spacing deep horizontal drains (sub-horizontal drains) to intercept the phreatic surface at the bedrock interface. Design criteria specified perforation patterns and inclination angles (typically 5° upward) to ensure gravity flow and effective depressurization of the slip zone. Surface drainage elements (concrete-lined ditches) were dimensioned to intercept runoff and prevent infiltration.

3.1.6.3. Structural support design

The structural support system was designed as a hybrid configuration tailored to varying overburden thicknesses and lithological units.

Active anchor system

High-capacity, 7-strand prestressed ground anchors were dimensioned to provide deep-seated restraint. The methodology explicitly mandated that these active structural reinforcement elements physically penetrate the anticipated deep active shear zones and be rigorously socketed with sufficient fixed bond lengths into the underlying competent bedrock, as shallow surficial supports were fundamentally insufficient for the observed deep-seated kinematics. The bond lengths within the competent bedrock (Chalky and Clayey Limestone) were determined in accordance with BS 8081:1989 and FHWA-IF-99-015 guidelines, utilizing specific rock-grout bond strength values derived from empirical correlations and field data. The tensile capacity of the steel strands was verified against ASTM A416 standards. Reinforced concrete spreader beams were designed to distribute anchor head loads and prevent punching failure in the weak colluvium, adhering to TS 500 standards.

Passive reinforcement

In zones of shallower overburden, soil nails were designed as passive tension elements. The bond capacity (grout-to-soil adherence) was estimated based on FHWA-NHI-14-007 recommendations for granular soils.

Surface protection

A facing system comprising shotcrete and steel wire mesh was designed to mitigate surficial weathering and raveling, supported by short pattern rock bolts.

3.1.6.4. Performance validation and analysis

The proposed remedial design was rigorously validated through a multi-stage analytical framework:

Global stability checks (LEM)

The reinforced slope was analyzed using the Spencer method in Slide2. Target Factors of Safety were established as FS ≥ 1.5 for static loading and FS ≥ 1.0 for pseudo-static seismic loading (k_h = 0.22).

Deformation and stress analysis (FEM)

Finite element simulations (PLAXIS 2D) were conducted to verify that the anchor loads remained within elastic limits and that serviceability displacements (particularly beneath the tunnel structure) were restricted to acceptable tolerances. The strength reduction factor (M_{sf}) was checked against a target of ≥ 1.50 and ≥ 1.00 for static and seismic analyses, respectively.

Sensitivity analysis

To account for potential maintenance issues or extreme events, the system's performance was evaluated under a "defective drainage" scenario (r_u = 0.15), with a reduced target safety factor (FS ≥ 1.25) accepted for this transient condition.

3.1.6.5. Construction sequence modeling

The numerical models explicitly simulated the top-down construction sequence, including staged excavation, support installation, and anchor stressing, to ensure stability was maintained throughout the execution phase.

Table 3.1 summarizes methodologies and tools applied in Case 1.

Table 3.1. *Summary of methodologies and tools applied in Case 1*

Method/ Test	Purpose/ Output (condensed)	Software/ Tool / Standard
Engineering geological mapping	Surface instability indicators (e.g., cracks) and seepage points	–
Rotary drilling	Stratigraphy; core recovery; RQD logging	Wireline T-76
Biaxial inclinometers	Cumulative displacement; shear-zone depth	ASTM D6230-21
Observation wells	Groundwater-level monitoring; hydrogeological assessment	–
Menard pressuremeter test (PMT)	In-situ deformation modulus; limit pressure (colluvium)	ASTM D4719
Uniaxial compressive strength (UCS)	Intact rock strength, σci (bedrock units)	TS EN 1926/2013
Point load test (PLT)	Indirect strength (Is50); UCS correlation	TS 699
Triaxial compression test	Shear strength (c, ϕ); failure envelope	TS 699 / ISRM
Physical property tests	Density, porosity, water absorption; E, ν	TS EN 1936 / TS EN 1926
GSI classification	Rock mass quality from fracturing & surface condition	–
Hoek–Brown criterion	Rock mass parameters (mb, s, a)	RocData
Limit equilibrium method (LEM)	Global stability (FS); Spencer; critical surface search (Cuckoo/PSO)	Slide2
Finite element method (FEM)	Stress–strain; strain localization; strength reduction (Msf)	PLAXIS 2D
Back-analysis	Calibrate c′, ϕ′; characterize interfaces	Slide2 / PLAXIS 2D
Support system design	Sizing/capacity checks (anchors, nails, concrete)	BS 8081:1989 / FHWA-IF-99-015 / FHWA-NHI-14-007 / ASTM A416 / TS 500

3.2. Case 2 – Landslide in a Mudstone–Fill–Radiolarite–Limestone Sequence (Partly Colluvial)

This section details the methodological framework employed for the geotechnical evaluation and rehabilitation design of the left abutment instabilities at a high Concrete-Faced Rockfill Dam (CFRD) situated within a complex active tectonic belt. The methodology integrates field investigations, laboratory testing, remote sensing, and advanced numerical modeling to calibrate shear strength parameters via back-analysis and validate remedial strategies under both static and dynamic loading conditions. Specifically, the investigation utilized Limit Equilibrium (LEM) analyses in Slide2 and Finite Element (FEM) simulations in PLAXIS 2D—incorporating the HS-Small constitutive model—to perform fully coupled dynamic time-history analyses and validate the effectiveness of the remedial rockfill buttress strategy. Furthermore, the design workflow optimized the passive stabilization geometry through staged construction simulations and internal drainage design to meet strict safety criteria.

3.2.1. Field investigation and monitoring program

A comprehensive site investigation program was executed to characterize the subsurface stratigraphy and define the geometric boundaries of the landslide masses.

3.2.1.1. Supplementary drilling

Research drilling was conducted to recover core samples and facilitate in-situ testing. Borehole logging included systematic recording of recovery and rock mass quality indices to support empirical classification and model parameterization. Drilling and logging were complemented by geophysical profiling to reduce uncertainty between borehole locations and to support continuous delineation of weathering thickness and competence transitions. Borehole logging procedures adhered to ISRM standards, specifically characterizing weathering grades (ranging from fresh to completely weathered) and discontinuity conditions based on visual inspection of core samples.

3.2.1.2. Instrumentation network

A robust network was installed to monitor slope kinematics. This system comprised inclinometer boreholes utilizing both automated In-Place Inclinometers (IPI) and manual units.

3.2.1.3. Surface deformation tracking

A geodetic network was established to track 3D surface displacement vectors on a monthly basis.

Table 3.2 details this instrumentation network.

Table 3.2. *Summary of site monitoring and instrumentation system*

Monitoring Method	Instrument Type	Purpose
Subsurface Displacement	Inclinometer Boreholes	Detect shear zone depth and rate
Subsurface Displacement	In-Place Inclinometer (IPI)	Continuous automated monitoring
Subsurface Displacement	Manual Inclinometer	Periodic manual verification
Surface Displacement	Geodetic Survey Points	Track 3D surface vectors
Remote Sensing	InSAR / LiDAR	Historical displacement tracking

3.2.2. In-situ testing and geophysical surveys

In-situ testing was conducted to assess the mechanical and hydraulic properties of the radiolarite, limestone, and serpentinite-peridotite sequences.

3.2.2.1. Standard penetration tests (SPT)

Performed within the overburden and weathered rock zones to correlate penetration resistance with relative density and strength parameters.

3.2.2.2. Pressuremeter tests (PMT)

Executed in selected boreholes to determine the in-situ deformation modulus of the rock mass. Pressuremeter testing utilized a Menard-type guard cell probe to record pressure-volume curves, from which the limit pressure and Menard modulus were calculated for stiffness evaluation (ASTM D 4719-07).

3.2.2.3. Permeability testing

Lugeon pressure water tests (Packer Test – PT) were conducted to profile hydraulic conductivity (British Standards Institution [BSI], 2015). These pressure water tests were executed in accordance with BS 5930, utilizing a wireline single-packer configuration to isolate specific rock mass intervals for step-wise pressure application and flow measurement. Permeability assessments in soil or highly weathered zones were supplemented by constant head permeability tests performed within the borehole casing in accordance with relevant standards (e.g., BS EN ISO 22282).

3.2.2.4. Geophysical exploration

Seismic refraction and Electrical Resistivity Tomography (ERT) were employed to map lithological boundaries. The Electrical Resistivity Tomography (ERT) surveys utilized a Wenner-Schlumberger electrode array configuration to optimize both vertical resolution and signal-to-noise ratio, with inversion processing conducted using 2D imaging software. Multi-channel Analysis of Surface Waves (MASW) was also executed to derive shear wave velocity (*Vs*) profiles for site classification. Additionally, PS-Logging (downhole seismic) was conducted to determine P-wave and S-wave velocities for dynamic analysis. Where geophysical surveys were available, shear-wave velocity profiling supported stiffness characterization inputs and improved continuity of stratigraphic interpretation between investigation points.

PS logging outputs were further used to support site classification workflows (e.g., PEER NGA West2 database target spectrum) and to derive small-strain stiffness indicators (e.g., G_{max} from density and shear-wave velocity) for dynamic modeling inputs.

3.2.3. Laboratory testing program

Laboratory testing was performed on recovered rock and soil samples to establish baseline physical and mechanical properties.

3.2.3.1. Rock mechanics

Tests on rock core samples were conducted to determine Uniaxial Compressive Strength (σ_{ci}) and Elastic Modulus. Point load strength index tests were performed in accordance with ISRM suggested methods on selected core samples to provide indirect strength correlations where full-scale uniaxial testing was not feasible.

3.2.3.2. Soil mechanics

For the soil-like landslide materials and fill, Consolidated-Undrained (CU) triaxial compression tests were performed in accordance with ASTM D4767 to define effective shear strength behavior. These mechanical tests were complemented by comprehensive index property characterization—including Atterberg limits and specific gravity determinations—to classify the fine-grained landslide matrix and fill materials. Accordingly, particle size distribution analyses were conducted in compliance with ASTM D6913 for sieve analysis, while hydrometer analyses for the fine-grained fraction followed ASTM D7928. Additionally, direct shear tests were conducted in accordance with TS EN ISO 17892-10, while physical property determinations including water content and unit weight complied with TS EN ISO 17892-1 and TS EN ISO 17892-2, respectively.

Image 3.1 illustrates a phase of the in-situ sampling process.

Image 3.1. *In-situ extraction of undisturbed samples from the exposed slope face*

3.2.4. Remote sensing and terrain modeling

To reconstruct the long-term displacement history and constrain the kinematics of the failure, remote sensing techniques were integrated with terrestrial data.

3.2.4.1. InSAR analysis

Interferometric Synthetic Aperture Radar was utilized to evaluate surface movements over a multi-year period. The analysis processed Sentinel-1 satellite data using LiCSAR automated processing chains and Small Baseline Subset (SBAS) interferometry techniques to minimize temporal decorrelation and isolate ground deformation signals.

3.2.4.2. LiDAR and photogrammetry

High-resolution point cloud data from LiDAR surveys and 3D photogrammetric analysis were used to verify landslide boundaries and track morphological changes. This involved the generation of high-resolution Digital Surface Models (DSMs) from stereo-pair aerial imagery and LiDAR point clouds, allowing for the calculation of vertical differential models between successive acquisition years.

3.2.5. Rock mass classification and parameter derivation

Geomechanical parameters for the bedrock units were derived using the Geological Strength Index (GSI) system and the Hoek-Brown failure criterion. For the critical landslide interfaces, shear strength parameters (cohesion c' and friction angle ϕ') were determined through static back-analysis. This iterative process involved adjusting strength values in numerical models until a Factor of Safety (FS) of approximately 1.0 was achieved. For the rockfill embankment materials, the internal friction angles (ϕ') were determined by considering the effective normal stress values at the midpoints of the respective rockfill zones. This derivation utilized the empirical relationships, charts, and tables provided in the Review of Shearing Strength of Rockfill (Leps, 1970), Haselsteiner (2017), and the AASHTO LRFD Bridge Design Specifications (2012).

3.2.6. Hydrogeological modeling

Hydraulic conductivity (K) values derived from field Lugeon tests were assigned to the geological units. The modeling focused on the permeability contrast between the fractured rock and the clayey shear zones.

3.2.7. Numerical analysis framework

The stability assessments for Case 2 were conducted using a multi-methodological approach that integrated both Limit Equilibrium (LEM) and Finite Element (FEM) methods. It should be noted that no forward static stability predictions were performed. Instead, the static framework was exclusively dedicated to the back analysis of the observed instability to calibrate the geomechanical parameters. Following this calibration, the primary predictive modeling was executed as a fully coupled time-history (dynamic) analysis to rigorously evaluate the stress-strain development, excess pore pressure generation, and permanent deformations under seismic loading.

3.2.7.1. Static back analysis

The primary intervention involved revising the slope geometry to reduce gravitational driving forces. The design incorporated a multi-benched excavation profile, optimized to unload the unstable upper colluvial mass while maintaining stability for the spillway infrastructure.

Limit equilibrium method (LEM)

Performed using Slide2 (v9.038), utilizing the Simplified Bishop and Spencer methods. Rather than calculating a predictive safety margin, these methods were strictly applied as back-analysis tools to determine the mobilized shear strength parameters at the onset of failure (Factor of Safety ≈ 1.0), satisfying both moment and force equilibrium.

Finite element method (FEM)

Conducted in PLAXIS 2D (v2024). Similar to the LEM approach, the ϕ-c reduction technique was employed strictly for back-calculation purposes. This allowed for the verification of the calibrated strength parameters, the identification of the exact failure mechanisms, and the establishment of an accurate initial stress state for the complex mudstone–fill–radiolarite sequence prior to the execution of the dynamic analysis.

3.2.7.2. Seismic hazard characterization and target spectrum generation

To define the seismic demand for the dynamic simulations, a site-specific target response spectrum was developed using the PEER NGA-West2 framework. This process addressed epistemic uncertainty through a weighted ensemble of Ground Motion Models (GMMs) and a precisely defined seismic scenario.

Seismic source and input parameters

The design earthquake was characterized by a Moment Magnitude (M_w) of 7.1 and a strike-slip faulting mechanism, reflecting the primary kinematic behavior of the region's active fault systems. Proximity to the rupture zone was defined by the following distance and geometry metrics:

- Rupture and Joyner-Boore distances (R_{rup}, R_{jb}): 2.0 km.
- Depth-to-top of rupture (Z_{tor}): 0.0 km (representing a surface-rupturing event).
- Dip angle: 90°.
- Site characterization: A measured shear wave velocity (V_{s30}) of 600 m/s was utilized (Site Class C (Dense Soil/Soft Rock) according to NEHRP standards and Site Class B per Eurocode 8).

For parameters where site-specific deep-basin data were unavailable—specifically the Rupture Width, Hypocentral Depth (Z_{hyp}), and Depths to the 1.0 km/s and 2.5 km/s isosurfaces ($Z_{1.0}$ and $Z_{2.5}$)—the values were set to the software's default (input as 999). This allowed the selected GMMs to calculate these variables based on established scaling laws and regional anelastic attenuation correlations specifically calibrated for Türkiye within the NGA-West2 framework.

Ground motion model (GMM) selection

The target spectrum was derived from the weighted average of four state-of-the-art GMMs: Abrahamson et al. (2014) (ASK14), Campbell and Bozorgnia (2014) (CB14), Chiou and Youngs (2014) (CY14), and Idriss (2014) (I14). Each model was assigned an equal weight of 0.25. The Boore et al. (2014) (BSSA14) model was excluded to ensure consistency with the regional seismic characterization due to its specific anelastic attenuation requirements.

Resulting spectral characteristics

The derived median response spectrum (5% damping) is anchored to a Peak Ground Acceleration (PGA) of 0.56835 g. As illustrated in Figure 3.1, the spectrum exhibits a peak pseudo-spectral acceleration (PS_a) of 1.25517 g at a period of 0.2 seconds. The discrete ordinates are summarized in Table 3.3.

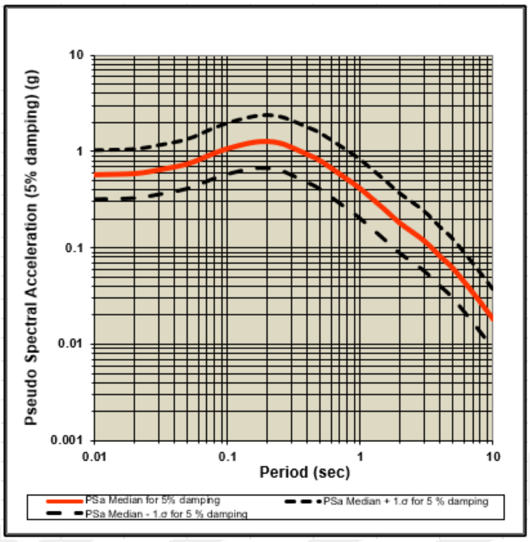

Figure 3.1. *Target acceleration response spectrum generated via the PEER NGA-West2 ensemble (M_w 7.1, V_{s30} = 600 m/s)*

Table 3.3. *Discrete target spectrum ordinates (5% damping)*

Period T (s)	Median PSa (g)	Period T (s)	Median PSa (g)
0.01	0.57012	0.4	0.91832
0.05	0.73874	0.5	0.79061
0.1	1.05748	1.0	0.40811
0.15	1.21518	2.0	0.17969
0.2	1.25517	5.0	0.06139
0.3	1.09443	10.0	0.01854

3.2.7.3. Dynamic time-history analysis and record selection

Fully coupled dynamic time-history analyses were performed in PLAXIS 2D to evaluate the performance of the remedial rockfill buttress. To ensure the simulations represent realistic ground shaking, seed records were selected based on their tectonic relevance, faulting mechanism, and site compatibility. A primary criterion was the alignment of the recording station's V_{s30} with the site's design value of 600 m/s.

Selection and justification of seed records

To capture a range of seismic effects, seed records were selected from the PEER NGA-West2 and AFAD (Disaster and Emergency Management Presidency) databases, with a priority placed on stations matching the site's design V_{s30}. The metadata for the prioritized AFAD recording stations, illustrating the event magnitudes and source-to-site distance metrics (R_{jb}, R_{rup}), is presented in Figure 3.2.

During the retrieval of horizontal acceleration-time histories from the databases, the two orthogonal horizontal components (East/North or H1/H2) were evaluated for each station. To ensure a conservative estimation of the seismic demand, the component exhibiting the larger Peak Ground Acceleration (PGA) was explicitly selected as the primary horizontal input for the subsequent analyses.

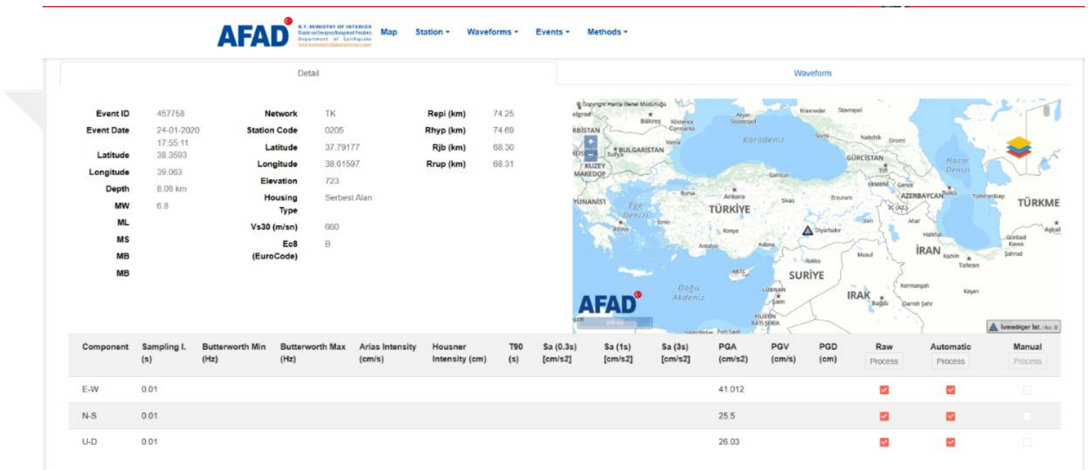

Figure 3.2. *AFAD station metadata illustrating event magnitudes, V_{s30} values, and source-to-site distances for seed record selection*

The specific seed records utilized for spectral matching and the engineering rationale for their selection are summarized in Table 3.4.

Table 3.4. *Summary of selected seed strong-motion records and selection rationale*

Event Name	Date	Station Name / Code	M_w	Vs30 (m/s)	RSN / Event ID	Selection Rationale
Elazığ-Sivrice, TR	2020	TK.0205	6.8	660.0	AFAD 457758	Near-field rupture proximity and site stiffness compatibility.
Darfield, NZ	2010	MECS	7.0	551.3	PEER 6949	Magnitude effects and representation of complex rupture sequence and energy release.
Tottori, Japan	2000	OKYH06	6.61	551.88	PEER 3924	Characterization of seismic duration effects and stiffness compatibility.
Düzce, TR	1999	Lamont 531	7.14	638.39	PEER 1618	Representative spectral characteristics for crustal events.
Hector Mine, USA	1999	Alhambra -Fremont School	7.13	549.75	PEER 3780	Evaluation of high-frequency content and significant energy release.
Kobe, Japan	1995	Nishi-Akashi	6.9	609	PEER 1111	Representative spectral characteristics and compatibility with target distance and strike-slip mechanism.

Processing and numerical implementation

To optimize computational efficiency and mitigate excessively prolonged dynamic analysis runtimes in PLAXIS 2D, the raw acceleration-time histories were initially truncated prior to any baseline correction and filtering. This truncation was systematically performed based on the significant duration concept derived from the Arias Intensity buildup (Trifunac and Brady, 1975). Specifically, the Elazığ and Hector Mine earthquake records were cropped to their $D_{5\text{-}75}$ significant duration as suggested by Husid (1969), whereas the Düzce, Kobe, Darfield, and Tottori records were truncated to their $D_{5\text{-}95}$ significant duration (Trifunac and Brady, 1975). During this cropping procedure, strict measures were taken to ensure that the maximum amplitudes, namely the Peak Ground Acceleration (PGA), of the original records were fully preserved.

Following this initial duration adjustment, the truncated accelerograms were processed using SeismoSignal to apply necessary baseline corrections and filtering.

Subsequently, spectral matching was executed via SeismoMatch, employing wavelet-based modifications introduced by Al Atik and Abrahamson (2010) to achieve tight convergence with the target spectrum (established in Section 3.2.7.2) while preserving the non-stationary characteristics of the modified time histories. During this procedure, the maximum matching period was strategically constrained to 3.0–4.0 seconds. This limitation ensures coverage of the geotechnical structures' predominant natural periods while strictly preventing artificial distortions in the signal tails that can occur when matched to excessively long periods (e.g., 10 s).

Numerical stability and boundary conditions

To ensure numerical accuracy and optimize mesh density, a low-pass filter (10 Hz) was applied. In accordance with the wave transmission criteria proposed by Kuhlemeyer and Lysmer (1973), the maximum element size (Δ) was restricted such that:

$$\Delta \leq \left(\frac{V_s}{10} \cdot f_{\max}\right) \tag{3.2}$$

Where f_{max} is the maximum oscillation frequency and V_s is the shear wave velocity of the respective soil layer. Dynamic boundary conditions utilized viscous absorbent formulations (Lysmer-type) to minimize spurious wave reflections.

To accurately capture the multidirectional nature of the seismic loading within the PLAXIS 2D environment, both horizontal and vertical dynamic excitations were applied simultaneously. The seismic input was prescribed at the model base as a line displacement, oriented at a 45° angle in the direction of the anticipated slope failure. Furthermore, to represent the vertical seismic demand, the vertical acceleration-time history for each respective earthquake record was generated by uniformly scaling the selected horizontal acceleration-time data by a factor of 0.5.

To facilitate the stabilization of excess pore water pressures and the accurate calculation of permanent deformations following the primary shaking, a free-vibration phase was integrated. This was achieved by extending the final processed acceleration-time histories with 5 seconds of zero amplitude at the end of each seismic record. Additionally, the default drift correction function within the finite element solver was explicitly disabled during the dynamic loading phase to rigorously preserve the precision of the baseline corrections previously applied in the signal processing stage.

Constitutive modeling and damping

The Hardening Soil-Small Strain (HS-Small) model was utilized for the rockfill and buttress materials to capture strain-dependent stiffness and hysteretic damping. To prevent numerical overdamping, Rayleigh damping coefficients (α and β) were calibrated for the bedrock units to provide approximately 5% damping at the fundamental frequency of the slope and at 10 Hz.

3.2.8. Remedial design and stabilization methodology

The rehabilitation strategy for the complex downstream instability necessitated a focused engineering approach, prioritizing passive mass-weighting to ensure long-term stability. In accordance with the established analytical framework where static models were exclusively utilized for the back-analysis of the initial failure, traditional forward static predictions were not performed. The design workflow involved incorporating the proposed counterweight fill into the finite element model, where the ultimate verification of the remedial design was achieved entirely through fully coupled dynamic time-history analyses. These dynamic simulations rigorously demonstrated that the rock buttress successfully mitigates excessive permanent deformations and provides the required stabilizing resistance under the design seismic event.

3.2.8.1. Passive stabilization (rock buttress design)

For the large-scale downstream instability, a passive stabilization strategy utilizing a massive rockfill buttress was adopted. The design methodology for this counterweight structure involved:

Geometry optimization

The buttress geometry was integrated into the PLAXIS 2D dynamic framework to maximize passive resistance against the sliding block during seismic excitation, effectively substituting conventional static sizing methods. The design modeled the buttress as extending from the valley floor to specific elevations, anchored against the competent bedrock of the opposite bank to provide effective toe support and strictly limit seismically induced displacements.

Staged construction modeling

To simulate the stress-strain development and effective stress initialization during implementation, the buttress construction was modeled in stages within the finite element framework. This allowed for the assessment of immediate settlement and deformation behavior during the placement of the fill prior to the application of the seismic motion.

Material constitutive modeling

The remedial rockfill material was modeled using the Hardening Soil Small Strain (HS-Small) constitutive model. This approach was selected to accurately capture the strain-dependent stiffness and hysteretic damping characteristics of the compacted rockfill under dynamic loading, ensuring that the seismic energy dissipation within the stabilization mass was physically realistic compared to the native landslide debris.

Internal drainage design

To prevent the saturation of the buttress and ensure the dissipation of excess pore water pressures from the hillside during both the construction and dynamic phases, graded filter drainage zones were integrated into the base of the remedial fill design.

Table 3.5 outlines the summary of methodologies and tools applied in Case 2.

Table 3.5. *Summary of methodologies and tools applied in Case 2*

Method/ Test	**Purpose/ Output (condensed)**	**Software/ Tool/ Standard**
Research drilling	Stratigraphy; core recovery; RQD logging	ISRM (1981) Suggested Methods
In-place inclinometers (IPI)	Continuous automated shear-zone depth & rate monitoring	–
Manual inclinometers	Periodic verification of subsurface displacement	–
Geodetic survey points	3D surface displacement vectors	–
Standard penetration test (SPT)	N-value correlations: relative density & strength	TS EN ISO 22476-3

Table 3.5. (Continued) *Summary of methodologies and tools applied in Case 2*

Method/ Test	Purpose/ Output (condensed)	Software/ Tool/ Standard
Menard pressuremeter test (PMT)	In-situ deformation modulus; limit pressure	ASTM D4719-20
Lugeon testing (PT)	Rock-mass hydraulic conductivity profiling	BS 5930
Constant-head permeability	Permeability in soil/weathered zones	BS EN ISO 22282
Seismic refraction & ERT	2D imaging of lithological boundaries	2D Earth Imager
MASW & PS-logging	Vs and small-strain stiffness (Gmax)	Seisimager2D / MLog
Laboratory rock mechanics	UCS (σci); elastic modulus; point load index	ISRM Suggested Methods
Laboratory soil mechanics	CU triaxial; direct shear; index tests (Atterberg; hydrometer/sieve)	ASTM D4767; ASTM D6913; ASTM D7928; TS EN ISO 17892-10
InSAR analysis	Long-term historical surface displacement (Sentinel-1)	LiCSAR / SBAS
LiDAR & photogrammetry	High-resolution DSMs; morphological change detection	–
GSI & Hoek–Brown criterion	Rock-mass strength parameters	RocData
Seismic hazard & GMM selection	Site target spectrum (Mw 7.1, Vs30 600)	PEER NGA-West2 / GMM Ensemble (2014)
Signal processing	Baseline correction; filtering of accelerograms	SeismoSignal v5.1.0
Spectral matching	Wavelet-based matching to NGA-West2 target spectrum	SeismoMatch v2026 / SeismoSignal v5.1.0

Table 3.5. (Continued) *Summary of methodologies and tools applied in Case 2*

Method/ Test	**Purpose/ Output (condensed)**	**Software/ Tool/ Standard**
Limit equilibrium method (LEM)	Back-analysis (FS)	Slide2 v9.038
Finite element method (FEM)	Stress–strain; staged construction; coupled dynamic time-history	PLAXIS 2D v2024
Constitutive modeling	HS-Small (rock buttress); Mohr–Coulomb (bedrock)	PLAXIS 2D v2024
Back-analysis	Calibrate c′, ϕ′ for critical interfaces	Slide2 v9.038 / PLAXIS 2D v2024

3.3. Case 3 – Instabilities at Diversion Tunnel Portals in Ophiolitic Mélange

This section details the methodological approach employed for the characterization and stabilization of diversion tunnel portals at a major Concrete-Faced Sand-Gravel Fill Dam (CFSGD) project. The investigation integrates extensive subsurface exploration—highlighted by in-situ pressuremeter testing—laboratory testing, and numerical back-analysis to define the hydro-mechanical behavior of the complex ophiolitic mélange (bimrock) matrix. Within this framework, Limit Equilibrium (LEM) slope stability analyses in Slide2 (v9.038) were utilized to calibrate shear strength parameters for the weathered surface zones and to validate the remedial cut-and-cover reinforced concrete conduit through iterative stability modeling of the backfill geometry and cover thickness under both static and extreme seismic loading conditions.

3.3.1. Field investigation and monitoring program

Subsurface characterization was conducted through a staged drilling program tailored to the complex geological conditions.

3.3.1.1. Drilling program

The investigation was executed in phases, providing high-density stratigraphic data necessary for geological modeling. Borehole logging workflows included rock mass quality indices (e.g., RQD and recovery) to support empirical classification systems and subsequent parameter derivation. The subsurface exploration program also incorporated

Standard Penetration Tests (SPT) and pressurized water (Lugeon) permeability tests performed at varying depth intervals to assess the hydraulic conductivity and relative density of the subsurface units.

3.3.1.2. Observational mapping

Field mapping was utilized to document the temporal evolution of slope instability, including tracking tension cracks parallel to excavation benches.

3.3.1.3. Post-event reconnaissance

Following the 2023 seismic sequence, a reconnaissance program was implemented to assess the performance of rehabilitated slopes.

3.3.2. In-situ testing program

To characterize the deformation characteristics of the weak mélange matrix, an extensive program of in-situ pressuremeter testing was implemented. These tests provided the elastic parameters required for subsequent soil-structure interaction analyses. Pressuremeter-derived stiffness parameters were treated as primary in-situ deformation inputs in units where core recovery and laboratory specimen preparation were limited.

3.3.3. Laboratory testing framework

Laboratory testing was performed on core samples to establish the physical and geomechanical properties of the Ophiolitic Complex.

3.3.3.1. Strength testing

A laboratory testing program encompassing Uniaxial Compressive Strength (UCS) and Point Load Index tests was executed to quantify the inherent strength range of the intact rock units. These strength evaluations were conducted in strict accordance with TS EN 1926, TS 699, and ISRM suggested methods to provide a reliable basis for geomechanical parameterization.

3.3.3.2. Physical properties

Laboratory analyses, including unit weight and natural moisture content determinations, were performed to establish the fundamental bulk properties required for numerical modeling inputs. These physical property tests adhered to the relevant sections of the TS EN ISO 17892 (specifically Part 1 and Part 2) or equivalent ASTM standards to ensure consistency and precision in material characterization.

3.3.4. Hydrogeological characterization

Groundwater conditions were monitored using borehole piezometers to identify the phreatic surface and its fluctuations. The investigation focused on the impact of concentrated surface runoff along the portal route.

3.3.5. Rock mass classification and parameter derivation

Rock mass quality was quantified using standard empirical systems to translate borehole data into design parameters.

3.3.5.1. Classification indices

RQD, RMR, GSI, and Q-system were applied to classify the rock mass. The Geological Strength Index (GSI) was estimated based on the specific charts for heterogeneous rock masses (Marinos and Hoek, 2001) given the block-in-matrix nature of the unit, and cross-verified using RMR correlations where the rock mass exhibited distinct jointed behavior.

3.3.5.2. Hoek-Brown criterion

Geomechanical parameters for the bedrock units were derived through the generalized Hoek-Brown failure criterion utilizing RocLab software. To facilitate the stability simulations within the limit equilibrium method framework, these non-linear parameters were subsequently converted into an equivalent linear Mohr-Coulomb strength envelope, defined by the effective cohesion (c') and the internal friction angle (ϕ'). An excavation disturbance factor (D) was applied to reflect the impact of the portal excavation methods.

3.3.6. Numerical stability and structural analysis

The stability of the portal slopes and the structural integrity of the remedial measures were evaluated through a multi-platform numerical approach.

Limit equilibrium method (LEM)

Analyses were conducted in Slide2 using the Simplified Bishop, Spencer, and GLE/Morgenstern-Price algorithms. Slide2-based analyses adopted cross-verification-oriented workflows and advanced slip surface search strategies where needed to identify critical non-circular mechanisms. The minimum required Factors of Safety (FS) for the remedial slope design—1.50 for static long-term conditions and 1.00 for pseudo-static loading—were established.

Back-analysis and calibration

A critical methodological step involved the back-analysis of observed failure states. The rock mass was modeled using two distinct material sets: a general Ophiolitic Complex set and an altered surface zone set to replicate moisture-induced degradation.

Seismic analysis

Performance was evaluated using pseudo-static analysis under both Operation Based Earthquake (OBE) levels and extreme seismic scenarios. The pseudo-static analysis methodology followed the approach outlined by Duncan and Wright (2005), treating seismic forces as equivalent static loads.

3.3.7. Support system design methodology

The methodology for support design involved a comparative evaluation of conventional reinforcement versus geometric modification.

3.3.7.1. Staged stability analysis

A systematic stability assessment was conducted along the alignment to evaluate critical conditions under distinct construction stages. For the analyzed cross-sections, comparative models were established to assess two primary configurations:

Surficial protection alone

The stability of the open cuts was evaluated where the rock mass was supported solely by surficial shotcrete and wire mesh, without the placement of backfill.

Backfill buttress support

The analyses were repeated for the final design configuration, incorporating the stabilizing buttress effect of the compacted granular fill and rockfill placed at ascending elevations around the cut-and-cover conduit.

3.3.7.2. Iterative validation

The final remedial design—a cut-and-cover reinforced concrete conduit backfilled with compacted granular fill—was validated through iterative stability modeling. This process involved calibrating the backfill geometry (maximum 1V:2H gradient) and cover thickness (1.00 m rockfill) to confirm compliance with static (FS≥1.5) and seismic (FS≥1.0) safety requirements. The structural dimensioning of the reinforced concrete conduit was performed in compliance with TS 500 (Requirements for Design and Construction of Reinforced Concrete Structures) and TS 498 (Design Loads for Buildings) standards.

Table 3.6 presents a summary of methodologies and tools applied in Case 3.

Table 3.6. *Summary of methodologies and tools applied in Case 3*

Method/ Test	Purpose/ Output (condensed)	Software/ Tool / Standard
Staged drilling program	Dense stratigraphic control; RQD logging	–
Observational mapping	Time-evolution of instability (e.g., tension cracks)	–
Post-event reconnaissance	Post-seismic slope performance (2023 sequence)	–
Standard penetration test (SPT)	Relative density assessment (soil units)	–
Lugeon testing	Depth-dependent hydraulic conductivity profiling	ISRM
Pressuremeter testing	In-situ deformation modulus Em; limit pressure PL (mélange matrix)	ASTM 4719-07
Borehole piezometers	Groundwater level and phreatic-surface fluctuations	–
Laboratory strength testing	Intact rock strength: UCS, point load index	TS EN 1926; TS 699; ISRM
Physical property tests	Unit weight; moisture content	TS EN ISO 17892 (Part 1, 2); ASTM
Rock mass classification	RQD, RMR, Q-system, GSI	Bieniawski (1989)
Hoek–Brown criterion	Rock-mass strength (incl. disturbance factor D)	RocLab v1.033
Limit equilibrium method (LEM)	Stability (FS): Bishop, Spencer, Morgenstern–Price	Slide2 v9.038
Pseudo-static analysis	Seismic performance (Duncan and Wright approach)	Slide2 v9.038
Back-analysis	Calibrate material sets (Ophiolitic Complex vs Altered Zone)	Slide2 v9.038
Reinforcement design	RC conduit sizing	TS 500 / TS 498

3.4. Case 4 – Landslide Triggered by Inadequate Drainage in a Radiolarite–Limestone–Mudstone Sequence

This section details the methodological approach utilized to investigate and remediate slope instabilities encountered during the construction of a spillway chute within highly weathered and tectonized flysch facies. The investigation focused on delineating the shear interface depth through inclinometer and piezometer monitoring. Using Limit Equilibrium Method (LEM) in Slide2—specifically the Simplified Bishop, Spencer, and GLE/Morgenstern-Price algorithms—the study focused on calibrating operative shear strength parameters via back-analysis to address instability mechanisms driven by seasonal saturation. Subsequently, the analytical framework evaluated the sensitivity of the slope to critical hydrogeological fluctuations and seismic loading. The methodology concludes with the design and numerical validation of a comprehensive remedial strategy—integrating geometric reconfiguration, hydraulic controls, and structural retention— to ensure long-term safety compliance. Specifically, the remedial design was optimized through iterative LEM analyses to achieve a target Static Factor of Safety (FS) $\geq$ 1.5 and Pseudo-static FS > 1.0 (k_h=0.18g), incorporating surcharge removal and the extension of the spillway shear key structure to seal the foundation interface against internal piping.

3.4.1. Field investigation and monitoring program

The site characterization program was structured to define the stratigraphic profile and monitor the kinematics of the unstable mass.

3.4.1.1. Subsurface exploration

Core-drilled boreholes were advanced to depths sufficient to penetrate the potential failure planes for geomechanical logging and instrumentation. Borehole logging included standardized recording of recovery and rock mass quality indices to support empirical parameter derivation and consistency across the investigation dataset. Rotary drilling was performed using XC-90 type rigs equipped with T-type (double) and B-type (single) core barrels to maximize recovery in the heterogeneous flysch units.

3.4.1.2. Deformation monitoring

Biaxial inclinometers were installed within selected boreholes to identify the precise depth of the shear interface and track the rate of displacement. Readings were collected using a standard inclinometer probe, with data interpretation focused on identifying shear zones activated by seasonal saturation.

3.4.1.3. Geomorphological mapping

Field mapping was employed to delineate the boundaries of the instability, focusing on tension cracks and mudflow activity.

Table 3.7 catalogs the deployed instruments.

Table 3.7. *Summary of instrumentation and monitoring parameters*

Instrument Type	Monitored Parameter	Objective
Biaxial Inclinometers	Lateral Displacement	Identification of slip surface depth and velocity
Observation Wells	Groundwater Elevation	Tracking of phreatic surface fluctuations
Surface Survey	Vector Displacement	Mapping of tension crack propagation

3.4.2. In-situ testing program

In-situ testing was performed to assess the mechanical properties of the weathered rock mass and residual soils in their natural state.

3.4.2.1. Standard penetration tests (SPT)

Conducted within the upper weathered horizons to correlate penetration resistance with material consistency. Recorded blow counts (N) were corrected for energy and overburden pressure to derive relative density and consistency indices according to Terzaghi and Peck (1967) and Das (1998) methodologies.

3.4.2.2. Pressuremeter testing (PMT)

Executed to evaluate the in-situ stiffness and deformation modulus (E_m), providing baseline elasticity data for numerical analysis. Tests were conducted using a Menard G-type probe, with pressure and volume calibrations performed on the control unit manometers and probe membrane prior to testing.

3.4.3. Laboratory testing framework

Laboratory testing on recovered materials was conducted to establish physical and geomechanical characteristics.

3.4.3.1. Physical and index properties

Testing determined unit weight, moisture content, and Atterberg Limits for USCS classification. Tests were performed in accordance with TS EN 17892 standards (parts 1, 2, 3, 4, and 12) or equivalent ASTM standards for moisture content, unit weight, particle size distribution, and Atterberg limits.

3.4.3.2. Strength characterization

The program included UCS and Point Load Index tests to quantify the strength of the rock mass units. Uniaxial compressive strength and Point Load Index tests adhered to TS EN 1926, TS 699, and ISRM suggested methods.

3.4.4. Hydrogeological characterization

Groundwater conditions were monitored using piezometric filter pipes. The program focused on tracking pore water pressure buildup and identifying potential artesian conditions for constructing phreatic surface profiles. Water level measurements were taken using a dip meter within 50 mm diameter PVC standpipes installed in completed boreholes.

3.4.5. Rock mass classification and parameter derivation

The geomechanical quality of the rock mass was characterized using the Geological Strength Index (GSI) system, supported by Rock Quality Designation (RQD) data obtained from core logs. GSI values were estimated based on the blockiness and surface conditions of the discontinuities observed in the flysch and ophiolitic units.

3.4.5.1. Hoek-Brown criterion

The Generalized Hoek-Brown criterion was utilized to characterize the non-linear strength behavior of the ophiolitic mélange and its constituent flysch-character sedimentary sequences.

3.4.5.2. Disturbance factor application

A disturbance factor (D) was incorporated into the numerical analysis to quantify the degradation of rock mass strength caused by weathering processes and excavation-induced relaxation.

3.4.6. Slope stability and numerical modeling

Stability analyses were conducted using the Limit Equilibrium Method (LEM) implemented within the Slide2 software environment.

3.4.6.1. Analysis algorithms

The Simplified Bishop, Spencer, and GLE/Morgenstern-Price methods were selected for calculating the Factor of Safety (FS).

3.4.6.2. Loading conditions

The models evaluated both static and pseudo-static conditions, incorporating maximum groundwater levels recorded during monitoring. Slide2 search workflows were applied to identify critical surfaces, particularly in heterogeneous weathered zones and along material interfaces where non-circular mechanisms may govern.

3.4.7. Calibration and back-analysis procedure

A back-analysis procedure was employed to calibrate the operative shear strength parameters of the landslide material.

3.4.7.1. Critical state simulation

Models were adjusted to represent the slope geometry at the time of failure (FS ≈ 1.0).

3.4.7.2. Parameter iteration

Shear strength parameters were iteratively refined until the model replicated the slip surface geometry identified by inclinometer data.

3.4.7.3. Validation

The accuracy of the calibrated model was verified against field-mapped boundaries and instrumental records.

3.4.8. Remedial design and verification methodology

The stabilization strategy for the spillway slopes was developed through an iterative process integrating hydraulic control, geometric optimization, and structural reinforcement. The design methodology focused on elevating the Factor of Safety (FS) to acceptable long-term levels by mitigating the primary instability triggers: elevated pore water pressure and critical surcharge loading.

3.4.8.1. Geometric and structural optimization

The remedial design was verified using Limit Equilibrium Method (LEM) analyses within the Slide2 software suite. To achieve the target stability criteria, the slope geometry was iteratively modified in the numerical model.

Slope reconfiguration

The design flattened critical slope sections (Sections A-A and B-B) and introduced a benching system with 4.0 m widths to enhance passive resistance and facilitate maintenance.

Surcharge unloading

The stability model simulated the complete removal of the anthropogenic excavation spoil (approximately 2,500 m^2 area, 10 m thickness) from the crest to quantify the reduction in driving moments.

Structural retention

Where geometric flattening was insufficient, structural elements were incorporated into the model. These included stone masonry gravity walls and reinforced concrete retaining walls at the toe. The structural dimensioning was validated by ensuring the global stability of the supported slope met the required safety factors.

3.4.8.2. Hydraulic control and interface design

A comprehensive drainage system was designed to lower the phreatic surface and prevent saturation of the weak rock mass.

Drainage system

The design included concrete head trenches (interceptors) to divert upland runoff and an increased density of weep holes within retaining structures to relieve internal hydrostatic pressure. The effectiveness of these measures was accounted for in stability analyses by modeling a controlled phreatic surface.

Foundation sealing

To address seepage risks at the spillway-foundation interface, a structural cut-off was designed. The existing concrete shear key ("tooth") was extended from a depth of 0.8 m to 2.5 m to seal the contact between the concrete structure and the weathered flysch foundation, preventing internal erosion and piping.

3.4.8.3. Verification criteria and loading conditions

The proposed remedial measures were validated against specific Factor of Safety targets established for the project.

Static condition

The design required a minimum Static FS of 1.50 under high groundwater conditions.

Seismic condition

Dynamic stability was verified using pseudo-static analysis with a horizontal seismic coefficient (k_h) of 0.18g, corresponding to approximately two-thirds of the Maximum Design Earthquake (MDE) for the region. The design targeted a seismic FS greater than 1.0 (achieving values ≈ 1.1) to ensure performance during seismic events.

Table 3.8 summarizes the methodologies and tools applied in Case 4.

Table 3.8. *Summary of methodologies and tools applied in Case 4*

Method/ Test	Purpose/ Output (condensed)	Software/ Tool/ Standard
Rotary drilling	Stratigraphy; core recovery; RQD logging	XC-90 / T & B Core Barrels
Geomorphological mapping	Instability limits (tension cracks, mudflows)	–
Biaxial inclinometers	Lateral displacement; shear-zone depth	Standard Inclinometer Probe
Observation wells / standpipes	Groundwater elevation; phreatic-surface fluctuations	Dipmeter
Standard penetration test (SPT)	N-value correlations: relative density & consistency	Terzaghi and Peck (1967) / Das (1998)
Menard PMT	In-situ stiffness; deformation modulus Em	Menard G-Type Probe
Lab physical property tests	Unit weight; moisture content; Atterberg limits; gradation	TS EN 17892/ ASTM
Rock strength tests	UCS; point load index Is50	TS EN 1926/ TS 699 / ISRM
Point-load conversion (k = 24)	UCS derived from point-load indices	–
Rock mass classification	Rock mass quality via GSI	–
Hoek–Brown criterion	Non-linear rock-mass strength parameters (incl. disturbance factor D)	RocLab
Limit equilibrium method (LEM)	Global stability (FS): Bishop, Spencer, GLE/Morgenstern–Price; remedial verification	Slide2 v9.038
Back-analysis	Calibrate operative shear strength (FS ≈ 1.0)	Slide2 v9.038

3.5. Case 5 – Design of Spillway Excavation in Arenized (Highly Weathered) Granodiorite

This section outlines the methodological framework employed for the stability assessment and support design of the spillway excavation, specifically addressing instability risks associated with deep-seated weathering profiles within the granodiorite unit. Given the challenges in recovering undisturbed core samples from the friable saprolite unit (arenized granodiorite), rock mass parameters were derived empirically based on the Generalized Hoek-Brown criterion. The stability analysis was conducted using the Finite Element Method (FEM) in RS2, utilizing Shear Strength Reduction (SSR) capabilities to evaluate global failure mechanisms within the fractured rock mass. The remedial design was subsequently optimized through iterative simulations to satisfy target safety criteria (Static SRF $\geq$ 1.5, Seismic SRF $\geq$ 1.0), integrating a multi-faceted stabilization strategy that combined geometric flattening (transitioning to conservative gradients in critical sections), systematic rock bolting with shotcrete facing for surface confinement, and deep drainage measures to mitigate pore pressure build-up.

3.5.1. Field investigation and subsurface mapping

A comprehensive drilling program was executed to define the stratigraphic profile and delineate the extent of the weathering zones.

3.5.1.1. Exploratory drilling

Core boreholes were utilized to map the contact between the arenized (saprolitic) granodiorite and the underlying massive bedrock. The drilling operations were executed using the rotary drilling method with a water flush system. However, due to the friable nature of the saprolite and the washing effect of the drilling fluid, core recovery was significantly limited, frequently resulting in the recovery of disaggregated, soil-like material rather than intact core.

3.5.1.2. Geomechanical logging

Field observations included calculating the RQD and assessing weathering grades based on core recovery.

3.5.1.3. Hydrogeological monitoring

PVC standpipe piezometers were installed to gather static groundwater level data.

3.5.2. In-situ hydraulic testing

To characterize the hydraulic properties of the heterogeneous rock mass, in-situ permeability testing was performed.

3.5.2.1. Testing methods

Pressurized Water (Packer-Lugeon) and infiltration tests were conducted to assess the hydraulic conductivity of both the massive discontinuity systems and the porous arenized matrix. Specifically, Packer Tests were utilized to evaluate the permeability of the fractured rock mass, while falling head (pressureless) tests were applied in the permeable upper zones.

3.5.3. Laboratory testing program

Laboratory testing was differentiated based on the integrity of the recovered core samples. Due to the friable nature of the arenized granodiorite, testing focused primarily on the competent sections.

3.5.3.1. Rock mechanics testing

Core samples retrieved from representative boreholes were subjected to standard tests to determine unit weight, UCS, and deformability parameters (Elastic Modulus and Poisson's ratio).

3.5.3.2. Soil mechanics testing

Grain size distribution analysis and Atterberg limits were conducted for material classification of the saprolitic horizons in accordance with the TS 1900-1 standard.

3.5.4. Hydrogeological modeling framework

The hydrogeological regime was modeled by integrating static water level data recorded from the piezometer network. These phreatic surfaces were incorporated into the stability models to simulate the impact of pore water pressure.

3.5.5. Empirical classification and parameter derivation

Due to the difficulty of laboratory testing for the arenized material, extensive use was made of empirical correlations.

3.5.5.1. Rock mass quality

The Volumetric Joint Count (J_v) was determined using the Palmström (2001) correlation for the massive granodiorite.

3.5.5.2. Geological strength index (GSI)

The modified GSI system was employed to quantify the rock mass quality for both massive and arenized horizons. The characterization of block size and discontinuity conditions for these classification systems was performed in accordance with ISRM (1981) guidelines.

3.5.5.3. Stiffness and strength derivation

For the arenized granodiorite, the intact modulus was derived using the Ocak (2008) correlation:

$$E_i = 0.4 \times \sigma_{ci}^{0.854} \tag{3.3}$$

The Generalized Hoek-Brown failure criterion was then applied to determine the overall rock mass strength.

3.5.6. Constitutive modeling

The numerical analysis employed a hybrid constitutive modeling framework within RS2 to accurately simulate the contrasting mechanical behaviors of the geological units:

3.5.6.1. Massive granodiorite

The Generalized Hoek-Brown failure criterion was utilized directly for the competent bedrock units to capture the non-linear, stress-dependent strength characteristics of the fractured rock mass.

3.5.6.2. Arenized (saprolitic) granodiorite

Due to its soil-like behavior and the limitations of GSI in granular residues, the highly weathered zone was modeled using the Mohr-Coulomb criterion. The effective shear strength parameters (c', ϕ') for this unit were derived by linearizing the non-linear strength envelope over the operative stress range calculated for the spillway slopes.

3.5.7. Numerical stability analysis

Slope stability was evaluated using FEM coupled with the SSR technique. This approach allowed for the calculation of the Strength Reduction Factor (M_{sf}) without pre-defining the failure surface geometry. The analysis evaluated both static and pseudo-static conditions, simulating staged excavation sequences and the sequential installation of support elements. Seismic design parameters were derived in compliance with the TBDY (Turkish Building Earthquake Code) 2018 regulations.

3.5.8. Support system and ground improvement design methodology

The remediation strategy for the spillway excavation was structured to address two concurrent stability threats: deep-seated global failure mechanisms governed by the thick, arenized (saprolitic) horizons, and the rapid surficial degradation of the exposed rock mass due to atmospheric weathering. The design methodology followed a multi-staged approach integrating geometric optimization, systematic structural reinforcement, and hydrogeological management.

3.5.8.1. Geometric optimization and slope flattening

The primary stabilization measure involved the optimization of the excavation geometry through iterative numerical simulations. The design methodology necessitated a transition from preliminary steep inclinations to flatter, more conservative gradients (slope regrading). This geometric easing was specifically adopted to reduce gravitational driving moments acting on critical slip surfaces and to accommodate the identified depth of the weathered profile within the safe excavation limits.

3.5.8.2. Systematic structural support strategy

To remediate the instability of the cut slopes, a systematic support system was designed to provide confinement and increase shear resistance across potential failure planes. The reinforcement methodology comprised two key components:

Systematic rock bolting

Passive rock bolts were employed on a regular grid pattern to knit the fractured rock mass and anchor the potentially unstable surface wedge into the competent bedrock. The methodology allowed for adaptive bolt lengths to ensure penetration beyond the critical weathering depth.

Surface protection and confinement

To prevent the unraveling of the friable arenized matrix and to isolate the moisture-sensitive saprolite from atmospheric exposure, a continuous structural facing was implemented. This consisted of reinforced shotcrete with steel wire mesh, acting as a unified shell to distribute bolt loads and preserve the residual strength of the excavation face.

3.5.8.3. Drainage and hydrogeological control

A comprehensive drainage strategy was integrated into the remediation design to mitigate the destabilizing effects of pore water pressure and seepage forces within the dispersible matrix. The methodology involved the installation of deep sub-horizontal drains (weep holes) to relieve internal hydrostatic pressures behind the shotcrete lining, coupled with a surface water management system comprising interceptor and toe ditches to minimize infiltration.

3.5.8.4. Foundation soil improvement

For spillway structures founded on variable granodiorite units, a ground improvement methodology was adopted to enhance bearing capacity and counteract uplift forces. This included the use of vertical anchorage elements to secure the concrete liner and intake structures against sliding and hydraulic uplift mechanisms.

3.5.8.5. Numerical verification criteria

The efficacy of the proposed remediation measures was verified using the Finite Element Method (FEM) with Shear Strength Reduction (SSR). The design was iteratively refined to ensure that the reinforced slopes met the rigorous project safety criteria: a Strength Reduction Factor (SRF) equivalent to FS $\geq$1.50 for static loading and FS $\geq$ 1.00 for pseudo-static seismic loading.

Design iterations were performed to ensure that the reinforcement successfully redistributed shear strains away from the critical weathered zones.

Table 3.9 illustrates the methodology and tools applied in Case 5.

Table 3.9. *Summary of methodology and tools applied in Case 5*

Method/ Test	Purpose/ Output (condensed)	Software/ Tool/ Standard
Rotary core drilling (water flush)	Stratigraphy; weathering zoning (massive vs. arenized); RQD logging	–
Standpipe piezometers	Static groundwater level; phreatic surface definition	–
Packer–Lugeon test	Hydraulic conductivity in fractured massive rock	–
Falling-head permeability test	Hydraulic conductivity in permeable/arenized upper zones	–
Laboratory rock mechanics	γ, UCS (σci), elastic modulus (E) on competent cores	–
Grain size distribution analysis	Material classification	TS 1900-1
Volumetric joint count	Jv for massive granodiorite (Eq 2.3)	Palmström (2001) correlation
Modulus of elasticity derivation	Intact modulus Ei for arenized granodiorite (Ei = 0.4 × σci^0.854)	Ocak (2008) correlation
Modified GSI system	Rock mass quality quantification	ISRM (1981)
Generalized Hoek–Brown	Non-linear rock-mass strength parameters	RocLab
Mohr–Coulomb criterion	Linearized parameters for material behavior	–
Constitutive modeling	Hybrid: Hoek–Brown (massive rock) + Mohr–Coulomb (arenized/saprolitic)	RS2
FEM (SSR)	Stability (Msf); staged excavation simulation	RS2
Pseudo-static analysis	Seismic stability evaluation	RS2 / TBDY 2018 parameters

3.6. Case 6: Intake Portal Stability and Rapid Drawdown Analysis

This section details the methodological framework employed for the stability assessment and support design of the intake portal excavations. The investigation specifically focuses on the moisture-induced strength degradation of the clay-rich sedimentary units and their response to reservoir level fluctuations. A multi-staged Rapid Drawdown (RDD) analysis was implemented, transitioning from a highly conservative "instantaneous" screening approach to a rigorous transient seepage simulation to evaluate the influence of pore pressure dissipation on global stability.

3.6.1. Field investigation and structural mapping

A targeted subsurface investigation was implemented to establish the geological model and identify critical lithological contacts.

3.6.1.1. Borehole exploration

Core boreholes were utilized to map the contact between the massive limestone and the underlying moisture-sensitive clay-rich sedimentary formation. In-situ Menard Pressuremeter Tests (PMT) were performed at regular intervals to determine the deformation modulus (E_{PMT}) and limit pressure (P_L) in accordance with the ASTM D4719-20 standard.

3.6.1.2. Structural mapping and monitoring

Surface mapping was conducted to characterize discontinuity orientations for kinematic analysis. Furthermore, a topographic displacement monitoring system was established to track surface deformations and validate numerical model predictions.

3.6.2. In-situ hydraulic characterization

To provide the necessary parameters for the transient seepage models, the hydraulic properties of the rock mass were characterized through in-situ testing:

3.6.2.1. Lugeon testing

Water pressure tests were conducted within selected borehole intervals to quantify the rock mass permeability.

3.6.2.2. Hydraulic conductivity derivation

The obtained Lugeon values (Lu) were converted to hydraulic conductivity (K) for implementation in the numerical analysis. The conversion followed the standard empirical approximation:

$$k \approx Lu \times 10^{-7} \text{m/s} \tag{3.4}$$

This parameter served as the primary input for simulating the time-dependent pore pressure response during reservoir drawdown stages.

3.6.3. Laboratory testing and water sensitivity analysis

Testing focused on the physical-mechanical properties of the sedimentary units, with a specific emphasis on their susceptibility to water-induced softening.

3.6.3.1. Standard rock mechanics

Tests included UCS, unit weight, and Poisson's ratio determination. Uniaxial compressive strength and deformability tests (elastic modulus and Poisson's ratio) were executed according to ASTM D7012-14 (TS 2030) standards, while unit weight and physical properties were determined following TS 1900-1 procedures. Triaxial compressive strength tests were conducted on selected intact rock core specimens to define shear strength envelopes (c', ϕ').

3.6.3.2. Saturation sensitivity

A critical methodological component involved Point Load Strength Index (Is_{50}) testing in both dry and 48-hour immersed states. The observed reduction from 4.93 MPa (dry) to 0.36 MPa (saturated) necessitated a design approach that explicitly accounts for saturated rock mass properties. The point load strength index tests were conducted in compliance with the TS 699 standard.

3.6.3.3. Durability

Slake Durability Index (I_{d2}) tests were utilized to quantify the disintegration rate of the clay-rich matrix under wetting-drying cycles (TS 699).

3.6.4. Empirical rock mass classification (dual-state GSI)

Geomechanical quality was assessed through a Dual-State GSI assignment to represent the moisture-induced degradation:

3.6.4.1. Dry state

Standard GSI values were derived based on the Hoek and Marinos (2000) charts.

3.6.4.2. Saturated state

Reflecting the high slaking susceptibility, reduced GSI values were assigned for saturated conditions, following the modifications suggested by Sönmez and Ulusay (2002).

3.6.4.3. Disturbance factor

A disturbance zone extending approximately 3.0 m from the excavation face was incorporated into the models to account for mechanical excavation-induced damage and stress relaxation.

3.6.5. Multi-stage slope stability and drawdown framework

The stability of the portal slopes was evaluated using the Limit Equilibrium Method (LEM) within Slide2. Seismic loading was represented through a pseudo-static approach in accordance with the Turkish Seismic Code provisions (DD-2), and the stability acceptance criteria were defined for both static and seismic conditions. The analysis followed a hierarchical approach to distinguish between theoretical worst-case risks and realistic performance:

3.6.5.1. Level 1: Conservative screening (instantaneous drawdown)

This stage simulated an "extremely conservative" scenario by assuming instantaneous reservoir drawdown. The rock mass was treated as fully saturated with the phreatic surface coinciding with the slope face, representing a condition where no pore pressure dissipation occurs. This stage was used to identify the maximum theoretical reinforcement requirements.

3.6.5.2. Level 2: Rigorous design (transient seepage analysis)

To evaluate slope stability during drawdown under physically representative conditions, transient finite element seepage simulations were conducted. By incorporating the hydraulic conductivity (k) derived from in-situ Lugeon tests and the storage characteristics of the rock mass, the model quantified the time-dependent pore pressure lag. This methodology enabled a more rigorous determination of the factor of safety as a function of the actual reservoir drawdown rate.

3.6.6. Remedial measure and support design methodology

The stabilization strategy for the intake portal was developed by contrasting the design outcomes of a preliminary conservative screening (Level 1) against a physically representative transient simulation (Level 2). This dual-stage methodology was employed to demonstrate that conventional "worst-case" assumptions lead to technically unreliable and over-engineered solutions in moisture-sensitive sedimentary units.

3.6.6.1. Reinforcement strategy (Level 1 - theoretical baseline)

The Level 1 "instantaneous drawdown" analysis, characterized by its disregard for pore pressure dissipation, dictated an intensive reinforcement strategy. To satisfy safety criteria under this purely theoretical state, the design required ϕ 32 mm rock bolts (L=12.0 m) with a minimum 8.0 m penetration into competent bedrock. While this design satisfied the FHWA-IF-03-017 guidelines for bond and tensile capacity, it represented an absolute upper bound of reinforcement rather than a realistic engineering requirement.

3.6.6.2. Design optimization and validation (Level 2 - rigorous analysis)

In contrast, the Level 2 transient seepage analysis—incorporating site-specific hydraulic conductivity (k) and reservoir drawdown rates—demonstrated that the slope is inherently stable without structural support. By capturing the realistic dissipation of pore water pressures, this rigorous approach revealed that the excess pore pressure lag remains well below critical thresholds. Consequently, the heavy reinforcement necessitated by the Level 1 screening was identified as redundant and based on a physically unrealistic hydraulic model.

3.6.6.3. Field validation and design standard

The methodology incorporates pre-production pull-out tests as a verification tool for bond strength assumptions within the clay-rich matrix. However, within the scope of this study, these tests and the associated FHWA-based dimensioning serve primarily to highlight the degree of over-engineering inherent in Level 1 approaches. The verification effort confirms that while a support system can be theoretically validated for worst-case conditions, its implementation is rendered unnecessary by the superior predictive accuracy of transient numerical modeling.

Table 3.10 synthesizes the methodology and tools applied in Case 6.

Table 3.10. *Summary of methodology and tools applied in Case 6*

Method/ Test	**Purpose/ Output (condensed)**	**Software/ Tool/ Standard**
Research boreholes	Lithological contacts (limestone / clay-rich units); RQD logging	–
Structural geological mapping	Discontinuity orientations for kinematic analysis	ISRM (1981)
Topographic displacement monitoring	Coordinate/elevation change tracking for model validation	–
RMR & Q-system classification	Rock-mass quality; support correlation (tunnel/shaft)	Bieniawski (1989) / Barton et al. (1974)
Generalized Hoek–Brown	Rock-mass strength parameters	RocLab (Hoek and Brown, 1997)
Rock mechanics (UCS, deformability)	Intact strength; E; ν	TS 2030 / ASTM D7012-14
Triaxial compressive strength	Strength envelope; intrinsic parameters (c, ϕ)	TS 2030 / ASTM D7012-14
Menard pressuremeter test (PMT)	In-situ deformability characteristics	ASTM D4719-20
Saturation sensitivity (PLT)	Wet/dry point-load strength reduction factor	TS 699
Slake durability index	Disintegration susceptibility (wetting–drying)	TS 699

Table 3.10. (Continued) *Summary of methodology and tools applied in Case 6*

Method/ Test	**Purpose/ Output (condensed)**	**Software/ Tool/ Standard**
Dual-State GSI	Rock mass characterization (dry vs saturated)	Hoek and Marinos (2000) / Sönmez and Ulusay (2002)
Seismic design parameters	Spectral acceleration coefficients for stability	TBDY (2018)
Reinforcement design	Bond-capacity validation	FHWA-IF-03-017
Limit equilibrium method (LEM)	Global stability (FS) for Level 1–2 scenarios	Slide2
Level 1: RDD screening	Worst-case instantaneous drawdown check	Slide2 (LEM)
Level 2: transient seepage	Time-dependent u-dissipation; phreatic lag	Slide2 (FEA)
Support optimization	Compare Level 1 (conservative) vs Level 2 (rigorous)	Slide

3.7. Software Tools and Computational Framework

A multi-software workflow was implemented to (i) enable cross-verification between independent numerical approaches and (ii) support the distinct analysis components required across the six case studies. The software tools were selected based on their specific strengths regarding limit equilibrium stability assessment, finite element strength reduction, transient seepage modeling, non-linear dynamic time-history simulation, and structural verification of remedial components. Case-specific implementations are described within the relevant case sections; this subsection summarizes the primary role of each tool within the overall methodology.

3.7.1. Slide2 v9.038 (Rocscience)

Slide2 was employed for Limit Equilibrium Method (LEM) analyses where force–moment equilibrium-satisfying methods (e.g., Spencer and GLE/Morgenstern–Price) were used to evaluate global stability under static and pseudo-static loading. Advanced critical surface search workflows (e.g., Automatic Refine Search and non-circular strategies such as Cuckoo Search and Particle Swarm Search) were applied where needed to identify governing mechanisms, particularly along soil–rock contacts and heterogeneous interfaces. Where relevant, Slide2's integrated seepage analysis capabilities were also utilized to support time-dependent drawdown-related pore pressure interpretation and to cross-check assumptions adopted in transient seepage assessments.

3.7.2. RS2 v11.005 (Rocscience)

RS2 was utilized for Finite Element Method (FEM) analyses based on the Shear Strength Reduction (SSR) technique, enabling the identification of critical failure mechanisms without the need to prescribe a slip surface a priori. The software was particularly valuable for simulating staged construction sequences (e.g., sequential excavation and support installation) and for soil-structure interaction for the support systems.

3.7.3. PLAXIS 2D v2024 (Bentley)

PLAXIS 2D was employed for FEM analyses under plane strain conditions, specifically for cases requiring fully coupled dynamic time-history simulations. While it was also used for strength reduction (ϕ-c reduction) checks, its primary role was the performance-based seismic assessment of complex slopes. Dynamic boundary conditions were represented using viscous absorbing boundary formulations to reduce spurious wave reflections (e.g., Lysmer-type boundaries; Lysmer and Kuhlmeyer, 1969). Rayleigh damping was applied where required to obtain physically plausible energy dissipation in time-domain simulations, ensuring consistency with the constitutive modeling framework adopted for the materials.

3.7.4. RocLab and RocData (Rocscience)

RocLab (v1.033) and RocData (v3.015) were used to support standardized rock mass characterization and parameter derivation workflows. These tools facilitated the GSI-based Generalized Hoek–Brown parameterization and subsequent conversion to equivalent Mohr–Coulomb parameters over relevant stress ranges. The specific software selected depended on the analysis timeframe of the respective case study. Both tools were utilized to ensure consistency and traceability in the scaling of intact rock properties to rock mass strength and stiffness parameters, including the incorporation of disturbance considerations (e.g., excavation disturbance factor, D, where applicable). The derived parameter sets were then used as inputs to the limit equilibrium and finite element analyses described in the case-specific methodology sections.

3.7.5. SeismoSignal (Strong-Motion Processing)

SeismoSignal was used to process strong-motion accelerograms prior to their use in dynamic analyses. Processing included baseline correction and digital filtering to obtain physically consistent acceleration, velocity, and displacement time-histories, effectively reducing low-frequency drift and high-frequency noise.

3.7.6. SeismoMatch (Spectrum Matching)

SeismoMatch was used to spectrally match selected seed earthquake records to the project-specific target response spectrum for dynamic time-history analyses. Wavelet-based modification methodologies proposed by Abrahamson (1992) and Hancock et al. (2006) were followed to adjust the frequency content to achieve convergence with the target spectrum while preserving the non-stationary characteristics of the original records. The matched time histories were then used as input motions for the coupled dynamic simulations described in the relevant case study section.

4. CASE STUDIES AND ANALYSES

This chapter presents the practical application of the comprehensive field investigation and computational methodology established in Chapter 3. To rigorously evaluate the static and dynamic stability of slopes adjacent to appurtenant hydraulic structures, six distinct case studies have been meticulously selected and analyzed. These specific cases were chosen because they encompass a broad and highly challenging spectrum of "intermediate" geological materials frequently encountered in complex topographical environments, ranging from thick heterogeneous colluvial deposits and highly weathered saprolitic granodiorite to tectonically disturbed ophiolitic mélanges and moisture-sensitive sedimentary sequences. By investigating these diverse geomorphological settings, this chapter provides a holistic perspective on a wide variety of failure kinematics—including deep-seated rotational slides, saturated flow-type failures, and massive tectonic mobilizations—triggered by excavation unloading, extreme seismic excitation, and adverse hydro-mechanical conditions. Consequently, the analyses demonstrate a comprehensive array of adaptive stabilization approaches, from high-capacity active anchoring and massive passive rockfill buttressing to geometric reconfiguration and advanced hydrogeological management.

The chapter is structured to guide the reader through a logical progression of these varied geotechnical challenges. Section 4.1 examines a deep-seated landslide within a colluvial matrix near a spillway chute, focusing on pore-pressure triggers and active anchor stabilization. Section 4.2 investigates a massive geohazard within a radiolarite-limestone-mudstone sequence, demonstrating the concept of "Absolute System Lock-in" via rockfill buttressing under extreme seismic loading. Section 4.3 details the rapid argillization and subsequent instability of diversion tunnel portals in an ophiolitic mélange, contrasting theoretical pseudo-static failures with actual dynamic resilience and topographic restoration. Section 4.4 explores a flysch facies landslide exacerbated by uncontrolled surcharging and inadequate drainage, necessitating structural and geometric mitigation. Section 4.5 assesses a critical spillway excavation in friable arenized granodiorite that required a dynamically adapted zoned support strategy. Finally, Section 4.6 addresses the complex hydro-mechanical behavior of clayey sedimentary units at an intake portal under rapid drawdown (RDD) conditions, vividly illustrating the critical difference between theoretical conservative screening and realistic transient seepage modeling.

4.1. Case 1 – Landslide in Colluvium

This section presents a comprehensive analysis of a deep-seated landslide that occurred within a thick colluvial deposit overlying weathered sedimentary bedrock during the excavation for a major hydraulic structure. The case study details the site characterization, geotechnical evaluation, back-analysis, and remedial design for the slopes adjacent to the spillway chute and associated access roads at the dam construction site. Specifically, the study area encompasses a critical segment of the right bank slope, analyzed through five representative cross-sections (labeled Section 1 through Section 5) spaced at 20-meter intervals. The primary objectives of this evaluation were to assess the observed failure mechanism, investigate trigger factors—particularly groundwater influence and surcharge loading on the loose colluvium—and confirm controlling geotechnical parameters through back-analysis. Consequently, a robust stabilization strategy was developed to ensure the long-term stability of the excavation and preserve the integrity of the nearby critical tunnel and transportation infrastructure.

4.1.1. Project setting, slope geometry, and instrumentation

The study area encompasses the right bank slope of the spillway chute and adjacent transportation infrastructure, including an upper cut-and-cover tunnel and access roads. The investigation specifically focuses on an active landslide segment that manifested during the final stages of excavation and surface protection. Field observations indicate that the instability is primarily concentrated between Section 2 and Section 3, with signs of movement extending towards Section 4. Consequently, the geotechnical assessment covers the entire critical alignment represented by Section 1 through Section 5.

The project necessitated a deep excavation for the construction of the spillway chute. However, significant discrepancies between the encountered geological conditions—specifically regarding unit thicknesses and geotechnical parameters—and the initial design assumptions led to slope instability. Furthermore, the proximity of the existing tunnel structure imposed strict spatial constraints, limiting the feasibility of extensive unloading excavations and necessitating critical revisions to the remedial design geometry.

Original design protocols stipulated that excavation should be halted upon encountering colluvial deposits to allow for the implementation of specific ground improvement measures. However, during the execution phase, excavation proceeded through four benches within the weak colluvial matrix without such interventions. Instead, a surface support system comprising wire mesh and shotcrete was installed directly onto the loose deposits. This application inadvertently contributed to destabilization by introducing additional surcharge loading onto the weak slope and, due to restricted permeability, facilitating the accumulation of pore water pressure behind the shotcrete facing. These conditions precipitated the initial slope failure, which was subsequently accelerated by uncontrolled surface water infiltration into the compromised ground beneath the shotcrete and wire mesh system.

4.1.1.1. Slope geometry and excavation profile

The slope geometry consists of a tiered, benched excavation extending from the upper access road and cut-and-cover tunnel level down to the spillway foundation. While the initial geotechnical designs for these spillway cuts proposed a 1V:2H inclination, the geometry was subsequently revised to a steeper 1V:1H (approximately 45°) slope angle across multiple benched levels to accommodate the significant vertical relief and site boundaries. The excavation stages are typically spaced at vertical intervals of 2.50 m to 4.0 m, varying according to localized reinforcement schemes and lithological conditions.

The schematic cross-section of Section 3 illustrates the pre-failure slope geometry, the observed deep-seated slip surface, and the originally planned design excavation profile. Figure 4.1 portrays this schematic cross-section.

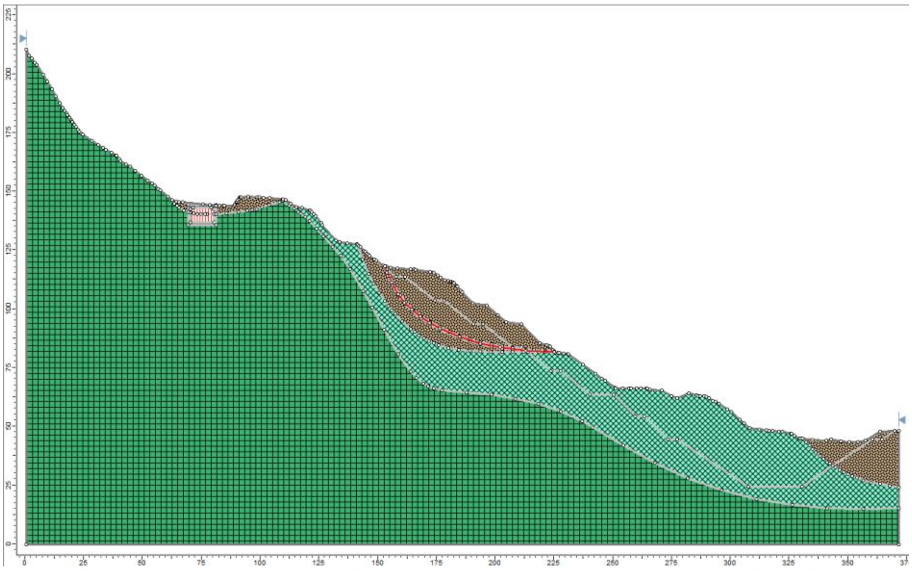

Figure 4.1. *Schematic cross-section of Section 3 illustrating the pre-failure slope geometry, the deep-seated slip surface (red), and the design excavation limits*

4.1.1.2. Geological setting and material properties

The general geological setting is characterized by a thick colluvial overburden, described as silty, sandy gravel containing limestone blocks up to 100 cm in size. This unit overlies a sequence of weathered carbonate rocks belonging to the local sedimentary formation, specifically comprising highly fractured chalky limestone and clayey limestone. The failure surface was subsequently identified as deep-seated, typically developing near the lithological contact between the colluvium and the underlying chalky limestone.

4.1.1.3. Instrumentation and monitoring program

To characterize the landslide kinematics and monitor its temporal evolution, a comprehensive site investigation and instrumentation program was implemented. This included the drilling of nine exploratory boreholes. Two of these were utilized strictly for lithological logging (coded BH-01 and BH-08), while the remaining seven were equipped with biaxial inclinometer casings (coded SI-02 through SI-07, and SI-09) to depths of up to 51.5 m.

Monitoring was conducted periodically over an observation period of approximately 12 months. Key findings from this period include:

Displacement

During a 180-day monitoring interval corresponding to the dry season, cumulative displacements ranging from 7.5 mm to 150 mm were recorded, indicating persistent, slow-moving instability. It was anticipated that these movements could accelerate significantly during the subsequent rainy season.

Shear zones

Inclinometer profiles identified distinct shear zones at depths reaching 25.0 m.

Groundwater

Although initial site investigations did not encounter a continuous groundwater table, the post-excavation period revealed significant seepage exiting through drainage weep holes and tension cracks on the shotcreted slope face. This indicated the presence of irregular perched water levels within the colluvium, exacerbated by the accumulation of pore water pressure behind the low-permeability shotcrete facing and the subsequent infiltration of uncontrolled surface water into the compromised ground. Groundwater levels were quantitatively monitored using 50 mm PVC observation wells installed in boreholes BH-01 and BH-08.

4.1.2. Geological and geotechnical characterization

The stratigraphic sequence at the study area is characterized by a thick, heterogeneous overburden of uncontrolled fill and colluvium overlying a local sedimentary bedrock sequence. The geological setting is structurally complex, governed by a paleo-landslide basin and a series of faults that have generated extensive brecciated and sheared zones within the underlying lithologies.

4.1.2.1. Overburden units: colluvium and fill

The colluvium is primarily described as a dirty beige, silty, and sandy gravel containing limestone blocks. While typical block diameters range from 20 to 30 cm, observational studies indicate the presence of blocks reaching 50 to 100 cm, with an overall gravel-block ratio of approximately 20–25%. The unit is generally non-plastic and exhibits a loose to medium-dense relative density. A critical engineering challenge presented by this unit is its significant lateral and vertical variability in thickness, which was not fully captured during initial site investigations due to topographic constraints.

4.1.2.2. Bedrock lithology

The bedrock sequence is differentiated into two primary units based on weathering grades and geomechanical strength characteristics:

Chalky limestone and breccia

This unit is characterized as highly weathered, intensely fractured, and weak to very weak rock. Discontinuities are predominantly horizontal to sub-horizontal, exhibiting medium surface roughness. The rock mass quality is relatively poor, with a Geological Strength Index (GSI) of 36.

Clayey limestone

Stratigraphically underlying the chalky unit, this layer consists of moderately to slightly weathered and fractured rock. It exhibits higher geomechanical competence compared to the overlying unit, characterized by a GSI value of 49.

4.1.2.3. Geotechnical investigation and laboratory testing

Geotechnical characterization was supported by a comprehensive suite of field and laboratory investigations, including a network of boreholes and inclinometer installations. To quantify rock mass strength, approximately 100 Uniaxial Compressive Strength (UCS) tests and over 50 Point Load Index (PLI) tests were conducted.

Chalky limestone

A series of UCS tests ($n > 40$) yielded an average strength of approximately 2.4 MPa. However, this value was deemed overly conservative due to sample disturbance effects on the weak rock. Consequently, a design UCS value of $\sigma_{ci} = 4.0$ MPa was adopted, justified by over 30 PLI tests (which are less susceptible to sampling disturbance) that indicated an equivalent UCS of approximately 4.4 MPa.

Clayey limestone

UCS testing (n > 50) yielded an average of approximately 11 MPa. This was supported by approx. 20 PLI data, establishing a design UCS value of σ_{ci} = 12.0 MPa.

Representative geological cross-section at Section 4 is presented in Figure 4.2.

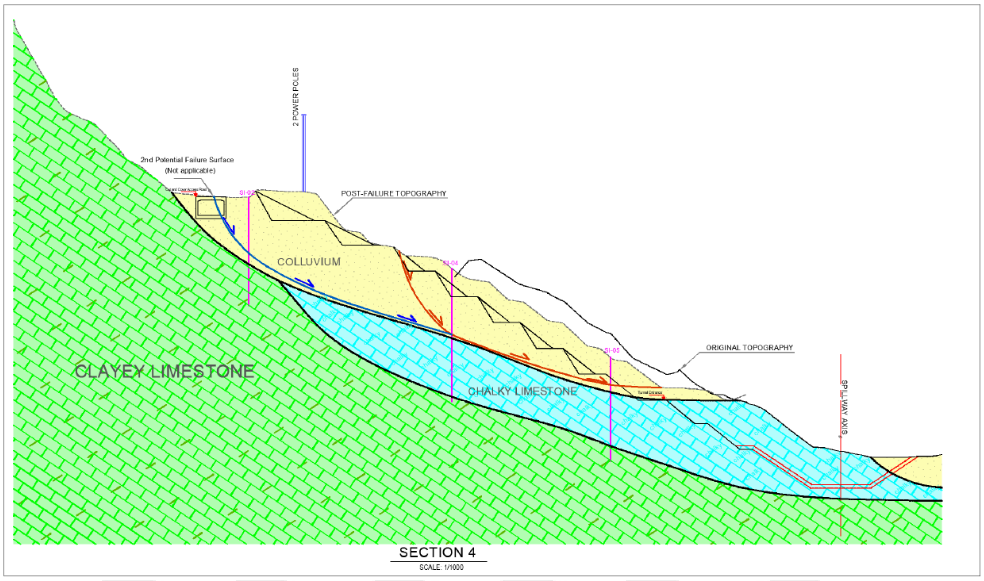

Figure 4.2. *Representative geological cross-section illustrating the colluvium thickness and bedrock interface at Section 4*

4.1.2.4. Constitutive modeling and design parameters

The stability analysis utilized the Generalized Hoek-Brown failure criterion for the rock mass units and the Mohr-Coulomb criterion for the soil units (colluvium and fill). For the rock mass, a disturbance factor of D = 0.5 was applied only to a depth of approximately 3.0 m from the excavation face to account for damage and stress relaxation, while D = 0 was applied to deeper, undisturbed units.

Initial design parameters for the colluvium (ϕ' = 28°, c' = 14 kPa) were found to be unconservative given the observed instability. Consequently, parameters were refined through back-analysis of the active failure, calibrating the colluvium's effective friction angle to ϕ' = 23°. Furthermore, the discrete slip surface identified by inclinometers—located near the colluvium-bedrock contact—was modeled using residual parameters (c_r' = 1 kPa, ϕ_r' = 23°) to account for the extreme shearing and pre-existing failure planes. Table 4.1 summarizes the utilized geotechnical design parameters.

Table 4.1. *Summary of geotechnical design parameters utilized in stability analyses*

Material	Color	Model Type	Unit Weight γ (kN/m³)	Eff. Cohesion c′ (kPa)	Friction Angle ϕ′ (°)	Stiffness E (MPa)	UCS (MPa)	GSI	Source/ Test Type
Colluvium		Mohr-Coulomb	18	23	23	350	-	-	Back-analysis
Slip Zone (Residual)		Mohr-Coulomb	18	1	23	-	-	-	Back-analysis
Chalky Limestone		Hoek-Brown	20	-	-	2100	4	36	Lab/GSI (m_i=9)
Clayey Limestone		Hoek-Brown	24	-	-	6600	12	49	Lab/GSI (m_i=9)

Shear strength for rock units was modeled using the Generalized Hoek-Brown criterion; therefore, c' and ϕ' are not direct inputs but are derived functions of normal stress. The deformation modulus (stiffness) for the rock mass units was estimated incorporating a disturbance factor of D=0.1 to conservatively account for excavation-induced damage; however, within the Limit Equilibrium Method (LEM) framework using Slide2, a depth-dependent approach was employed, assigning D=0.5 to the uppermost 3 m to reflect immediate surface disturbance, and D=0 for the underlying intact rock.

4.1.3. Failure mechanism, observed deformations, and groundwater conditions

The landslide mechanism is characterized as a deep-seated rotational failure, primarily developing within the thick, heterogeneous colluvial overburden and extending to the lithological contact with the underlying weathered chalky limestone. Significant instability was observed along the critical alignment spanning Section 1 through Section 5, where ground movement accelerated during the final stages of the multi-bench excavation and surface protection works.

4.1.3.1. Kinematics and observed deformations

Monitoring data acquired from these instruments (specifically SI-03, SI-04, and SI-06) localized the active shear zone at depths reaching 25.0 m. Due to the heterogeneous nature and high block content of the colluvial matrix, a thin, uniform residual shear plane was not anticipated. Instead, the failure mechanism is best characterized as a distributed shear band where shear strength was mobilized toward a residual state.

The temporal evolution of the slope behavior indicates a transition from marginal stability to active instability. Monitoring data obtained over an observation period of approximately 12 months revealed cumulative displacements ranging from 7.5 mm to 150 mm within a specific 180-day interval corresponding to the dry season. Although the significant block content initially contributed to a degree of structural interlocking, the steepened slope gradient (1V:1H) ultimately exceeded the available shear strength of the mass. Surface distress was extensively documented, characterized by the propagation of numerous tension cracks across the shotcreted slope face and along the upper bench levels. Geological cross-section at Section 3 illustrating the deep-seated failure surface identified by the inclinometer data is illustrated in Figure 4.3.

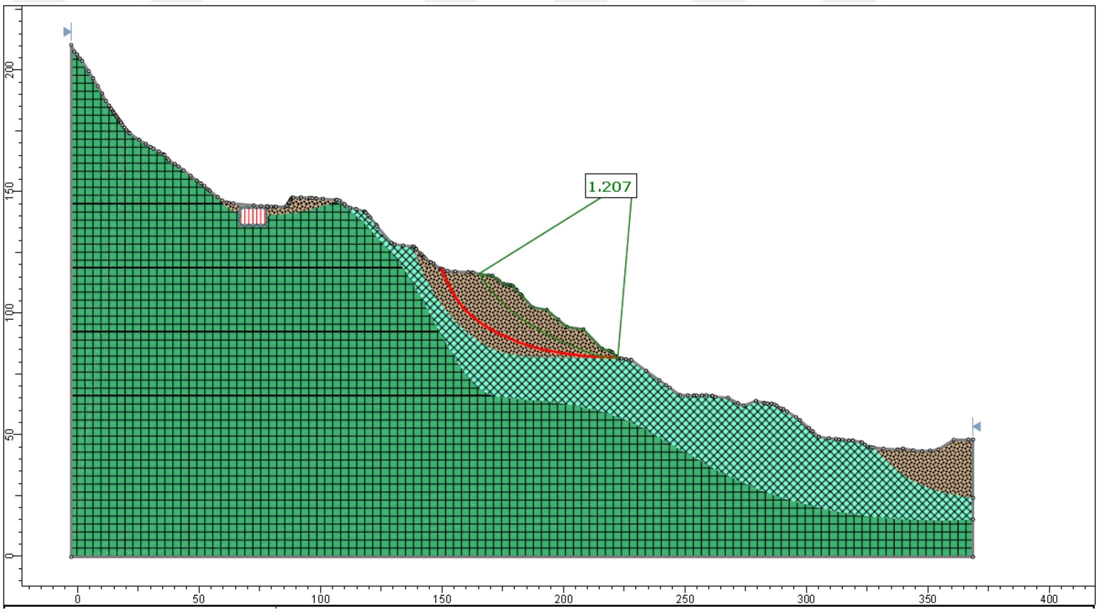

Figure 4.3. *Geological cross-section at Section 3 illustrating the deep-seated failure surface identified by inclinometer data (non-circular analysis)*

4.1.3.2. Hydrogeological triggers

Groundwater conditions, compounded by the operational deviations from design protocols, were identified as a primary triggering factor for the observed instability. Although initial site investigations did not detect a continuous phreatic surface, post-excavation observations revealed significant seepage exiting through tension cracks and drainage weep holes. Assessments indicated that approximately 90% of the seepage flow bypassed the 3.0 m weep holes, primarily because the restricted permeability of the shotcrete facing facilitated the accumulation of pore water pressure rather than its controlled discharge. This suggests that groundwater, likely originating from higher elevations near the tunnel portals, traveled through high-permeability pathways within the blocky gravel matrix and became trapped behind the support system. Furthermore, the uncontrolled infiltration of surface water into the compromised ground, coupled with the additional surcharge loading from the shotcrete layer, drastically reduced the effective stress and accelerated the degradation of shear strength within the saturated clayey matrix of the colluvium.

4.1.3.3. Execution and support sequence

The progression of the excavation and the timing of support installation played a critical role in the slope's destabilization. Original design protocols stipulated that excavation should be halted upon encountering unforeseen thick colluvial deposits to allow for the implementation of specific ground improvement measures. However, during the execution phase, the excavation proceeded through four consecutive benches within the weak colluvial matrix without such interventions. Instead, a surface support system comprising wire mesh and shotcrete was installed directly onto the loose deposits. This application inadvertently contributed to instability through two mechanisms: (1) it introduced additional surcharge loading onto the weak slope face, and (2) the relatively impermeable shotcrete shell restricted natural face drainage, facilitating the accumulation of pore water pressure behind the facing.

4.1.4. Back-analyses using limit equilibrium (Slide2) and finite element (PLAXIS) methods

To verify the postulated failure mechanisms discussed in Section 4.1.3 and to calibrate the geotechnical parameters governing the instability, a comprehensive back-analysis was conducted. The numerical modeling approach consolidated the 2D Limit Equilibrium Method (LEM) via Slide2 (Rocscience) and the Finite Element Method (FEM) through PLAXIS 2D.

4.1.4.1. Numerical modeling strategy and setup

The model geometry was constructed based on the tiered spillway excavation, utilizing a plane strain assumption for the deep-seated rotational failure. Boundary conditions in the FEM models were established with standard fixed-base and laterally constrained settings. Constitutive modeling employed the Mohr-Coulomb failure criterion for the colluvium and fill units, while the underlying bedrock units were represented by the Generalized Hoek-Brown criterion.

Within the scope of this study, the linear elastic-perfectly plastic Mohr-Coulomb (MC) constitutive model was employed to simulate the deformation and failure mechanisms of the colluvial slope debris. Based on back-analyses calibrated with field inclinometer measurements, the effective shear strength parameters of the weak matrix—which govern the overall stability of the mass and the kinematics of the critical slip surface—were conservatively established as c' = 23 kPa and φ' = 23°. Conversely, the MC model inherently possesses a structural limitation in its stress-strain formulation, as it relies on a single, constant stiffness modulus (E). Consequently, to accurately capture the relatively small-magnitude field deformations recorded by the inclinometers within the finite element (FEM) model, the mass elasticity modulus was intentionally assigned a high value (E = 350 MPa). This adopted approach comprehensively reflects both the mechanical contribution of the high volumetric block proportion to the macroscopic mass stiffness and the high initial stiffness exhibited by the geomaterial in the small-strain domain, considering that the slope mass in the field has not yet reached an ultimate catastrophic failure state.

Groundwater representation was a critical component of the model setup. Because site investigations did not reveal a clear phreatic surface despite observed seepage, pore-water pressure was simulated using a pore-pressure ratio (r_u) of 0.15, representing approximately 30% saturation of the unstable mass cross-section.

4.1.4.2. Calibration of failure mechanism

The calibration logic followed an iterative back-analysis procedure to reproduce the active failure state (FS ≈ 1.0) identified by the inclinometer data and surface tension cracks across the representative critical cross-sections.

Dry conditions

Initial LEM analyses using the Spencer method in a dry state yielded a factor of safety of FS = 1.207 (non-circular) - 1.215 (circular). Since the theoretical failure condition requires FS ≤ 1.0, it was analytically confirmed that dry conditions alone could not explain the observed landslide.

Saturated state

By introducing the pore water pressure ratio (r_u = 0.15), and calibrating the colluvium to effective parameters of c' = 23 kPa and φ' = 23°, the calculated safety factor decreased significantly to FS ≈ 1.038.

Residual conditions

Further analysis modeled the distinct shear strip identified by inclinometers near the colluvium-bedrock contact. Utilizing residual strength parameters (c'_r = 1.0 kPa, φ'_r = 23°) under saturated conditions (r_u = 0.15), the LEM factor of safety dropped to a critical range of 0.944 – 1.009 across various sections. This confirms that the presence of elevated pore water pressures, combined with the mobilization of residual strength along the deep-seated interface, was the primary mechanism driving the slope failure.

FEM validation

Initial PLAXIS FEM simulations indicated that the system was unable to reach numerical equilibrium, confirming the active failure state. Furthermore, FEM deviatoric strain plots accurately localized the shear band at the weathered bedrock interface (depths up to 25.0 m), aligning with the inclinometer-detected shear zones.

Figure 4.4 displays the comparative dry vs. saturated analysis.

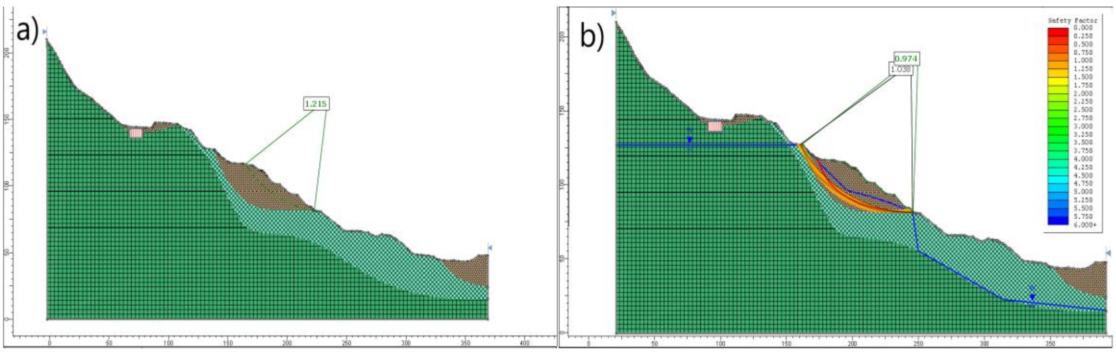

Figure 4.4. *Comparison of limit equilibrium back-analysis results for section Section 3, showing (a) the stable dry case (FS = 1.215) (circular surface) and (b) the critical failure case induced by pore water pressure (FS ≈ 1.0)*

Figure 4.5 depicts the back analysis accounting for residual shear zone at Section 2.

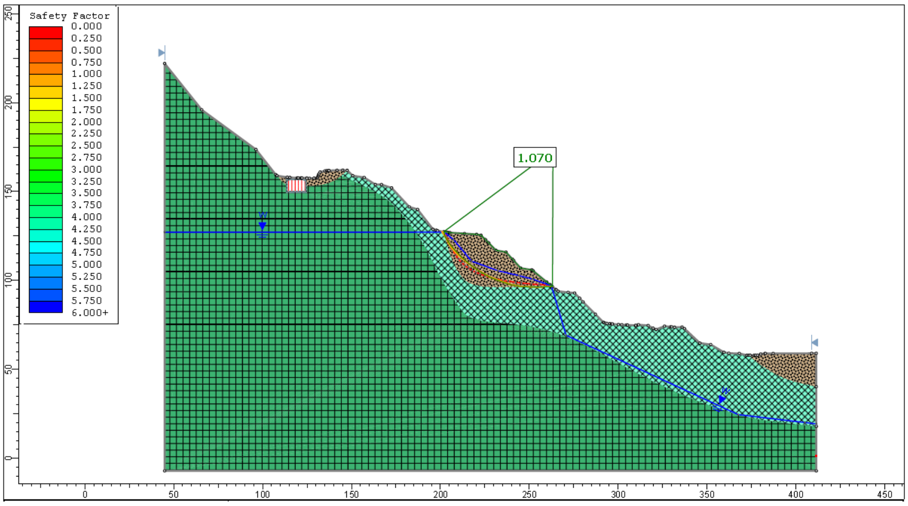

Figure 4.5. *Back analysis accounting for residual shear zone at Section 2 (fully saturated assumption, FS=1.070)*

A modified parameter set is evaluated in Figure 4.6.

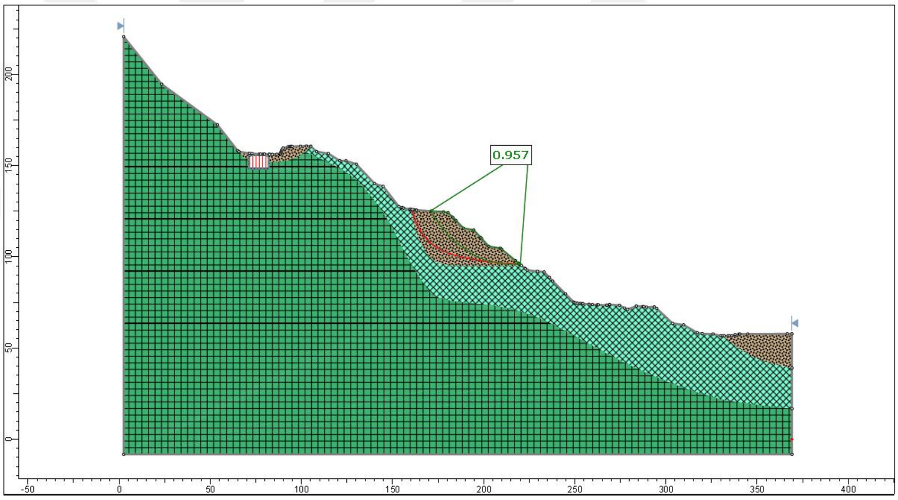

Figure 4.6. *Back analysis accounting for residual shear zone at Section 2 (r_u=0.15, FS=0.957)*

Figure 4.7 models the back analysis accounting for residual shear zone at Section 3 (r_u=0.15).

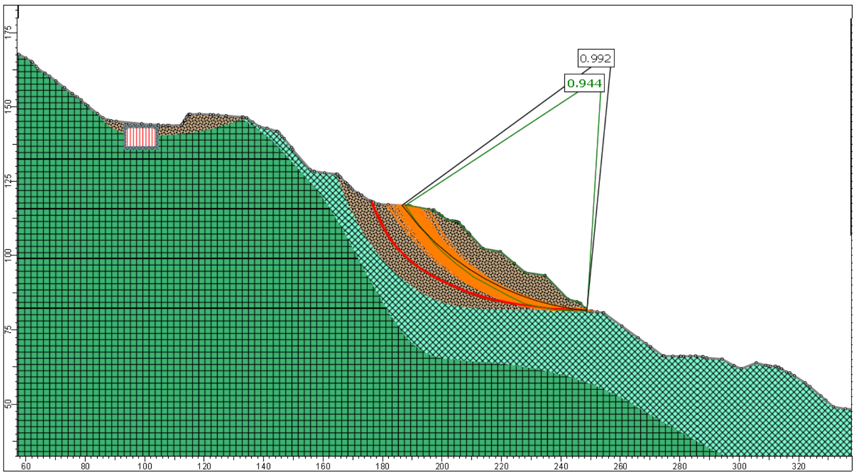

Figure 4.7. *Back analysis accounting for residual shear zone at Section 3 (r_u=0.15, FS=0.944-0.992)*

Back analysis accounting for residual shear zone at Section 4 (r_u=0.15) is outlined in Figure 4.8.

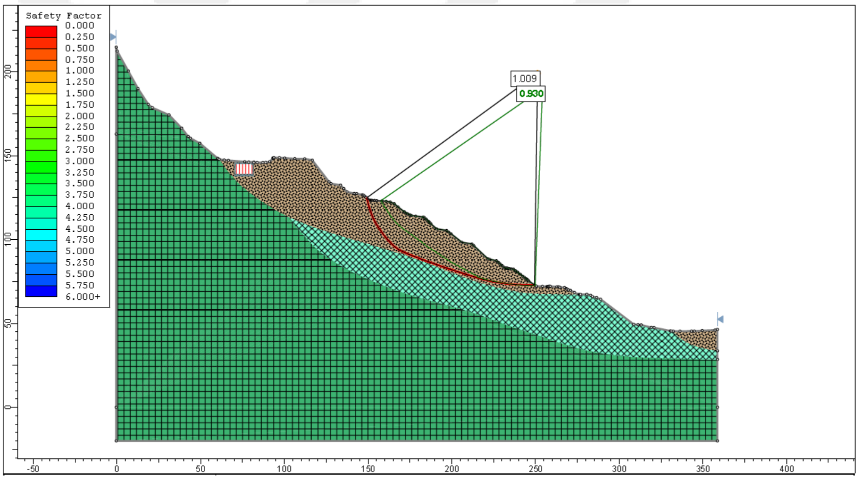

Figure 4.8. *Back analysis accounting for residual shear zone at Section 4 (r_u=0.15, FS=1.009)*

Figure 4.9 presents the back analysis results accounting for the residual shear zone at Section 5, with r_u = 0.15.

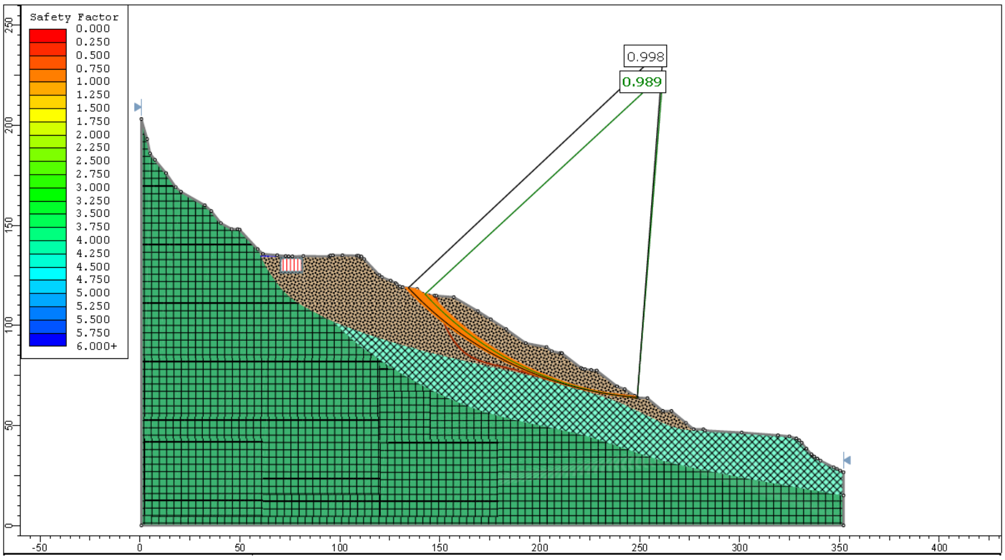

Figure 4.9. *Back analysis accounting for residual shear zone at Section 5 (r_u=0.15, FS=0.989-0.998)*

Initial FEM safety factor (M_{Sf}) evaluations for Section 4 and 5 are captured in Figure 4.10.

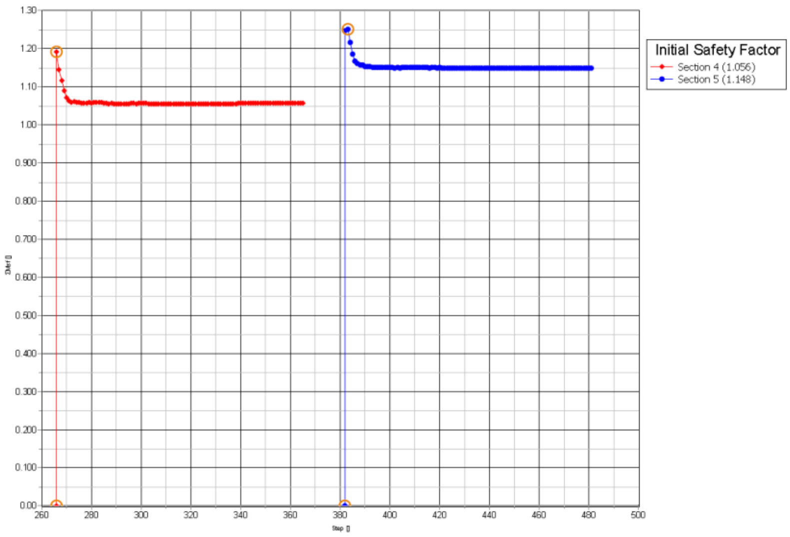

Figure 4.10. *Initial FEM safety factors (Msf) for Section 4 and 5 (FS=1.056-1.148)*

Figure 4.11 compares LEM slip surface and FEM deviatoric strain at Section 4.

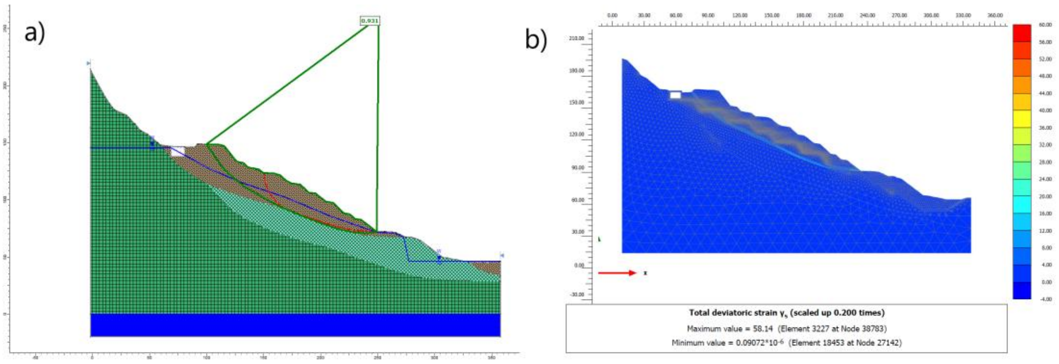

Figure 4.11. *(a) LEM slip surface and (b) FEM deviatoric strain comparison showing the localization of shear bands at the colluvium-bedrock interface at section 4*

Table 4.2 summarizes the comparison between LEM and FEM results during the back-analysis phase.

Table 4.2. *Comparison of LEM and FEM results for the back-analysis of the failure state*

Analysis Mode	**Condition / Trigger**	**Slide2 FS (Spencer)**	**Observed State**
LEM	Dry State (Static)	1.215	Stable (Pre-seepage)
LEM	Saturated (r_u=0.15)	0.944 – 1.009	Active Movement
FEM	Static	1.056 – 1.148	Near-Failure Condition

4.1.5. Remedial measures, support system, and post-remediation performance

The remedial strategy for the right bank landslide prioritized a holistic combination of geometric modification, comprehensive drainage, and deep reinforcement to stabilize the active colluvial mass. The primary intervention involved the maximum possible excavation of the unstable colluvium from the upper benched levels to reduce the driving mass. This geometric improvement was integrated with a phased, top-down construction of a hybrid ground support system supported by mandatory, aggressive groundwater control.

4.1.5.1. Structural support system

The geotechnical solution utilized three principal support elements tailored to the varying lithological conditions:

Active support system (pre-stressed anchored beams)

To ensure deep-seated stability in the most critical zones, an active reinforcement system was implemented, targeting the middle and lower elevations of the slope profile (Section 3, Section 4, and Section 5). These locations correspond to the areas where the remaining colluvial overburden (following remedial excavation) reaches its maximum thickness. The remedial design incorporates high-capacity, 7-strand pre-stressed ground anchors installed within 200 mm diameter drill holes, typically oriented at an inclination of 30° below the horizontal.

The technical specifications of this active support system are as follows:

- Load capacity: The system utilizes anchors with an ultimate tensile capacity of 1820 kN. The design specifies working loads of 983 kN for static conditions and 1310 kN for seismic loading scenarios.
- Geometry and bond: Total anchor lengths range from 15.0 m to 35.0 m to effectively intercept the deep-seated failure surface. To generate the required pull-out resistance, a minimum fixed bond length of 7.0 m is strictly socketed into the competent bedrock units. The design adopted specific bond strength values based on the socket lithology: 209.4 kN/m for chalky limestone (corresponding to a grout-ground adhesion of 333.3 kN/m²) and 377.0 kN/m for clayey limestone (corresponding to an adhesion of 600.0 kN/m²).
- Load distribution: To prevent punching failure within the weak soil matrix, anchor head loads are transferred to the slope face through 190 cm × 50 cm reinforced concrete spreader beams. This configuration ensures that bearing pressures remain within the allowable limits of the loose colluvium.

Passive support systems (soil nails and rock bolts)

In the upstream regions characterized by relatively variable overburden thickness (Section 1 and Section 2), a hybrid passive reinforcement strategy was adopted. While all elements consisted of ϕ32 mm steel bars installed within 65 mm diameter drill holes with a typical length of 12.0 m, their functional classification and design parameters were adapted based on the specific lithological profile encountered at each borehole location:

- Soil nails: Utilized where the reinforcement remained entirely within the loose colluvial matrix. For these elements, the design relied on a conservative grout-to-soil bond strength of 20 kN/m.

- Rock bolts: Employed within the same alignment (Section 1 and Section 2) wherever most of the reinforcement by length penetrated through the colluvium and socketed into the competent bedrock. By utilizing the rock socket, these elements mobilized a higher design bond strength of 68 kN/m (corresponding to a grout-ground adhesion of 333.3 kN/m²).

Surface protection and constructive reinforcement

Independent of the global stability measures, a comprehensive surface protection system was specified for the entire excavation face to mitigate surficial unraveling, prevent atmospheric weathering, and inhibit water infiltration. This system comprises steel-mesh reinforced shotcrete (Q188/188 mesh, 10–20 cm thickness) anchored by short constructive rock bolts (typically 3.0 m length applied in a 2.0 m × 2.0 m pattern). These short bolts are primarily designed to secure the facing elements and ensure local stability against wedge failures in exposed cuts, rather than contributing to deep-seated slope stability.

4.1.5.2. Drainage system design

Subsurface drainage was identified as the most critical component for long-term performance. Initial observations revealed that standard 3.0 m drainage weep holes were insufficient, with approximately 90% of seepage bypassing them through high-permeability pathways in the blocky gravel. Consequently, the revised design implemented a three-tier system:

Surface drainage

Concrete-lined channels and ditches (minimum 1% gradient) to intercept runoff.

Shallow drainage

Standard weep holes behind shotcrete to prevent water column buildup.

Deep horizontal drains

Long perforated PVC drains installed at a 5° upward inclination, extending to the lithological contact with the underlying chalky limestone. Every third weep hole in a horizontal row was extended to reach this interface, effectively intercepting the perched water table responsible for the failure.

Table 4.3 catalogs a summary of support system components and design specifications.

Table 4.3. *Summary of support system components and design specifications*

Support Category	**Support Type**	**Specification / Material**	**Spacing (V x H)**	**Length / Depth**
Active Support System	Pre-stressed Anchored Beams	Anchor: 7-strand steel (1820 kN ult. capacity); Working loads: 983 kN (static) / 1310 kN (seismic); Ø200 mm drill hole. Head: 190 cm × 50 cm reinforced concrete spreader beams.	2.5–4.0 m × 1.5–5.0 m	Total: 15.0–35.0 m (Bond: Min. 7.0 m fixed length in bedrock)
Passive Support Systems	Soil Nails (In loose colluvium)	Bar: Ø32 mm steel bar; Ø65 mm drill hole. Bond: Grout-to-soil bond strength of 20 kN/m.	2.0–3.5 m × 2.0–3.5 m*	12.0 m
	Rock Bolts (Socketed into bedrock)	Bar: Ø32 mm steel bar; Ø65 mm drill hole.Bond: Rock socket bond strength of 68 kN/m (Mobilized via rock socket).	2.0–3.5 m × 2.0–3.5 m*	12.0 m
Surface Protection & Constructive Reinforcement	Constructive Rock Bolts	Short rock bolts designed to secure facing elements against wedge failures.	2.0 m × 2.0 m	3.0 m
	Shotcrete & Mesh	Steel-mesh reinforced shotcrete (Q188/188 mesh).	Continuous	10–20 cm thickness
Drainage	Horizontal Drains	Perforated PVC (Long-reach).	Variable (1 in 3 rows)	Bedrock interface

4.1.5.3. Post-remediation stability and seismic deformation assessment

Following the implementation of the remedial design, comprehensive stability requirements were established as FS > 1.50 for static loading and FS > 1.0 for seismic loading. A horizontal seismic coefficient (k_h) of 0.22 was utilized for both LEM and FEM analyses, representing the Operating Basis Earthquake (OBE = 0.22), while the Maximum Design Earthquake was defined as MDE = 0.44. The stability assessment in FEM used the Phi-c reduction technique to calculate the safety factor (ΣM_{sf}), accounting for the method's ability to model complex, interconnected failure mechanisms.

Performance evaluation using updated Limit Equilibrium (LEM) and Finite Element (FEM) simulations confirmed the adequacy of the proposed measures.

- Static stability: Under effective drainage conditions ($r_u = 0$), the Factor of Safety (FS) for critical sections improved significantly, ranging from 1.599 to 1.725, surpassing the design requirement. Post-remediation stability analyses for the critical alignment (Section 3, Section 4, and Section 5) demonstrated full compliance with the mandated design safety criteria.
- Sensitivity analysis: To account for potential drainage clogging, analyses were performed with a pore-pressure ratio of $r_u = 0.15$. The system maintained a temporary FS between 1.383 and 1.399 (e.g., Section 3 achieved an FS of 1.383), providing a sufficient safety margin for maintenance interventions.
- Seismic stability: Pseudo-static analyses ($k_h = 0.22$) yielded safety factors exceeding unity (e.g., 1.005 – 1.448) across all sections in Slide2.

Crucially, while LEM analyses demonstrated safety factors exceeding the acceptable limits, Section 4 and Section 5—characterized by the thickest colluvial deposits and the highest potential for deformation impacting the critical tunnel structure—were further evaluated using PLAXIS 2D to assess soil-structure interaction and permanent deformations. FEM analysis confirmed that under seismic loading ($k_h = 0.22$), the calculated maximum permanent displacements for Section 4 and Section 5 were 0.2334 m and 0.2766 m, respectively. Furthermore, the seismically induced displacement at the critical lower-right corner of the cut-and-cover road structure was recorded at approximately 0.20 m.

To evaluate the safety and serviceability of the structure under these specific displacements, it is essential to contextualize the numerical results within established empirical and analytical frameworks. According to the seminal work by Hynes-Griffin and Franklin (1984) on rationalizing the seismic coefficient method for earth structures, permanent earthquake-induced displacements up to 1.0 m are generally considered a "tolerable upper limit" that would not immediately threaten the overall integrity or stability of the primary retaining or impounding systems. Their comprehensive study established that if the safety factor remains above 1.0 when applying a pseudo-static coefficient equivalent to half of the peak ground acceleration ($k_h = 0.5 \times PGA/g$), the resulting deformations will remain within acceptable, non-catastrophic limits.

Additionally, as illustrated in the empirical displacement regression charts based on Newmark sliding block models developed by Hynes-Griffin and Franklin (1984) shown in Figure 4.12, the ratio of the critical yield acceleration to the maximum peak acceleration (k_y/k_{max} or N/A) heavily dictates the expected permanent slip. For a critical yield acceleration of $k_y = 0.22$ under a Maximum Design Earthquake (MDE) peak ground acceleration of 0.44g, the resulting seismic coefficient ratio is N/A = 0.50. At this specific ratio, the estimated permanent displacement corresponding to the upper bound curve is approximately 22 cm, with the mean and mean+σ predictions falling significantly lower (well below 10 cm).

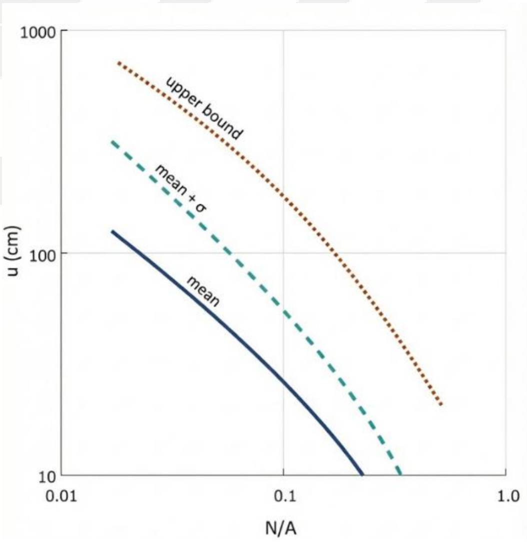

Figure 4.12. *Permanent seismic displacement versus critical seismic coefficient ratio (N/A) based on empirical sliding block regression models (Hynes-Griffin and Franklin, 1984)*

The displacements calculated via the rigorous pseudo-static finite element approach in PLAXIS 2D (≈20 cm) fall significantly below the 1.0 m catastrophic threshold. When evaluated at the specific seismic coefficient ratio of N/A = 0.50, the empirical upper-bound conservative estimate derived from the chart is approximately 22 cm. The PLAXIS 2D results align remarkably well with this empirical upper-bound prediction. Given that the numerical model computes a comprehensive continuum-based total displacement—incorporating cumulative static deformations from preceding phases and distributed elastoplastic strains induced by the sustained inertial force, rather than merely isolated rigid-block slip—this correlation is highly consistent and mathematically sound. Therefore, it can be concluded that the structural integrity of the cut-and-cover structure and the overall slope stability are reliably preserved. The predicted deformations are well within tolerable limits for serviceability, indicating that the chosen stabilization measures and the current geomechanical configuration provide robust resistance against the anticipated seismic demand. Figure 4.13 visualizes a static limit equilibrium analysis of Section 1 for the proposed stabilization, while Figure 4.14 presents the seismic analysis for the section.

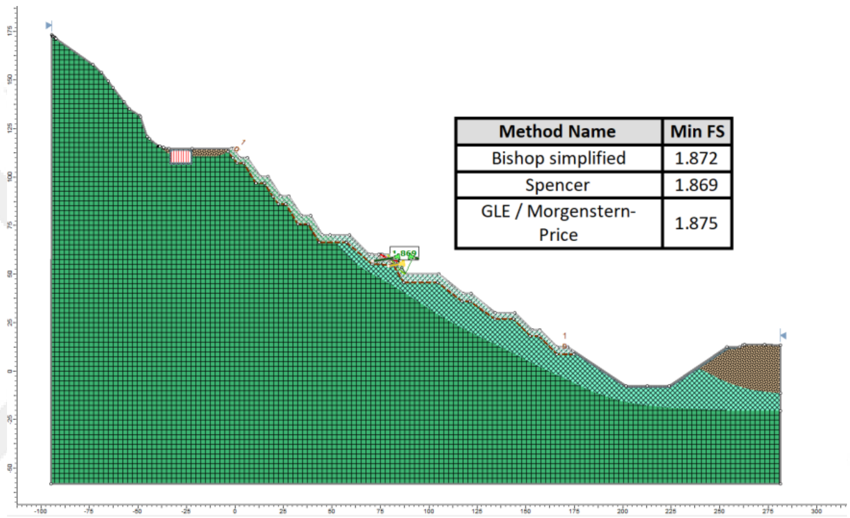

Figure 4.13. *Static limit equilibrium analysis of Section 1 for the proposed stabilization*

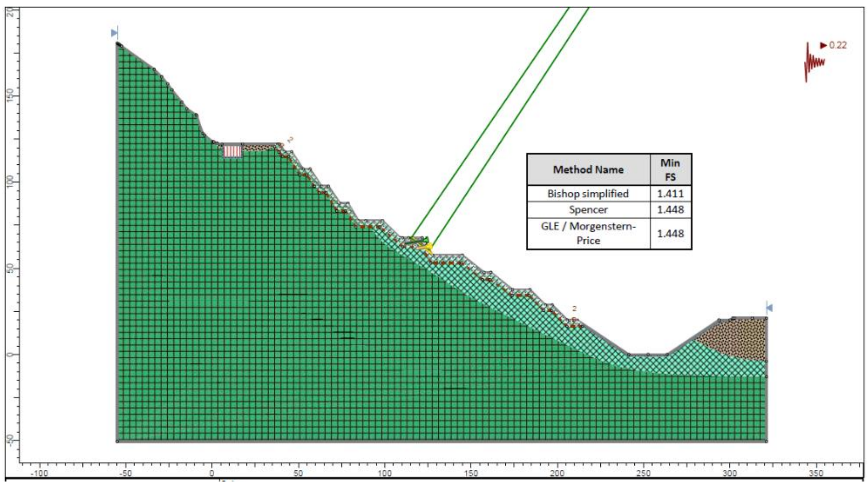

Figure 4.14. *Seismic limit equilibrium analysis of Section 1 for the proposed stabilization*

Figure 4.15, and Figure 4.16 feature static and seismic limit equilibrium analyses of Section 2 for the proposed stabilization, respectively.

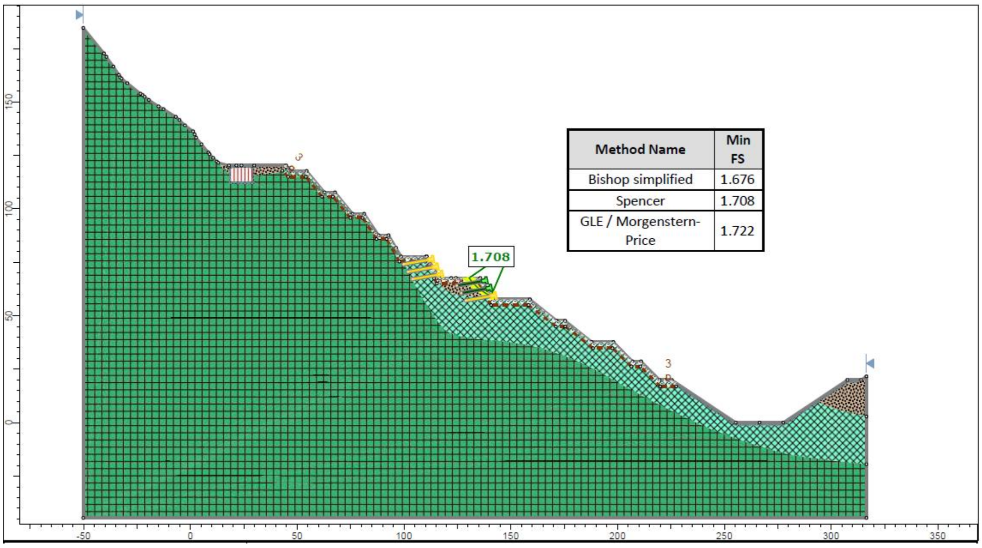

Figure 4.15. *Static limit equilibrium analysis of Section 2 for the proposed stabilization*

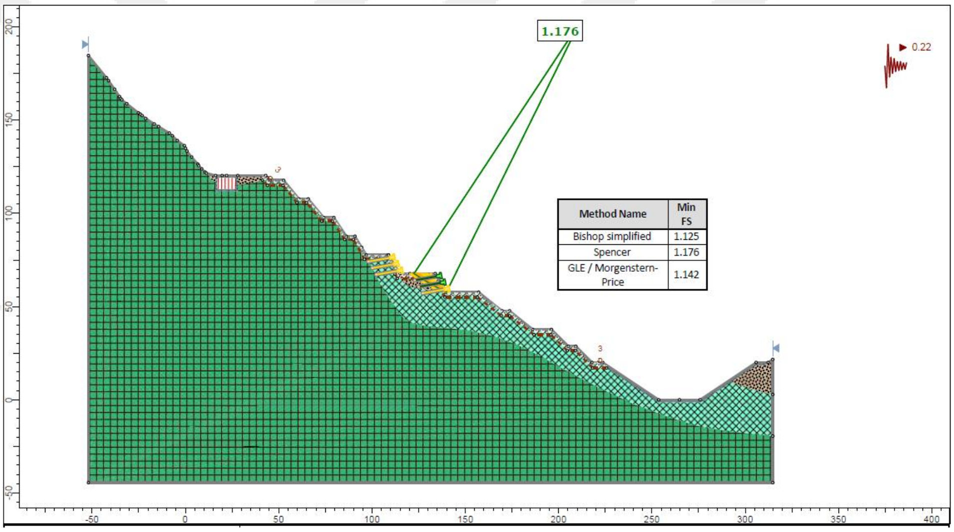

Figure 4.16. *Seismic limit equilibrium analysis of Section 2 for the proposed stabilization*

Figure 4.17 demonstrates a limit equilibrium analysis of the representative critical cross-section, Section 3, detailing the achieved Factor of Safety under static loading conditions, while Figure 4.18 displays the seismic limit equilibrium equivalent.

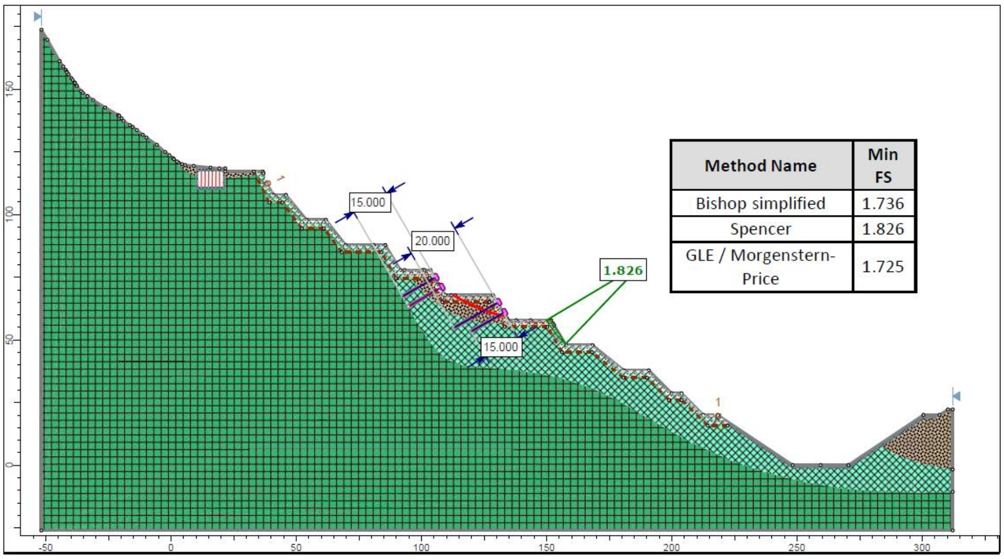

Figure 4.17. *Limit Equilibrium analysis of the representative critical cross-section, Section 3, demonstrating the achieved Factor of Safety for the proposed stabilization measures under static loading conditions*

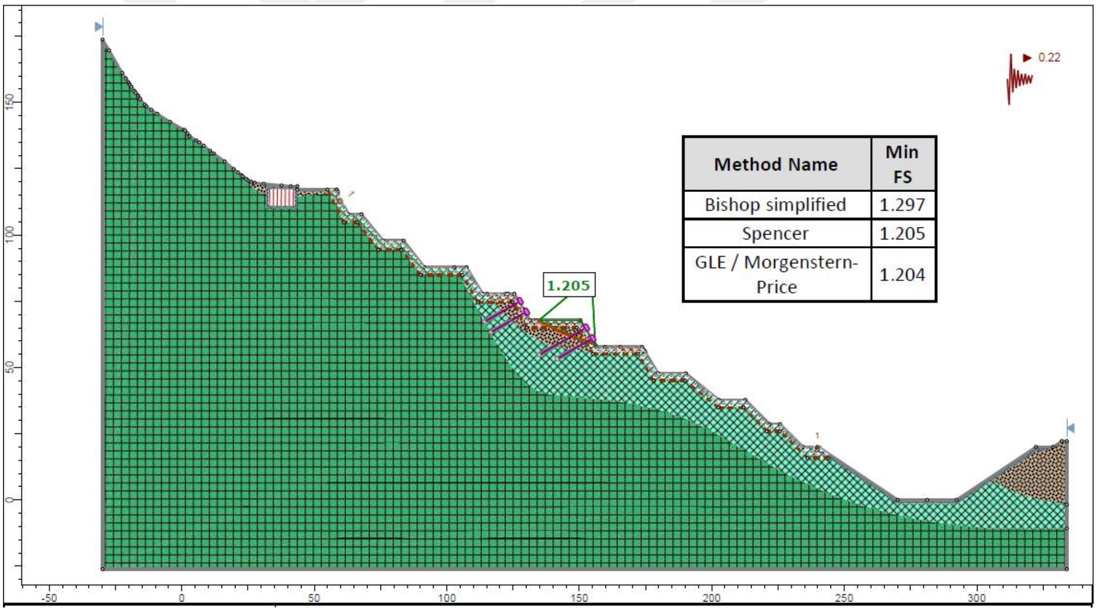

Figure 4.18. *Limit Equilibrium analysis of the representative critical cross-section, Section 3, demonstrating the achieved Factor of Safety for the proposed stabilization measures under seismic loading conditions*

Figure 4.19 expresses a static limit equilibrium analysis of Section 4 for the proposed stabilization, and Figure 4.20 details the seismic limit equilibrium analysis.

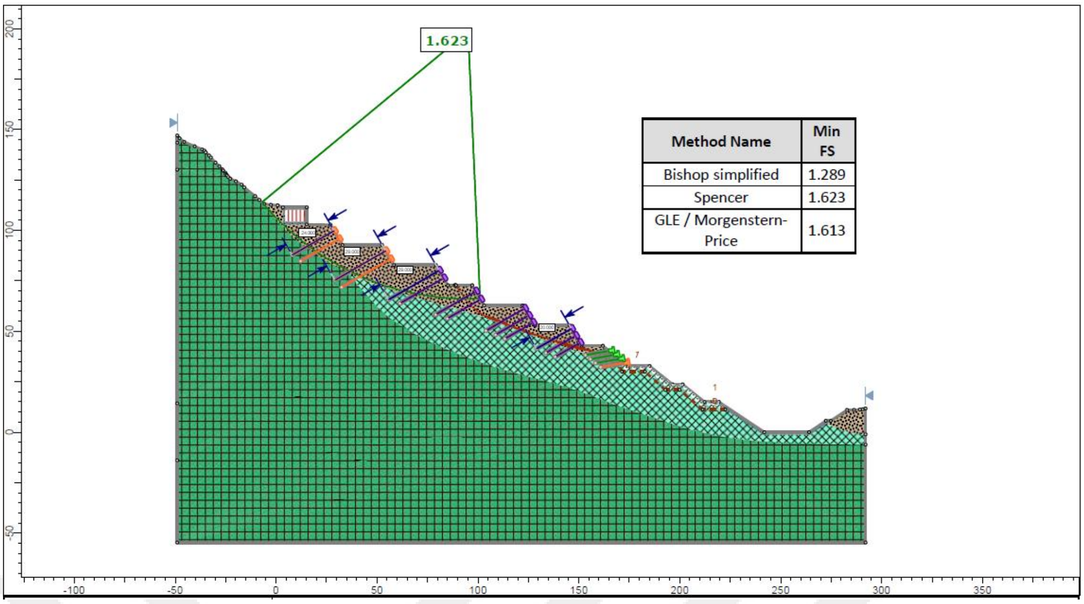

Figure 4.19. *Static limit equilibrium analysis of Section 4 for the proposed stabilization*

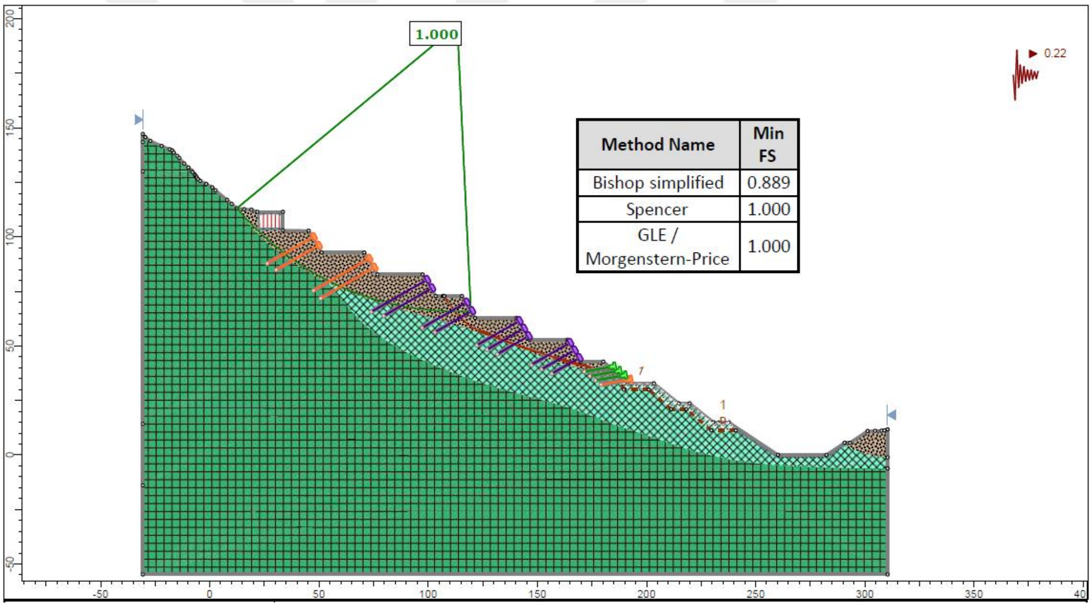

Figure 4.20. *Seismic limit equilibrium analysis of Section 4 for the proposed stabilization*

Figure 4.21 presents the static limit equilibrium analysis of Section 5 for the proposed stabilization, while Figure 4.22 outlines the seismic limit equilibrium analysis for the section.

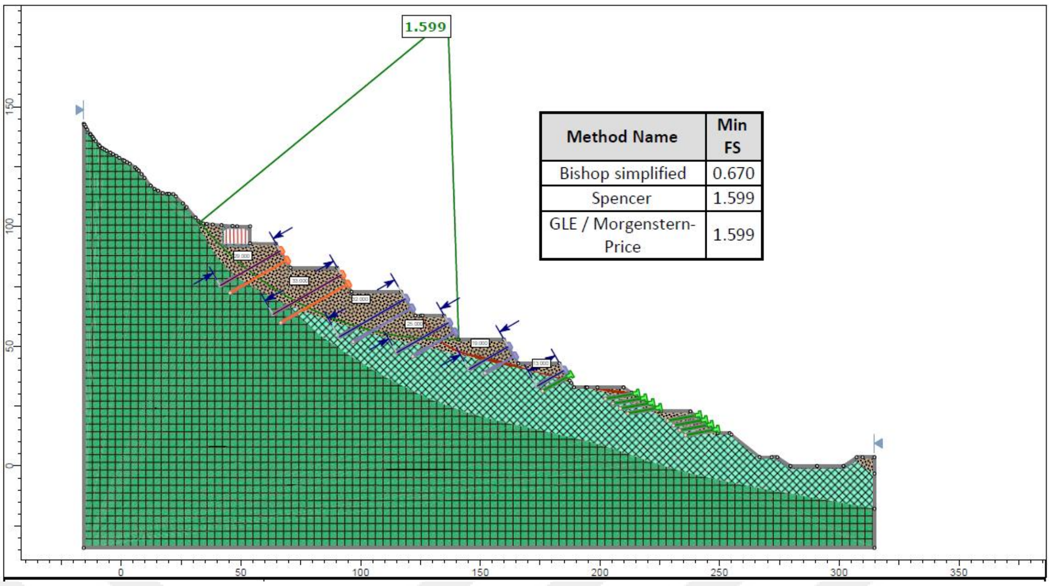

Figure 4.21. *Static limit equilibrium analysis of Section 5 for the proposed stabilization*

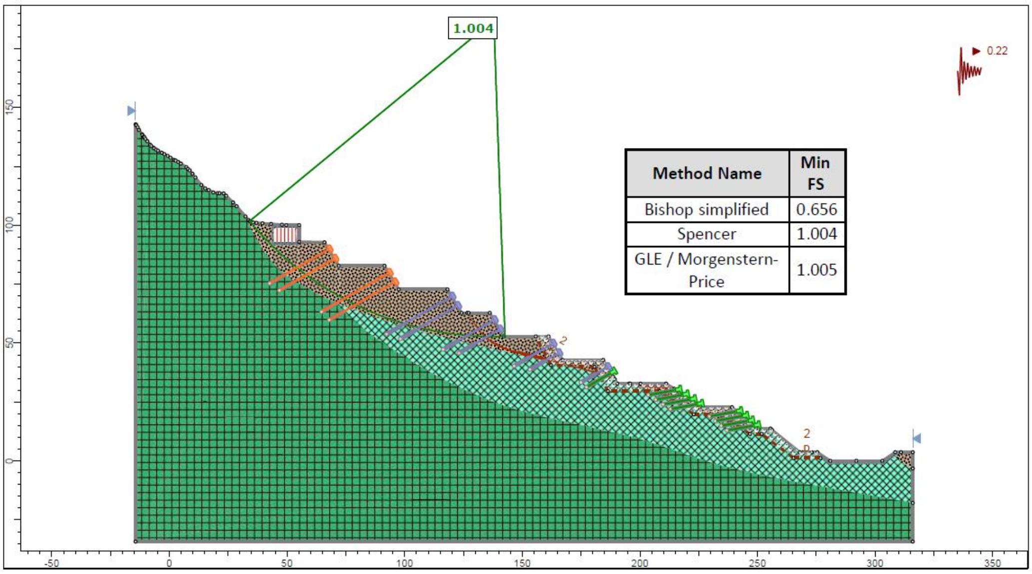

Figure 4.22. *Seismic limit equilibrium analysis of Section 5 for the proposed stabilization*

Figure 4.23 portrays FEM analysis models for Section 4 and Section 5 at the final construction stage.

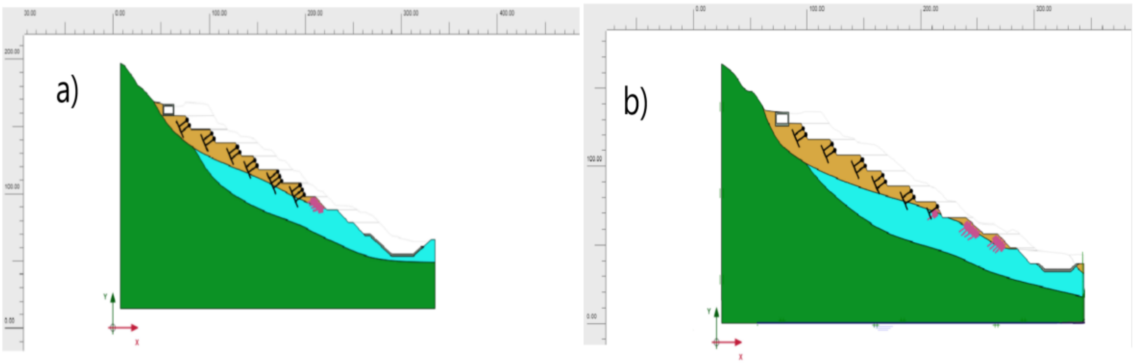

Figure 4.23. *FEM analysis models for (a) Section 4 and (b) Section 5 at final construction stage*

Figure 4.24 presents the Finite Element Method (FEM) analysis results for Section 4 under static conditions, illustrating the effectiveness of the support system.

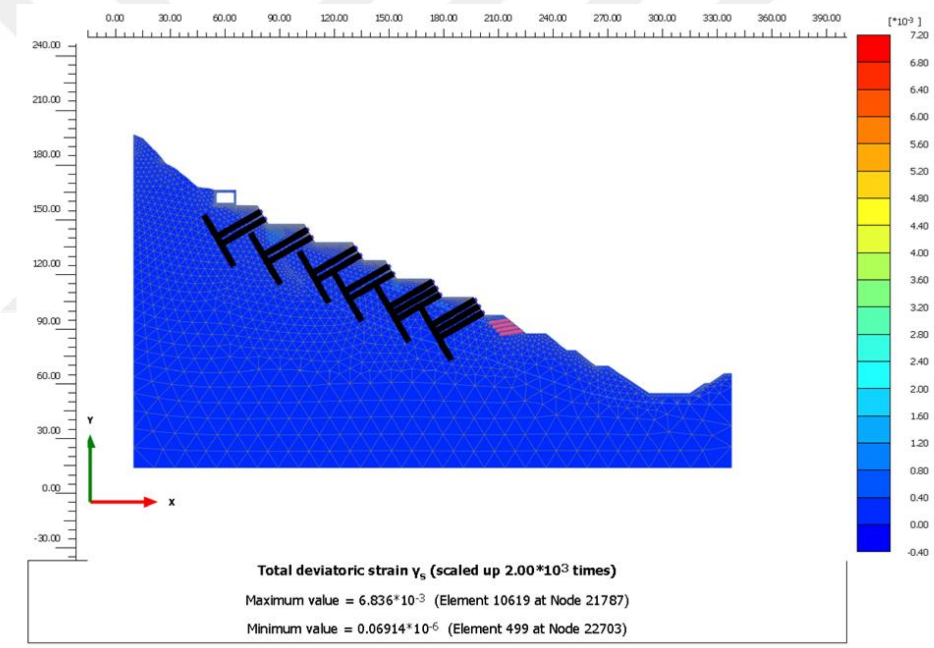

Figure 4.24. *Finite Element Method (FEM) analysis results for Section 4 under static conditions (Calculated FS ≈ 1.55). The deviatoric strain contours illustrate the effectiveness of the support system in limiting shear strain development and preventing failure mechanism formation*

Table 4.4 tabulates a summary of factors of safety for the remediated slope at critical sections.

Table 4.4. *Summary of factors of safety for the remediated slope at critical sections*

Section	Static FS (Dry)	Seismic FS (k_h=0.22)	Static FS (r_u=0.15)
3	1.725	1.204	1.383
4	1.613	1.000	1.399
5	1.599	1.005	1.386

Figure 4.25 shows the limit equilibrium analysis result at Section 3, and Figure 4.26 presents the limit equilibrium analysis result at Section 4.

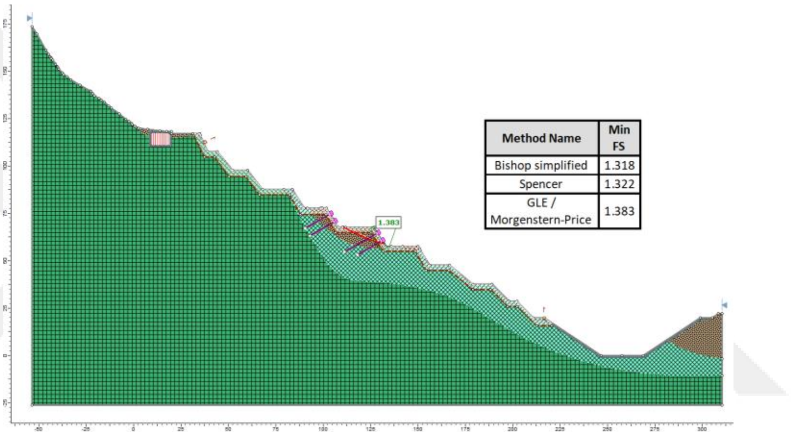

Figure 4.25. *Limit equilibrium analysis result at Section 3 (r_u=0.15, FS=1.383)*

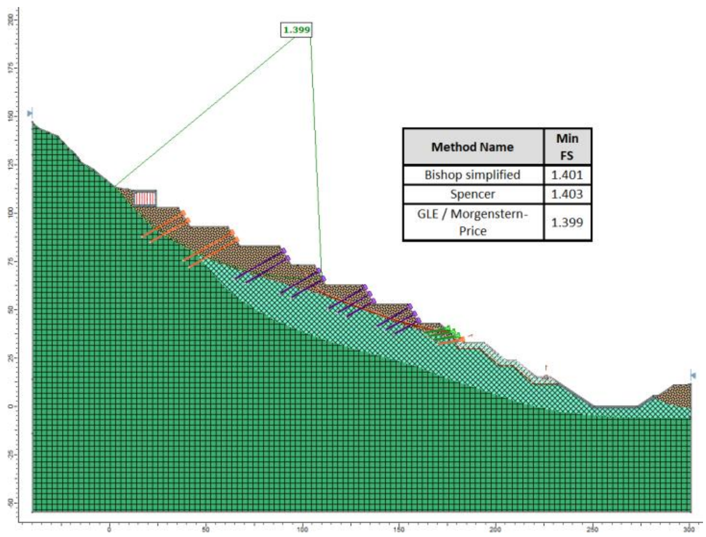

Figure 4.26. *Limit equilibrium analysis result at Section 4 (r_u=0.15, FS=1.399)*

Figure 4.27 presents the limit equilibrium analysis result at Section 5.

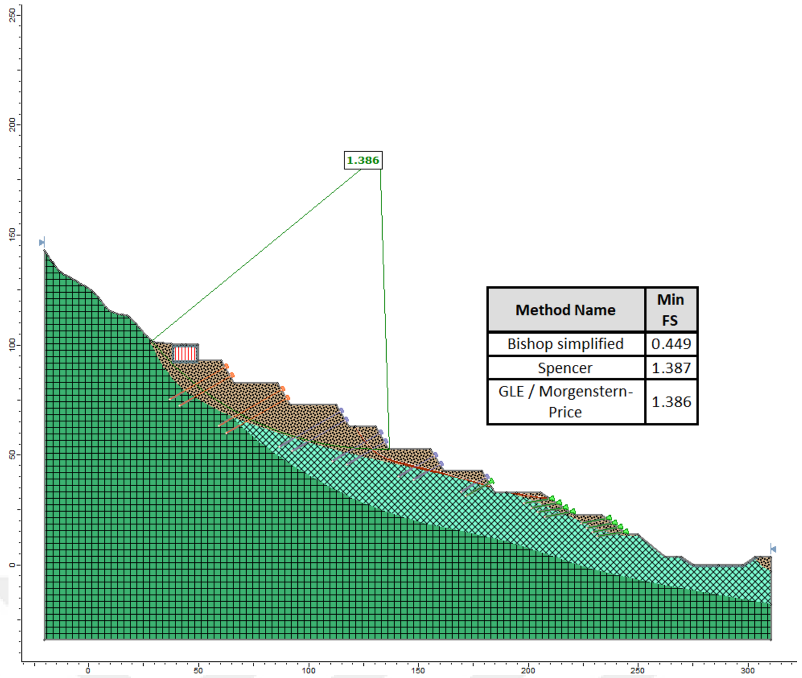

Figure 4.27. *Limit equilibrium analysis result at Section 5 (r_u=0.15, FS=1.386)*

Table 4.5 compiles a comparison of safety factors before and after remediation.

Table 4.5. *Comparison of safety factors before and after remediation*

Analysis Condition	Analysis Method	Pre-Remediation FS	Post-Remediation FS
Static (Drained)	Slide2 (Spencer)	1.215	1.599 – 1.725
Static (Saturated, r_u=0.15)	Slide2 (Spencer)	0.944 – 1.009	1.383 – 1.399
Pseudo-static (k_h=0.22)	Slide2 (Spencer)	< 1.0	1.005 – 1.448
Seismic Displacement	PLAXIS (FEM)	Unstable	≈ 20 cm (Acceptable, under tolerable limits)

Figure 4.28 clarifies the static and seismic safety factors (Msf) after remediation for Sections 4 and 5.

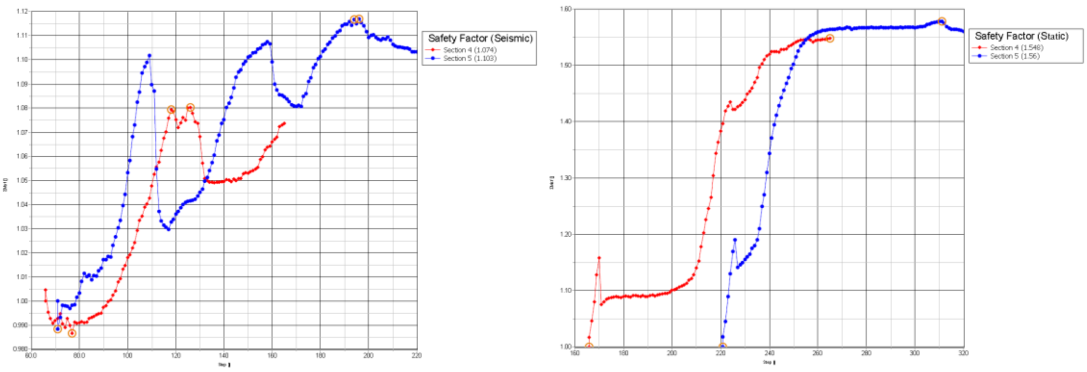

Figure 4.28. *Static and seismic safety factors (M_{sf}) after remediation for Section 4 (M_{sf}^{static}=1.548; $M_{sf}^{seismic}$=1.074) and Section 5 (M_{sf}^{static}=1.56; $M_{sf}^{seismic}$=1.103)*

Figure 4.29 displays the finite element displacement vectors for the remediated slope under seismic loading, confirming stability of the tunnel foundation at Section 4.

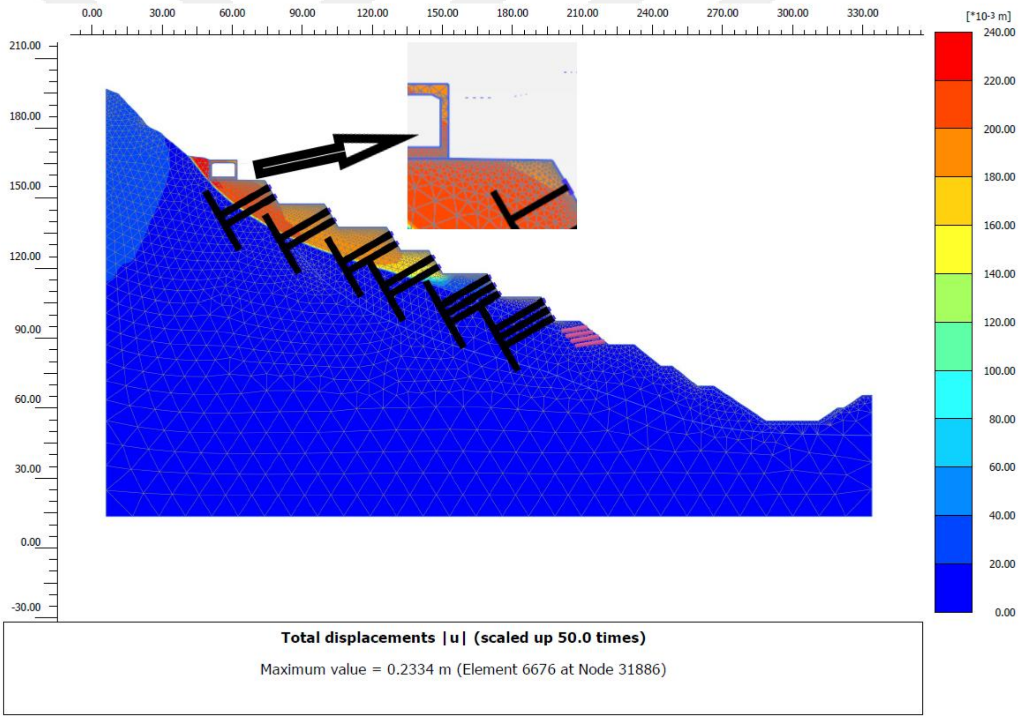

Figure 4.29. *Finite element displacement vectors for the remediated slope under seismic loading, confirming stability of the tunnel foundation (Section 4)*

Figure 4.30 shows the finite element displacement vectors for the remediated slope under seismic loading, confirming stability of the tunnel foundation at Section 5.

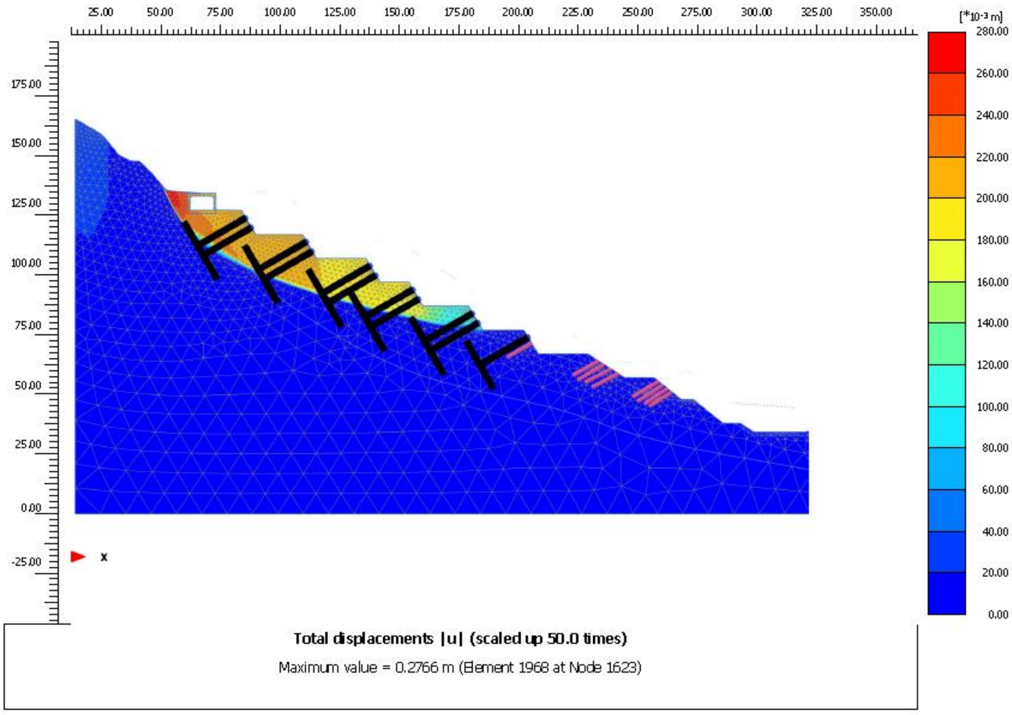

Figure 4.30. *Finite element displacement vectors for the remediated slope under seismic loading, confirming stability of the tunnel foundation (Section 5)*

4.1.6. Lessons learned

The primary lesson learned from this case study is that conventional investigation densities may fail to resolve the complex variability of colluvium thickness and the presence of ancient landslide features. The back-analysis confirmed that the mobilization of the shear band to a residual state ($c'_r \approx 1$ kPa, $\varphi'_r \approx 23°$) rendered the slope highly sensitive to pore-pressure fluctuations. Consequently, in blocky gravel environments, short drainage weep holes are inherently inadequate; stabilization requires deep interceptor drains.

Furthermore, this study underscores the absolute necessity of employing high-capacity tieback anchors in thick colluvial deposits governed by deep-seated kinematics. When anticipated failure surfaces propagate at significant depths, shallow surficial supports—such as standard soil nails or short constructive bolts—are fundamentally insufficient to halt mass movement. To ensure global stability and effectively mobilize resisting tensile forces, active structural reinforcement elements must physically penetrate the deep active shear zones and be rigorously socketed with sufficient fixed bond lengths into the underlying competent bedrock.

Additionally, the successful remediation highlights the necessity of early instrumentation, which allowed for the accurate calibration of residual strength parameters before catastrophic acceleration occurred.

Finally, this study demonstrates the paramount importance of adopting a deformation-based approach for the seismic assessment of critical infrastructure. While traditional Limit Equilibrium Methods (LEM) are sufficient for verifying global stability thresholds, coupling them with advanced Finite Element Methods (FEM) is strictly necessary to evaluate complex soil-structure interactions and quantify permanent ground displacements. Benchmarking these numerical deformations against established empirical criteria—such as the tolerable displacement limits defined by Hynes-Griffin and Franklin (1984)—provides a highly robust and verifiable framework. This dual-methodology ensures not only the prevention of catastrophic failure but also guarantees that the structural components will maintain strict serviceability standards under the Maximum Design Earthquake (MDE) demand, characterized by a Peak Ground Acceleration (PGA) of 0.44g and a corresponding critical yield acceleration of $k_y = 0.22$.

4.2. Case 2 – Landslide in a Mudstone–Fill–Radiolarite–Limestone Sequence (Partly Colluvial)

This section presents a comprehensive analysis of the slope instability encountered at the downstream left bank of a Concrete-Faced Rockfill Dam (CFRD) project with a structural height exceeding 100 m. Situated within a highly complex and active tectonic belt at the convergence of two major continental plates, the project involves substantial excavations for the main embankment and appurtenant hydraulic structures. The primary objective of this study was to assess the kinematic failure mechanisms affecting these critical structures—specifically the spillway and the diversion tunnel—calibrate shear strength parameters through rigorous back-analysis, and develop a robust remediation strategy centered on rockfill buttressing to ensure long-term stability under both static and extreme seismic loading conditions.

4.2.1. Project setting, slope geometry, and instrumentation

The natural topography of the left abutment is characterized by a steep vertical relief, extending from the valley floor to the dam crest elevation, with a total height differential exceeding 130 m. Construction of the facility commenced in the previous decade, involving significant excavations.

The geological setting is characterized by a complex tectonic sequence (ophiolitic mélange), which primarily consists of an ultramafic unit (Serpentinite–Peridotite) and a pelagic sedimentary unit (Radiolarite–Limestone–Mudstone). These units are frequently sheared, folded, and imbricated due to their proximity to major active fault zones, resulting in a foundation mass that is highly weathered and fragmented. Much of the unstable slope is covered by Quaternary colluvium and landslide debris comprising clay mixed with gravel and large limestone blocks.

Geotechnical evaluations identified slope instability on the left bank causing structural distress to the existing concrete spillway chute and the diversion tunnel outlet. This study focuses on the downstream landslide, which represents a large, complex kinematic system approximately 435 m in length and 160 m in width, formed by three nested landslide masses. The failure surface depth ranges between 28 m and 40 m, with a distinct shear zone identified at around 18–30 m. This mass directly impacts the serviceability of the spillway channel and the exit portal of the diversion tunnel. While the landslide toe partially overlaps with the downstream toe of the main dam embankment in a limited area, the primary dam structure is not directly intersected by the failure surface.

Figure 4.31 highlights an illustration of the general plan view of the dam structures and identified landslide areas.

Figure 4.31. *Illustration of general plan view of the dam structures and identified landslide areas*

To characterize the slope behavior and temporal evolution, a comprehensive site investigation and monitoring program was executed. Subsurface investigations included approximately 850 m of supplementary investigative drilling, nearly 100 Standard Penetration Tests (SPT), pressuremeter tests (PMT), and Lugeon permeability tests. Geophysical surveys employed seismic refraction, Electrical Resistivity Tomography (ERT), and PS-logging in selected boreholes.

The monitoring network established to track slope movements comprises:

1. Subsurface monitoring: Eleven research boreholes were equipped with inclinometers (10 units at 50 m depth and one at 40 m depth). The system utilizes a combination of 7 automated In-Place Inclinometers (IPI) and 4 manual inclinometers. These instruments identified distinct shear surfaces at depths consistent with the landslide geometry described above.
2. Surface monitoring: A geodetic network of 48 deformation points is surveyed monthly to track horizontal and vertical geometric variations.
3. Remote sensing: Long-term displacement history was derived using multi-temporal InSAR (Synthetic Aperture Radar Interferometry) analysis spanning a period of over a decade, supplemented by 3D Photogrammetric studies using LiDAR cloud data.

Table 4.6 documents a summary of the site monitoring and instrumentation system.

Table 4.6. *Summary of the site monitoring and instrumentation system*

Instrumentation Type	**Quantity**	**Installation/Monitoring Details**	**Purpose**
In-Place Inclinometers (IPI)	7	Automated; depths up to 50 m	Continuous monitoring of deep shear displacements
Manual Inclinometers	4	Depths up to 40–50 m	Periodic verification of shear zones
Geodetic Deformation Points	48	Surface network; monthly surveys	Tracking surface vectors (horizontal/vertical)
InSAR & LiDAR	N/A	Analysis period: Multi-year observation (>13 years)	Long-term historical displacement & topology

Table 4.7 registers a summary of landslide geometry and recorded shear surface depths.

Table 4.7. *Summary of landslide geometry and recorded shear surface depths*

Landslide Location	**Length (m)**	**Width (m)**	**Estimated Depth (m)**	**Shear Zone Depth (m)**	**Primary Observed Damage**
Downstream	435	160	28 – 40	18 – 30	Spillway chute, Diversion outlet

4.2.2. Geological and geotechnical characterization of the composite sequence

The geological environment of the project site is defined by a complex tectonic arrangement within a major regional suture zone, characterized by intense regional compression, folding, thrusting, and imbrication dating from the Late Cretaceous to the present. The lithological sequence at the left abutment primarily belongs to an ophiolitic complex, which comprises two dominant formations that have been tectonically juxtaposed:

- Pelagic sedimentary unit (Unit-1): This unit represents the primary unstable sequence, consisting of interlayered radiolarite, pelagic limestone, and mudstone/shale. Due to severe tectonic deformation, these sedimentary units are frequently wedged, imbricated, or segmented in both lateral and vertical directions.

- Ultramafic basement unit (Unit-2): Forming the basement, this unit consists of basic volcanics, specifically serpentinite and peridotite. It is stratigraphically divided into a highly weathered, fractured surface zone (Unit-2a) and a deeper, more competent base rock (Unit-2b).

The contacts between these units are primarily tectonic, characterized by shearing and slicing, which results in low Rock Quality Designation (RQD) values typically ranging between 0% and 30%. The bedrock is mantled by Quaternary deposits, including colluvium and paleo-landslide material (LM), with thicknesses ranging from 0.5 m to 5.0 m. These materials consist of an unsorted clay matrix enclosing gravels and large silicified limestone or ophiolitic blocks.

Figure 4.32 depicts a representative geological cross-section along the downstream landslide.

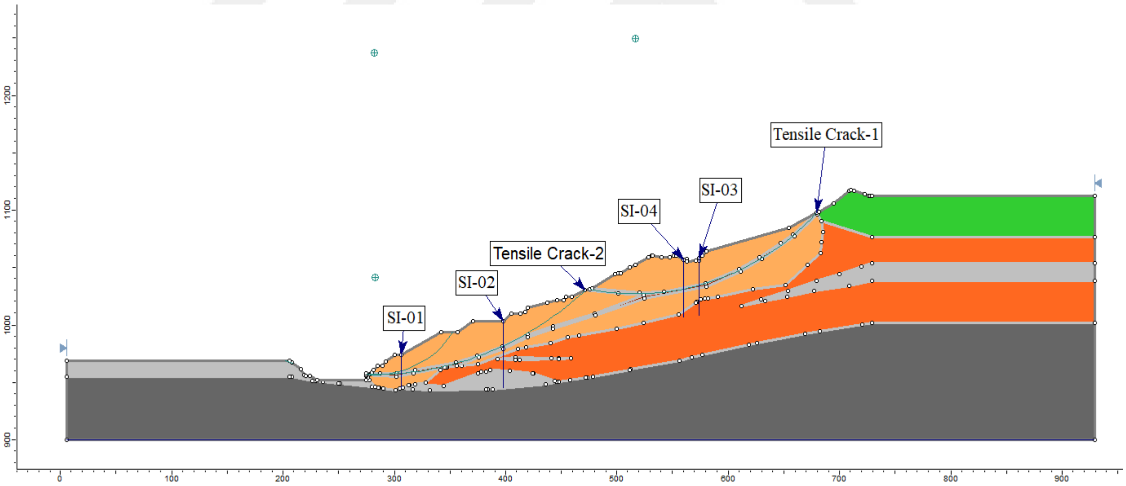

Figure 4.32. *Representative geological cross-section along the downstream landslide*

4.2.2.1. Geotechnical units and material properties

Based on extensive in-situ testing (including approximately 100 SPTs, pressuremeter tests, and Lugeon permeability tests) and laboratory analysis (UCS and triaxial tests), four main geotechnical units were defined for the rock mass, alongside specific parameters for the overburden and shear zones:

Radiolarite (Unit-1a)

Typically reddish-brown, medium to highly weathered (W3–W4), and very weak. It is highly fractured, often degrading to a clayey-silt mass at identified shear depths (18–30 m).

Limestone (Unit-1b)

Pink to white, micritic, and exhibiting karstic features such as small voids and manganese coatings. While no large caverns were encountered, the unit is characterized as highly permeable.

Sheared Serpentinite/Peridotite (Unit-2a)

Weak to very weak, with UCS values as low as 0.90 MPa in weathered sections. This unit is generally impermeable to slightly permeable ($k \approx 1.1 \times 10^{-6}$ m/s).

Competent Peridotite (Unit-2b)

The stable foundation rock, characterized by higher stiffness (E > 2500 MPa) and RQD values up to 100%.

4.2.2.2. Paleo-landslide indicators and shear interfaces

A critical feature of the site geology is the presence of residual clayey interfaces along slip surfaces, referred to in the literature as "fault clay" or "weakness zones." These interfaces act as impermeable boundaries that facilitate the accumulation of perched water and govern the kinematic failure mechanism. Back-analyses using both Limit Equilibrium (Slide2) and Finite Element (PLAXIS 2D) methods confirmed that these zones possess residual shear strength significantly lower than the surrounding rock mass.

The adopted geotechnical design parameters, derived from the Hoek-Brown failure criterion (using GSI) for rock masses and back-analysis for slip surfaces, are summarized in Table 4.8.

Table 4.8. *Geotechnical design parameters for the composite sequence units*

Material	Unit	Color	UCS (MPa)/ GSI/ m_i	Unit Weight γ (γ_{sat}) (kN/m^3)	Cohesion c' (kPa)	Friction Angle ϕ' (°)	Stiffness E (MPa)	Source
Radiolarite	Unit-1a		25/ 18/ 8	20 (20)	600	20	415	RocData / Lab
Limestone	Unit-1b		30/ 35/ 10	21 (22)	1200	25	1361	RocData / Lab
Sheared Serpentinite	Unit-2a		15/ 24/ 12	20 (22)	500	25	339	RocData / Lab
Basic Volcanics (Base)	Unit-2b		40/ 40/ 25	22 (22)	2000	35	2554	RocData / Lab
Landslide Material	LM		-	19 (20)	1 – 5	26	30	Back-Analysis
Shear Zone	SZ		-	18 (19)	1 – 3	18.0 – 20.0	15	Back-Analysis

Shear zone parameters represent the residual strength range identified during calibration; specific values (c'=1 kPa, ϕ'=18° vs. c'=3 kPa, ϕ'=20°) vary slightly between LE and FE sensitivity analyses.

4.2.3. Failure mechanism, observed deformations, and hydrogeological conditions

The failure mechanism identified in the left abutment slopes, particularly the extensive downstream landslide, is categorized as a complex kinematic system. Geomorphologically, the movement is classified as a combination of rotational and translational slide types, comprising three nested landslide masses. The critical sliding surface is a deeply seated, pre-existing structural weakness within the highly fragmented rock mass, characterized as an impermeable, clayey interface presumed to be at residual shear strength.

4.2.3.1. Triggering mechanisms

Instability at the site is governed by a multi-factorial process where changes in the stress field and environmental conditions have exacerbated movement over a ten-year timeline:

Excavation unloading

The progress of excavations at the slope toes during the primary construction phase removed passive resistance, reactivating ancient slide masses.

Seismic loading

The temporal evolution of the landslide was punctuated by a major regional seismic sequence in 2023 (Mw 7.7 and 7.6). These events delivered Peak Ground Accelerations (PGA) estimated at 0.6g to 0.7g to the facility, mobilizing locked-in stresses resulting from prior tectonic deformation.

Hydrogeological pressures

The relationship between triggering rainfall and slope movement functions analogously to a 'hydraulic brake system.' The fractured rock mass exhibits high secondary permeability (Lugeon values of 25–50), allowing rapid infiltration. This water is trapped by low-permeability clayey shear zones, creating a 'ponded water' effect. This accumulation generates excess pore water pressure that overcomes the frictional resistance of the mechanical 'locked segments' along the slip surface.

Figure 4.33 conceptualizes a model of locked segment triggers.

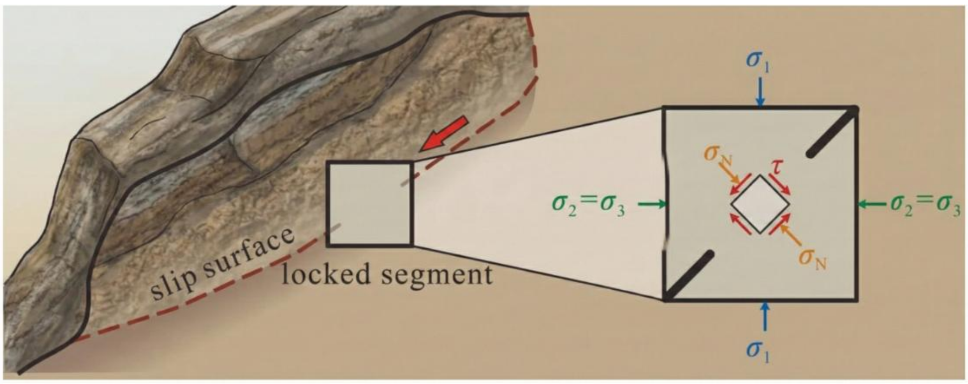

Figure 4.33. *Conceptual model of locked segment triggers (Chen et al., 2018)*

Figure 4.34 illustrates a conceptual model of incremental pore pressure.

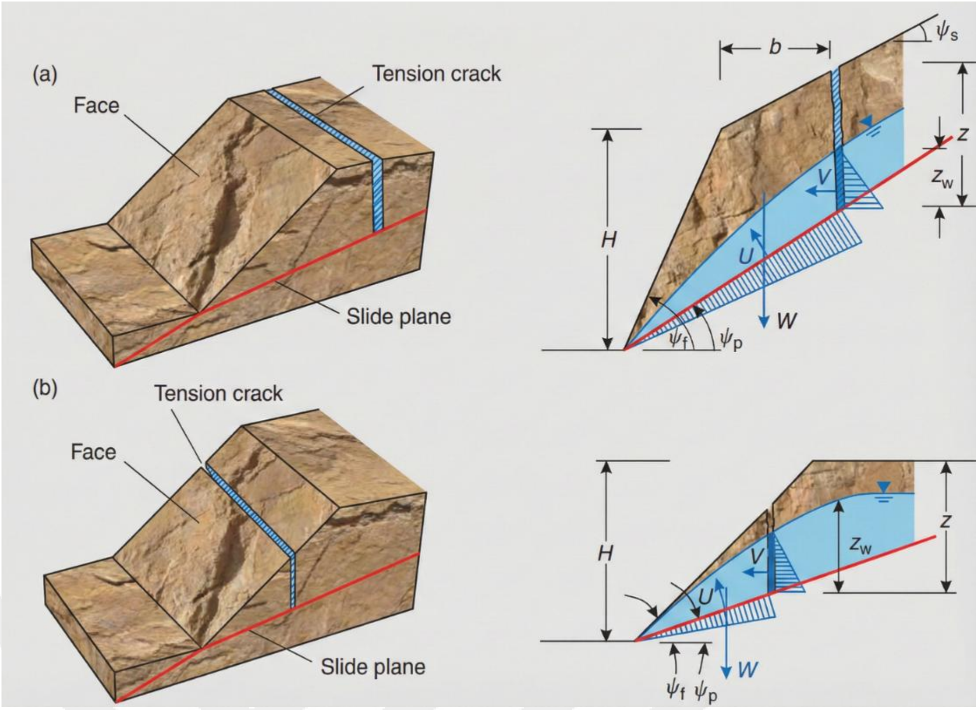

Figure 4.34. *Conceptual model of incremental pore pressure (Wyllie and Mah, 2004)*

4.2.3.2. Observed deformations and damage

Observed physical deformations confirm the ongoing movement and critical stability status. The downstream landslide has induced extensive cracking and structural separation within the existing concrete spillway chute. Furthermore, the movement propagated to the exit portal of the diversion tunnel, resulting in significant structural distress and a localized collapse during the post-seismic period.

Monitoring data from inclinometers and surface geodesy defined the depth of the shear band (18–30 m), which is consistent with the failure plane adopted in numerical back-analyses. While slow creep had been documented throughout the pre-seismic monitoring period, these instruments registered sudden increments in shear deformation—reaching 85–90 mm at depth and over 100 mm at the surface—immediately following the 2023 seismic sequence.

4.2.4. Static back-analyses and seismic response assessment

4.2.4.1. Static back-analysis and parameter calibration

To characterize the residual strength of the composite sequence and the pre-existing landslide interfaces, static back-analyses were conducted on the representative critical cross-section using both Limit Equilibrium (LEM) and Finite Element (FEM) methods.

The primary objective was to calibrate shear strength parameters for the actively sliding mass (LM) and the underlying clayey shear interface by reproducing the observed "critical" state of the slope (where the Factor of Safety, FS ≈ 1.0).

Limit equilibrium (Slide2)

Utilizing the Simplified Bishop, Spencer, and GLE/ Morgenstern-Price methods, the analysis returned an FS of 0.956-1.055 for the existing slope configuration.

Finite element (PLAXIS 2D)

Utilizing the Mohr-Coulomb model with the Strength Reduction Method (SRM), the analysis yielded an FS of 0.914, indicating a condition of marginal stability consistent with the observed creep and structural distress.

These analyses effectively constrained the residual strength parameters for the critical slip surface. The back-calculated effective cohesion (c') ranged from 1 to 3 kPa, and the effective internal friction angle (ϕ') ranged from 18° to 20°. These calibrated values were subsequently adopted for the design of rehabilitation measures. Figure 4.35 exposes the existing downstream landslide profile used for static back-analysis.

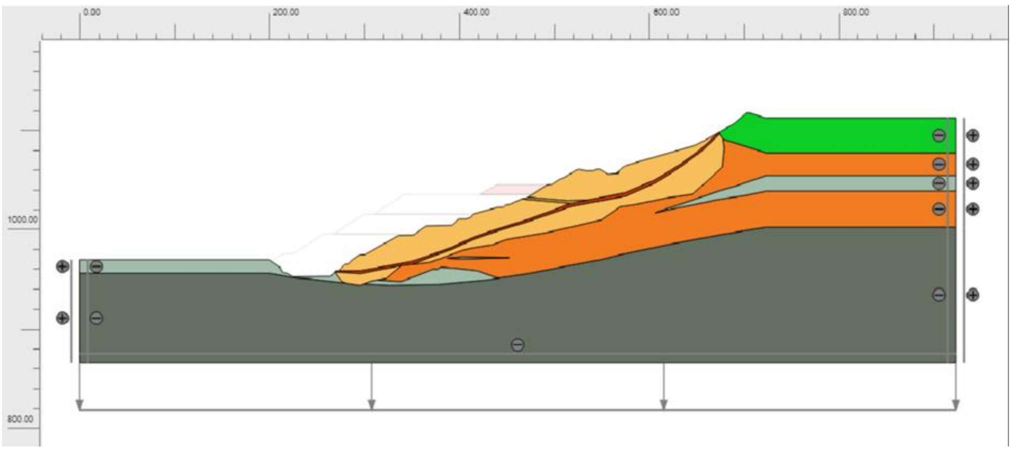

Figure 4.35. *Existing downstream landslide profile used for static back-analysis (PLAXIS 2D)*

Figure 4.36 outlines the back-analysis result via Slide2.

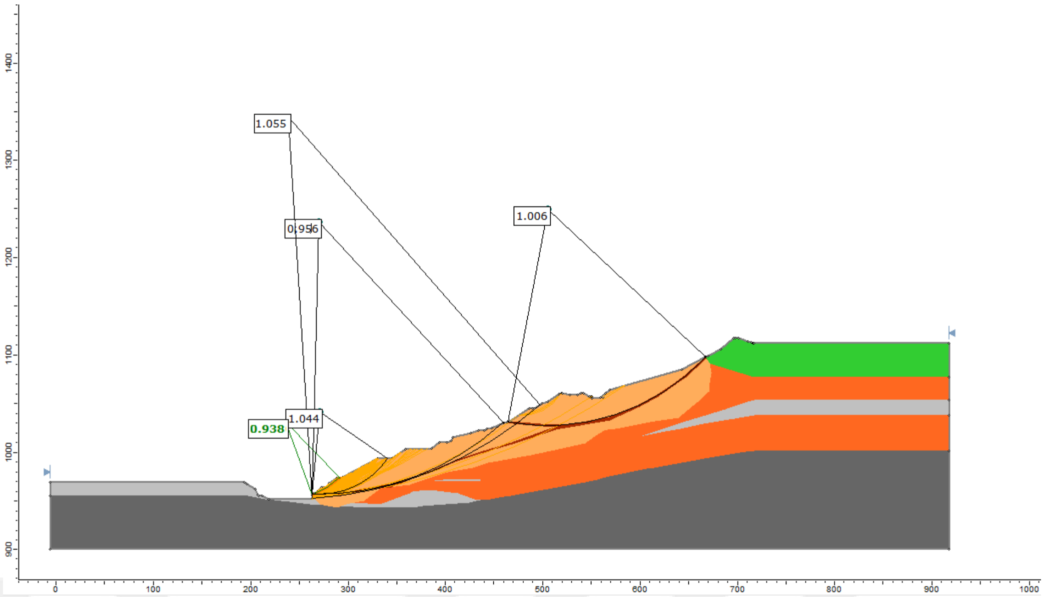

Figure 4.36. *Back-analysis result (Slide2) (FS ≈ 1.0)*

Figure 4.37 confirms the initial safety factor of ΣMsf=0.914 obtained from PLAXIS 2D.

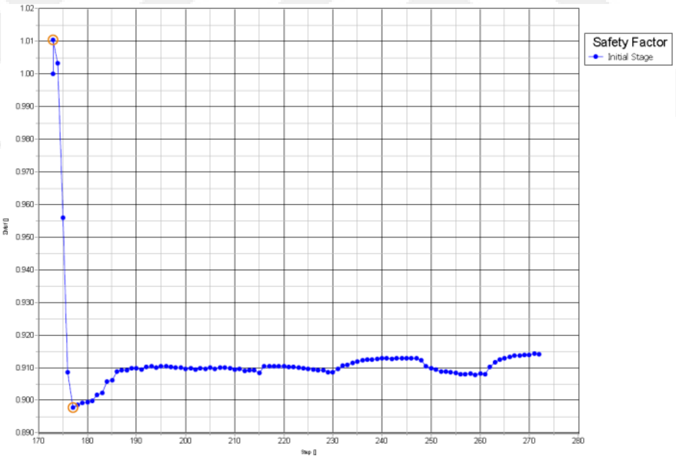

Figure 4.37. *Initial ΣM_{sf}=0.914 (PLAXIS 2D)*

Table 4.9 quantifies calibrated shear strength parameters for sliding materials based on back-analysis.

Table 4.9. *Calibrated shear strength parameters for sliding materials based on back-analysis*

Material	Modeling Method	γ_{sat} (kN/m^3)	c′ (kPa)	ϕ′ (∘)	E (MPa)	ν	Calculated FS
Clayey Shear Zone	Slide (LEM; M-C)	19.0	1	17	N/A	N/A	0.956-1.055

Table 4.9. (Continued) *Calibrated shear strength parameters for sliding materials based on back-analysis*

Material	**Modeling Method**	**γ_{sat} (kN/m^3)**	**c′ (kPa)**	**ϕ′ (∘)**	**E (MPa)**	**ν**	**Calculated FS**
Landslide Material	Slide (LEM; M-C)	20.0	5	25	N/A	N/A	
Clayey Shear Zone	PLAXIS (FEM; M-C)	19.0	3	20	15	0.35	0.914
Landslide Material	PLAXIS (FEM; M-C)	20.0	5	26	30	0.35	

4.2.4.2. Dynamic response assessment

The seismic response of the slope was evaluated through fully coupled time-history dynamic analyses in PLAXIS 2D. Six real earthquake records—Elazığ, Düzce, Kobe, Tottori, Darfield and Hector Mine—were spectrally matched to the project design target spectrum.

To capture the non-linear, elasto-plastic behavior of the materials under cyclic loading:

Rockfill components

To represent the elasto-plastic behavior of the rockfill materials under cyclic loading, the Hardening Soil Small Strain Stiffness (HS-Small) model was employed, incorporating hysteretic damping through the evolution of shear modulus.

Natural landslide/bedrock

Modeled using the Mohr-Coulomb criterion.

4.2.4.3. Results of dynamic simulation

Dynamic results for the unreinforced landslide mass indicated significant permanent deformations. Examination of the deformed mesh reveals that plastic strains and shear concentrations are localized precisely along the tectonic contacts and residual clay interfaces, confirming that these geological features constrain the kinematic response. The analysis predicted true-scale maximum displacements reaching more than 2.0 m during the evaluated earthquake events (Figure 4.38). Examination of the deformed mesh reveals that plastic strains and shear concentrations are localized precisely along the tectonic contacts and residual clay interfaces, confirming that these geological features constrain the kinematic response.

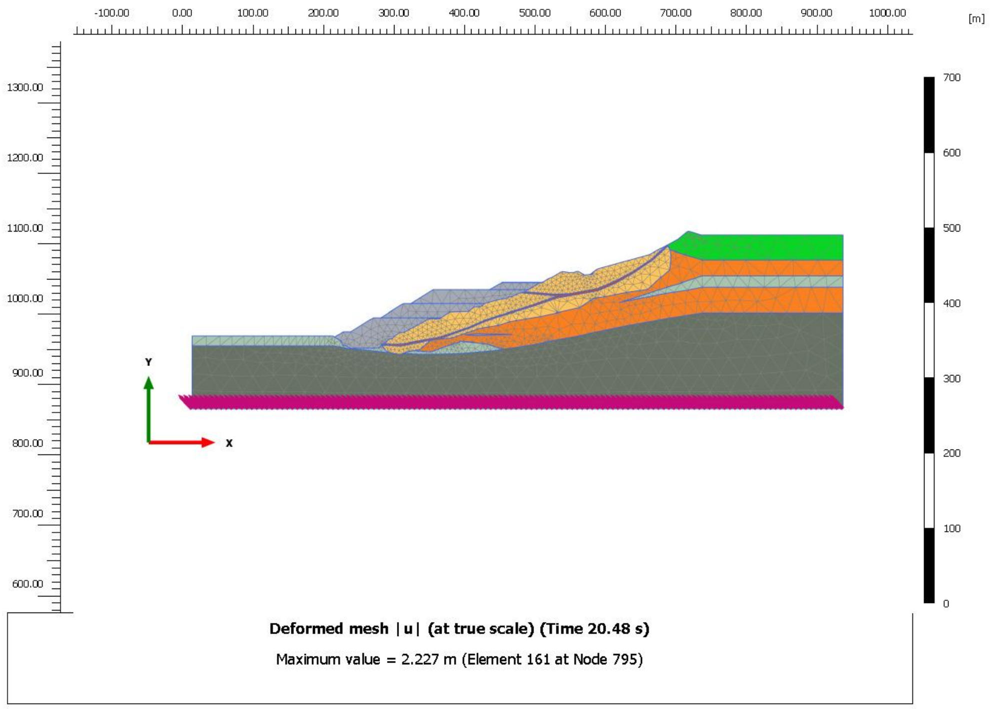

Figure 4.38. *Deformed mesh under Düzce dynamic loading*

4.2.5. Remedial measures, support system, and seismic performance evaluation

4.2.5.1. Remediation strategy and support design

The rehabilitation of the left abutment landslide complex necessitated a multi-faceted support strategy. The design integrated heavy civil engineering measures with strategic structural rehabilitations and extensions to ensure long-term stability under extreme loading conditions. The intervention was divided into two primary components:

Landslide stabilization (rock buttress)

The primary stabilization element and the ultimate structural support solution for the large downstream mass was the construction of a substantial Rockfill Buttress. This buttress extends from the valley floor up to an elevation of approximately half the dam height and is anchored against the stable rock environment of the right bank. This configuration provides massive passive resistance to the sliding block, effectively neutralizing the driving geostatic forces and securing the global stability of the left abutment. The rockfill material was modeled using the HS-Small constitutive model to capture strain-dependent stiffness, utilizing the parameters listed in Table 4.10.

Structural measures

Leveraging the global kinematic stability achieved by the massive toe buttress (where ΣMsf is improved to approximately 1.10), two strategic alternatives are evaluated for the hydraulic structures. While the stabilization effectively prevents catastrophic global failure under extreme dynamic loads, the achieved static safety margin remains below conventional long-term design thresholds (typically ΣMsf $\geq$ 1.5). Consequently, one viable option is that the original concrete spillway chute could be retained in its current alignment and subjected to comprehensive structural rehabilitation to repair the displacement-induced damage along with additional ground improvement. However, given the marginal safety factors and the complex geological setting, the option to completely relocate the spillway structure to the more competent rock mass on the right abutment is strictly preserved as a definitive alternative. Similarly, the diversion tunnel was planned to extend to ensure the exit portal is founded beyond the mapped extent of the landslide.

Figure 4.39 sketches a conceptual cross-section of the downstream slope showing rock buttress support.

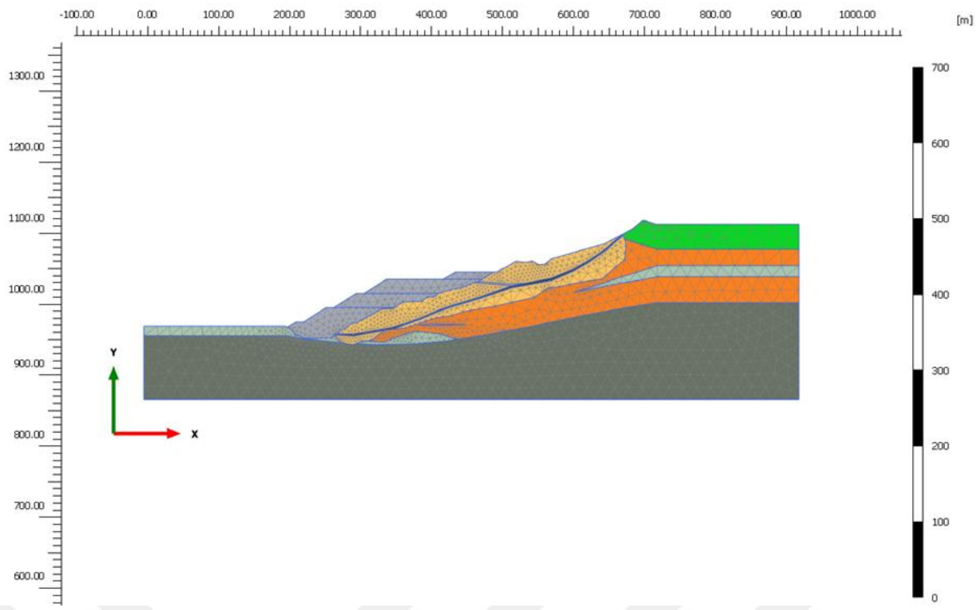

Figure 4.39. *Conceptual cross-section of the downstream slope showing rock buttress support*

Table 4.10. *Key design parameters for rock buttress material*

Parameter	Symbol	Value	Unit	Material Model
Saturated Unit Weight	γ_{sat}	22	kN/m^3	HS-Small
Effective Cohesion	c'	5	kPa	HS-Small
Effective Friction Angle	ϕ'	45	°	HS-Small
Secant Stiffness	E_{50}	75,000	kPa	HS-Small

4.2.5.2. Static stability verification

Numerical verification using Slide2 (LEM) and PLAXIS 2D (FEM) indicates that the proposed interventions significantly enhance the stability of the slope. In its natural state, the site exists in an actively unstable condition, characterized by a Factor of Safety (ΣM_{sf}) of 0.914. This indicates that the natural slope geometry, governed by the residual friction angle (φ'_{res}) along the pre-existing slip surface, is incapable of maintaining static equilibrium without external intervention. However, the implementation of the designed rockfill toe buttress successfully stabilized the system. Elevating the static ΣM_{sf} from 0.914 to 1.100 prior to any seismic loading represents a substantial stabilization achievement, demonstrating the massive passive resistance mobilized by the rockfill structure. Figure 4.40 validates the static rock buttress supported ΣMsf of 1.10 from PLAXIS 2D.

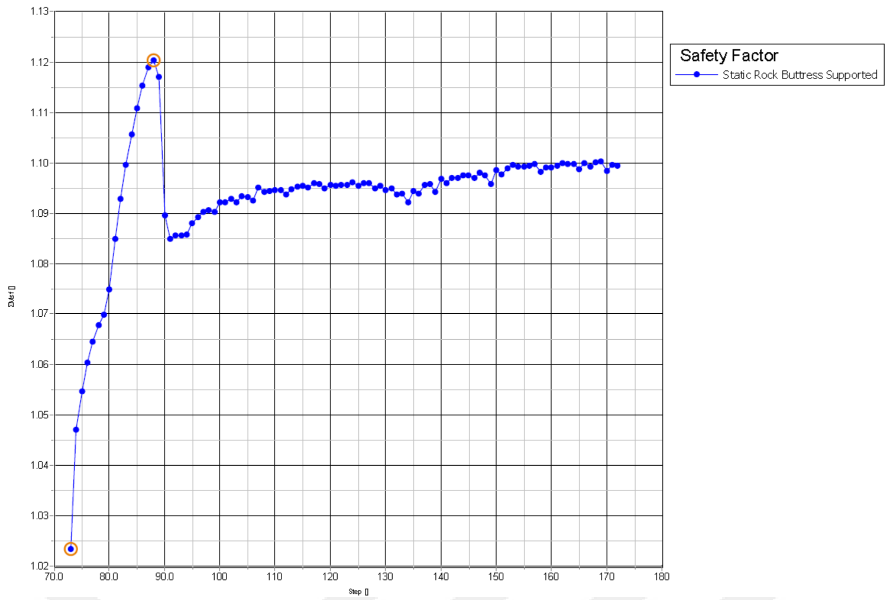

Figure 4.40. *Static rock buttress supported ΣM_{sf}=1.10 (PLAXIS 2D)*

4.2.5.3. Post-earthquake stability and stabilization efficacy

Seismic performance was rigorously assessed through fully coupled time-history analyses. The primary engineering achievement lies in the system's robust capacity to withstand severe seismic excitations without experiencing any degradation in global stability. During the dynamic phase, the application of six distinct ground motions (scaled to 0.56g)—specifically Elazığ, Düzce, Kobe, Tottori, Darfield and Hector Mine—induced manageable permanent displacements primarily in the range of 11-21 cm.

To evaluate the risk of delayed failure and structural degradation, post-earthquake safety analyses were systematically conducted. The assessments for the Elazığ, Düzce, Kobe, Tottori, Darfield and Hector Mine seismic events yielded ultimate ΣM_{sf} values of 1.099, 1.099, 1.098, 1.098, 1.102 and 1.101, respectively (summarized in Table 4.11).

Table 4.11. *Summary of pre-earthquake, dynamic, and post-earthquake stability assessments (ΣM_{sf})*

Analysis Phase	Geotechnical State / Event	Factor of Safety (FS=ΣMsf)	Principal Geotechnical Observation
Pre-Support	Natural State (No Rock Buttress)	0.914	Actively unstable condition ($\Sigma M_{sf} < 1.0$); pre-existing failure mechanism and residual slip surface confirmed.
Post-Support	Static Stabilization (Pre-EQ)	1.100	Successful stabilization; passive resistance effectively mobilized via rockfill toe buttress.
Post-Earthquake (Following 0.56g Dynamic Excitation)	Elazığ Düzce Kobe Tottori Darfield Hector Mine	1.099 1.099 1.098 1.098 1.102 1.101	Absolute System Lock-in: The global stability margin is completely preserved across all six seismic events ($\Delta\Sigma M_{sf} \approx 0$). The structure exhibits absolute resilience against extreme inertial forces and severe dynamic shear stress cycles. Permanent displacements are strictly confined to superficial kinematic adjustments, while the critical slip surface remains mechanically locked by the mobilized passive resistance. Consequently, extreme transient oscillations are fully absorbed, rendering the final post-earthquake static equilibrium practically indistinguishable from the pre-EQ state.

This stability performance reveals a critical geotechnical phenomenon: Absolute System Lock-in. The post-earthquake ΣM_{sf} values are remarkably constant and practically indistinguishable from the pre-seismic static baseline of 1.100 (with variances limited to a negligible ± 0.002). This proves that the seismic displacements observed during the dynamic phase are strictly superficial kinematic adjustments that do not alter the global resisting forces.

Unlike typical earth structures that exhibit strain-softening or stability degradation post-excitation, the proposed rockfill buttress provides a rigid boundary condition that effectively "locks" the pre-existing residual slip surface. The results unequivocally confirm that the extreme inertial forces and the induced dynamic shear stress cycles during the 0.56g shaking were fully absorbed by the structural configuration without triggering any progressive failure mechanism. Consequently, the designed stabilization measure not only prevents catastrophic failure during extreme dynamic loading but ensures that the structure completely retains its designated safety margin (1.100) in the post-seismic state.

Figure 4.41 exhibits post-earthquake safety factor variations across multiple seismic events.

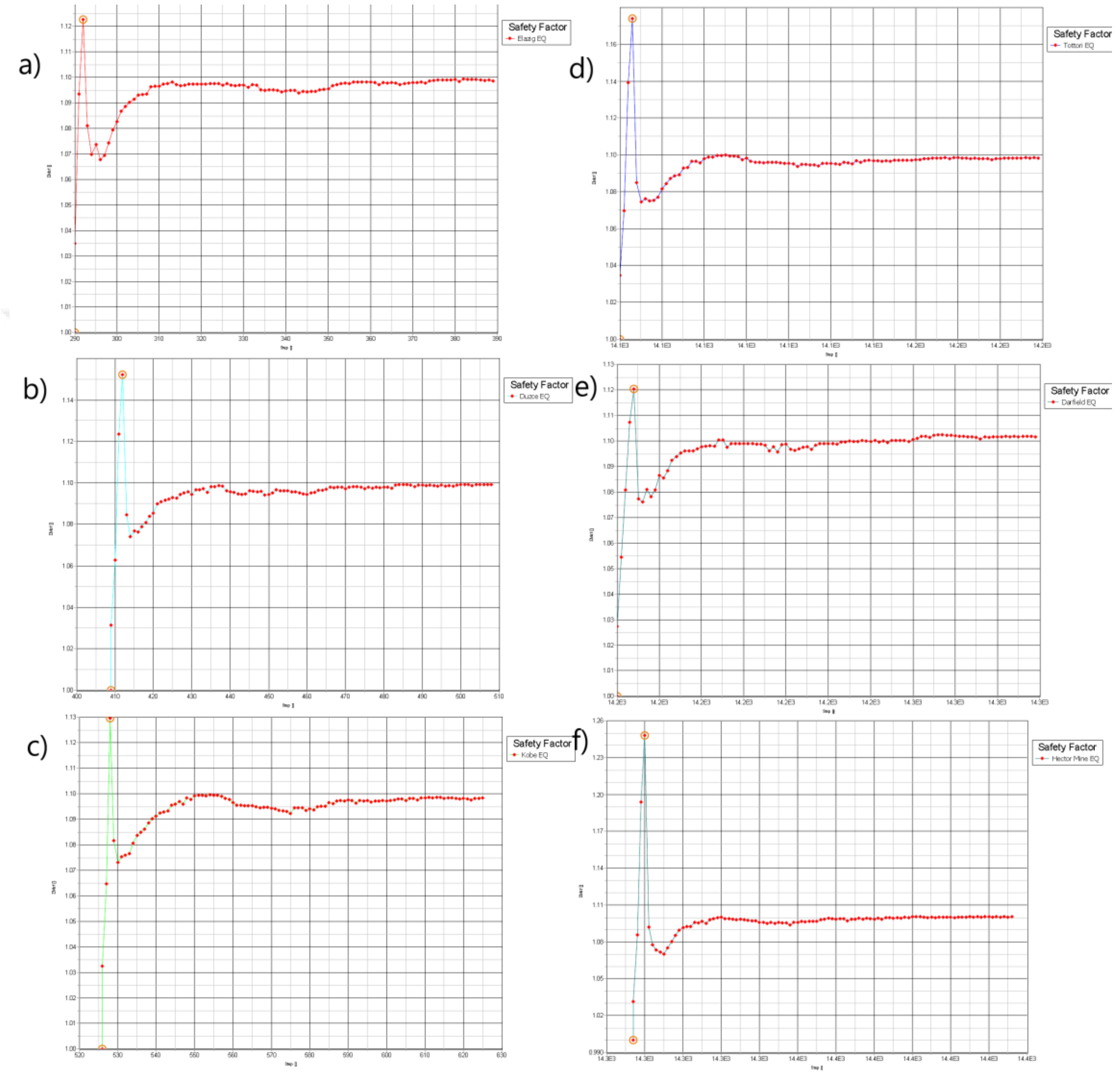

Figure 4.41. *Post-earthquake safety factor variations: a) Elazığ EQ (Σ Msf = 1.099), b) Düzce EQ (Σ Msf = 1.099), c) Kobe EQ (Σ Msf = 1.098), d) Tottori EQ (Σ Msf = 1.098), e) Darfield EQ (Σ Msf = 1.102), f) Hector Mine EQ (Σ Msf = 1.101)*

Figure 4.42 illustrates the initial geotechnical conditions of the natural slope prior to the implementation of any stabilization measures. The contour plot clearly reveals the development of a continuous, deep-seated shear band (highlighted by the strain concentration arc) propagating along the pre-existing residual slip surface. The unimpeded daylighting of this failure mechanism towards the valley floor perfectly correlates with the calculated actively unstable state (ΣM_{sf} = 0.914). The dashed outlines indicate the intended geometry of the subsequent rockfill toe buttress, which was strategically designed to intercept and passively resist this exact kinematic mechanism.

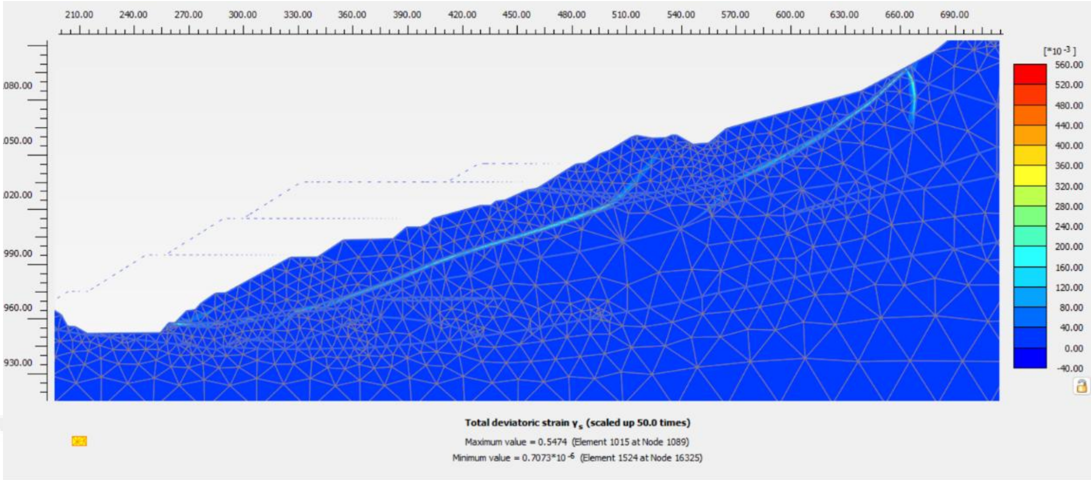

Figure 4.42. *Total deviatoric strain (γ_s) distribution at the initial (pre-construction) stage, scaled up 50.0 times*

Figure 4.43 illustrates the accumulation of shear strains within the slope mass following the Elazığ dynamic excitation. The contour plot reveals that strain accumulation is strictly localized near the surface of the upper slope benches, representing minor superficial yielding. Crucially, no continuous shear band developed along the deep-seated residual slip surface. The rockfill buttress remained entirely undeformed, effectively absorbing the induced dynamic shear stresses and preventing global instability. These superficial strain concentrations perfectly correlate with the limited permanent crest displacements (11-21 cm) and the absolute retention of the static safety margin (ΣM_{sf} = 1.099), confirming that the seismic response of the stabilized structure remains well within acceptable serviceability limits without experiencing any progressive failure during this specific excitation.

Furthermore, dynamic stability analyses incorporating the remaining five seismic records (Düzce, Kobe, Tottori, Darfield and Hector Mine) yielded exceptionally consistent results, as summarized in Table 4.12. The permanent displacements across all five benches for these events were restricted to a range of 3.7 cm to 21.2 cm, with the average bench displacements varying between 9.4 cm and 13.3 cm. These analyses consistently demonstrated analogous surficial strain localization, the complete absence of deep-seated yielding, and overall structural resilience, thereby comprehensively verifying the long-term dynamic performance of the system.

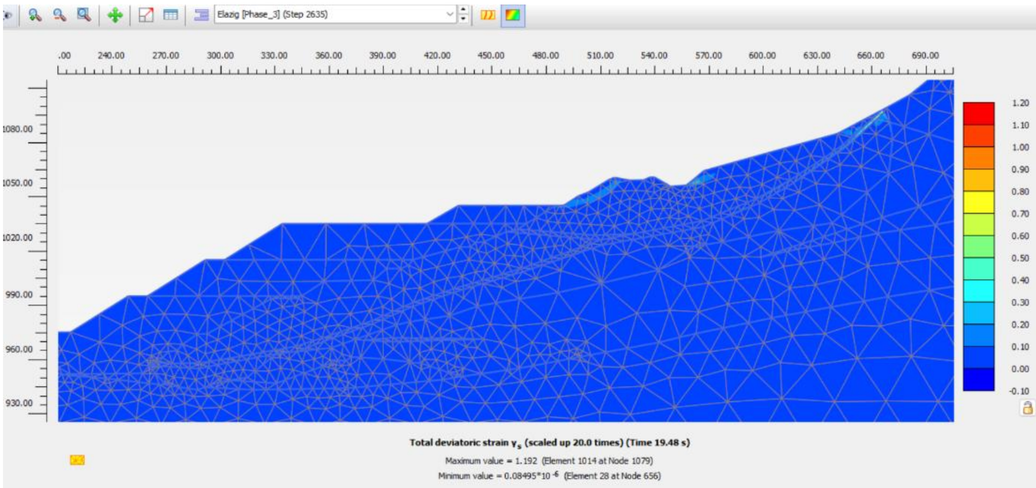

Figure 4.43. *Total deviatoric strain (γ_s) distribution at the end of the Elazığ earthquake dynamic phase (deformations scaled up 20.0 times for visibility)*

To rigorously validate the efficacy of the proposed stabilization measures under extreme seismic demands, a comparative visual evaluation of the induced shear strains was conducted. Figure 4.43 presents the total deviatoric strain (γ_s) profiles for the Elazığ earthquake—representing the general stabilized seismic response—alongside the Düzce record (Figure 4.44), which represents the most critical dynamic loading scenario characterized by severe transient oscillations.

As clearly illustrated in Figure 4.44, even under the most demanding inertial forces and extreme transient displacements, strain accumulation remains strictly confined to the superficial zones of the upper slope benches. The most critical geotechnical observation is the complete absence of a continuous shear band along the pre-existing, deep-seated residual slip surface. The rockfill toe buttress successfully neutralizes the driving forces in both the moderate and extreme scenarios, fully preventing the reactivation of the landslide mass. This visual evidence robustly supports the numerical post-earthquake Factor of Safety (ΣM_{sf}) results (maintaining the ≈ 1.100 baseline), unequivocally confirming that the stabilization design is highly resilient against global failure mechanisms. The system effectively absorbs the severe dynamic shear stress cycles without initiating any progressive failure, restricting seismic damage to acceptable, localized superficial kinematic adjustments.

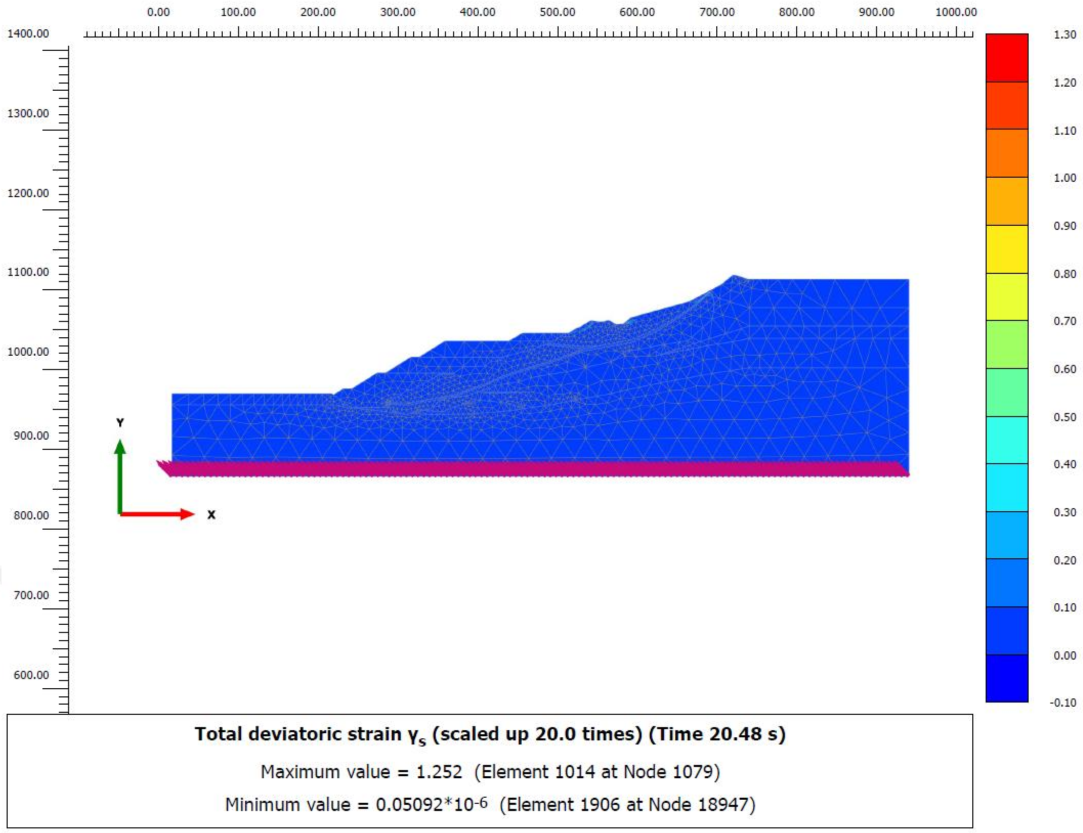

Figure 4.44. *Total deviatoric strain (γ_s) distribution at the end of the Düzce earthquake dynamic phase*

Figure 4.45 depicts the selected nodes for dynamic analysis.

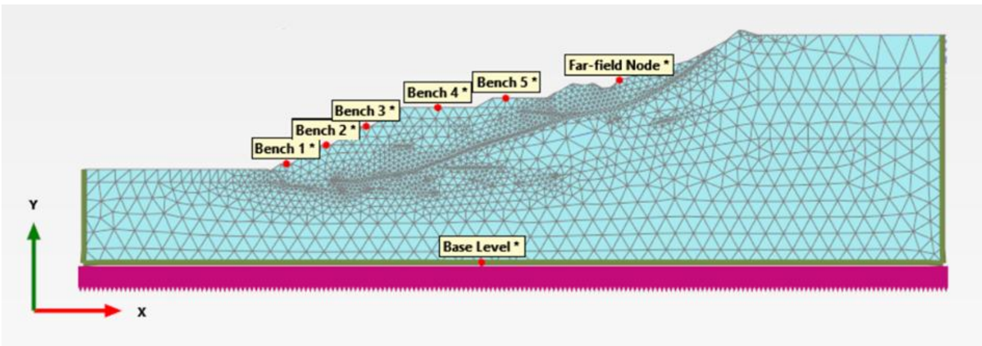

Figure 4.45. *Selected nodes for dynamic analysis*

Figure 4.46 represents the displacement time-history for critical points on the landslide mass during the Elazığ Earthquake.

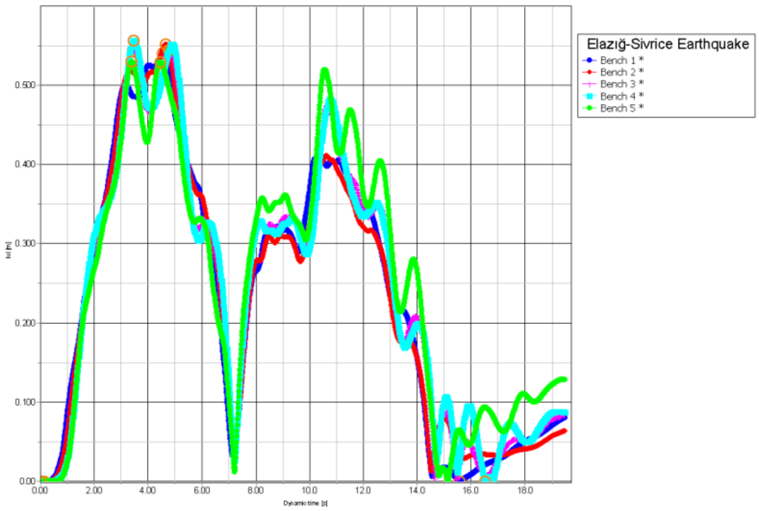

Figure 4.46. *Displacement time-history for critical points on the landslide mass (Elazığ Earthquake)*

Figure 4.47 displays the displacement time-history for critical points on the landslide mass during the Düzce Earthquake.

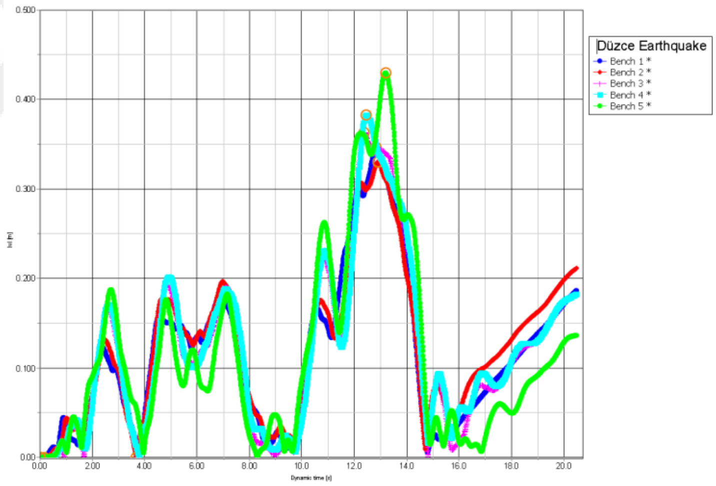

Figure 4.47. *Displacement time-history for critical points on the landslide mass (Düzce Earthquake)*

Figure 4.48 illustrates the displacement time-history for critical points on the landslide mass during the Kobe Earthquake.

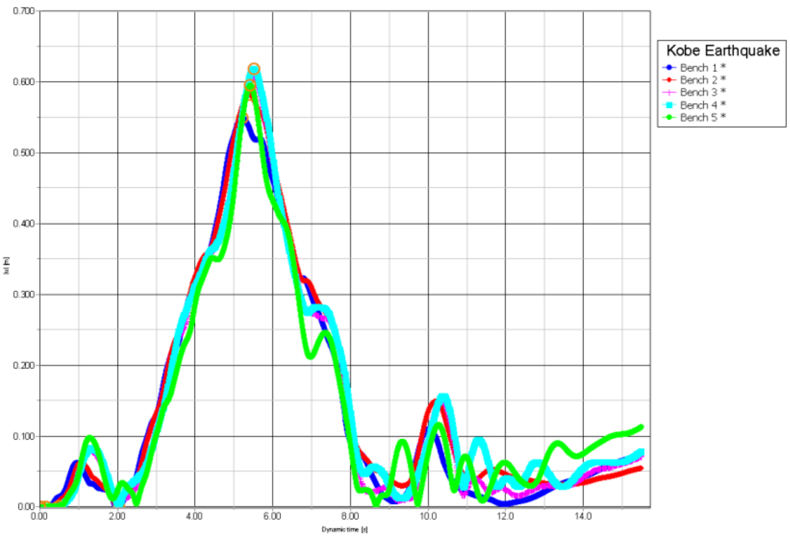

Figure 4.48. *Displacement time-history for critical points on the landslide mass (Kobe Earthquake)*

Figure 4.49 presents the displacement time-history for critical points on the landslide mass during the Tottori Earthquake.

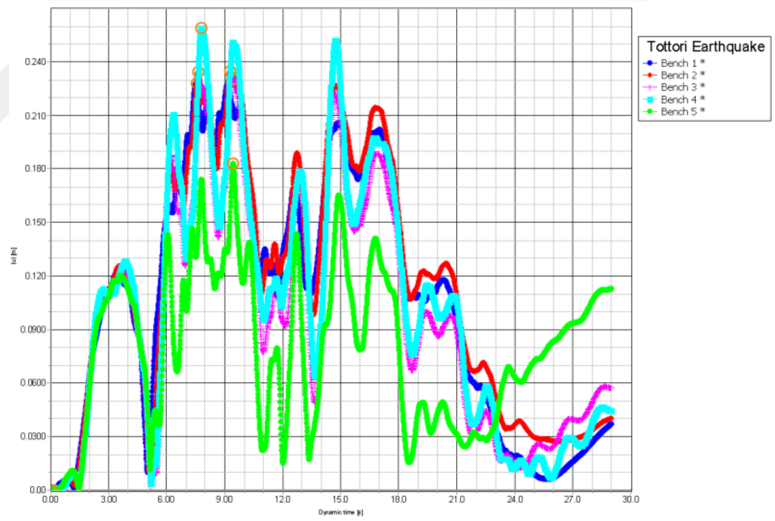

Figure 4.49. *Displacement time-history for critical points on the landslide mass (Tottori Earthquake)*

Figure 4.50 depicts the displacement time-history for critical points on the landslide mass during the Darfield Earthquake.

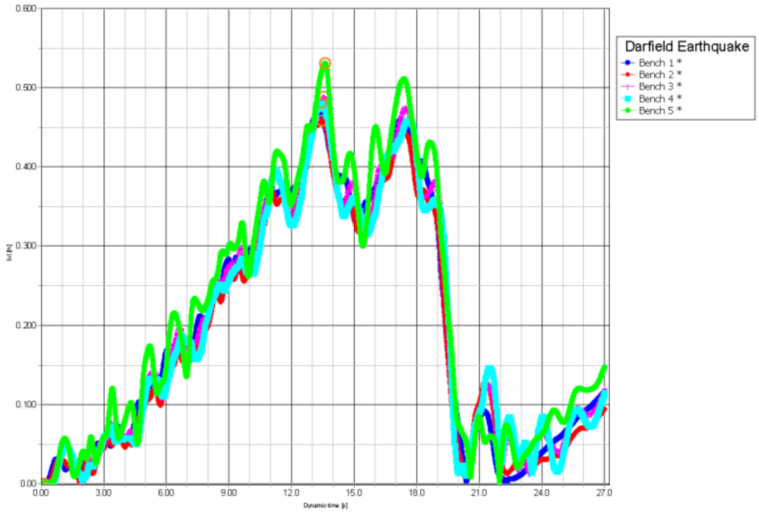

Figure 4.50. *Displacement time-history for critical points on the landslide mass (Darfield Earthquake)*

Figure 4.51 illustrates the displacement time-history for critical points on the landslide mass during the Hector Mine Earthquake.

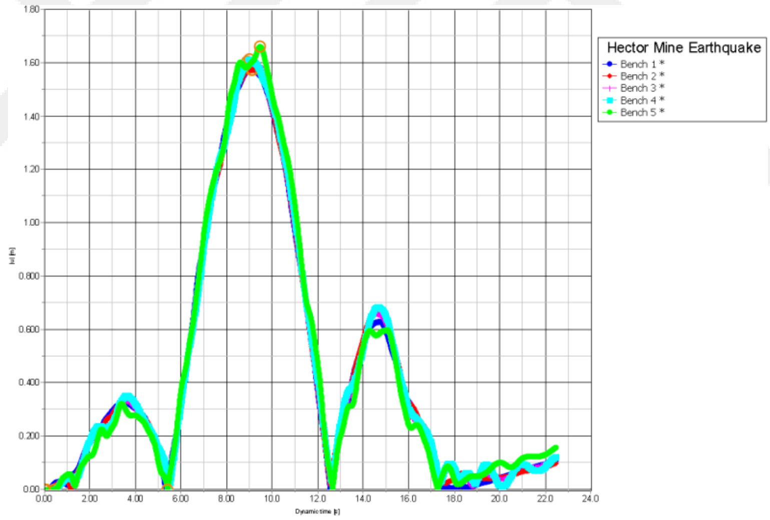

Figure 4.51. *Displacement time-history for critical points on the landslide mass (Hector Mine Earthquake)*

Table 4.12. *Summary of maximum permanent displacements for selected points*

Seismic Record	Bench 1 (cm)	Bench 2 (cm)	Bench 3 (cm)	Bench 4 (cm)	Bench 5 (cm)
Elazığ	8.1	6.4	8.4	8.8	**12.9**
Düzce	18.7	**21.2**	18.2	18.3	13.7
Kobe	7.5	**5.5**	7.1	7.9	11.3

Table 4.12. (Continued) *Summary of maximum permanent displacements for selected points*

Seismic Record	Bench 1 (cm)	Bench 2 (cm)	Bench 3 (cm)	Bench 4 (cm)	Bench 5 (cm)
Tottori	3.7	4.0	5.8	4.4	**11.3**
Darfield	11.7	9.5	11.9	11.5	**14.8**
Hector Mine	11.1	10.0	12.4	12.4	**15.8**
Average	10.1	9.4	10.6	10.6	13.3

Table 4.13 arrays a summary of dynamic performance indicators and calculated displacements.

Table 4.13. *Summary of dynamic performance indicators and calculated displacements*

Metric / Record	Value / Range	Performance Classification
Max. Slope Displacement (Downstream)	10 – 20.0 cm (approximate)	Acceptable (Eurocode 8)
Overall Damage Class	–	Non-Catastrophic / Repairable

4.2.6. Conclusion and lessons learned

The integration of long-term monitoring data (InSAR and LiDAR) with numerical predictions suggests that the slope behavior is transitioning from active creep to a stable state following the remediation phases. A key lesson learned from this case study is that complex instabilities in tectonic mélange environments—where sedimentary and ultramafic units are interfingered—may benefit from a passive stabilization approach. This strategy relies primarily on massive mass-weighting (rockfill buttresses) to counterbalance driving forces, rather than rigid structural retention systems which are prone to shearing in such heterogeneous masses.

Furthermore, the study demonstrates that the 'locked segment' behavior of the hillside necessitates a coupled hydro-mechanical modeling approach to accurately predict seismic response. The rigorous post-earthquake verifications conclusively show that a properly dimensioned passive buttress can induce "Absolute System Lock-in," completely protecting deep-seated failure interfaces against dynamic shear degradation and limiting permanent seismic deformations to strictly superficial zones.

Crucially, this case study highlights the practical realities of remediating massive landslides in active tectonic margins. Attaining conventional long-term static safety factors (e.g., ΣMsf ≥ 1.5) is often economically and practically unfeasible for such large-scale geohazards. Instead, securing a reliable, albeit lower, safety margin (ΣMsf ≈ 1.10) that robustly guarantees global stability under both static and extreme dynamic loading conditions is a substantial engineering accomplishment. This stabilization approach prevents catastrophic collapse and provides critical flexibility for infrastructural planning.

Finally, due to the susceptibility of rigid liners to structural distress within these deforming geological masses and the accepted marginal safety factors, support designs must prioritize flexible buttressing and, where feasible, actively maintain the option for the relocation of appurtenant structures to the opposite bank or other isotropic rock environments.

4.3. Case 3 – Instabilities at Diversion Tunnel Portals in Ophiolitic Mélange

This section presents a comprehensive analysis of the slope instabilities encountered at the inlet and outlet portals of a diversion tunnel associated with a major Concrete-Faced Sand-Gravel Fill Dam (CFSGD) project. Situated in a seismically active terrain with a hydraulic height of approximately 70 m, the diversion infrastructure is founded within Ophiolitic Complex Sediments—a highly heterogeneous, weak, mélange-like rock mass that is exceptionally prone to rapid weathering, argillization, and subsequent strength degradation upon atmospheric exposure.

The primary objectives of this evaluation were to assess the observed failure mechanisms—specifically deep-seated rotational sliding and surficial mass wasting triggered by adverse hydrogeological conditions—and to verify the inadequacy of the initial design parameters through numerical back-analysis. Furthermore, the study aims to develop and evaluate the performance of remedial measures, focusing on a cut-and-cover conduit structure and slope stabilization using a compacted granular backfill cover in conjunction with rockfill, under both static and extreme seismic loading conditions, including the implications of the 2023 seismic sequence evaluated under varying peak ground acceleration (PGA) scenarios (0.48g, 0.36g, and 0.24g).

4.3.1. Project setting, portal geometry, and excavation details

The diversion infrastructure comprises a circular tunnel (approx. 250 m) that transitions into a reinforced concrete conduit. The conduit length varies by design stage, ranging significantly from approximately 200 m to 400 m. Both structures were designed with an inner diameter of 3.50 m and a reinforced concrete liner thickness of 0.35 m (C25). The tunnel traverses mountainous terrain with a maximum overburden of approximately 60 m, while the downstream conduit is situated behind the dam body, covered by shallow backfill. Figure 4.52 illustrates the general plan view of the diversion tunnel portal excavations and conduit route.

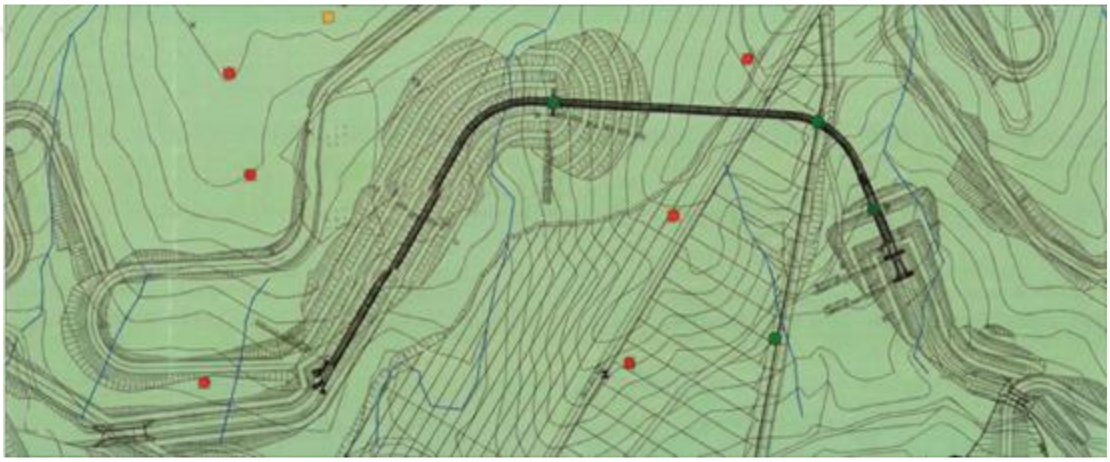

Figure 4.52. *General plan view of the diversion tunnel portal excavations and conduit route*

4.3.1.1. Geological and hydrogeological context

The portals are situated along an ephemeral stream channel (dry stream route), a critical drainage path where seasonal precipitation and surface runoff naturally flow across the portal slopes. This drainage condition causes the weak rock unit to undergo argillization, making it highly susceptible to instability. Geological conditions are dominated by Ophiolitic Complex Sediments, a lithologically heterogeneous unit exhibiting flysch-like characteristics. The formation consists of a clay-altered, sheared matrix enclosing blocks of serpentinite, silicified radiolarite, and conglomeratic limestone.

Subsurface characterization was supported by an extensive drilling program, which included more than 35 boreholes with a total depth of approximately 1,500 m, and over 60 in-situ pressuremeter tests to constrain the deformation modulus of the weak rock mass. The investigation confirmed the poor quality of the rock mass, yielding Rock

Quality Designation (RQD) values of 0% and core recovery ratios between 42% and 71%. Piezometric data indicated groundwater levels at depths of 3.60 m at the tunnel entrance (BH-6) and 1.10 m along the tunnel route (BH-5). Seismic hazard analysis indicates peak ground accelerations of MDE (Maximum Design Earthquake) = 0.28g and OBE (Operation Based Earthquake) = 0.14g.

4.3.1.2. Excavation geometry and geometric constraints

The portal slope geometry was initially established using temporary excavation gradients of 1V:1H (45°). Geotechnical reports for the permanent design necessitated flattening these slopes to a 1V:1.5H ratio (approximately 33.7°), incorporating 6.0 m high benches to enhance global stability and facilitate a transition to a 1V:2H embankment.

However, as displayed in Figure 4.53, implementing the required permanent 1V:1.5H slopes proved structurally infeasible due to severe spatial constraints:

Inlet portal

Extending the slopes to the required inclination would have caused the excavation footprint to encroach upon the alignment of the dam’s plinth line and the dam body itself.

Outlet portal

Excavations were similarly positioned near the dam body skirt, departing from standard standoff practices for hydraulic structures.

These geometric conflicts forced the retention of the steep 1V:1H temporary slopes for extended periods, preventing the timely implementation of the permanent design profile.

Figure 4.53. *Schematic plan illustrating the the infeasible permanent 1V:1.5H slope at the diversion tunnel inlet*

4.3.1.3. Excavation sequence and instability evolution

The excavation sequence involved the completion of open-cut excavations for both the inlet and outlet portals. A critical factor in the evolution of instability was the prolonged exposure of these cut slopes without the implementation of requisite primary support systems. While the initial benches of the inlet portal received mesh-reinforced shotcrete, the majority of the excavation faces remained unsupported.

This exposure led to rapid weathering and argillization of the ophiolitic units upon contact with atmospheric conditions and seasonal precipitation. The progression of instability was characterized by surface mass wasting and deep-seated movements:

Outlet failure

At the outlet portal, progressive sliding eventually caused the complete closure of the tunnel exit in early 2020.

Inlet instability

Tension cracks appeared parallel to the benches, with deformations extending toward critical infrastructure, including the valve chamber access route.

These failures necessitated a fundamental design change. The open channel segment at the portal approach was replaced with a cut-and-cover conduit structure (e.g., the 85.00 m conduit at the inlet) followed by granular backfilling along with rockfill. Additionally, the intake tower was set back 10.00 m from its original location to mitigate long-term slope slippage risks.

Post-seismic evaluations following the 2023 seismic sequence—where the nearest strong motion stations recorded Peak Ground Accelerations (PGA) of approximately 0.48g, significantly exceeding the Operation Based Earthquake (OBE) design level of 0.14g—relied on visual mapping to assess the performance of these stabilized slopes, supplemented by subsequent parametric pseudo-static numerical models simulating fractional PGA levels (0.36g and 0.24g) to better understand the seismic margin of safety. Table 4.14 lists a summary of diversion tunnel portal geometry and excavation parameters.

Table 4.14. *Summary of diversion tunnel portal geometry and excavation parameters*

Structure / Component	Parameter	Value	Unit
Diversion Tunnel	Length	~ 260	m
Diversion Conduit	Length	~ 225	m
Excavation Slope (Temp)	Gradient	1V:1H	-
Excavation Slope (Perm)	Gradient	1V:1.5H	-
Bench Details	Height	6.0	m
Tunnel Liner	Thickness	0.35	m

Figure 4.54 delineates a longitudinal profile of the diversion tunnel and conduit system showing the transition from tunnel to cut-and-cover conduit.

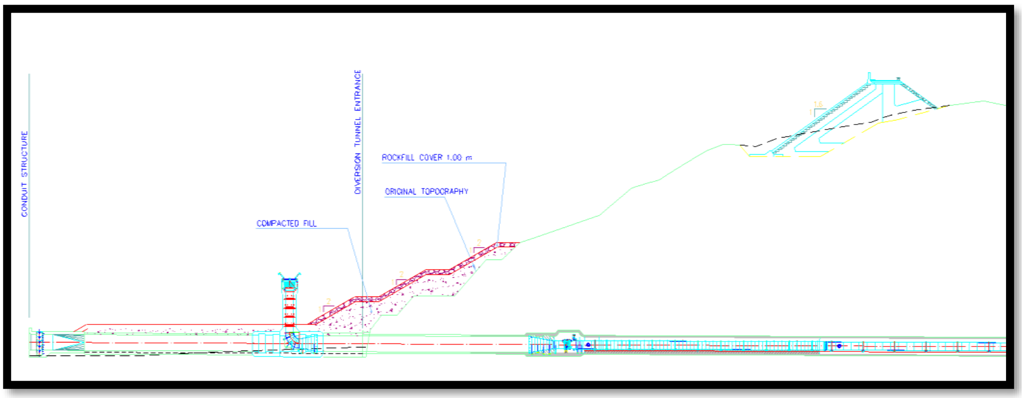

Figure 4.54. *Longitudinal profile of the diversion tunnel and conduit system showing the transition from tunnel to cut-and-cover conduit*

4.3.2. Geological and geotechnical conditions of the Ophiolitic Mélange

The geological framework of the portal area is defined by Ophiolitic Complex Sediments, an allochthonous unit exhibiting a typical flysch character and extreme lithological heterogeneity. Structurally, this formation is identified as a complex tectonic mélange, consisting of a highly altered, sheared, and clay-rich matrix enclosing embedded tectonic blocks of varying sizes. The lithology includes silicified radiolarite, conglomeratic limestone, serpentinite, and siliceous shale, interspersed with marl bands and conglomerate alternations.

The structural integrity of this unit can be conceptualized using a 'block-in-matrix' (bimrock) model, where hard, lithified blocks are embedded within a soft, cohesive, weak matrix. Consequently, the global mechanical behavior of the rock mass is governed not by the strength of the individual blocks, but by the shear strength properties of the weaker surrounding matrix. The formation is heavily influenced by regional tectonic activity associated with major active fault systems, resulting in a rock mass that is intensely fractured and traversed by vertical and reverse faults.

4.3.2.1. Rock mass characterization

Geotechnical site investigations, including extensive core drilling and more than 60 in-situ pressuremeter tests, confirmed the poor quality of the rock mass. Core recovery percentages typically ranged between 40% and 70%, while the Rock Quality Designation (RQD) was consistently reported as 0% across all boreholes, underscoring the inherently fragmented nature of the material.

The rock mass is governed by a high density of discontinuities. Joint spacings are typically less than 60 mm, with persistence ranging between 1 m and 3 m. Joint surfaces are generally rough and pockmarked, with apertures of 1 mm to 5 mm frequently filled with soft clay or calcareous material. Based on these observations, standard rock mass classification systems yielded the following indices:

Rock mass rating (RMR)

Values between 30 and 34, classifying the unit as Class IV (Weak Rock).

Geological strength index (GSI)

Estimated between 32 and 36.

Q-system

Values between 0.03 and 0.09, corresponding to an "Extremely Poor" rock mass classification.

4.3.2.2. Hydro-mechanical behavior and alteration

A critical geotechnical characteristic of the ophiolitic mélange unit is its extreme sensitivity to hydro-mechanical variations. The matrix contains a significant proportion of clay minerals prone to rapid weathering, argillization, and swelling upon atmospheric exposure and saturation. Site investigations delineated a heavily weathered surface zone extending to a depth of approximately 10–12 m along the tunnel alignment.

When exposed to seasonal precipitation and surface runoff, this near-surface material undergoes a drastic degradation in shear strength. This process drives the formation of a distinct 'surficial alteration zone' capable of generating flow-type failures and shallow landslides, kinematically distinct from the global stability of the deeper rock mass.

4.3.2.3. Geotechnical design parameters

To accurately model the slope stability, two distinct sets of shear strength parameters were established.

Altered surface zone

Representing the critical failure interface where residual strength governs stability.

General ophiolitic complex

Representing the underlying, less weathered rock mass.

Laboratory testing indicated a broad range in Uniaxial Compressive Strength (UCS), from as low as 2.11 kg/cm² (~0.2 MPa) in weathered sections to 162.9 kg/cm² (~16 MPa) in intact blocks. However, back-analyses of the observed instabilities suggested that the operative strength in the wetted surface zone was significantly lower.

Consequently, the altered zone was modeled with a cohesion (c') of 25 kPa and an internal friction angle (ϕ') of 3°, reflecting near-residual conditions. Table 4.15 collects a summary of geotechnical design parameters for the ophiolitic mélange.

Table 4.15. *Summary of geotechnical design parameters for the ophiolitic mélange*

Material	Parameter	Value	Unit	Source / Test Type
Altered Surface Zone	Unit Weight (γ)	20	kN/m³	Back-analysis
	Cohesion (c')	25	kPa	Back-analysis (Residual)
	Friction Angle (ϕ')	3	°	Back-analysis (Residual)
Ophiolitic Complex	Unit Weight (γ)	25	kN/m³	Lab tests
	Cohesion (c')	75	kPa	Back-analysis / Lab Correlation
	Friction Angle (ϕ')	20	°	Back-analysis / Lab Correlation
	Def. Modulus (E_m)	3.16	GPa	Pressuremeter / Empirical
	Hoek-Brown (m_i)	7	-	RocLab

Figure 4.55 supplies the Hoek-Brown failure envelope and RocLab material characterization for the ophiolitic mélange.

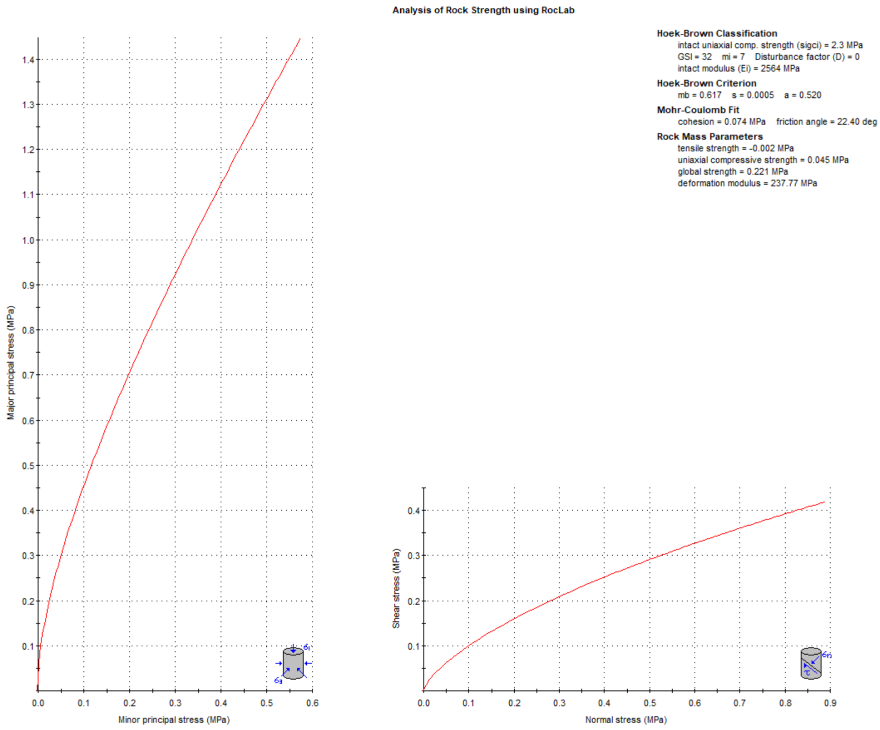

Figure 4.55. *Hoek-Brown failure envelope and RocLab material characterization for the ophiolitic mélange*

4.3.3. Failure mechanisms, observed deformations, and excavation-induced effects

The instability mechanisms governing the diversion tunnel portals were driven by the rapid geotechnical degradation of the ophiolitic mélange unit upon atmospheric exposure. The failure mode is characterized by a transition from rock mass behavior to a soil-like continuum. The critical phenomenon observed in the field involved surficial mass wasting propagating into deep-seated rotational landslides.

This degradation sequence is initiated by the infiltration of meteoric water (rainfall and snowmelt) into the clay-rich matrix. The absorption of moisture triggers swelling and softening, which simultaneously increases the driving mass weight (bulk unit weight) and drastically reduces the available shear strength. This process results in the formation of a highly degraded 'Altered Surface Zone' (typically 3.0 m to 5.0 m thick) that exhibits viscoplastic flow characteristics, behaving effectively as a weak, remolded soil.

4.3.3.1. Mechanics of instability and support ineffectiveness

The geometry of the unstable mass was constrained by wide sliding arcs extending deep into the rock mass. This failure geometry rendered the initially specified 4.0 m long rock bolts ineffective. Technical evaluations indicated that these bolts failed to provide stabilization because:

Geometric bypass

The failure envelopes were sufficiently deep and wide to encompass the entire length of the bolts, meaning the reinforcement was floating within the active sliding mass rather than anchoring it.

Lack of anchorage

The intensely fractured and heterogeneous nature of the ophiolitic unit provided no competent rock blocks or sound horizons for the bolts to anchor into beyond the failure plane.

4.3.3.2. Observed deformations and timeline

Field monitoring documented a clear progression from discrete fracturing to catastrophic mass movement. The deformation timeline is summarized as follows:

Portal closure event (Early 2020)

The outlet portal slopes suffered a major slide during the construction phase. This failure occurred on slopes that had been excavated to the temporary profile but left entirely unsupported. The volume of the displaced mass was sufficient to physically obstruct the tunnel exit, necessitating extensive remedial earthworks.

Crack propagation (subsequent month)

Monitoring records identified the development of wide tension cracks and parallel fissures on the upper benches. These fissures, aligned parallel to the tunnel axis, progressively increased in aperture and persistence.

Structural threat

The deformation zone expanded retrogressively, eventually threatening critical infrastructure by extending toward the valve chamber complex and access routes, critically approaching the alignment of the dam plinth.

Figure 4.56 uncovers an illustration of the diversion tunnel exit portal closure and associated slope failure.

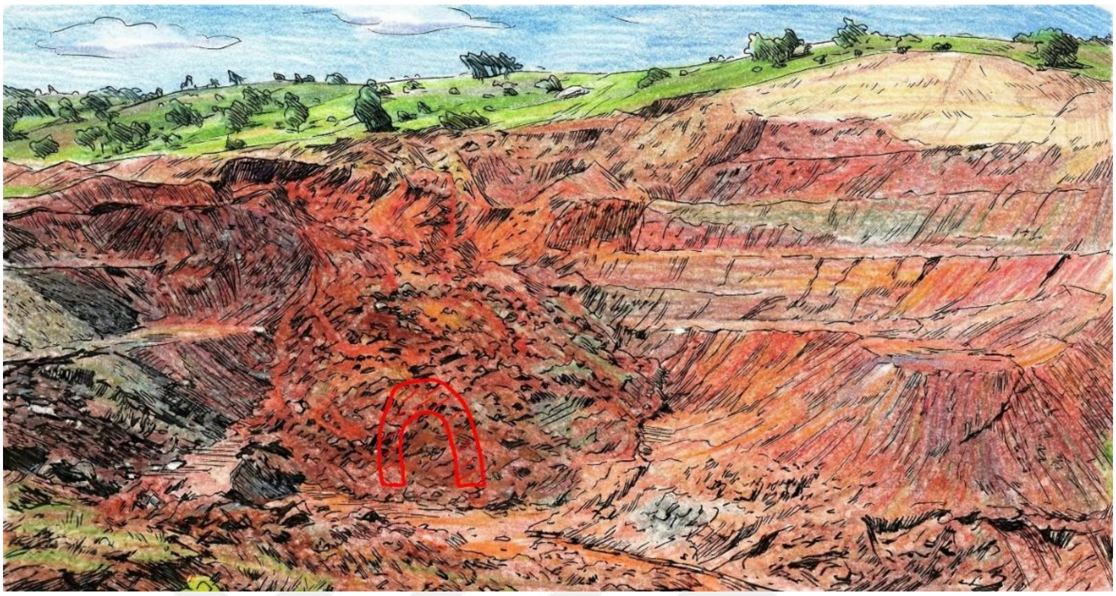

Figure 4.56. *Illustration of the diversion tunnel exit portal closure and associated slope failure*

4.3.3.3. Triggers and excavation effects

The primary trigger for these instabilities was hydro-mechanical. The portal's location within a dry stream bed served as a preferential flow path for surface runoff, accelerating the saturation and argillization of the silicified-radiolarite units. Piezometric data confirmed groundwater levels as shallow as 1.10 m to 3.60 m below the surface.

Excavation-induced stress relief further exacerbated the instability. The retention of steep 1V:1H temporary slopes without immediate shotcrete application allowed for rapid weathering and stress relaxation. Geometric constraints, particularly the proximity of the cut slopes to the dam body skirt, prevented the implementation of flatter gradients or effective toe support.

While post-seismic field inspections following the 2023 seismic sequence revealed no new major physical deformations on the rehabilitated slopes, pseudo-static assessments utilizing the recorded Peak Ground Acceleration (PGA) of approximately 0.48g, as well as intermediate scaled accelerations, indicated that the slopes exhibited theoretical vulnerability under such extreme dynamic loads. Table 4.16 indicates a summary of observed instabilities, triggers, and documented timeline.

Table 4.16. *Summary of observed instabilities, triggers, and documented timeline*

Event / Observation	Timeline	Mechanism / Trigger
Initial Portal Closure	Early 2020	Surface flow and sliding triggered by environmental exposure and lack of support.
Bench Tension Cracks	Mid-2020 (Subsequent Month)	Deep-seated sliding and moisture-induced swelling creating parallel fissures.
Progression of Fissures	Mid-2020 (Continued)	Documented advancement of cracks toward the valve chamber complex and access routes.
Seismic Assessment	Post-Seismic Phase (2023)	Seismic reassessment (approx. 0.48g PGA) indicating theoretical vulnerability despite lack of visual failure.

4.3.4. Back-analyses of portal slope stability (limit equilibrium and finite element methods)

The stability of the diversion tunnel portal slopes was evaluated using numerical back-analyses to distinguish the failure mechanisms and validate remedial designs. The primary assessment utilized the Limit Equilibrium Method (LEM) via the Slide2 software suite, incorporating the Simplified Bishop, Spencer, and GLE/Morgenstern-Price algorithms to determine the critical Factor of Safety (FS). Finite Element Method (FEM) tools (SAP2000) were utilized to assess the structural interaction between the conduit and the dam body under embankment loads.

4.3.4.1. Parameter calibration and material modeling

The analytical core of this study involved a rigorous calibration process where shear strength parameters were back-analyzed to replicate the observed instabilities on the temporary 1V:1H slopes. Initial rock mass properties were estimated using the RocLab software based on a Geological Strength Index (GSI) of 32–36 and an intact Uniaxial Compressive Strength (σ_{ci}) of 2.3 MPa.

However, to replicate the documented surface flows and landslides, a dual-layer material model was required:

Altered surface zone (shallow)

To account for the rapid argillization and swelling observed upon contact with atmospheric moisture and surface runoff, a near-surface "altered zone" was modeled with degraded, residual-like parameters (c' = 25 kPa, ϕ' = 3°).

Ophiolitic complex (deep)

The underlying, less weathered rock mass was modeled with an effective cohesion (c') of 75 kPa and an internal friction angle (ϕ') of 20°.

Table 4.17 incorporates calibrated shear strength parameters used for back-analysis.

Table 4.17. *Calibrated shear strength parameters used for back-analysis*

Material	Color	Unit Weight (γ) [kN/m³]	Cohesion (c′) [kPa]	Friction Angle (ϕ′) [°]	Source / Analysis Type
Altered Surface Zone		20	25	3	Back-analysis (Residual)
Compacted Fill		19	5	25	Design Parameter
Rockfill Cover		22	0	40	Design Parameter
Concrete		20	400	35	Design Parameter
Ophiolite Complex		25	75	20	Back-analysis / Lab Correlation

4.3.4.2. Stability of temporary excavations (1V:1H)

Static back-analyses of the unsupported 1V:1H temporary excavations confirmed the critical instability observed in the field.

Inlet portal

The unsupported static FS was calculated at 1.185, falling significantly below the permanent design requirement of 1.50. Figure 4.57 shows a static LEM analysis for the unsupported 1V:1H inlet portal slope.

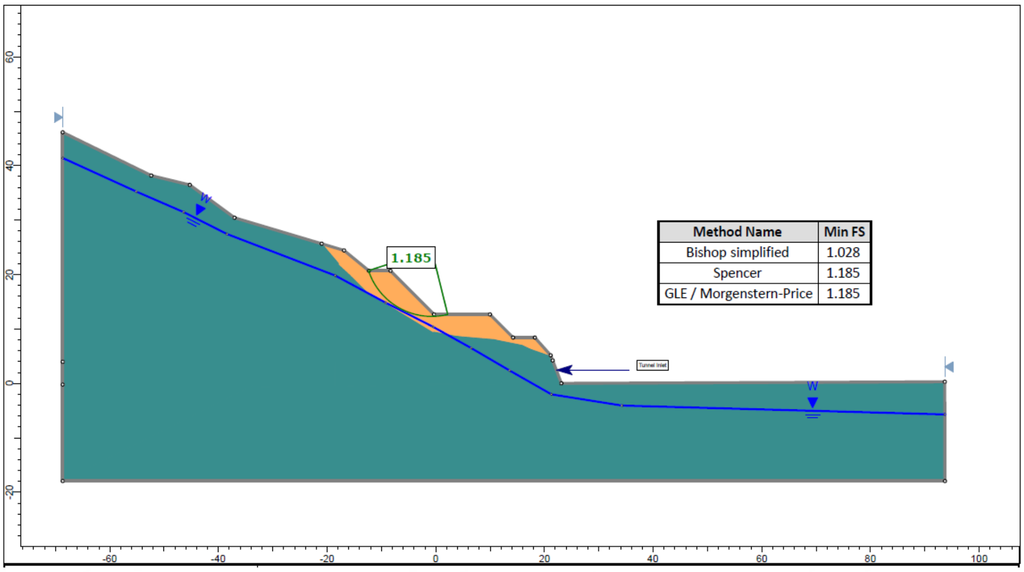

Figure 4.57. *Static LEM analysis for the unsupported 1V:1H inlet portal slope (FS=1.185)*

Numerical simulations indicated that the application of primary support (shotcrete and wire mesh) provided only marginal improvement, raising the static FS to approximately 1.361. Crucially, under the pseudo-static Operation Based Earthquake (OBE) load of 0.14g, the FS for the supported slopes dropped to 0.972. Figure 4.58 renders a static LEM analysis for the shotcrete and wire mesh supported 1V:1H inlet portal slope, while Figure 4.59 simulates a seismic LEM analysis for the same settings.

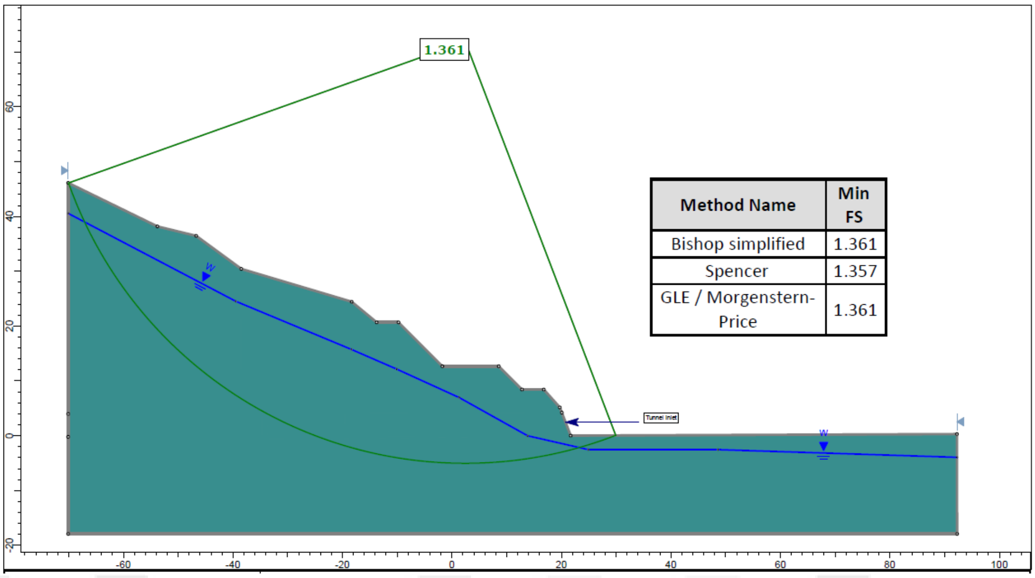

Figure 4.58. *Static LEM analysis for the shotcrete and wire mesh supported 1V:1H inlet portal slope (FS=1.361)*

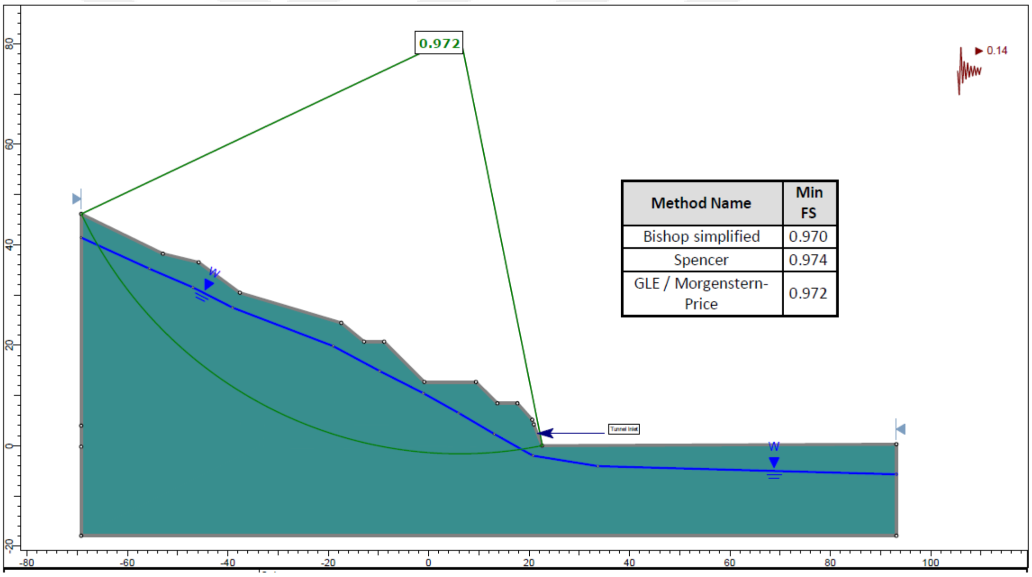

Figure 4.59. *Seismic LEM analysis for the shotcrete and wire mesh supported 1V:1H inlet portal slope (FS=0.972)*

Outlet portal

Analysis of the critical cross-section yielded a static Factor of Safety (FS) of 1.184, with failure surfaces propagating entirely through the heavily degraded zone. Figure 4.60 presents a static LEM analysis for the unsupported 1V:1H outlet portal slope, while Figure 4.61 displays a static LEM analysis for the shotcrete and wire mesh supported 1V:1H outlet portal slope.

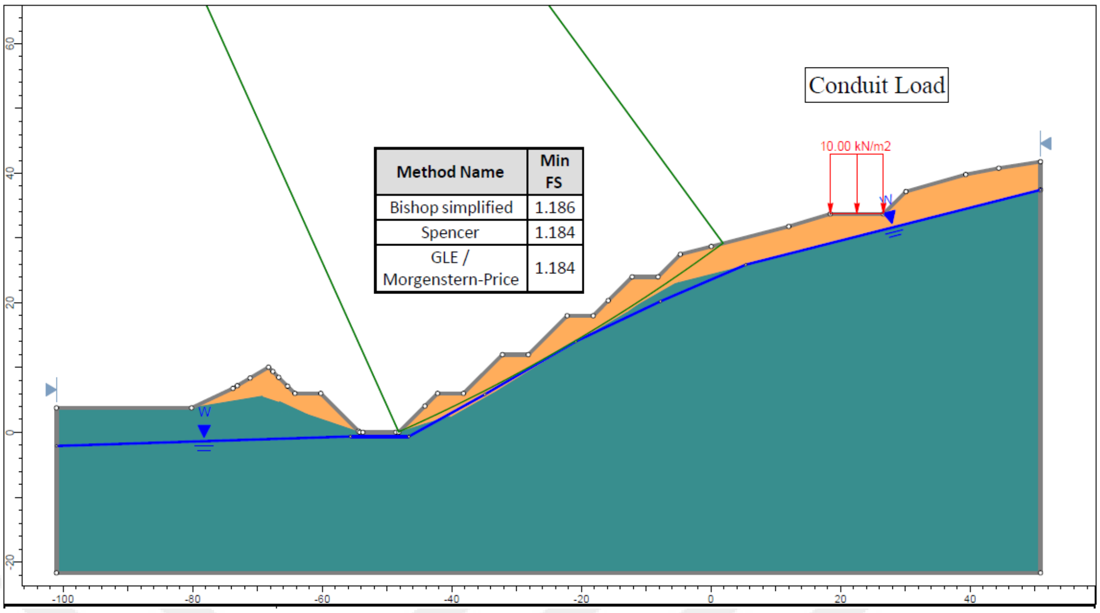

Figure 4.60. *Static LEM analysis for the unsupported 1V:1H outlet portal slope (FS=1.184)*

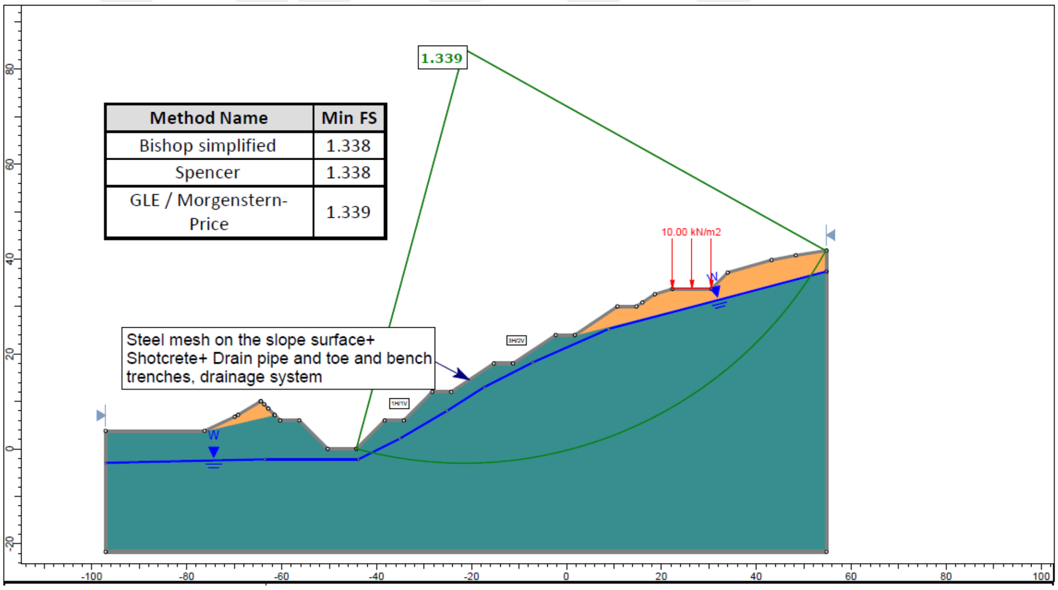

Figure 4.61. *Static LEM analysis for the shotcrete and wire mesh supported 1V:1H outlet portal slope (FS=1.339)*

4.3.4.3. Failure geometry and bolt ineffectiveness

Kinematic checks and LEM simulations revealed that the instability was governed by a "wide circle" rotational mechanism extending deep into the weak matrix. This geometry explains the failure of the initially installed 4.0 m rock bolts; the bolts were situated entirely within the active plastic zone of the sliding mass and failed to penetrate into competent anchorage material.

4.3.5. Support system design, implementation, and performance evaluation

The initial support strategy for the portal slopes relied on standard rock reinforcement techniques, comprising steel wire mesh, a minimum of 5+5 cm of shotcrete, and systematic 4.0 m long rock bolts. To mitigate the sensitivity of the ophiolitic mélange to water, a surface drainage network was designed, including head and bench ditches, toe drains, and weep holes.

Failure of the Initial System: Visual monitoring and numerical back-analyses revealed critical deficiencies in this approach:

Inconsistent implementation

Support was often applied partially or delayed, allowing atmospheric weathering to degrade the exposed rock face.

Ineffective bolting

The 4.0 m rock bolts were fundamentally ineffective. Kinematic analyses demonstrated that failure surfaces in the weak mélange followed deep, "wide circle" arcs that extended beyond the bolt length. Furthermore, the disintegrated, clay-rich matrix provided no competent rock blocks for effective mechanical anchoring.

Analytical inadequacy

Even with the full application of shotcrete and bolts, the static Factor of Safety (FS) for the 1V:1H slopes remained between 1.34 and 1.36, failing to meet the permanent design requirement of 1.50. Under seismic loading (0.14g), the FS dropped to 0.972, indicating a high probability of failure.

4.3.5.1. Remedial strategy: geometric modification

Recognizing the limitations of internal reinforcement, the stabilization strategy shifted to a comprehensive structural and geometric modification. The open trapezoidal channel approach was replaced with a cut-and-cover reinforced concrete conduit (approximately 85 m long at the inlet).

This structure served as a rigid core, allowing the slopes to be stabilized via backfilling rather than excavation. The area was filled with compacted granular material to achieve a stable permanent inclination of 1V:2H. To prevent erosion and reduce surface infiltration, a 1.00 m thick rockfill cover was placed over the final embankment.

Table 4.18 groups a summary of portal support and rehabilitation components.

Table 4.18. *Summary of portal support and rehabilitation components*

Component	Specification	Function
Conduit Liner	0.35 m Reinforced Concrete (C25)	Structural conveyance & rigid core
Embankment	Compacted Granular Fill (1V:2H)	Restoring natural topography
Surface Protection	1.00 m Rockfill	Erosion control & runoff protection
Primary Support	Mesh + 5+5 cm Shotcrete	Surface sealing (preventing alteration)
Drainage	Weep holes, head& bench ditches, toe drains	Pore pressure management

4.3.5.2. Performance evaluation and validation of remedial measures

The remedial design was rigorously evaluated using Limit Equilibrium Methods (LEM) and validated by post-earthquake field observations. To ensure long-term stability, the designed cut-and-cover solution—involving the reinforced concrete conduit and backfilling with compacted granular fill to achieve the flatter 1V:2H slope profile capped with a rockfill toe weight—was thoroughly analyzed. The remediated 1V:2H slopes achieved static safety factors satisfying the long-term stability criterion (FS > 1.50), and maintained stability under the Operation Based Earthquake (OBE) load of 0.14g. Specifically, the remedial design satisfied all stability criteria across the following domains:

Inlet portal

The remediated slope achieved a static FS of 1.512. Under OBE seismic loading (0.14g), the FS remained stable at 1.130. Figure 4.62 exhibits a static, Figure 4.63 a seismic LEM analysis for the inlet portal slope after remediation.

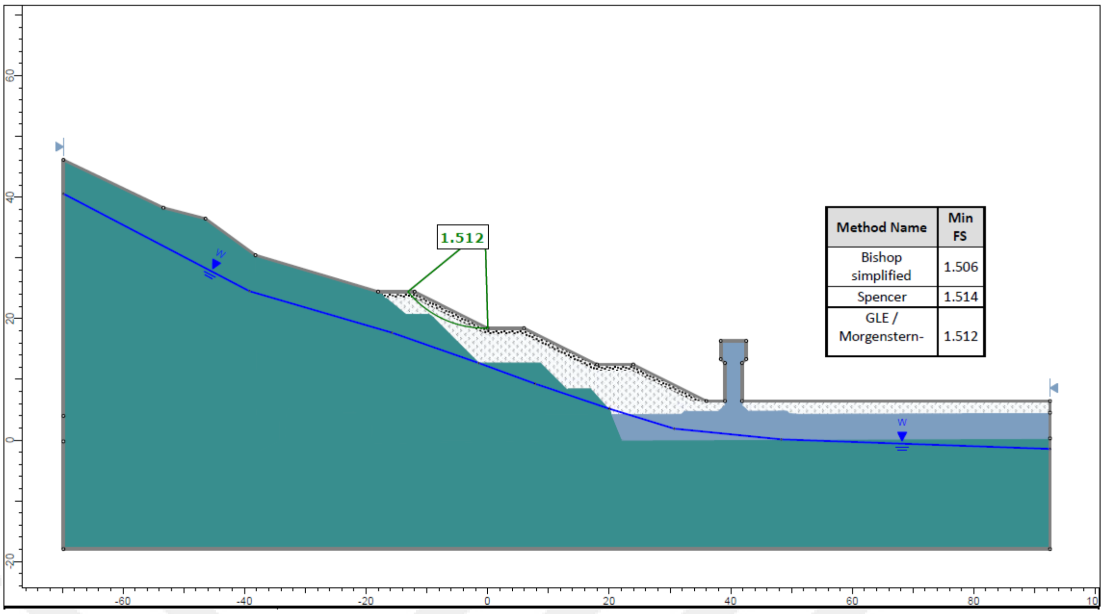

Figure 4.62. *Static LEM analysis for the inlet portal slope after remediation (FS=1.512)*

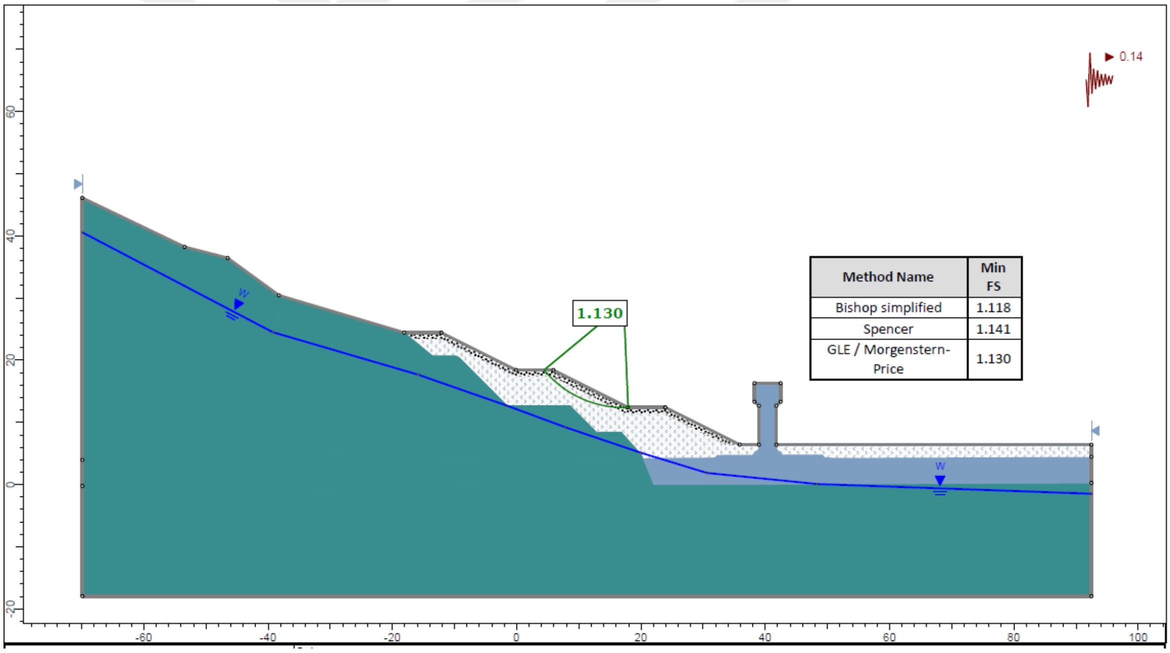

Figure 4.63. *Seismic LEM analysis for the inlet portal slope after remediation (FS=1.130)*

Outlet portal

Comprehensive backfilling resulted in a static FS of 1.504 and a pseudo-static FS of 1.168. Figures 4.64 and 4.65 present the static and seismic LEM analyses for the outlet portal slope after remediation, respectively.

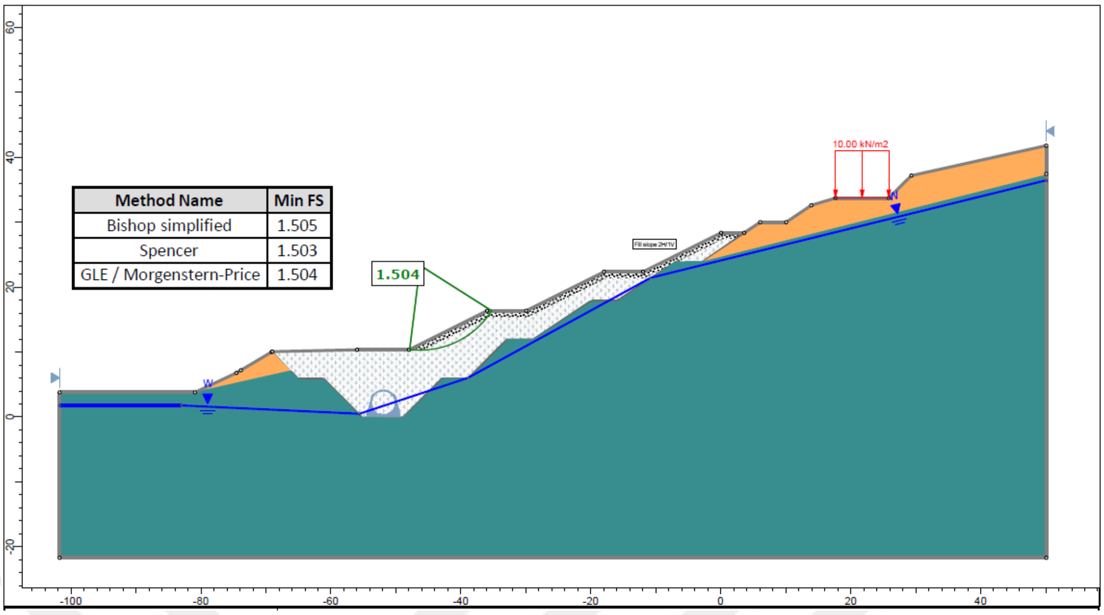

Figure 4.64. *Static LEM analysis for the outlet portal slope after remediation (FS=1.504)*

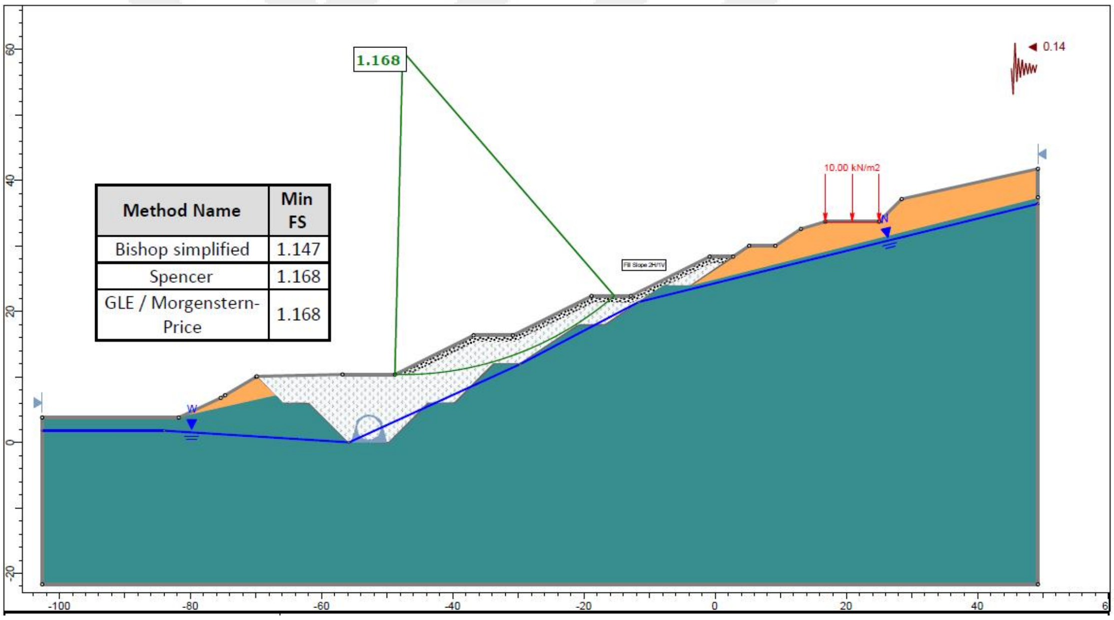

Figure 4.65. *Seismic LEM analysis for the outlet portal slope after remediation (FS=1.168)*

Structure-dam interaction

Structural analysis verified that the conduit remains stable under the surcharge load of the dam embankment (approx. 400 kN/m²).

- Inlet portal: Backfill support resulted in a static FS of 1.899 and a pseudo-static FS of 1.183. Figures 4.66 and 4.67 illustrate the static and seismic interaction with the body after conduit backfill at the inlet.

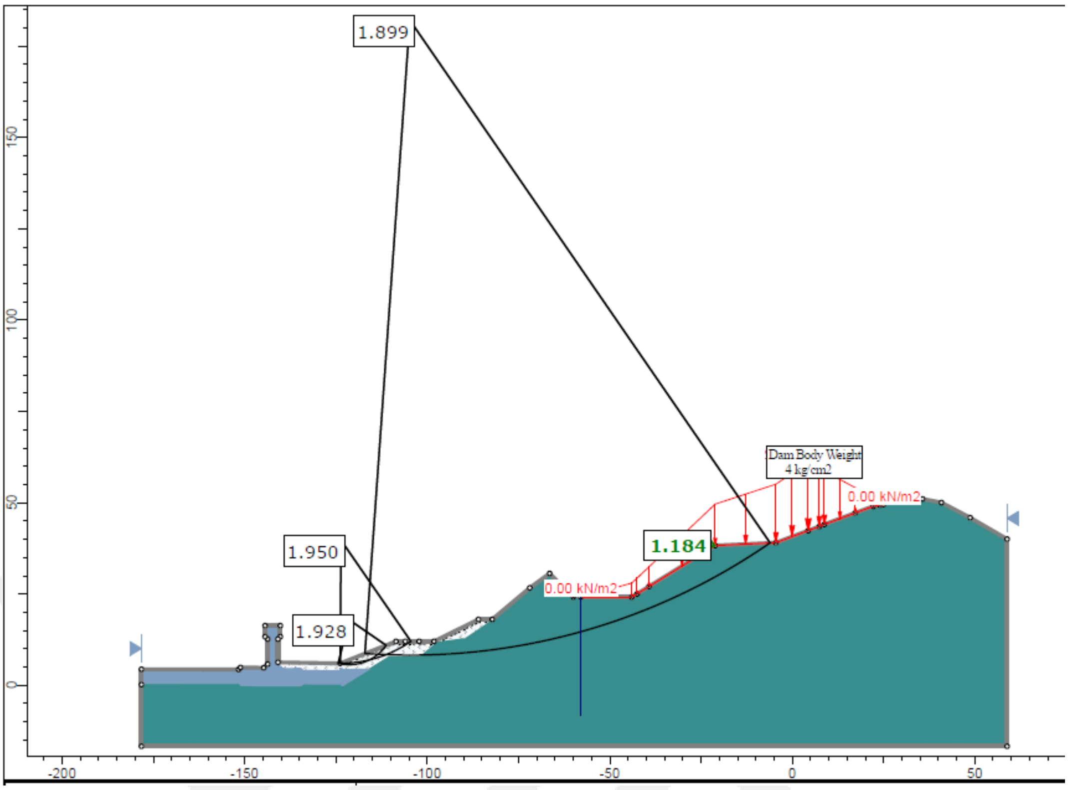

Figure 4.66. *Interaction with the body after conduit backfill at the inlet for static case (FS=1.899)*

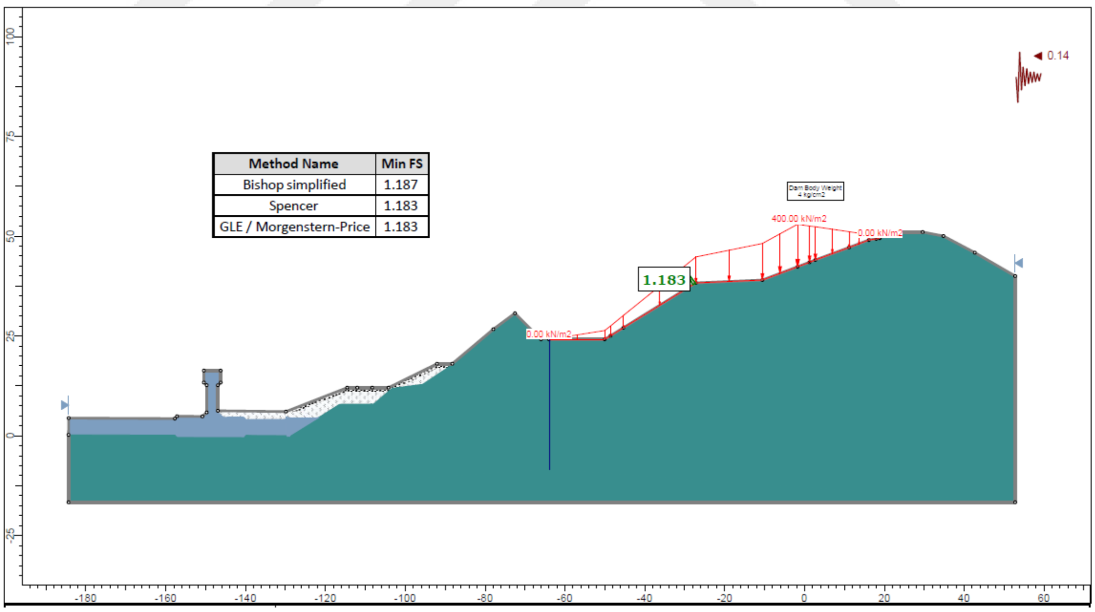

Figure 4.67. *Interaction with the body after conduit backfill at the inlet for seismic case (FS=1.183)*

- Outlet portal: The remediated slope achieved a static FS of 1.697 and a seismic FS of 1.179. Figures 4.68 and 4.69 present the static and seismic stability analyses of the diversion outlet profile with fill support, respectively.

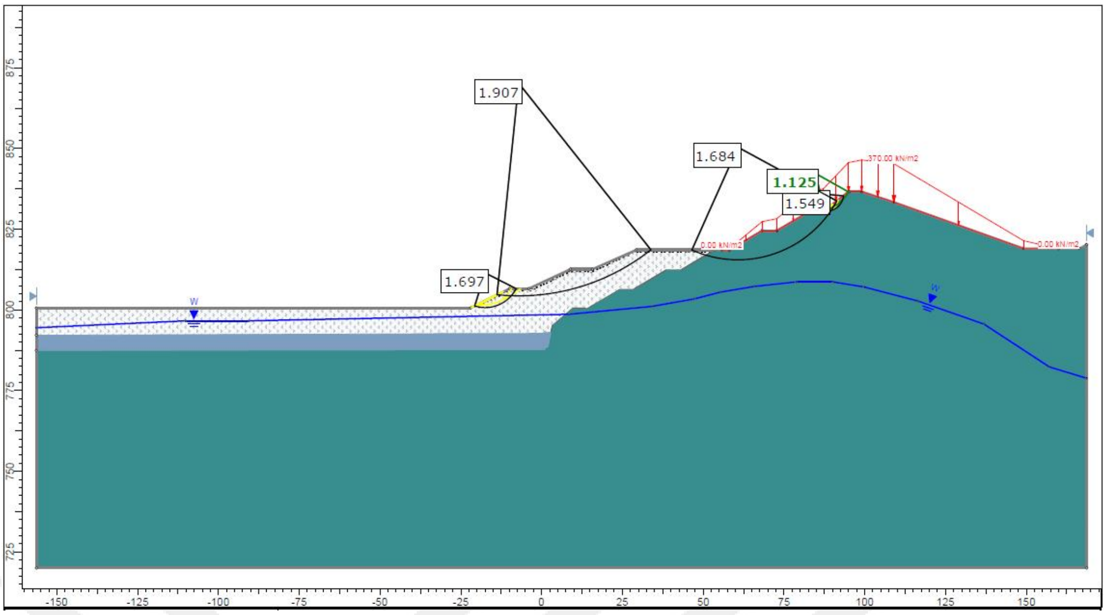

Figure 4.68. *Static stability analysis of diversion outlet profile with fill support (FS=1.697)*

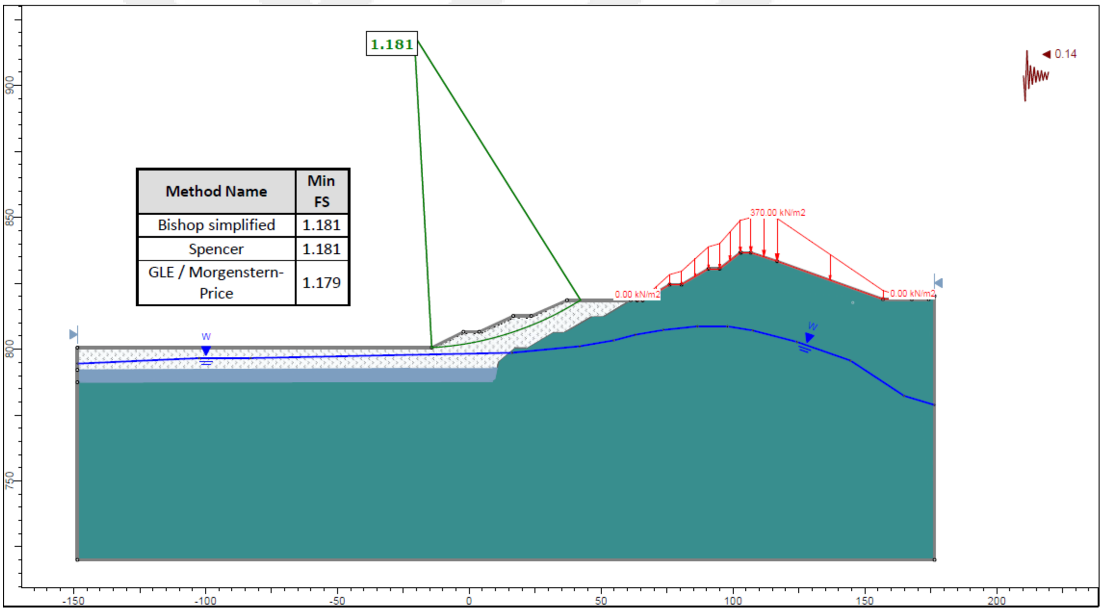

Method Name	Min FS
Bishop simplified	1.181
Spencer	1.181
GLE / Morgenstern-Price	1.179

Figure 4.69. *Seismic stability analysis of diversion outlet profile with fill support (FS=1.179)*

4.3.5.3. Extreme seismic assessment and field validation (the 0.48g discrepancy)

Beyond the standard design parameters, a critical evaluation was performed using the actual Peak Ground Acceleration (PGA) of approximately 0.48g recorded during the 2023 seismic sequence, alongside scaled accelerations of 0.36g (3/4 PGA) and 0.24g (1/2 PGA) to systematically assess the sensitivity of the slope performance under varying dynamic load intensities.

The LEM analyses predicted widespread failure under the maximum extreme load of 0.48g, with safety factors dropping to 0.62–0.70. However, extended pseudo-static analyses utilizing reduced seismic coefficients demonstrated a clear transition toward equilibrium. Specifically, simulations applying 0.36g resulted in safety factors ranging from FS = 0.75 - 0.80, whereas analyses employing 0.24g yielded FS = 0.94 - 1.00, indicating a near-stable condition.

Despite these analytical models predicting failure (FS < 0.7) under the extreme PGA of 0.48g and scaled accelerations of 0.36g (FS $\leq$ 0.8), post-earthquake site inspections revealed no significant physical deformations on the rehabilitated slopes. This outcome practically validated the near-stable conditions (FS $\approx$ 1.00) calculated at 0.24g (1/2 PGA). This discrepancy highlights a major limitation in the standard pseudo-static method for ophiolitic terrains: the method treats seismic force as a constant, unidirectional load, neglecting the transient nature of ground motion and the high damping capacity of the clay-rich mélange matrix. This outcome demonstrates the resilience of the cut-and-cover solution against transient dynamic loads, further supporting the premise that the effective seismic energy transferred to the sliding mass was significantly dampened.

Outlet portal

Applying a pseudo-static load of 0.24g produced an FS of 0.944, whereas increasing the seismic coefficient to 0.36g and 0.48g reduced the FS to 0.789 and 0.698, respectively. Figure 4.70 shows the results of the pseudo-static stability analysis for a seismic coefficient of 0.24g.

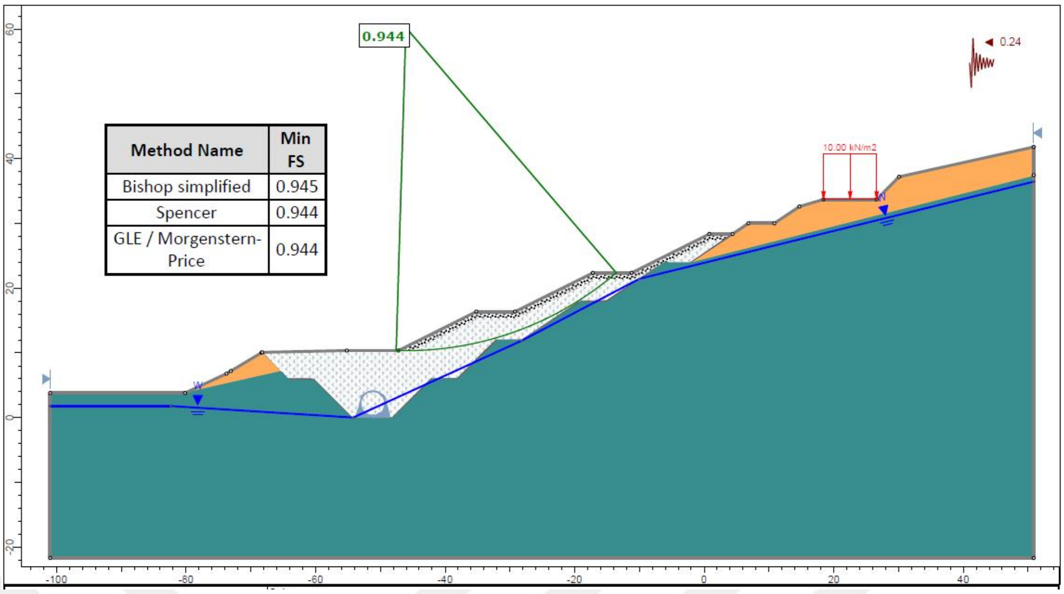

Figure 4.70. *Results of the pseudo-static stability analysis for a seismic coefficient of 0.24g, producing an FS of 0.944*

Figure 4.71 presents the results of the pseudo-static stability analysis for an increased seismic coefficient of 0.36g.

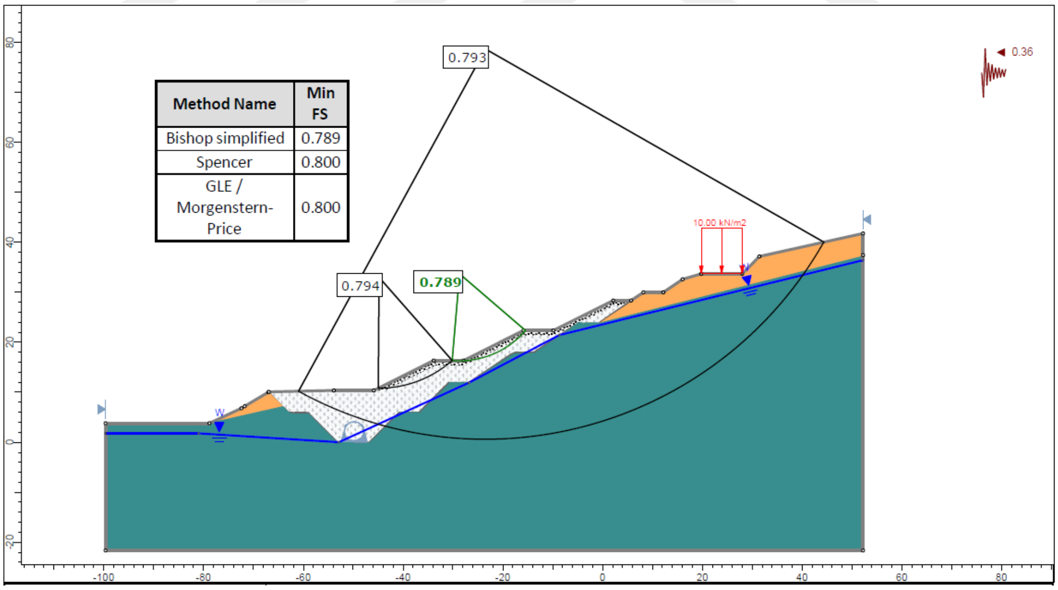

Figure 4.71. *Results of the pseudo-static stability analysis for an increased seismic coefficient of 0.36g, reducing the FS to 0.789*

Figure 4.72 illustrates the results of the pseudo-static stability analysis for a maximum seismic coefficient of 0.48g.

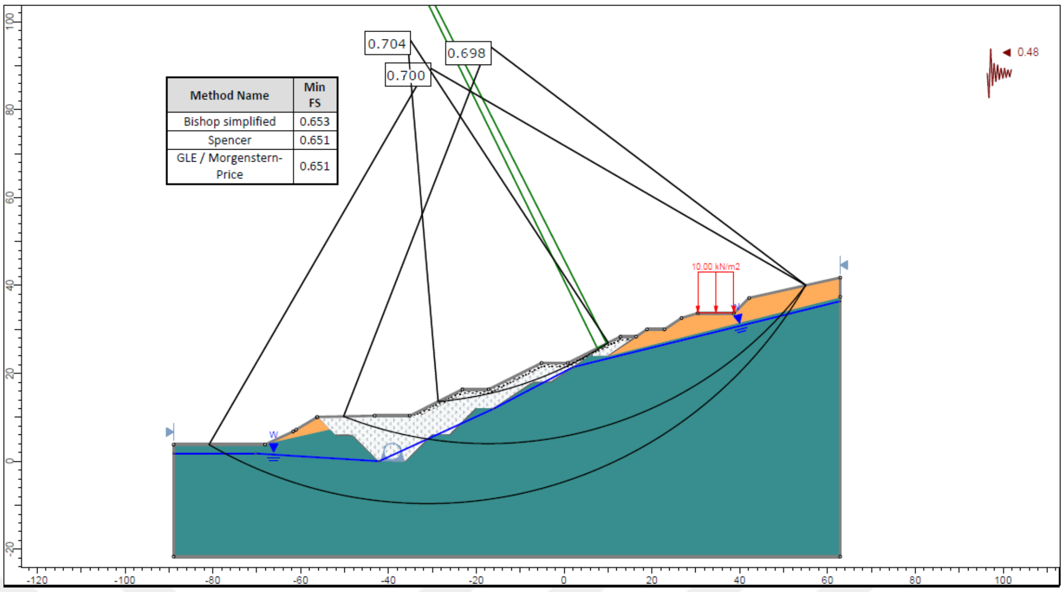

Figure 4.72. *Results of the pseudo-static stability analysis for a maximum seismic coefficient of 0.48g, further reducing the FS to 0.698*

Support-dam interaction

Below are the supported inlet and outlet portals under extreme seismic conditions, along with their interactions with the dam body.

- Inlet portal: As the pseudo-static load intensified from 0.24g to 0.36g and ultimately 0.48g, the corresponding FS values progressively declined from 1.01 to 0.81 and 0.66. Figure 4.73 outlines the computed FS of 1.01 for the potential slope instability under an initial pseudo-static seismic coefficient of 0.24g.

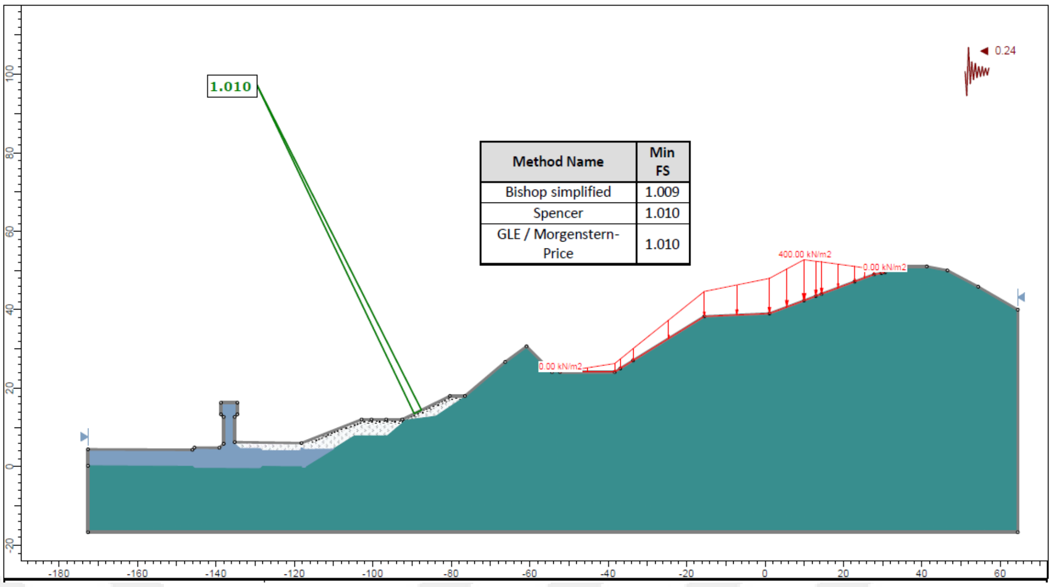

Figure 4.73. *Computed FS of 1.01 for the potential slope instability under an initial pseudo-static seismic coefficient of 0.24g*

Figure 4.74 captures the reduction of the computed FS to 0.81 following an increase in the pseudo-static seismic coefficient to 0.36g.

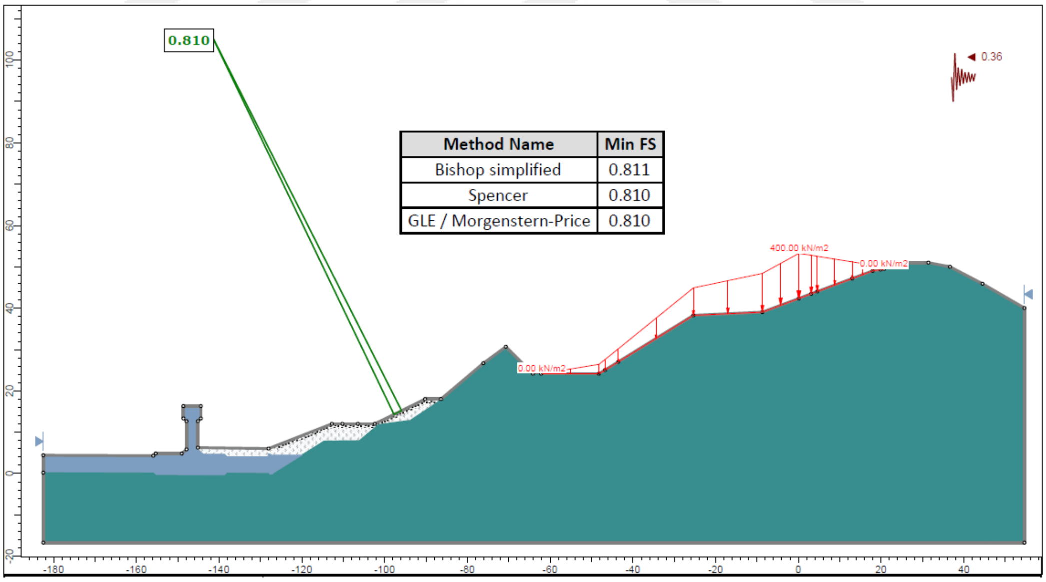

Figure 4.74. *Reduction of the computed FS to 0.81 following an increase in the pseudo-static seismic coefficient to 0.36g*

Figure 4.75 exhibits the critical decline of the computed FS to 0.659 when subjected to the maximum pseudo-static seismic coefficient of 0.48g.

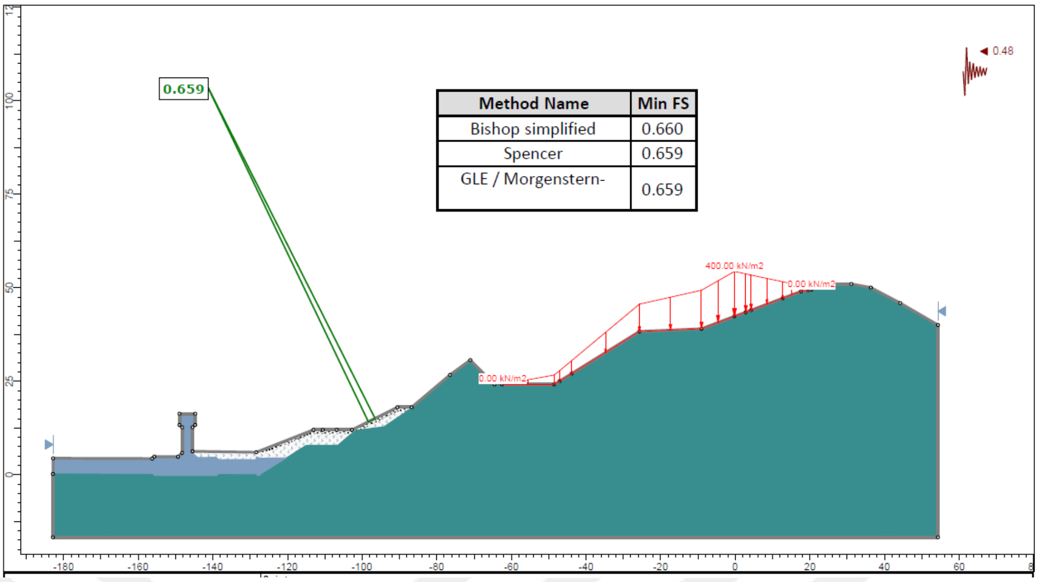

Figure 4.75. *Critical decline of the computed FS to 0.659 when subjected to the maximum pseudo-static seismic coefficient of 0.48g*

- Outlet portal: The stability analysis yielded an FS of 0.942 under an initial seismic coefficient of 0.24g; subsequent increases to 0.36g and 0.48g reduced the FS to 0.748 and 0.62, respectively. Figure 4.76 proves the results of the 2-D pseudo-static stability analysis showing an FS of 0.942 for an applied seismic load of 0.24g.

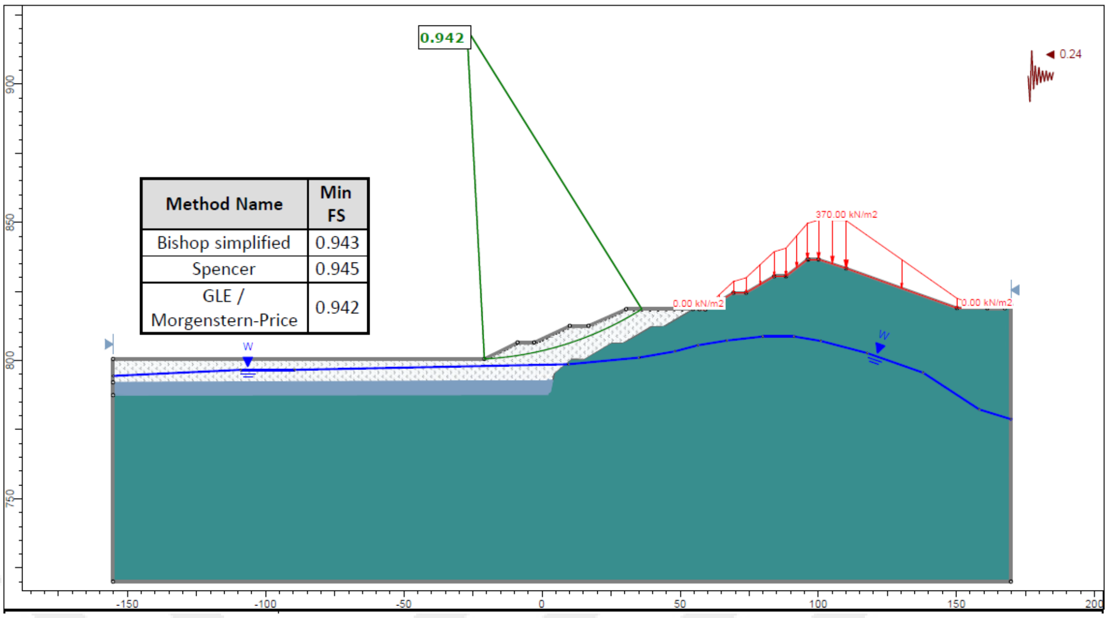

Figure 4.76. *Results of the 2-D pseudo-static stability analysis demonstrating an FS of 0.942 for an applied seismic load of 0.24g*

Figure 4.77 displays the results of the 2-D pseudo-static stability analysis demonstrating a reduced FS of 0.748 following an increase in the seismic coefficient to 0.36g.

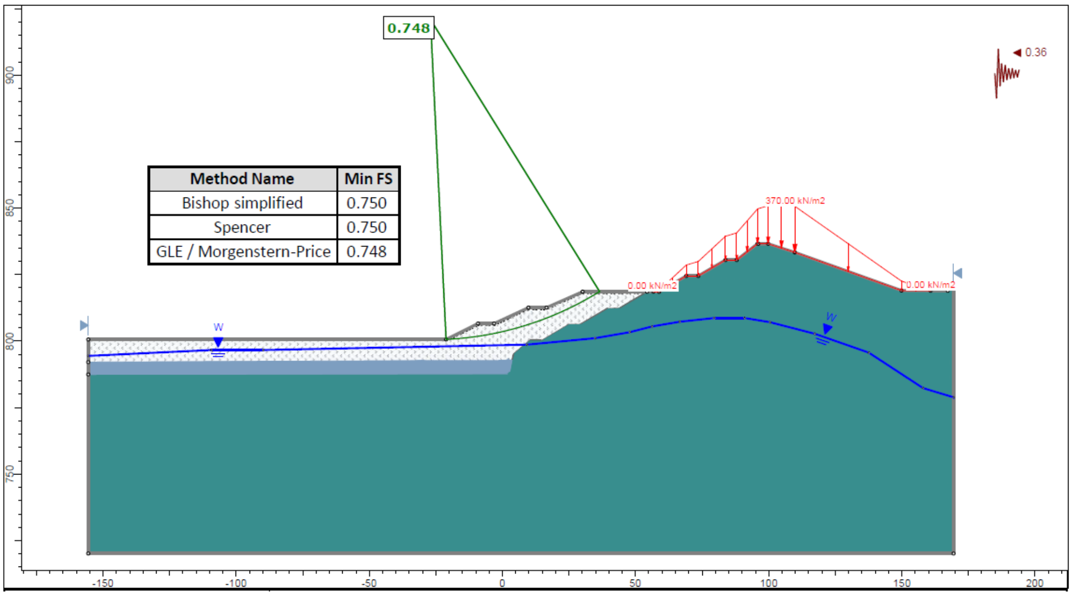

Figure 4.77. *Results of the 2-D pseudo-static stability analysis demonstrating a reduced FS of 0.748 following a subsequent increase in the seismic coefficient to 0.36g*

Figure 4.78 reflects the results of the 2-D pseudo-static stability analysis demonstrating a critical FS of 0.62 under the maximum applied seismic coefficient of 0.48g.

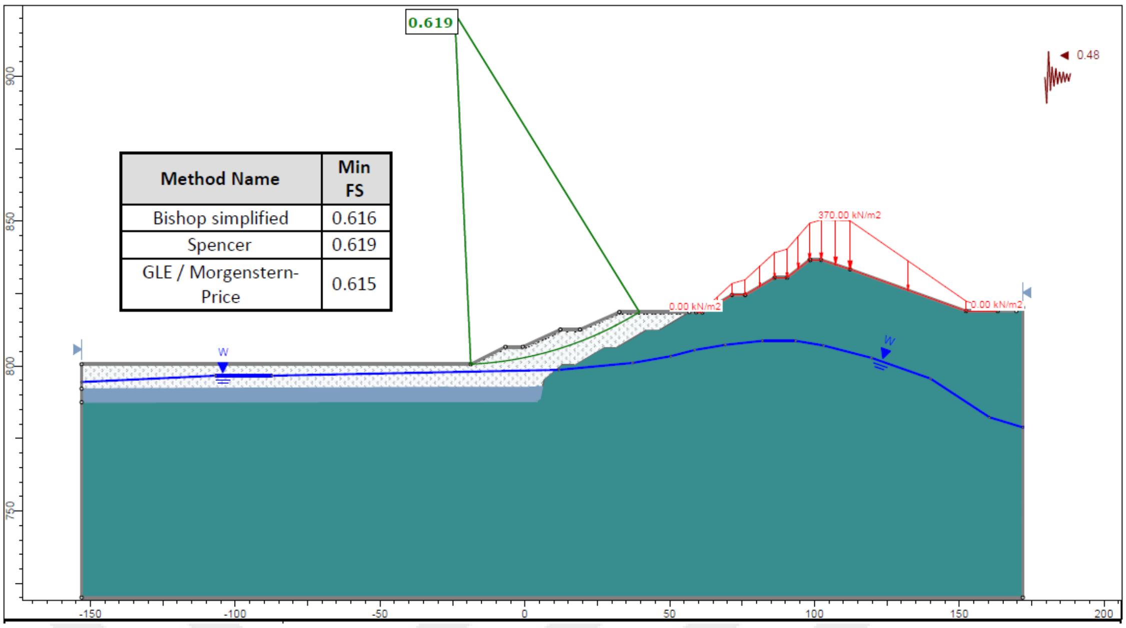

Figure 4.78. *Results of the 2-D pseudo-static stability analysis demonstrating a critical FS of 0.62 under the maximum applied seismic coefficient of 0.48g*

Table 4.19 combines a consolidated summary of safety factors for portal configurations.

Table 4.19. *Consolidated summary of safety factors (FS) for portal configurations*

Analysis Scenario	**Support**	**Loading Condition**	**Computed FS (LEM)**	**Min. Required FS**	**Outcome**
Unsupported 1V:1H	-	Static	1.185	1.50	Unstable / Failed
Supported 1V:1H	Mesh+ Shotcrete	Static	1.339-1.361	1.50	Marginal
Supported 1V:1H	Mesh+ Shotcrete	Pseudo-static (0.14g)	0.972	1.10	Unstable
Remediated (1V:2H)	Conduit+ Backfill	Static	1.504 – 1.512	1.50	Stable

Table 4.19. (Continued) *Consolidated summary of safety factors (FS) for portal configurations*

Analysis Scenario	Support	Loading Condition	Computed FS (LEM)	Min. Required FS	Outcome
Remediated (1V:2H)	Conduit+ Backfill	Pseudo-static (0.14g)	1.13 – 1.18	1.00	Stable
Remediated (1V:2H)	Conduit+ Backfill	Pseudo-static (0.24g)	0.942-1.01	1.00	Analytical Failure/ Marginally Stable
Remediated (1V:2H)	Conduit+ Backfill	Pseudo-static (0.36g)	0.748-0.81	1.00	Analytical Failure
Remediated (1V:2H)	Conduit+ Backfill	Pseudo-static (0.48g)	0.62 – 0.70	1.00	Analytical Failure

Despite analytical failure under 0.48g, 0.36g, and near-failure at 0.24g, slopes remained physically stable post-2023 earthquakes.

4.3.6. Lessons learned

The primary geotechnical lesson from this case study is that conventional internal reinforcement (short rock bolts) is unsuitable for stabilizing ophiolitic mélange formations where failures are governed by deep-seated, rotational mechanisms. The mélange behaves analogously to a "loose sandcastle" protected by a thin shell of shotcrete; while the shell prevents immediate weathering, it cannot restrain a deep mass movement if the underlying matrix is saturated and weak.

In such geological settings, permanent stability is most reliably achieved through topographic restoration—specifically, the use of cut-and-cover conduits that allow for slope flattening and toe weighting—rather than attempting to reinforce an inherently fragmented and weak rock mass. Additionally, the discrepancy between the pseudo-static failure predictions at 0.48g and the observed post-seismic stability suggests that traditional simplified seismic coefficients may be overly conservative for these materials, likely due to the high damping characteristics of the clay-altered matrix.

Furthermore, these analytical outcomes provide compelling evidence that could help justify the use of k_h = PGA/2 as an appropriate seismic coefficient in literature, suggesting that even such a reduction might remain conservative in highly damped ophiolitic formations. It is also crucial to emphasize that the direction of seismic waves resulting from fault rupture, along with potential directivity effects, plays a significant role in the actual dynamic response of the slopes.

The actual PGA peak may have been too brief to induce the full-scale deformation predicted by the model. Furthermore, the analysis is influenced by:

- Conservative parameters: The selection of geotechnical parameters for the ophiolitic terrain may have been conservative.
- Idealized models: The models rely on simplified topographic representations and idealized stress-strain responses for materials, which may not capture the complex three-dimensional site geometry and material behavior.
- Undetected movement: It is also possible that minor slope movements or deformations occurred that were below the threshold of visual detection during site surveys.

Ultimately, this study's extended pseudo-static analyses confirm that while conventional methods provide essential insights, their results must be interpreted with caution, especially in seismically active regions with challenging geological conditions like ophiolitic terrains. For critical infrastructure, the integration of advanced numerical modeling with robust observational data remains essential for a comprehensive and reliable assessment of slope stability.

4.4. Case 4 – Landslide Triggered by Inadequate Drainage in a Radiolarite–Limestone–Mudstone Sequence

This section presents a comprehensive analysis of the slope instability encountered during the construction of the spillway and discharge channel of a major embankment dam project located in a tectonically complex region of Türkiye. The case study details the geotechnical evaluation and remediation of slopes situated within a challenging geological setting characterized by highly weathered flysch facies and allochthonous ophiolitic mélange units.

The primary investigation focuses on active and potential mass movements observed along a critical segment of the alignment (approx. 75 m), which threatened the integrity of the hydraulic structure and associated access roads. The objective of this study was to assess the failure mechanisms—triggered by a combination of construction-induced toe excavation, crest surcharging, and seasonal hydraulic events—through the use of inclinometer monitoring and limit equilibrium back-analysis. Subsequently, a remedial strategy involving geometric re-grading, structural support, and comprehensive drainage improvements was developed to ensure long-term stability under both static and design seismic conditions.

4.4.1. Project setting, slope geometry, and drainage layout

The case study examines the geotechnical challenges encountered during the construction of the spillway structure and discharge channel for a major embankment dam (specifically a Concrete-Faced Sand-Gravel Fill Dam) located in a seismically active region of Türkiye. The dam, designed primarily for irrigation, features a crest length of more than 800 m and a maximum height of approximately 80 m from the foundation level.

The appurtenant spillway structure is situated on the right abutment and consists of a broad-crested weir discharging into a channel extending nearly 490 m. Given the project's location, the stability analysis for these critical components was designed to account for a Maximum Design Earthquake (MDE) with a horizontal peak ground acceleration of 0.28 g, an Operating Basis Earthquake (OBE) with a peak ground acceleration of 0.14 g for operational design (assuming a 100-year economic life, a 50% probability of exceedance, and a 144-year return period), and a horizontal seismic design coefficient (k_h) selected as 0.18 g (≅2/3MDE).

4.4.1.1. Geological and tectonic setting

The geological setting of the spillway excavation is dominated by allochthonous ophiolitic mélange units and associated flysch facies. These units represent a sequence derived from the closure of the Neotethys ocean, which was tectonically emplaced onto the stable continental platform during the Upper Cretaceous-Miocene interval. The lithological sequence is characterized by an intensely fractured, folded, and altered succession of radiolarian chert, mudstone, and micritic limestone interlayers, alongside localized intrusions of ultramafic rocks (harzburgite, serpentinite, pyroxenite) and gabbro.

Due to the site's proximity to major regional suture zones and active fault systems, the rock mass exhibits severe tectonic deformation. Furthermore, substantial chemical weathering and physical decomposition have affected the upper geological profile, resulting in residual soil layers and landslide debris ranging from approximately 3 to 10 m in thickness, with weathering effects extending up to 30 m in depth.

4.4.1.2. Slope geometry and instability mechanisms

The slope geometry in the critical failure zones was established through major excavations into the natural hillside, where the existing topography typically exhibited a slope ratio of approximately 1V:1.5H. Long-term design specifications recommended excavation inclinations of 1.5H:1V, integrated with 4.0 m wide benches at vertical intervals of 6.0 to 7.5 m. However, short-term temporary cuts were permitted at steeper 1V:1H inclinations.

Instability was concentrated in two primary zones: the area immediately adjacent to the spillway crest structure and a substantial segment of the discharge channel sidewalls. These instabilities were exacerbated by construction activities, specifically the excavation for a realignment road near the control structure and the uncontrolled placement of excavated spoil material on the upper slope benches. This surcharge load acted as a destabilizing force, significantly reducing the factor of safety, particularly when the material became saturated.

4.4.1.3. Hydrogeology and instrumentation

The critical failure mechanism was directly attributed to the inadequate management of surface water and subsurface pore pressures. The hydrogeological regime is characterized by high seasonal variability, perennial springs, and multiple ephemeral watercourses traversing the slope alignment. Geotechnical investigations also indicated localized pressurized groundwater conditions.

In the absence of effective surface drainage, seasonal precipitation resulted in the rapid saturation of the fine-grained, highly weathered matrix, leading to a drastic reduction in effective stress and significant softening, effectively triggering flow-like behavior in the saturated mass.

To characterize these mechanisms, a robust monitoring system was implemented, comprising a network of core-drilled boreholes (with depths ranging from approximately 25 to 40 m) equipped with piezometric filter pipes. Additionally, three strategic inclinometer stations (designated as BH-3, BH-4, and BH-5) were installed to depths sufficient to intersect the potential failure surface. Monitoring conducted over a critical 6-month period encompassing the wet season captured the transition from dormant to active displacement driven by precipitation events. Figure 4.79 displays the general layout of the spillway excavation and discharge channel.

Figure 4.79. *General layout of the spillway excavation and discharge channel*

4.4.2. Geological and geotechnical characterization

The geological sequence at the project site is primarily composed of allochthonous ophiolitic mélange units and associated flysch facies. These units were tectonically emplaced onto the stable continental platform during the Upper Cretaceous-Miocene interval. The sedimentary sequence is characterized by deep-sea sediments, including alternating sequences of thin-to-medium bedded dark red-to-brown radiolarian chert, yellowish mudstone, and micritic limestone. The ophiolitic component represents a complex assemblage containing harzburgite, serpentinite, pyroxenite, and gabbro.

4.4.2.1. Structural and weathering framework

The structural framework of the slope is heavily influenced by intense tectonism associated with the proximity to major regional active fault systems and suture zones. The rock mass is characterized by intensive folding, fracturing, and the presence of serpentinitic intrusions along discontinuity surfaces, which significantly degrade the rock mass strength.

Weathering is pervasive, extending deep into the bedrock profile. Geotechnical investigations using cored boreholes (BH-1 through BH-7) consistently demonstrated extremely low rock quality, with RQD (Rock Quality Designation) values often registering 0%. Core samples were frequently categorized as 'fragmented', 'highly weathered' (W4), or 'completely weathered' (W5). This severe alteration results in a thick mantle of residual soil and landslide debris, typically ranging from 3 to 10 m in thickness, transitioning into a very weak rock mass profile at greater depths. Quaternary deposits, including poorly graded alluvial blocks, gravels, and silts (approximately 6 to 12 m thick), unconformably overlie these units in the valley floor.

4.4.2.2. Geotechnical parameters

Geotechnical characterization was established through a combination of in-situ testing and laboratory analysis.

Laboratory testing

The average natural unit weight of the rock materials was approximately 21 kN/m^3. Uniaxial Compressive Strength (UCS) values, derived from converted Point Load Tests, averaged 5.57 MPa, with a mean point load strength index (Is_{50}) of 0.23 MPa.

Soil characterization

The fine-grained residual soils exhibited high plasticity, with Plasticity Index (PI) values ranging from 22.9% to 33.0%, classifying them as low (CL) to high (CH) plasticity clays.

In-situ testing

Standard Penetration Tests (SPT) in weathered horizons typically yielded "very stiff" to "hard" consistencies, often reaching refusal. Pressuremeter testing (e.g., in borehole BH-1) provided variable Menard Elasticity Modulus (E_M) values, ranging from 10.9 MPa to 563 MPa in the transition zones, while competent rock layers at depth exceeded 5000 MPa. For design purposes, these moduli were typically reduced by 40% to account for geological complexity and saturation.

4.4.2.3. Hydrogeology

The hydrogeological condition is critical to stability. While the intact rock matrix is generally impermeable or exhibits very low permeability, the dense network of tectonic discontinuities facilitates localized groundwater storage and the formation of seasonal springs. The low RQD values and the argillaceous nature of the flysch unit create a setting where water ingress rapidly reduces effective stress and frictional resistance along discontinuities, leading to failure when saturation occurs.

Figure 4.80 exhibits a photo showing the highly fractured ophiolitic mélange matrix and residual soil mantle.

Figure 4.80. *Photo showing the highly fractured ophiolitic mélange matrix and residual soil mantle*

The material parameters adopted for stability analyses, derived from back-analysis and laboratory testing, are summarized in Table 4.20.

Table 4.20. *Summary of geotechnical design parameters for the spillway sequence*

Material	Color	Unit Weight γ (kN/m³)	Cohesion c′ (kPa)	Friction Angle ϕ′ (°)	Source / Test Type
Landslide Material		18.0	5.0	20.0–28.0	Back-analysis
Residual Soil (D=0.2)		21.3	34.0	15.0	Lab/ Hoek-Brown
Dam Body		20	Infinite Strength		Design Value
Type-II Weak Rock (Flysch Facies)		25.0	137.0	37.0	Lab/ Hoek-Brown
Stone Retaining Wall		22.0	200.0	40.0	Design Value
Fill Material		19.0 - 20.0	-	20.0	Design Value

4.4.3. Failure mechanism, hydrogeological conditions, and role of pore water pressure

The instability within the spillway excavation sequence is characterized by a compound failure mechanism, which transitioned from a state of incipient instability (creep) to active mass movement during the seasonal high-precipitation period. The failure primarily involved the mobilization of highly weathered residual soil and landslide debris derived from the flysch facies of the ophiolitic mélange.

4.4.3.1. Failure kinematics and triggers

Deformations manifested as complex movements, encompassing deep-seated rotational shearing, shallow slope failures, and saturated flow-type failures. Prior to primary mobilization, the slope exhibited distress in the form of longitudinal tension cracks ranging from 20 to 35 m in length. One active slide sector reached a lateral width of approximately 75 m.

At the critical cross-section, the material transitioned into a viscous fluid state, moving parallel to the spillway axis until an adjacent competent limestone block acted as a structural barrier, diverting the displaced mass into the discharge channel.

The primary triggers of instability were a combination of anthropogenic interventions and adverse climatic conditions:

Toe excavation

The construction sequence necessitated extensive excavation for the realignment of access routes and the spillway channel, effectively removing the buttressing passive resistance at the slope toe.

Surcharge loading

An uncontrolled spoil disposal area was established on the upper slope benches, covering a substantial footprint with an approximate thickness of 10 m. This loose, uncompacted excavation waste imposed a significant destabilizing load (driving moment) and functioned as a permeable reservoir, facilitating infiltration.

Climatic forcing

Intense seasonal precipitation and snowmelt served as the immediate hydraulic trigger. This saturation caused the fine-grained matrix to undergo drastic softening and loss of effective stress, leading to flow-like failure mechanisms.

4.4.3.2. Hydrogeological conditions

Hydrogeological conditions played a governing role in the failure mechanism. The slope is traversed by perennial springs and ephemeral watercourses, which facilitate sustained infiltration into the slope mass. Despite the low primary permeability of the intact rock matrix, the dense network of tectonic discontinuities creates high secondary permeability, allowing for significant localized groundwater transmission.

Piezometric monitoring confirmed that the shallow groundwater table (GWT) is highly dynamic and sensitive to precipitation events, with levels fluctuating from near-surface horizons to depths of approximately 11–12 m. Historical records from a key exploratory borehole (BH-8) indicated localized artesian conditions, evidencing high confined pore water pressures.

The absence of a comprehensive drainage network facilitated the rapid saturation of the weathered profile. This hydrogeological response significantly reduced effective stresses along potential slip interfaces, ultimately leading to the structural distress and rupture of initial support measures, including shotcrete facings.

Figure 4.81 depicts the front view of the excavation slope before the main failure.

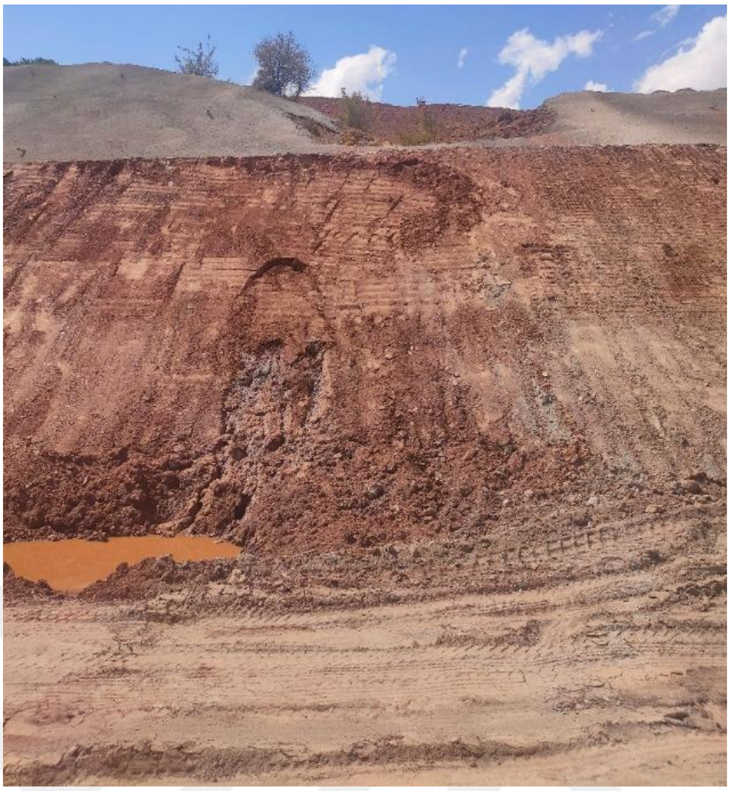

Figure 4.81. *Front view of the excavation slope before the main failure*

4.4.3.3. Instrumentation and monitoring results

Subsurface instrumentation provided quantitative evidence of the failure evolution and the depth of critical slip surfaces. Inclinometer readings indicated that the slope remained relatively dormant during the initial monitoring phase. However, rapid acceleration was recorded during the subsequent wet season, coinciding with snowmelt events.

Deep-seated movement (BH-3 & BH-4)

Inclinometers located near the spillway crest detected distinct shear zones at depths of approximately 14 m and 18–19 m, respectively. Cumulative lateral displacements reached significant magnitudes (>75 mm) before readings ceased.

Shallow active failure (BH-5)

Located in the most active instability zone, this instrument recorded initial movement at a shallow depth of approximately 4.5 m. The magnitude of the flow-type movement sheared the casing during the peak precipitation period, rendering the instrument inoperable.

These measurements confirm that while surface manifestations were shallow flow failures, the overall failure mechanism involved deep-seated saturated horizons within the flysch facies. Table 4.21 summarizes the groundwater levels and inclinometer-detected slip surface depths.

Table 4.21. *Summary of groundwater levels and inclinometer-detected slip surface depths*

Instrument	Surface Elevation (m)	Groundwater Depth (m)	Slip Surface Depth (m)	Max. Observed Displacement (mm)
BH-3	870	11.40	14.0	75
BH-4	871	10.00	18.0 - 19.0	60
BH-5	821	1.00	4.5	30 (prior to breaking)
BH-8	808	Artesian	N/A	N/A

4.4.4. Back-analyses: sensitivity of factor of safety to groundwater level and pore pressure

The stability of the spillway excavation was evaluated using the Limit Equilibrium Method (LEM) via the Slide2 software suite, employing the Simplified Bishop, Spencer and GLE/Morgenstern-Price methods to assess both existing and proposed slope geometries. A critical component of this numerical investigation involved back-analysis to calibrate the shear strength parameters of the active landslide material, specifically targeting the highly weathered horizons within the flysch facies.

4.4.4.1. Back-analysis and parameter calibration

Through the back-analysis process, assuming a limit equilibrium state (Factor of Safety, FS ≈ 1.0) under the observed high-precipitation conditions, the landslide material was characterized by a unit weight (γ) of 18 kN/m^3, a cohesion (c') of 5 kPa, and internal friction angles (ϕ') ranging between 20° and 28°. These values effectively simulate the observed failure surfaces at depths between 4.5 m and 19.0 m.

To accurately represent the rock mass behavior, the modeling utilized a disturbance factor (D) of 0.2 for the residual soil layer, yielding rock mass deformation modulus of 34.02 MPa.

4.4.4.2. Sensitivity to hydrogeological conditions

The sensitivity of the FS to hydrogeological conditions was identified as the governing stability factor. Stability analyses integrated high phreatic levels recorded in the field—varying from 0.80 m to 11.40 m depth—and accounted for the elevated pore water pressures generated by snowmelt.

Under these critical groundwater conditions, back-analyses of the existing topography (typically 1V:1.5H) yielded factor of safety (FS) values calculated as 1.069, 1.122, and 1.016 for the analyzed cross-sections (designated as Sections A-A, B-B, and C-C, Figures 4.82, 4.83, 4.84, respectively,). These results indicate a marginal state of equilibrium, consistent with the observed transition from dormant to active movement.

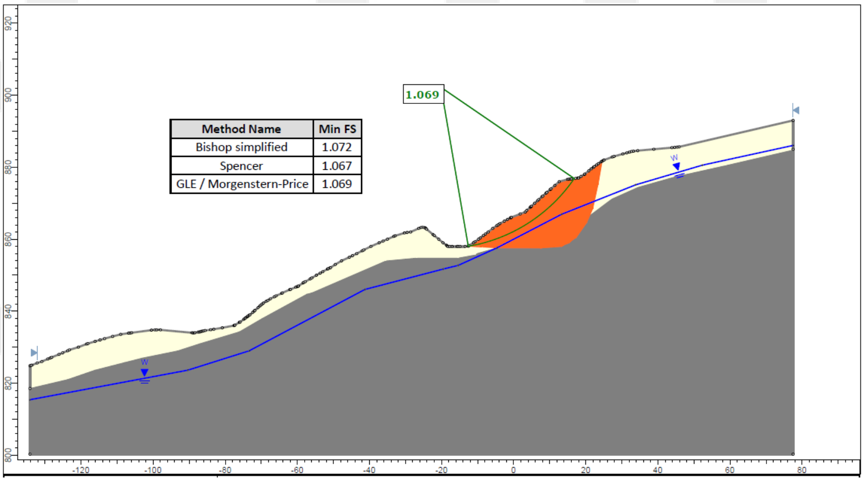

Figure 4.82. *Limit equilibrium back-analysis for Section A-A under static conditions, demonstrating the critical slip surface (FS=1.069)*

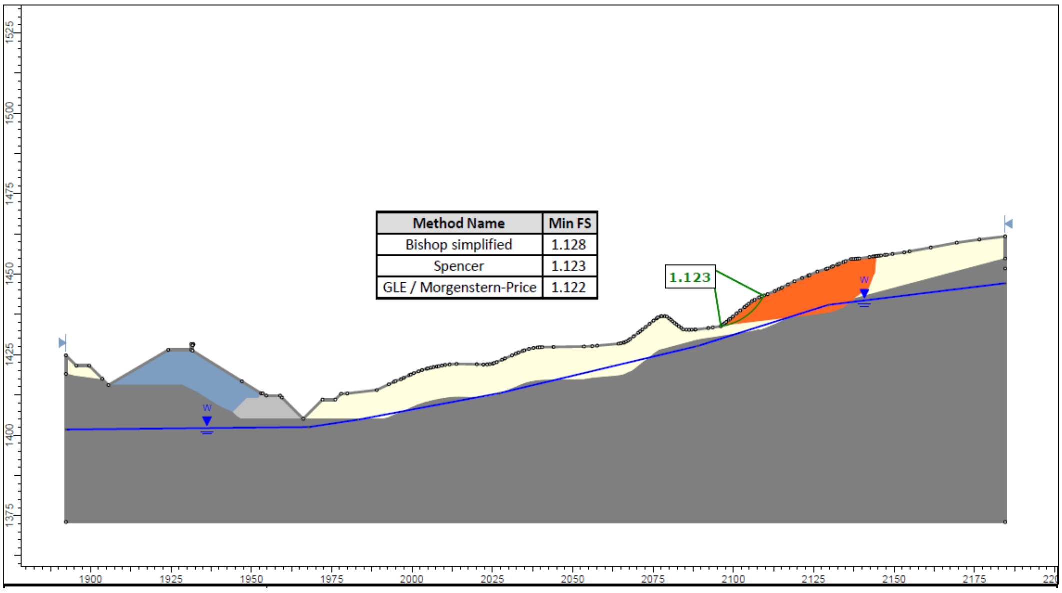

Figure 4.83. *Slide2 back-analysis results for Section B-B under static conditions (FS=1.122)*

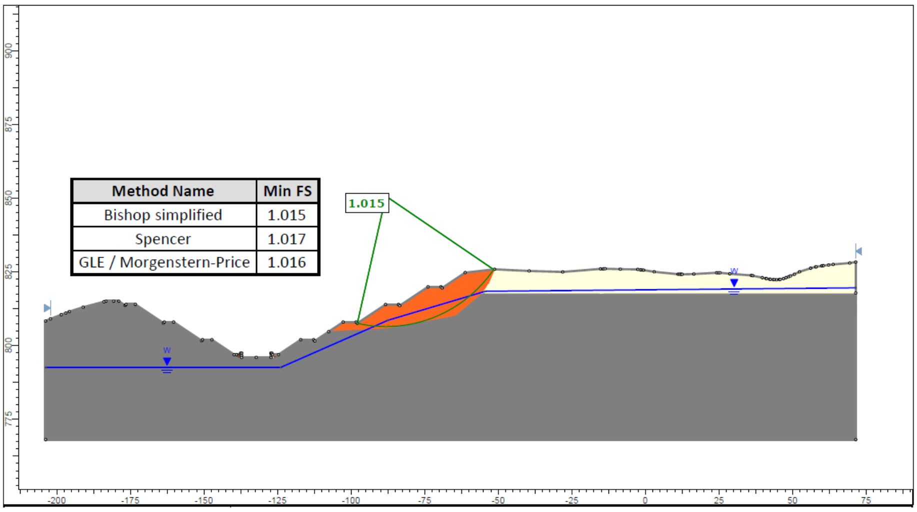

Figure 4.84. *Limit equilibrium back-analysis identifying the deep-seated failure mechanism at Section C-C (FS=1.016)*

Table 4.22 outlines the summary of Slide2 back-analysis results for critical sections.

Table 4.22. *Summary of Slide2 back-analysis results for critical sections*

Analysis Section	Groundwater Depth (m)	Factor of Safety (FS)
A-A	10.0	1.07
B-B	11.4	1.12
C-C	3.0	1.06

4.4.4.3. Stability assessment of pre-remediation geometries

Following the calibration of the shear strength parameters, a forward stability assessment was conducted on the existing topography and temporary excavation geometries (1V:1H, 1V:1.5H with wall, 1V-1.73H (corresponding to 30°, without wall) and 1V:2H). The objective of this phase was to quantify the extreme vulnerability of these pre-remediation profiles to both static groundwater fluctuations and anticipated seismic demands.

Under the critical groundwater conditions established during the back-analysis, the evaluation of the pre-remediation geometries yielded the following results (Figures 4.85-4.94):

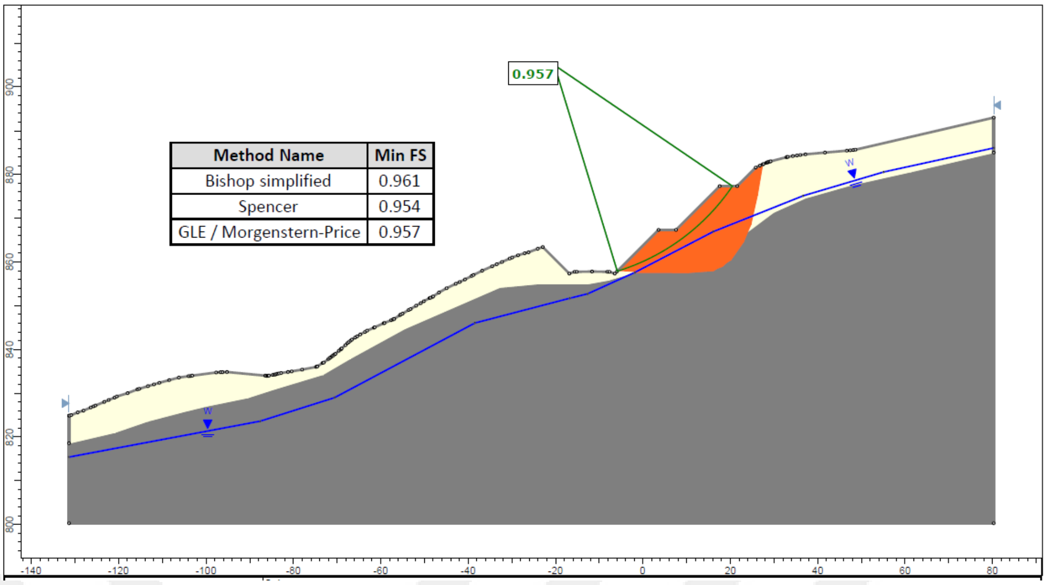

Figure 4.85. Stability analysis of Section A-A under temporary 1V:1H excavation geometry for static conditions (FS=0.957)

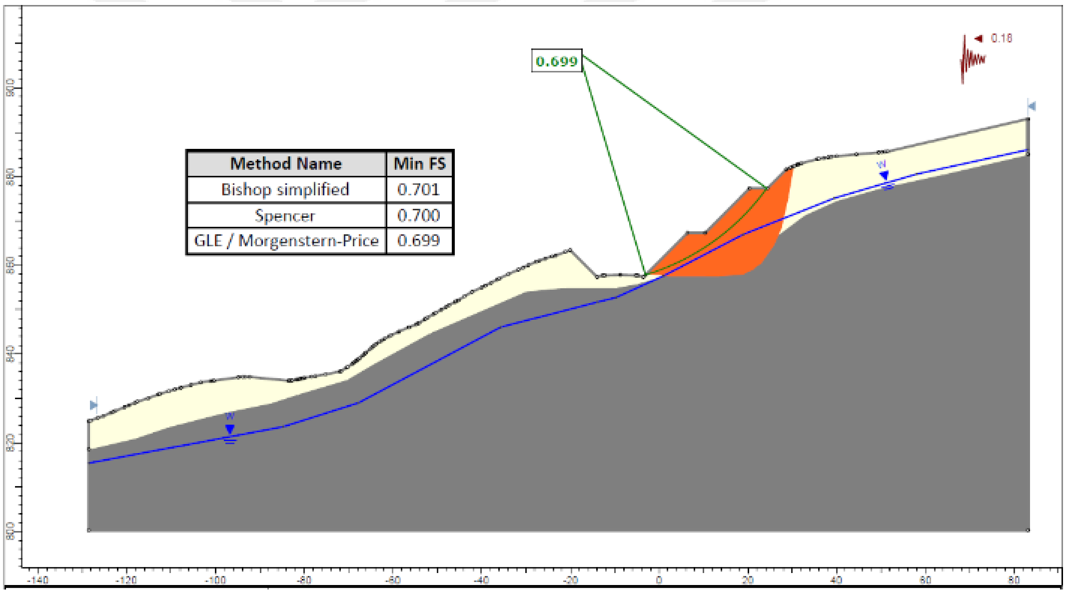

Figure 4.86. Stability analysis of Section A-A under temporary 1V:1H excavation geometry for pseudo-static conditions (k_h = 0.18g) (FS=0.699)

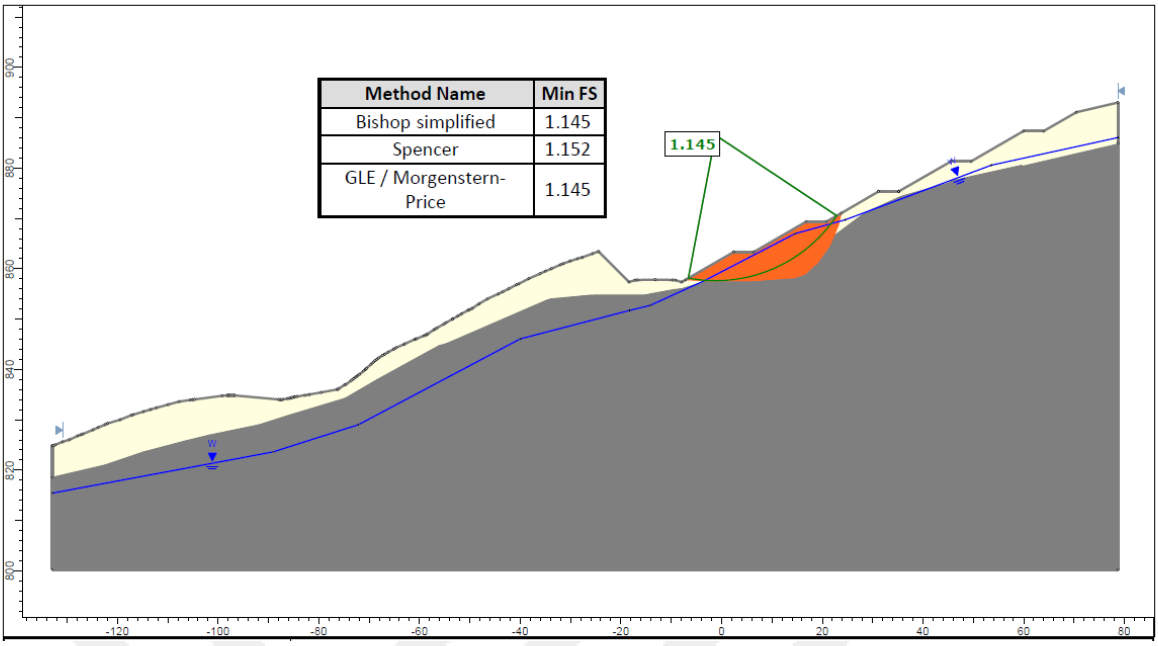

Figure 4.87. *Static evaluation of the 30° flattened (1V-1.73H) slope at Section A-A without structural support (FS=1.145)*

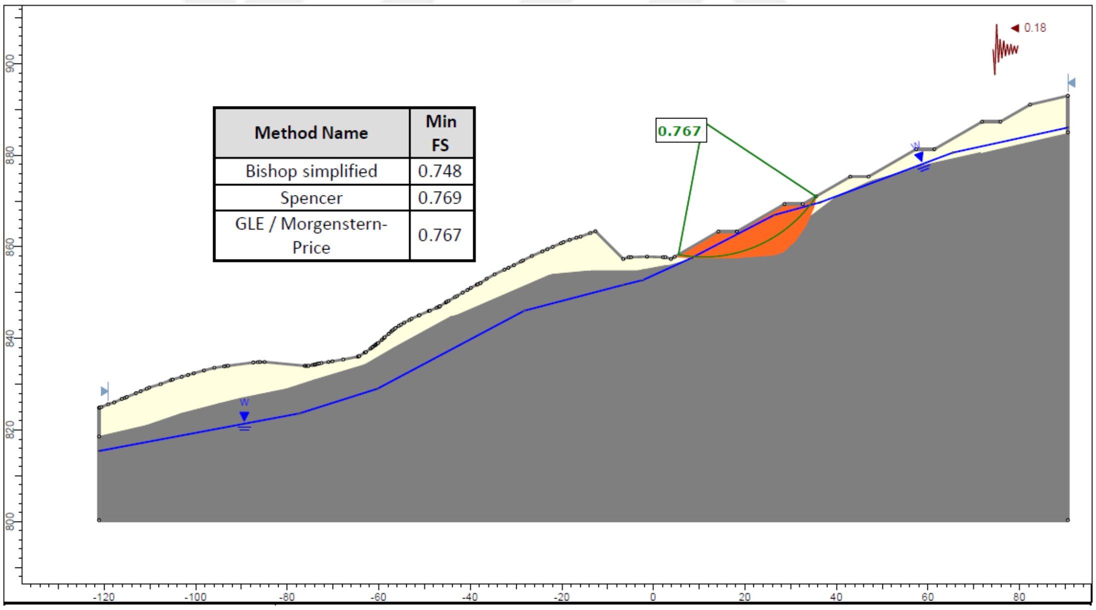

Figure 4.88. *Seismic evaluation of the 30° flattened (1V-1.73H) slope at Section A-A without structural support (FS=0.767)*

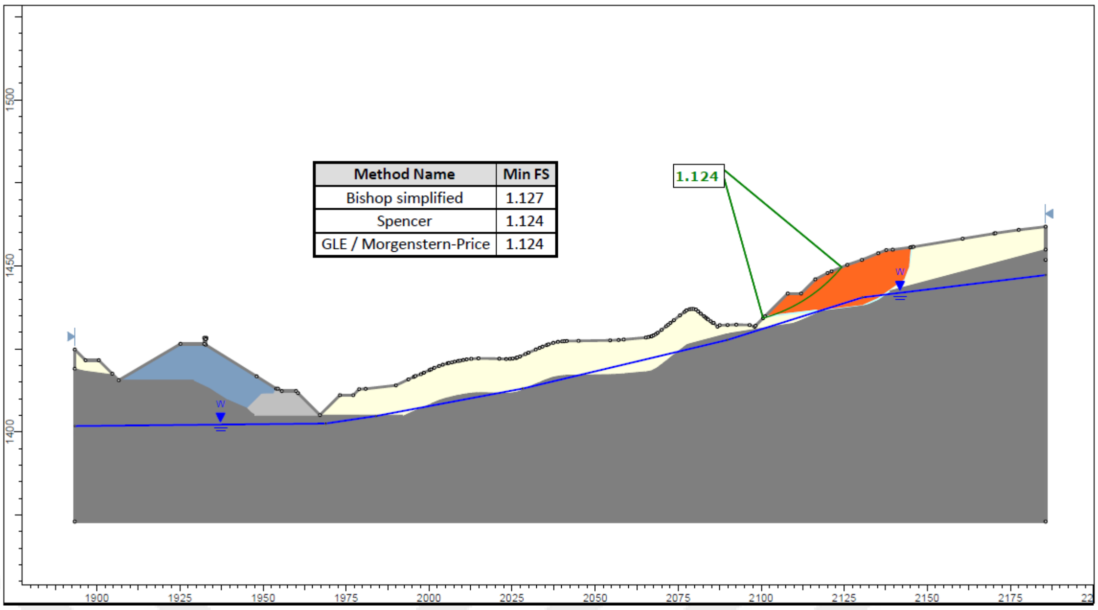

Figure 4.89. *Stability analysis for Section B-B illustrating the insufficiency of existing geometries under static conditions for 1V:1H profile (FS=1.124)*

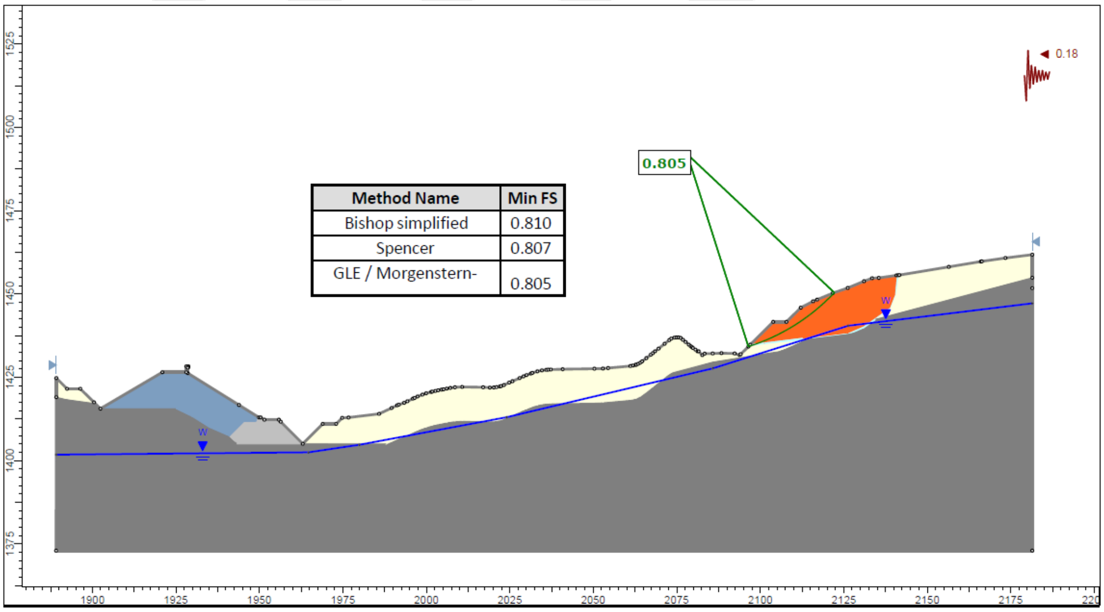

Figure 4.90. *Stability analysis for Section B-B illustrating the insufficiency of existing geometries under pseudo-static loading (k_h = 0.18g) for 1V:1H profile (FS=0.805)*

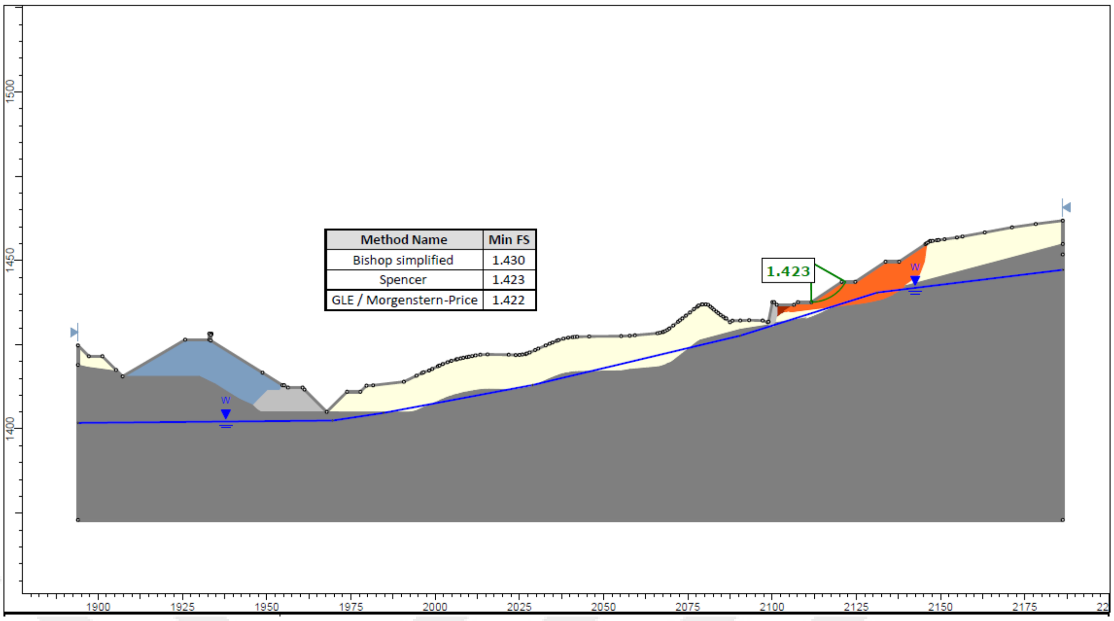

Figure 4.91. *Static evaluation of the 1V:1.5H profile with stone retaining wall at Section B-B (FS=1.423)*

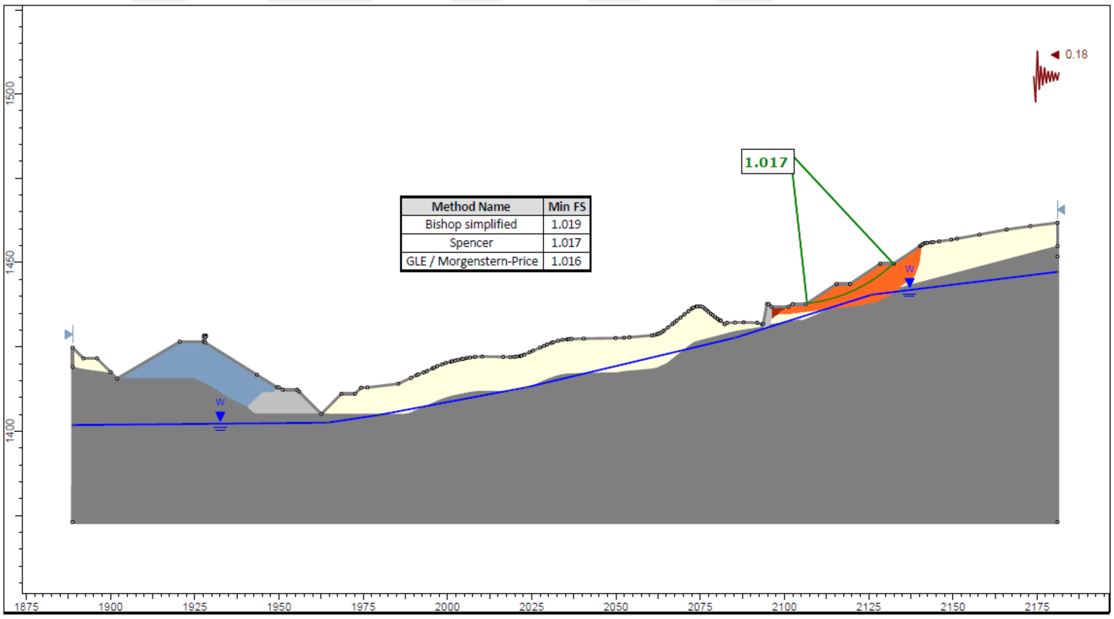

Figure 4.92. Seismic evaluation of the 1V:1.5H profile with stone retaining wall at Section B-B (FS=1.017)

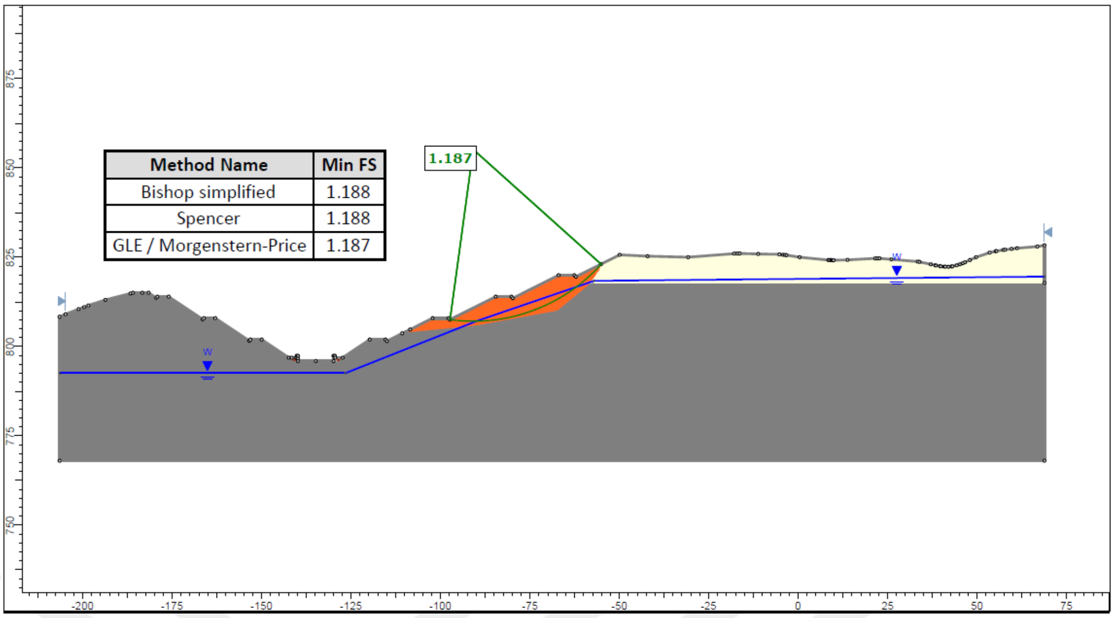

Figure 4.93. *Stability assessment of Section C-C under 1V:2H slope geometry for static conditions (FS=1.187)*

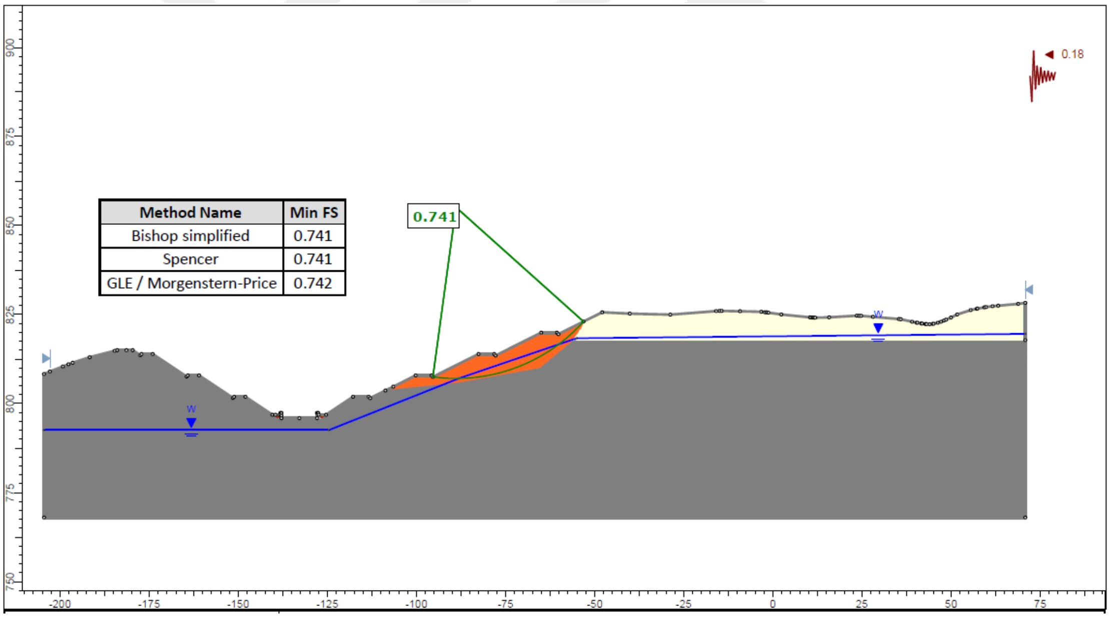

Figure 4.94. *Stability assessment of Section C-C under 1V:2H slope geometry for pseudo-static (k_h = 0.18g) conditions (FS=0.741)*

4.4.4.4. Evaluation of remedial measures

The limit equilibrium analysis firmly established that simple geometric re-grading (e.g., flattening to 1V:1.5H without support) was often insufficient to meet the required seismic safety factor of 1.00. Consequently, aggressive stabilization measures were modeled. The results demonstrated that acceptable stability (Static FS ≥ 1.5, Seismic FS

≈ 1.0) could be achieved by flattening slopes to 30° combined with the construction of stone masonry gravity toe walls.

4.4.5. Drainage improvements, support measures, and performance evaluation

The critical instability observed in the spillway slopes was fundamentally linked to elevated pore water pressure (PWP) resulting from inadequate surface water diversion and the geometric imbalance caused by anthropogenic modifications. Consequently, a comprehensive remedial strategy was developed focusing on hydraulic control, geometric reconfiguration, and structural support. The proposed interventions were designed to address the specific failure mechanisms identified in the crest and discharge channel zones.

4.4.5.1. Proposed remedial strategy

The remedial design incorporates the following specific measures:

Geometric reconfiguration and unloading

- Spoil removal: The primary unloading measure involves the complete removal of the uncontrolled spoil material located at the slope crest. This mass, covering a substantial footprint with a thickness of approximately 10 m, acted as both a driving surcharge and a reservoir for water infiltration.
- Slope reshaping: For the slopes near the spillway weir (Sections A-A and B-B), the geometry is flattened to an inclination of 30° (approx. 1.7H:1V) integrated with 4.0 m wide benches at vertical intervals of 6.0 to 7.5 m. For the discharge channel (Section C-C), a gentler inclination of 1V:3H is applied.
- Surface replacement: In areas where the surface material was remolded and highly disturbed, excavation to a depth of approximately 5.0 m is required, followed by backfilling with concrete to secure the slope face.

Structural support

- Toe retention: Implementation of structural retention at the toe, utilizing reinforced concrete walls, stone masonry gravity walls, or mortared riprap, depending on the specific section requirements.

- Foundation sealing: A critical structural enhancement involves extending the spillway's concrete shear key (cut-off wall) from its original depth of approx. 0.8 m to 2.5 m. This extension is designed to effectively seal the contact between the concrete structure and the weathered foundation, preventing seepage and internal piping.

Hydraulic control system

- Surface drainage: Construction of concrete interceptor ditches to capture upland runoff before it enters the slope, and reinforced channels on benches to prevent infiltration into tension cracks, along with toe drains.
- Internal drainage: Installation of an increased density of weep holes within all retaining structures to relieve hydrostatic pressure behind the walls.
- Stream rehabilitation: Construction of concrete culverts to manage the permanent flow from springs and ephemeral watercourses.

Table 4.23 outlines the summary of proposed support and drainage measures.

Table 4.23. *Summary of proposed support and drainage measures*

Measure Type	Description	Objective
Drainage	Concrete head and bench ditches, toe drains, weep holes and culverts	Surface runoff interception and stream management
Unloading	Removal of 10 m thick spoil tip (2,500 m^2)	Reduction of driving force and infiltration potential
Reshaping	Flattening to 30° or 1V:3H with 4.0 m benches	Geometric stabilization and passive resistance increase
Structural	Reinforced concrete walls and rock mass barbicans	Toe support and pore pressure relief
Interface Fix	Extension of concrete shear key to 2.5 m	Sealing spillway-foundation contact against piping

4.4.5.2. Performance evaluation of remedial measures

The effectiveness of these measures was validated through updated Limit Equilibrium Method (LEM) analyses using the Simplified Bishop, Spencer and

GLE/Morgenstern-Price algorithms. The results demonstrate that the proposed interventions successfully raise the Factor of Safety (FS) above the required static (FS ≥ 1.5) and dynamic (FS > 1.0) thresholds.

Sections A-A and B-B

The integration of a 30° slope with a stone retaining wall increased the static FS from marginal values (0.957-1.12) to robust values of 1.57 and 1.62, respectively. Under seismic loading (k_h=0.18g), the FS improved from failure conditions to stable values of 1.121 and 1.082. Figure 4.95 illustrates the final remedial design for Section A-A incorporating a 30° slope with a stone masonry retaining wall under static conditions, while Figure 4.96 depicts the same configuration under pseudo-static conditions.

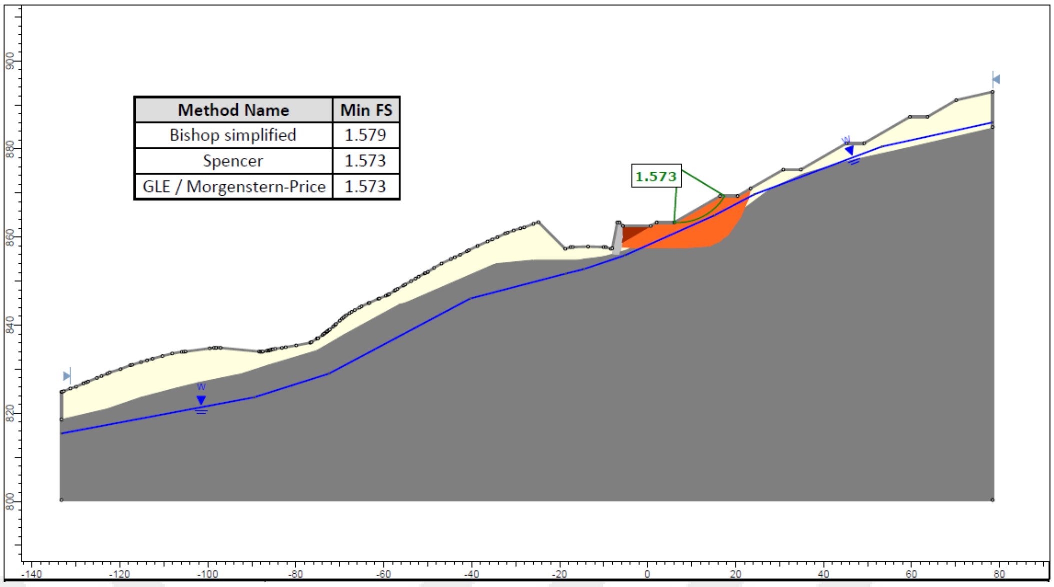

Figure 4.95. *Final remedial design for Section A-A incorporating a 30° slope with a stone masonry retaining wall, achieving target safety factors under static conditions (FS=1.573)*

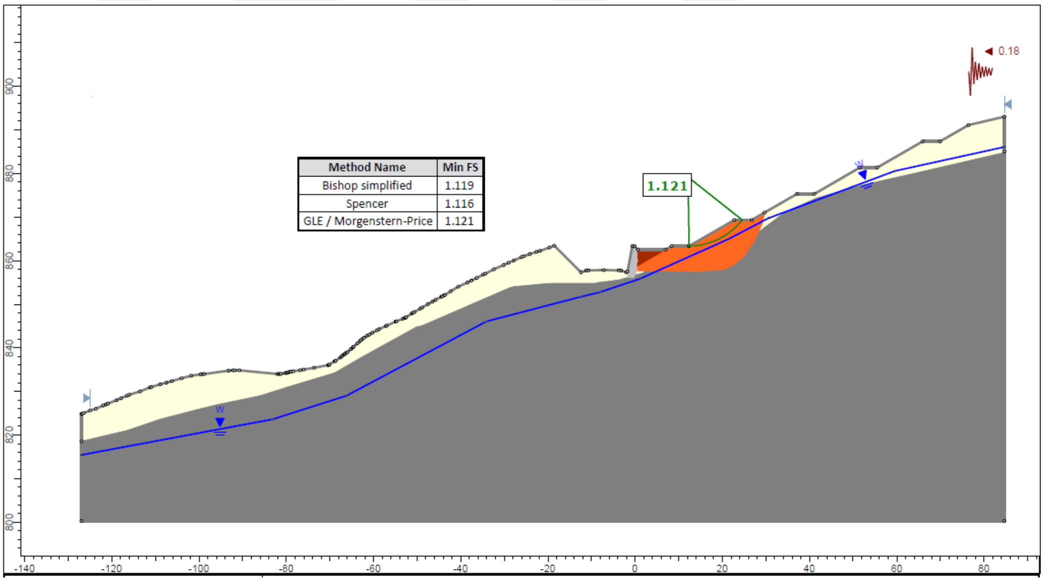

Figure 4.96. *Final remedial design for Section A-A incorporating a 30° slope with a stone masonry retaining wall, achieving target safety factors under pseudo-static (k_h = 0.18g) conditions (FS=1.121)*

Figure 4.97 presents the final remedial design for Section B-B featuring a 30° slope with a stone masonry retaining wall under static conditions, while Figure 4.98 displays the performance of the same configuration under pseudo-static conditions.

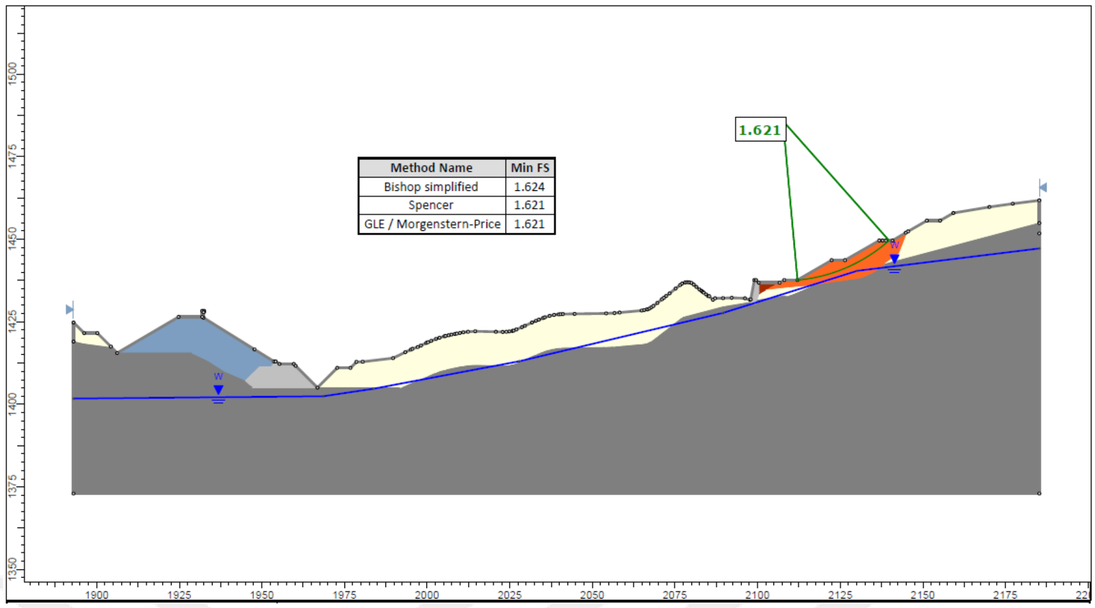

Figure 4.97. *Final remedial design for Section B-B featuring a 30° slope with a stone masonry retaining wall under static conditions (FS=1.621)*

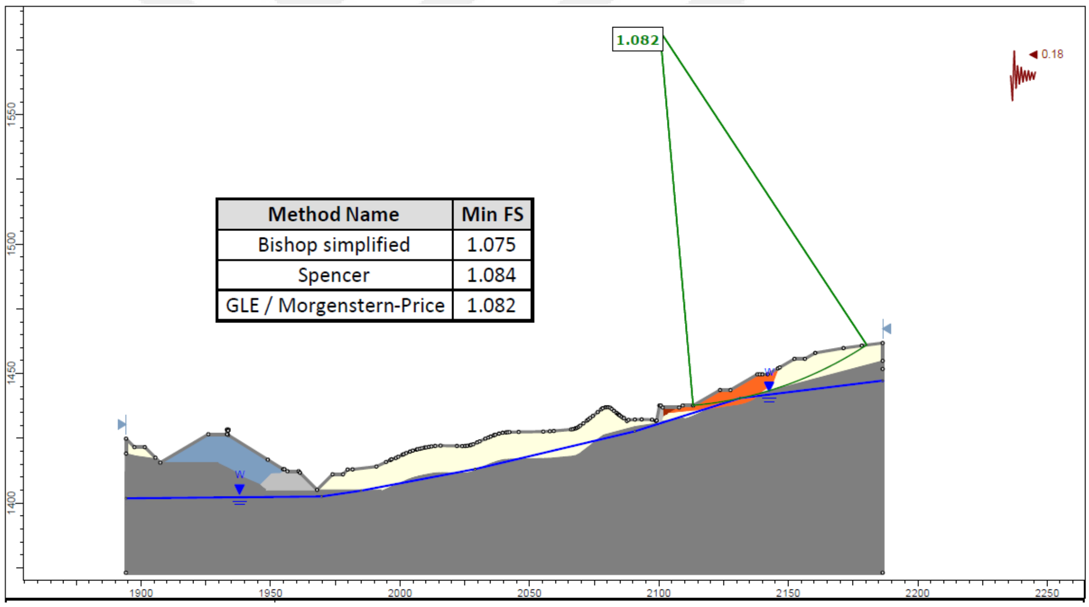

Figure 4.98. *Final remedial design for Section B-B featuring a 30° slope with a stone masonry retaining wall under pseudo-static (k_h = 0.18g) conditions (FS=1.082)*

Section C-C

Geometric re-grading to 1V:3H improved the static FS to 1.671, ensuring a safety margin (FS=1.030) even under design earthquake loading. Figure 4.99 exhibits the static stability verification for the remediated 1V:3H profile by the discharge channel at Section C-C, while Figure 4.100 displays the stability verification for the same profile under pseudo-static conditions.

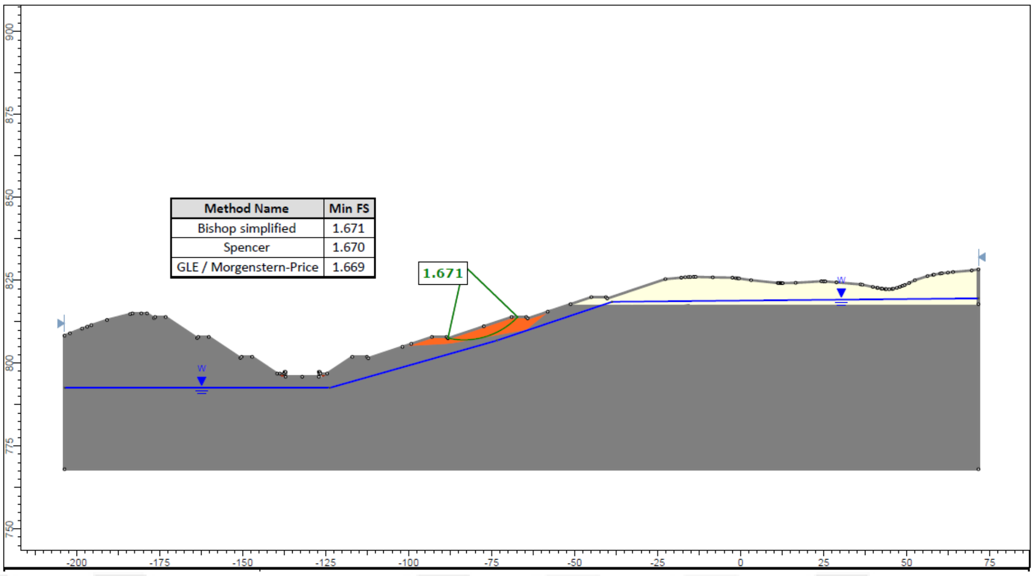

Figure 4.99. *Static stability verification for the remediated 1V:3H profile by the discharge channel (Section C-C) (FS=1.671)*

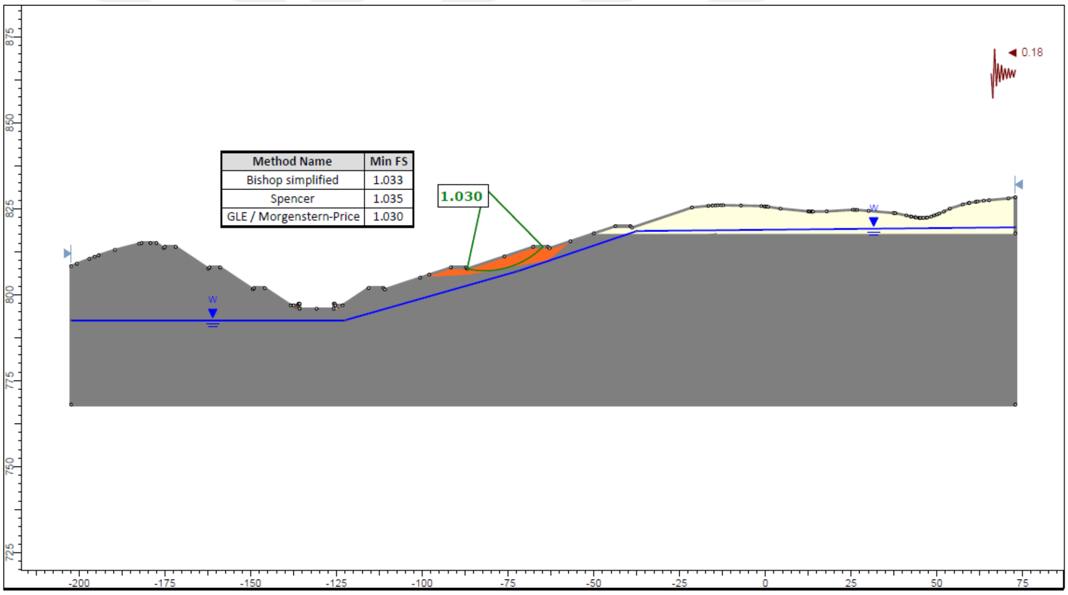

Figure 4.100. *Pseudo-static (k_h = 0.18g) stability verification for the remediated 1V:3H profile by the discharge channel (Section C-C) (FS=1.030)*

Table 4.24 presents a comprehensive summary of the stability analysis results.

Table 4.24. *Summary of Stability Analysis Results*

Cross-Section	Slope Condition / Stability Control	Static FS	Seismic FS (k_h=0.18g)	Required FS (Static/Seismic)	Stability Assessment
A-A	Existing Topography (1V:1.5H)	1.069	0.760	1.5 / 1.0	Unstable
A-A	1V:1H	0.957	0.699	1.5 / 1.0	Unstable
A-A	30° Slope without Wall	1.145	0.767	1.5 / 1.0	Unstable
A-A	**30° Slope with Wall**	**1.573**	**1.121**	**1.5 / 1.0**	**Stable**
B-B	Existing Topography	1.122	0.840	1.5 / 1.0	Unstable
B-B	1V:1H	1.124	0.805	1.5 / 1.0	Unstable
B-B	1V:1.5H Re-grade (w/ wall)	1.423	1.017	1.5 / 1.0	Marginally Stable
B-B	**30° Slope with Wall**	**1.621**	**1.08**	**1.5 / 1.0**	**Acceptable***
C-C	Existing Topography (1V:1.5H)	1.016	0.69	1.5 / 1.0	Unstable
C-C	1V:2H Re-grade	1.187	0.741	1.5 / 1.0	Unstable
C-C	**1V:3H Re-grade**	**1.671**	**1.03**	**1.5 / 1.0**	**Acceptable***

**The seismic FS values of 1.08 and 1.03 are accepted as marginally compliant given the conservative selection of input parameters.*

4.4.6. Lessons learned

This case study highlights the extreme vulnerability of tectonized flysch sequences to changes in the moisture regime. The failure demonstrated that conventional surface protection, such as shotcrete and wire mesh, can be counterproductive if internal drainage is insufficient to relieve pore water pressures; in such cases, the lining acts as an impermeable barrier that traps pressure, leading to structural rupture.

Furthermore, the placement of uncompacted excavation waste on the crest of a potentially unstable slope was identified as a critical management error that directly triggered the transition from slow creep to active flow-type movement. Future designs in similar geological settings must prioritize the early installation of drainage interceptors and the sealing of hydraulic interfaces between concrete structures and weathered rock masses to prevent progressive strength degradation and internal erosion.

Finally, the stability assessments demonstrated that in highly weathered, saturated ophiolitic mélanges, relying solely on geometric slope flattening (e.g., re-grading to 1V:1.5H or 30°) is often insufficient to achieve required safety margins, particularly under seismic demands (k_h = 0.18g). To ensure long-term stability and prevent retrogressive failure, geometric modifications must be coupled with robust structural interventions, such as massive stone masonry retaining walls, to provide necessary passive toe resistance.

4.5. Case 5 – Design of Spillway Excavation in Arenized (Highly Weathered) Granodiorite

This case study presents a comprehensive geotechnical evaluation, stability assessment, and support design for the spillway excavation of a hydraulic structure located in a mountainous region of Türkiye. The project is designed for municipal drinking water supply and features a concrete-faced rockfill dam (CFRD) with a maximum height of approximately 40 m.

The spillway, situated on the left abutment, is designed as a side-channel free overflow structure with a total length of approximately 115 m. The primary geotechnical objective was to investigate the stability of excavation slopes intersecting deep horizons of 'arenized' (completely weathered) granodiorite. This involved evaluating potential failure mechanisms through numerical back-analysis and developing a robust stabilization strategy to ensure a Factor of Safety (FS) of ≥ 1.50 for static loading and ≥ 1.00 for pseudo-static seismic conditions.

4.5.1. Project setting, spillway excavation geometry, and design objectives

The spillway excavation features a multi-benched profile with total cut heights reaching approximately 40 m. During the initial planning phase, the cut slopes were provisionally projected with a steep 1V:0.33H geometry. However, recognizing critical geological constraints during the execution phase—specifically the presence of highly weathered 'arenized' granodiorite—the design was revised. To ensure overall slope stability, the governing critical sections (inlet area) were flattened to a significantly gentler 1V:1.33H geometry, while the inherently stable lower (downstream) sections were maintained at a 1V:1H inclination.

The geological setting is dominated by a Cretaceous-aged granodiorite intrusive, which exhibits a complex weathering profile. A critical geotechnical constraint is the 'arenatization' (saprolitization) of the granodiorite, where intense physical and chemical weathering has transformed the parent rock into a friable, sandy matrix (grus). This arenized horizon extends to depths ranging from approximately 15 to 20 m and is highly sensitive to moisture, exhibiting a rapid loss of shear strength and structural integrity upon saturation.

Construction scheduling delays, including the suspension of works during winter seasons, resulted in prolonged exposure of the excavation faces to atmospheric conditions. This vulnerability was exacerbated by the absence of pre-installed drainage measures (head, bench, and toe ditches), subjecting the slopes to the abrasive and erosive effects of surface water runoff. Consequently, the technical administration mandated a robust constructive support system capable of stabilizing both the fractured rock mass and the critical arenized zones.

Hydrogeological conditions were characterized through an extensive network of 29 exploratory boreholes, which were instrumented with PVC filter pipes for long-term monitoring. Based on the investigation program, the boreholes were categorized into preliminary planning (BH series) and supplementary design (SB series) investigation phases.

Monitoring data indicated that static groundwater levels in the spillway area typically range between 12.0 m and 17.5 m below the surface. The design criteria adopted for the slope stability assessment required a Factor of Safety (FS) of ≥ 1.50 for static loading conditions and ≥ 1.00 for pseudo-static seismic conditions.

4.5.2. Geological and geotechnical characterization of arenized granodiorite

The regional geological setting is dominated by a magmatic arc sequence, specifically a Cretaceous-aged granodiorite intrusive. The lithological framework is characterized by a complex, heterogeneous weathering profile that transitions from a competent, massive rock mass to a highly decomposed saprolitic material. A critical geotechnical feature influencing the spillway excavation is the 'arenatization' (saprolitization) of the granodiorite. This intense chemical and physical weathering process (classified as W5: Completely Weathered) transforms the parent rock into a friable, sandy matrix often referred to as granite sand or 'arena'.

Borehole logs (e.g., SB-4/1, BH-1) indicate that this arenized horizon extends to depths ranging from approximately 15 to 20 m. Although the matrix is highly disintegrated, it frequently incorporates robust, residual massive blocks of granodiorite (core-stones) that can reach several meters in diameter, exhibiting exfoliation patterns reminiscent of 'onion-skin' weathering. A significant characteristic of the arenized material is its high sensitivity to moisture; while it displays soil-like consistency in core samples, it undergoes a dramatic loss of shear strength and structural integrity upon saturation, behaving effectively as a cohesionless soil.

The underlying competent granodiorite is described as gray-beige, medium-hard to hard, with moderate to high intact strength. Structural characterization reveals a massive structure intersected by three primary discontinuity sets typically dipping steeply at 70°–80°. Discontinuities are generally closed, with apertures narrowing from approximately 5 mm at the surface to 0.1–1.0 mm at depth. Fracture surfaces vary from rough to very rough and frequently exhibit limonitization, kaolinized coatings, or quartz and calcite fillings. The rock mass quality was categorized as "blocky to disturbed" or "small blocky" (J_v = 16), with an average Rock Quality Designation (RQD) of 60%.

Hydrogeological conditions are governed by the secondary porosity of the joint systems within the massive rock mass and the primary porosity of the saprolitic (arenized) horizons. Based on field permeability tests, the hydraulic conductivity is categorized as low to moderate. Groundwater flow patterns generally follow the topographic gradient, migrating from the upper slopes toward the valley floor.

Long-term monitoring via PVC-instrumented observation wells (e.g. BH and SB series) established that the static groundwater table (GWT) typically resides at depths ranging from approximately 12 m to 18 m below the natural ground surface. These levels exhibit seasonal fluctuations in response to regional precipitation patterns. Figure 4.101 provides a visual illustration of arenized granodiorite (W5) intermixed with massive blocks, adapted from site photos.

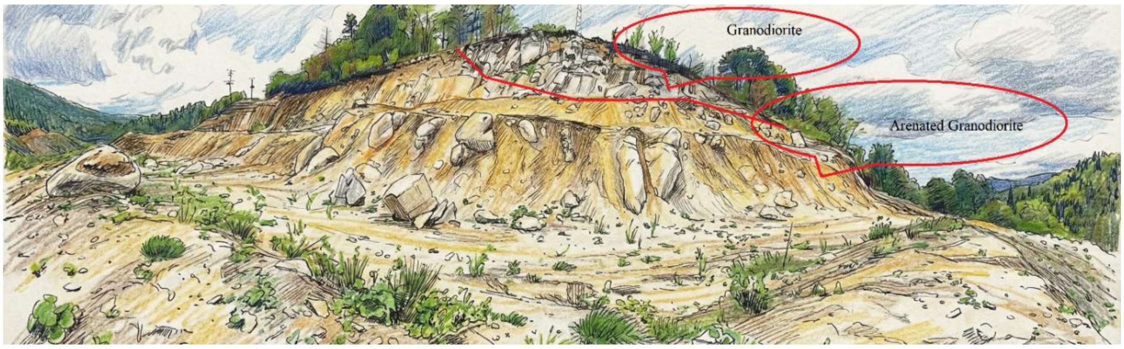

Figure 4.101. *Visual illustration of arenized granodiorite (W5) intermixed with massive blocks – adapted from site photos*

4.5.3. Laboratory test data and parameter calibration for numerical analyses (RS2)

To accurately conduct the baseline slope stability assessment, the geotechnical parameterization for the numerical models was first established through a rigorous combination of direct laboratory testing on competent rock cores and empirical correlations for the highly weathered (arenized) zones. Laboratory investigations were conducted on intact rock core samples recovered from boreholes BH-1, IT-1, and IT-3 during the site investigation phase.

4.5.3.1. Competent granodiorite characterization

Direct laboratory testing on the massive granodiorite unit yielded the following mean intact properties:

- Unit weight (γ): 24 kN/m³
- Uniaxial compressive strength (σci): 51 MPa
- Intact elastic modulus (Ei): 12 GPa
- Poisson's ratio (ν): 0.28

4.5.3.2. Arenized granodiorite characterization

The saprolitic nature of the arenized granodiorite (W5) prevented the extraction of high-quality undisturbed samples for standard laboratory testing. Consequently, its properties were derived using conservative geotechnical assumptions to represent the transition between a cohesionless soil and a weak rock:

Strength

A nominal σ_{ci} of 1 MPa was adopted. In estimating the uniaxial compressive strength (UCS) of the arenized granodiorite horizon, two observations were treated as key indicators of very low intact strength and advanced disintegration: (i) the practical soil–rock transition was assumed to occur at approximately 1 MPa, and (ii) the material was observed to crumble and fragment readily, even under weak hammer impacts. Collectively, these field-based descriptors were considered critical in justifying a low UCS range for the unit.

Stiffness

The intact modulus (E_i) was calibrated using the empirical relationship proposed by Ocak (2008) (Eq 3.3), yielding an initial modulus of 400 MPa.

Unit weight

An empirical value of 22 kN/m³ was assigned.

4.5.3.3. Rock mass parameter calibration (Hoek-Brown to Mohr-Coulomb)

The translation of these intact values into rock mass parameters (c', ϕ', E_m) for use in the RS2 and Slide2 analyses was achieved via the Generalized Hoek-Brown (2002) failure criterion within the RocLab software environment.

Competent Granodiorite

The calibration incorporated a Geological Strength Index (GSI) of 45 and a material constant (m_i) of 25. The GSI was derived from RQD = 60%, J_v = 16, SCR = 12, and SR = 32 (calculated utilizing the empirical relationship:

$$SR = -17.5 \ln(J_v) + 79.8 \tag{4.1}$$

To account for construction-induced damage and stress relief near the excavation face, a disturbance factor (D) of 0.2 was applied to approximately the uppermost 3.0 m of the slope profile during specific analysis stages.

Figure 4.102 displays the RocLab analysis for the competent granodiorite, illustrating the Hoek-Brown and Mohr-Coulomb failure envelopes.

Arenized Granodiorite

A GSI of 30 and an m_i of 9 (correlated to tuffaceous materials due to similar disintegration patterns) were selected to characterize the weathered mass, with a disturbance factor (D) of 0.0, since the material is thought to be already disintegrated.

Figure 4.103 depicts the RocLab analysis for the conversion of Hoek-Brown to Mohr-Coulomb parameters for arenized granodiorite.

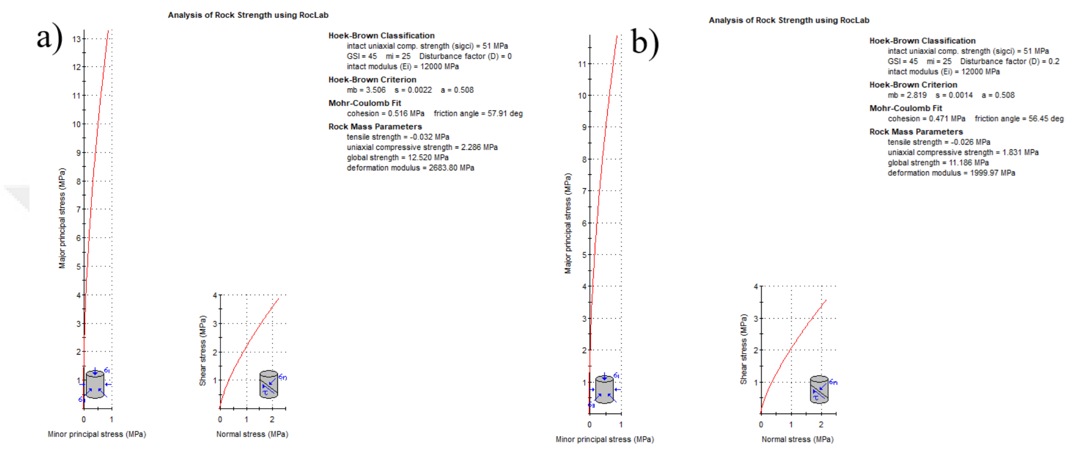

Figure 4.102. *RocLab analysis for the competent granodiorite (a) for D=0; and (b) for D=0.2*

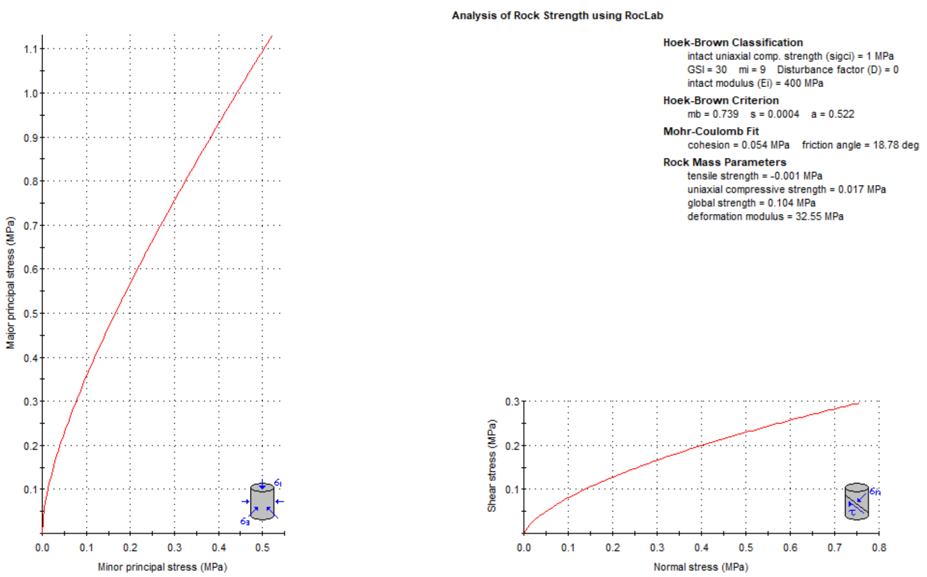

Figure 4.103. *RocLab analysis for the conversion of Hoek-Brown to Mohr-Coulomb parameters for arenized granodiorite (UCS=1 MPa, D=0)*

Table 4.25 presents a summary of the geotechnical design parameters for the granodiorite units.

Table 4.25. *Summary of geotechnical design parameters for granodiorite units*

Material	Color	Parameter (symbol)	Value (unit)	Source / derivation
Arenized Granodiorite (W5)		Unit weight (γ)	22.0 kN/m³	Design input
		UCS (σci)	1 MPa	Assumption / Field Obs.
		Intact modulus (Ei)	400 MPa	Empirical (Ocak, 2008)
		GSI	30 (–)	Field characterization
		Hoek–Brown constant (mi)	9 (–)	Selected (based on tuff)
		Derived rock mass params (Hoek–Brown)	(RocLab)	RocLab (Hoek–Brown)
		Cohesion (c′, D = 0.0)	54 kPa	Calculated
		Friction angle (ϕ′, D = 0.0)	19°	Calculated
		Rock mass modulus (Em, D = 0.0)	33 MPa	Calculated
Competent Granodiorite		Unit weight (γ)	24 kN/m³	Lab tests
	D=0.2	UCS (σci)	51 MPa	Lab tests
		GSI	45 (–)	Field characterization (SR= 32, SCR= 12)
		Hoek–Brown constant (mi)	25 (–)	Lab tests / RocLab
		Derived rock mass params (Hoek–Brown)	(RocLab)	RocLab (Hoek–Brown)
		Cohesion (c′)	516 kPa (471; D = 0.2)	Calculated
		Friction angle (ϕ′)	58° (57; D = 0.2)	Calculated
		Rock mass modulus (Em)	2684 MPa (2000; D = 0.2)	Calculated

4.5.4. Baseline slope stability assessment under static and seismic conditions

Following the derivation of the geomechanical parameters, the baseline stability of the planned spillway excavation—comprising the 1V:1.33H geometry at the critical inlet section and the steeper 1V:1H geometry at the inherently stable downstream section—was evaluated using the Finite Element Method (FEM) within the RS2 software environment. The Shear Strength Reduction (SSR) technique was employed to determine the critical Strength Reduction Factor (SRF), which corresponds to the Factor of Safety (FS). The numerical models integrated site-specific hydrogeological conditions, including pore water pressure effects derived from the observation well data.

The stability acceptance criteria were established as $FS_{static} \geq 1.50$ and $FS_{seismic} \geq 1.00$. For the Earthquake Ground Motion Level–2 (DD-2), the Turkish Seismic Hazard Map was adopted to define the design seismic inputs at the study site. The maximum expected peak ground acceleration at outcropping rock was taken as $PGA_{rock,outcrop}$=0.254 g. The short-period design spectral acceleration parameter S_{DS} was evaluated as a function of the local site class; for the site conditions considered herein, S_{DS}=0.755. The corresponding peak ground acceleration at the ground surface was then estimated using the prescribed relationship;

$$PGA_{\mathrm{ground}} = 0.4\, S_{\mathrm{DS}} \tag{4.2}$$

resulting in $PGA_{ground}=0.4\times0.755\cong0.30$ g. Finally, the design horizontal seismic acceleration to be used in the analyses was computed following the $0.40\times S_{DS}\times0.5$ approach, yielding:

$$kh = 0.40 \times S_{DS} \times 0.5 \tag{4.3}$$

$$\approx 0.15$$

This value was adopted as the representative horizontal seismic action in the subsequent design calculations.

Two characteristic cross-sections were selected for analysis to represent the heterogeneity of the geological conditions:

4.5.4.1. Critical control section (inlet area)

This section represents the most vulnerable zone of the excavation, where exploratory boreholes (BH-1, SB-4/1, and SB-20) identified a deep weathering profile with arenized granodiorite extending up to approximately 18 m.

Analysis result

The baseline analysis for the unsupported slope yielded a critical Factor of Safety of 1.14.

Failure mechanism

This result indicates that the slope is at a state of limit equilibrium under static conditions. Numerical strain contours demonstrated a potential for global instability, characterized by a deep-seated circular failure surface propagating through the weak arenized (saprolitic) horizon and daylighting at the toe of the excavation.

Seismic implication

Given that the slope yields an unsupported static FS of 1.14 and only achieves a supported seismic FS of 1.09, it can be logically deduced that the slope in its unsupported state is implicitly unstable under pseudo-static loading conditions (anticipated $FS_{seismic} < 1.00$), significantly violating the minimum design criterion of ≥ 1.00.

Figure 4.104 illustrates the baseline stability assessment of the critical Inlet Section in its unsupported state under static conditions.

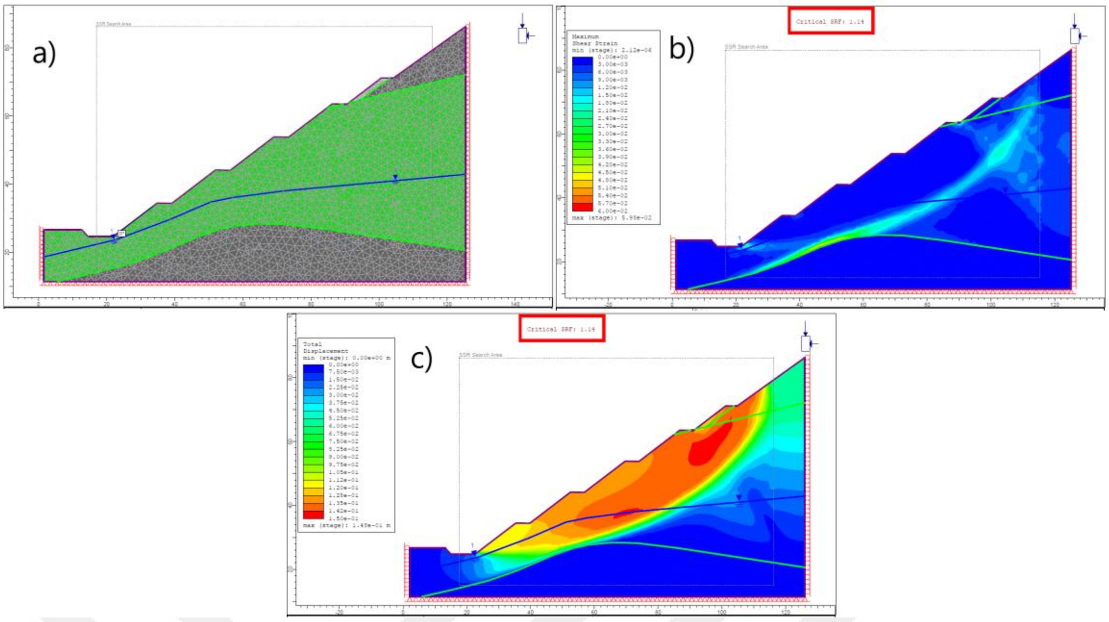

Figure 4.104. *Baseline stability assessment of the critical Inlet Section in its unsupported state under static conditions: (a) numerical model geometry, (b) maximum shear strain contours, and (c) total displacement vectors (FS = 1.14)*

4.5.4.2. Stable control section (downstream)

This section represents areas where the excavation intersects massive, competent granodiorite with negligible arenation.

Analysis result

The baseline analysis for the unsupported slope yielded a high Factor of Safety of 2.45.

Failure mechanism

While the section is inherently stable against global shear failure, the rock mass remains susceptible to surface degradation. The primary risks in this zone are surface spalling and localized rockfalls due to atmospheric exposure (weathering) and the erosive effects of surface water runoff.

Figure 4.105 presents the baseline stability assessment of the inherently stable Downstream Section in its unsupported state under static loading.

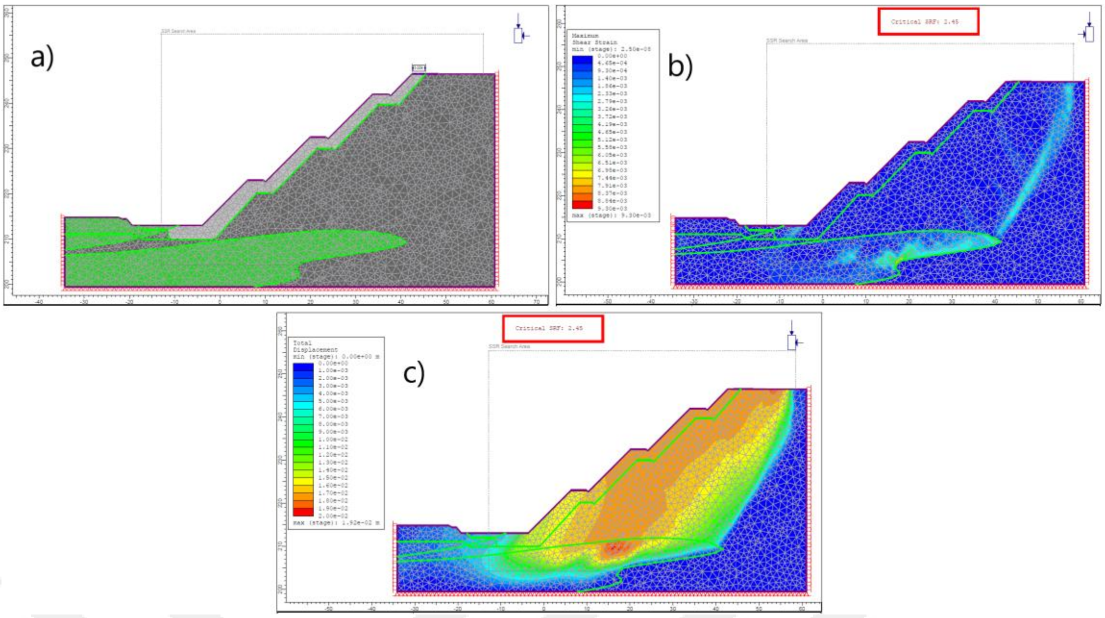

Figure 4.105. *Baseline stability assessment of the inherently stable Downstream Section in its unsupported state under static loading: (a) numerical model setup, (b) maximum shear strain contours, and (c) total displacement vectors (FS = 2.45)*

4.5.4.3. Conclusion of baseline assessment

The analyses confirmed that without systematic reinforcement, the spillway excavation—particularly at the governing control section (Inlet Area)—fails to meet the mandatory safety requirements. Consequently, a robust stabilization system is required to prevent deep-seated global failure within the saprolitic (arenized) horizons and to mitigate progressive surface weathering in the more competent rock zones.

Table 4.26 presents a summary of baseline stability factors and design parameters.

Table 4.26. *Summary of baseline stability factors and design parameters*

Section	Condition	Analysis Type	FS Result	Design Criterion	Stability Assessment
Inlet Section (Critical)	Unsupported	Static (FEM/SSR)	1.14	≥ 1.5	Unsafe: Deep-seated global failure through saprolitic (arenized) horizon.
Downstream Section (Stable)	Unsupported	Static (FEM/SSR)	2.45	≥ 1.5	Safe (Global): Requires constructive measures for surface protection.
Regional Parameters	Design Input	Seismic Coeff. (k_h)	0.15	-	Derived from regional peak ground acceleration (PGA ≈ 0.30g).
Governing Section	Design Constraint	Pseudo-static	< 0.99*	≥ 1.0	Unsafe: Seismic safety requirements not met (*below static threshold).

4.5.5. Improvement scenarios, support options, and comparative performance evaluation

To remediate the critical instability identified at the governing control section (Inlet Area) and to provide comprehensive surface protection against the rapid atmospheric degradation characteristic of the saprolitic (arenized) granodiorite, a robust structural stabilization system was engineered. The design strategy necessitated a transition from the initial steep geometry to a 1V:1.33H inclination, supplemented by a composite reinforcement system anchored into the underlying competent rock mass.

4.5.5.1. Support system specifications

The selected stabilization measures were designed to provide both structural confinement and drainage relief:

Systematic rock bolting and surface support

The application of the support system was specifically tailored to the stability requirements of the distinct spillway zones:

- Downstream section: In this region, where the rock mass exhibited inherent global stability, the reinforcement was limited to surficial protection. A 15 cm thick layer of shotcrete, reinforced with a single layer of Q221/221 steel wire mesh, was applied to isolate the rock face from atmospheric exposure and prevent progressive degradation.

- Inlet area (critical section): To remediate the critical instability posed by the deep-seated saprolitic profile, a composite reinforcement system was implemented. This integrated system combined surficial protection (15 cm shotcrete and wire mesh) with heavy-duty structural reinforcement. The primary reinforcement in this zone consisted of ϕ 32 mm diameter rock bolts with a length of 12.0 m, installed in a systematic 2.0 m × 2.0 m grid pattern with a bond strength of 48 kN/m. The bolts were inclined at 15° below the horizontal to effectively intercept potential failure surfaces and ensure secure anchorage into the competent granodiorite bedrock.

Drainage strategy

Recognizing the extreme moisture sensitivity of the saprolitic material, a passive drainage system was implemented to manage hydrostatic conditions. This includes ϕ 50 mm perforated sub-drainage pipes (weep holes), 6.0 m in length, installed at 4.0 m horizontal and vertical intervals to relieve pore water pressure behind the shotcrete lining. Surface runoff is further managed via a comprehensive network of reinforced concrete interceptor (head), bench, and toe ditches to minimize infiltration into the slope mass.

Table 4.27 provides a summary of the selected stabilization measures.

Table 4.27. *Summary of selected stabilization measures*

Support Detail	Component	Dimension	Value	Unit	Purpose/Function
Rock Bolt	Diameter	φ	32	mm	Primary Stabilization
Rock Bolt	Length	L	12.0	m	Primary Stabilization
Rock Bolt	Spacing (V x H)	S	2.0 x 2.0	m	Primary Stabilization
Shotcrete	Thickness	t	15	cm	Surface Protection
Drainage (Weep Hole)	Length	L	6.0	m	Long-term Drainage (where required)

4.5.5.2. Performance evaluation and verification

Numerical verification using RS2 (Finite Element Method) demonstrated that the implemented support system successfully mitigates the risk of deep-seated failure by redistributing shear strains away from the critical arenized zones.

The implementation of the composite reinforcement system resulted in a significant improvement in the safety margins for both critical and stable sections:

Governing control section (inlet area)

The support system increased the static factor of safety (FS) from a critical 1.14 to 1.69, satisfying the long-term stability criterion. Under pseudo-static seismic loading ($k_h \approx 0.15$), the reinforced slope yielded an FS of 1.09, exceeding the mandatory threshold of 1.00.

Figure 4.106 illustrates the evaluation of the remediated Inlet Section featuring rock bolts and shotcrete under static conditions.

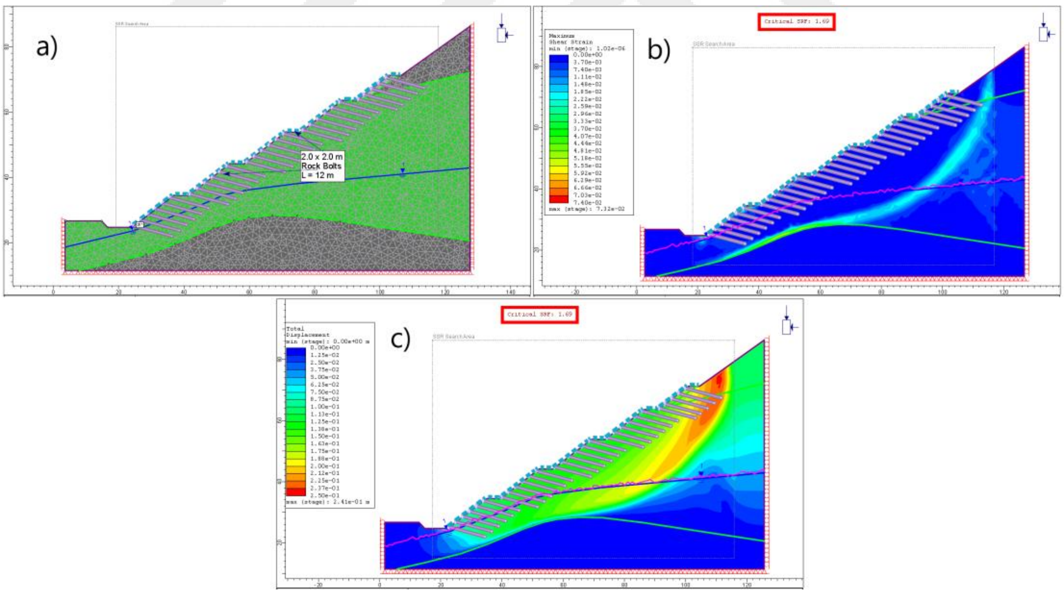

Figure 4.106. *Evaluation of the remediated Inlet Section featuring rock bolts and shotcrete under static conditions: (a) support system model geometry, (b) maximum shear strain contours, and (c) total displacement vectors (FS = 1.69)*

Figure 4.107 presents the performance verification of the heavily reinforced Inlet Section under pseudo-static seismic loading.

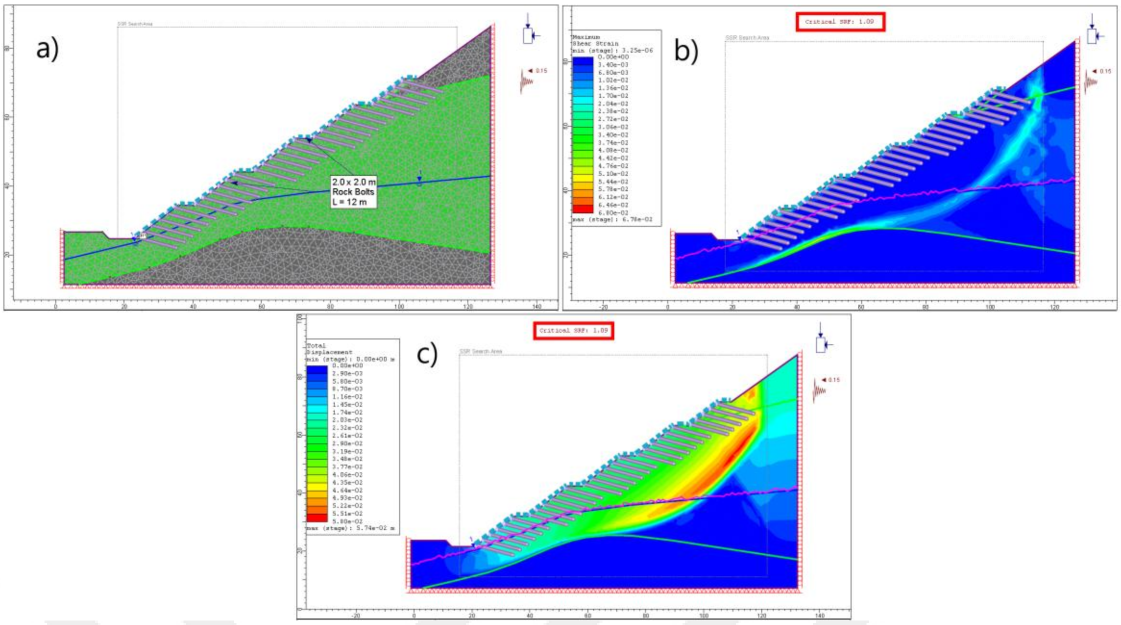

Figure 4.107. *Performance verification of the heavily reinforced Inlet Section under pseudo-static seismic loading ($k_h \approx 0.15$): (a) seismic model geometry, (b) maximum shear strain contours, and (c) total displacement vectors (FS = 1.09)*

Downstream section (stable)

While inherently stable against global failure (Unsupported FS = 2.45), the application of support ensured uniform surface integrity and long-term protection against progressive weathering. The reinforced section maintained high safety margins, with an FS of 2.56 under static conditions and 1.62 under seismic loading.

Figure 4.108 presents the stability verification of the Downstream Section incorporating surficial shotcrete protection under static conditions.

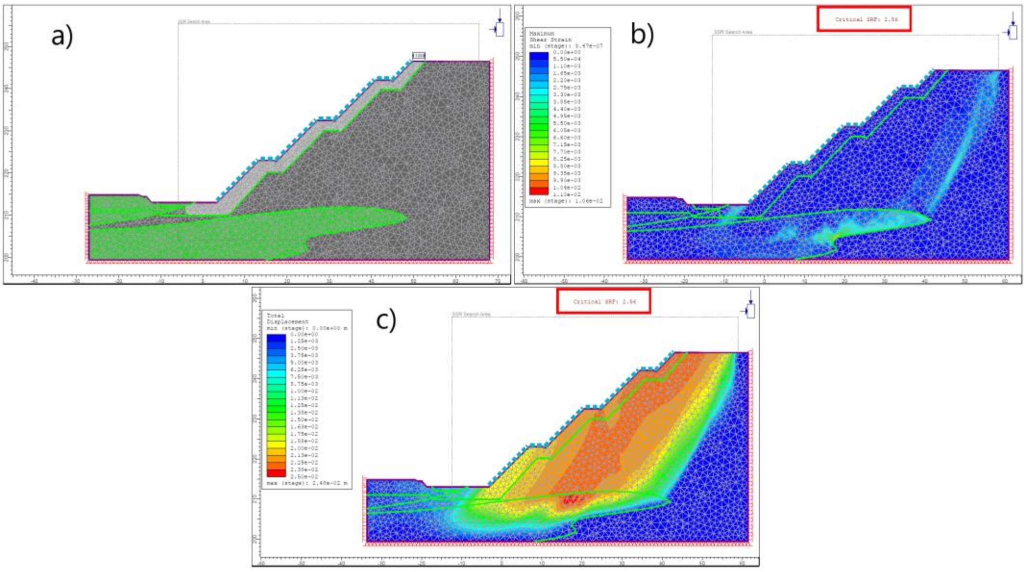

Figure 4.108. *Stability verification of the Downstream Section incorporating surficial shotcrete protection under static conditions: (a) support model geometry, (b) maximum shear strain contours, and (c) total displacement vectors (FS = 2.56)*

Figure 4.109 presents the pseudo-static seismic stability verification the shotcrete-lined Downstream Section.

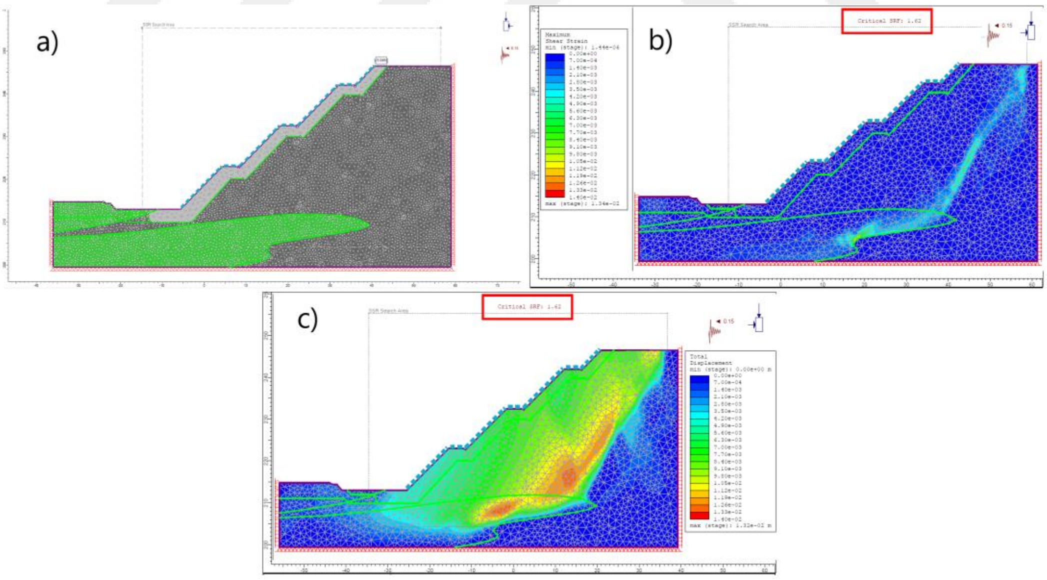

Figure 4.109. *Pseudo-static seismic stability verification ($k_h \approx 0.15$) of the shotcrete-lined Downstream Section: (a) seismic model geometry, (b) maximum shear strain contours, and (c) total displacement vectors (FS = 1.62)*

Table 4.28 provides a comparative stability performance summary, detailing the factors of safety before and after the implementation of stabilization measures.

Table 4.28. *Comparative stability performance summary*

Section	Condition	Analysis Type	FS Result	Design Criterion	Stability Assessment
Inlet Section (Critical)	Unsupported	Static (SSR)	1.14	≥ 1.5	Unsafe: Global failure risk in saprolite.
Inlet Section (Critical)	Unsupported	Pseudo-static (SSR)	<1.00	≥ 1.0	Unsafe: Seismic Failure risk.
Inlet Section (Critical)	Reinforced	Static (SSR)	1.69	≥ 1.5	Safe: Target safety requirements met.
Inlet Section (Critical)	Reinforced	Pseudo-static (SSR)	1.09	≥ 1.0	Safe: Seismic stability requirements met.
Downstream Section (Stable)	Unsupported	Static (SSR)	2.45	≥ 1.5	Safe: Requires surface protection only.
Downstream Section (Stable)	Supported	Static (SSR)	2.56	≥ 1.5	After surface protection.
Downstream Section (Stable)	Reinforced	Pseudo-static (SSR)	1.62	≥ 1.0	Safe: High seismic safety margin (Surface protection applied).

4.5.6. Lessons learned

This case highlights a fundamental challenge in geotechnical engineering: the characterization of highly disturbed or weathered rock masses, such as saprolitic granodiorite. Because the friable nature of the material often precludes the extraction of high-quality intact samples for traditional shear strength testing, the Generalized Hoek-Brown failure criterion serves as a vital analytical framework to empirically derive equivalent Mohr-Coulomb parameters (c' and ϕ') for numerical modeling.

Furthermore, the project underscores that in saprolitic environments, mechanical reinforcement alone may be insufficient. The spatial variability of the weathering profile—which can reach significant depths (up to approximately 20 meters) in this geological setting—requires a flexible design approach adaptable to real-time geological observations (Observational Method). Moreover, the successful remediation demonstrates the technical and economic necessity of a "zoned" support strategy. Rather than applying a uniform reinforcement scheme across the entire spillway, tailoring the intervention to the local geological reality—utilizing extensive geometric flattening (from

1V:0.33H to 1V:1.33H) and deep rock bolting for the critical saprolitic inlet, while applying only surficial shotcrete sealing for the inherently stable downstream rock—optimizes both safety and constructability.

Crucially, due to the rapid loss of shear strength in saturated weathered rock, the installation of drainage systems and the immediate sealing of the excavated face (e.g., via shotcrete) must occur concurrently with earthworks. This proactive strategy is essential to prevent progressive strength degradation and surficial mass wasting before the primary reinforcement can reach full capacity. Finally, the stability assessments reveal that in these highly friable, arenized materials, pseudo-static seismic demands often govern the ultimate design. Even when a slope maintains a marginal static equilibrium (e.g., FS = 1.14), the degraded cohesion in the matrix renders it implicitly unstable under dynamic loading, mandating heavy structural reinforcement to satisfy strict seismic safety criteria.

4.6. Case 6 – Intake Portal Stability and Rapid Drawdown Analysis

This section presents a comprehensive geotechnical stability assessment for the excavated slopes surrounding the upstream intake portal and control shaft of a large-scale water conveyance infrastructure project. The analysis specifically addresses the critical interaction between the massive limestone unit and the underlying moisture-sensitive clay-rich sedimentary formation under reservoir fluctuations. Following the hierarchical methodology defined in Section 3.6, the results are presented in two stages: a Level 1 conservative screening (instantaneous drawdown) and a Level 2 rigorous transient simulation.

4.6.1. Project setting, slope geometry, and operating water levels

The intake portal is situated on steep natural slopes that will be subjected to full submersion during reservoir impoundment. The excavation involves the portal face (Sections 1-1' and 2-2') and side slopes (Section 3-3').

4.6.1.1. Slope geometry and excavation

The slope geometry is categorized into sections relative to a reference shaft collar elevation (approximately +800 m). The upper section, established during previous construction phases, consists of five excavation stages forming four distinct benches.

These benches are characterized by a height of 10 m and a width of 4 m, resulting in a cumulative section height ranging from approximately 30 m to 50 m.

Below the reference elevation (Ref. El. +800 m), the current design involves deep excavations for the tunnel portal and associated control shaft structures. These slopes are critical for the tunnel face and the side slopes:

Portal face slopes (sections 1-1' and 2-2')

These slopes reach a maximum vertical height of approximately 48 m (Section 1-1') and 35 m (Section 2-2'). They are designed with an inclination of 1V:2H (26.6°) to ensure stability within the weaker geological units.

Portal side slopes (section 3-3')

These slopes reach maximum heights of up to 40 m and are designed with a steeper inclination of 1V:1H (45°).

Operating levels

The stability was evaluated for a critical Rapid Drawdown (RDD) scenario, simulating a 32 m reservoir decline from the Maximum Reservoir Level (MRL: +802 m) to the Minimum Operating Level (MOL: +770 m).

4.6.1.2. Geological and hydrogeological context

Geologically, the project site features an upper sequence of massive cream-grey limestone (Middle Eocene), which conformably overlies a Paleocene–Lower Eocene sedimentary complex. The lower critical slopes are predominantly excavated within this underlying complex, which consists of interbedded red-colored conglomerate, sandstone, siltstone, and claystone. The primary bedding is oriented approximately perpendicular to the slope face and dips into the slope at a shallow angle of 5° to 15°. While this orientation generally favors global stability against daylighting discontinuities, the formation is highly susceptible to surface degradation and moisture-induced softening.

Hydrogeologically, the high clay content within the underlying sedimentary formation is of significant concern. These lithologies exhibit low hydraulic conductivity and poor drainage characteristics. Consequently, during rapid drawdown events, pore water pressures within the slope cannot dissipate at a rate commensurate with the reservoir level decline. This lag effect maintains high internal pore pressures while the stabilizing hydrostatic pressure of the reservoir is removed, leading to a temporary but critical reduction in effective stress and overall factor of safety (FS). Figure 4.110 displays the illustration of general site layout.

Figure 4.110. *Illustration of general site layout*

4.6.1.3. Operating water levels and monitoring

Stability analyses were conducted for four distinct hydraulic conditions to evaluate the factor of safety (FS) throughout the operational life of the structures:

Initial construction stage

Represents the short-term stability of the unsupported and supported excavations prior to reservoir impoundment.

Minimum operating level (MOL)

Analyzed at a reference elevation of +770 m, representing the lower operational boundary of the reservoir.

Maximum reservoir level (MRL)

Analyzed at a reference elevation of +802 m, where the slopes are subjected to maximum hydrostatic confinement and saturation.

Rapid drawdown (RDD) scenario

The most critical condition, simulating a transient decline from +802 m to +770 m. Due to its complexity and impact on safety, this scenario was evaluated through a hierarchical approach (Level 1 Screening and Level 2 Transient Analysis) to distinguish between theoretical risks and physically representative behavior.

Figure 4.111 illustrates the time-dependent reservoir boundary function simulating the 32-meter rapid drawdown (RDD) operational cycle over a 270-day period (from MRL +802 m to MOL +770 m).

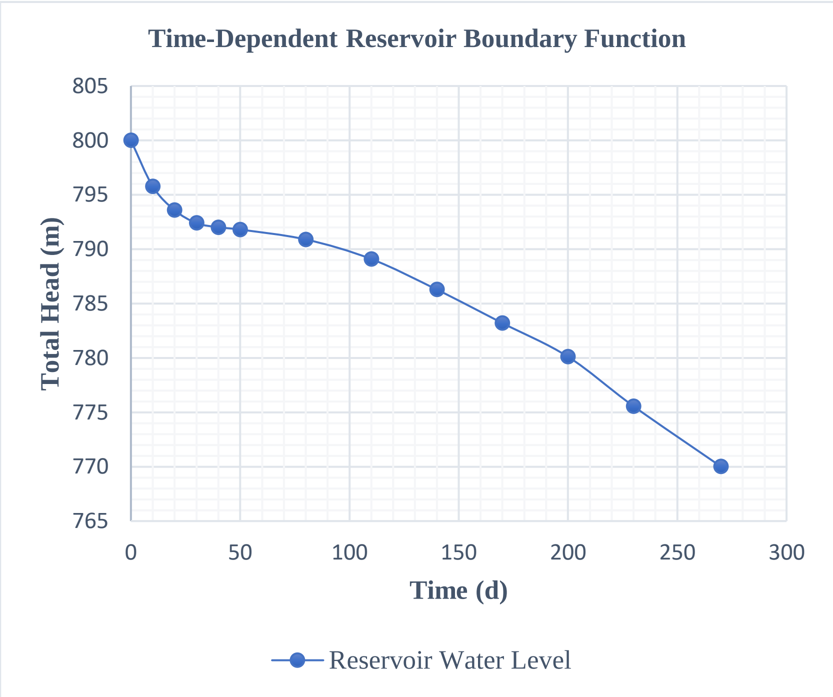

Figure 4.111. *Time-dependent reservoir boundary function simulating the 32-meter rapid drawdown (RDD) operational cycle over a 270-day period (from MRL +802 m to MOL +770 m)*

To validate the geotechnical model and monitor long-term performance, topographic measurement points have been installed across the slope faces. These instruments, referenced against stable benchmarks outside the zone of influence, provide continuous data on displacement trends, with increased monitoring frequency mandated during periods of significant reservoir fluctuation or intense precipitation. Figure 4.112 presents the general view of the intake portal excavation and slope geometry.

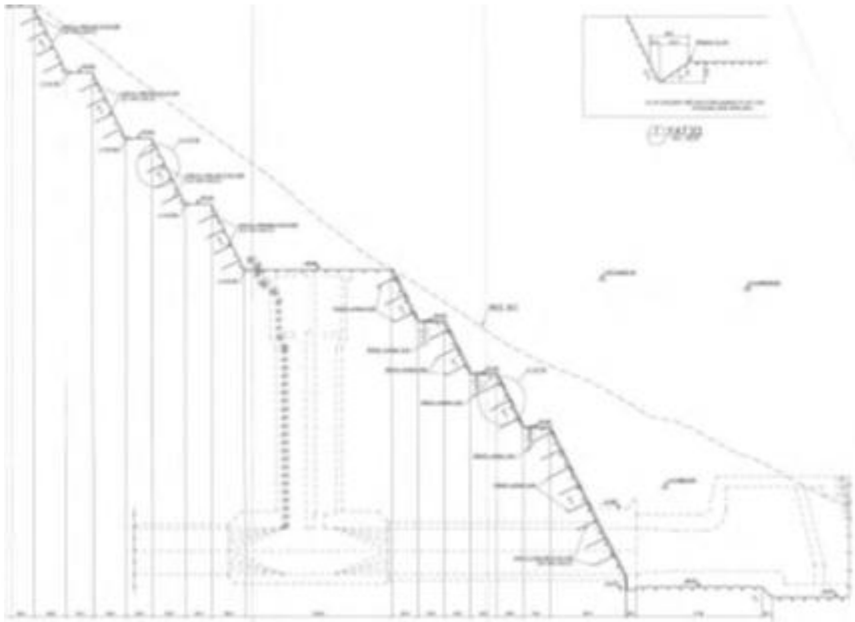

Figure 4.112. *General view of the intake portal excavation and slope geometry*

Table 4.29 tabulates the summary of key geometrical and operational parameters for the upstream slope.

Table 4.29. *Summary of key geometrical and operational parameters for the upstream slope*

Parameter	Value	Unit
Maximum Slope Height	48	m
Face Slope Inclination	1V:2H	—
Side Slope Inclination	1V:1H	—
Bench Height	10	m
Bench Width	4	m
Maximum Reservoir Level (MRL)	+802	m
Minimum Operating Level (MOL)	+770	m
Drawdown Range	32	m

4.6.2. Geological and geotechnical characterization

The site stratigraphy features a massive limestone unit conformably overlying a clay-rich sedimentary complex (conglomerate, sandstone, mudstone), separated by a distinct lithological transition zone.

4.6.2.1. Stratigraphy and structural geology

Massive limestone

The upper slope sections are dominated by an approximately 150 m thick, hard, cream-to-grey limestone. Hydrogeologically, this unit functions as a permeable aquifer, facilitating groundwater recharge into the lower horizons.

Sedimentary complex

Conformably underlying the limestone is an interbedded sequence of conglomerate, sandstone, mudstone, and claystone.

Transition zone

An approximately 15 m thick zone of highly weathered, low-strength argillaceous limestone and claystone marks the contact. With RQD values ranging from 0% to 25%, this zone is characterized as a very poor rock mass, necessitating a shift from structural kinematic control to rock mass behavior modeling.

Structural orientation

The primary bedding dips into the slope at 5° to 15°. While this generally prevents planar failures, the presence of the weakened sedimentary matrix favors deep-seated circular or composite failure surfaces.

4.6.2.2. Water sensitivity and geotechnical investigation

The geotechnical characterization was based on a drilling program totaling more than 550 m of core recovery. A critical finding of the investigation was the extreme moisture sensitivity of the clay-rich sedimentary formation. Slake durability tests (TS 699) revealed that these lithologies are prone to rapid degradation and disintegration upon exposure to wetting-drying cycles. This sensitivity was further quantified through comparative point load testing: while the average Is_{50} for dry samples reached up to 4.93 MPa, samples subjected to 48-hour saturation exhibited a drastic reduction, with values dropping as low as 0.36 MPa.

This significant loss of strength confirmed that the rock mass integrity is fundamentally compromised upon contact with reservoir water. During rapid drawdown (RDD) events, the poor drainage characteristics of the clay-rich units prevent the rapid dissipation of pore water pressures. This creates a critical condition where internal hydraulic pressures remain high while the stabilizing hydrostatic confinement of the reservoir is removed, leading to a significant reduction in the effective stress within the slope mass. Consequently, this experimental evidence justified the necessity of adopting saturated rock mass parameters for the subsequent Level 1 and Level 2 stability assessments to represent the most adverse operational conditions.

4.6.2.3. Design parameter derivation

Rock mass parameters were derived using the Generalized Hoek-Brown failure criterion. To accurately capture the moisture-induced degradation observed in the clay-rich sedimentary complex, a Dual-State Parameter Assignment was implemented for the numerical models:

Dry/standard state

Representing the rock mass prior to saturation, a GSI of 34 and an intact rock strength (q_u) of 30 MPa were assigned based on core logging and standard UCS tests.

Saturated state (governing condition)

To account for the drastic softening observed in the saturation sensitivity tests, the parameters were reduced to a GSI of 29 and a q_u of 18 MPa. This state was used as the primary input for all drawdown scenarios to ensure a conservative representation of the weakened rock matrix.

Transition zone modeling

The lithological contact zone was modeled as a distinct geomechanical unit with significantly lower strength and stiffness (GSI = 15) to account for its highly weathered and sheared state.

Hydraulic conductivity

Lugeon values (Lu) were converted to hydraulic conductivity using the approximation (Eq. 3.4), serving as the primary input for the Level 2 transient models.

These parameters, summarized in Table 4.30, were utilized to assess slope performance across the different hydraulic stages. While the Level 1 analysis utilized these saturated parameters under instantaneous drawdown assumptions, the Level 2 transient analysis combined these strength values with in-situ hydraulic conductivity (k) to evaluate the realistic pore pressure response. Table 4.30 outlines the summary of derived rock mass design parameters for stability analysis.

Table 4.30. *Summary of derived rock mass design parameters for stability analysis*

Geological Unit	Color	Unit Weight γ [kN/m³]	Hydraulic Conductivity (m/s)	UCS q_u [MPa]	GSI	m_i	Cohesion c′ [kPa]	Friction Angle ϕ′ [°]	Modulus E [MPa]
Limestone		25	1e-6	38	46	12	432	50	2865
Transition Zone		21	1e-07	10	15	7	72	24	437
Mudstone/ Conglomerate (Dry)		23.5	5e-06	30	34	8	270	40	1271
Mudstone/ Conglomerate (Saturated)		24.5	5e-08	18	29	6	180	30	916

Parameters derived using Generalized Hoek-Brown and Mohr-Coulomb mapping in RocLab based on BH series borehole data and laboratory testing. A disturbance factor (D) of 0.30 was applied within approximately 3 m of the surface.

4.6.3. Level 1: Conservative screening and theoretical support requirements

Aligned with the hierarchical framework detailed in Section 3.6.5, the preliminary stability assessment focused on a Level 1 Conservative Screening. This stage was performed under 'instantaneous drawdown' conditions to establish the theoretical lower-bound safety factors of the slope by discounting any potential drainage or seepage dissipation effects.

4.6.3.1. Seismic loading assumptions and acceptance criteria

The seismic design inputs were grounded in the Turkish Seismic Hazard Map (TBDY 2018) for Earthquake Ground Motion Level–2 (DD-2). Based on this standard, the peak ground acceleration at the rock outcrop ($PGA_{rock,outcrop}$) was established as 0.254

g. Accounting for the specific local site classification, the short-period design spectral acceleration coefficient (S_{DS}) was determined to be 0.755. Consequently, the expected peak ground acceleration at the surface was derived as (from Eq. 4.2):

$$PGA_{ground} = 0.4 \times 0.755 \approx 0.302 \text{ g}$$

For the limit equilibrium stability analyses, the representative horizontal seismic coefficient (k_h) was calculated via Eq. 4.3 as:

$$k_h = 0.40 \times 0.755 \times 0.5 \approx 0.151$$

While this coefficient was adopted as the governing horizontal seismic load for the baseline stability assessments, the simultaneous occurrence of a peak seismic event and a critical rapid drawdown (RDD) represents an extremely low-probability, compounded hazard.

Consequently, to avoid evaluating an overly conservative and extreme scenario, explicit pseudo-static RDD results are not presented herein. Nevertheless, given the substantially high static factor of safety (FS) margins achieved in the Level 2 transient analyses due to effective pore pressure dissipation, the slopes are anticipated to maintain adequate seismic stability (FS ≥ 1.0) even under such severe hypothetical conditions.

4.6.3.2. Hydro-geotechnical mechanism of instability

The critical nature of this scenario is driven by the hydrogeological properties of the clay-rich sedimentary formation. Due to the high clay content and low hydraulic conductivity, pore water drainage cannot occur synchronously with the rapid decline in reservoir level.

In this Level 1 screening, the rock mass units below the initial saturation line (+802 m) are assumed to remain in a fully saturated state. This creates a severe loading condition where excess pore water pressures (u) persist while the stabilizing hydrostatic confinement on the slope face is removed. The resulting temporary but significant reduction in effective stress ($\sigma' = \sigma - u$) leads to a critical drop in the factor of safety (FS).

4.6.3.3. Level 1 (instantaneous RDD) analysis results (original design failure)

The preliminary screening evaluated the performance of the slopes under the originally proposed constructive support (ϕ 20 mm, L=3.0 m rock bolts at 3.0 × 3.0 m spacing). The results highlighted a severe inadequacy in this design for the portal face:

Portal face slopes (sections 1-1' and 2-2')

These sections exhibited total instability. The FS_{min} for Section 1-1' was calculated as 0.843 (unsupported) and 0.914 (original support). Similarly, Section 2-2' yielded an FS of 0.794 (unsupported) and 0.951 with the original support. Figure 4.113 highlights the critical slip surface showing instability for unsupported Section 1-1' under Level 1 rapid drawdown. Figure 4.114 demonstrates the Level 1 RDD scenario for Section 1-1' with original support.

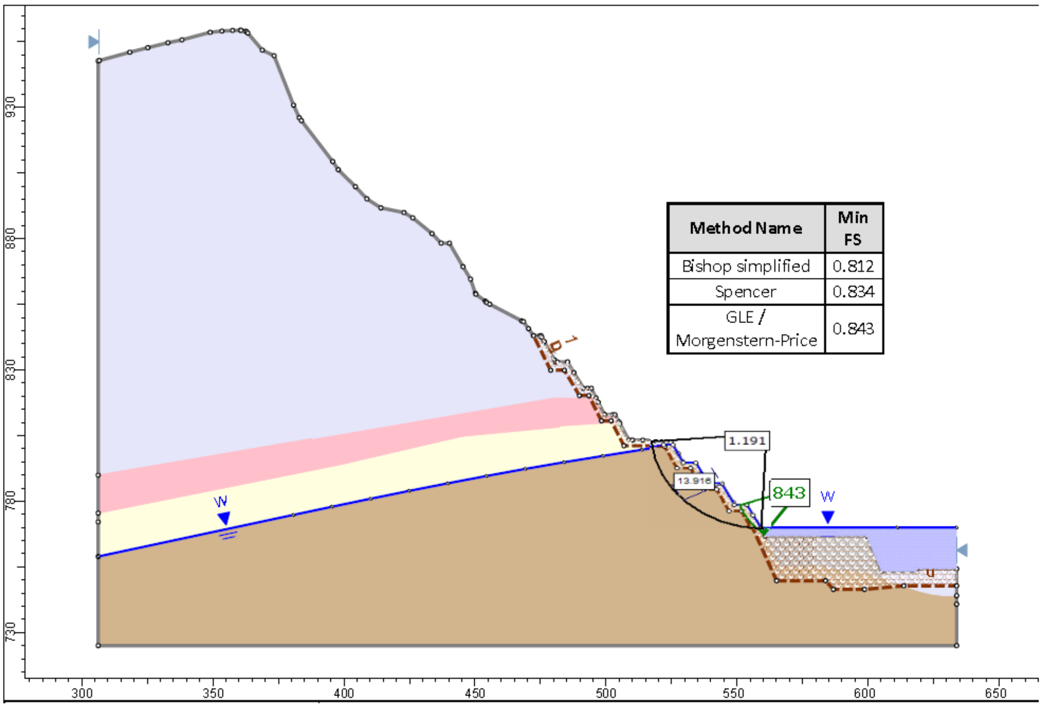

Figure 4.113. *Critical slip surface showing instability for unsupported Section 1-1' under Level 1 rapid drawdown (FS=0.843)*

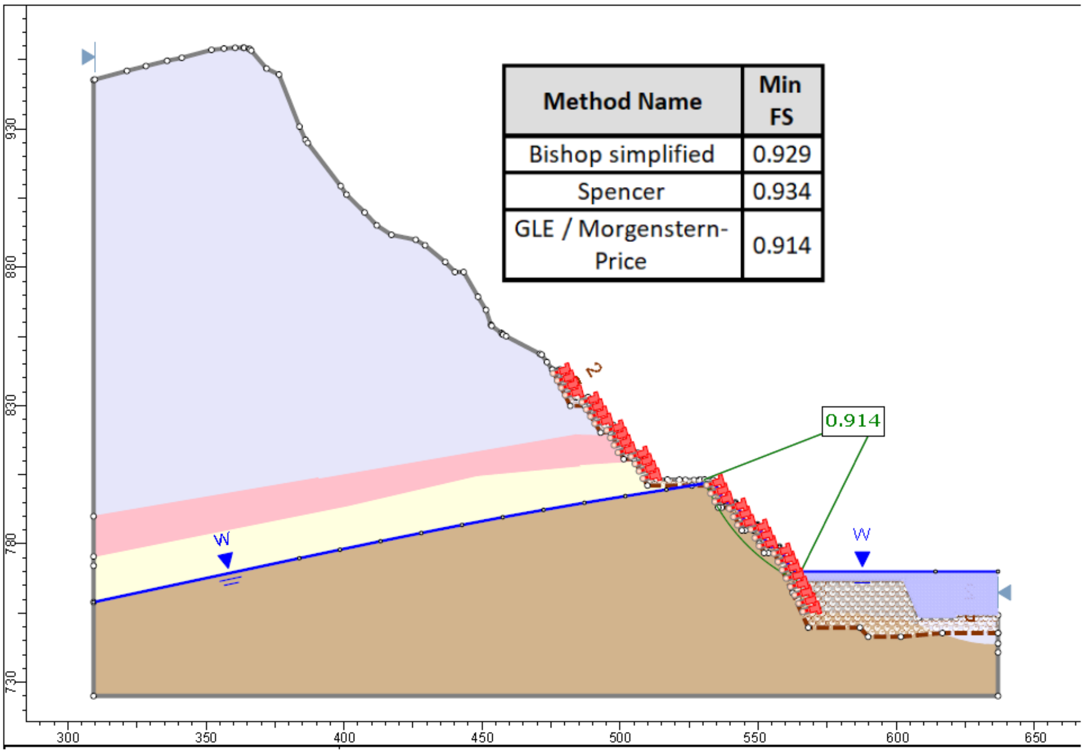

Figure 4.114. *Level 1 RDD scenario for Section 1-1' with original support (FS=0.914)*

Figure 4.115 depicts the Level 1 RDD scenario for unsupported Section 2-2'.

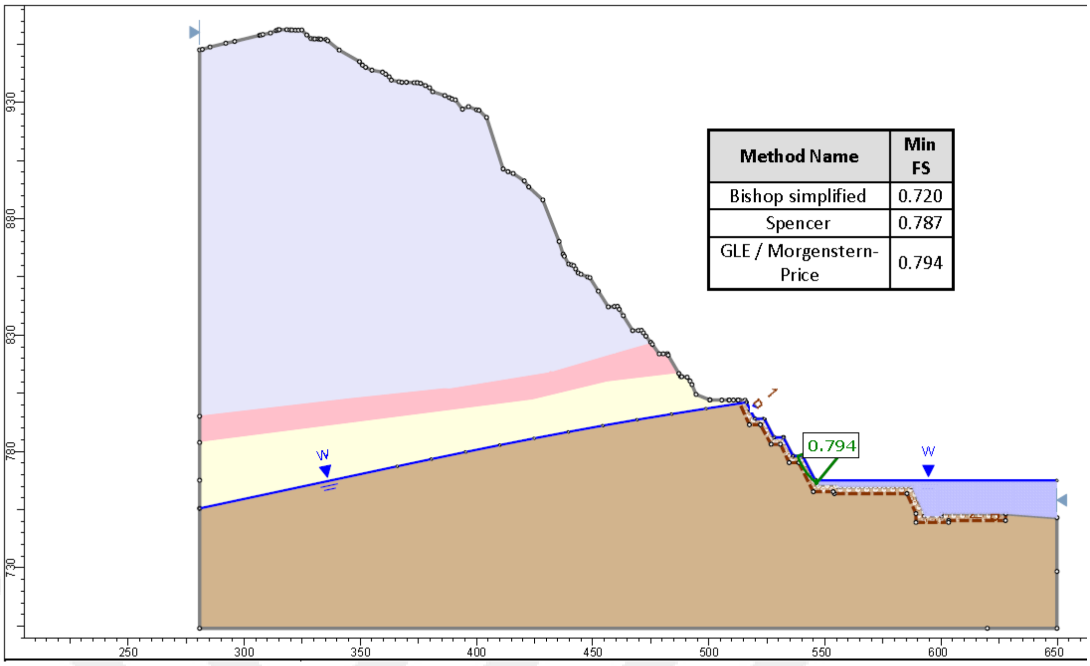

Figure 4.115. *Level 1 RDD scenario for unsupported Section 2-2' (FS=0.794)*

Figure 4.116 represents the Level 1 RDD scenario for Section 2-2' with original support.

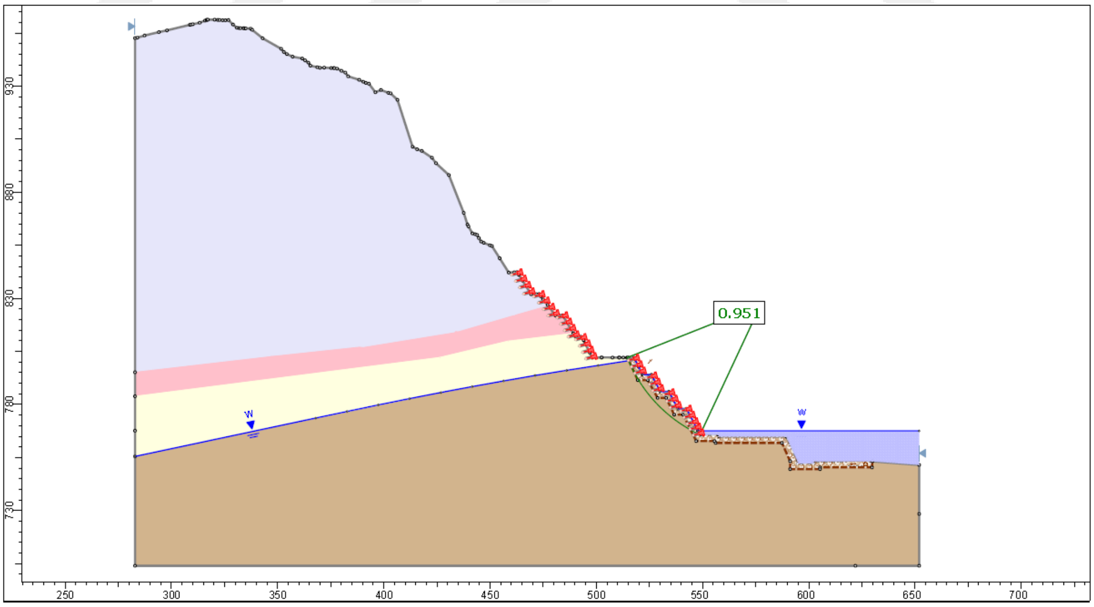

Figure 4.116. *Level 1 RDD scenario for Section 2-2' with original support (FS=0.951)*

Deep-seated failure

The critical slip surfaces extended approximately 14 m into the slope face (e.g., in Section 1-1' for FS=1.19), confirming that the 3 m bolts were insufficient to intercept the failure planes driven by the saturation-induced weakness.

Theoretical requirement

To satisfy Level 1 safety criteria (FS ≥ 1.0 seismic, 1.5 static), this "worst-case" screening dictated the theoretical necessity for a heavy-duty reinforcement system, specifically ϕ 32 mm bolts with 12.0 m length on a 2.0 m × 2.0 m grid, ensuring at least 8.0 m of penetration into the competent bedrock beyond the failure zone. While this design was validated using FHWA-IF-03-017 guidelines for bond and pull-out resistance, it represented a significant over-engineering of the slope.

Side slopes (section 3-3')

In contrast, the side slopes remained inherently stable under rapid drawdown, achieving an FS of 1.823, satisfying the project requirements without further intervention.

Figure 4.117 portrays the Level 1 RDD scenario for unsupported Section 3-3'.

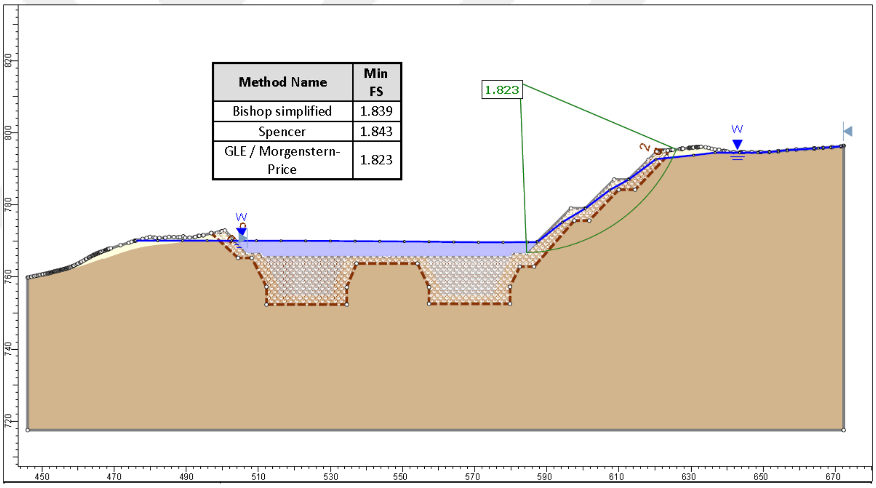

Figure 4.117. *Level 1 RDD scenario for unsupported Section 3-3' (FS=1.823)*

Table 4.31 enumerates the summary of initial stability analysis results for critical sections under level 1 rapid drawdown conditions.

Table 4.31. *Summary of initial stability analysis results for critical sections under level 1 rapid drawdown conditions*

Section	Condition	Calculated Factor of Safety (FS)	Required FS	Stability
1-1'	Unsupported	0.843	1.20	Unstable
1-1'	Original Design Support (L=3 m)	0.914	1.20	Unstable

Table 4.31. (Continued) *Summary of initial stability analysis results for critical sections under level 1 rapid drawdown conditions*

Section	Condition	Calculated Factor of Safety (FS)	Required FS	Stability
2-2'	Unsupported	0.794	1.20	Unstable
2-2'	Original Design Support (L=3 m)	0.951	1.20	Unstable
3-3' (Side Slope)	Rapid Drawdown	1.823	1.20	Stable

4.6.4. Level 2: Rigorous transient seepage modeling and optimization

To evaluate the slope's performance under physically representative conditions, a Transient Finite Element Seepage analysis was conducted in Slide2. This model simulated the reservoir decline over a realistic 270-day operational cycle.

4.6.4.1. Seepage mechanism and boundary conditions

The numerical framework assumes that all geological units located below the Maximum Reservoir Level (MRL) reach a state of full saturation during high-pool stages. This steady-state saturation serves as the initial condition for the transient seepage analysis.

The critical instability mechanism is driven by the stark contrast in hydraulic conductivity between the primary lithologies. While the overlying massive limestone unit functions as a highly permeable aquifer, the underlying clay-rich sedimentary formation exhibits significantly lower permeability. During reservoir fluctuations, this hydrogeological heterogeneity leads to differential drainage rates. The limestone unit drains relatively rapidly, whereas the low-permeability sedimentary layers retain high internal pore water pressures, creating a destabilizing hydraulic gradient directed towards the excavated face.

During the drawdown phase, the external stabilizing hydrostatic pressure acting on the slope face is removed. However, due to the low hydraulic diffusivity of the underlying clay-rich sedimentary formation, pore water drainage cannot occur synchronously with the declining reservoir level. This results in a pronounced "lag" in the phreatic surface response, where high residual pore water pressures are maintained within the slope mass.

This transient condition generates steep hydraulic gradients directed toward the excavated face, significantly reducing the effective stress ($\sigma' = \sigma - u$) along potential failure surfaces. Consequently, the temporary imbalance between the internal seepage forces and the reduced external confinement creates the most critical stability window for the portal structures.

The transient analysis focused on quantifying this lag over a realistic 270-day drawdown period (from +802 m to +770 m), accounting for:

Hydraulic conductivity (k)

Derived from in-situ Lugeon tests and implemented using the empirical approximation (Eq. 3.4):

Specific storage (Ss)

Defining the rock mass's ability to release water as pore pressure declines.

Effective stress calculation

Utilizing the transient pore pressure distribution (u(t)) to determine the safety factor at each time step through the effective stress relationship:

$$\sigma' = \sigma - u \tag{4.4}$$

4.6.4.2. Modeling approach

Unlike the Level 1 approach, which lumped drawdown effects into an instantaneous "pseudo-static" saturation event, the Level 2 analysis explicitly solved the time-dependent diffusion equation. This allowed the model to capture the realistic dissipation rate of excess pore water pressures. By simulating the actual 270-day operational cycle, the analysis provided a much more accurate representation of the hydraulic gradients directed toward the excavated face.

4.6.4.3. Analysis results: optimization and inherent stability

The transient results revealed a fundamental shift in the stability assessment. By calculating the actual pore pressure dissipation rather than assuming zero drainage:

Pore Pressure dissipation

The analysis demonstrated that despite the low permeability of the mudstone units, the drawdown rate of the reservoir allows for a sufficient dissipation of internal pressures. The phreatic lag, while present, does not reach the critical levels assumed in Level 1.

Inherent stability

The most significant finding was that the unsupported slope remains stable throughout the entire drawdown process. The calculated Factor of Safety (FS) remained above the mandatory thresholds (Static FS > 1.5) at every critical time step.

Support redundancy

Consequently, the intensive support system necessitated by Level 1 (ϕ 32 mm, L=12.0 m rock bolts) was identified as structurally redundant. The Level 2 results verify that the slope’s natural drainage capacity—combined with its geometric optimization—is sufficient to maintain global integrity during extreme reservoir fluctuations.

Table 4.32 summarizes the summary of transient seepage boundary conditions and stability results.

Table 4.32. *Summary of transient seepage boundary conditions and stability results*

Parameter / Condition	**Level 1 (Instantaneous Screening)**	**Level 2 (Transient FEA)**
Seepage Duration	t = 0 (Instantaneous)	~ 270 days
Saturation Assumption	Full saturation below MRL (+802 m)	Time-dependent dissipation based on k
Calculated FS (Unsupported)	< 1.20 (Failed)	> 1.50 (Stable)
Support Requirement	Ø 32 mm, L=12.0 m rock bolts	Structurally redundant

Figure 4.118 delineates the Level 2 transient rapid drawdown (RDD) stability analysis for the critical portal face (Section 1-1'), illustrating pore pressure dissipation and inherent stability over the operational cycle.

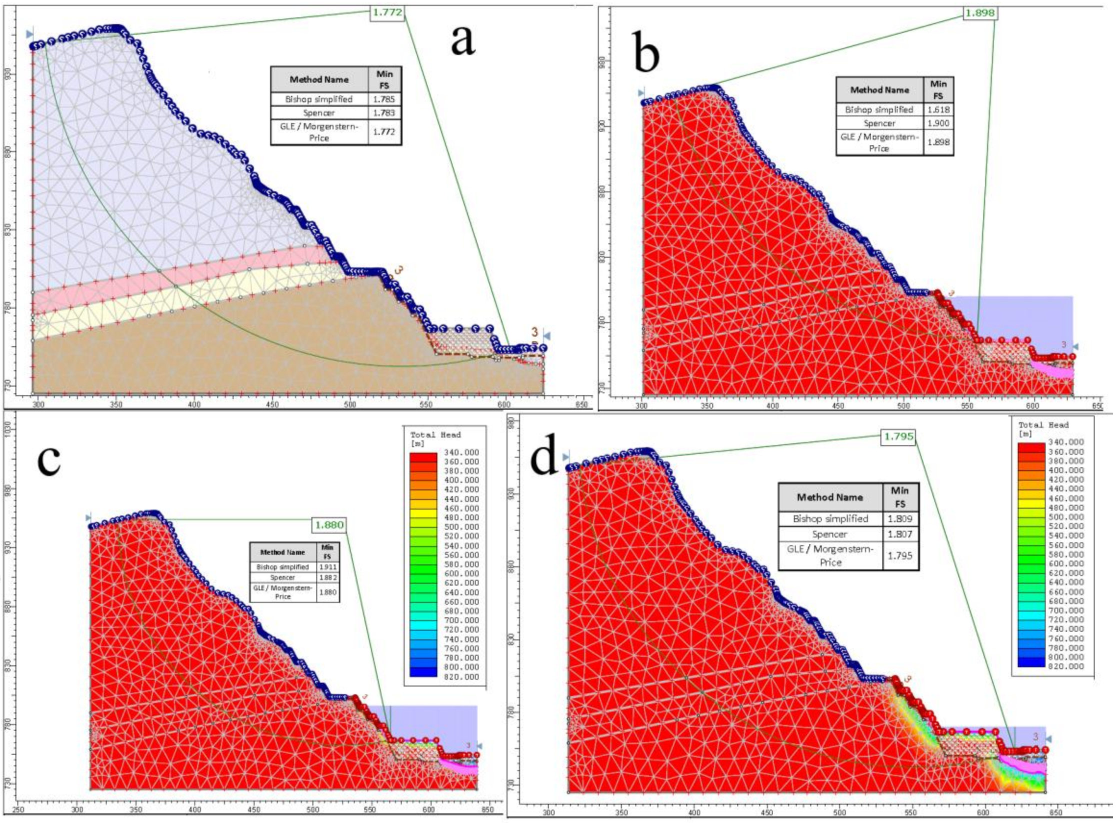

Figure 4.118. *Level 2 transient rapid drawdown (RDD) stability analysis for the critical portal face (Section 1-1'), illustrating pore pressure dissipation and inherent stability over the operational cycle: (a) baseline dry condition (global stability, FS=1.772), (b) Stage 1 at Maximum Reservoir Level (t = 0 days, MRL +802 m) (FS=1.898), (c) Stage 2 during early drawdown (t = 10 days) (FS=1.880), and (d) Stage 13 at Minimum Operating Level (t = 270 days, MOL +770 m) (FS=1.795)*

Figure 4.119 presents the evolution of phreatic surfaces and the corresponding Factor of Safety (FS) for Section 2-2' under Level 2 transient seepage conditions.

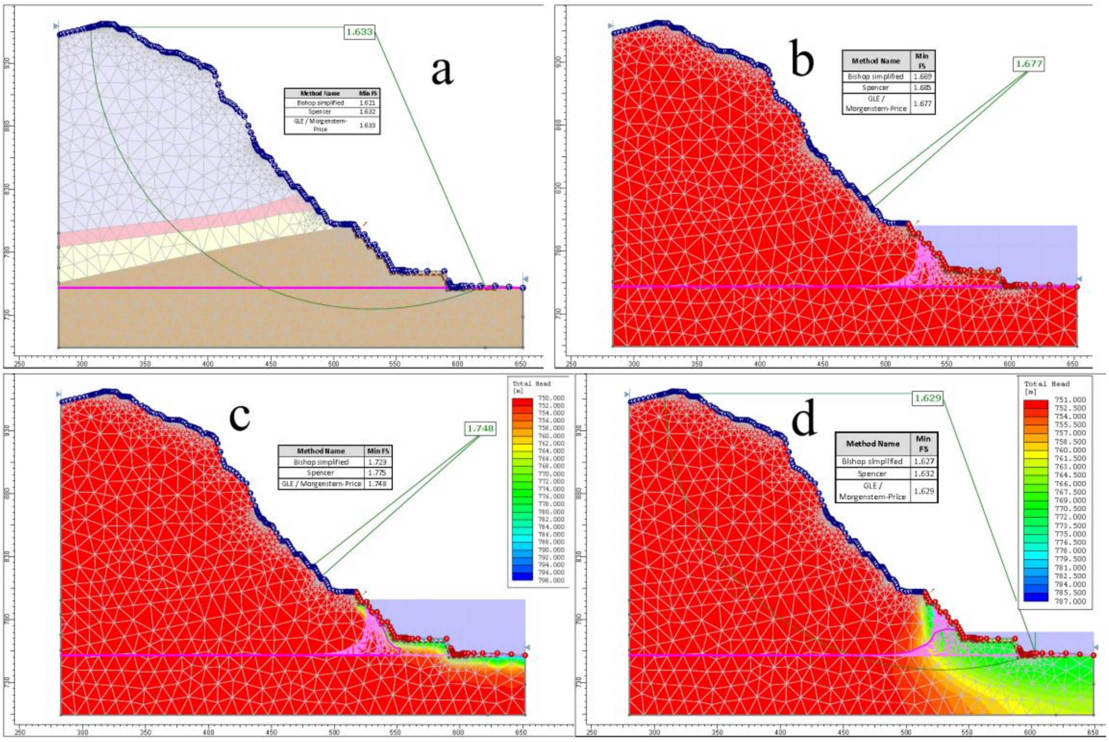

Figure 4.119. *Evolution of phreatic surfaces and the corresponding Factor of Safety (FS) for Section 2-2' under Level 2 transient seepage conditions: (a) initial dry state (global stability, FS=1.633), (b) Stage 1 steady-state saturation (t = 0 days) (FS=1.677), (c) Stage 2 intermediate drawdown response (t = 10 days) (FS=1.748), and (d) Stage 13 final drawdown state (t = 270 days) (FS=1.629)*

Figure 4.120 verifies the Level 2 transient seepage and stability evaluation for the side slope (Section 3-3'), confirming the preservation of high safety margins throughout the reservoir decline.

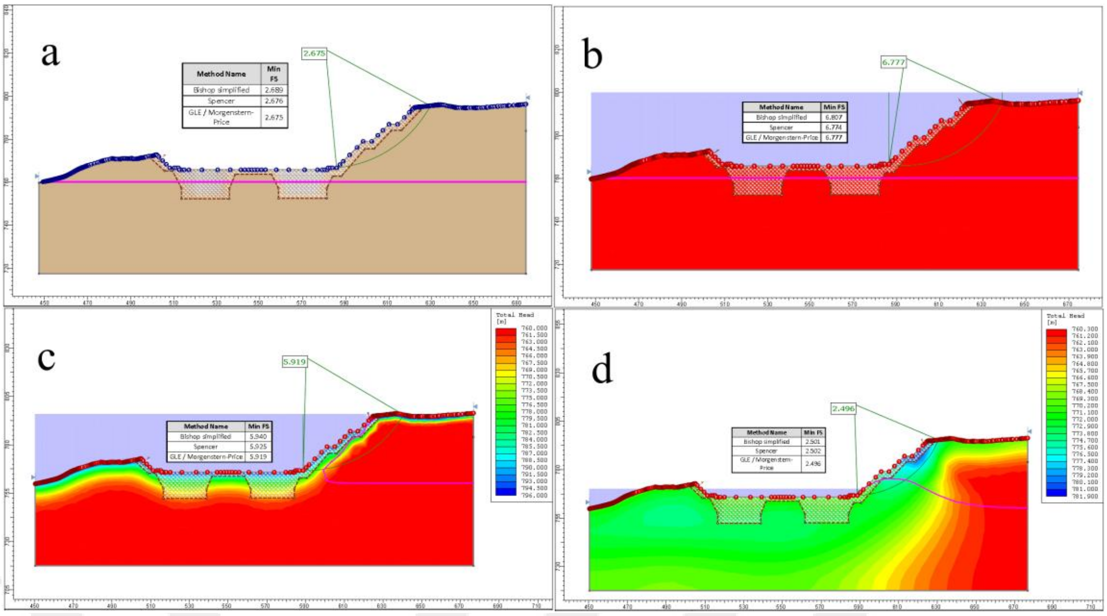

Figure 4.120. *Level 2 transient seepage and stability evaluation for the side slope (Section 3-3'), confirming the preservation of high safety margins throughout the reservoir decline: (a) dry condition (FS=2.675), (b) Stage 1 high-pool state (t = 0 days) (FS=6.777), (c) Stage 2 transient response (t = 10 days) (FS=5.919), and (d) Stage 13 low-pool state (t = 270 days) (FS=2.496)*

4.6.5. Evaluation of support strategies

The stabilization of the intake portal slopes under Rapid Drawdown (RDD) conditions represents a critical case study in the transition from conservative "worst-case" screening to optimized, physically representative design. The evaluation highlights that modeling philosophy directly dictates the scale of engineering intervention, where the disregard for time-dependent pore pressure dissipation leads to significant over-engineering.

Numerical simulations indicate that this imbalance results in critical failure circles extending approximately 14 m into the rock mass. The depth of these failure surfaces underscores the transition from surficial weathering-related issues to a deep-seated global instability governed by the reduced effective stress regime at the contact and within the saturated sedimentary matrix.

4.6.5.1. Evaluation of remedial alternatives: geometry vs. reinforcement

Prior to detailing the support measures, geometry modification was evaluated as a potential strategy to enhance long-term stability. However, extensive regrading of the upper slopes was deemed technically and economically impractical:

Morphological constraints

The cliff-like morphology of the massive limestone unit posed a severe constraint for slope flattening.

Volume and logistics

Achieving a naturally stable angle through full excavation would have necessitated the removal of approximately 1,000,000 m^3 of material. Such a massive earthwork operation presented prohibitive trade-offs, including excessive disposal requirements and the potential disturbance of the pristine upper limestone cap.

Consequently, the design focus shifted toward a structural stabilization approach, utilizing deep reinforcement to minimize the excavation footprint while attempting to satisfy safety criteria under saturated conditions.

4.6.5.2. Theoretical support implementation (Level 1 requirement)

Under the Level 1 Conservative Screening (instantaneous drawdown), the portal face exhibited severe global instability, with failure surfaces penetrating 14 m into the slope. To satisfy safety criteria under this purely theoretical state, an intensive reinforcement strategy was developed:

Deep reinforcement (portal face)

The primary measure involved ϕ 32 mm rock bolts (L=12.0 m) installed on a dense 2.0 m × 2.0 m grid. This length was specifically dimensioned to penetrate at least 8.0 m beyond the identified critical failure zone. The use of self-drilling technology was considered mandatory to prevent borehole collapse within the weathered, saturated claystone layers.

Surface support

The system included a robust facing consisting of a 20 cm temporary shotcrete layer reinforced with double steel wire mesh (Q443/443), followed by a permanent 30 cm concrete lining to isolate the sensitive rock mass from hydraulic cycles.

Drainage system

To manage the pore pressure response, a systematic network was designed, including ϕ 100 mm weep holes and ϕ 50 mm perforated PVC horizontal drains installed at 6.0 m horizontal and 3.5 m vertical intervals to accelerate pressure dissipation.

4.6.5.3. Performance verification and the "Over-Engineering Trap"

The effectiveness of the 12.0 m rock bolts was confirmed by Level 1 numerical analyses, which raised the safety factors above required thresholds. However, as demonstrated by the Level 2 Transient Analysis, this intensive reinforcement is physically redundant.

Table 4.33 compares the slope stability effectiveness for original vs. improved support systems.

Table 4.33. *Comparison of slope stability effectiveness for original vs. improved support systems*

Analysis Section	Scenario	Original Support FS (L=3 m)	Level 1 Design FS (L=12 m)	Level 2 (Transient) FS (Unsupported)	Status
1-1'	Static RDD	0.843	1.183 (≈1.20)	1.795	Compliant
2-2'	Static RDD	0.951	1.233	1.629	Compliant
3-3'	Static RDD	1.823 (Unsupported)	-	2.496	Compliant

While Level 2 analysis indicates inherent stability without support, the revised FS values for the 12 m bolts demonstrate the safety margins achieved under the theoretical Level 1 design configuration. The transient results confirm that the 12 m bolts are a product of over-engineering caused by neglecting drainage.

4.6.6. Lessons learned

The primary takeaway from this case study is the critical importance of evaluating rock mass parameters in both dry and saturated states when dealing with clay-cemented sedimentary formations. The findings emphasize that stability in moisture-sensitive environments is a function of both material degradation and hydraulic response:

- Material degradation and safety overestimation: The substantial strength degradation observed—where the Geological Strength Index (GSI) dropped from

34 to 29 and the Uniaxial Compressive Strength (q_u) decreased from 30 MPa to 18 MPa upon saturation—highlights that conventional dry-parameter analysis significantly overestimates the factor of safety. Ignoring these moisture-induced changes can lead to a false sense of security during initial design phases.

- The Power of Transient Modeling: While the drastic intact strength reduction (I_{s50} drop from 4.93 to 0.36 MPa) suggests an extreme risk, the Level 2 transient analysis proved that actual stability is governed by the rate of pore pressure dissipation. Even with degraded parameters, the slope's inherent natural drainage capacity during the 270-day operational cycle prevents the "theoretical failure" predicted by instantaneous, lumped-parameter models.
- Overcoming morphological constraints via advanced analysis: When site conditions—such as the cliff-like massive limestone unit and the prohibitive 1,000,000 m^3 excavation volume—render geometric slope flattening impossible, conventional "instantaneous" drawdown analyses (Level 1) force designers into an "over-engineering trap" requiring massive structural reinforcement (e.g., 12.0 m ϕ 32 rock bolts). Rigorous transient seepage modeling provides a justifiable, scientifically sound exit from this trap, validating the inherent stability of the slope and eliminating the need for unfeasible earthworks or intensive structural support.
- Modeling precision and optimization: Conventional "instantaneous" drawdown analyses (Level 1) significantly overestimate reinforcement needs by ignoring the time-dependent nature of groundwater flow. Future designs in clay-rich sedimentary units should prioritize rigorous transient seepage (FEA) modeling to avoid excessive construction costs and redundant structural interventions.
- Remediation hierarchy: If active remediation is strictly required in similar low-permeability environments, the design should focus on hydrogeological mitigation (horizontal drainage) rather than solely relying on deep-seated structural support. Managing the "phreatic lag" by accelerating drainage is more technically sound than attempting to mechanically reinforce a theoretically saturated mass. This approach not only ensures a higher degree of safety but also prevents the implementation of costly, over-engineered reinforcement systems.

4.7. Summary and Cross-Case Synthesis

The comprehensive evaluation of the six case studies presented in this chapter uncovers fundamental physical and analytical truths governing the stability of slopes adjacent to appurtenant hydraulic structures. Across a diverse spectrum of "intermediate" geomaterials—ranging from thick colluvial deposits and highly weathered flysch to saprolitic granodiorites and tectonized ophiolitic mélanges—the most persistent catalyst for instability is extreme hydro-mechanical sensitivity. Upon exposure to atmospheric conditions or reservoir saturation, these complex matrices undergo rapid argillization, arenization, or severe softening, resulting in a drastic degradation of intact rock strength and global mass parameters (e.g., GSI and UCS drops in Cases 5 and 6). Consequently, the failure modes consistently manifest as deep-seated rotational or compound slides propagating 14 to 40 meters into the slope mass. Furthermore, the entrapment of pore water pressure—whether artificially induced by impermeable shotcrete facings without adequate deep drainage (Case 1), or naturally occurring due to low-permeability fault clays (Case 2) and uncontrolled surcharging (Case 4)—acts as the primary kinematic trigger, rapidly eroding effective shear strength and driving the slopes from dormant creep to active failure.

A critical comparative finding across the remediation strategies is the absolute kinematic incompatibility of standard, shallow structural support in these environments. The back-analyses explicitly demonstrated that conventional 3.0 to 4.0-meter pattern rock bolts were fundamentally obsolete, acting merely as "floating" elements within the massive, deep-seated active sliding arcs (Cases 1 and 3). Instead, successful stabilization strictly necessitated two divergent but highly effective approaches based on site constraints: deep active reinforcement or massive passive structural restoration. Where spatial constraints required the retention of steep profiles, deep, high-capacity actively prestressed anchors (15–35 m) socketed well into competent bedrock were mandatory to modify the internal stress field (Case 1). Conversely, in highly fragmented, weak matrices where internal anchorage was unfeasible, physical stability was achieved through topographic restoration and mass weighting. Interventions such as massive rockfill toe buttresses (Case 2), cut-and-cover concrete conduits (Case 3), and rigorous geometric flattening combined with stone masonry retaining walls (Case 4) provided the unparalleled passive resistance required to neutralize massive geohazards.

Analytically, the cross-case synthesis reveals a stark divergence between simplified conservative screening models and true physical field performance, heavily influencing Factor of Safety (FS) trends. Conventional limit equilibrium and pseudo-static evaluations frequently projected overly pessimistic outcomes that either failed to materialize or dictated massive "over-engineering." For instance, in Case 3, theoretical pseudo-static models predicted catastrophic failure (FS < 0.7) under an extreme 0.48g seismic load, yet the physical slopes exhibited absolute resilience, indicating that simplified models drastically neglect the high hysteretic damping capacity of clay-rich mélange matrices. Similarly, in Case 6, relying on instantaneous Level 1 rapid drawdown (RDD) assumptions falsely forced the theoretical necessity of highly expensive 12.0-meter anchoring systems; however, rigorous Level 2 transient seepage modeling proved that the slope's inherent time-dependent pore pressure dissipation naturally maintained a stable FS (> 1.50) without structural intervention.

Ultimately, these six cases collectively demonstrate that reliance on deterministic, "dry" parameters and standard constructive support protocols is critically inadequate for hydraulic infrastructure situated in complex geology. The stabilization of such slopes demands an adaptive, deformation-based approach that couples rigorous hydrogeological management with advanced numerical methods capable of capturing realistic soil-structure interactions and transient hydraulic behaviors, as perfectly exemplified by the "Absolute System Lock-in" achieved dynamically in Case 2. Having established these site-specific kinematic realities and stabilization benchmarks, the fundamental discrepancies between analytical predictions and physical slope performances require broader contextualization. The subsequent chapter (Chapter 5) will critically discuss these divergent analysis methodologies, parameter sensitivities, and the overarching implications of the "Safety Factor Gap" between Limit Equilibrium and Finite Element methods in the realm of modern geotechnical engineering.

To synthesize the findings of this chapter, Table 4.34 presents a comprehensive summary of each case study, outlining the failure mechanisms and the results of the proposed remedial analyses.

Table 4.34. *Comprehensive summary of geotechnical case studies and remedial analyses*

Case	Site + analysis (loading; initial condition)	Remedial design + final performance
1	Colluvium (silty/sandy gravel + limestone blocks) over weathered clayey limestone; deep rotational → shear band at bedrock; trapped high pore pressures. LEM (Slide2), FEM (PLAXIS 2D); static back-analysis (sat., r_u = 0.15) + pseudo-static (k_h = 0.22). FS ≈ 1.0 (sat. back-calculated 0.94–1.01; active).	Unloading excavation + pre-stressed anchored beams + soil nails/rock bolts + shotcrete + deep horizontal drains. Static FS = 1.60–1.73; Seismic FS = 1.01–1.45; max permanent disp. ≈ 20 cm (< 1.0 m).
2	Tectonized ophiolitic mélange (serpentinite/peridotite) + pelagic sediments; residual fault-clay interfaces; nested rotational/translational with locked segments. LEM (Slide2), FEM (PLAXIS 2D); static back-analysis + fully coupled dynamic time-history (6 records, scaled to 0.56 g). FS ≈ 0.91 (FEM); 0.96–1.06 (LEM) (actively unstable).	Massive rockfill toe buttress (HS-Small) for passive mass-weighting. Static FS = 1.10; post-earthquake FS ≈ 1.10 (system lock-in); permanent disp. 3.7–21.2 cm (acceptable).
3	Ophiolitic bimrock; matrix rapidly argillizes/weakens on exposure; surficial wasting → deep rotational sliding. LEM (Slide2), FEM (SAP2000 for conduit); static back-analysis + pseudo-static (OBE k_h = 0.14; checks up to 0.48). FS ≈ 1.18 (unsupported; unstable → portal closure).	Cut-and-cover RC conduit + compacted granular backfill (1V:2H) + drained rockfill cover. Static FS = 1.50–1.51; Pseudo-static FS = 1.13–1.18 (k_h = 0.14); physically stable post-2023 earthquakes despite extreme analytical predictions.
4	Allochthonous ophiolitic mélange/flysch; deep weathering (thick residual soil); compound (rotational + saturated flow) from toe excavation, crest surcharge, seasonal saturation. LEM (Slide2: Bishop/Spencer/GLE); static back-analysis (elevated u) + pseudo-static (k_h = 0.18). FS ≈ 1.0 (back-calculated 1.02–1.12; transitioning to active).	Reshaping (1V:3H) + crest unloading + masonry gravity toe walls + comprehensive drainage. Static FS = 1.57–1.67; Pseudo-static FS = 1.03–1.12 (marginally compliant).

Table 4.34. (Continued) *Comprehensive summary of geotechnical case studies and remedial analyses*

Case	Site + analysis (loading; initial condition)	Remedial design + final performance
5	Granodiorite with deep saprolitization; moisture-sensitive; deep circular shear in weak saprolite at inlet + downstream weathering/spalling. FEM (RS2, SSR); static + pseudo-static ($k_h \approx 0.15$ from 0.30 g PGA). Inlet: Static FS = 1.14; pseudo-static FS < 1.00.	Zoned stabilization: flattening (1V:1.33H) + deep reinforcement (12.0 m φ32 mm rock bolts) in saprolite; shotcrete/wire mesh in competent rock. Inlet: Static 1.69, Seismic 1.09; Downstream: Static 2.56, Seismic 1.62.
6	Permeable limestone over low-permeability clay-rich complex; reduced effective stress + phreatic lag during rapid drawdown. Level 1: LEM (instantaneous RDD). Level 2: transient FEM seepage (Slide2). Loading: RDD 32 m / 270 days. Level 1 FS = 0.79–0.84 (theoretical failure).	Level 1 suggested heavy support (12.0 m φ32 mm bolts), but Level 2 shows natural drainage capacity sufficient → deep support redundant. Level 2 transient FS = 1.63–1.80 (stable under realistic transient seepage).

5. DISCUSSION

Building upon the site-specific numerical modeling, back-analyses, and observational data presented in Chapter 4, this chapter synthesizes the analytical findings of this dissertation within the broader context of the geotechnical literature established in Chapter 2. By comparing the diverse failure mechanisms, analytical discrepancies, and remediation strategies across the six case studies, this discussion highlights the limitations of conventional analytical paradigms, validates advanced numerical approaches, and introduces novel perspectives on the static and dynamic stability assessment of slopes adjacent to appurtenant hydraulic structures.

5.1. Case Comparisons

The six case studies analyzed in this dissertation represent a broad spectrum of geomorphological and hydro-geotechnical challenges common to appurtenant hydraulic structures. A comparative assessment reveals that while each site exhibits unique kinematics, instabilities are universally governed by the interaction between heterogeneous lithologies, spatial variability, and fluctuating hydraulic regimes, which corroborates the foundational principles outlined by Phoon and Kulhawy (1999).

5.1.1. Structural control vs. matrix control (bimrock behavior)

A fundamental distinction arises between failures governed by the internal strength of a weak matrix and those constrained by geological interfaces, directly echoing the literature on rock mass classification for complex formations.

5.1.1.1. Matrix-controlled failures

Case 3 (Ophiolitic Mélange) and Case 5 (Saprolitic Granodiorite) demonstrate typical "block-in-matrix" (bimrock) and saprolitic behavior. In these scenarios, global stability is dictated by the shear strength of the weak, weatherable matrix rather than the competent blocks. This firmly supports the assertions by Marinos and Hoek (2001) that standard classification systems are often inadequate for tectonically disturbed, heterogeneous formations, necessitating customized Geological Strength Index (GSI) approaches.

5.1.1.2. Compound and deep-seated failures

Case 1 (Colluvium) and Case 4 (Flysch Sequence) represent failures where deep weathering profiles dictate the scale of instability. In Case 1, the failure was strictly defined by the deep lithological contact (25 m) between the colluvium and bedrock, requiring residual strength parameterization (c'r = 1 kPa, ϕ'r = 23°). Similarly, Case 4 exhibited a compound mechanism: while surface manifestations presented as shallow flow slides (4.5 m), inclinometer data revealed deep-seated rotational movements (up to 19.0 m). This strongly supports the literature emphasizing that treating pre-existing shear planes with peak strength parameters is highly unconservative, requiring the adoption of fully softened or residual strengths to accurately capture progressive failure, as dictated by Skempton (1964) and Stark et al. (2005).

5.1.2. Hydro-mechanical triggers: infiltration vs. drawdown

The trigger mechanisms observed across the case studies illustrate the multifaceted role of water, universally recognized next to gravity as the most significant factor influencing slope stability.

5.1.2.1. Saturation-induced softening

Case 1 and Case 4 exemplify failures triggered by external saturation (rainfall/snowmelt) and blocked natural drainage. In Case 4, the saturation of the high-plasticity flysch matrix caused a drastic reduction in effective stress, triggering flow-type behavior. This perfectly aligns with the hydro-mechanical coupling principles discussed by Ali et al. (2022) and Gariano and Guzzetti (2016), where rainfall percolation reduces matric suction and diminishes frictional shear strength. In Case 1, the application of a shotcrete layer without adequate deep drainage trapped groundwater, artificially elevating pore water pressures (r_u = 0.15) and triggering collapse.

5.1.2.2. Transient internal pressure

Conversely, Case 6 represents a "bottom-up" instability driven by rapid drawdown (RDD). Unlike the infiltration cases, the critical condition arose from the lag in pore pressure dissipation during reservoir unloading. The findings provide a new perspective by demonstrating that traditional "instantaneous" drawdown assumptions (Level 1) create an "over-engineering trap," whereas physically realistic transient seepage analysis (Level

2) proves that inherent time-dependent drainage often manages the phreatic lag naturally, maintaining stability without massive structural intervention. This extends the discourse on RDD by Fredlund and Rahardjo (1993) by explicitly linking modeling conservatism to financial and structural redundancy.

5.1.3. Active vs. passive stabilization strategies

The remediation approaches adopted across the case studies reveal a strategic divergence based on the stabilization mechanism and the scale of the instability, reinforcing the necessity of a holistic, systems-based approach.

5.1.3.1. Active support (pre-stressed systems)

For deep-seated failures where limiting deformation was critical to preserve adjacent infrastructure, active reinforcement was the governing solution. In Case 1, 35.0 m long pre-stressed anchors were utilized to actively apply clamping loads, modifying the stress field before further deformation occurred, consistent with standard active anchor design philosophies.

5.1.3.2. Passive reinforcement (untensioned internal support)

In Case 5, the shallow global instability within the arenized profile was successfully managed with systematic rock bolting (12.0 m) combined with shotcrete facing. These elements act passively to stitch the weathered zone, conforming to the soil nailing and passive dowel stabilization mechanisms detailed in the literature.

5.1.3.3. Geometric and mass stabilization (external passive measures)

For instabilities where internal reinforcement was technically unfeasible due to "weak matrix" behavior or excessive volume, geometric stabilization proved superior. In Case 2 (Tectonic Mélange), internal reinforcement could not be reliably bonded; thus, a massive rockfill buttress was constructed. In Case 3, the solution was a cut-and-cover conduit with compacted backfill, restoring the natural slope geometry. This supports the literature stating that massive earth buttresses increase the normal force and frictional resistance at the toe, offering the most reliable defense for massive active slides.

5.2. Parameter Sensitivities

Numerical sensitivity analyses and back-calculations reveal that slope stability is governed by a complex interplay of critical parameter groups, frequently subjected to high epistemic uncertainty.

5.2.1. Sensitivity to rock mass degradation (GSI and UCS)

The most profound sensitivity observed in bimrock and sedimentary formations is the degradation of rock mass parameters due to weathering and saturation. In Case 6, the analysis quantified a "saturation-induced softening" mechanism, where the GSI dropped from 34 to 29 and the UCS decreased from 30 MPa to 18 MPa upon saturation. This parametric reduction validates the recommendations by Sönmez and Ulusay (2002) to adjust GSI for moisture content, proving that treating clay-bearing rock masses as static, non-degradable materials yields highly unconservative safety factors. Similarly, in Case 5, the stability was entirely controlled by the depth of the arenatization profile, dropping the FS to a critical 1.14 prior to geometric regrading.

5.2.2. Sensitivity to effective friction angle (ϕ')

In soil-like and colluvial units, stability is governed by the mobilized friction angle. In Case 1, back-analysis revealed that an initial design assumption of $\phi' = 28°$ was unconservative; a reduction to the residual value of $\phi' = 23°$ eroded the safety margin completely. In Case 2, sensitivity analyses on the shear zone interface showed that the variation between peak and residual (ϕ'=18°-20°) strength parameters determined the scale of the required rockfill buttress, emphasizing the necessity of probabilistically defining residual conditions in progressive failure scenarios as highlighted by Stark et al. (2005).

5.2.3. Sensitivity to hydrogeological regime (r_u and phreatic level)

The impact of pore water pressure creates a non-linear "tipping point" for stability. In Case 4, pseudo-static safety factors established a direct correlation with groundwater depth, where a phreatic rise of a few meters disproportionately compromised seismic stability, dropping the FS from 0.84 to 0.69. Even in the absence of a distinct water table in Case 1, introducing a pore pressure ratio (r_u=0.15) to simulate partial saturation from blocked drainage reduced the FS from 1.215 to roughly 1.00, validating the assertion by Hopkins et al. (1975) that unmanaged water is the primary catalyst for mass movements.

5.2.4. Sensitivity to seismic input characteristics

Dynamic analyses revealed that stability is strictly sensitive to the frequency content, energy flux, and duration of the seismic record, not just the Peak Ground Acceleration (PGA). In Case 2, fully coupled time-history analyses utilizing six spectrally matched records (including Elazığ, Düzce, and Kobe) produced varying permanent displacements ranging from approximately 3.7 cm to 21.2 cm. This variability indicates that performance-based design is highly sensitive to total seismic energy (e.g., Arias Intensity), which a singular pseudo-static coefficient cannot capture, corroborating the findings of Jibson (2007) and Kwong and Chopra (2015).

5.3. Differences Between Limit Equilibrium and Finite Element Methods

The comparative implementation of LEM (Slide2) and FEM (RS2/PLAXIS 2D) across the case studies provided critical insights into numerical reliability, corroborating the evolutionary trajectory of slope stability analysis documented by Zienkiewicz et al. (1975) and Griffiths and Lane (1999).

5.3.1. Kinematic freedom vs. predefined geometry

FEM demonstrated superior capability in identifying failure mechanisms without a priori geometric assumptions. In Case 2, while LEM required specific search algorithms to approximate the nested slip surface, FEM Strength Reduction (SRM) naturally localized the shear bands through the weak clayey matrix, revealing a more complex and critical mechanism. Conversely, for simpler rotational failures in homogeneous masses (Case 4), LEM proved computationally efficient and highly accurate.

5.3.2. Soil-structure interaction (active vs. passive)

A fundamental discrepancy was observed in supported scenarios. While LEM simplifies reinforcement into a point force, FEM captures strict stress-strain compatibility. In Case 1, FEM revealed that the 35.0 m pre-stressed anchors actively modified the normal stress distribution and strain localization in the colluvium, a phenomenon LEM cannot physically resolve.

5.3.3. The "Safety Factor Gap" and conservatism

Consistently, FEM-derived safety factors were more conservative than LEM results, confirming recent comparative studies by Babar et al. (2021). In Case 2, the LEM back-analysis yielded a stable upper bound FS of 1.055, whereas the FEM analysis indicated a distinctly critical condition with FS = 0.914—a discrepancy of approximately 13%. This conservatism stems from FEM's ability to simulate localized yielding, progressive failure, and internal stress redistributions prior to the formation of a global slip surface.

5.4. Pseudo-static vs. Time-Dependent Dynamic Methods

The findings highlight a fundamental divergence between the binary "pass/fail" criterion of the conventional pseudo-static approach and the deformation-based reality of time-dependent dynamic analysis, challenging the historical reliance on Terzaghi's (1950) simplified pseudo-static coefficient.

5.4.1. The "0.48g Paradox" (Case 3)

The limitation of the pseudo-static method is starkly illustrated in Case 3. Analytical models utilizing the recorded PGA (0.48g) predicted catastrophic failure (FS < 0.70). However, post-earthquake field inspections revealed absolute physical stability. This discrepancy offers a novel perspective to the literature: the pseudo-static method, by treating transient peak accelerations as sustained static loads, drastically neglects the high hysteretic damping capacity of the clay-rich ophiolitic matrix. It demonstrates that standard pseudo-static analyses are excessively conservative for highly damped bimrocks, supporting arguments for advanced displacement-based evaluations.

5.4.2. Serviceability vs. failure (Case 1 and Case 2)

Time-history analyses in Case 2 demonstrated that temporary yielding does not equate to collapse. Similarly, in Case 1, while pseudo-static results indicated a critical state (FS ≈ 1.0 at k_h=0.22) prior to optimization, rigorous pseudo-static FEM confirmed that the active anchor system restricted cumulative displacements to ≈ 20 cm at the critical base of the cut-and-cover structure. Under the Maximum Design Earthquake (MDE) assumed as having a Peak Ground Acceleration (PGA) of 0.44g, the critical acceleration ratio (k_y/PGA=N/A) is exactly 0.50. According to the empirical sliding block models by

Hynes-Griffin and Franklin (1984), the upper-bound permanent displacement for this ratio is approximately 22 cm.

While the numerical result aligns remarkably well with the empirical upper bound, it is critical to distinguish the fundamental mechanics governing these values. The empirical displacement (u) derived from the Newmark-based charts represents strictly the permanent slip of a rigid block along a predefined failure surface. In contrast, the total displacement computed in PLAXIS 2D using pseudo-static analysis is fundamentally more comprehensive; it encapsulates cumulative deformations from preceding construction and static phases, the continuous superposition of both elastic and plastic strains, and localized volumetric settlements coupled with distributed shear deformations. Consequently, the approximate 20 cm FEM prediction represents a highly realistic, continuum-based response rather than a simplistic rigid-block approximation. By remaining well below general catastrophic failure thresholds (typically defined as ≥ 1.0 m for such infrastructure), these results conclusively prove that the active stabilization measures restrict deformations within tolerable serviceability limits, ensuring robust structural resistance against extreme dynamic demands.

5.4.3. Absolute system lock-in (Case 2)

A completely new perspective introduced in this research is the concept of "Absolute System Lock-in" achieved via passive mass stabilization. In Case 2, time-history analyses using the advanced HS-Small constitutive model revealed that the massive rockfill buttress entirely absorbed the 0.56g dynamic excitation. Post-earthquake stability (ΣMsf = 1.098 to 1.102 across all six records) was practically indistinguishable from the pre-earthquake static baseline (ΣMsf = 1.100). This confirms that a properly dimensioned passive buttress can rigidly lock a deep-seated residual slip surface, preventing any dynamic shear degradation and isolating deformations strictly to superficial kinematic adjustments.

5.5. Support Applications and Real-Field Adaptations

The retrospective analysis demonstrates that stabilization efficacy is strictly governed by the kinematic compatibility between reinforcement length and failure surface depth, demanding a holistic "systems approach" to stabilization.

5.5.1. Kinematic incompatibility of shallow reinforcement

In Case 3 and Case 6, the initially designed 3.0–4.0 m rock bolts proved fundamentally ineffective. Numerical back-analyses revealed that critical failure circles extended 14–25 m deep. Consequently, short bolts merely "floated" within the active sliding mass. This provides a strong validation of literature warning that shallow pattern bolting is futile when deep matrix degradation or massive residual shear interfaces govern the failure plane.

5.5.2. The "Over-Engineering Trap" (Case 6)

Following strict regulatory guidelines (Level 1 rapid drawdown analysis) forced a theoretical requirement for massive 12.0 m, ϕ 32 mm rock bolts. However, implementing Level 2 transient seepage modeling proved the slope was inherently stable due to phreatic lag management. This provides a critical industry perspective: advancing from conservative screening to fully coupled numerical modeling eliminates redundant, multi-million-dollar structural interventions, aligning with modern mandates for cost-benefit optimized geotechnical design (Robson et al., 2024).

5.5.3. The observational method and systems approach

The necessity of real-field adaptation is exemplified by Case 5 and Case 4. In Case 5, the initial steep design (1V:0.33H) was dynamically revised to 1V:1.33H combined with zoned rock bolting based directly on the observed depth of the arenized saprolite. In Case 4, unloading the crest surcharge was combined with extending a shear key and improving drainage. These interventions validate the "Systems Approach" to stabilization (Cornforth, 2005) and the Observational Method: design assumptions in highly weathered geological environments must remain flexible, continuously adapting geometry, hydraulic control, and structural retention to real-time subsurface data to achieve whole-life cost-effective safety.

6. CONCLUSIONS AND RECOMMENDATIONS

This dissertation has successfully achieved its primary research objectives by systematically evaluating the stability of critical excavated slopes surrounding appurtenant hydraulic structures through a multi-methodological framework encompassing six complex case studies. By bridging the critical gap between deterministic limit equilibrium calculations and performance-based dynamic and hydrogeological numerical assessments, this research has provided a comprehensive understanding of the complex failure kinematics governing heterogenous, water-sensitive geomaterials.

6.1. Main Findings of the Thesis

The investigation yielded several pivotal findings regarding the hydro-mechanical behavior and seismic response of complex geological formations. The critical outcomes derived from the analytical and observational data are categorized into static and dynamic stability findings.

6.1.1. Static stability and hydro-mechanical findings

6.1.1.1. Severe hydro-mechanical sensitivity and strength degradation

A primary driver of instability in clay-cemented sedimentary and ophiolitic lithologies is the drastic degradation of rock mass strength upon saturation. Laboratory testing and back-analyses quantified this sensitivity, revealing that the Point Load Index ($I_{s(50)}$) can decrease by over 90% (e.g., from 4.93 MPa to 0.36 MPa in Case 6), accompanied by substantial drops in rock mass parameters, such as the GSI decreasing from 34 to 29 and the UCS dropping by approximately 40% necessitating a 'Dual-State' strength characterization approach. Consequently, conventional designs relying strictly on "dry" or peak parameters are inherently unconservative for hydraulic structures subject to wetting.

6.1.1.2. Deep-seated failure geometry in bimrocks and colluvium

Instabilities in thick colluvial deposits and block-in-matrix (bimrock) formations are predominantly deep-seated, governed by underlying lithological contacts or weak matrix zones rather than superficial weathering. Numerical models and inclinometer data confirmed critical slip surfaces extending from 14 meters (Case 4 and Case 6) up to 40 meters (Case 2) into the slope mass. This kinematic reality renders standard constructive reinforcement methods (e.g., 3.0–4.0 m rock bolts) functionally obsolete, as they merely "float" within the active sliding mass.

6.1.1.3. Transient hydraulic effects and "Pore Pressure Lag"

In low-permeability sedimentary units subjected to Rapid Drawdown (RDD), a critical "pore pressure lag" dictates stability. During rapid reservoir unloading (e.g., a 32 m drop), the inability of the rock mass to dissipate internal pressures synchronously removes the stabilizing hydrostatic force while high destabilizing pore pressures remain within the slope. However, Level 2 transient seepage analyses demonstrated that the inherent time-dependent drainage often manages this lag naturally, preventing the theoretical failure predicted by overly conservative instantaneous (Level 1) assumptions and eliminating the 'over-engineering trap' inherent in simplified models.

6.1.2. Dynamic stability and seismic response findings

6.1.2.1. Dynamic resilience and damping capacity discrepancy

A fundamental discrepancy exists between conventional pseudo-static predictions and real-world physical seismic performance. In Case 3, slopes that were analytically predicted to fail (FS < 0.80) under extreme peak ground accelerations (PGA ≈ 0.48g) during the 2023 Seismic Sequence remained physically stable. This confirms that clay-rich ophiolitic matrices possess a high hysteretic damping capacity, and transient peak inertial forces do not directly translate to large-scale mass displacements, challenging the validity of simplified force-based pseudo-static coefficients for highly ductile materials.

6.1.2.2. "Absolute System Lock-in" via passive mass weighting

Fully coupled time-history dynamic analyses using advanced constitutive models (HS-Small) demonstrated that passive stabilization structures, such as massive rockfill buttresses, can induce an "Absolute System Lock-in". In Case 2, the rockfill buttress entirely absorbed extreme dynamic excitations (0.56g), perfectly preserving the pre-earthquake static safety margin (ΣMsf = 1.100) post-earthquake (ΣMsf ≈ 1.098 - 1.102). This proves that properly dimensioned passive masses can rigidly lock deep-seated residual slip surfaces against dynamic shear degradation.

6.1.2.3. Seismic serviceability tolerances

Advanced numerical simulations—encompassing both fully coupled dynamic and rigorous pseudo-static FEM—validated that permanent earthquake-induced displacements (e.g., the approximate 20 cm continuum-based prediction in Case 1) strongly correlate with the ≈ 22 cm empirical upper-bound limit specifically derived for the site's critical acceleration ratio (N/A = 0.50). By maintaining deformations far below general catastrophic failure thresholds (typically defined as ≥ 1.0 m for massive earth structures, per Hynes-Griffin and Franklin, 1984), these results, along with the findings of the fully-coupled time-history dynamic analysis in Case 2, verify that temporary yielding under extreme seismic loads does not equate to catastrophic structural collapse.

6.2. Application and Stabilization Recommendations from a Field Engineering Perspective

Based on the synthesized numerical data and field observations, the following targeted stabilization recommendations are provided to guide future geotechnical engineering practices for slopes around hydraulic structures:

6.2.1. Transition to deep reinforcement strategies

In geological environments exhibiting thick colluvium or deep weathering profiles (e.g., arenized granodiorites and bimrocks), standard pattern bolting (3.0--6.0 m) is kinematically incompatible. Stabilization must prioritize deep reinforcement strategies designed to extend sufficiently beyond the critical failure plane—specifically maintaining a minimum setback of at least 1.5 m (or 0.2H of the total slope height for anchors) in accordance with FHWA guidelines—to ensure the bond zone is established within competent bedrock.

6.2.1.1. Active support

For critical cuts where strict deformation control is paramount to protect adjacent infrastructure, high-capacity pre-stressed active anchors (up to 35.0 m lengths, as successfully implemented in Case 1) must be utilized to modify the internal stress field.

6.2.1.2. Passive support

In collapsing or running ground conditions where standard borehole stability cannot be maintained, the use of self-drilling IBO bolts should be strictly adopted.

6.2.2. Integrated drainage as a mandatory structural component

Structural support should never serve as the sole line of defense in water-sensitive lithologies. Standard shallow weep holes are frequently bypassed by groundwater in highly permeable blocky colluvium. Therefore, deep horizontal drains must be designed to physically intercept the phreatic surface behind the failure wedge. This active hydrogeological control functions as a primary "stress improver" and is mandatory to mitigate pore pressure lag during rapid drawdown or intense infiltration scenarios.

6.2.3. Geometric stabilization for "Un-Reinforceable" masses

When internal structural reinforcement is technically unfeasible due to the severe degradation of the matrix (e.g., ophiolitic mélanges) or the massive volume of the active landslide, external passive geometric strategies should be prioritized over rigid retention systems.

6.2.3.1. Mass weighting

Implementation of massive rockfill toe buttresses (as in Case 2) to provide unparalleled passive frictional resistance against global sliding.

6.2.3.2. Topographic restoration

Utilization of cut-and-cover reinforced concrete conduits (as in Case 3) to function as a rigid core, allowing the hazard to be buried and the slope restored to a stable, gentle inclination (e.g., 1V:2H) with compacted backfill.

6.2.4. The observational method and adaptive design

The spatial heterogeneity of saprolitic and ophiolitic units makes rigid, preliminary design assumptions highly risky. Engineers must implement the Observational Method, utilizing real-time inclinometer and geodetic monitoring to execute "on-the-fly" adaptations. This proactive approach includes revising slope gradients dynamically (e.g., flattening a failing 1V:0.33H cut to a stable 1V:1.33H profile, as done in Case 5) and extending support lengths immediately as true lithological contacts are revealed during earthworks.

6.3. Scientific Contribution of the Thesis

This dissertation provides a multi-dimensional contribution to the field of geotechnical engineering by explicitly bridging the existing disconnect between theoretical geomechanical principles and the practical execution of complex stabilization measures for slopes adjacent to critical hydraulic infrastructure:

6.3.1. Benchmarking analysis methodologies (The "Safety Factor Gap")

This thesis provides a rare, quantitative benchmarking of Limit Equilibrium (LEM) and Finite Element (FEM) methods applied to identical, highly complex tectonic geometries. By documenting a consistent "safety factor gap" (e.g., FEM yielding results approximately 13% more conservative than LEM in tectonic mélanges in Case 2), this work elucidates the limitations of LEM in capturing localized stress relaxation and progressive failure mechanisms in strain-softening materials.

6.3.2. Validating performance-based seismic design

Through forensic numerical back-analysis of the 2023 Seismic Sequence, the research provides crucial empirical evidence supporting displacement-based dynamic (time-history) analysis over traditional force-based pseudo-static methods. It proves that highly damped ophiolitic matrices can sustain extreme accelerations without collapse, demanding an evolution in how seismic coefficients (k_h) are selected and applied in practice.

6.3.3. Characterization of "Intermediate" geomaterials

The study expands the geotechnical knowledge base on "intermediate" geomaterials—such as arenized saprolites, tectonized flysch, and complex colluvial mixtures—that defy standard soil or rock classification systems. The research captures the "block-in-matrix" behavior often ignored in idealized constitutive models, supplying specific operational parameter ranges for these challenging lithologies.

6.3.4. Holistic evaluation of appurtenant structures

Unlike general slope stability literature, this dissertation isolates the unique boundary conditions of hydraulic appurtenances. It rigorously evaluates the coupled effect of rapid-drawdown forces combined with deep excavation unloading, filling a conspicuous lacuna regarding the specific interactions between rigid concrete hydraulic structures and deformable, water-sensitive geologic masses.

6.4. Recommendations for Future Research

While this dissertation establishes a robust two-dimensional analytical framework, future research should expand upon these findings to further enhance predictive geotechnical capabilities:

6.4.1. 3-D kinematic effects and arching

Hydraulic structures situated within narrow topographical gorges may experience significant lateral confinement and three-dimensional stress redistribution that 2-D plane strain models cannot capture. Future studies should employ 3-D numerical modeling to explicitly represent these spatial confinement ("arching") effects, enabling more rigorous and cost-effective optimization of support systems in valley constrictions and abutment zones.

6.4.2. Long-term creep modeling

Incorporating time-dependent viscoplastic constitutive models within the finite element framework could provide superior insights into the slow-moving, continuous creep mechanisms observed in heavily sheared tectonic mélange zones (e.g., Case 2) over decadal operational timescales.

6.4.3. Probabilistic drawdown analysis

Integrating Monte Carlo simulation with transient seepage analyses would help quantify the reliability of slopes under varying operational drawdown rates, explicitly accounting for epistemic uncertainty in hydraulic conductivity, boundary conditions, and the degradation/variability of shear strength parameters.

6.4.4. Real-time monitoring integration

Future mega-infrastructure projects are strongly encouraged to develop automated "early-warning" systems. By integrating real-time inclinometer and piezometer telemetry with dynamically updated numerical models (digital twins), engineers can establish proactive tools to mitigate construction- and operation-induced risks before they reach critical thresholds.

6.4.5. Climate-resilient stability assessment

Considering the increasing frequency of extreme weather patterns, future models should integrate regional climate change projections into transient seepage analyses. Investigating the impact of PMP (Probable Maximum Precipitation) and multi-day storm sequences on the phreatic surface (z_w) and pore water pressure (u) distribution will be critical for the long-term climate-resilience of hydraulic infrastructure.

6.4.6. Machine learning-aided parameter estimation

To address the inherent uncertainties in geotechnical parameters, future studies could employ hybrid frameworks combining numerical modeling with Machine Learning (ML) algorithms. Deep learning models, such as Physics-Informed Neural Networks (PINNs), could be utilized to back-calculate soil strength parameters from observed slope deformations, thereby enhancing the calibration of complex constitutive models.

REFERENCES

Abrahamson, N. A., Silva, W. J., and Kamai, R. (2014). Summary of the ASK14 ground motion relation for active crustal regions, *Earthquake Spectra, 30,* 1025–1055. https://doi.org/10.1193/070913eqs198m

Abrahamson, N. A. (1992). Non-stationary spectral matching. *Seismological Research Letters*, *63*(1), 30.

Abramson, L. W., Lee, T. S., Sharma, S., and Boyce, G. M. (2002). *Slope stability and stabilization methods* (2nd ed.). John Wiley & Sons.

Agostini, R., Bizzarri, A., Masetti, M., Papetti, A., and Polo, M. (1987). *Flexible gabion and Reno mattress structures in river and stream training works*. Officine Maccaferri.

Ahmed, J., Ghazali, M. A., Mukhlisin, M., Alias, M. N., and Taha, M. R. (2012). Effectiveness of horizontal drains in improving slope stability: A case study of landslide event in Putrajaya Precinct 9, Malaysia. In *Unsaturated Soils: Theory and Practice* (pp. 753–758).

Akin, M. (2013). Slope stability problems and back analysis in heavily jointed rock mass: A case study from Manisa, Türkiye. *Rock Mechanics and Rock Engineering*, *46*(2), 359–371. https://doi.org/10.1007/s00603-012-0262-x

Al-Ameri, S. S., and Al-Ameri, A. S. (2018). Slope stability analysis under rapid drawdown condition and seismic loads of earth dam (Case study: Mandali Dam). *Journal of Engineering and Sustainable Development*, *22*(6), 1–12.

Al Atik, L., and Abrahamson, N. (2010). An improved method for nonstationary spectral matching. *Earthquake Spectra*, *26*(3), 601–617. https://doi.org/10.1193/1.3459159

Al-Homoud, A. S., and Tal, A. B. (1995). Mitigative design for colluvial slope instability, Wadi Es-Sir sewage treatment plant, Jordan. *Environmental and Engineering Geoscience, 1*(3), 313–326. https://doi.org/10.2113/gseegeosci.I.3.313

Al-Homoud, A. S., Tal, A. B., and Taqieddin, S. A. (1997). A comparative study of slope stability methods and mitigative design of a highway embankment landslide with a potential for deep seated sliding. *Engineering Geology*, *47*(1–2), 157–173. https://doi.org/10.1016/S0013-7952(97)00016-1

Al-Homoud, A. S., Tubeileh, F. K., and Hamdan, F. H. (1999). Assessment of slope stability and stabilization measures. *Building and Environment*, *34*(3), 305–318.

Al-Zayadi, A. A. (2022). Slope stability and soil liquefaction analysis of earth dams with a proposed method of geotextile reinforcement. *Journal of Engineering*, *28*(6), 1–18.

Ali, A., ur Rehman, H., and Ajmal, M. (2022). Effect of rainfall on stability of soil slope. *Civil Engineering Journal*, *8*(3), 573–586.

Alonso, E. E., and Pinyol, N. M. (2016). Numerical analysis of rapid drawdown: Applications in real cases. *Water Science and Engineering*, *9*(3), 175–182. https://doi.org/10.1016/j.wse.2016.11.003

Alonso, E. E., and Pinyol, N. M. (2010) Criteria for rapid sliding I. A review of Vaiont case. *Engineering Geology*, *114(*3-4*)*, 198-210.

Alonso, E., and Pinyol, N. M. (2009). Slope stability under rapid drawdown conditions. In *Rainfall-induced landslides: Proceedings of the First Italian Workshop on Landslides* (pp. 11–27). https://upcommons.upc.edu/handle/2117/11200 (accessed June 22, 2025).

Amarasinghe, M. P., Robert, D., Kulathilaka, S. A. S., Zhou, A., and Jayathissa, H. A. G. (2024). Slope stability analysis of unsaturated colluvial slopes based on case studies of rainfall-induced landslides. *Bulletin of Engineering Geology and the Environment*, *83*, Article 476. https://doi.org/10.1007/s10064-024-03933-1

American Association of State Highway and Transportation Officials. (2012). *AASHTO LRFD bridge design specifications* (6th ed.). AASHTO.

American Society of Civil Engineers. (2016). *Minimum design loads and associated criteria for buildings and other structures* (ASCE/SEI 7-16).

American Society of Civil Engineers. (2023). *Seismic evaluation and retrofit of existing buildings* (ASCE/SEI 41-23).

Ancheta, T. D., Darragh, R. B., Stewart, J. P., Seyhan, E., Silva, W. J., Chiou, B. S.-J., Wooddell, K. E., Graves, R. W., Kottke, A. R., Boore, D. M., Kishida, T., and Donahue, J. L., (2014). NGA-West2 database, *Earthquake Spectra*, *30*, 989–1005. https://doi.org/10.1193/070913eqs197m

Anderson, D. W., & Bass, A. (2008). *A dam incident at Sugar Creek Site L44*. In *Association of State Dam Safety Officials annual conference proceedings*. https://damfailures.org/sites/default/files/wp-content/uploads/2018/10/A-Dam-Incident-at-Sugar-Creek-L-44.pdf (accessed June 17, 2025).

Ang, A. H. S., and Tang, W. H. (1975). *Probability concepts in engineering planning and design, Vol. I: Basic principles*. John Wiley & Sons.

Arias, A. (1970). A measure of earthquake intensity. In R. J. Hansen (Ed.), *Seismic design for nuclear power plants* (pp. 438–483). MIT Press.

Armstrong, R., Kishida, T., and Park, D. S. (2021). Efficiency of ground motion intensity measures with earthquake-induced earth dam deformations. *Earthquake Spectra*, *37*(1), 5–25. https://doi.org/10.1177/8755293020938811

Ashford, S. A., and Sitar, N. (1997). Analysis of topographic amplification of inclined shear waves in a steep coastal bluff. *Bulletin of the Seismological Society of America*, *87*(3), 692–700.

Assaad, R. H., & El-Adaway, I. H. (2020). Evaluation and prediction of the hazard potential level of dam infrastructures using computational artificial intelligence algorithms. *Journal of Management in Engineering, 36*(5), 04020051. DOI: 10.1061/(ASCE)ME.1943-5479.0000810.

ASTM International. (2020). *Standard test methods for prebored pressuremeter testing in soils* (ASTM D4719-20). West Conshohocken, PA. https://doi.org/10.1520/D4719-20

ASTM International. (2011). *Standard test method for standard penetration test (SPT) and split-barrel sampling of soils* (ASTM D1586-11). West Conshohocken, PA.

ASTM International. (2014). *Standard test methods for compressive strength and elastic moduli of intact rock core specimens under varying states of stress and temperatures* (ASTM D7012-14). West Conshohocken, PA.

ASTM International. (2016). *Standard test method for slake durability of shales and other similar weak rocks* (ASTM D4644-16). https://doi.org/10.1520/D4644-16

ASTM International. (2017). *Standard test methods for particle-size distribution (gradation) of soils using sieve analysis* (ASTM D6913/D6913M-17). West Conshohocken, PA.

ASTM International. (2020). *Standard test method for consolidated undrained triaxial compression test for cohesive soils* (ASTM D4767-11(2020)). West Conshohocken, PA.

ASTM International. (2021). *Standard test method for particle-size distribution (gradation) of fine-grained soils using the sedimentation (hydrometer) analysis* (ASTM D7928-21). West Conshohocken, PA.

ASTM International. (2021). *Standard test method for monitoring ground movement using probe-type inclinometers* (ASTM D6230-21). West Conshohocken, PA.

Azadi, A., and Momayez, M. (2024). Review on Constitutive Model for Simulation of Weak Rock Mass. *Geotechnics*, *4*(3), 872–892. https://doi.org/10.3390/geotechnics4030045

Azarafza, M., Nikoobakht, S., Rahnamarad, J., Asasi, F., and Derakhshani, R. (2020). An empirical method for slope mass rating-Qslope correlation for Isfahan province, Iran. *MethodsX*, *7*, Article 101069. https://doi.org/10.1016/j.mex.2020.101069

Azeze, A. (2020). Comparison of general limit equilibrium methods for slope stability analysis. *Engineering, Technology & Applied Science Research*, *10*(6), 6482–6487.

Azizi, M. A., Marwanza, I., Hartanti, N. A., Ghifari, M. K., Anugrahadi, A., and Zulfahmi, Z. (2020). Application of Cuckoo Search method in 3D slope stability analysis for limestone quarry mine. *Indonesian Mining Journal*, *23*(2), 57–65. https://doi.org/10.30556/imj.Vol23.No2.2020.1120

Babar, M. S., Israr, J., Ali, S. U., and Gang, Z. (2021). Semi empirical slope stability analyses of Mohmand Dam using limit equilibrium and finite element methods. Preprint. *Research Square*. https://doi.org/10.21203/rs.3.rs-998184/v1

Baecher, G. B., and Christian, J. T. (2003). *Reliability and statistics in geotechnical engineering*. John Wiley & Sons.

Baez, J. I., Alonso, E., De Beer, F., and Van der Veen, C. (1992). Lime/fly ash injection for levee stabilization. *Transportation Research Record*, *1362*, 20–27.

Baguelin, F., Jézéquel, J.-F., and Shields, D. H. (1978). *The pressuremeter and foundation engineering*. Trans Tech Publications.

Bakır, B. S., and Akış, E. (2005). Analysis of a highway embankment failure associated with the 1999 Düzce, Türkiye earthquake. *Soil Dynamics and Earthquake Engineering*, *25*(3), 251–260. https://doi.org/10.1016/j.soildyn.2003.05.001

Baker, J. W. (2008). *Probabilistic seismic hazard analysis*. White paper version 2.0.1. Stanford University.

Baker, J. W. (2011). Conditional mean spectrum: Tool for ground-motion selection. *Journal of Structural Engineering*, *137*(3), 322–331. https://doi.org/10.1061/(ASCE)ST.1943-541X.0000215

Baker, J. W. (2013). *Introduction to probabilistic seismic hazard analysis (PSHA)* (Version 2.0). Stanford University.

Baker, J. W., and Cornell, C. A. (2006). Spectral shape, epsilon and record selection. *Earthquake Engineering & Structural Dynamics*, *35*(9), 1077–1095. https://doi.org/10.1002/eqe.571

Baker, R. and Leshchinsky, D. (1987) "Stability Analysis of Conical Heaps," *Soils and Foundations*, *27*(4), 99-110. https://doi.org/10.3208/sandf1972.27.4_99

Baker, R., Shukha, R., Operstein, V., and Frydman, S. (2006). Stability charts for pseudo-static slope stability analysis. *Soil Dynamics and Earthquake Engineering*, *26*(9), 813–823. https://doi.org/10.1016/j.soildyn.2006.01.023

Baron, I., Cilek, V., Krejci, O., Melichar, R., and Hubatka, F. (2004). Structure and dynamics of deep-seated slope failures in the Magura Flysch Nappe, outer Western Carpathians (Czech Republic). *Natural Hazards and Earth System Sciences*, *4*(4), 549–562.

Barton, N., Lien, R., and Lunde, J. (1974). Engineering classification of rock masses for the design of tunnel support. *Rock Mechanics*, 6(4), 189–236.

Bayati, Z., Saeidi, A., and Payan, M. (2025). Approaches to the stability analysis of slopes subjected to seismic loading: A review. *Results in Engineering*, *26*, 105362. https://doi.org/10.1016/j.rineng.2025.105362

Bazzurro, P., and Cornell, C. A. (1999). Disaggregation of seismic hazard. *Bulletin of the Seismological Society of America*, *89*(2), 501–520.

Bentley Systems. (2023). *PLAXIS 2D material models manual*. Bentley Systems, Incorporated.

Benz, T. (2007). *Small-strain stiffness of soils and its numerical consequences*. Doctoral dissertation. Universität Stuttgart. Institut für Geotechnik, Mitteilung 55.

Berg, R. R., Christopher, B. R., and Samtani, N. C. (2009). *Design and construction of mechanically stabilized earth walls and reinforced soil slopes* (FHWA NHI-10-024, Vol. 1). Federal Highway Administration.

Berg, R. R., Christopher, B. R., & Samtani, N. C. (2009). *Design of mechanically stabilized earth walls and reinforced soil slopes—Volume II* (Report No. FHWA-NHI-10-025). Federal Highway Administration. https://rosap.ntl.bts.gov/view/dot/49730 (accessed June 17, 2025).

Bieniawski, Z. T. (1989). *Engineering rock mass classifications: A complete manual for engineers and geologists in mining, civil, and petroleum engineering*. John Wiley & Sons.

Bieniawski, Z. T. (1973). Engineering classification of jointed rock masses. *Transactions of the South African Institution of Civil Engineers, 15*(12), 335–344.

Birid, K. C. (2015, May). *Interpretation of pressuremeter tests in rock*. Paper presentation. *International Symposium for the 60th Anniversary of the Pressuremeter (ISP7-PRESSIO)*, Tunisia.

Bishop, A. W. (1955). The use of the slip circle in the stability analysis of slopes. *Géotechnique*, *5*(1), 7–17. https://doi.org/10.1680/geot.1955.5.1.7

Bjerrum, L. (1967). Progressive failure in slopes of overconsolidated plastic clay and clay shales. *Journal of the Soil Mechanics and Foundations Division*, *93*(5), 1–49.

Bjerrum, L. (1973). Problems of soil mechanics and construction on soft clays. In *Proceedings of the 8th International Conference on Soil Mechanics and Foundation Engineering* (*Vol. 3*, pp. 111–159), Moscow.

Blacklock, J. R., and Wright, P. J. (1986). Restoration of failed highway embankments by lime-flyash injection. *Transportation Research Record*, (1104), 7–18. https://onlinepubs.trb.org/Onlinepubs/trr/1986/1104/1104.pdf (accessed April 17, 2025).

Bolla, S., and Paronuzzi, P. (2021). Seismic stability of earth-rock dams using finite element limit analysis. *Geosciences*, *11*(4), 154. https://doi.org/10.3390/geosciences11040154

Boore, D. M., Stewart, J. P., Seyhan, E., and Atkinson, G. M. (2014). NGA-West2 equations for predicting PGA, PGV, and 5% damped PSA for shallow crustal earthquakes, *Earthquake Spectra*, *30*, 1057–1085. https://doi.org/10.1193/070113eqs184m

Boore, D. M. (2005). On pads and filters: Processing strong-motion data. *Bulletin of the Seismological Society of America*, 95(2), 745–750.

Boynton, S. S., and Blacklock, J. (1985). Lime stabilization of clay soil slopes by injection. *Ground Engineering*, *18*(4), 10–15.

Bozovic, A. (1989). *Selecting seismic parameters for large dams—Guidelines* (ICOLD Bulletin 72). International Commission on Large Dams. https://damsafety.org/content/selecting-seismic-parameters-large-dams-guidelines (accessed May 12, 2025).

Brabhaharan, P. (2010). Research into seismic design and performance of high cut slopes in New Zealand. In *Proceedings of the 15th World Conference on Earthquake Engineering*. International Society for Soil Mechanics and Geotechnical Engineering.

Bradley, B. A. (2010). A generalized conditional intensity measure approach and holistic ground-motion selection. *Earthquake Engineering & Structural Dynamics*, *39*(12), 1321–1342. https://doi.org/10.1002/eqe.995

Bradley, B. A. (2011). Correlation of significant duration with amplitude and cumulative intensity measures and its use in ground motion selection. *Journal of Earthquake Engineering*, *15*(6), 809–832. https://doi.org/10.1080/13632469.2011.557140

Bradley, B. A. (2012). A ground motion selection algorithm based on the generalized conditional intensity measure approach. *Soil Dynamics and Earthquake Engineering*, *40*, 48–61. https://doi.org/10.1016/j.soildyn.2012.04.007

Bradley, B. A. (2014). *Online open-source applications for ground motion selection using the GCIM method*. Paper presented at the New Zealand Society for Earthquake Engineering (NZSEE) Conference, Auckland, New Zealand.

Bray, J. D., and Macedo, J. (2023). Performance-based seismic assessment of slope systems. *Soil Dynamics and Earthquake Engineering*, *168*, 107835. doi:10.1016/j.soildyn.2023.107835.

Bray, J. D., and Travasarou, T. (2007). Simplified procedure for estimating earthquake-induced deviatoric slope displacements. *Journal of Geotechnical and Geoenvironmental Engineering*, *133*(4), 381–392.

Bray, J. D., and Travasarou, T. (2009). Pseudostatic coefficient for use in simplified seismic slope stability evaluation. *Journal of Geotechnical and Geoenvironmental Engineering*, *135*(9), 1336–1340.

Bray, J. D., and Travasarou, T. (2011). *Pseudostatic slope stability procedure*. New Zealand Geotechnical Society.

Briaud, J.-L. (1989). *The pressuremeter test for highway applications* (Publication No. FHWA-IP-89-008). Federal Highway Administration. https://rosap.ntl.bts.gov/view/dot/74774/dot_74774_DS1.pdf (accessed February 21, 2025).

Brinkgreve, R. B. J. (2021). *PLAXIS 2D – Material models manual*. PLAXIS/Bentley Systems.

British Standards Institution. (1989). *Code of practice for ground anchorages* (BS 8081:1989).

British Standards Institution. (2012). *Geotechnical investigation and testing - Geohydraulic testing - Part 2: Water permeability tests in a borehole using open systems* (BS EN ISO 22282-2:2012).

British Standards Institution. (2015). *Code of practice for ground investigations* (BS 5930:2015).

British Standards Institution. (2018). *Code of practice for grouted anchors* (BS 8081:2015+A2:2018).

Broms, B. B., and Bennermark, H. (1967). Stability of clay at vertical openings. *Journal of the Soil Mechanics and Foundations Division*, *93*(1), 71–94.

Bruce, D. A. (2012, September). 40 years of rock anchors for dams in North America. *Proceedings of the Canadian Dam Association Annual Conference*, Montreal, QC, Canada.

Bruce, D. A., and Juran, I. (1998). *Drilled and grouted micropiles: State-of-practice review*. Federal Highway Administration.

Bruce, D.A., Wolfhope, J.S. (2007). “Rock Anchors for North American Dams: The National Research Program Bibliography and Database,” *Ground Anchorages and Anchored Structures*, Proceedings of the International Conference, Institution of Civil Engineers, London, U.K.

Butterworth, S. (1930). On the theory of filter amplifiers. *Experimental Wireless and the Wireless Engineer*, *7*, 536–541.

Campbell, K. W., and Bozorgnia, Y. (2014). NGA-West2 ground motion model for the average horizontal components of PGA, PGV, and 5% damped linear acceleration response spectra, *Earthquake Spectra*, *30*,1087–1115. https://doi.org/10.1193/062913eqs175m

Campbell, K. W., and Bozorgnia, Y. (2010). A ground motion prediction equation for the horizontal component of cumulative absolute velocity (CAV) based on the PEER-NGA strong motion database. *Earthquake Spectra*, *26*(3), 635–650.

Cao, V. V., Ronagh, H. R., and Baji, H. (2019). Selecting and scaling of energy-compatible ground motion records. *Frontiers in Built Environment*, *5*, 140. https://doi.org/10.3389/fbuil.2019.00140

Cascini, L., Cuomo, S., and Guida, D. (2010). Classification and mechanics of rainfall-induced shallow landslides in coarse-grained soils. *Geomorphology*, *120*(3-4), 200–211.

Cedergren, H. R. (1989). *Seepage, drainage, and flow nets* (3rd ed.). Wiley.

Central Water Commission (CWC). (2017). *Guidelines for instrumentation of large dams* (Doc. No. CDSO_GUD_DS_02_v1.0). Ministry of Water Resources, River Development & Ganga Rejuvenation, Government of India.

Cepero, J. A. (2023). *Saving the Guajataca Dam spillway: Emergency actions and interim risk reduction measures (IRRMs)*. Association of State Dam Safety Officials. https://damfailures.org/wp-content/uploads/2023/02/Cepero_Saving-the-Guajataca-Dam-Spillway.pdf (accessed June 17, 2025).

Chakraborty, R., Dey, A. Probabilistic slope stability analysis: state-of-the-art review and future prospects. *Innov. Infrastruct. Solut. 7*, 177 (2022). https://doi.org/10.1007/s41062-022-00784-1

Chaturvedi, S., and Dutt, D. (2015). Landslide hazard zonation mapping using frequency ratio method in a part of the Himalayas, India. *Natural Hazards, 79*, 109–127.

Chávez, J. A., Landa, E., and Silva, C. (2016). Stability analysis of the right abutment of Tablachaca Dam. *International Journal of Rock Mechanics and Mining Sciences, 85*, 1–10.

Chen, H., Qin, S., Xue, L., Yang, B., and Zhang, K. (2018). A physical model predicting instability of rock slopes with locked segments along a potential slip surface. *Engineering Geology*, *242*, 34–43. https://doi.org/10.1016/j.enggeo.2018.05.012

Chen, Q., and Xia, J. (2016). Real-time dynamic Newmark analysis for earthquake-induced landslide displacements. *Landslides*, *13*(5), 1177–1186. https://doi.org/10.1007/s10346-015-0639-9

Chen, W. F. (1975). *Limit analysis and soil plasticity*. Elsevier.

Chen, X., Li, Y., and Zhang, Z. (2024). Nonlinear seismic response analysis of slopes considering the coupled effect of slope geometry and soil stratigraphy. *Geophysical Journal International*, *238*(1), 616–630.

Chiaradonna, A. (2022). Defining the boundary conditions for seismic response analysis—A practical review of some widely-used codes. *Geosciences, 12*(2), 83. doi:10.3390/geosciences12020083.

Chiou, B. S.-J., and Youngs, R. R. (2014). Update of the Chiou and Youngs NGA model for the average horizontal component of peak ground motion and response spectra, *Earthquake Spectra, 30*, 1117–1153. https://doi.org/10.1193/072813eqs219m

Cho, Y., and Rathje, E. (2022). Generic predictive model of earthquake-induced slope displacements derived from finite element analysis. *Journal of Geotechnical and Geoenvironmental Engineering*, *148*(4), 04022012.

Christian, J. T., Ladd, C. C., and Baecher, G. B. (1994). Reliability applied to slope stability analysis. *Journal of Geotechnical Engineering*, *120*(12), 2180–2207.

Clague, J. J., and Stead, D. (Eds.). (2012). *Landslides: Types, mechanisms, and modeling*. Cambridge University Press.

Claret, F., Prasianakis, N. I., Baksay, A., et al. (2024). EURAD state-of-the-art report: development and improvement of numerical methods and tools for modeling coupled processes in the field of nuclear waste disposal. *Frontiers in Nuclear Engineering*, *3*. https://doi.org/10.3389/fnuen.2024.1437714

Clayton, C. R. I., Milititsky, J., and Woods, R. I. (1993). *Earth pressure and earth-retaining structures* (2nd ed.). Blackie Academic & Professional.

Coe, J. T., Brandenberg, S. J., Ahdi, S., & Kordaji, A. (2018). *Geophysical methods for determining the geotechnical engineering properties of earth materials*. California Department of Transportation. https://dot.ca.gov/-/media/dot-media/programs/research-innovation-system-information/documents/final-reports/ca17-2111-finalreport-a11y.pdf (accessed June 17, 2025).

Collin, J. G., Leshchinsky, D., and Hung, C.-J. (2005). *Soil slope and embankment design: Reference manual* (Publication No. FHWA NHI-05-123). Federal Highway Administration.

Conte, E., Donato, A., and Troncone, A. (2014). Two- and three-dimensional numerical analysis of the progressive failure that occurred in a slope of stiff clay. *Engineering Geology*, *183*, 205–214.

Cornell, C. A. (1968). Engineering seismic risk analysis. *Bulletin of the Seismological Society of America*, *58*(5), 1583–1606.

Cornforth, D. H. (2005). *Landslides in practice: Investigation, analysis, and remedial/preventative options in soils*. Wiley.

Cruden, D. M., and Varnes, D. J. (1996). Landslide types and processes. In A. K. Turner and R. L. Schuster (Eds.), *Landslides: Investigation and mitigation* (Special Report 247, pp. 36–75). Transportation Research Board, National Research Council.

Cundall, P. A. (1988). Formulation of a three-dimensional distinct element model—Part I. A scheme to detect and represent contacts in a system composed of many polyhedral blocks. *International Journal of Rock Mechanics and Mining Sciences & Geomechanics Abstracts*, *25*(3), 107–116.

Cundall, P. A., and Strack, O. D. L. (1979). A discrete numerical model for granular assemblies. *Géotechnique*, *29*(1), 47–65.

Das, B. M. (1998). *Principles of geotechnical engineering* (4th ed.). PWS Publishing Company.

Das, B. M. (2010). *Principles of foundation engineering* (7th ed.). Cengage Learning.

Das, S., and Maheshwari, B. K. (2022). Topographic amplification of seismic ground motion in hills. In *Proceedings of the 4th International Conference on Performance Based Design in Earthquake Geotechnical Engineering (Beijing 2022)* (*Vol. 52*). Springer Nature. https://doi.org/10.1007/978-3-031-11898-2_63

Dávalos, H., and Miranda, E. (2019). Evaluation of bias on the probability of collapse from amplitude scaling using spectral-shape-matched records. *Earthquake Engineering & Structural Dynamics*, *48*(8), 970–986. https://doi.org/10.1002/eqe.3161

Dawson, E. M., Roth, W. H., and Drescher, A. (1999). Slope stability analysis by strength reduction. *Géotechnique*, *49*(6), 835–840.

Deere, D. U. (1968). Geological considerations. In K. G. Stagg and O. C. Zienkiewicz (Eds.), *Rock mechanics in engineering practice* (pp. 1-20). Wiley.

Deere D. U., Deere D. W. (1989) Rock quality designation (RQD) after twenty years. U.S. Army Corps of Engineers Contract Report GL-89-1. Waterways Experiment Station, Vicksburg, MS 67.

Dennis, N. D., and Nguyen, H. N. (2015). *Geosynthetic drains for slope stability and rehabilitation* (Final Report TRC-0506). Arkansas Department of Transportation.

Deoda, V., Adhikary, S., and Raju, V. S. (2020). Seismic analysis of earthen dams subjected to spectrum compatible and conditional mean spectrum time histories. *Jordan Journal of Civil Engineering*, *14*(1), 82–96. https://jjce.just.edu.jo/ (accessed June 17, 2025).

Dhakal, R. P., Singh, S., and Mander, J. B. (2007). Effectiveness of earthquake selection and scaling method in New Zealand. *Bulletin of the New Zealand Society for Earthquake Engineering*, *40*(3), 160–171.

Deravi, G., Tayyari, S., Hafezquran, A., and Mahrofi, A. (2021, February 24–27). *A study of Lugeon test distribution and uncertainty, with an overview to the test advantage and limitation*. Paper presentation. 5th Asia-Pacific Group - International Symposium on Water and Dams, New Delhi, India.

Desjarlais, C. (2022). *Analysis of piezometer measurements and stratigraphy at Sugar Lake Dam*. Master's thesis. University of British Columbia. UBC cIRcle. https://dx.doi.org/10.14288/1.0406301 (accessed October 01, 2025).

Ding, Y., Xu, Y., and Miao, H. (2024a). Mathematical and physical characteristics of the phase spectrum of earthquake ground motions. *Buildings*, *14*(5), 1250. https://doi.org/10.3390/buildings14051250

Ding, C., Xue, K., and Zhou, C. (2024b). Case study on long-term deformation monitoring and numerical simulation of layered rock slopes on both sides of Wudongde dam reservoir area. *Scientific Reports*, *14*, 6909. https://doi.org/10.1038/s41598-024-57598-7

Disaster and Emergency Management Presidency (AFAD). (2018). *Türkiye bina deprem yönetmeliği* (TBDY-Turkish building earthquake code). Ministry of Interior.

Dobry, R., Idriss, I. M., and Ng, E. (1978). Duration characteristics of horizontal components of strong-motion earthquake records. *Bulletin of the Seismological Society of America*, *68*(5), 1487–1520. https://doi.org/10.1785/BSSA0680051487

Drucker, D. C. (1952). A more fundamental approach to plastic stress-strain relations. In *Proceedings of the 1st U.S. National Congress of Applied Mechanics* (pp. 487–491), ASME.

Duncan, J. M. (1996). State of the art: Limit equilibrium and finite-element analysis of slopes. *Journal of Geotechnical Engineering*, *122*(7), 577–596. https://doi.org/10.1061/(ASCE)0733-9410(1996)122:7(577)

Duncan, J. M., and Stark, T. D. (1992). Soil strengths from back analysis of slope failures. In *Stability and Performance of Slopes and Embankments II* (pp. 890–904). ASCE.

Duncan, J. M., and Wright, S. G. (2005). *Soil strength and slope stability*. John Wiley & Sons.

Duncan, J. M., Wright, S. G., and Brandon, T. L. (2014). *Soil strength and slope stability* (2nd ed.). John Wiley & Sons.

Dunnicliff, J. (1993). *Geotechnical instrumentation for monitoring field performance*. Wiley.

Dwitya, R., Pratomo, A. H., Cahyadi, T. A., Nugroho, A. R. B., Utomo, D. P., and Sulo, C. (2024). Slope stability monitoring of hydroelectric dam and upstream watershed areas utilizing satellite interferometric synthetic aperture radar (InSAR). *IOP*

Conference Series: Earth and Environmental Science, *1339*(1), Article 012037. https://doi.org/10.1088/1755-1315/1339/1/012037

Dykes, A. P., and Bromhead, E. N. (2021). Lessons from the Vaiont landslide. In M. A. Cabrera, L. F. Prada-Sarmiento, and J. Montero (Eds.), *Proceedings of the 13th International Symposium on Landslides*. International Society for Soil Mechanics and Geotechnical Engineering.

Edil, T. B. (1992). Terraced concrete debris berm for slope stabilization. *Transportation Research Record*, *1343*, 108–113.

Ehrlich, M., da Costa, D. P., and Silva, R. C. (2018). Behavior of a colluvial slope located in Southeastern Brazil. *Landslides*, *15*(8), 1595–1613. https://doi.org/10.1007/s10346-018-0964-6

El-Ramly, H., Morgenstern, N. R., and Cruden, D. M. (2002). Probabilistic slope stability analysis for practice. *Canadian Geotechnical Journal*, *39*(3), 665–683.

Elias, V., and Juran, I. (1991). *Soil nailing for stabilization of highway slopes and excavations* (Report No. FHWA-RD-89/198). Federal Highway Administration.

Erguler, Z. A., and Ulusay, R. (2009). Water-induced variations in mechanical properties of clay-bearing rocks. *International Journal of Rock Mechanics and Mining Sciences*, 46(3), 355-370.

Ermatov, I. I., and Ermatova, Y. S. (2023). Ecological condition of the adjacent territories of the Charvak reservoir in the aftermath of possible earthquakes. *International Journal of Geology, Earth & Environmental Sciences*, *13*, 19–23.

Ersöz, T. (2017). *Kuzey Batı Karadeniz Bölgesi'ndeki (Türkiye) ayrışmanın etkisinde olan çeşitli yol yarmalarının şev stabilitesinin değerlendirmesi (Evaluation of the slope stability of various road cuts under the effect of weathering in the North West Black Sea Region (Türkiye))*. Master's thesis. Middle East Technical University. Avesis.

European Committee for Standardization (CEN). (2004). *Eurocode 7: Geotechnical design - Part 1: General rules* (EN 1997-1:2004).

European Committee for Standardization (CEN). (2004). *Eurocode 8: Design of structures for earthquake resistance* (EN 1998-1:2004).

Failmezger, R. A., Zdinak, A. L., Darden, J. N., and Fahs, R. (2005). Use of rock pressuremeter for deep foundation design. In M. Gambin, J. P. Magnan, and P. Mestat (Eds.), *50 ans de pressiomètres* (50 years of pressuremeters) (Vol. 1, pp. 301–309). Presses de l'ENPC/LCPC.

Fallah, A., and Noferesti, H. (2015). Stability assessment of the Farrokhi earth embankment dam using the pseudo-static and deformation-based methods. *International Journal of Mining and Geo-Engineering*, *49*(2), 205–220.

Fan, X., Scaringi, G., Domènech, G., Yang, F., Guo, Z., Dai, L., He, C., and Xu, Q. (2019). Two large-scale rainfall-induced landslides in the southeastern Tibetan Plateau, China. *Landslides*, *16*(8), 1749–1756.

Fang, K., Tang, H., Li, C., Su, X., An, P., and Sun, S. (2023). Centrifuge modelling of landslides and landslide hazard mitigation: A review. *Geoscience Frontiers, 14*(1), 101493. https://doi.org/10.1016/j.gsf.2022.101493

Fay, L., Akin, M., and Shi, X. (2012). *Cost-effective and sustainable road slope stabilization and erosion control* (NCHRP Synthesis 430). Transportation Research Board.

Federal Emergency Management Agency. (2009). *Quantification of building seismic performance factors* (FEMA P-695). U.S. Department of Homeland Security.

Federal Energy Regulatory Commission (FERC). (2017). *Engineering guidelines for the evaluation of hydropower projects: Chapter 13 - Evaluation of seismic hazards*. Office of Energy Projects.

Federal Energy Regulatory Commission (FERC). (1991). *Engineering guidelines for the evaluation of hydropower projects: Chapter V—Geotechnical investigations and studies (dams, dam sites, or appurtenant structures).* https://www.ferc.gov/sites/default/files/2020-04/chap5.pdf (accessed May 28, 2025).

Federal Energy Regulatory Commission (FERC). (2014). *FERC engineering guidelines: Risk-informed decision making, Chapter R20—Probabilistic seismic hazard analysis*. Draft. https://www.ferc.gov/sites/default/files/2020-04/chapter-R20.pdf (accessed May 21, 2025).

Fell, R., Ho, K. K. S., Lacasse, S., and Leroi, E. (2005). A framework for landslide risk assessment and management. In O. Hungr, R. Fell, R. Couture, and E. Eberhardt (Eds.), *Landslide risk management* (pp. 3–25). Taylor & Francis.

Fell, R., MacGregor, P., Stapledon, D., Bell, G., and Foster, M. (2014). *Geotechnical engineering of dams* (2nd ed.). CRC Press/Balkema.

Fellenius, W. (1936). Calculation of the stability of earth dams. In *Transactions of the 2nd Congress on Large Dams* (*Vol. 4*, pp. 445–462), Washington DC.

Feng, C., and Yin, Y. (2025). Stability and displacement analysis of interlayered soft-hard slopes under seismic loading. *Scientific Reports*, *15*, Article 19260.

Finn, W. D. L. (1988). Dynamic analysis in geotechnical engineering. *Earthquake Engineering & Structural Dynamics*, *17*(4), 591–611. https://doi.org/10.1002/eqe.4290170406

Fluixá-Sanmartín, J., Altarejos-García, L., Morales-Torres, A., & Escuder-Bueno, I. (2018). Review article: Climate change impacts on dam safety. *Natural Hazards and Earth System Sciences, 18*(9), 2471–2488. DOI: 10.5194/nhess-18-2471-2018.

Forbes, K., and Broadhead, J. (2013). *Forests and landslides: The role of trees and forests in the prevention of landslides and rehabilitation of landslide-affected areas in Asia* (RAP Publication 2013/02). Food and Agriculture Organization of the United Nations, Regional Office for Asia and the Pacific.

Foschaar, J. C., Baker, J. W., and Deierlein, G. G. (2012, September 24–28). *Preliminary assessment of ground motion duration effects on structural collapse*. Paper presentation. 15th World Conference on Earthquake Engineering, Lisbon, Portugal.

Foster, M., Fell, R., and Spannagle, M. (2000). The statistics of embankment dam failures and accidents. *Canadian Geotechnical Journal*, *37*(5), 1000–1024. https://doi.org/10.1139/t00-030

Franklin, J. A., and Chandra, R. (1972). The slake-durability test. *International Journal of Rock Mechanics and Mining Sciences & Geomechanics Abstracts*, *9*(3), 325–341. https://doi.org/10.1016/0148-9062(72)90001-0

Fredlund, D. G., and Krahn, J. (1977). Comparison of slope stability methods of analysis. *Canadian Geotechnical Journal*, *14*(3), 429–439.

Fredlund, D. G., and Rahardjo, H. (1993). *Soil mechanics for unsaturated soils*. John Wiley & Sons.

Fu, X., Gu, C.-S., Su, H.-Z., & Qin, X.-N. (2018). Risk analysis of earth-rock dam failures based on fuzzy event tree method. *International Journal of Environmental Research and Public Health*, *15*(5), 886. DOI: 10.3390/ijerph15050886.

Gaidzik, K., Żaba, J., and Ciesielczuk, J. (2020). Tectonic control on slow-moving Andean landslides in the Colca Valley, Peru. *Journal of Mountain Science*, *17*(8), 1807–1825. https://doi.org/10.1007/s11629-020-6099-y

Gariano, S. L., and Guzzetti, F. (2016). Landslides in a changing climate. *Earth-Science Reviews*, *162*, 227–252.

Geli, L., Bard, P. Y., and Jullien, B. (1988). The effect of topography on earthquake ground motion: A review and new results. *Bulletin of the Seismological Society of America*, *78*(1), 42–63.

Gedney, D. S., and Weber, W. G. (1978). Design and Construction of Soil Slopes. In Special Report *176:* Landslides: Analysis and *Control* (R. L. Schuster and R. J. Krizek, eds.), TRB, National Research Council, Washington, D.C., Chapter 8, pp. 172-191.

Gens, A., Hutchinson, J. N., and Cavounidis, S. (1988). Three-dimensional stability analysis of slopes. *Géotechnique, 38*(1), 1–23.

Geotechnical Control Office (GCO). (1984). *Geotechnical manual for slopes* (2nd ed.). Government of Hong Kong.

Geotechnical Control Office. (1984). *Guide to surface drainage in hill slopes*. Hong Kong Government.

Ghafoori, M., Lashkaripour, G. R., and Ghafoori, M. (2011). Stability analysis of the rock slope of the Gabric Dam spillway trench head in south of Iran. *Journal of Earth and Space Physics*, *37*(2), 145–156.

Glueer, F., Mreyen, A.-S., Cauchie, L., Havenith, H.-B., Bergamo, P., Halló, M., and Fäh, D. (2024). Integrating Seismic Methods for Characterizing and Monitoring Landslides: A Case Study of the Heinzenberg Deep-Seated Gravitational Slope Deformation (Switzerland). *Geosciences*, *14*(2), 28. https://doi.org/10.3390/geosciences14020028

Gokceoglu, C., Ulusay, R., and Sonmez, H. (2000). Factors affecting the durability of selected weak and clay-bearing rocks from Türkiye, with particular emphasis on the influence of the number of drying and wetting cycles. *Engineering Geology*, *57*(3-4), 215-237.

Gordan, B., Armaghani, D. J., Hajihassani, M., and Monjezi, M. (2016). Prediction of seismic slope stability using an optimization-based artificial neural network. *Journal of Mining and Environment*, *7*(2), 231–242.

Gou, P., Zhang, S., Xie, H., Chen, W., and Luo, J. (2012). Fully coupled dynamic analysis of an earth dam. *Applied Mechanics and Materials*, *170–173*, 1111–1114.

Goughnour, R. R., Sung, J. T., and Ramsey, J. S. (1991). Slide correction by stone columns. In M. I. Esrig and R. C. Bachus (Eds.), *Deep foundation improvements: Design, construction, and testing* (ASTM STP 1089, pp. 131–147). ASTM International. https://doi.org/10.1520/STP25056S

Gör, M. (2022). Evaluation of a mass movement occurred after slope excavation. *Geotechnical and Geological Engineering*, *40*, 2393–2408. https://doi.org/10.1007/s10706-021-02035-7

Gör, M. (2021). Limit denge analizi (Bishop Yöntemi) ile kütle hareketinin mekanizması ve önlem yapısının analizi: Van ili örneği (Mechanism of mass movement and analysis of precaution structure with limit equilibrium analysis (Bishop's Method): A case study of Van province). *Gümüşhane Üniversitesi Fen Bilimleri Dergisi*, *11*(2), 597–608. https://doi.org/10.17714/gumusfenbil.850560

Gray, D. H., and Sotir, R. B. (1996). *Biotechnical and soil bioengineering slope stabilization: A practical guide for erosion control*. John Wiley & Sons.

Greenwood, J. R., Norris, J., and Wint, J. (2004). Assessing the contribution of vegetation to slope stability. *Geotechnical Engineering*, *157*(4), 199–207. https://doi.org/10.1680/geng.2004.157.4.199

Griffiths, D. V. (1980). *Finite element analyses of walls, footings and slopes*. Doctoral dissertation. University of Manchester.

Griffiths, D. V., and Fenton, G. A. (2004). Probabilistic slope stability analysis by finite elements. *Journal of Geotechnical and Geoenvironmental Engineering*, *130*(5), 507–518.

Griffiths, D. V., and Lane, P. A. (1999). Slope stability analysis by finite elements. *Géotechnique*, *49*(3), 387–403.

Guzzetti, F., Gariano, S. L., Peruccacci, S., Brunetti, M. T., Marchesini, I., Rossi, M., and Melillo, M. (2020). Geographical landslide early warning systems. *Earth-Science Reviews, 200*, 102973. https://doi.org/10.1016/j.earscirev.2019.102973

Han, Y., Liu, H., and Wu, J. (2017). Analysis of the influence of tunnel portal section construction on slope stability. *Geomatics, Natural Hazards and Risk*, *8*(2).

Hancock, J., Watson-Lamprey, J., Abrahamson, N. A., Bommer, J. J., Markatis, A., McCoy, E., and Mendis, R. (2006). An improved method of matching response spectra of recorded earthquake ground motion using wavelets. *Journal of Earthquake Engineering*, *10*(Sup1), 67–89. https://doi.org/10.1080/13632460609350629

Harle, S. M., and Wankhade, R. L. (2025). Machine learning techniques for predictive modelling in geotechnical engineering: A succinct review. *Discover Civil Engineering*, *2*(1), 86.

Harr, M. E. (1987). *Reliability-based design in civil engineering*. McGraw-Hill.

Harrison, J., and Hepler, T. (2019). Spillway chute joints – the devil's in the details. *Journal of Dam Safety, 16*(3). https://damfailures.org/wp-content/uploads/2021/08/Spillway-Chute-Joints-16.3.pdf (accessed June 17, 2025).

Haselsteiner, R., Pamuk, R., and Ersoy, B. (2017). Aspects concerning the shear strength of rockfill material in rockfill dam engineering. *Geotechnik*, *40*(3), 193–203. https://doi.org/10.1002/gete.201600099

Haselton, C. B., Baker, J. W., Stewart, J. P., Whittaker, A. S., Luco, N., and Goulet, C. A. (2010). *Practical guidelines to select and scale earthquake records for nonlinear response history analysis of structures* (U.S. Geological Survey Open-File Report 2010-1068). U.S. Geological Survey.

Hausmann, M. R. (1990). *Engineering principles of ground modification*. McGraw-Hill.

Havenith, H. B., Strom, A., Jongmans, D., Abdrakhmatov, K., Delvaux, D., and Tréfois, P. (2003). Seismic triggering of landslides, Part A: Field evidence from the Northern Tien Shan. *Natural Hazards and Earth System Sciences*, *3*(1/2), 135–149.

Havenith, H.-B., Strom, A., Calvetti, F., and Jongmans, D. (2003). Seismic triggering of landslides. Part B: Simulation of dynamic failure processes. *Natural Hazards and Earth System Sciences*, *3*(6), 663–682. https://doi.org/10.5194/nhess-3-663-2003

Hiller, D. M., and MacNeil, D. J. (2001). *A review of the use of live willow poles for stabilising highway slopes* (TRL Report 508). Transport Research Laboratory.

Hoek, E. (2007). *Practical rock engineering*. E-book. Rocscience. https://www.rocscience.com/assets/resources/learning/hoek/Practical-Rock-Engineering-Full-Text.pdf (accessed August 28, 2025).

Hoek, E. (1999). Support for very weak rock associated with faults and shear zones. In: *Proceedings of the international symposium on rock support and reinforcement practice in mining*, Kalgoorlie, Australia.

Hoek, E., and Bray, J. W. (1981). *Rock slope engineering* (3rd ed.). CRC Press.

Hoek, E., and Brown, E. T. (2019). The Hoek–Brown failure criterion and GSI – 2018 edition. *Journal of Rock Mechanics and Geotechnical Engineering*, 11(3), 445-463.

Hoek, E., and Brown, E. T. (1997). Practical estimates of rock mass strength. *International Journal of Rock Mechanics and Mining Sciences*, *34*(8), 1165–1186. https://doi.org/10.1016/S1365-1609(97)80069-X

Hoek, E., and Brown, E. T. (1980). *Underground excavations in rock*. Institution of Mining and Metallurgy.

Hoek, E., Carranza-Torres, C., and Corkum, B. (2002). Hoek-Brown failure criterion - 2002 edition. In R. Hammah, W. Bawden, J. Curran, and M. Telesnicki (Eds.), *Mining and tunnelling innovation and opportunity: Proceedings of the 5th North American Rock Mechanics Symposium and the 17th Tunnel Association of Canada Conference* (*Vol. 1*, pp. 267–273). University of Toronto Press.

Hoek, E., and Diederichs, M. S. (2006). Empirical estimation of rock mass modulus. *International Journal of Rock Mechanics and Mining Sciences, 43*(2), 203-215.

Hoek, E., and Marinos, P. (2000). Predicting tunnel squeezing problems in weak heterogeneous rock masses. *Tunnels and Tunnelling International*, *32*(11), 45–51.

Holtz, R. D., and Schuster, R. L. (1996). Stabilization of soil slopes. In A. K. Turner and R. L. Schuster (Eds.), *Landslides: Investigation and mitigation* (Transportation Research Board Special Report No. 247, pp. 439–473). National Academy Press.

Hopkins, T. C., Allen, D. L., and Deen, R. C. (1975). *Effects of water on slope stability* (Research Report No. 435). Kentucky Department of Highways.

Houlsby, A. C. (1976). Routine interpretation of the Lugeon water-test. *Quarterly Journal of Engineering Geology and Hydrogeology*, *9*(4), 303–313. https://doi.org/10.1144/gsl.qjeg.1976.009.04.03

Hsieh, S. Y., and Lee, C. T. (2011). Empirical estimation of the Newmark displacement from the Arias intensity and critical acceleration. *Engineering Geology*, *122*(1–2), 34–42. https://doi.org/10.1016/j.enggeo.2010.12.006

Hu, H.-P., Jiang, S.-H., Chen, D., Huang, J.-S., and Zhou, C.-B. (2024). Probabilistic back analysis of slope parameters and reliability evaluation using improved Bayesian updating method. *Rock and Soil Mechanics*, *45*(3), 835–845. https://doi.org/10.16285/j.rsm.2023.5485

Huang, Y. H. (2014). *Slope stability analysis by the limit equilibrium method: Fundamentals and methods*. American Society of Civil Engineers Press.

Huang, Y.-N., Whittaker, A. S., and Luco, N. (2011). Assessing adequacy of spectrum-matched ground motions for response history analysis. *Earthquake Engineering & Structural Dynamics*, *40*(2), 113–129.

Hungr, O. (1987). An extension of Bishop's simplified method of slope stability analysis to three dimensions. *Géotechnique*, *37*(1), 113–117.

Hungr, O., Salgado, F. M., and Byrne, P. M. (1989). Evaluation of a three-dimensional method of slope stability analysis. *Canadian Geotechnical Journal*, *26*(4), 679–686.

Husid, R. (1969). Análisis de terremotos: Análisis general. *Revista del IDIEM*, 8, 21-42. Santiago, Chile.

Hynes-Griffin, M. E., and Franklin, A. G. (1984). *Rationalizing the seismic coefficient method* (Miscellaneous Paper GL-84-13). U.S. Army Corps of Engineers Waterways Experiment Station.

Idriss, I. M. (2014). An NGA-West2 empirical model for estimating the horizontal spectral values generated by shallow crustal earthquakes, *Earthquake Spectra*, *30*, 1155–1177. https://doi.org/10.1193/070613eqs195m

Idriss, I. M., and Boulanger, R. W. (2008). *Soil liquefaction during earthquakes*. Earthquake Engineering Research Institute.

Independent Forensic Team. (2018). *Independent forensic team report: Oroville Dam spillway incident*. Association of State Dam Safety Officials & United States Society on Dams.

International Organization for Standardization. (2019). *Geotechnical investigation and testing — Laboratory testing of soil — Part 11: Permeability tests* (ISO Standard No. 17892-11:2019).

International Society for Rock Mechanics. (1981). *Rock characterization, testing and monitoring: ISRM suggested methods* (E. T. Brown, Ed.). Pergamon Press.

Irinyemi, A. K., Owusu, A., and Atsu, D. K. (2021). Dynamic stability of large embankment dams and a case study. *International Journal of Advanced Research*, *9*(10), 639–655. http://dx.doi.org/10.21474/IJAR01/13532

Itasca. (2024a). *Dynamic modeling considerations*. In *FLAC3D 9.1 documentation*. https://docs.itascacg.com/itasca910/flac3d/docproject/source/options/dynamic/considerations/considerations.html (accessed January 20, 2025).

Itasca. (2024b). *Dynamic damping*. In *FLAC3D 9.1 documentation*. https://docs.itascacg.com/itasca910/flac3d/docproject/source/options/dynamic/considerations/considerations.html (accessed January 20, 2025).

Ito, T., and Matsui, T. (1975). Methods to estimate lateral force acting on stabilizing piles. *Soils and Foundations*, *15*(4), 43–59.

Janbu, N. (1954) Application of Composite Slip Surface for Stability Analysis. In: *Proceedings of European Conference on Stability of Earth Slopes*, Sweden, 43-49.

Japan Landslide Society. (2008). *Landslides in Japan*. National Conference of Landslide Control.

Jefferies, M. G. (1993). Nor-Sand: A simple critical state model for sand. *Géotechnique*, *43*(1), 91–103.

Jeng, C.-J., and Lin, T.-A. (2011). A case study on the in-situ matrix suction monitoring and undisturbed-sample laboratory test for the unsaturated colluvium slope. *Soils and Foundations*, *51*(2), 321–331. https://doi.org/10.3208/sandf.51.321

Ji, J., Zhang, C., Gao, Y., and Low, B. K. (2010). Practical reliability analysis of slope stability by advanced Monte Carlo simulations in a spreadsheet. *Canadian Geotechnical Journal*, *47*(8), 902–913.

Jia, Y., Luan, S., Asheghabadi, M. S., Xing, D., Yuan, H., and Liu, J. (2024). Slope stability analysis of coastal geotechnical structures under combined effects of earthquake and rainfall. *Frontiers in Earth Science, 11*, 1335756. https://doi.org/10.3389/feart.2023.1335756

Jibson, R. W. (1993). Predicting earthquake-induced landslide displacements using Newmark's sliding block analysis. *Transportation Research Record*, *1411*, 9–17.

Jibson, R. W. (2011). Methods for assessing the stability of slopes during earthquakes—A retrospective. *Engineering Geology*, *122*(1–2), 43–50.

Kalatehjari, R., and Ali, N. (2013). The comparison between 2-D and 3-D slope stability analysis based on reinforcement requirements. *Electronic Journal of Geotechnical Engineering*, *18*, 2795–2804.

Kamran, M. (2023). *Predictive modeling of slope stability using hybrid machine learning approaches: PCA-GMM based WOA-XGBoost*. Preprint. Research Square. https://doi.org/10.21203/rs.3.rs-3726217/v1

Karaman, K., Özyazıcıoğlu, Ş., and Kesimal, A. (2015). Bir kireçtaşı ocağında şev stabilitesi durum çalışmalarının değerlendirilmesi (Evaluation of slope stability case studies in a limestone quarry). *Avrupa Bilim ve Teknoloji Dergisi*, *2*(4), 118–122.

Karikari-Yeboah, O., and Gyasi-Agyei, Y. (2000). *Stability of slopes characterized by colluvium: Investigation, analysis and stabilization.* GeoEng 2000:105, International Conference on Geotechnical and Geological Engineering.

Karol, R. H. (2003). *Chemical grouting and soil stabilization* (3rd ed.). Marcel Dekker.

Kasani, H. A., and Selvadurai, A. P. S. (2023). *A review of techniques for measuring the Biot coefficient and other effective stress parameters for fluid-saturated rocks*. *Applied Mechanics Reviews*, *75*(2), 020801. https://doi.org/10.1115/1.4055888

Kaya, A. (2019). Yamaç duraylılığı araştırmalarında 2D ve 3D FEM-SSR yöntemlerinin uygulanması: Borçka (Artvin) yöresinden örnek bir çalışma (Application of 2D and 3D FEM-SSR methods in slope stability investigations: A case study from Borçka (Artvin) region). *Gümüşhane Üniversitesi Fen Bilimleri Dergisi*, *9*(2), 272–283. https://doi.org/10.17714/gumusfenbil.428667

Keefer, D. K. (1984). Landslides caused by earthquakes. *Geological Society of America Bulletin*, *95*(4), 406–421.

Khakimov, K. A., Janizakova, G. M., Sharipov, S. M., Safarov, E., and Boymurodov, D. O. (2024). Exploring the classification, dynamics, and control measures of landslide processes in the Charvak free tourist zone. In *PAMIR-2 2023 Proceedings* (pp. 1033–1036). Scitepress. https://doi.org/10.5220/0012949100003882

Klimeš, J., Novotný, J., Cochacin Rapre, A., Balek, J., Zahradníček, P., Strozzi, T., Sana, H., Frey, H., René, M., Štěpánek, P., Meitner, J., and Junghardt, J. (2021). Paraglacial rock slope stability under changing environmental conditions, Safuna Lakes, Cordillera Blanca Peru. *Frontiers in Earth Science*, *9*, 607277. https://doi.org/10.3389/feart.2021.607277

Klimeš, J., Novotný, J., Balek, J., Hanzlík, P., Cochacin Rapre, A., Štěpánek, P., Strozzi, T., and Hovadik, J. (2024). Landslide hazard assessment and risk reduction in the rural community of Rampac Grande, Cordillera Negra, Peru. *Environmental Earth Sciences*, *83*, 27. https://doi.org/10.1007/s12665-023-11307-1

Klimeš, J., Vilímek, V., and Opluštil, D. (2012). Implications of geomorphological research for the assessment of natural hazards in the Safuna Lakes area (Cordillera Blanca, Peru). *Geomorphology*, *156*, 69–84.

Koerner, R. M. (2012). *Designing with geosynthetics* (6th ed.). Xlibris Corporation.

Kolapo, P., Oniyide, G. O., Said, K. O., Lawal, A. I., Onifade, M., and Munemo, P. (2022). An overview of slope failure in mining operations. *Mining, 2*(2), 350–384. https://doi.org/10.3390/mining2020019

Kouroussis, G., Verlinden, O., and Conti, C. (2011). Finite-dynamic model for infinite media: Corrected solution of viscous boundary efficiency. *Journal of Engineering Mechanics*, *137*(7), 509–511. https://doi.org/10.1061/(ASCE)EM.1943-7889.0000250

Kramer, S. L. (1996). *Geotechnical earthquake engineering*. Prentice Hall.

Kropp, A., and Thomas, M. (1992). Partial landslide repair by buttress fill. *Transportation Research Record*, *1343*, 108–113.

Kwong, N. S., and Chopra, A. K. (2015). *Selection and scaling of ground motions for nonlinear response history analysis of buildings in performance-based earthquake engineering* (PEER Report 2015/11). Pacific Earthquake Engineering Research Center.

Landis, T. D., Wilkinson, K. M., Steinfeld, D. E., Riley, S. A., and Fekaris, G. N. (2005). Roadside revegetation of forest highways: New applications for native plants. *Native Plants Journal, 6*(3), 297–305. https://doi.org/10.2979/NPJ.2005.6.3.297

Lazarte, C. A., Robinson, H., Gómez, J. E., Baxter, A., Cadden, A., and Berg, R. (2015). *Geotechnical Engineering Circular No. 7: Soil nail walls reference manual* (Report No. FHWA-NHI-14-007). National Highway Institute, U.S. Department of Transportation.

Lazarte, C. A., Elias, V., Espinoza, R. D., and Sabatini, P. J. (2003). *Geotechnical engineering circular No. 7: Soil nail walls* (Publication No. FHWA-IF-03-017). Federal Highway Administration.

Lee, K. Z.-Z., Gillette, D. R., and Gutierrez, A. (2025). A comparison of return periods of design ground motions for dams from different agencies and organizations. *Infrastructures*, *10*(5), Article 105. https://doi.org/10.3390/infrastructures10050105

Lempérière, F. (2017). Dams and floods. *Engineering*, *3*(1), 144–149. https://doi.org/10.1016/J.ENG.2017.01.018

Leps, T. M. (1970). Review of shearing strength of rockfill. *Journal of the Soil Mechanics and Foundations Division*, *96*(4), 1159–1170. https://doi.org/10.1061/JSFEAQ.0001433

Lewis, L. (2000). *Soil bioengineering: An alternative for roadside management: A practical guide* (Technical Report 0077-1801-SDTDC). U.S. Department of Agriculture, Forest Service, San Dimas Technology and Development Center.

Li, S., Feng, X.-T., Wang, C. Y., and Hudson, J. A. (2013). ISRM suggested method for rock fractures observations using a borehole digital optical televiewer. *Rock Mechanics and Rock Engineering*, *46*(3), 635–644. https://doi.org/10.1007/s00603-012-0344-9

Li, X., Xu, W., and Gao, M. (2021). Characteristics of Arias intensity and Newmark displacement of strong ground motion in Lushan earthquake. *Acta Seismologica Sinica*, *43*(6), 768–786. https://doi.org/10.11939/jass.20200180

Liang, C., Chen, J., Xu, Q., and Li, J. (2023). Evaluation of nonlinear response biases of arch dams due to amplitude scaling via three-component record selection based on conditional spectra. *Engineering Structures*, *287*, Article 116169. https://doi.org/10.1016/j.engstruct.2023.116169

Lin, H., Li, L., Qiang, Y., Zhang, Y., Liang, S., Xu, X., Li, H., and Hu, S. (2024). Sensitivity analysis of slope stability based on eXtreme gradient boosting and SHapley Additive exPlanations: An exploratory study. *Heliyon*, *10*(16), e35871. https://doi.org/10.1016/j.heliyon.2024.e35871

Lin, T., Harmsen, S. C., Baker, J. W., and Luco, N. (2013). Conditional spectrum computation incorporating multiple causal earthquakes and ground-motion prediction models. *Bulletin of the Seismological Society of America*, *103*(2A), 1103–1116.

Littlejohn, G. S., and Bruce, D. A. (1977). *Rock anchors: State of the art*. Foundation Publications.

Liu, F., Qian, F., Liu, J., Guo, C., Liu, H., Deng, Y., and Zhang, M. (2025). Using the Newmark sliding block method to construct the empirical model of permanent displacement for earthquake-induced landslides in China. *Applied Sciences*, *15*(8), Article 4152.

Liu, J., and Feng, D. (2023). A multiscale finite element method for soil-rock mixture. *Frontiers in Materials*, *10*. https://doi.org/10.3389/fmats.2023.1116544

Liu, S. (2009). Application of in situ direct shear device to shear strength measurement of rockfill materials. *Water Science and Engineering*, *2*(3), 48–57. https://doi.org/10.3882/j.issn.1674- 2370.2009.03.005

Liu, S. Y., Shao, L. T., & Li, H. J. (2015). Slope stability analysis using the limit equilibrium method and two finite element methods. *Computers and Geotechnics*, *63*, 291–298. doi:10.1016/j.compgeo.2014.10.008.

Liu, W., Sheng, G., Kang, X., Yang, M., Li, D., and Wu, S. (2024). Slope stability analysis of open-pit mine considering weathering effects. *Applied Sciences*, *14*(18), 8449. https://doi.org/10.3390/app14188449

Liu, Z., L'Heureux, J. S., Glimsdal, S., and Lacasse, S. (2021). Modelling of mobility of Rissa landslide and following tsunami. *Computers and Geotechnics*, *140*, 104388. https://doi.org/10.1016/j.compgeo.2021.104388

Lorig, L. J. (2009, November). *Challenges in current slope stability analysis methods*. In *Slope Stability 2009, Santiago, Chile*. https://www.lopproject.com/wp-content/uploads/2018/12/Challenges-in-current-slope-stability-analysis-methods.pdf (accessed August 28, 2025).

Kuhlemeyer, R. L., and Lysmer, J. (1973). Finite element method accuracy for wave propagation problems. *Journal of the Soil Mechanics and Foundations Division*, *99*(5), 421-427.

Lysmer, J., and Kuhlemeyer, R. L. (1969). Finite dynamic model for infinite media. *Journal of the Engineering Mechanics Division*, *95*(4), 859-877.

Macedo, J., Abrahamson, N., and Bray, J. D. (2019). Arias intensity conditional scaling ground-motion models for subduction zones. *Bulletin of the Seismological Society of America*, *109*(4), 1343–1357. https://doi.org/10.1785/0120180297

Makdisi, F. I., and Seed, H. B. (1978). Simplified procedure for estimating dam and embankment earthquake-induced deformations. *Journal of the Geotechnical Engineering Division*, *104*(7), 849–867. https://doi.org/10.1061/AJGEB6.0000668

Maleki Javan, M. R., Gholami, R., and Khosravi, M. H. (2015). Stability analysis of the rock slope of the Gabric Dam spillway trench head in south of Iran. *Earth and Statistics*, *1*(1), 1–10. https://jes.arakut.ac.ir/article_708803_ca07905918ffd2e2d517e7cd19e936a7.pdf (accessed April 28, 2025).

Malhotra, S., and Lee, T. S. (2008). Reinforcement of slopes for seismic stability. In *Proceedings of the 6th International Conference on Case Histories in Geotechnical Engineering*. Missouri University of Science and Technology. https://scholarsmine.mst.edu/icchge/6icchge/session03/22 (accessed May 20, 2025).

Marinos, P., and Hoek, E. (2001). Estimating the geotechnical properties of heterogeneous rock masses such as flysch. *Bulletin of Engineering Geology and the Environment*, *60*(2), 85-92.

Marinos, V. (2019). A revised, geotechnical classification GSI system for tectonically disturbed heterogeneous rock masses, such as flysch. *Bulletin of Engineering Geology and the Environment*, *78*, 899–912. https://doi.org/10.1007/s10064-017-1151-z

Marinos, V., Marinos, P., and Hoek, E. (2005). The geological strength index: applications and limitations. *Bulletin of Engineering Geology and the Environment*, *64*(1), 55-65.

Matsui, T., and San, K. C. (1992). Finite element slope stability analysis by shear strength reduction technique. *Soils and Foundations, 32*(1), 59–70.

McGuire, R. K. (2004). *Seismic hazard and risk analysis* (MNO-10). Earthquake Engineering Research Institute.

Mejia, L. H., Sun, J. I., & Leung, K. K. (2005). *Seismic upgrade of hydraulic fill dam by buttressing*. *Soil Dynamics and Earthquake Engineering*, *25*(7–10), 571–579. https://doi.org/10.1016/j.soildyn.2004.11.028

Millet, R. A., Lawton, G. M., Repetto, P. C., and Garga, V. K. (1992). Stabilization of Tablachaca Dam landslide. *In R. B. Seed and R. W. Boulanger (Eds.), Stability and performance of slopes and embankments* (*Vol. 2*, pp. 1365–1381). American Society of Civil Engineers, Reston, VA, USA.

Mirus, B. B., Bogaard, T., Greco, R., and Stähli, M. (2025). Invited perspectives: Integrating hydrologic information into the next generation of landslide early warning systems. *Natural Hazards and Earth System Sciences*, *25*(1), 169–182. https://doi.org/10.5194/nhess-25-169-2025

Montgomery, D. R., Schmidt, K. M., Greenberg, H. M., and Dietrich, W. E. (2000). Forest clearing and regional landsliding. *Geology*, *28*(4), 311–314. https://doi.org/10.1130/0091-7613(2000)28<311:FCARL>2.0.CO;2

Moradi, S., Huisman, J. A., Vereecken, H., and Class, H. (2024). Comparing different coupling and modeling strategies in hydromechanical models for slope stability assessment. *Water*, *16*(2), Article 312. https://doi.org/10.3390/w16020312

Morgenstern, N. R., and Price, V. E. (1965). The analysis of the stability of general slip surfaces. *Géotechnique*, *15*(1), 79–93.

Müller, L. (1964). The rock slide in the Vaiont valley. *Rock Mechanics and Engineering Geology*, *2*(1), 148–212.

Naeim, F., Alimoradi, A., and Pezeshk, S. (2004). Selection and scaling of ground motion time histories for structural design using genetic algorithms. *Earthquake Spectra*, *20*(2), 413–426.

Nanehkaran, Y. A., Licai, Z., Chengyong, J., Chen, J., Anwar, S., Azarafza, M., and Derakhshani, R. (2023). Comparative analysis for slope stability by using machine learning methods. *Applied Sciences*, *13*(3), 1555.

Nanehkaran, Y. A., Pusatli, T., Chengyong, J., Chen, J., Cemiloglu, A., Azarafza, M., and Derakhshani, R. (2022). Application of machine learning techniques for the estimation of the safety factor in slope stability analysis. *Water, 14*(22), 3743. https://doi.org/10.3390/w14223743

Narimani, S., Davarpanah, S. M., Bar, N., and Vásárhelyi, B. (2025). Analyzing drill core logging using rock quality designation–60 years’ experience from modifications to applications. *Applied Sciences*, *15*(3), Article 1309. https://doi.org/10.3390/app15031309

NEHRP Consultants Joint Venture. (2011). *Selecting and scaling earthquake ground motions for performing response-history analyses* (NIST GCR 11-917-15). National Institute of Standards and Technology.

Newmark, N. M. (1965). Effects of earthquakes on dams and embankments. *Géotechnique*, *15*(2), 139–160. https://doi.org/10.1680/geot.1965.15.2.139

Ng, C. W. W., and Shi, Q. (1998). A numerical investigation of the stability of unsaturated soil slopes subjected to transient seepage. *Computers and Geotechnics*, *22*(1), 1–28.

Nguyen, T. A. (2021). *A new approach for slope stability analysis: Combining the limit equilibrium method and finite element method*. Master's thesis. Delft University of Technology. TU Delft Repository.

Norbury, D. (2016). *Soil and rock description in engineering practice* (2nd ed.). Whittles Publishing.

Norrish, A., Lo, S., Luke, K., and Lu, P. (1998). *Slope stabilization of a highway cut using soil nails – case study*. Geotechnical Special Publication.

North Carolina Department of Transportation. (2021). *Geotechnical investigation and recommendations manual*. https://connect.ncdot.gov/resources/Geological/Documents/Geotechnical%20Investigation%20and%20Recommendations%20Manual.pdf (accessed August 28, 2025).

Ocak, I. (2008). Estimating the modulus of elasticity of the rock material from compressive strength and unit weight. *Journal of the Southern African Institute of Mining and Metallurgy*, *108*(10), 621–626.

Olgun, M., and Acar, M. H. (2009). Deprem kuvvetleri etkisi altındaki şevlerin stabilitesini etkileyen faktörlerin incelenmesi (Investigation of factors affecting the stability of slopes subjected to earthquake forces). *S.Ü. Mühendislik-Mimarlık Fakültesi Dergisi*, *24*(2), 11-19

Ozyurek, S., Yildiz, A., and Toğrol, E. (2022). A case study on the stability of a tunnel portal in a landslide area. *Geomechanics and Engineering*, *28*(2), 177–187.

Özyürek, Y., Can, A., Acar, K., and Gökçeoğlu, C. (2022). Paleo-heyelan malzemesi içinde açılan tünel portalı için önerilen mühendislik önlemleri ve çözümlemeleri: Bahçe-Nurdağ Tüneli, Türkiye (Proposed engineering measures and analyses for a tunnel portal opened in paleo-landslide material: Bahçe-Nurdağ Tunnel, Türkiye). *Yerbilimleri*, *43*(3), 263-286. https://doi.org/10.17824/yerbilimleri.1078716

Palmström, A. (1982). The volumetric joint count—a useful and simple measure of the degree of rock mass jointing. In *Proceedings of the 4th Congress, International Association of Engineering Geology* (Vol. 2, pp. 221–228).

Palmström, A. (2001). Measurement and characterization of rock mass jointing. In V. M. Sharma and K. R. Saxena (Eds.), *In-situ characterization of rocks* (pp. 49–97). A.A. Balkema.

Palmström, A. and Singh, R. (2001) The Deformation Modulus of Rock Masses: Comparisons between in Situ Tests and Indirect Estimates. *Tunnelling and Underground Space Technology, 16*, 115-131. https://doi.org/10.1016/S0886-7798(01)00038-4

Paolucci, R. (2002). Amplification of earthquake ground motion by steep topographic irregularities. *Earthquake Engineering and Structural Dynamics*, *31*(10), 1831–1853.

Pardeshi, S. S., Singh, R. P., and Kumar, R. (2023). Machine learning in the stochastic analysis of slope stability: A state-of-the-art review. *Archives of Computational Methods in Engineering*, *30*(2), 1–32.

Parmar, S. P. (2025). Contemporary approaches to slope stability back analysis. *Journal of Advances in Geotechnical Engineering*, *8*(3), 13–33. https://doi.org/10.5281/zenodo.15589554

Paronuzzi, P., Rigo, E., and Bolla, A. (2013). Influence of filling–drawdown cycles of the Vajont reservoir on Mt. Toc slope stability. *Geomorphology*, *191*, 75–93.

Paronuzzi, P., Bolla, A., Pinto, D., Lenaz, D., and Soccal, M. (2021). The clays involved in the 1963 Vajont landslide: Genesis and geomechanical implications. *Engineering Geology*, *294*, 106376. https://doi.org/10.1016/j.enggeo.2021.106376

Paz, M. C., Alcalá, F. J., Medeiros, A., Martínez-Pagán, P., Pérez-Cuevas, J., and Ribeiro, L. (2020). Integrated MASW and ERT Imaging for Geological Definition of an Unconfined Alluvial Aquifer Sustaining a Coastal Groundwater-Dependent Ecosystem in Southwest Portugal. *Applied Sciences*, *10*(17), 5905. https://doi.org/10.3390/app10175905

Peck, R. B., and Ireland, H. O. (1953). Investigation of stability problems. *Proceedings of the American Railway Engineering Association*, *54*, 1116–1128.

Phillips, M. (2020, May 12–15). *Keynote lecture: Hydraulic structures – learning from recent (partial) failures and the opportunities they present*. Keynote address. 8th IAHR International Symposium on Hydraulic Structures (ISHS 2020), Santiago, Chile. https://doi.org/10.14264/uql.2020.515

Phoon, K. K., and Ching, J. (2018). *Probabilistic approaches for geotechnical site characterization and slope stability analysis*. Springer.

Phoon, K.-K., and Kulhawy, F. H. (1999). Characterization of geotechnical variability. *Canadian Geotechnical Journal*, *36*(4), 612–624.

Pinyol, N. M., Di Carluccio, G., and Alonso, E. E. (2022). A slow and complex landslide under static and seismic action. *Engineering Geology*, *297*, 106478. https://doi.org/10.1016/j.enggeo.2021.106478

Porterfield, J. A., Cotton, D. M., and Byrne, R. J. (1994). *Soil nailing field inspectors manual* (Report No. FHWA-SA-93-068). Federal Highway Administration.

Poşluk, E., Dalgıç, S., Kuşku, İ., and Apaydın Poşluk, E. (2014). Heyelan ıslahında gereken dayanma kuvvetinin limit denge yöntemi ile belirlenmesi (Determining support force for landslide amendment with limit equilibrium method). *IMO Teknik Dergi*, *25*(1), 6677-6692.

Potts, D. M., and Zdravković, L. (2001). *Finite element analysis in geotechnical engineering: Application*. Thomas Telford. https://doi.org/10.1680/feaigea.27831

Potts, D. M., and Zdravković, L. (1999). *Finite element analysis in geotechnical engineering: Theory*. Thomas Telford.

Poulos, H. G. (1995). Design of reinforcing piles to increase slope stability. *Canadian Geotechnical Journal*, *32*(5), 808–818.

Qu, M., and Dang, F. (2022). Numerical analysis of instability mechanism of a high slope under excavation unloading and rainfall. *Applied Sciences*, *12*(16), 7990. https://doi.org/10.3390/app12167990

Quilodrán, C., and Campaña, J. (2024). *Pseudostatic seismic coefficients for stability analysis of dams, further discussion*. Paper presentation. 17th Pan-American Conference on Soil Mechanics and Geotechnical Engineering (XVII PCSMGE), La Serena, Chile. https://www.issmge.org/uploads/publications/84/130/FV_12_-_MT_2_-_FV.pdf (accessed May 15, 2025).

Rafiei Renani, H., and Cai, M. (2022). Forty-year review of the Hoek-Brown failure criterion for jointed rock masses. *Rock Mechanics and Rock Engineering*, *55*, 439–461.

Ragam, P., Kumar, N. K., Ajith, J. E., Karthik, G., Himanshu, V. K., Machupalli, D. S., and Murlidhar, B. R. (2024). Estimation of slope stability using ensemble-based hybrid machine learning approaches. *Frontiers in Materials*, *11*, 1399978.

Raghuvanshi, T. K. (2017). Plane failure in rock slopes – A review on stability analysis techniques. *Journal of King Saud University - Science*, *31*(1), 101–109. https://doi.org/10.1016/j.jksus.2017.06.004

Ran, S., Zhou, W., Weng, Y., Chi, F., Wang, D., Cao, X., and Ma, G. (2026). Causative environment-informed active landslide detection with InSAR monitoring: Empowering reservoir slope hazard management. *International Journal of Applied*

Earth Observation and Geoinformation, *146*, 105079. https://doi.org/10.1016/j.jag.2025.105079

Ranysakol, T. (2023). Static and pseudostatic analysis of embankment slope stability of Bener Dam, Purworejo Regency, Central Java. *IOP Conference Series: Earth and Environmental Science*, *1233*(1), 012014. https://doi.org/10.1088/1755-1315/1233/1/012014

Rathje, E. M. (2025). Evolution of approaches to evaluate the seismic performance of earth slopes. *Indian Geotechnical Journal*. https://doi.org/10.1007/s40098-025-01181-y

Rathje, E. M., and Antonakos, G. (2011). A unified model for predicting earthquake-induced sliding displacements of rigid and flexible slopes. *Engineering Geology*, *122*(1–2), 51–60.

Rathje, E. M., and Bray, J. D. (1999). An examination of simplified earthquake-induced displacement procedures for earth structures. *Canadian Geotechnical Journal*, *36*(1), 72–87.

Rathje, E. M., and Bray, J. D. (2000). Nonlinear coupled seismic sliding response of earth structures. *Journal of Geotechnical and Geoenvironmental Engineering*, *126*(11), 1002–1014.

Rathje, E. M., and Saygili, G. (2008). Probabilistic seismic hazard analysis for the sliding displacement of slopes: I. Development of seismic hazard curves. *Journal of Geotechnical and Geoenvironmental Engineering*, *134*(6), 804–814.

Regmi, S., and Dahal, R. K. (2024). Consequences of slope instability and existing practices of mitigation in hydropower projects of Nepal. *Geoenvironmental Disasters*, *11*, Article 26. https://doi.org/10.1186/s40677-024-00289-2

Richards, G. L., Schweiger, P. G., & Israel-Devadason, B. P. (2017, September 10–14). What happens downstream stays downstream, or does it? Potential failure modes from spillway exit flows. Paper presented at *Dam Safety 2017 – 34th Annual Conference*, San Antonio, Texas. Association of State Dam Safety Officials. https://damsafety.org/content/what-happens-downstream-stays-downstream-or-does-it-potential-failure-modes-spillway-exit (accessed December 07, 2025).

Riquelme, A. J., Abellán, A., Tomás, R., and Jaboyedoff, M. (2014). A new approach for semi-automatic rock mass joints recognition from 3D point clouds. *Computers & Geosciences*, *68*, 38–52. https://doi.org/10.1016/j.cageo.2014.03.014

Romana, M. (1985). *New adjustment ratings for application of Bieniawski classification to slopes*. In *Proceedings of the International Symposium on the Role of Rock Mechanics in Excavations for Mining and Civil Works* (pp. 49–53). International Society for Rock Mechanics.

Sabatini, P. J., Pass, D. G., and Bachus, R. C. (1999). *Ground anchors and anchored systems for highway structures* (Report No. FHWA-IF-99-015). Federal Highway Administration.

Sánchez-Fernández, J., Fernández-Landa, A., Hernández Cabezudo, Á., and Molina Sánchez, R. (2025). Critical factors for the application of InSAR monitoring in ports. *Remote Sensing*, *17*(23), Article 3900. https://doi.org/10.3390/rs17233900

Salyamova, K., An, E., Nishonov, N., Toshmatov, K., and Turdikulov, K. (2023). Long-term monitoring of earth dam of the Charvak hydroelectric power plant (HPP) considering the water level of the reservoir. *E3S Web of Conferences*, *462*, 02050. https://doi.org/10.1051/e3sconf/202346202050

Sarma, S. K. (1973). Stability analysis of embankments and slopes. *Géotechnique, 23*(3), 423–433. https://doi.org/10.1680/geot.1973.23.3.423

Sarma, S. K. (1975). Seismic stability of earth dams and embankments. *Géotechnique, 25*(4), 743–761. https://doi.org/10.1680/geot.1975.25.4.743

Sari, M., Seren, A., and Alemdag, S. (2020). Determination of geological structures by geophysical and geotechnical techniques in Kırklartepe Dam Site (Turkey). *Journal of Applied Geophysics*, *182*, 104174. doi:10.1016/j.jappgeo.2020.104174

Satıcı, Ö., and Ünver, B. (2015). Assessment of tunnel portal stability at jointed rock mass: A comparative case study. *Computers and Geotechnics*, *64*, 72–82. https://doi.org/10.1016/j.compgeo.2014.11.002

Sasanakul, I., and Gassman, S. (2019). *Deep soil test borings to determine shear wave velocities across South Carolina* (Report No. FHWA-SC-19-04). South Carolina Department of Transportation.

Schanz, T., Vermeer, P. A., and Bonnier, P. G. (1999). The hardening soil model: Formulation and verification. In R. B. J. Brinkgreve (Ed.), *Beyond 2000 in computational geotechnics* (pp. 281–296). Balkema.

Schlosser, F., and Unterreiner, P. (1991). Soil nailing in France: Research and practice. *Transportation Research Record, 1330*, 20–27.

Schofield, A. N., and Wroth, C. P. (1968). *Critical state soil mechanics*. McGraw-Hill.

Seed, H. B., and Idriss, I. M. (1971). Simplified procedure for evaluating soil liquefaction potential. *Journal of the Soil Mechanics and Foundations Division*, *97*(9), 1249–1273.

Seed, H. B., and Lee, K. L. (1966). Liquefaction of saturated sands during cyclic loading. *Journal of the Soil Mechanics and Foundations Division*, *92*(6), 105–134. https://doi.org/10.1061/JSFEAQ.0000913

Seed, H. B., and Martin, G. R. (1966). The seismic coefficient in earth dam design. *Journal of the Soil Mechanics and Foundations Division, 92*(3), 25–58. https://doi.org/10.1061/JSFEAQ.0000871

Seed, R. B., Cetin, K. O., Moss, R. E. S., Kammerer, A. M., Wu, J., Pestana, J. M., Riemer, M. F., Sancio, R. B., Bray, J. D., Kayen, R. E., & Faris, A. (2003). *Recent advances in soil liquefaction engineering: A unified and consistent framework* (Report No. EERC 2003-06). Earthquake Engineering Research Center, University of California, Berkeley.

Serafim, J.L., and Pereira, J.P. (1983). Considerations on the Geomechanical Classification of Bieniawski. In *Proceedings of International Symposium on Engineering Geology and Underground Openings*, Lisbon, Portugal, 1133-1144.

Sevaldson, R. A. (1956). The slide in Lodalen, October 6th, 1954. *Géotechnique, 6*(4), 167–182. https://doi.org/10.1680/geot.1956.6.4.167

Shobeir, H., Mofid, H., and Alavi, S. A. (2017). The effect of reservoir impounding on the stability of the slopes: A case study of the Seymareh Dam reservoir. *Geotechnical and Geological Engineering*, *35*(2), 805–817.

Sidle, R. C., Pearce, A. J., and O'Loughlin, C. L. (1985). *Hillslope stability and land use* (Water Resources Monograph No. 11). American Geophysical Union. https://doi.org/10.1029/WM011

Singh, R., Kaur, H., and Garg, A. (2020). Earth dam slope stability analysis under rapid drawdown condition using finite element method. *International Research Journal of Engineering and Technology*, *7*(10), 825–829.

Skempton, A. W. (1970). First-time slides in over-consolidated clays. *Géotechnique, 20*(3), 320–324. https://doi.org/10.1680/geot.1970.20.3.320

Skempton, A. W. (1964). Long-term stability of clay slopes. *Géotechnique*, *14*(2), 77–102.

Sloan, S. W. (2013). Geotechnical stability analysis. *Géotechnique*, *63*(7), 531–572.

Song, Y., Feng, M., and Chen, P. (2023). Modified minimum principal stress estimation formula based on Hoek–Brown criterion and equivalent Mohr–Coulomb strength parameters. *Scientific Reports*, *13*, Article 6409. https://doi.org/10.1038/s41598-023-33053-x

Sonmez, H., and Ulusay, R. (2002). A discussion on the Hoek-Brown failure criterion and suggested modifications to the criterion verified by slope stability Case Studies. *Bulletin of Earth Sciences Application and Research Centre of Hacettepe University*, *26*, 77-99.

Sonmez, H., and Ulusay, R. (1999). Modifications to the geological strength index (GSI) and their applicability to stability of slopes. *International Journal of Rock Mechanics and Mining Sciences*, *36*(6), 743-760.

Sordo, B., Rathje, E., and Kumar, K. (2024). Sequential hybrid finite element and material point method to simulate slope failures. *Computers and Geotechnics*, *173,* Article 106525.

Somerville, P., Skarlatoudis, A., and Thio, H. K. (2016, November 25–27). *Design ground motion time histories using the conditional mean spectrum*. Paper presentation. Australian Earthquake Engineering Society 2016 Conference, Melbourne, VIC, Australia.

Song, K., Zhang, Y., and Li, J. (2024). Study on construction mechanic characteristics and construction optimization of super-large cross-section tunnel portal under shallow buried depth and asymmetrical loading: A case study in Southwest China. *Frontiers in Earth Science*.

Spencer, E. (1967). A method of analysis of the stability of embankments assuming parallel inter-slice forces. *Géotechnique*, *17*(1), 11–26.

Spiga, M., Mura, M., and Calvi, G. M. (2022). Analysis of ground motion intensity measures and selection techniques for estimating building response. *Applied Sciences*, *12*(23), 12089.

Stark, T. D., and Eid, H. T. (1998). Performance of a 3D slope stability analysis method in practice. In *Slope stability and landslides* (pp. 1-15). ASCE.

Stark, T. D., Choi, H., and McCone, S. (2005). Drained shear strength parameters for analysis of landslides. *Journal of Geotechnical and Geoenvironmental Engineering*, *131*(5), 575–588.

Stark, T. D., Jafari, N. H., and Baghdady, A. (2020). Case history summaries of five slope failures: Missed predictions and lessons learned. In *Geo-Congress 2020: Geotechnical Special Publication, 318* (pp. 206–215). ASCE.

Stead, D., and Wolter, A. (2015). A critical review of rock slope failure mechanisms: The importance of structural geology. *Journal of Structural Geology*, *74*, 1–23. https://doi.org/10.1016/j.jsg.2015.02.002

Steedman, R. S., and Zeng, X. (1990). The influence of phase on the calculation of pseudo-static earth pressure on a retaining wall. *Géotechnique*, *40*(1), 103–112.

Sulsky, D., Chen, Z., and Schreyer, H. L. (1994). A particle method for history-dependent materials. *Computer Methods in Applied Mechanics and Engineering*, *118*(1–2), 179–196.

Sulsky, D., Zhou, S. J., and Schreyer, H. L. (1995). Application of a particle-in-cell method to solid mechanics. *Computer Physics Communications*, *87*(1–2), 236–252.

Şeker, P. N. (2010). *Kırıkkale - Kalecik (Ankara) karayolundaki heyelanın jeoteknik değerlendirmesi (Geotechnical evaluation of the landslide on the Kırıkkale - Kalecik (Ankara) highway).* Master's thesis. Ankara Üniversitesi.

Tanchev, L. (2014). *Dam failures and incidents: A global perspective*. Taylor & Francis.

Taşkıran, T., Aslan Fidan, A. (2019). *Doymamış koşullardaki bir şevin yağış etkisindeki duraylılığını etkileyen parametrelerin incelenmesi (Investigation of parameters affecting the stability of an unsaturated slope under rainfall effect)*. *Teknik Dergi, 30*(5), 9489-9512. https://doi.org/10.18400/tekderg.399877

Taylor, D. W. (1937). Stability of earth slopes. *Journal of the Boston Society of Civil Engineers*, *24*(3), 197–246.

Taylor, D. W. (1948). *Fundamentals of soil mechanics*, Wiley, New York.

Terzaghi, K. (1943). *Theoretical soil mechanics*. John Wiley & Sons, Inc. https://doi.org/10.1002/9780470172766

Terzaghi, K. (1950). Mechanism of landslides. In S. Paige (Ed.), *Application of geology to engineering practice* (Berkey Volume, pp. 83–123). Geological Society of America. https://doi.org/10.1130/berkey.1950.83

Terzaghi, K., and Peck, R. B. (1967). *Soil mechanics in engineering practice* (2nd ed.). John Wiley & Sons.

Toker, M., Kasım, E., and Ünlü, G. (2006). *(Elmadag-Kırıkkale) Ayr.- Kalecik Yolu Km:17+200 Heyelanı İyilestirme Projesi Hazırlanması İşi ((Elmadag-Kırıkkale) Jct.- Kalecik Road Km:17+200 Landslide Remediation Project Preparation Work)*.

Topal, T., and Akin, M. (2009). Geotechnical assessment of a landslide along a natural gas pipeline for possible remediations (Karacabey-Türkiye). *Environmental Geology*, *58*(6), 1339–1352. https://doi.org/10.1007/s00254-008-1630-6

Topsakal, E., and Topal, T. (2015). Slope stability assessment of a re-activated landslide on the Artvin-Savsat junction of a provincial road in Meydancik, Türkiye. *Arabian Journal of Geosciences*, *8*(3), 1769–1786. https://doi.org/10.1007/s12517-013-1210-0

Trifunac, M.D. and Brady, A.G. (1975). On the correlation of seismic intensity scales with the peaks of recorded strong ground motion. *Bulletin of the Seismological Society of America*, *65*, 139-162.

Turkish Standards Institute. (1997). *Design loads for buildings* (Standard No. TS 498).

Turkish Standards Institute. (2000). *Requirements for design and construction of reinforced concrete structures* (Standard No. TS 500).

Turkish Standards Institute. (2006). *Methods of testing soils for civil engineering purposes - Part 2: Determination of mechanical properties* (Standard No. TS 1900-2).

Turkish Standards Institute. (2010). *Natural stones - Test methods - Determination of real density and apparent density, and of total and open porosity* (TS EN 1936).

Turkish Standards Institute. (2013). *Natural stone test methods - Determination of uniaxial compressive strength* (TS EN 1926).

U.S. Army Corps of Engineers (USACE). (1997). *Risk-based analysis in geotechnical engineering for support of planning studies, engineering and design*. US Army Corps of Engineers, Department of the Army, Washington, DC 1997. 20314–100.

U.S. Army Corps of Engineers. (2003). *Slope stability* (EM 1110-2-1902). Department of the Army.

U.S. Army Corps of Engineers. (2016). *Requirements for seismic analysis of dams* (EM 1110-2-6050). Department of the Army.

U.S. Army Corps of Engineers. (2024). *Strong motion instrumentation for civil works projects* (ER 1110-2-103). Department of the Army.

U.S. Bureau of Reclamation (USBR). (2001). *Engineering geology field manual* (2nd ed., Vol. II). U.S. Government Printing Office.

U.S. Bureau of Reclamation. (2021). *Design standards no. 14: Appurtenant structures for dams (spillway and outlet works) (Chapter 3: General Structural Design)*. U.S. Department of the Interior.

Ün, B., and Yıldız, A. (2021). Şev stabilitesi probleminin geri analizle çözümü: Örnek bir vaka (Solution of slope stability problem with back analysis: A case study). Academic Platform *Journal of Engineering and Science*, *9*(1), 174–181. https://doi.org/10.21541/apjes.740867

VandenBerge, D. R., Duncan, J. M., and Brandon, T. L. (2015). Limitations of transient seepage analyses for calculating pore pressures during external water level changes. *Journal of Geotechnical and Geoenvironmental Engineering*, *141*(5), Article 04015011. https://doi.org/10.1061/(ASCE)GT.1943-5606.0001283

Vanmarcke, E. H. (1977). *Probabilistic modeling of soil profiles*. *Journal of the Geotechnical Engineering Division*, *103*(11), 1227–1246. https://doi.org/10.1061/AJGEB6.0000517

Vanmarcke, E. H. (1983). *Random fields: Analysis and synthesis*. MIT Press.

Varnes, D. J. (1978). Landslide types and processes. In R. L. Schuster and R. J. Krizek (Eds.), *Landslides: Analysis and control* (Special Report 176, pp. 11–33). Transportation Research Board.

Vaskou, P., de Quadros, E. F., Kanji, M. A., Johnson, T., and Ekmekci, M. (2019). ISRM suggested method for the Lugeon test. *Rock Mechanics and Rock Engineering*, *52*, 4155–4174. https://doi.org/10.1007/s00603-019-01954-x

Vassileva, M., Motagh, M., Roessner, S., and Xia, Z. (2023). Reactivation of an old landslide in north–central Iran following reservoir impoundment: Results from multisensor satellite time-series analysis. *Engineering Geology*, *327*, 107337. https://doi.org/10.1016/j.enggeo.2023.107337

Vidal, H. (1969). The principle of reinforced earth. *Highway Research Record*, *282*, 1–16.

Wahl, T. L., and Heiner, B. J. (2024). Discharge through open offset joints and cracks in spillway chutes. *Journal of Hydraulic Engineering*, *150*(5). https://doi.org/10.1061/JHEND8.HYENG-13898

Wang, J., Wang, Z., Sun, G., & Luo, H. (2024). Analysis of three-dimensional slope stability combined with rainfall and earthquake. *Natural Hazards and Earth System Sciences*, *24*, 1741–1756. https://doi.org/10.5194/nhess-24-1741-2024

Wang, L. (2013). *Probabilistic back analysis of geotechnical systems*. Master's thesis. Clemson University. TigerPrints. https://open.clemson.edu/all_theses/1727 (accessed July 12, 2025).

Wang, L., Zhang, X., Geng, X., and Lei, Q. (2023). Nodal integration-based particle finite element method (N-PFEM) for poro-elastoplastic modelling of saturated soils under large deformation. *Computers and Geotechnics*, *161*, 105567. https://doi.org/10.1016/j.compgeo.2023.105567

Wang, Y., and Wittel, F. (2026). *Moisture-induced degradation of clay-bearing sandstone*. engrXiv. https://doi.org/10.31224/6381

Washington State Department of Transportation. (2013). *Geotechnical design manual M 46-03: Chapter 4 - Soil and rock classification and logging*. https://wsdot.wa.gov/publications/manuals/fulltext/m46-03/chapter4.pdf (accessed May 12, 2025).

Washington State Department of Transportation. (2022). *Geotechnical design manual* (M 46-03.16).

Whitman, R. V. (1984). Evaluating calculated risk in geotechnical engineering. *Journal of Geotechnical Engineering*, *110*(2), 143–188.

Whitman, R. V., and Bailey, W. A. (1967). Use of computers for slope stability analysis. *Journal of the Soil Mechanics and Foundations Division*, *93*(4), 475–498.

Wu, T. H., McKinnell III, W. P., and Swanston, D. N. (1979). Strength of tree roots and landslides on Prince of Wales Island, Alaska. *Canadian Geotechnical Journal*, *16*(1), 19–33.

Wyllie, D. C. (1992). *Foundations on rock*. E & FN Spon.

Wyllie, D. C. (2018). *Rock slope engineering: Civil applications* (5th ed.). CRC Press.

Wyllie, D. C., and Mah, C. W. (2004). *Rock slope engineering: Civil and mining* (4th ed.). Spon Press.

Wyllie, D. C., and Norrish, N. I. (1996). Stabilization of rock slopes. In A. K. Turner and R. L. Schuster (Eds.), *Landslides: Investigation and mitigation* (Transportation Research Board Special Report 247, pp. 474–504). National Academy Press.

Xanthakos, P. P. (1991). *Ground anchors and anchored structures*. Wiley-Interscience.

Yang, X. S., and Deb, S. (2009). Cuckoo search via Lévy flights. *World Congress on Nature & Biologically Inspired Computing (NaBIC)*, 210-214. IEEE.

Yerro, A., Alonso, E., and Pinyol Puigmartí, N. M. (2013). The material point method: A promising computational tool in geotechnics. In *Proceedings of the 18th International Conference on Soil Mechanics and Geotechnical Engineering*, Paris.

Yerro, A., González-Pérez, C., and Alonso, E. E. (2021). The material point method for the analysis of large-scale landslides: The Aznalcóllar dam failure and the Fundão tailings dam failure. *Engineering Geology*, *294*, 106382. https://doi.org/10.1016/j.enggeo.2021.106382

Yow, J. L., Jr. (1993). Borehole dilatometer testing for rock engineering. In J. A. Hudson (Ed.), *Comprehensive rock engineering: Principles, practice and projects: Vol. 3. Rock testing and site characterization* (pp. 671–682). Pergamon Press. https://doi.org/10.1016/B978-0-08-042066-0.50034-3

Yuan, R., Deng, Q., Cunningham, D., Han, Z., and Zhang, B. (2016). Newmark displacement model for landslides induced by the 2013 Ms 7.0 Lushan earthquake, China. *Frontiers of Earth Science*, *10*(4), 740–750. https://doi.org/10.1007/s11707-015-0547-y

Xing, Z. (1990) Closure: Three-dimensional stability analysis of concave slopes in plan view. *Journal of Geotechnical Engineering*, *116*(2), 345-346.

Zabala, F., and Alonso, E. E. (2011). Progressive failure of Aznalcóllar dam using the material point method. *Géotechnique*, *61*(9), 795–808. https://doi.org/10.1680/geot.9.P.134

Zeng, X., and Steedman, R. S. (1993). On the behaviour of quay walls in earthquakes. *Géotechnique*, *43*(3), 417–431. https://doi.org/10.1680/geot.1993.43.3.417

Zerouali, B., Bailek, N., Tariq, A., Kuriqi, A., Guermoui, M., Alharbi, A. H., Khafaga, D. S., and El-kenawy, E.-S. M. (2024). Enhancing deep learning-based slope stability classification using a novel metaheuristic optimization algorithm for feature selection. *Scientific Reports*, *14*, 21812. https://doi.org/10.1038/s41598-024-72588-5

Zhang, G., Tu, F., Tang, Y., Chen, X., Xie, K., and Dai, S. (2023). Application of geophysical prospecting methods ERT and MASW in the landslide of Daofu County, China. *Frontiers in Earth Science*, *10*, Article 1054394. https://doi.org/10.3389/feart.2022.1054394

Zhang, W., Wang, L., and Dai, Z. (2019). MPM modeling of Fundão dam failure: A study of failure mechanisms and run-out analysis. *Engineering Geology*, *261*, 105267.

Zhang, Y., Chen, G., Zheng, L., Li, Y., and Zhuang, X. (2013). Effects of geometries on three-dimensional slope stability. *Canadian Geotechnical Journal*, *50*(3), 233–249.

Zhao, J., Yu, Y., Xu, H., Zhang, R., Ma, Y., and Li, J. (2024). Multi-directional viscous damping absorbing boundary in numerical simulation of elastic wave dynamic response. *Applied Sciences*, *14*(5), Article 2183. https://doi.org/10.3390/app14052183

Zhong, Q., Wang, L., Chen, S., Chen, Z., Shan, Y., Zhang, Q., Ren, Q., Mei, S., Jiang, J., Hu, L., and Liu, J. (2021). Breaches of embankment and landslide dams: State of the art review. *Earth-Science Reviews*, *216*, 103597. https://doi.org/10.1016/j.earscirev.2021.103597

Zhou, Y., Chen, X., and Wang, F. (2025). Amplitude-scaling bias analysis of ground motion record set in strip method for structural seismic fragility assessment. *Buildings*, *15*(3), 401.

Zhuang, Y., Hu, X., He, W., Shen, D., and Zhu, Y. (2024). Stability analysis of a rocky slope with a weak interbedded layer under rainfall infiltration conditions. *Water, 16*(4), 604. https://doi.org/10.3390/w16040604

http-1: https://www.ice.org.uk/what-is-civil-engineering/infrastructure-projects/aberfan-disaster-lessons-learned (accessed June 14, 2025).

http-2: https://www.epa.gov/environmental-geophysics/borehole-optical-televiewer-otv (accessed September 25, 2025).

http-3: https://www.epa.gov/environmental-geophysics/borehole-acoustic-televiewer-atv (accessed September 25, 2025).

http-4: https://www.usbr.gov/tsc/techreferences/mands/rockmanual/green_uniqueUSBR/6515.pdf (accessed September 10, 2025).

http-5:
https://www.precisiondrillingaustralia.com.au/blog/vibrating-wire-pizeometer/ (accessed September 10, 2025).

http-6:
https://smemonitoring.co.za/a-practical-guide-for-geotechnical-and-groundwater-monitoring/ (accessed December 20, 2025).

http-7:
https://www.geosense.com/wp-content/uploads/2021/04/Piezometers-In-depth-V1.0.pdf (accessed September 10, 2025).

http-8:
https://www.conetec.com/services/geophysical-testing/p-s-logging (accessed September 16, 2025).

http-9:
https://forneyonline.com/simple-guide-astm-d7012/ (accessed September 15, 2025).

http-10:
https://isrm.net/isrm/page/show/1305 (accessed November 15, 2025).

http-11:
https://www.usbr.gov/tsc/techreferences/mands/rockmanual/rockmanual.html (accessed September 15, 2025).

http-12:
https://www.tensarinternational.com/resources/articles/remote-sensing-in-geotechnics (accessed November 12, 2025).

http-13:
https://www.ciria.org/CIRIA/news/CIRIA_news2/Beyond_the_boundaries_-_slope_design_and_management.aspx (accessed October 18, 2025).

http-14:
https://www.rocscience.com/learning/facilitating-geotechnical-engineering-problems-using-metaheuristic-optimization-algorithms (accessed October 22, 2025).

http-15:
https://www.rocscience.com/help/slide2/overview/technical-specifications (accessed July 16, 2025).

http-16:
https://www.rocscience.com/help/rs2/overview/technical-specifications (accessed July 16, 2025).

http-17:
https://www.seequent.com/products-solutions/plaxis-2d/ (accessed July 16, 2025).

http-18:
https://www.seequent.com/products-solutions/plaxis-3d/ (accessed July 16, 2025).

http-19: https://www.itascainternational.com/software/flac-constitutive-models (accessed July 16, 2025).

http-20:
https://docs.itascasoftware.com/itasca900/flac3d/docproject/source/modeling/introduction/generalfeatures.html (accessed July 16, 2025).

http-21:
https://www.seequent.com/products-solutions/geostudio-2d/ (accessed July 16, 2025).

http-22:
https://www.finesoftware.eu/geotechnical-software/slope-stability/ (accessed July 16, 2025).

http-23:
https://www.finesoftware.eu/geotechnical-software/fem-earthquake/ (accessed July 16, 2025).

http-24:
https://docs.itascacg.com/flac3d700/3dec/docproject/source/theory/3dectheory/theory_background.html (accessed July 16, 2025).

http-25:
https://www.itascacg.com/software/udec (accessed July 16, 2025).

http-26:
https://www.ensoftinc.com/products/utexas/ (accessed June 05, 2025).

http-27:
https://damtoolbox.org/wiki/Pseudo-Dynamic_Analysis (accessed September 9, 2025).

http-28:
https://blogs.agu.org/landslideblog/2008/12/11/the-vaiont-vajont-landslide-of-1963/ (accessed September 13, 2025).

http-29:
https://ncfi.com/case-studies/neshoba-spillway-rehabilitation (accessed May 30, 2025).

http-30:
https://damsafety.org/dam-failures (accessed July 22, 2025).

http-31:
https://damfailures.org/case-study/oroville-dam-california-2017/ (accessed July 11, 2025).

http-32:
https://damfailures.org/case-study/guajataca-dam-puerto-rico-2017/ (accessed September 09, 2025).

http-33:
https://damfailures.org/case-study/teton-dam-idaho-1976/ (accessed August 05, 2025).

http-34:
https://damfailures.org/case-study/sugar-creek-watershed-dam-no-l-44-oklahoma-2007/ (accessed April 20, 2025).

http-35:
https://damfailures.org/lessons-learned/dams-located-in-seismic-areas-should-be-evaluated-for-liquefaction-cracking-potential-fault-offsets-deformations-and-settlement-due-to-seismic-loading (accessed July 22, 2025).

http-36:
https://damfailures.org/case-study/hebgen-dam-montana-1959/ (accessed July 22, 2025).

http-37:
https://damsafety.org/content/dam-failure-case-study-fontenelle-dam-wyoming-1965 (accessed July 22, 2025).

http-38:
https://www.ciria.org/CIRIA/News/blog/reusing_poor_marginal_soil.aspx (accessed October 09, 2025).

http-39:

https://chatgpt.com (accessed January 1, 2025).

http-40:

https://gemini.google.com (accessed January 1, 2025).

http-41:

https://notebooklm.google.com (accessed January 1, 2025).

APPENDIX

DISCLAIMER (Institutional Independence)

This dissertation has been prepared by the author in an academic and personal capacity. The analyses, interpretations, conclusions, and any opinions expressed herein are solely those of the author. They do not necessarily reflect, and should not be attributed to, the views of the General Directorate of State Hydraulic Works of Türkiye (DSİ) or any other institution. Nothing in this dissertation should be construed as an official statement, policy, guidance, or position of DSİ, nor as institutional endorsement of any kind.

AI TRANSPARENCY STATEMENT

Some illustrative (non-data) visual elements included in this dissertation (e.g., conceptual schematics, graphical abstractions, and figure layout assistance), as well as the wording refinement of non-technical passages, were prepared with the support of generative AI/ large language model (LLM) tools, including ChatGPT (OpenAI; GPT-3.5/4.0/5.0/5.1/5.2 models)[60], Gemini (Google; 1.5 Flash/2.5/3.0/3.0 Pro/3.1 Pro models)[61], and NotebookLM (Google)[62]. The utilization of these tools was strictly limited to Chapter 2 (Literature Review) and occurred predominantly during the year 2025. The author has meticulously reviewed, edited, and verified all AI-assisted outputs and remains fully responsible for the content of this dissertation. No confidential or restricted information was provided to these AI tools. Generative AI tools were not used to create, alter, or fabricate research data, monitoring records, numerical calculations, analysis outputs, or conclusions; all such data were generated strictly through the stated methods and supported by the cited sources.

[60]http-39: https://chatgpt.com (accessed January 1, 2025).
[61]http-40: https://gemini.google.com (accessed January 1, 2025).
[62]http-41: https://notebooklm.google.com (accessed January 1, 2025).

CURRICULUM VITAE

ORCID NO **:** 0000-0001-9205-488X

Name Surname **: Ahmet Ali Mert**

Foreign Language **: English (C2)**

Education and Professional Background:

- 2019–Present, **Senior Civil (Geotechnical) Engineer**, General Directorate of State Hydraulic Works (DSİ), Dams & Hydroelectric Power Plants Dept., Ankara, Türkiye.
- 2014–2016, **Civil Works & Construction Manager**, Huawei Technologies Co. Ltd., Istanbul, Türkiye.
- 2012–2013, **Geotechnical Design Engineer**, Emay International Engineering & Consultancy Inc., İstanbul, Türkiye.
- 2020–2026, **PhD in Civil Engineering (Geotechnical)**, Eskişehir Technical University, Türkiye. Dissertation: *Static and Dynamic Stability Assessment of Slopes Adjacent to Appurtenant Hydraulic Structures and Stabilization Recommendations.*
- 2017–2019, **MSc in Geotechnical Engineering**, The University of Texas at Austin, USA. Thesis: *Geotechnical Properties, One-Dimensional Consolidation Behavior and Liquefaction Susceptibility of Glaciolacustrine Clay Samples from the Oso Landslide.*
- 2013–2015 **MSc in Soil Mechanics & Geotechnical Engineering** (all requirements completed except thesis; degree not awarded), Istanbul Technical University, Türkiye.
- 2007–2012, **BSc in Civil Engineering** (**5th in department**) (Double Major: **BSc in Environmental Engineering — 1st in department**), Anadolu University, Türkiye.

Publications and/or Scientific/Artistic Activities:

- 2026, Mert, A.A., Salman, M. and Çalışkan, F. “Overcoming Geological Challenges in the Construction of a CFSGD Diversion Tunnel.” Accepted for ITA-AITES World Tunnel Congress (WTC 2026), Montreal. [Conference Paper]
- 2024, Mert, A.A. and Çalışkan, F. “Stability of Portal Slopes of a Diversion Tunnel after the Kahramanmaraş Earthquakes.” ITA-AITES WTC 2024, Shenzhen. [Conference Paper]
- 2024, Demirdöğen, S., Mert, A.A., et al. “Performance of Sürgü, Kartalkaya and Tahtaköprü Dams During Feb 6, 2023 Earthquakes.” 7th Meeting of EWG, ICOLD, Athens. [Symposium Paper]
- 2021, Karslioğlu, A., Mert, A.A. and Onur, M.İ. “New Trends in Determination of Soil Properties.” *European Journal of Science and Technology*, Special Issue 28. [Journal Article]
- 2020, Wooten, R.L., Mert, A.A., et al. “Geotechnical Effects of Hurricane Harvey.” *ISSMGE Intl. Journal of Geoengineering Case Histories*, 5(4). [Journal Article]

Awards:

- 2016–2019, MoNE/DSİ Graduate Sponsorship (UT Austin).
- 2018, Graduate Dean's Prestigious Fellowship Supplement (UT Austin).
- 2012, TÜBİTAK 2nd Prize for Bachelor Thesis on Flood Mapping (GIS + Hydrologic + Hydraulic Modeling).

Professional Union/Association/Organization Memberships:

- Turkish Chamber of Civil Engineers (İMO).
- Turkish Chamber of Environmental Engineers (ÇMO).